DOE/NV/10461--T46

EVALUATION OF THE GEOLOGIC RELATIONS AND SEISMOTECTONIC STABILITY OF THE YUCCA MOUNTAIN AREA NEVADA NUCLEAR WASTE SITE INVESTIGATION (NNWSI)

PROGRESS REPORT

30 SEPTEMBER 1994

CENTER FOR NEOTECTONIC STUDIES

MACKAY SCHOOL OF MINES

UNIVERSITY OF NEVADA, RENO

Table of Contents

Annual Progress Report----General Task
Prepared by Steven G. Wesnousky

October 1, 1993 to September 30, 1994

Introduction

This report provides a summary of progress for the project "Evaluation of the Geologic Relations and Seismotectonic Stability of the Yucca Mountain Area, Nevada Nuclear Waste Site Investigation (NNWSI)." A similar report was previously provided for the period of 1 October 1992 to 30 September 1993. The report initially covers the activities of the General Task and is followed by sections that describe the progress of the other ongoing Tasks which are listed below.

Task 1:	Quaternary Tectonics
Task 3.	Mineral Deposits, Volcanic Geology
Task 4:	Seismology
Task 5:	Tectonics
Task 8:	Basinal Studies

General Task

Staff

Steven G. Wesnousky, Project Director; Nina G. Krob, Administrative Assistant

Administrative Activities

The General Task continued the (1) coordination and oversight of the research of Tasks 1, 3, 5, and 8, the (2) oversight of budgets and (3) the collation and preparation of required monthly reports. As well, Dr. Wesnousky has continued to represent NWPO at meetings with the National Academy of Sciences, the Nuclear Regulatory Commission, and the Department of Energy.

Steven G. Wesnousky attended the following meetings and provided the following seminars for NWPO:

Nov. 9-10, 1993, Lecture to the National Academy of Sciences' Committee on the Technical Bases for Yucca Mountain Standards in Las Vegas entitled 'Uncertainties in Seismic Hazard Analysis'.

Nov. 17, 1993, Nuclear Regulatory Commission/DOE Technical Exchange on Seismic Hazard Methodology in Washington, D.C.

Dec. 22-23, 1993, Field Trip to examine Neotectonic studies of Paintbrush, Solitario, Ghost Dance, and Bare Mountain Faults at Yucca Mountain with NWPO

Jan. 30-31, 1994, AC&W field trip to Yucca Mountain.

March 8-9, 1994, Invited lecture to Nuclear Waste Technical Review Board Panel on Structural Geology & Geoengineering entitled 'How Good is Probabilistic Seismic Hazard Analysis?' in San Francisco.

April 28, 1994, Seminar to Las Vegas section of the Geological Society of Nevada describing earth science studies related to Yucca Mountain overseen by the Center for Neotectonic Studies.

May 2-5, 1994, Field trip with NWPO sponsored investigators to examine fault lineaments at Yucca Mountain.
June 29-30, 1994, Attend ACNW meeting and provide presentation "Low Sun Angle Photography as it relates to Tectonics of Yucca Mountain"
July 14, 1994--Meeting of PI's of NWPO sponsored technical programs in Carson City.

Technical Activities

Technical activities have been divided between research activities and review of technical reports.

Technical Reports Reviewed:

Sept. 23, 1994--DOE Topical Report on Seismic Hazard Analysis Methodology

Research Activities:

Projects Completed:

Subsequent to the Little Skull Mountain earthquake of June 1992, NWPO sponsored the collection of a set of high-altitude 1:12,000 scale low-sun-angle aerial photographs. During the year, graduate student Takashi Kumamoto, under the supervision of Steven G. Wesnousky, completed a first analysis of the photos. The results of the analysis are provided as a set of 1:12,000 fault lineament maps in the appendix accompanying this report. The analysis includes all or part of the following 7.5 minute topographic quadrangles in Nevada: Cane Spring, Camp Desert Rock, Specter Range, Jackass Flats, Striped Hills, and Skull Mountain. The maps have not been field-checked. Future work could entail mapping of Quaternary units offset by faults in the vicinity of Yucca Mountain to place limits on the most recent time of motion and, possibly, slip rate of these faults.

Ongoing Projects:

The General Task currently is overseeing two projects, each being conducted through partial support of graduate students Takashi Kumamoto and Mike Sleeman. Each is related to the analysis of seismic hazard at Yucca Mountain.

A. Estimation of Earthquake Size.

Estimation of the size of expected earthquakes along mapped faults is generally determined from empirically derived relationships between fault length and seismic moment or magnitude for historical earthquakes. There are numerous of these compilations, including a most recent by Wells and Coppersmith (BSSA, v.84, 974-1003, 1994). Many of these compilations and resulting regressions of earthquake size versus fault length tend to ignore an observation that has been in the seismological literature for some time, which is that the relationship of earthquake size versus rupture length in earthquakes is a function of the repeat time or fault slip rate on which the earthquake occurs (e.g. Scholz et al, BSSA, v. 76, 65-70, 1986; Kanamori and Allen, in Earthquake Source Mechanics, v. 6, 1985; Wesnousky, JGR,

v. 91, 12,587-12,631, 1986). For that reason, in collaboration with John Anderson, we have begun to quantify the relationship between earthquake rupture length, fault slip rate, and earthquake size for a data set of historical earthquakes using a least-squares multivariate regression on those three variables. Table 1 is a synthesis of historical earthquakes for which there exist estimates of moment-magnitude, fault rupture length, and the slip rate of the fault on which the respective earthquake occurred. The result of a least squares regression on the data is shown in Figure 1. The results of the regression actually results in a reduction of the misfit of predicted to observed values as compared to the predictions of a two-variable regression on moment-magnitude versus length. Moreover, the result indicates that slow slipping faults will generally produce a larger moment-magnitude earthquake than a faster slipping fault, by as much as .3 to .4 magnitude units when considering faults slipping at .01 to 10 mm/yr, respectively. Ongoing work will entail a rigorous review of the input. If the review supports the data, the resulting analytic regressions will be the firm basis to suggest that information regarding fault slip rate should be used in assessing the expected size of future earthquakes.

B. Analysis of Seismic Hazard.

Mike Sleeman, under the supervision of Steven G. Wesnousky, has implemented a synthesis of currently available data bearing on the location and activity of mapped faults and the instrumental record of seismicity in the Yucca Mountain area which will be the basis to begin assessing the uncertainties in seismic hazard analysis of the region attendant to the assumption of various models of fault behavior and empirical relations between earthquake size, source-to-site distance, and strong ground motion.

Principally funded by other sources but of important consequence to understanding the tectonic framework and style of earthquake faulting in the Basin and Range, and more generally the mechanics of earthquake faults, as well as the state of the art in seismic hazard analysis, Steven G. Wesnousky along with graduate students Janice Murphy, John Caskey, Mark Stirling, and Takashi Kumamoto and former Research Associate Craig Jones have presented the following abstracts at professional meetings and published the following papers.

Meetings and Abstracts:

1993 AGU Annual Fall Meeting, San Francisco, CA

Hirabayashi, C. K., T. K. Rockwell, S. G. Wesnousky, Clustering of Seismic Activity on the San Miguel Fault, Baja, California, *EOS Supplement, Program and Abstracts,* Oct. 26, 1993, p. 428.

Stirling*, M. W., S. G. Wesnousky, and M. D. Petersen, Slip Rates, Paleoearthquake Histories, Earthquake Frequency Distributions, and Seismic Hazard in Southern California, *EOS supplement, Programs and Abstracts,* Oct. 26, 1993, p. 575.

Jackson, D. D., K. Aki, C. A. Cornell, J. Dieterich, T. Heaton, T. Henyey, Y. Kagan, M. Mahdyiar, k. McNally, S. Park, S. Salyards, D. Schwartz, S. Ward, R. Weldon, and S. G. Wesnousky, Future Seismic Hazards of Southern California, *EOS Supplement, Programs and Abstracts,* Oct. 26, 1993, p. 426.

1994 SSA Annual Meeting, Pasadena, CA

Caskey*, S. J., S. G. Wesnousky, and P. Z. Zhang, Surface Rupture Characteristics and Slip Distribution for the 16 December 1954 Fairview Peak (Ms=7.2) and Dixie Valley (Ms=6.8) Earthquakes, Central Nevada, Seismological Research Letters, v. 65, no. 1, 1994, p. 31.

Kumamoto, T., S. G. Wesnousky, N. Chida, T. Nakata, K. Shimazaki, and m. Okamura, High Resolution Seismic Reflection Survey in Lake Tahoe: Preliminary Evidence of Faulting in Young Sediments, Seismological Research Letters, V. 65, no. 1, 1994, p. 31.

1994 Paleoseismology Conference, Sept. 16-18, Monterey

Caskey*, S. J., S. G. Wesnousky, and P. Z. Zhang, Surface Rupture Characteristics and Slip Distribution for the 16 December 1954 Fairview Peak (Ms=7.2) and Dixie Valley (Ms=6.8) Earthquakes, Central Nevada.

Publications

Guang*, Y., S. G. Wesnousky, and G. Ekstrom (1993), Slip Partitioning along Major Convergent Plate Boundaries, Journal of Geophysical Research, Pure and Applied Geophysics (PAGEOPH), 140, 183-210.

Murphy*, J., and S. G. Wesnousky (1994), Seismic Hazard within the Greater San Francisco Bay Region: A Reevaluation after the Loma Prieta Earthquake, U.S. Geological Survey Professional Paper 1551-A, A255-A272.

Wesnousky, S. G. (1994), The Gutenberg-Richter or Characteristic Earthquake Distribution, Which is it?, Bulletin of the Seismological Society of America, v. 84, no. 6., in press.

Wesnousky, S. G. and C. H. Jones (1994), Slip Partitioning, Spatial and Temporal Changes in the Regional Stress Field, and the Relative Strength of Active Faults in the Basin and Range, GEOLOGY, v. 22, no. 11, 1031-1034.

References

Kumamoto, T., and S. G. Wesnousky, 1994, Low Sun Angle Aerial Photo Reconnaissance of Active Faults in Vicinity of Little Skull Mountain, Nye County, Nevada, Cane Spring Quadrangle, U.S. Geological Survey.

_____, 1994, Low Sun Angle Aerial Photo Reconnaissance of Active Faults in Vicinity of Little Skull Mountain, Nye County, Nevada, Camp Desert Rock Quadrangle, U.S. Geological Survey.

_____, 1994, Low Sun Angle Aerial Photo Reconnaissance of Active Faults in Vicinity of Little Skull Mountain, Nye County, Nevada, Specter Range, NW Quadrangle, U.S. Geological Survey.

_____, 1994, Low Sun Angle Aerial Photo Reconnaissance of Active Faults in Vicinity of Little Skull Mountain, Nye County, Nevada, Jackass Flats Quadrangle, U.S. Geological Survey.

_____, 1994, Low Sun Angle Aerial Photo Reconnaissance of Active Faults in Vicinity of Little Skull Mountain, Nye County, Nevada, Striped Hills Quadrangle, U.S. Geological Survey.

_____, 1994, Low Sun Angle Aerial Photo Reconnaissance of Active Faults in Vicinity of Little Skull Mountain, Nye County, Nevada, Skull Mountain Quadrangle, U.S. Geological Survey.

General Task Table 1. Fault Slip Rates and Earthquake Sizes

EQ number	yr mo day	Location	Mo	Mw	L. range	Length	min	max	srate
1	1811 12 16	New Madrid, MO		8.2	60-250	250.0	0.9	1.7	1.7
2	1848 10 16	Marlborough, New Zealand		7.1	95	95.0	5.0	10.0	7.5
3	1857 01 09	Fort Tejon, CA	7.00e+27	7.9	360-400	380.0	16.0	43.0	24.0
4	1868 10 21	Hayward,CA	1.56e+26	6.8	48	48.0	9.0	9.0	9.0
5	1872 03 26	Owens Valley, CA	3.10e+27	7.6	108	108.0	1.0	3.0	2.0
6	1888 09 01	N. Canterbury, New Zealand		7.2	25-35	30.0	11.0	25.0	18.0
7	1891 10 28	Nobi, Japan	1.50e+27	7.4	80	80.0	1.0	2.0	2.0
8	1896 08 31	Rikuu, Japan	1.40e+27	7.4	36-50	43.0	2.3	2.3	2.3
9	1906 04 18	San Francisco, CA	3.90e+27	7.7	420-470	445.0	7.5	32.0	19.0
10	1915 10 03	Pleasant Valley, NV	6.60e+26	7.2	34	34.0	0.3	1.0	0.5
11	1927 03 07	Tango, Japan	4.60e+26	7.1	33	33.0	0.2	0.2	0.2
12	1930 11 25	N. Izu, Japan	2.70e+26	6.9	22	22.0	1.0	2.0	2.0
13	1933 03 11	Long Beach, CA	4.10e+25	6.4	23	23.0	0.1	6.0	0.6
14	1934 06 07	Parkfield, CA	1.50e+25	6.1	20	20.0			33.9
15	1939 12 26	Erzihcan, Turkey	4.50e+27	7.7	350	350.0	5.0	8.0	6.5
16	1940 05 19	Imperial Valley, CA	2.70e+26	6.9	60	60.0	15.0	20.0	17.5
17	1942 12 20	Erbaa Niksar, Turkey	2.50e+26	6.9	50	50.0	5.0	8.0	6.5
18	1944 02 01	Gerede-Bolu, Turkey	2.40e+27	7.6	190	190.0	5.0	8.0	6.5
19	1952 07 21	Kern County, CA	1.10e+27	7.3	75	75.0	3.0	8.5	5.7
20	1953 03 18	Golen-Yenice, Turkey	7.30e+26	7.2	58	58.0	5.0	8.0	6.5
21	1954 12 16	Fairview Peak, NV	6.40e+26	7.2	46-63	46.0	0.1	0.1	0.1
22	1954 12 16	Dixie Valley, NV	2.90e+26	6.9	46	46.0	0.3	1.0	0.5
23	1956 02 09	San Miguel, Mexico	1.00e+26	6.6	22	22.0	0.2	0.5	0.3
24	1959 08 18	Hebgen Lake, MT	1.03e+27	7.3	26	26.0	0.8	2.5	1.4
25	1964 06 16	Niigata, Japan	3.20e+27	7.6	80	80.0			0.5
26	1966 06 28	Parkfield, CA	1.50e+25	6.1	37	37.0			33.9
27	1967 07 22	Mudurnu Valley, Turkey	8.80e+26	7.3	80	80.0	5.0	8.0	6.5
28	1968 04 09	Borrego Mtn, CA	1.20e+26	6.7	30-45	37.5	1.6	5.0	3.3
29	1969 04 28	Coyote Mtn., CA	3.80e+24	5.7	10	10.0	1.6	5.0	3.3
30	1971 02 09	San Fernando, CA	1.04e+26	6.6	16-17	17.0	2.0	7.5	5.0
31	1973 02 06	Luhuo, China	1.90e+27	7.5	89-110	90.0	5.0	10.0	7.0
32	1979 08 06	Coyote Lake, CA	5.10e+24	5.8	14	14.0	15.0	31.0	17.0
33	1979 10 15	Imperial Valley, CA	6.00e+25	6.5	30.5	30.5	15.0	20.0	17.5
34	1981 01 23	Daofu, China	1.30e+26	6.7	46	46.0	5.0	10.0	7.0
35	1983 05 02	Coalinga, CA	5.40e+25	6.5	25	25.0	1.0	7.0	1.0
36	1983 10 28	Borah Peak, ID	2.80e+26	6.9	30-39.5	30.0	0.1	0.3	0.3
37	1984 04 24	Morgan Hill, CA	2.00e+25	6.2	30	30.0	3.0	25.0	8.0
38	1986 07 08	N. Palm Springs, CA	1.62e+25	6.1	9-16	16.0	14.0	25.0	19.5
39	1987 03 02	Edgecumbe, New Zealand	6.30e+25	6.5	18-32	32.0	1.3	2.8	2.0
40	1987 11 24	Superstition Hills, CA	1.10e+26	6.7	27	27.0	2.0	6.0	4.0
41	1989 10 18	Loma Prieta, CA	3.00e+26	7.0	34	34.0	7.5	32.0	12.0
42	1990 07 16	Luzon, Phillippines	3.90e+27	7.7	110-120	120.0	10.0	20.0	15.0
43	1992 06 28	Landers, CA	8.20e+26	7.2	70-85	70.0	0.8	2.0	1.3
44	1994 01 17	Northridge, CA	1.38e+26	6.7	8-16	11.0	1.0	1.0	1.0

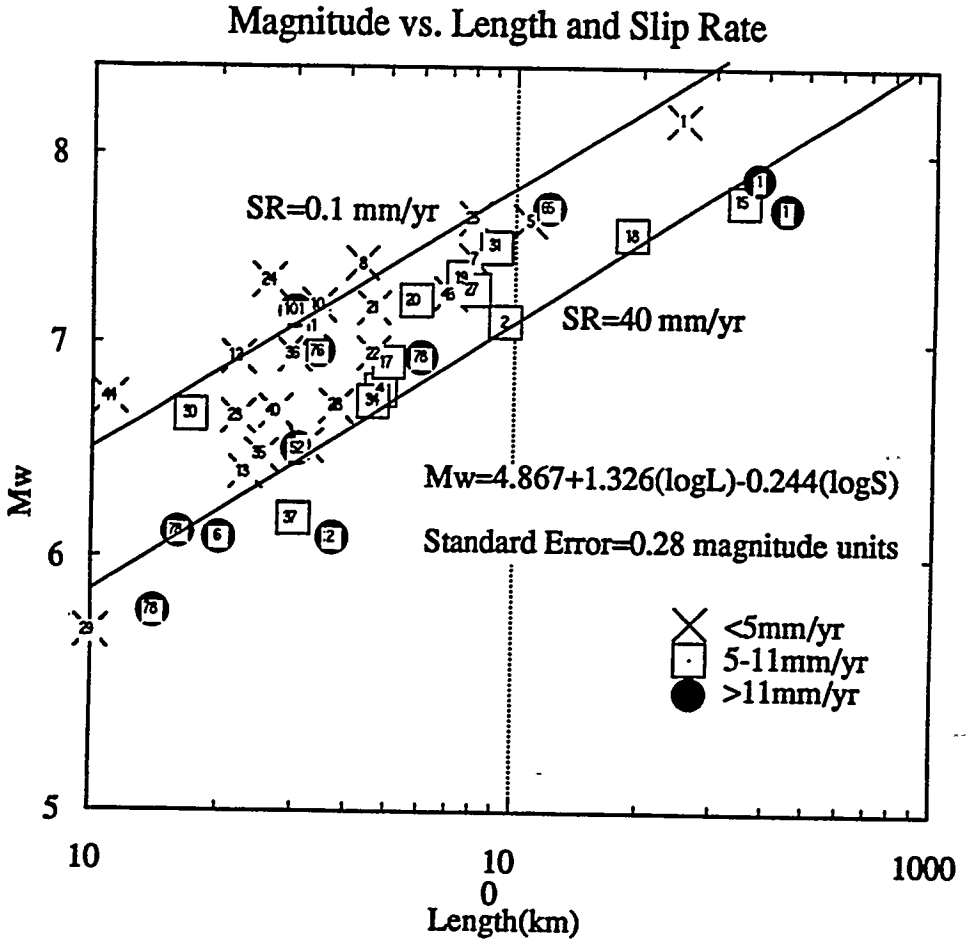

General Task Figure 1.

Appendix A

UNITED STATES
DEPARTMENT OF THE INTERIOR
GEOLOGICAL SURVEY

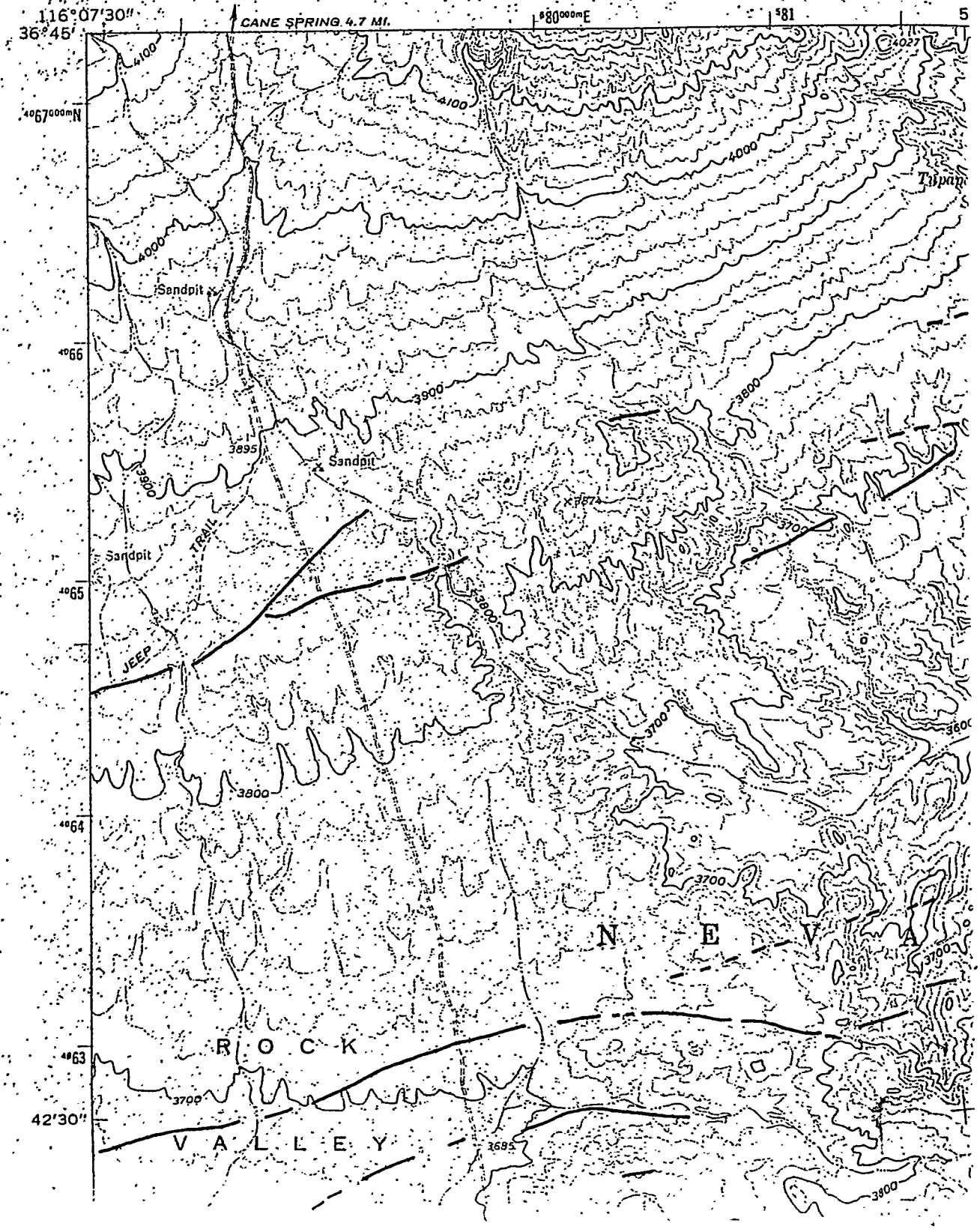

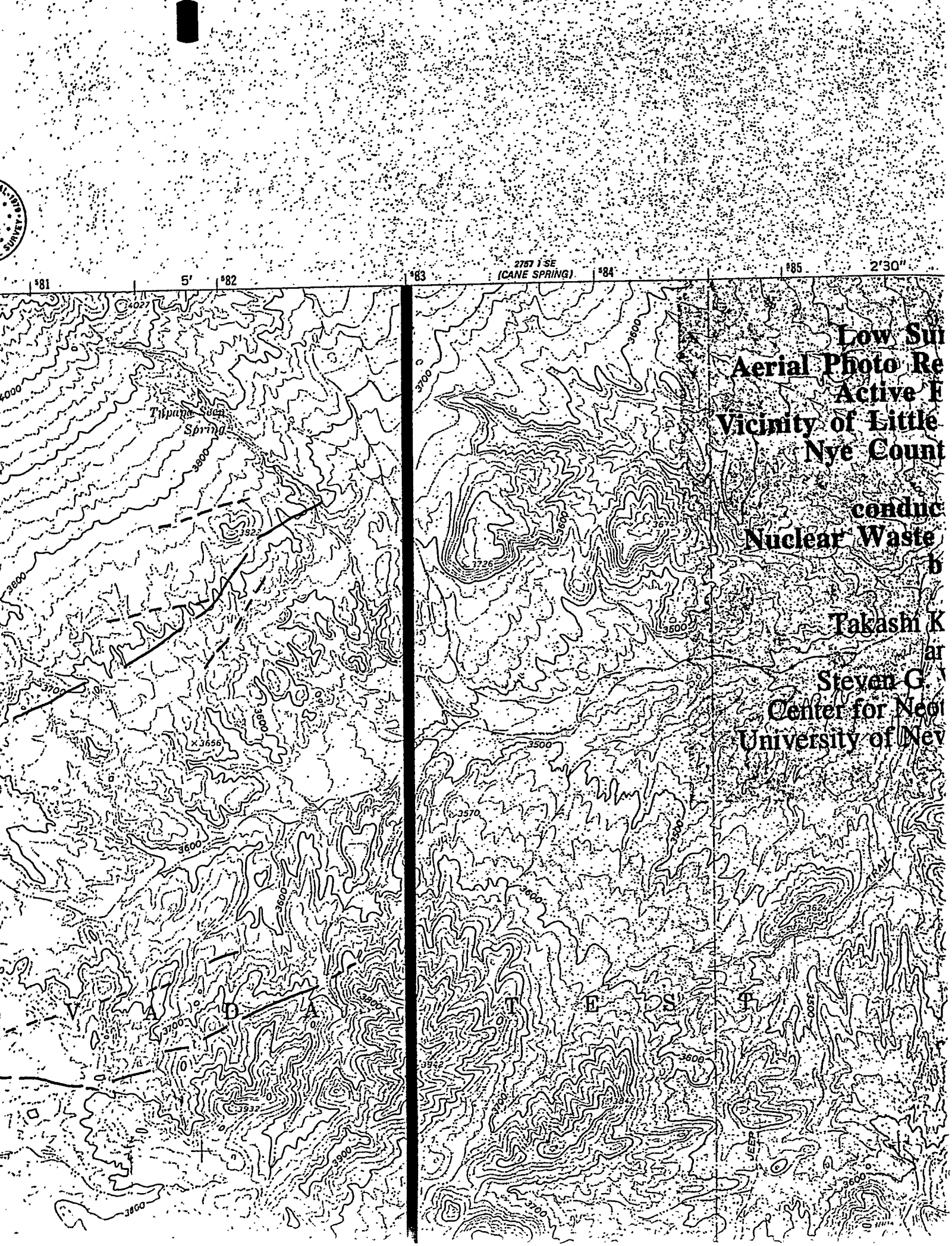

Low Sui
Aerial Photo Re
Active F
Vicinity of Little
Nye Count

condnc
Nuclear Waste
b

Takashi K
ar

Steven G.
Center for Neo
University of Nev

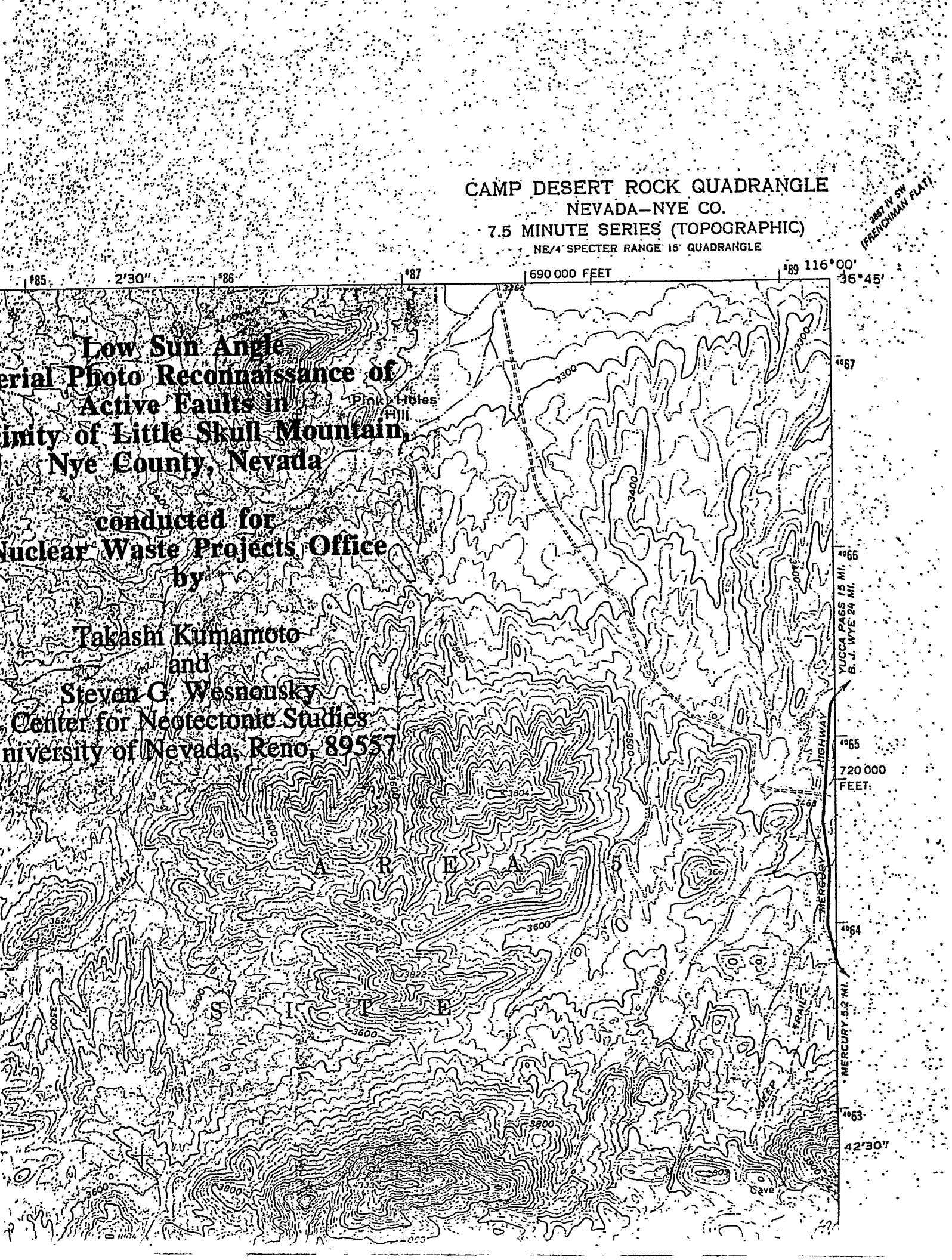
CAMP DESERT ROCK QUADRANGLE
NEVADA—NYE CO.
7.5 MINUTE SERIES (TOPOGRAPHIC)
NE/4 SPECTER RANGE 15' QUADRANGLE
2867 IV SW
(FRENCHMAN FLAT)
116°00'
36°45'
690 000 FEET
720 000 FEET
2'30"
Low Sun Angle
erial Photo Reconnaissance of
Active Faults in
inity of Little Skull Mountain,
Nye County, Nevada
conducted for
Nuclear Waste Projects Office
by
Takashi Kumamoto
and
Steven G. Wesnousky
Center for Neotectonic Studies
niversity of Nevada, Reno, 89557
Pink Holes
Hill
AREA 5
SITE
YUCCA PASS 15 MI.
B.J. WYE 24 MI.
HIGHWAY
MERCURY
MERCURY 5.2 MI.
FRAILE
Cave
42'30"

CAMP DESERT ROCK QUADRANGLE
NEVADA—NYE CO.
7.5 MINUTE SERIES (TOPOGRAPHIC)
NE/4 SPECTER RANGE 15' QUADRANGLE

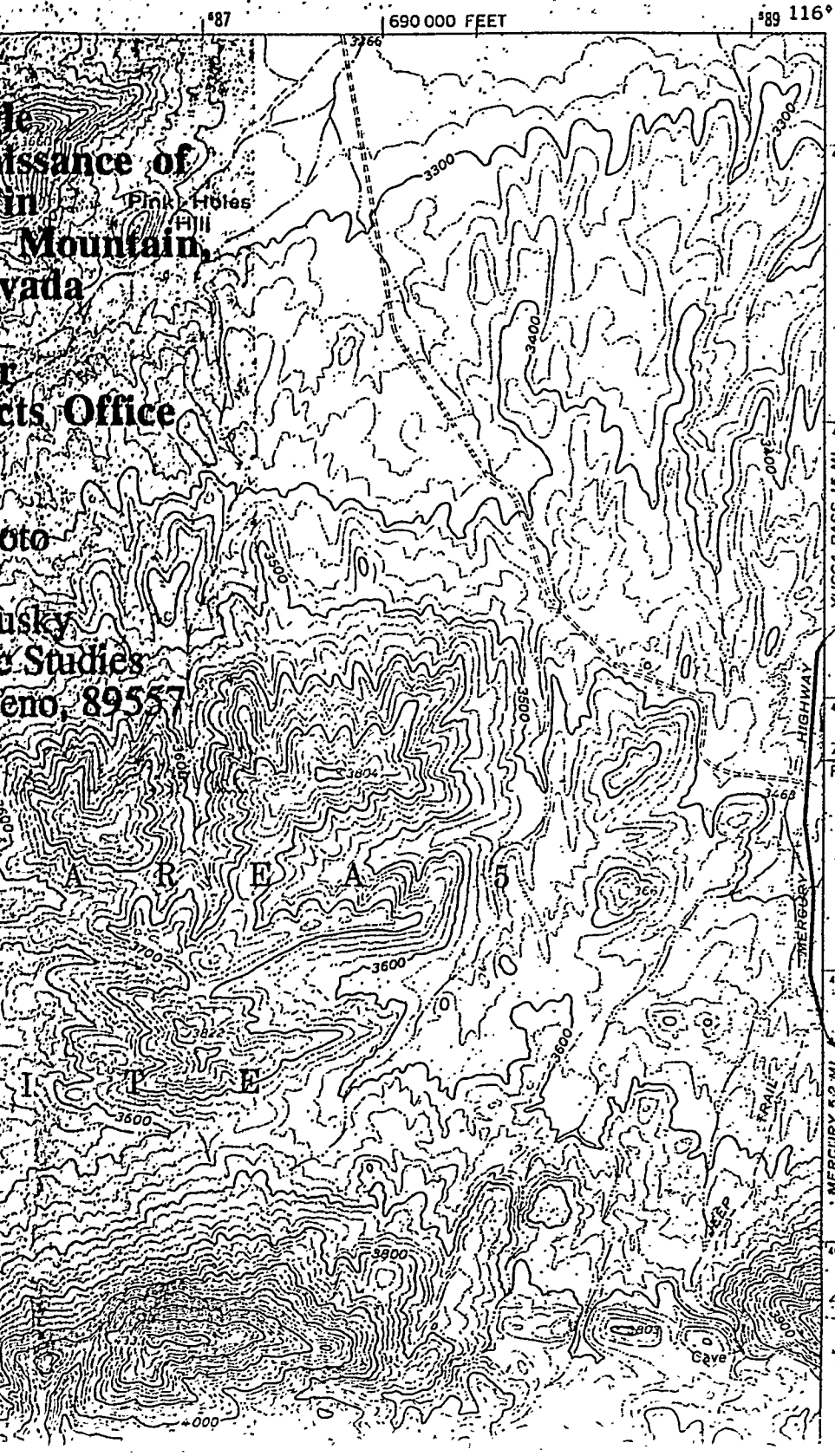

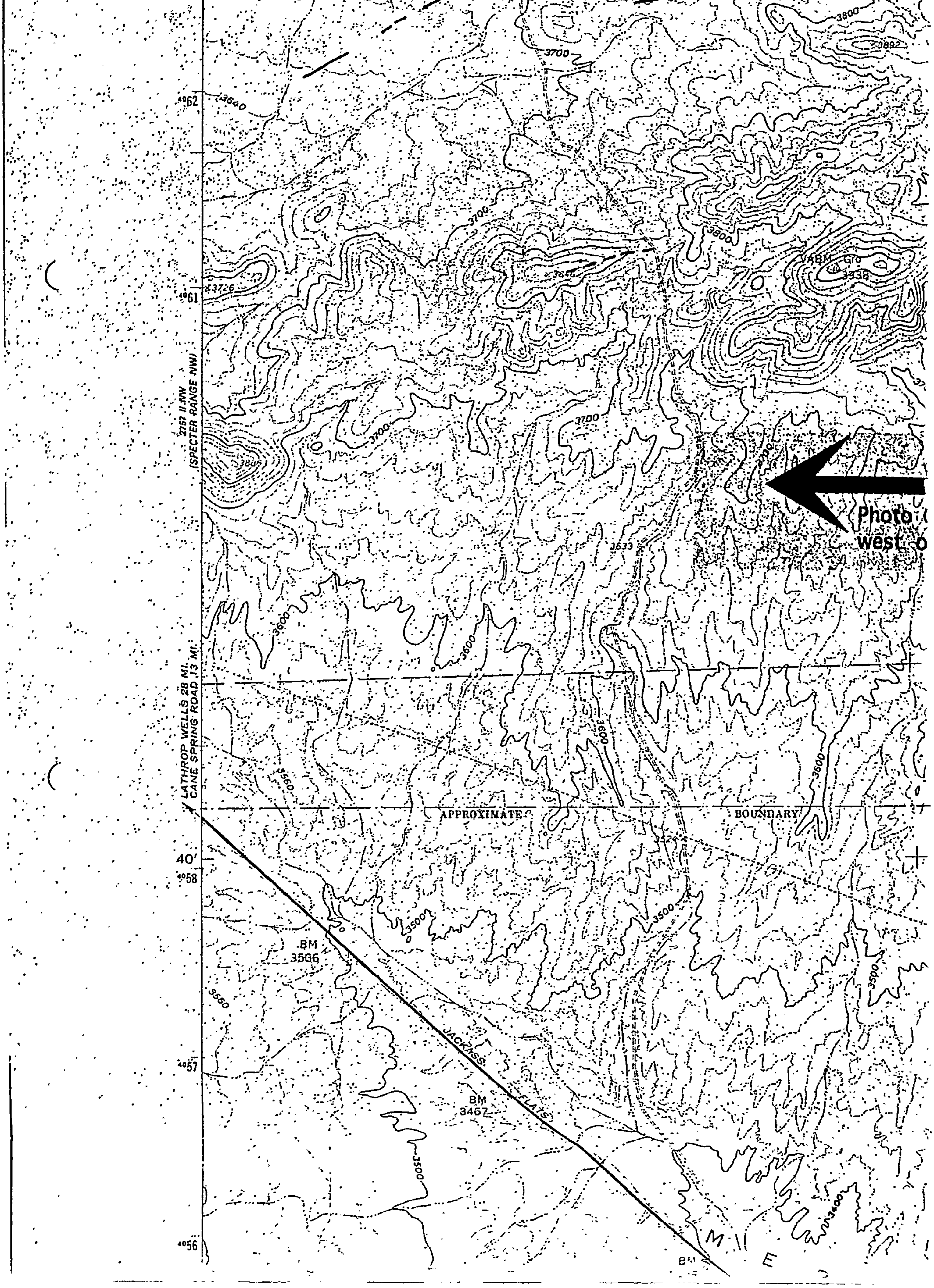

Photo
west
APPROXIMATE
BOUNDARY
JACKASS FLATS
LATHROP WELLS 28 MI.
CANE SPRING ROAD 13 MI.
2757 II NW
(SPECTER RANGE NW)
BM
3566
BM
3467
VABM
3938
3700
3800
3640
3600
3500
3560
3633
3524
40′

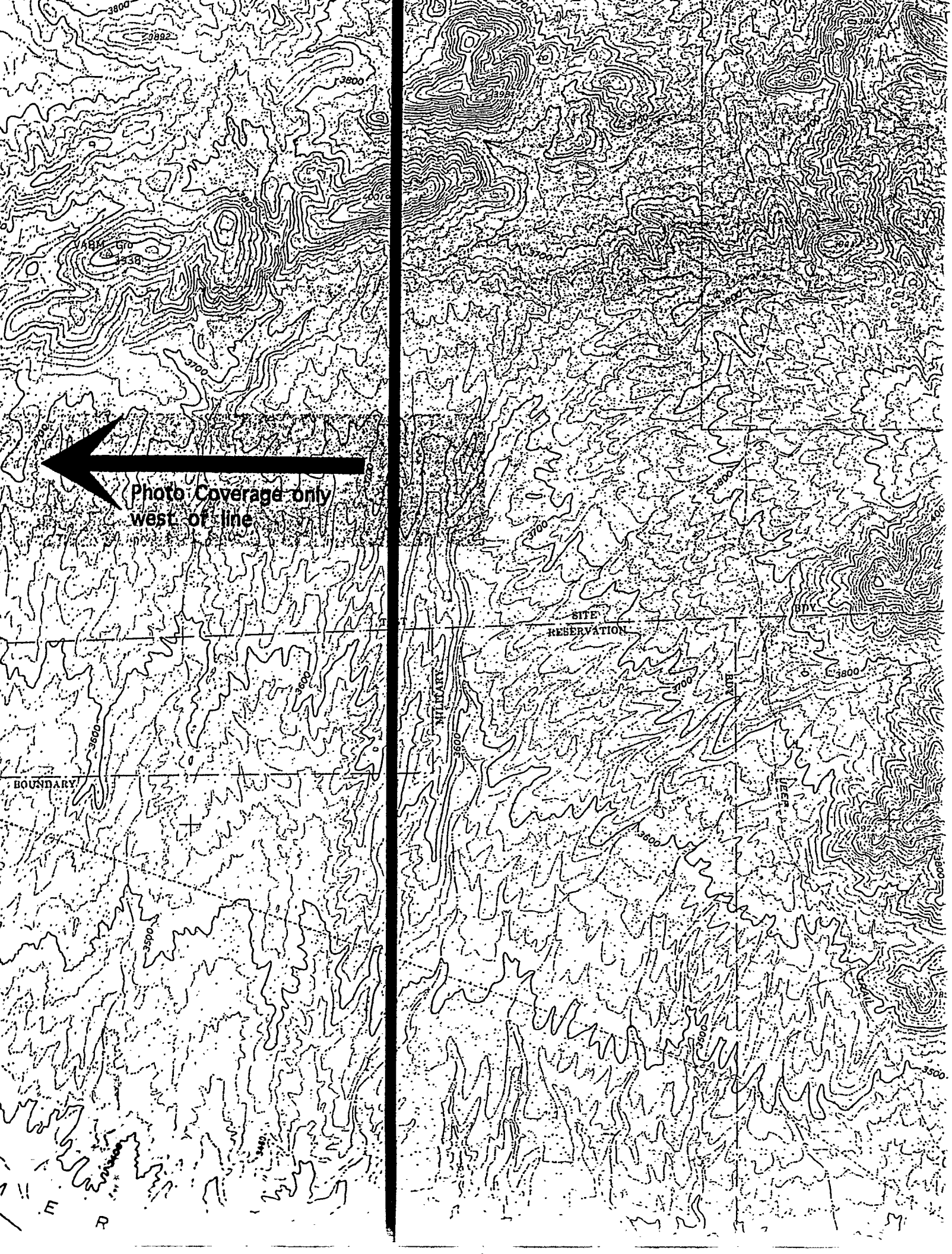
Photo Coverage only
west of line
SITE
RESERVATION
BOUNDARY
MILITARY
BUY
LEER
3800
3700
3600
3500

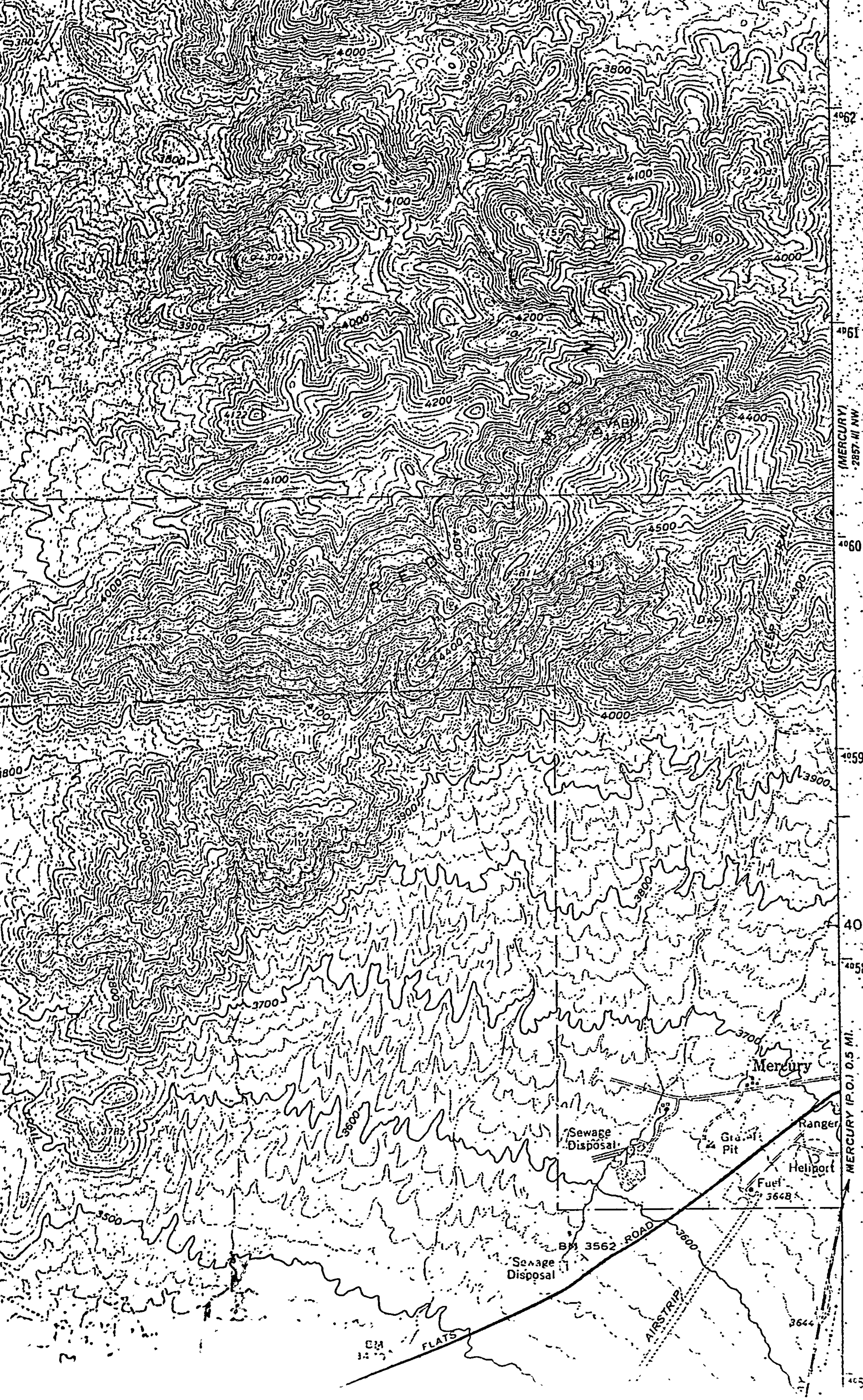
Mercury
Sewage Disposal
Gravel Pit
Ranger
Heliport
Fuel
3648
BM 3562
ROAD
FLATS
AIRSTRIP
3644
MERCURY (P.O.) 0.5 MI.
(MERCURY)
2857 II NW
4062
4061
4060
4059
40'
4058
4056
4100
4200
4500
4400
4000
3900
3800
3700
3600
3500

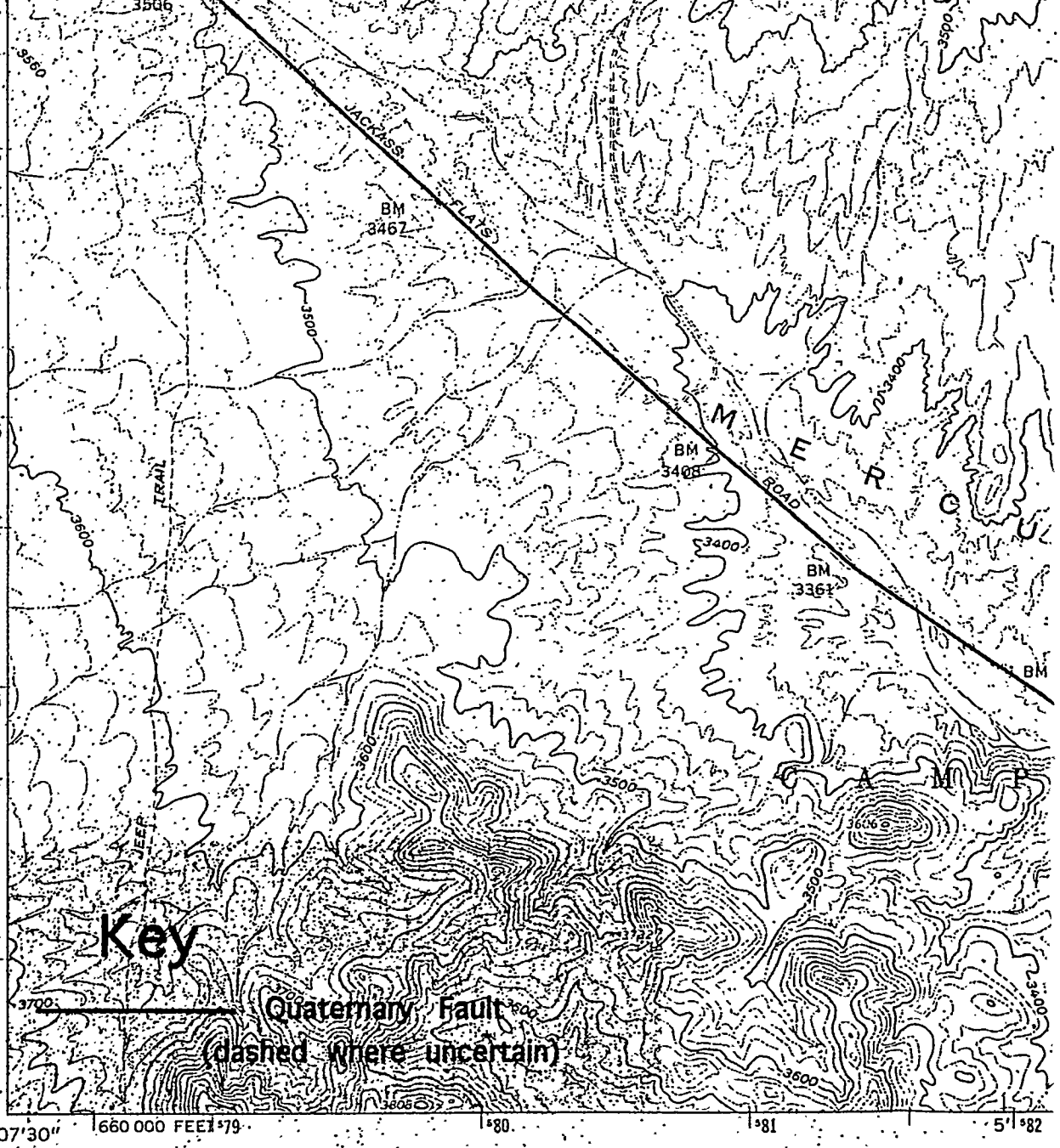

Mapped, edited, and published by the Geological Survey
in cooperation with the Atomic Energy Commission

Control by USGS, USC&GS, and the Atomic Energy Commission

Topography from aerial photographs by photogrammetric methods
Aerial photographs taken 1959. Field check 1961

Polyconic projection. 1927 North American datum
10,000-foot grid based on Nevada coordinate system, central zone
1000-meter Universal Transverse Mercator grid ticks,
zone 11, shown in blue
To place on the predicted North American Datum 1983
move the projection lines 7 meters north and
77 meters east as shown by dashed corner ticks

There may be private inholdings within the boundaries of
the National or State reservations shown on this map

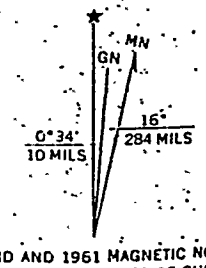

UTM GRID AND 1961 MAGNETIC NORTH
DECLINATION AT CENTER OF SHEET

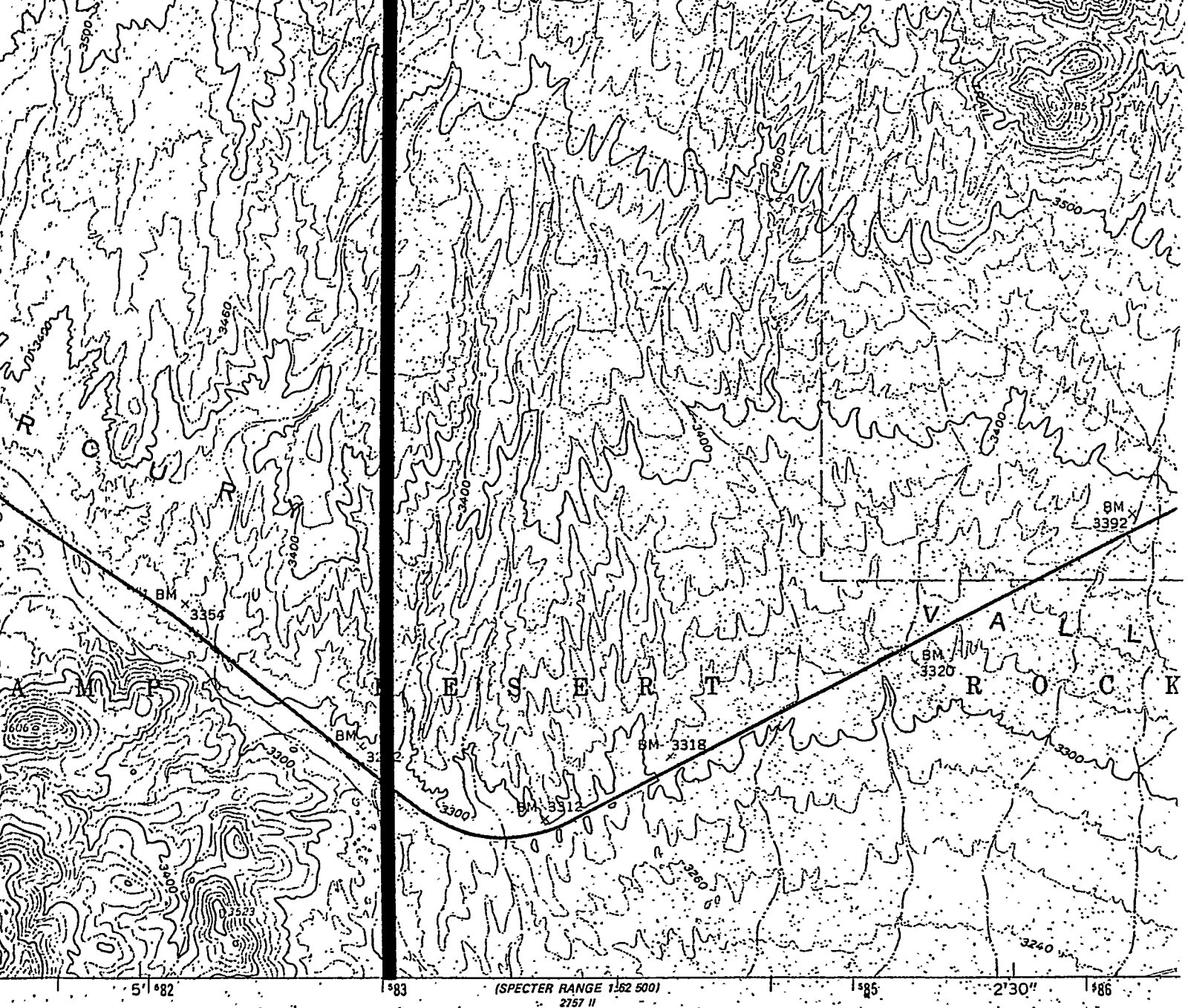

(SPECTER RANGE 1:62 500)
2757 II

SCALE 1:24 000

1 MILE
1000 0 1000 2000 3000 4000 5000 6000 7000 FEET
1 KILOMETER

CONTOUR INTERVAL 20 FEET
NATIONAL GEODETIC VERTICAL DATUM OF 1929

16°
34 MILS

NETIC NORTH
R OF SHEET

QUADF

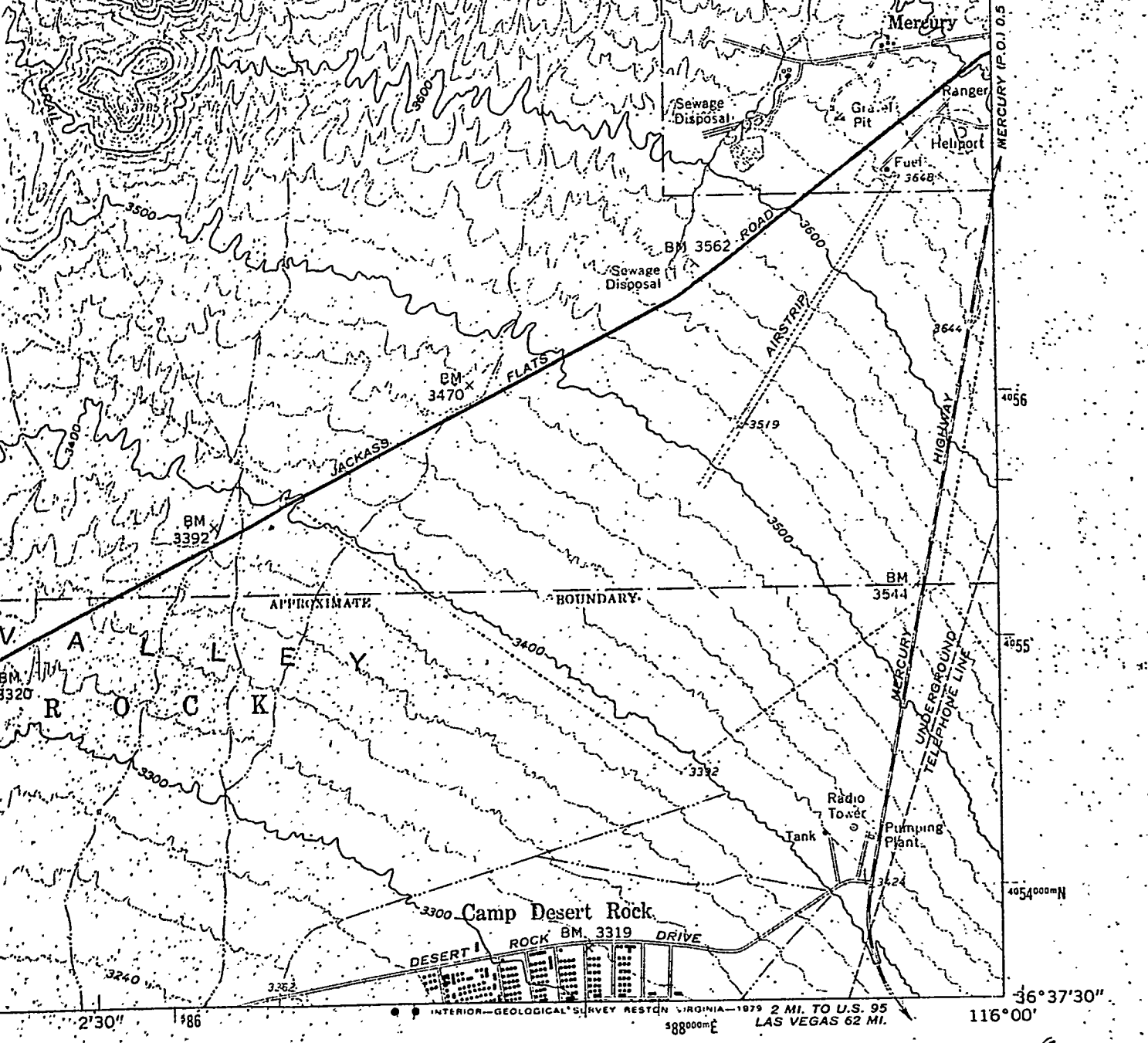

CAMP DESERT ROCK, NEV.

NE/4 SPECTER RANGE 15' QUADRANGLE

N3637.5—W11600/7.5

1961

DMA 2757 II NE—SERIES V896

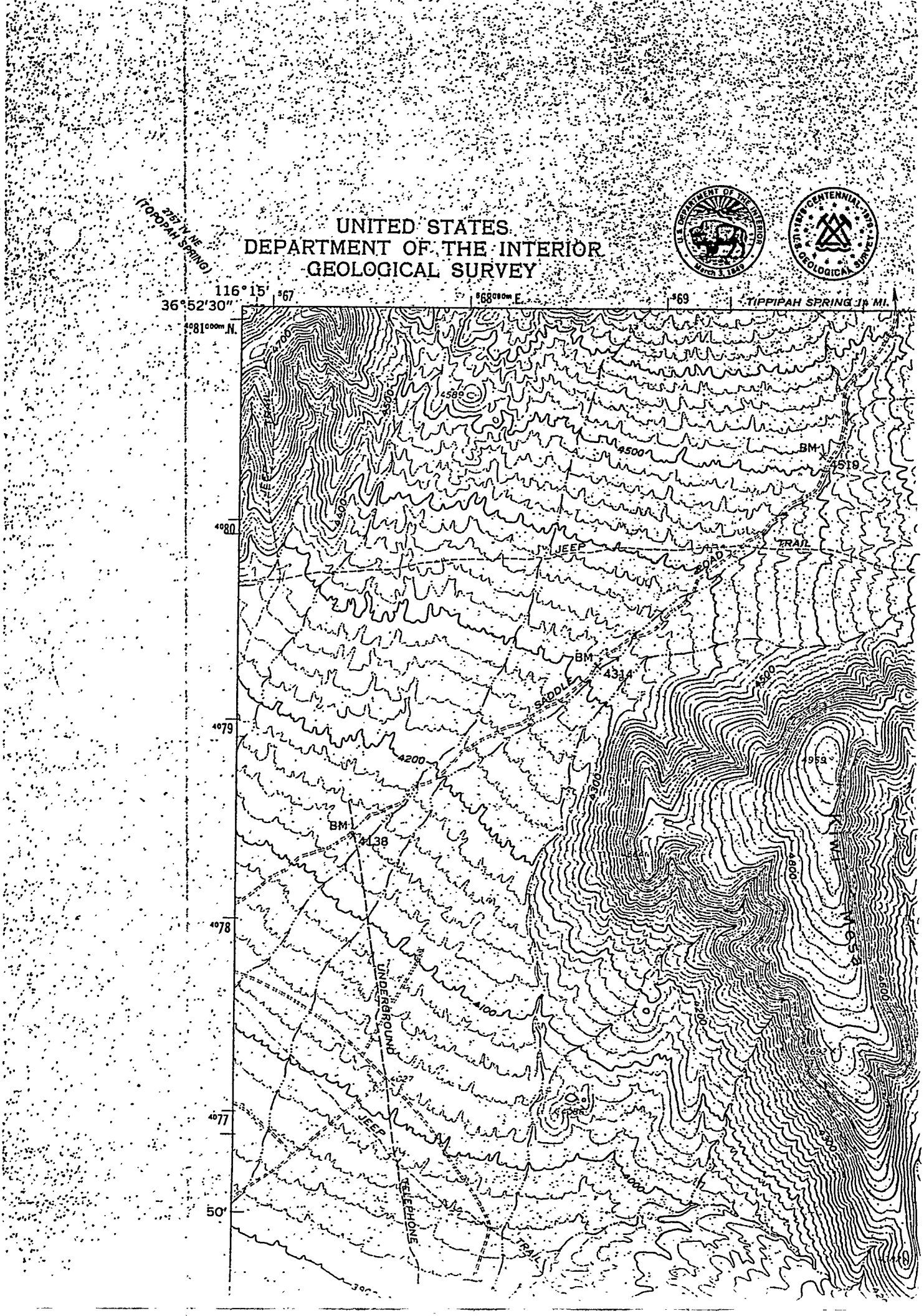
UNITED STATES
DEPARTMENT OF THE INTERIOR
GEOLOGICAL SURVEY
2757 IV NE
(TOROPAH SPRING)
116°15'
36°52'30"
567
568000m E.
569
TIPPIPAH SPRING 1⅛ MI.
4081000m N.
4080
4079
4078
4077
50'
4700
4600
4500
4400
4300
4200
4100
4000
3900
BM
4519
BM
4314
BM
4138
JEEP
TRAIL
ROAD
SADDLE
UNDERGROUND
JEEP
TELEPHONE
TRAIL
1959
4588
4588


TIPPIPAH SPRING 1½ MI.
12'30"
2757 I NW
(MINE MOUNTAIN)
BM 1519
TRAIL
5407
5298
5374
5462
5662
4959
4976
4736
4992
Lookout Peak

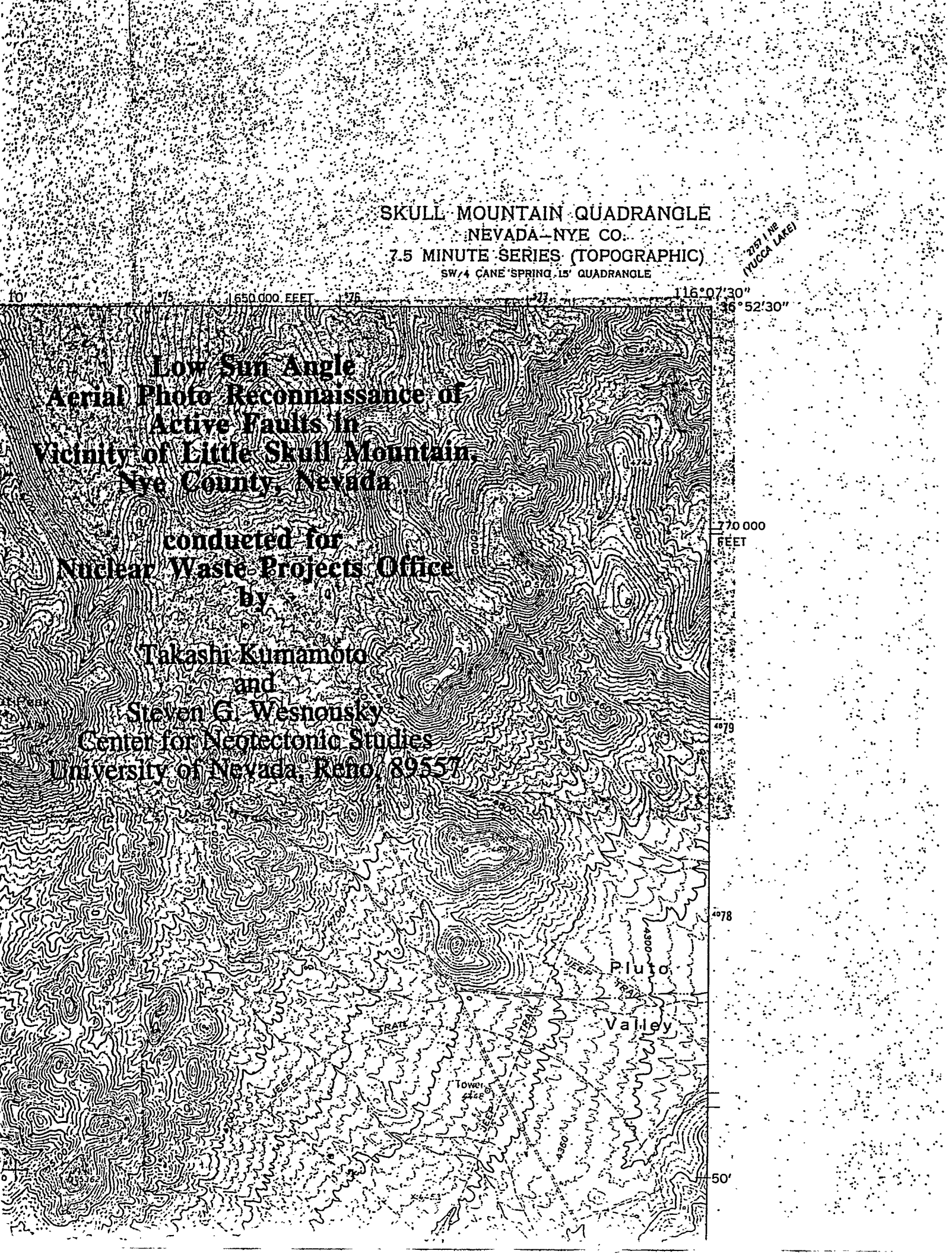
SKULL MOUNTAIN QUADRANGLE
NEVADA—NYE CO.
7.5 MINUTE SERIES (TOPOGRAPHIC)
SW/4 CANE SPRING 15' QUADRANGLE
2757 I NE
(YUCCA LAKE)
116°07'30"
36°52'30"
650 000 FEET
770 000
FEET
Low Sun Angle
Aerial Photo Reconnaissance of
Active Faults in
Vicinity of Little Skull Mountain,
Nye County, Nevada
conducted for
Nuclear Waste Projects Office
by
Takashi Kumamoto
and
Steven G. Wesnousky
Center for Neotectonic Studies
University of Nevada, Reno, 89557
Pluto
Valley
Tower
4078
4079
50'

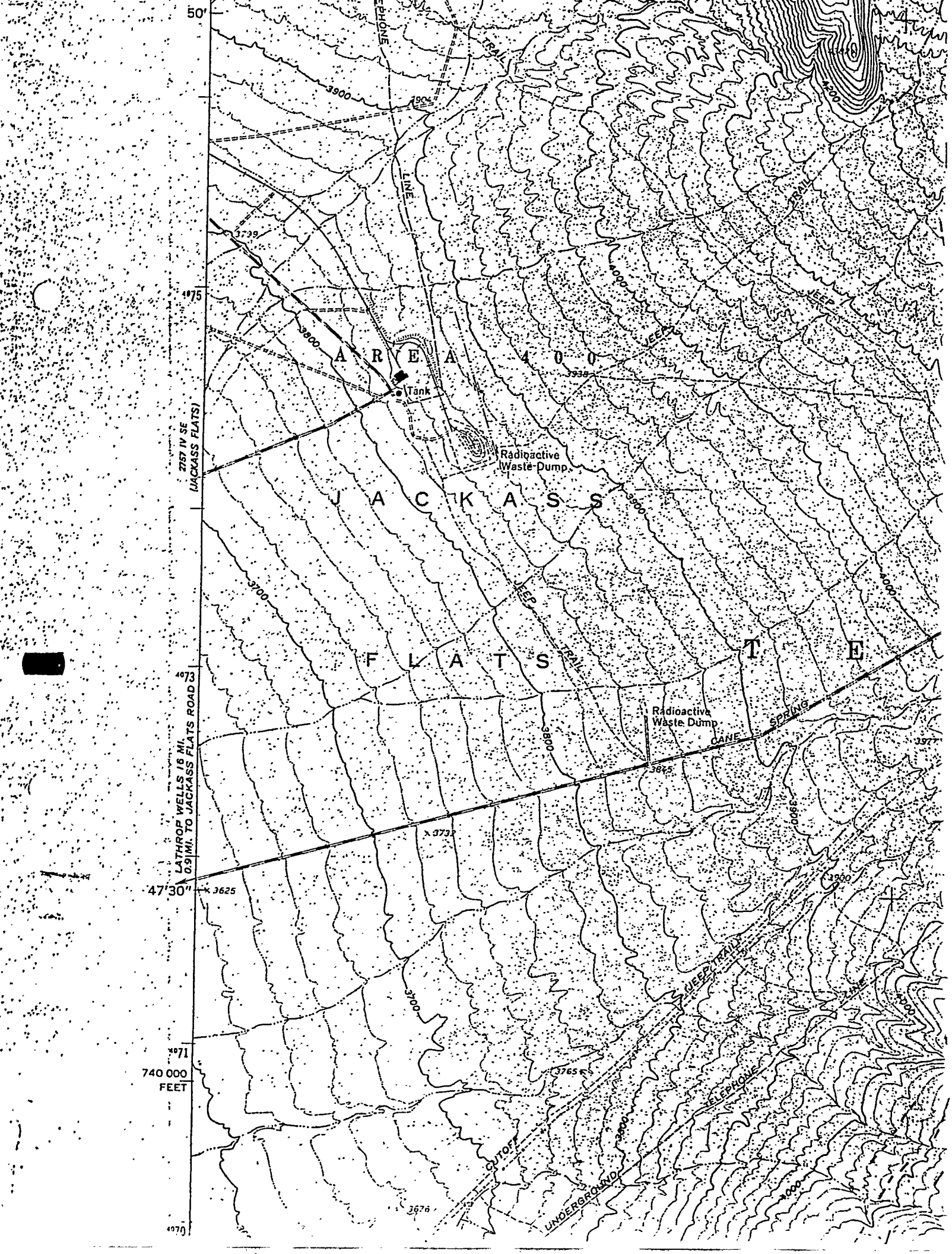
50'
TELEPHONE LINE
TRAIL
3900
4000
4200
3739
4075
JEEP TRAIL
3800
AREA 400
3938
Tank
Radioactive Waste Dump
2757 IV SE (JACKASS FLATS)
JACKASS FLATS
3700
4000
3900
4073
Radioactive Waste Dump
CANE SPRING
3845
3971
3900
3739
LATHROP WELLS 16 MI.
0.9 MI. TO JACKASS FLATS ROAD
47'30"
3625
3900
3700
4000
4071
740 000 FEET
3765
TELEPHONE LINE
CUTOFF
UNDERGROUND
3800
3676
4070

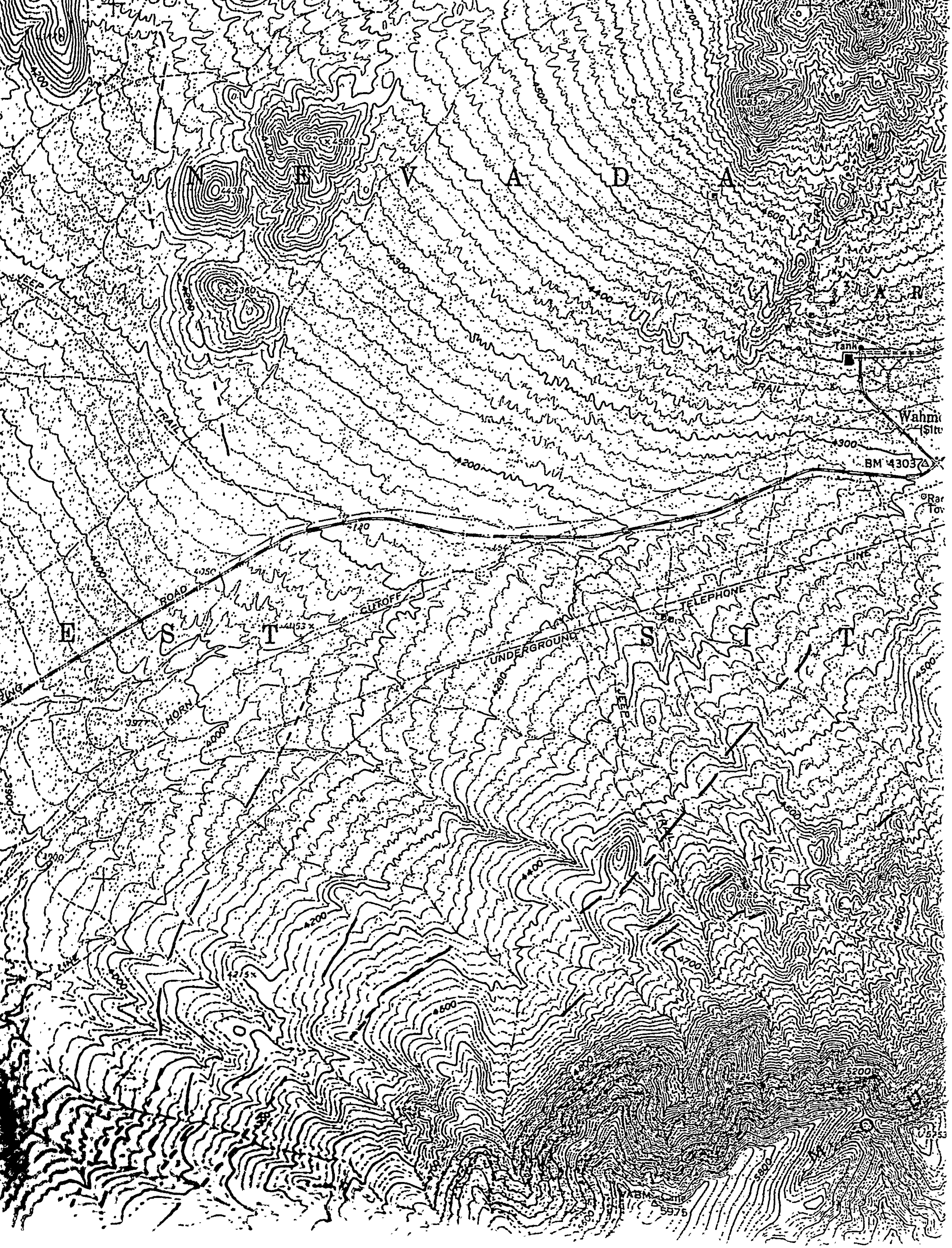
N E V A D A
E S T
S I T
JEEP
TRAIL
JEEP
TRAIL
Tank
BM 4303
ROAD
CUTOFF
UNDERGROUND TELEPHONE LINE
HORN
LINE
JEEP
4580
4200
4300
4400
4600
4000
3900
4050
4453
3977
4500
4800
5200
5976
BM


50'
4076
Tower
4298
MERCURY 23 MI.
(CANE SPRING)
WAHMONIE
CANE SPRING ROAD
Cane Spring Wash
FLAT
Tank
Wahmonie
(Site)
4300
BM 4303
Radio Tower
LINE
4500
4700
5208
5302
4073
4072
47'30"
5000
5200
5400
4900
4600
4071

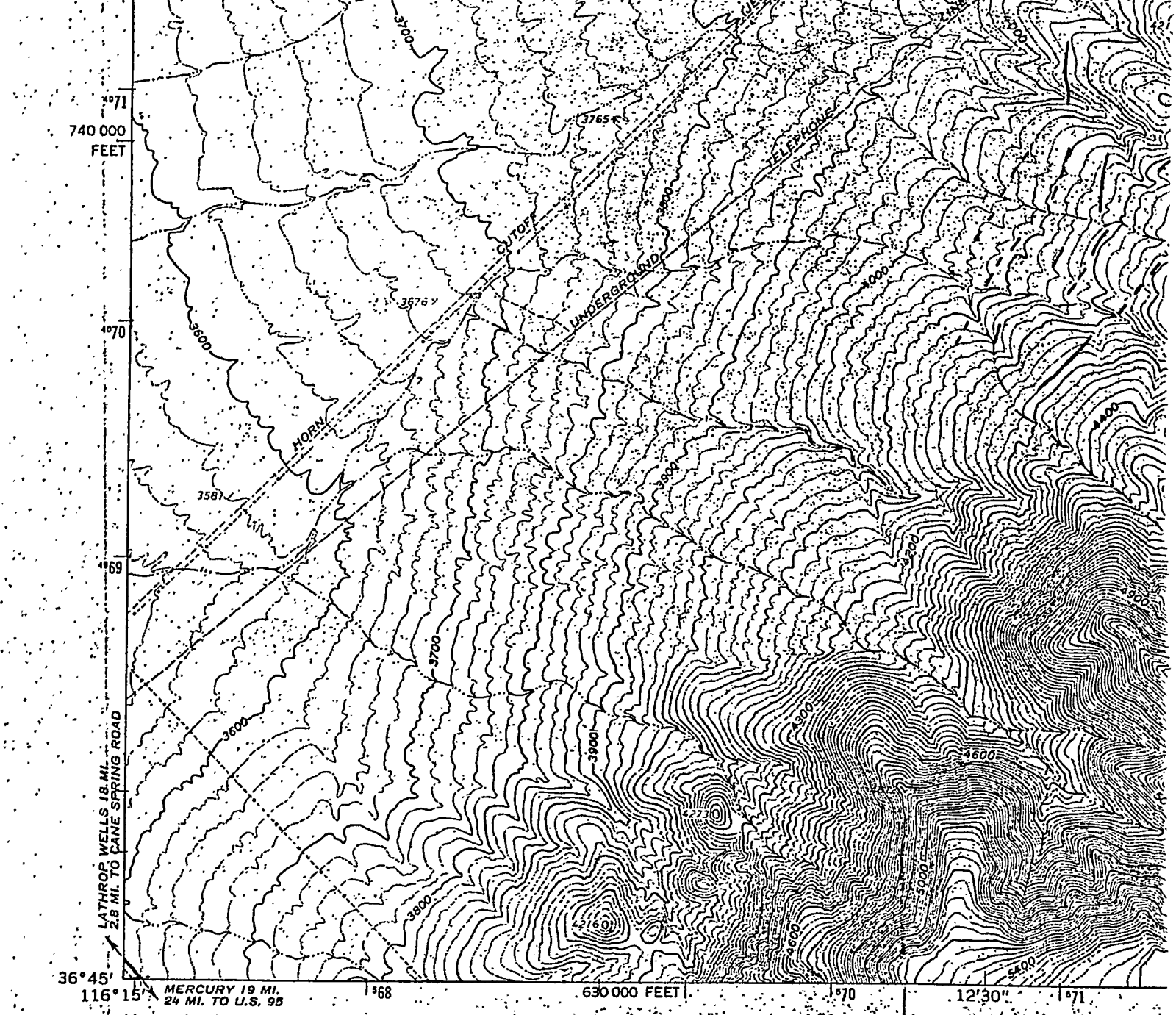

Mapped, edited, and published by the Geological Survey
in cooperation with the Atomic Energy Commission

Control by USGS, USC&GS, and Atomic Energy Commission

Topography from aerial photographs by photogrammetric methods
Aerial photographs taken 1959. Field check 1961

Polyconic projection. 1927 North American datum.
10,000-foot grid based on Nevada coordinate system, central zone
1000-meter Universal Transverse Mercator grid ticks,
zone 11, shown in blue

To place on the predicted North American Datum 1983,
move the projection lines 8 meters north and
78 meters east as shown by dashed corner ticks

There may be private inholdings within the boundaries of
the National or State reservations shown on this map

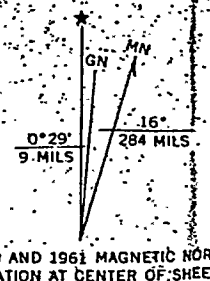

UTM GRID AND 1961 MAGNETIC NORTH
DECLINATION AT CENTER OF SHEET

1
1000.

SCALE 1:24 000

1 0 1 MILE

1000 0 1000 2000 3000 4000 5000 6000 7000 FEET

1 .5 0 1 KILOMETER

CONTOUR INTERVAL 20 FEET
NATIONAL GEODETIC VERTICAL DATUM OF 1929

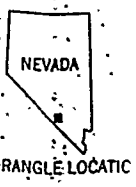

QUADRANGLE LOCATIC

THIS MAP COMPLIES WITH NATIONAL MAP ACCURACY STANDARDS
FOR SALE BY U. S. GEOLOGICAL SURVEY, DENVER, COLORADO 80225, OR RESTON, VIRGINIA 22092
A FOLDER DESCRIBING TOPOGRAPHIC MAPS AND SYMBOLS IS AVAILABLE ON REQUEST

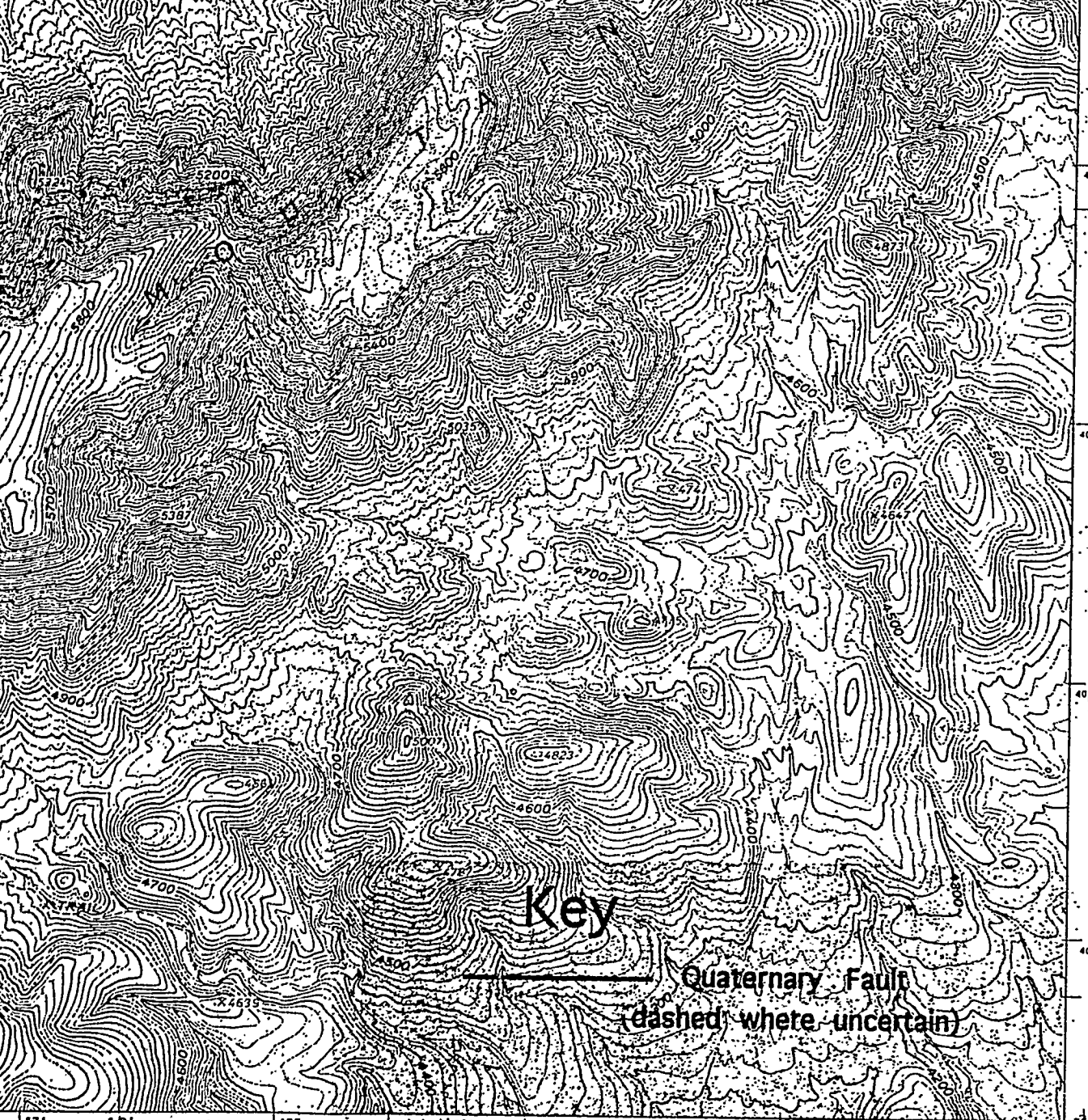

1 MILE

ROAD CLASSIFICATION

Heavy-duty — Light-duty

Medium-duty — Unimproved dirt

NEVADA

QUADRANGLE LOCATION

(CAMP DESERT ROCK) 2757 II NE

A 22092

SKULL MOUNTAIN, NEV.

SW/4 CANE SPRING 15' QUADRANGLE

N3645—W11607.5/7.5

1961

DMA 2757 I SW—SERIES V896

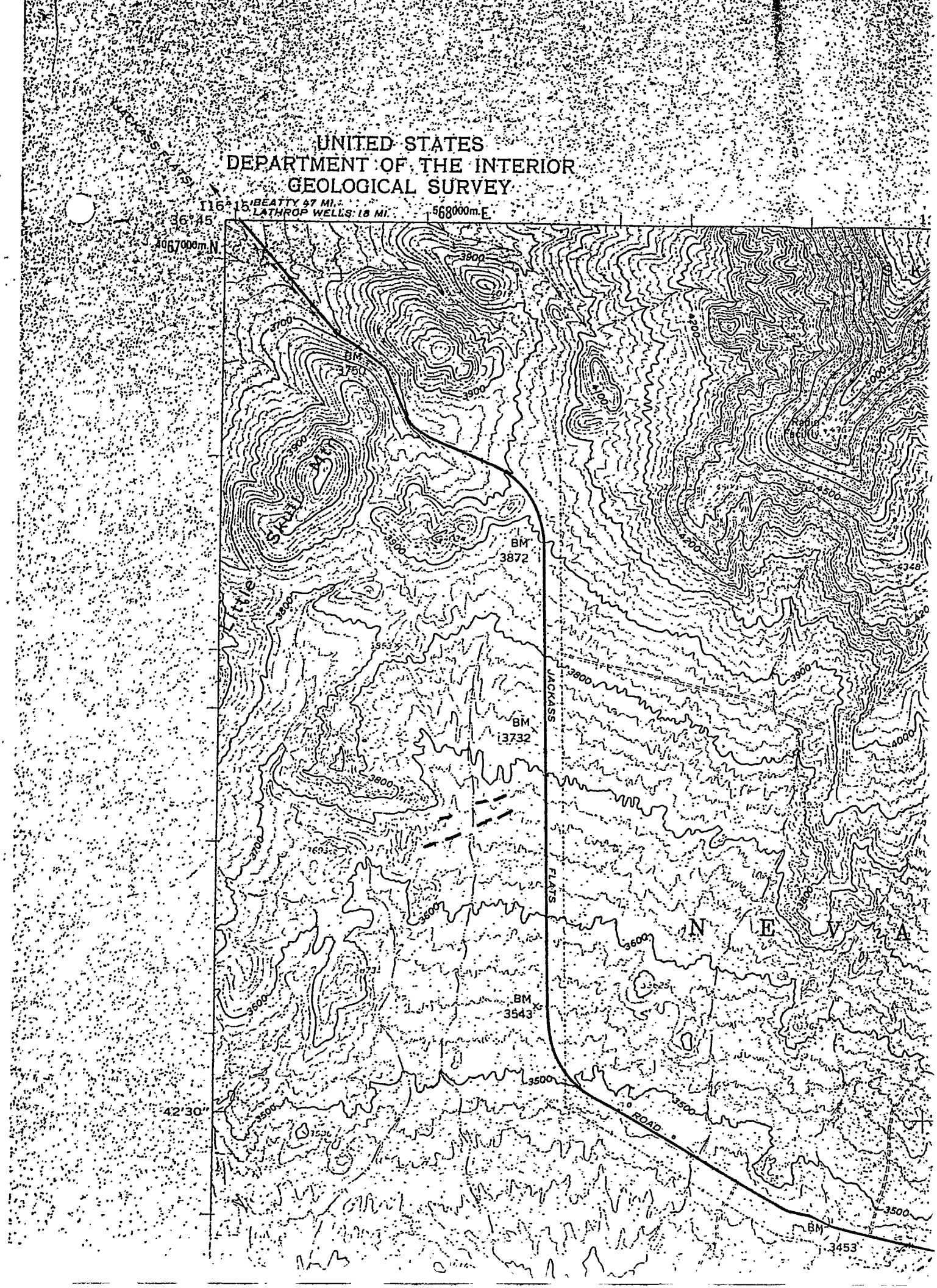
UNITED STATES
DEPARTMENT OF THE INTERIOR
GEOLOGICAL SURVEY
BEATTY 47 MI.
LATHROP WELLS 18 MI.
116° 15'
36° 45'
4067000m.N.
568000m.E.
Little SKULL MTS.
JACKASS FLATS
BM 3750
BM 3872
BM 3732
BM 3543
BM 3453
Radio
ROAD
NEVADA
42'30"

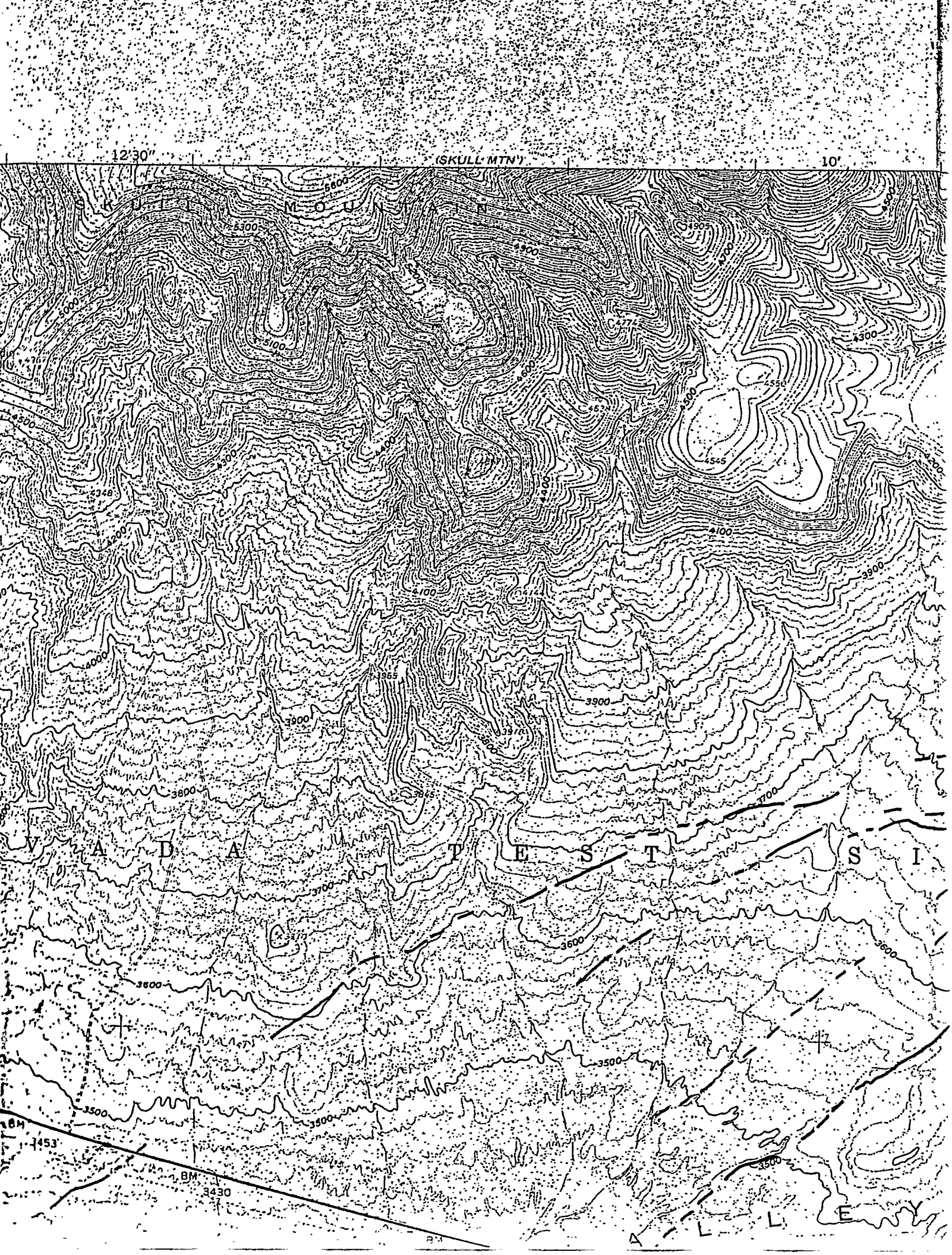
12'30"
(SKULL MTN)
10'
SKULL MOUNTAIN
5600
5300
5000
5100
4900
4700
4500
4300
4600
4400
4200
4100
4000
3900
3800
3700
3600
3500
3965
3970
3845
4545
4550
4477
4348
4453
BM
3430
VADA
TESTSI
ALLEY

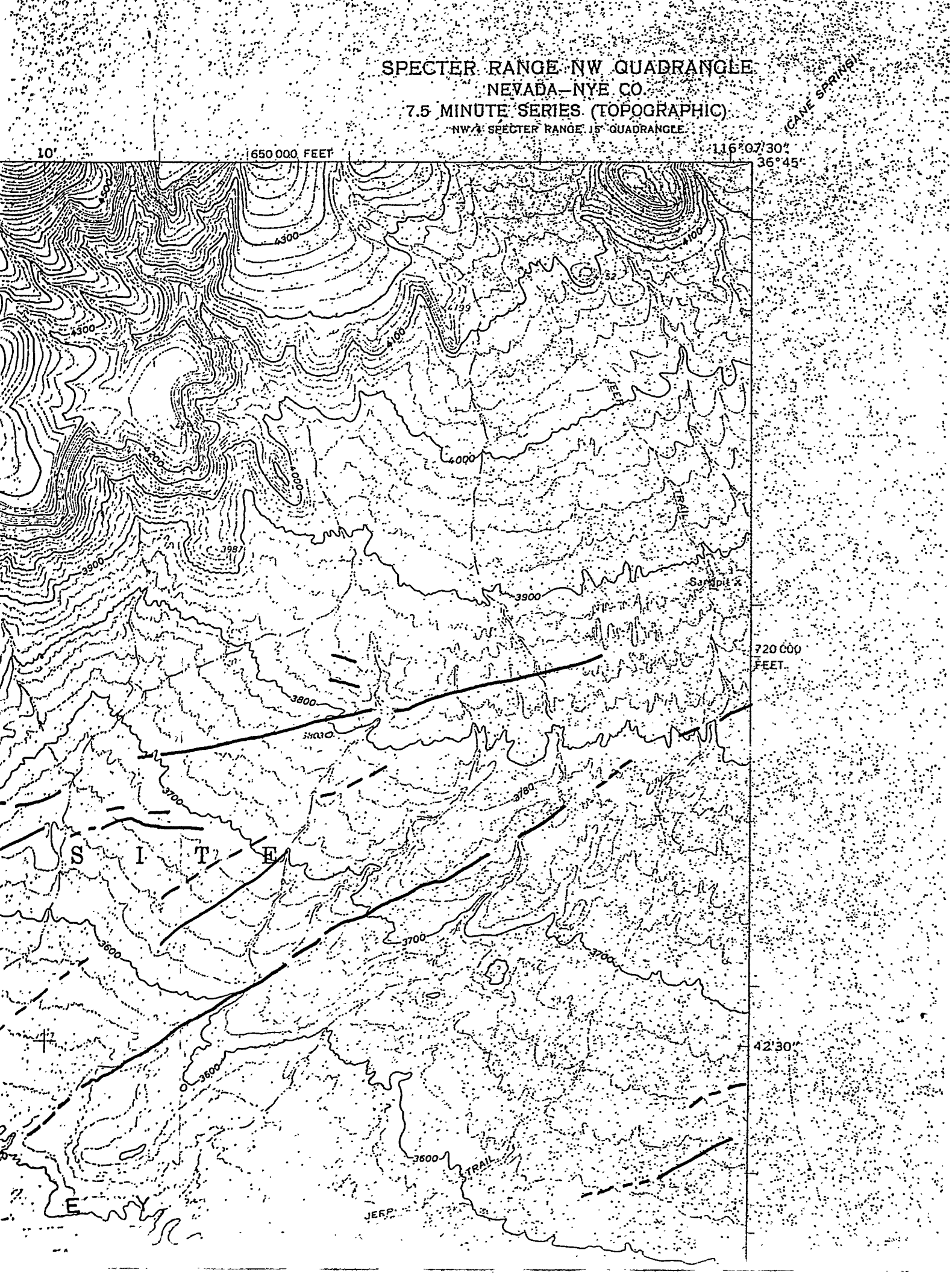
SPECTER RANGE NW QUADRANGLE
NEVADA—NYE CO.
7.5 MINUTE SERIES (TOPOGRAPHIC)
NW/4 SPECTER RANGE 15' QUADRANGLE
10'
650 000 FEET
116°07'30"
36°45'
(CANE SPRING)
4300
4100
4000
3900
3800
3700
3600
4139
3987
3780
JEEP TRAIL
Sandpit
720 000 FEET
42'30"
S I T E
JEEP TRAIL

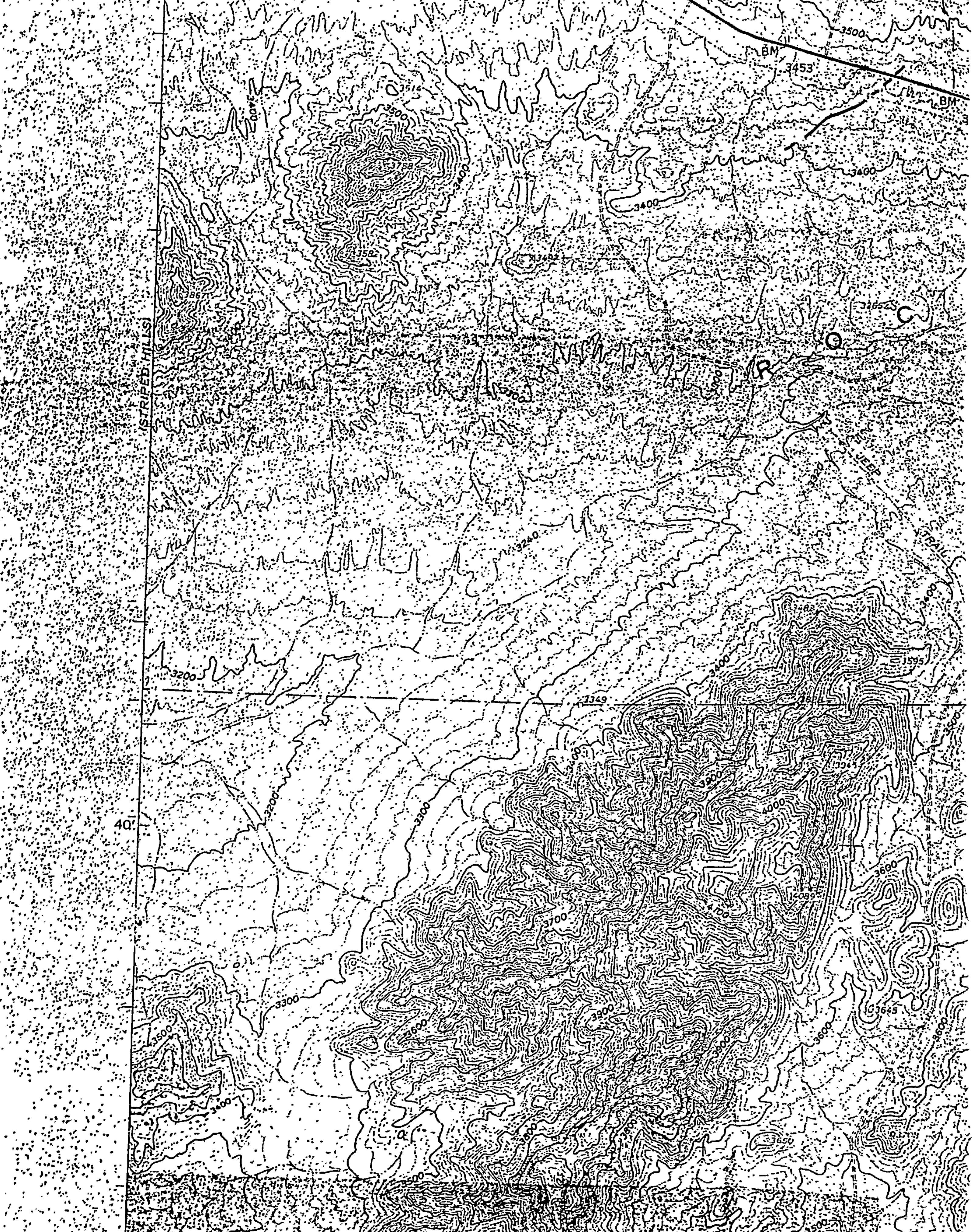

Low Sun Angle

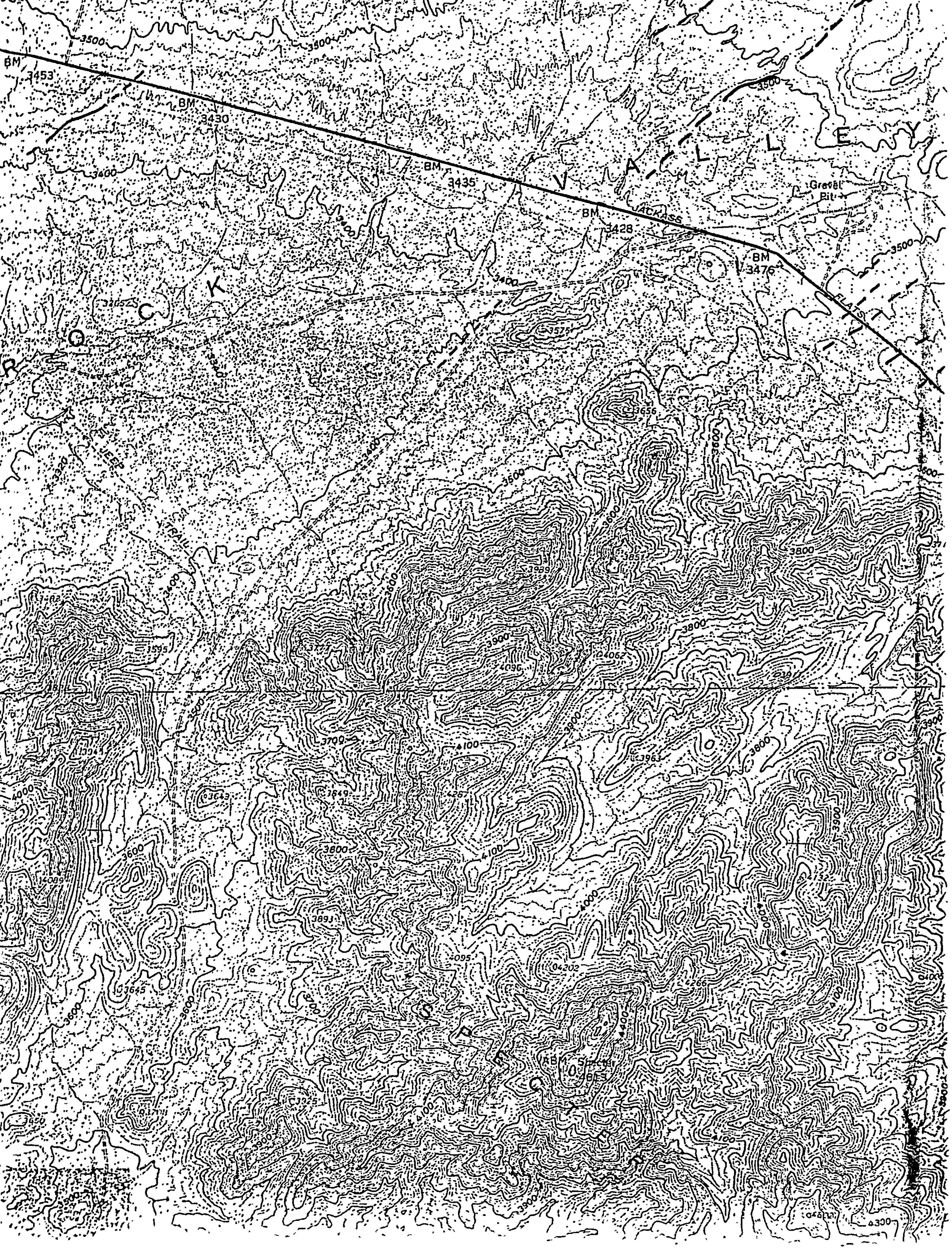

BM 3453
3500
BM 3430
3400
BM 3435
V A L L E Y
Gravel Pit
JACKASS
BM 3428
BM 3476
FLATS
3500
R O C K
3400
3575
3656
JEEP
TRAIL
3600
3500
3851
3989
3800
3900
4096
4062
3595
3700
4100
3963
3643
3649
4000
4089
3645
3891
4095
4202
4266
4400
4100
3900
4300

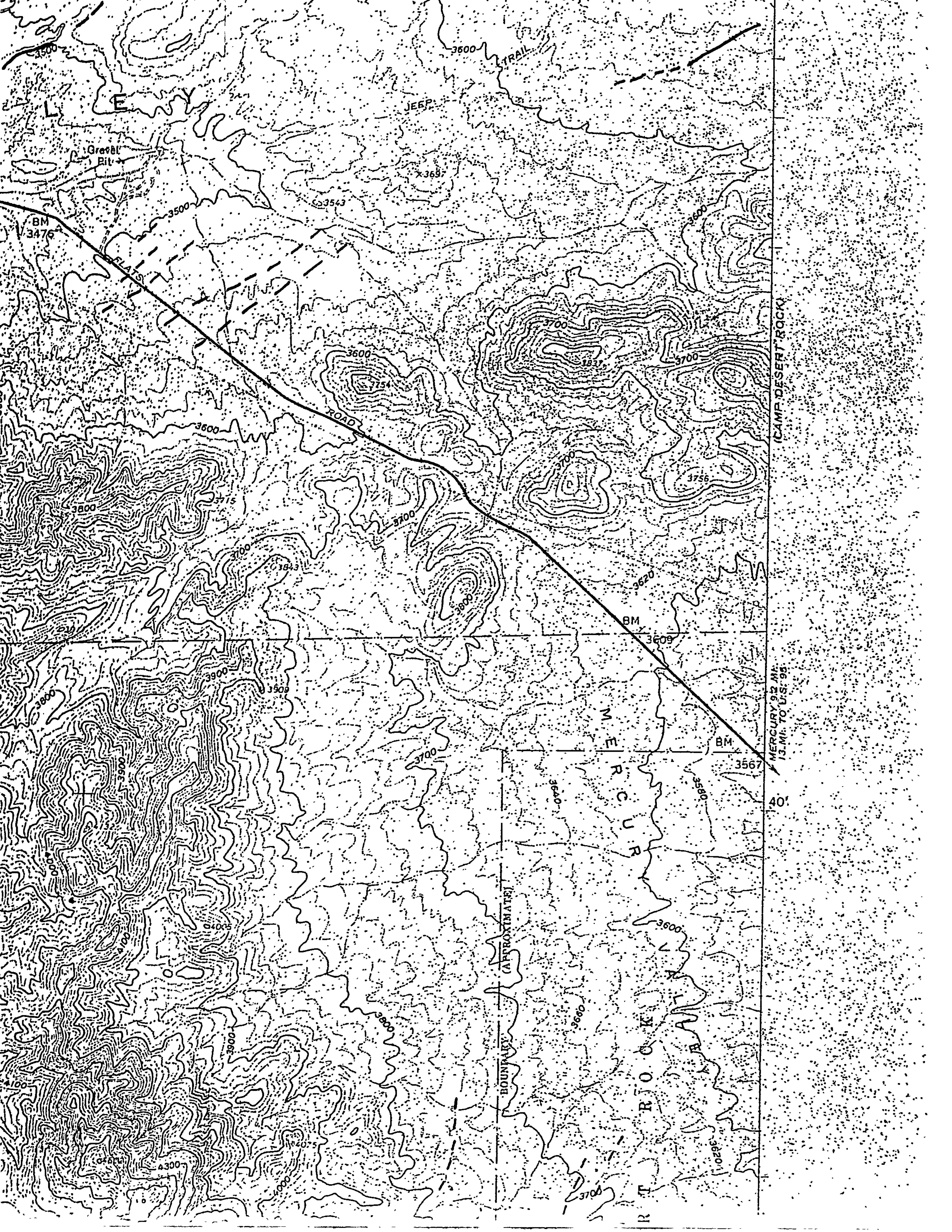
L E Y
Gravel Pit
3500
3600
JEEP
TRAIL
x 3697
3543
BM
3476
FLATS
ROAD
3700
3754
3600
3756
(CAMP DESERT ROCK)
3715
3800
3843
3620
BM
3609
3900
3909
M E R C U R
BM
3567
MERCURY 9.2 MI.
13 MI. TO U.S. 95
40'
3640
3580
BOUNDARY (APPROXIMATE)
R O C K V A L L E Y
4005
4100
4300
3660
3620
4000

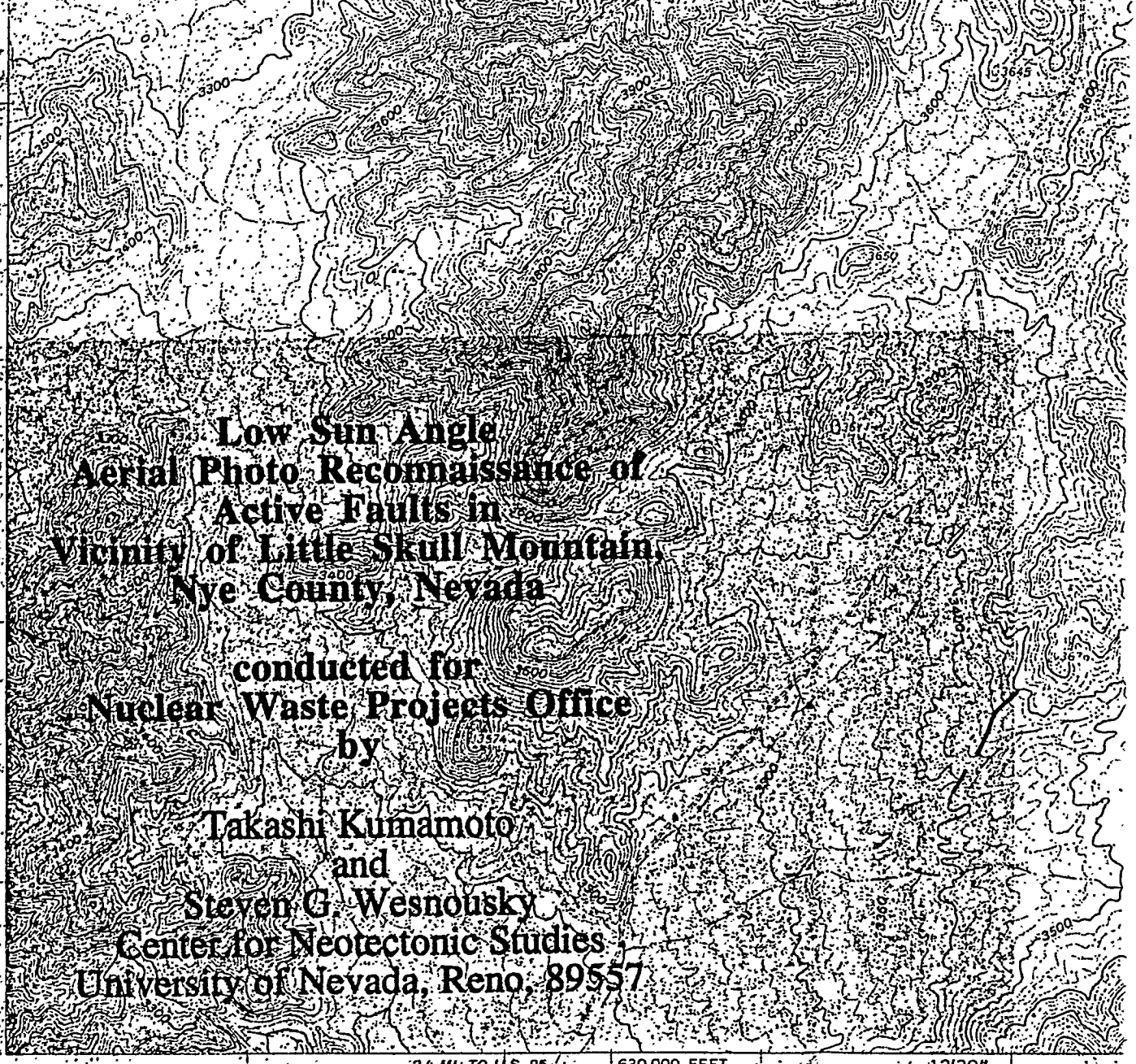

Low Sun Angle Aerial Photo Reconnaissance of Active Faults in Vicinity of Little Skull Mountain, Nye County, Nevada

conducted for

Nuclear Waste Projects Office

by

Takashi Kumamoto
and
Steven G. Wesnousky
Center for Neotectonic Studies
University of Nevada, Reno, 89557

690 000 FEET

36°37'30"

116°15'

2.4 MI. TO U.S. 95

630 000 FEET

12'30"

(LATHROP WELLS) 1:62 500

Mapped, edited, and published by the Geological Survey in cooperation with the Atomic Energy Commission

Control by USGS, USC&GS, and Atomic Energy Commission

Topography from aerial photographs by photogrammetric methods
Aerial photographs taken 1959. Field checked 1961

Polyconic projection. 1927 North American datum
10,000-foot grid based on Nevada coordinate system, central zone
1000-meter Universal Transverse Mercator grid ticks,
zone 11, shown in blue

16°

TRUE NORTH

MAGNETIC NORTH

APPROXIMATE MEAN DECLINATION, 1961

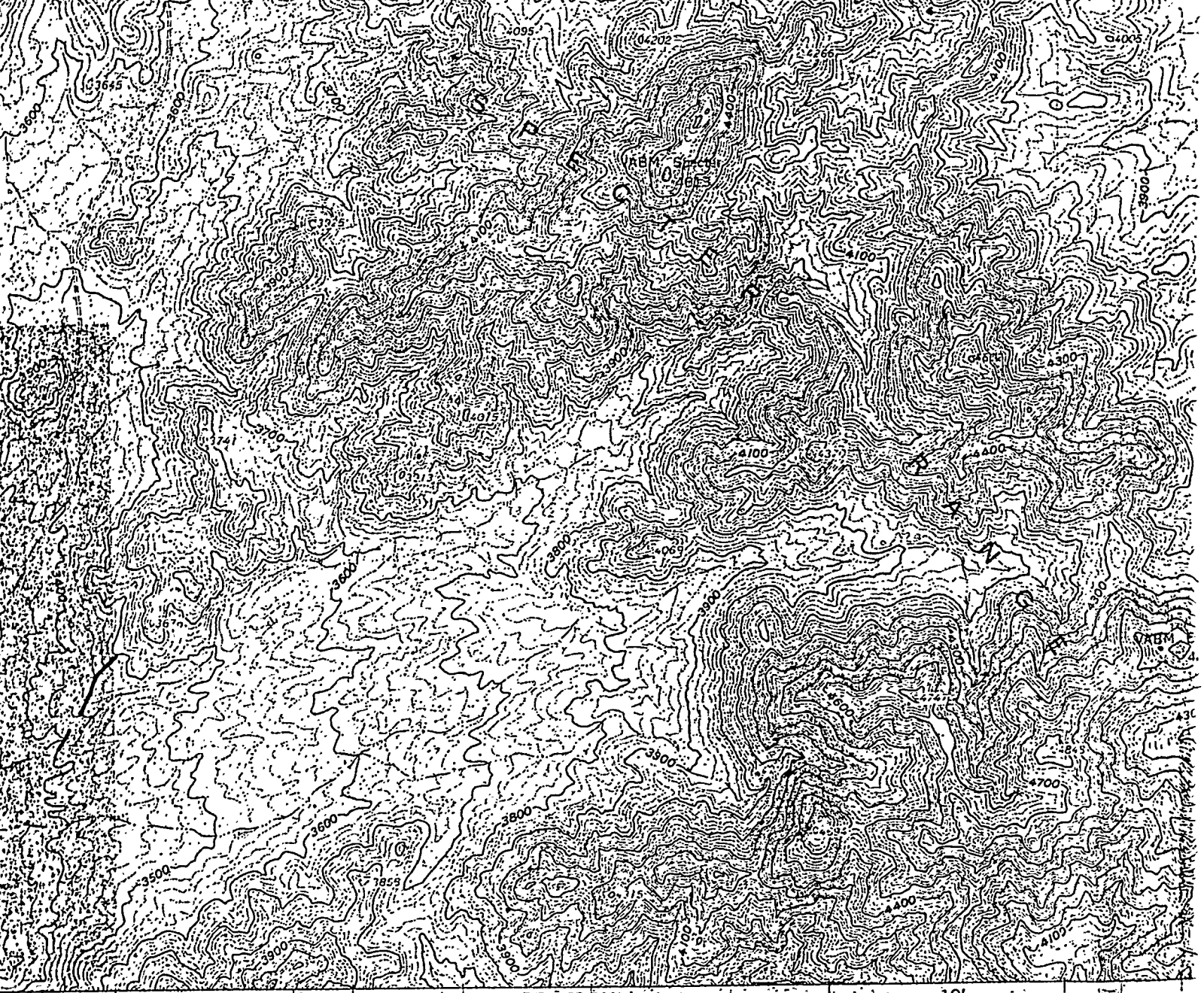
12'30"
(SPECTER RANGE 1:62 500)
10'
SCALE 1:24 000
1 MILE
1000 0 1000 2000 3000 4000 5000 6000 7000 FEET
1 5 0 1 KILOMETER
CONTOUR INTERVAL 20 FEET
DATUM IS MEAN SEA LEVEL
NEVADA
QUADRANGLE LOCAT

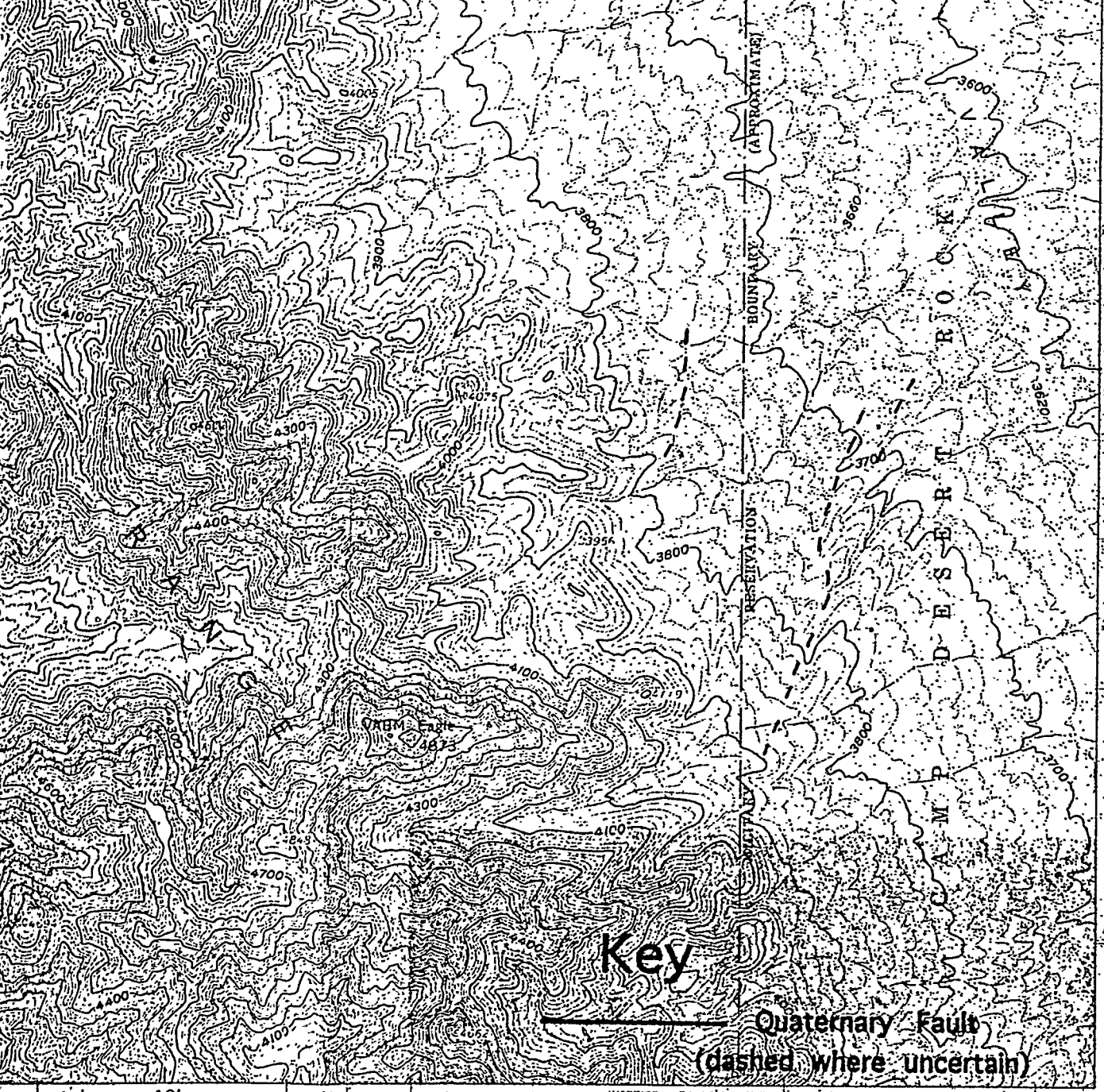

10'

INTERIOR—GEOLOGICAL SURVEY, WASHINGTON, D. C.—1962
NP-2179

1 MILE

(SPECTER RANGE)
1,162,500

ROAD CLASSIFICATION

Heavy-duty ——— Unimproved dirt

NEVADA

QUADRANGLE LOCATION

SPECTER RANGE NW, NEV.

NW/4 SPECTER RANGE 15' QUADRANGLE
N3637.5—W11607.5/7.5

1961

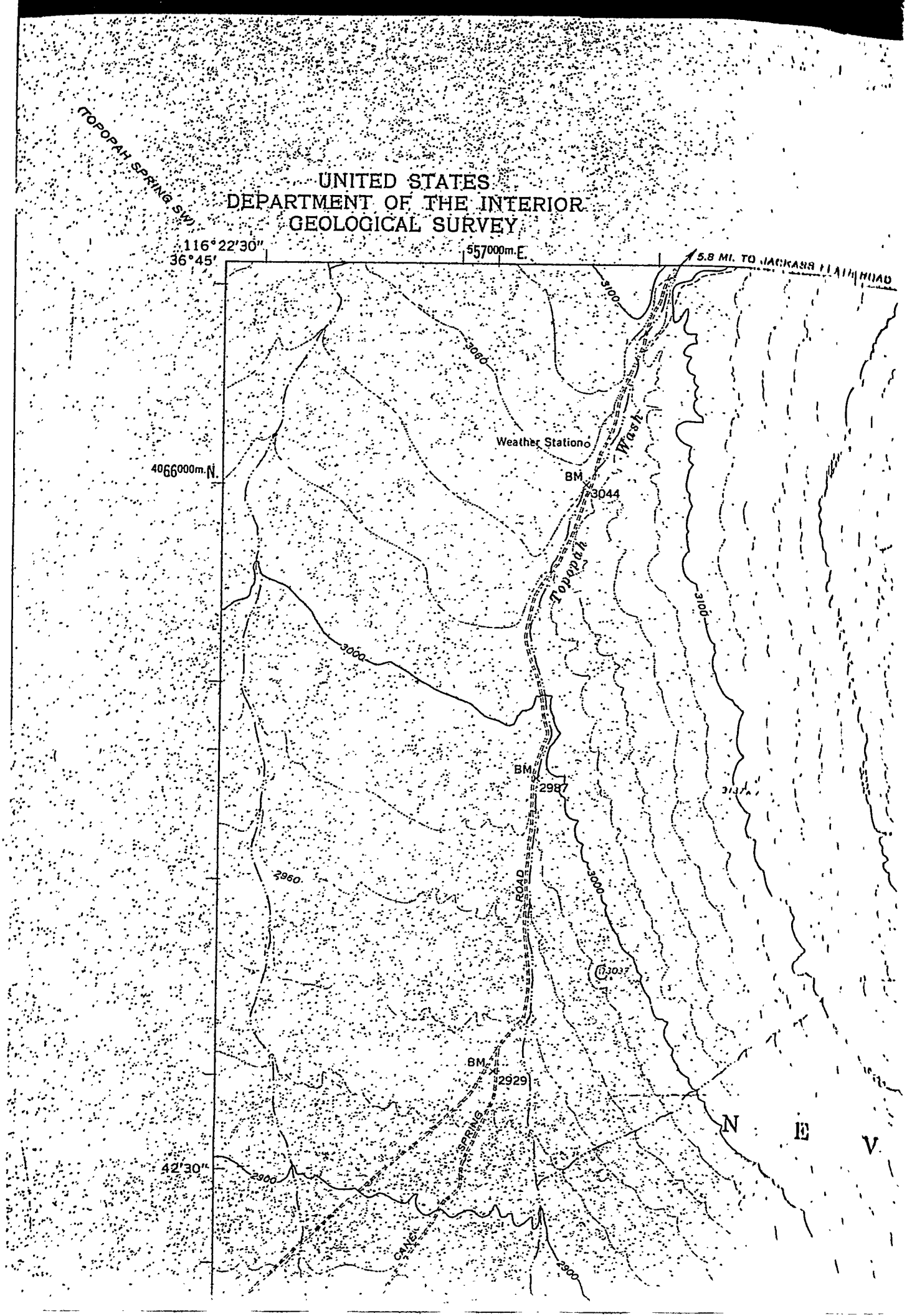
TOPOPAH SPRING SW.
UNITED STATES
DEPARTMENT OF THE INTERIOR
GEOLOGICAL SURVEY
116°22'30"
36°45'
557000m.E.
5.8 MI. TO JACKASS FLATS ROAD
4066000m.N.
42'30"
3100
3060
3000
2960
2900
Weather Station
BM 3044
Topopah Wash
BM 2987
BM 2929
ROAD
SPRING
CANYON
N E V

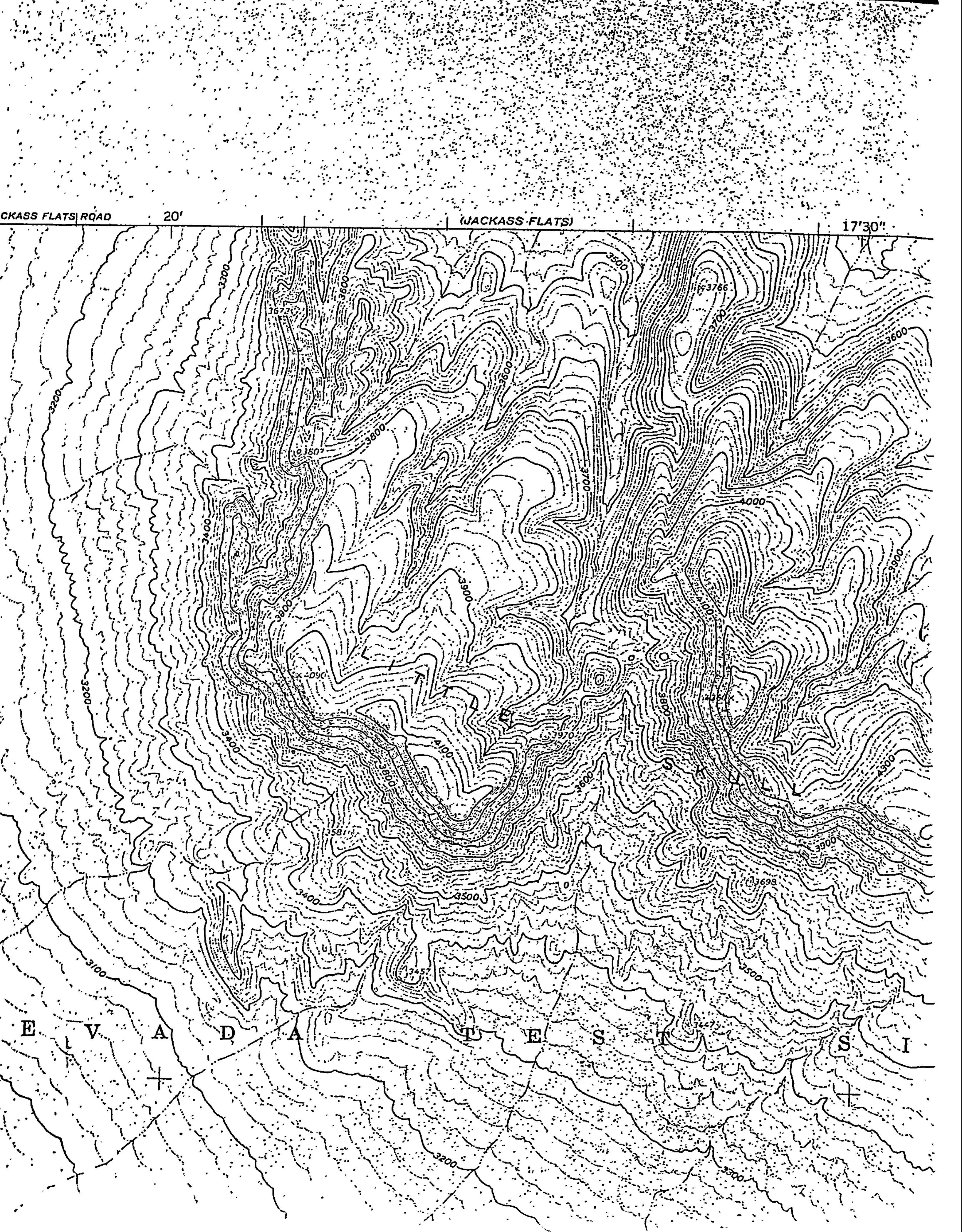
CKASS FLATS ROAD
20'
(JACKASS FLATS)
17'30"
3300
3500
3766
3600
3200
3600
3800
3700
4000
3400
3900
3900
3800
4100
3200
3400
4100
3970
3800
3600
4300
3800
3900
3400
3500
3698
3100
3500
3200
3300
L I T T L E
S K U L L
E V A D A T E S T S I

STRIPED HILLS QUADRANGLE
NEVADA—NYE CO.
7.5 MINUTE SERIES (TOPOGRAPHIC)
NE/4 LATHROP WELLS 15' QUADRANGLE

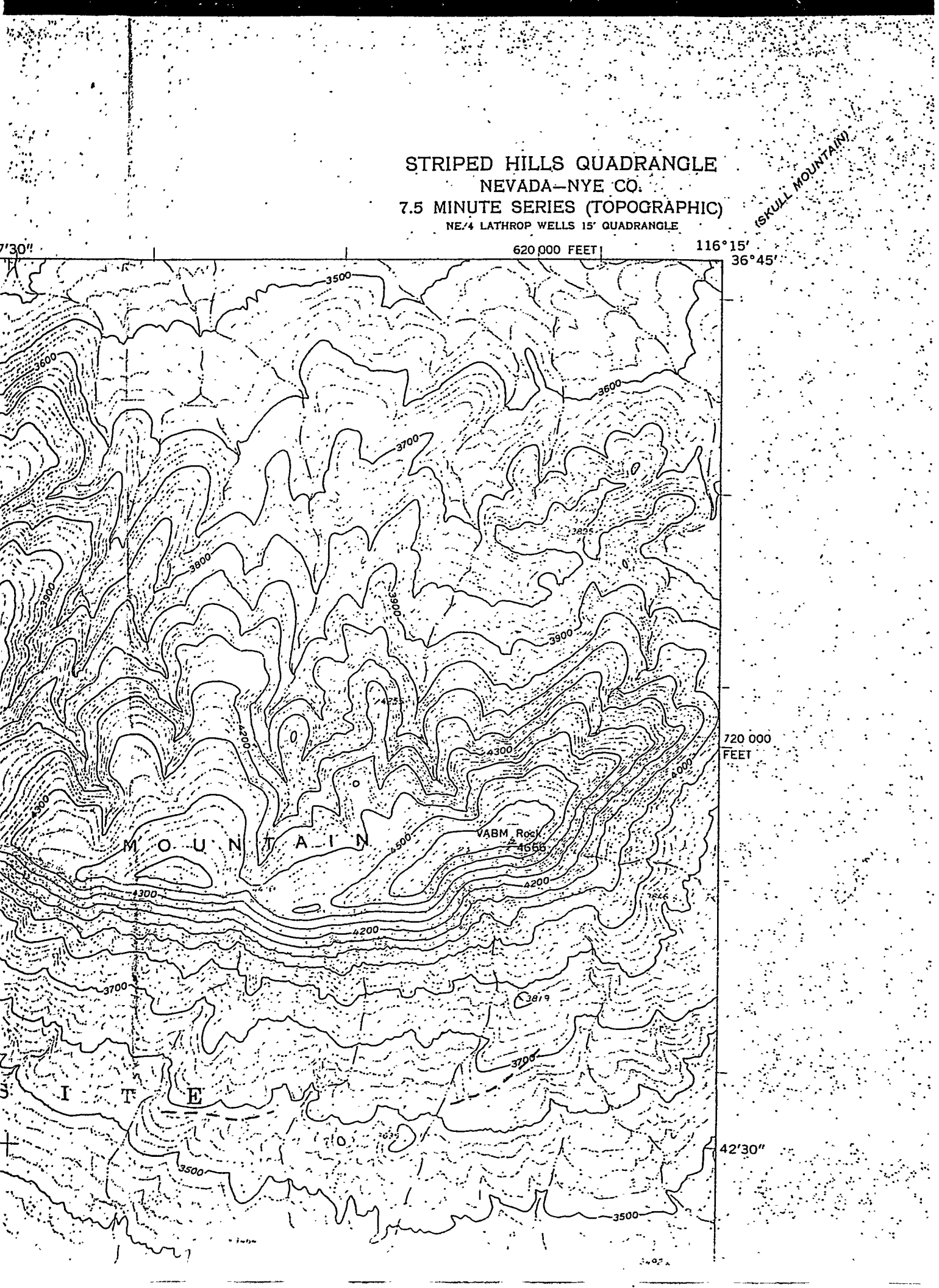

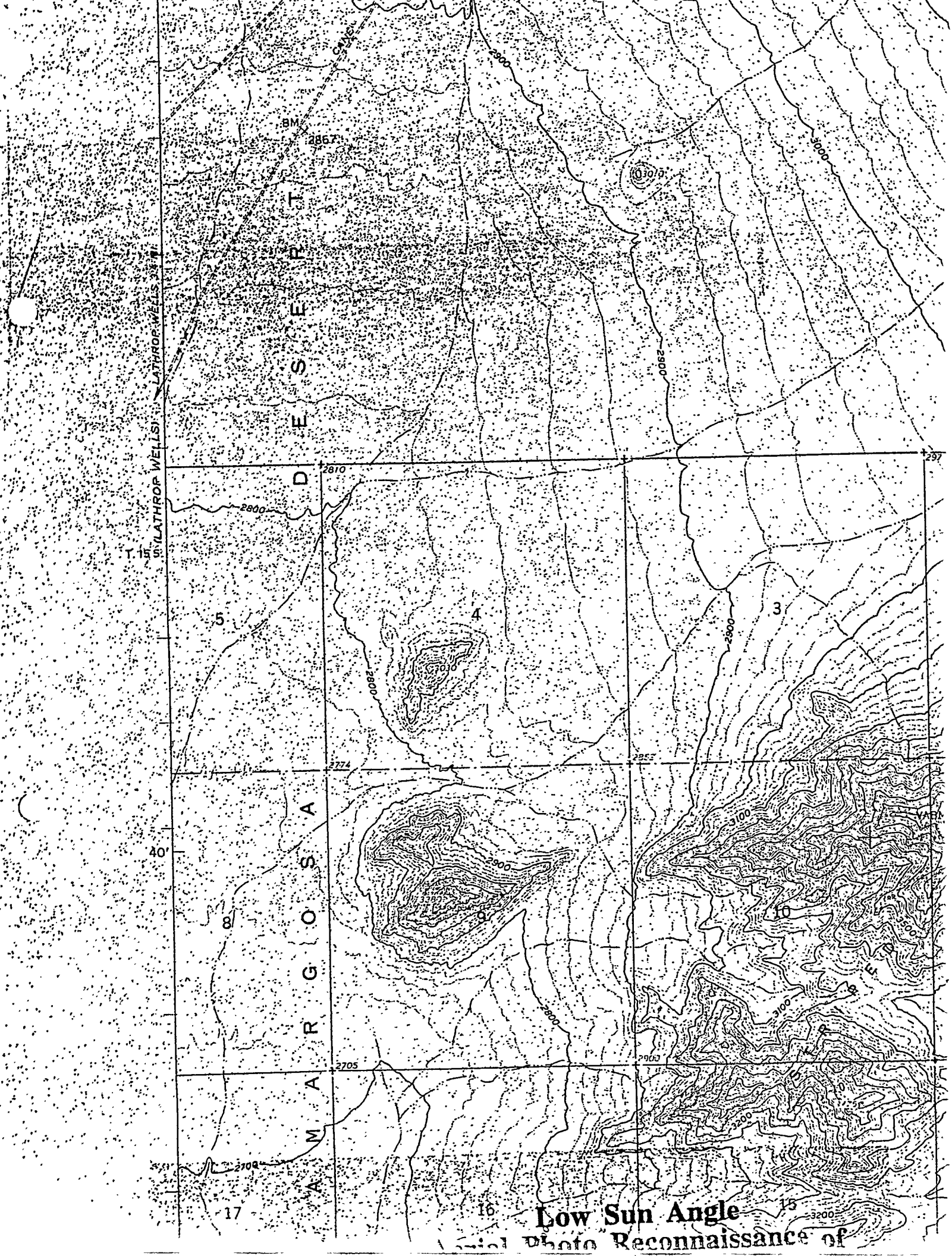

Low Sun Angle

Aerial Photo Reconnaissance of

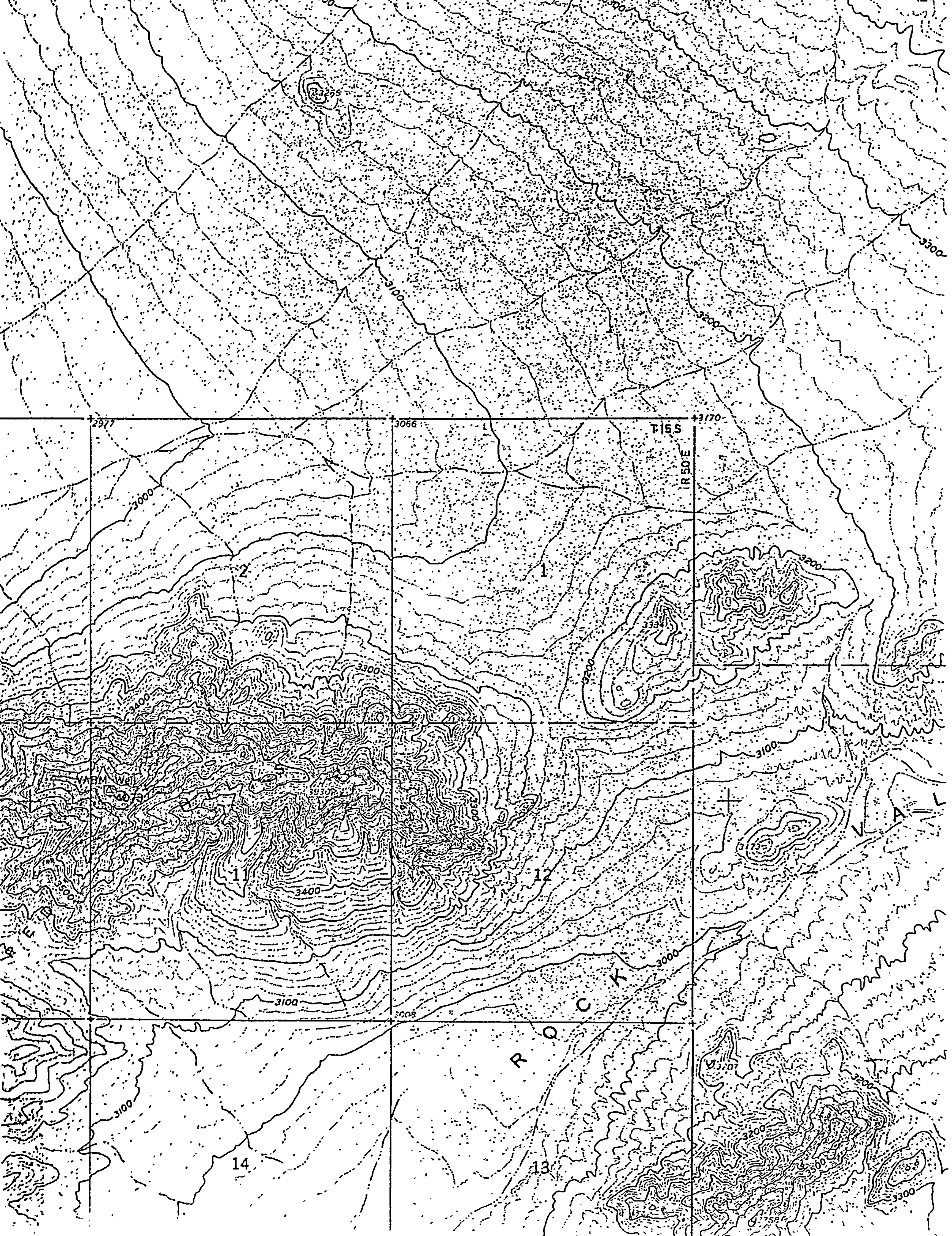

3100
3200
3300
2977
3066
3170
T 15 S
R 50 E
3000
2
1
3334
3200
3300
3400
Warm Well
3100
3000
3500
11
12
3400
3000
3100
3005
R O C K
V A L
3173
3100
3200
3300
14
13

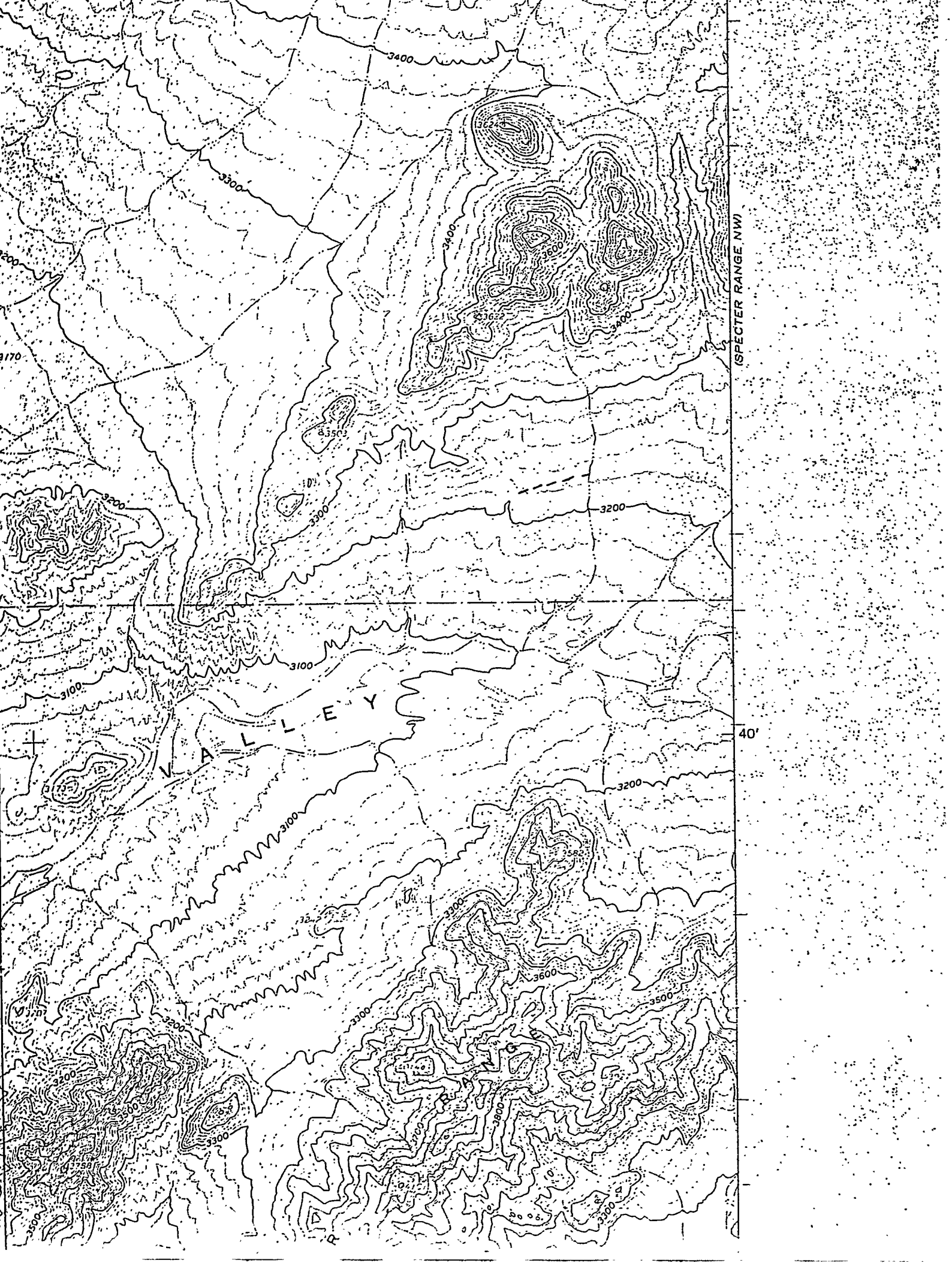
3400
3300
3400
3600
3622
3400
3503
3200
3300
3200
3100
3100
VALLEY
40'
3200
3100
3300
3600
3500
3300
3200
3200
3300
3758
3500
3300
3800
3700
RANGE
(SPECTER RANGE NW)

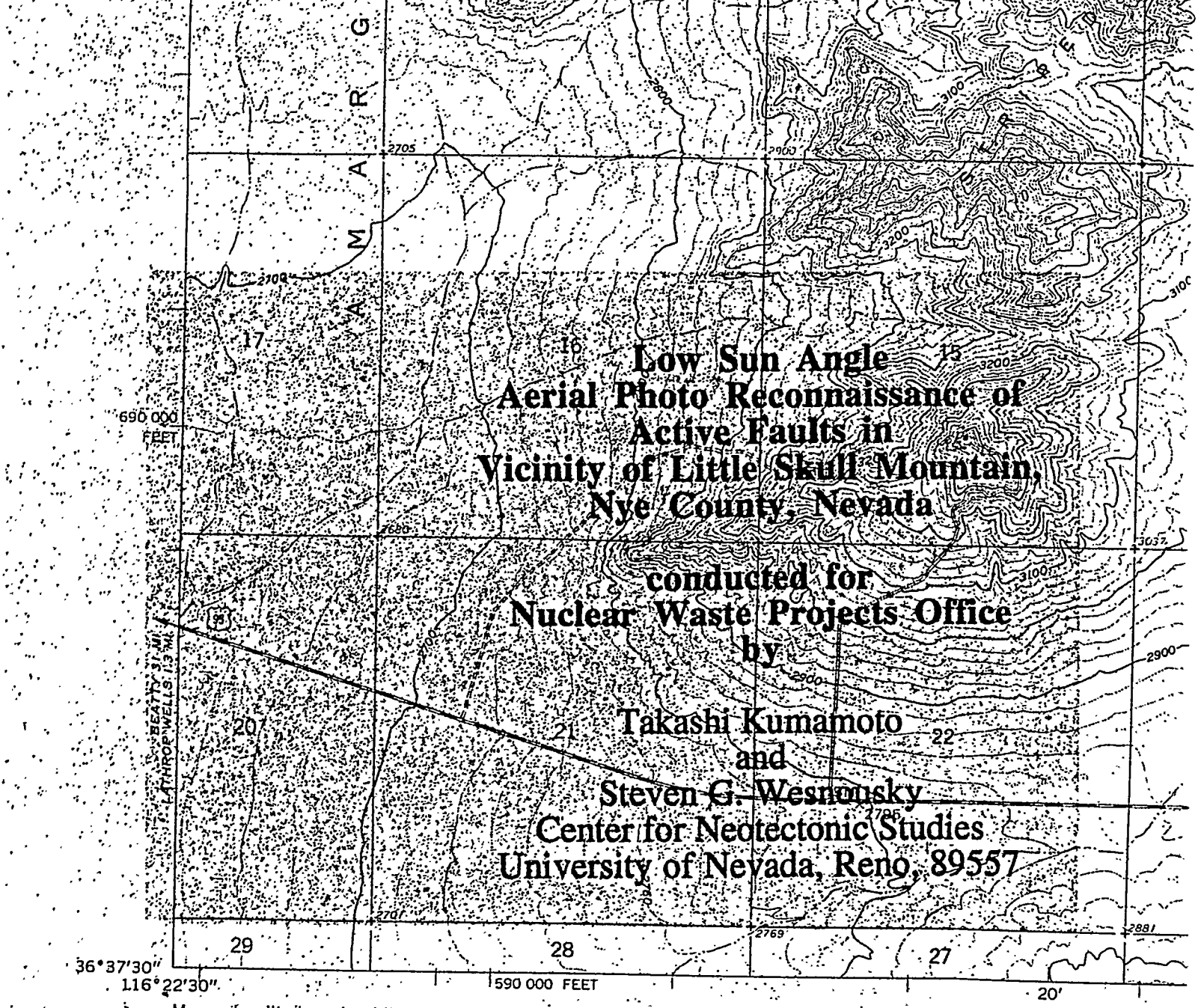

Low Sun Angle Aerial Photo Reconnaissance of Active Faults in Vicinity of Little Skull Mountain, Nye County, Nevada

conducted for
Nuclear Waste Projects Office
by

Takashi Kumamoto
and
Steven G. Wesnousky
Center for Neotectonic Studies
University of Nevada, Reno, 89557

LATHROP WELLS 1:62 500

Mapped, edited, and published by the Geological Survey
in cooperation with the Atomic Energy Commission

Control by USGS, USC&GS, USCE, and Atomic Energy Commission

Topography by photogrammetric methods from aerial photographs taken 1959. Field checked 1961

Polyconic projection. 1927 North American datum
10,000-foot grid based on Nevada coordinate system, central zone
1000-meter Universal Transverse Mercator grid ticks,
zone 11, shown in blue

1
1

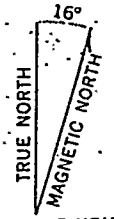

APPROXIMATE MEAN
DECLINATION, 1961

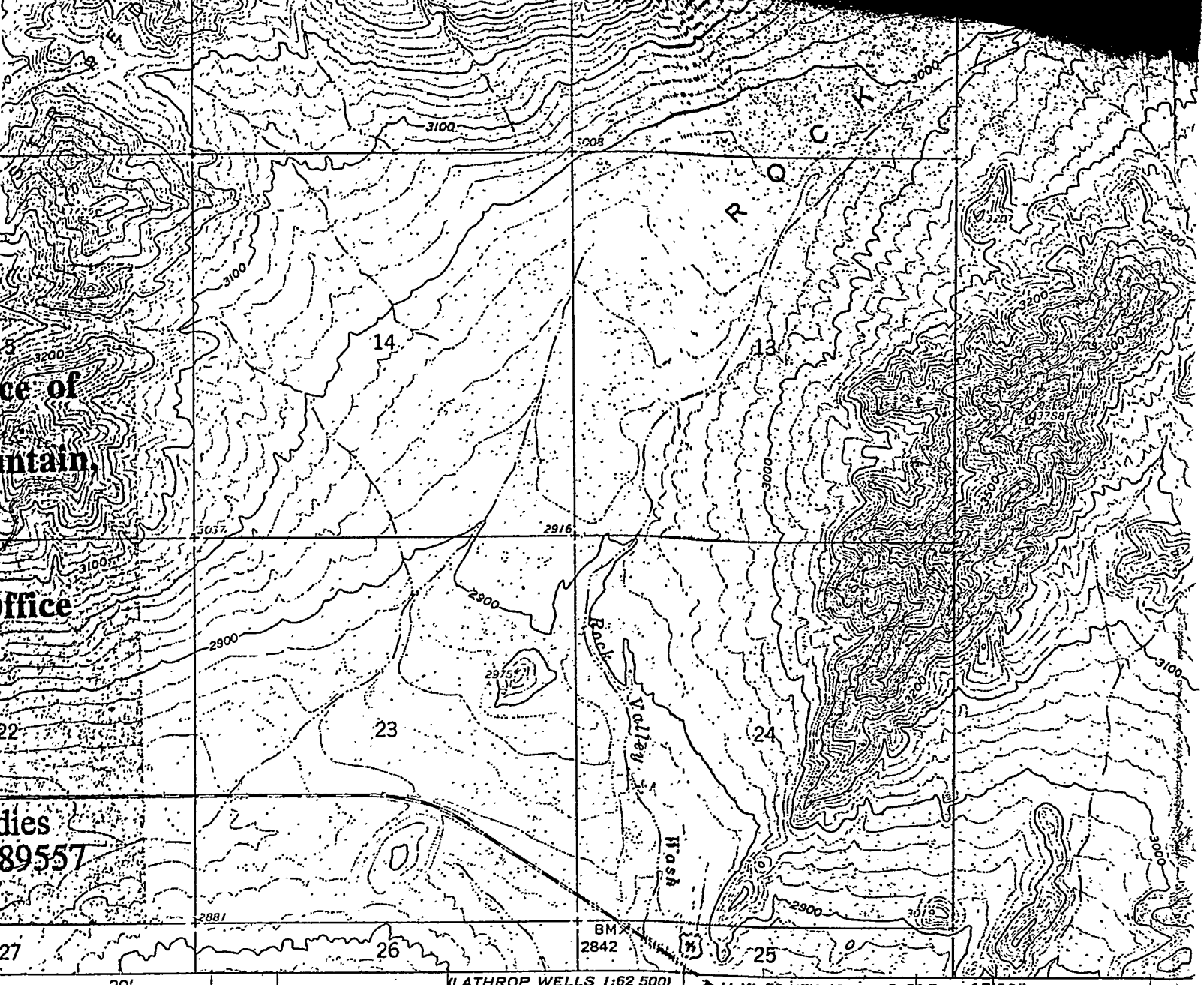

SCALE 1:24000

1 0 1 MILE

1000 0 1000 2000 3000 4000 5000 6000 7000 FEET

1 5 0 1 KILOMETER

CONTOUR INTERVAL 20 FEET

DOTTED LINES REPRESENT 10-FOOT CONTOURS

DATUM IS MEAN SEA LEVEL

NEVAD

QUADRANGLE

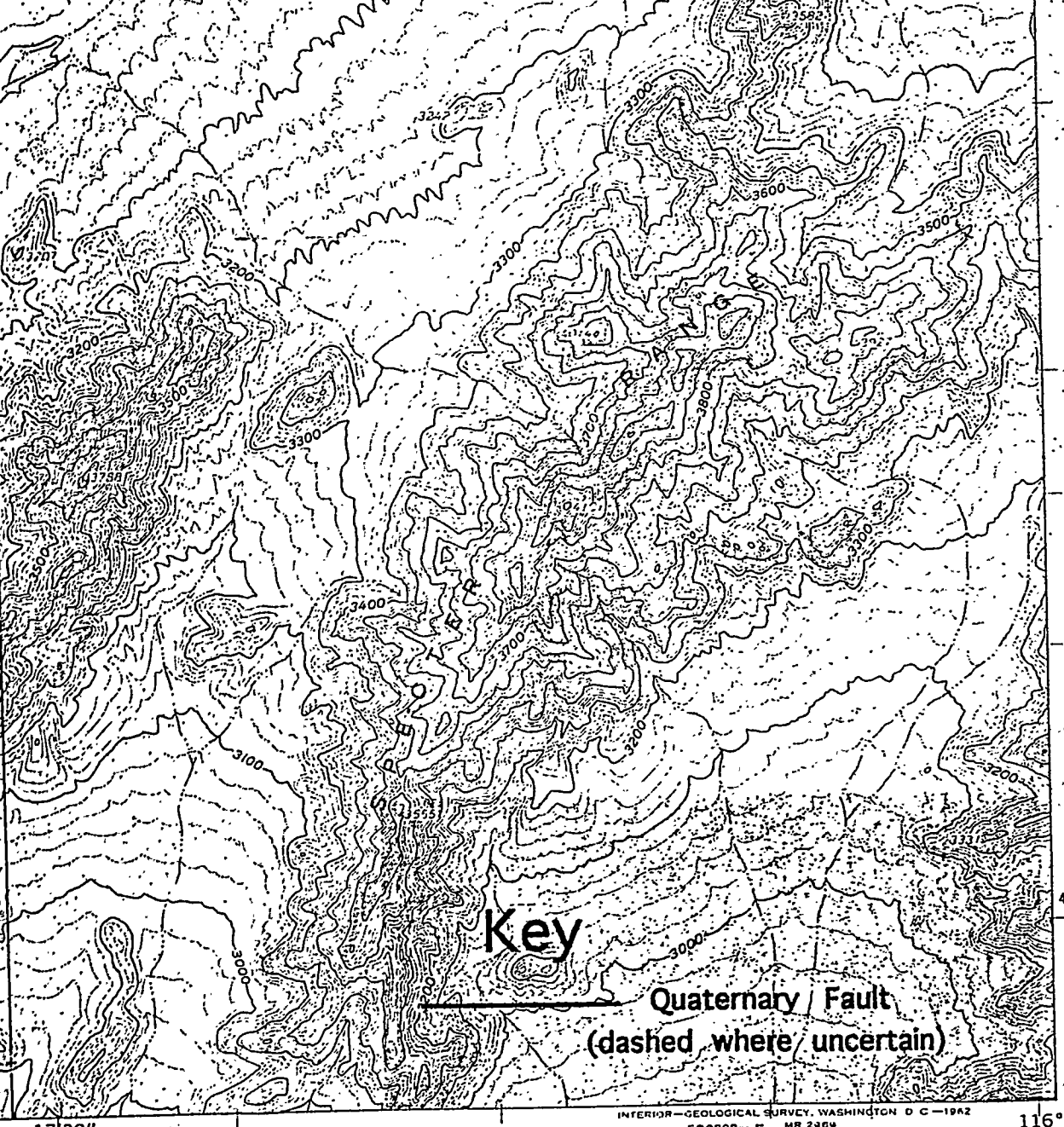

ROAD CLASSIFICATION

Medium-duty — Light-duty

Unimproved dirt

U.S. Route

(SPECTER RANGE 1:62 500)

MILE

NEVADA

QUADRANGLE LOCATION

STRIPED HILLS, NEV.

NE/4 LATHROP WELLS 15' QUADRANGLE

N3637.5—W11615/7.5

1961

2757 I NW
(MINE MOUNTAIN)

UNITED STATES
DEPARTMENT OF THE INTERIOR
GEOLOGICAL SURVEY

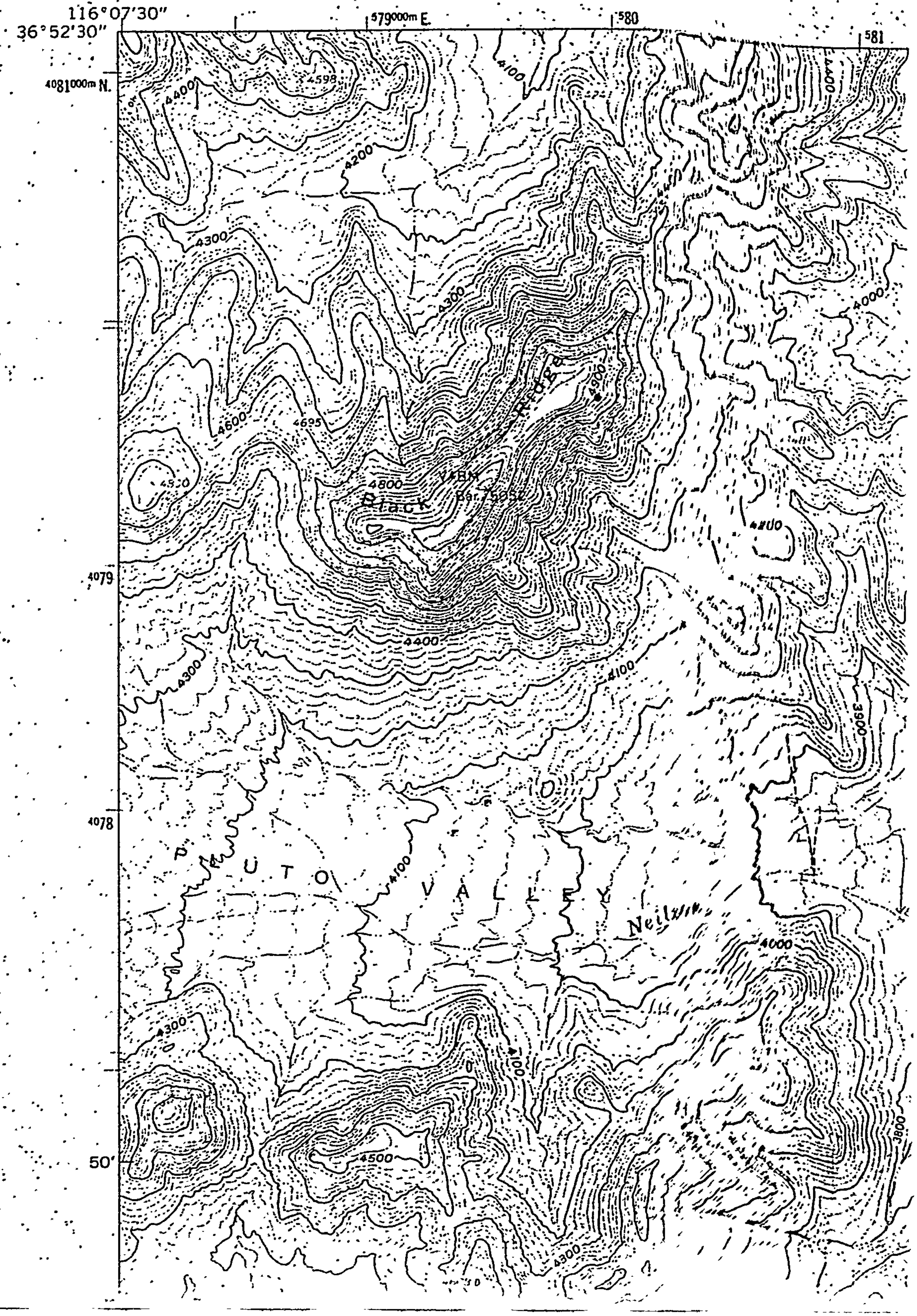

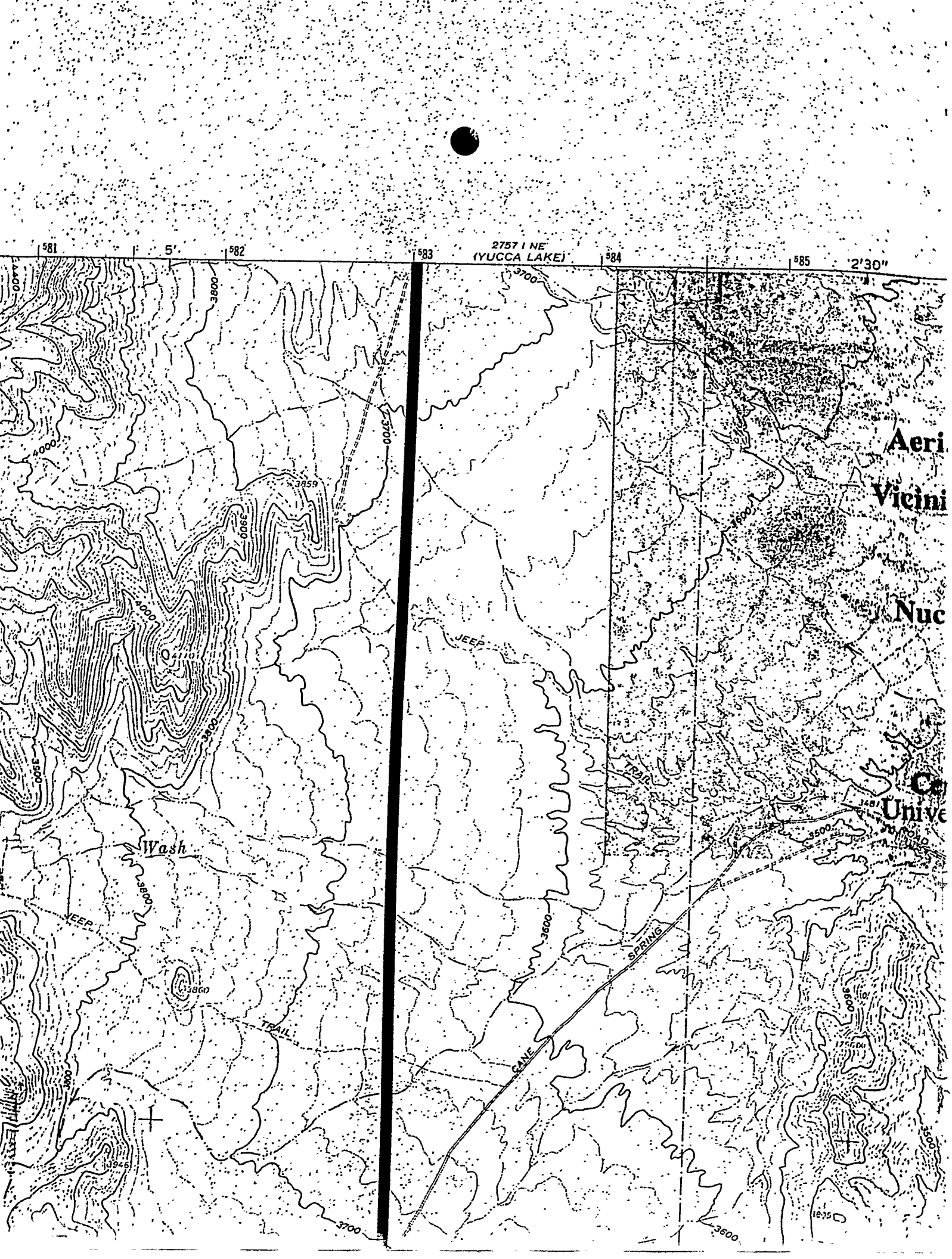
581
5'
582
583
2757 I NE
(YUCCA LAKE)
584
585
2'30"
3700
3800
4000
3900
3859
3600
3500
JEEP
TRAIL
Wash
3860
SPRING
CANE
3946
Aeri
Vicini
Nuc
Unive

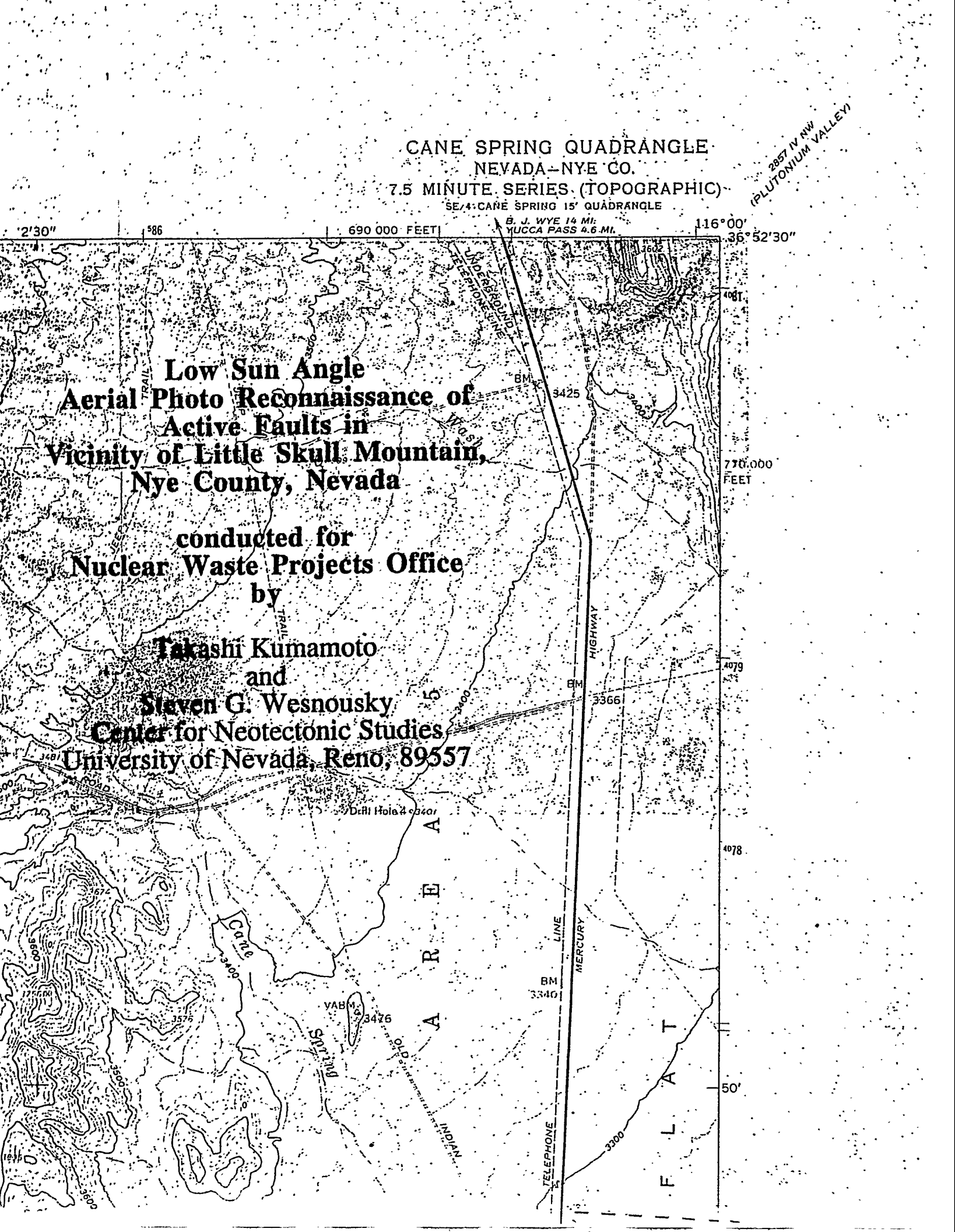
CANE SPRING QUADRANGLE
NEVADA—NYE CO.
7.5 MINUTE SERIES (TOPOGRAPHIC)
SE/4 CANE SPRING 15' QUADRANGLE
2857 IV NW
(PLUTONIUM VALLEY)
B. J. WYE 14 MI.
YUCCA PASS 4.6 MI.
116°00'
36°52'30"
690 000 FEET
2'30"
586
Low Sun Angle
Aerial Photo Reconnaissance of
Active Faults in
Vicinity of Little Skull Mountain,
Nye County, Nevada
conducted for
Nuclear Waste Projects Office
by
Takashi Kumamoto
and
Steven G. Wesnousky
Center for Neotectonic Studies
University of Nevada, Reno, 89557
TELEPHONE LINE
UNDERGROUND
TRAIL
BM
3425
3400
HIGHWAY
95
4079
BM
3366
4078
ROAD
Drill Hole 4
3401
AREA
Cane
Spring
MERCURY
LINE
BM
3340
VABM
3476
OLD
INDIAN
TELEPHONE
3300
FLAT
50'
3500
3600


Wahmonie Flat
JACKASS FLATS ROAD 8.4 MI.
(SKULL MOUNTAIN) 2757 I SW
CANE SPRING
Cane
Cane Spring
Gravel
JEEP
Photo
west
T
E
47'30"
4076
4073
4071
4070

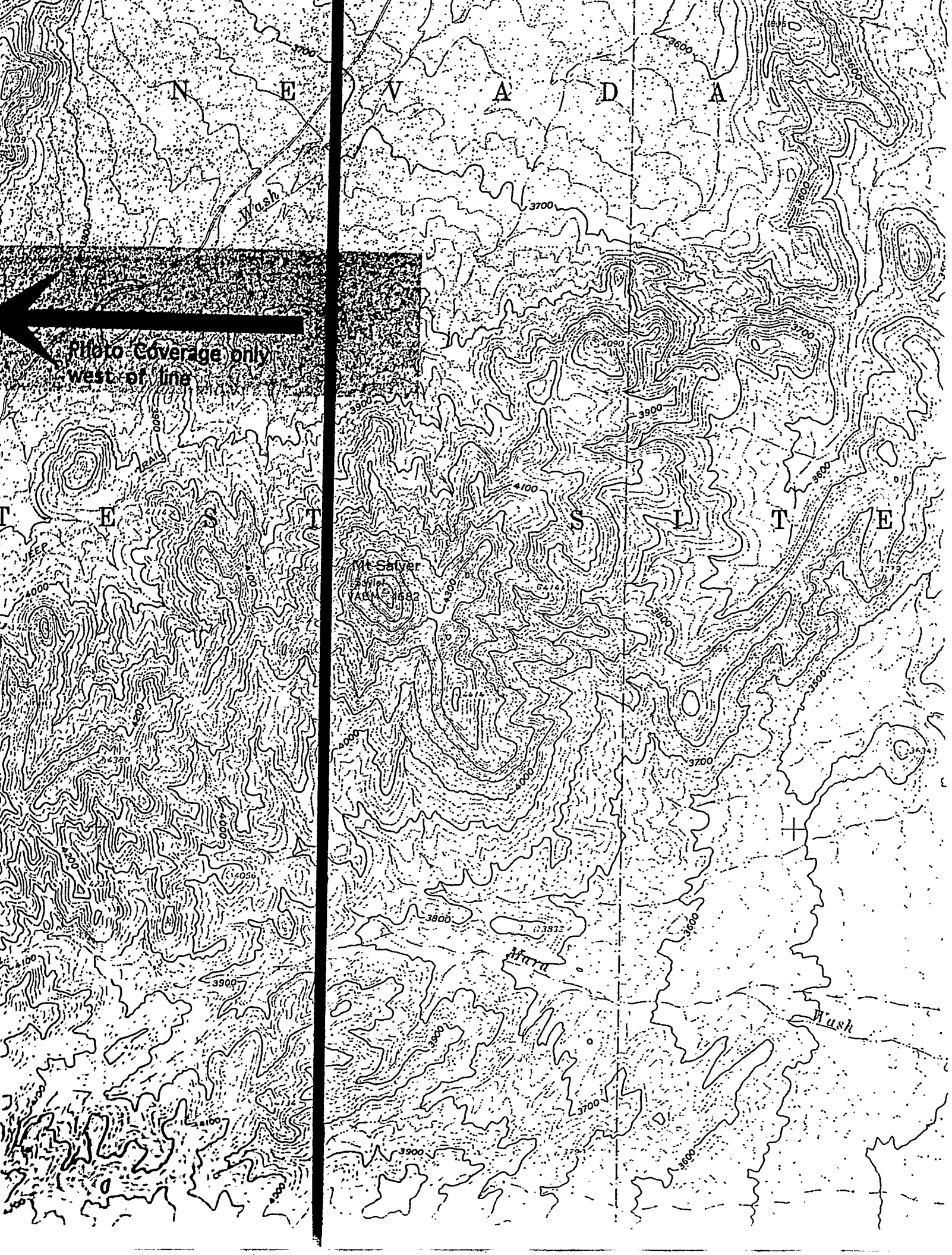
N E V A D A
T E S T S I T E
Wash
Rubio Coverage only
west of line
Mt Salyer
Wash

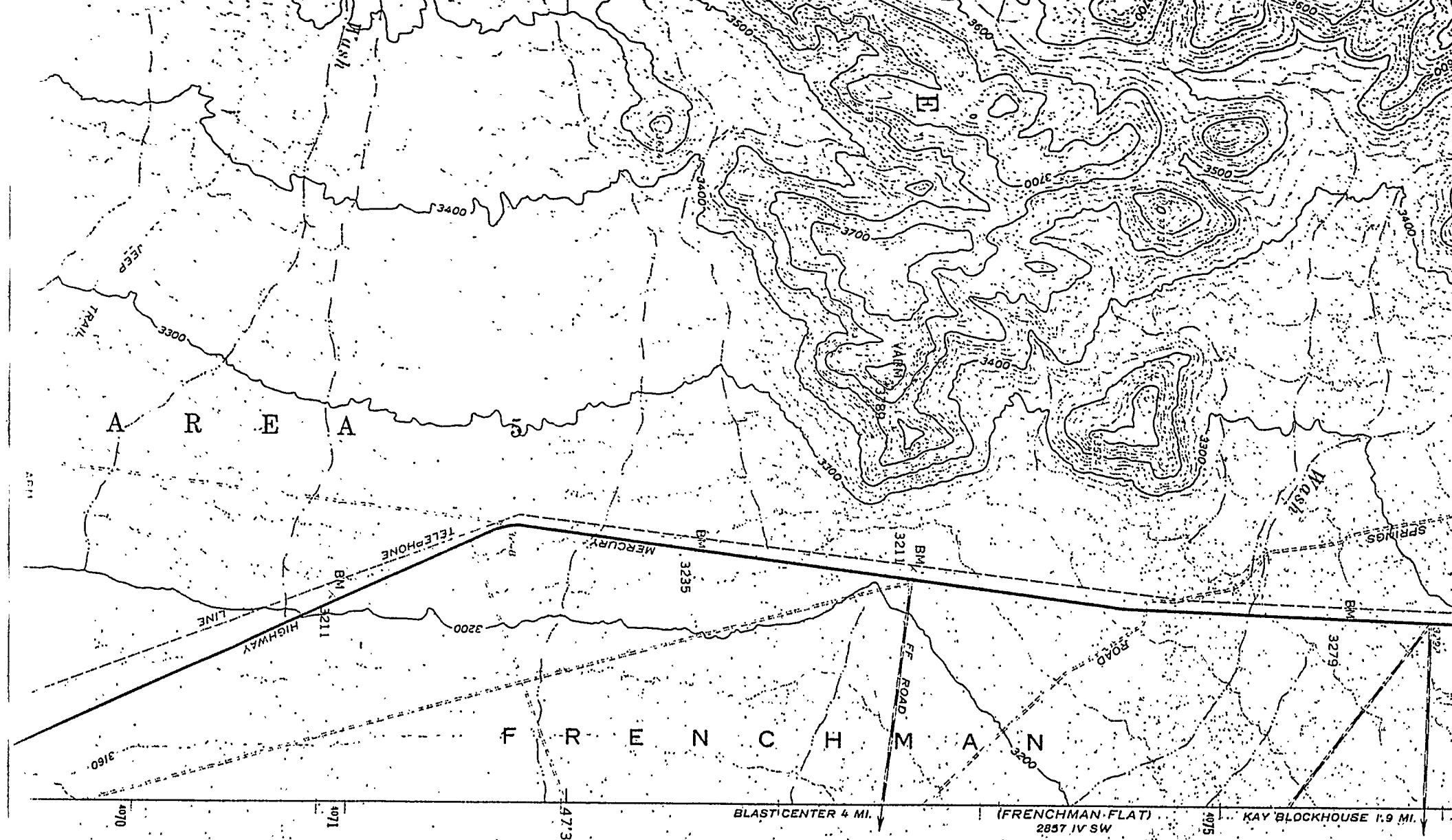
AREA 5
FRENCHMAN
TELEPHONE LINE
HIGHWAY
MERCURY
WASH
SPRINGS
FF ROAD
ROAD
TRAIL
JEEP
BM 3211
BM 3235
BM 3279
3400
3500
3600
3700
3200
3300
3160
4070
711
47'30"
BLAST CENTER 4 MI.
(FRENCHMAN FLAT)
2857 IV SW
KAY BLOCKHOUSE 1.9 MI.

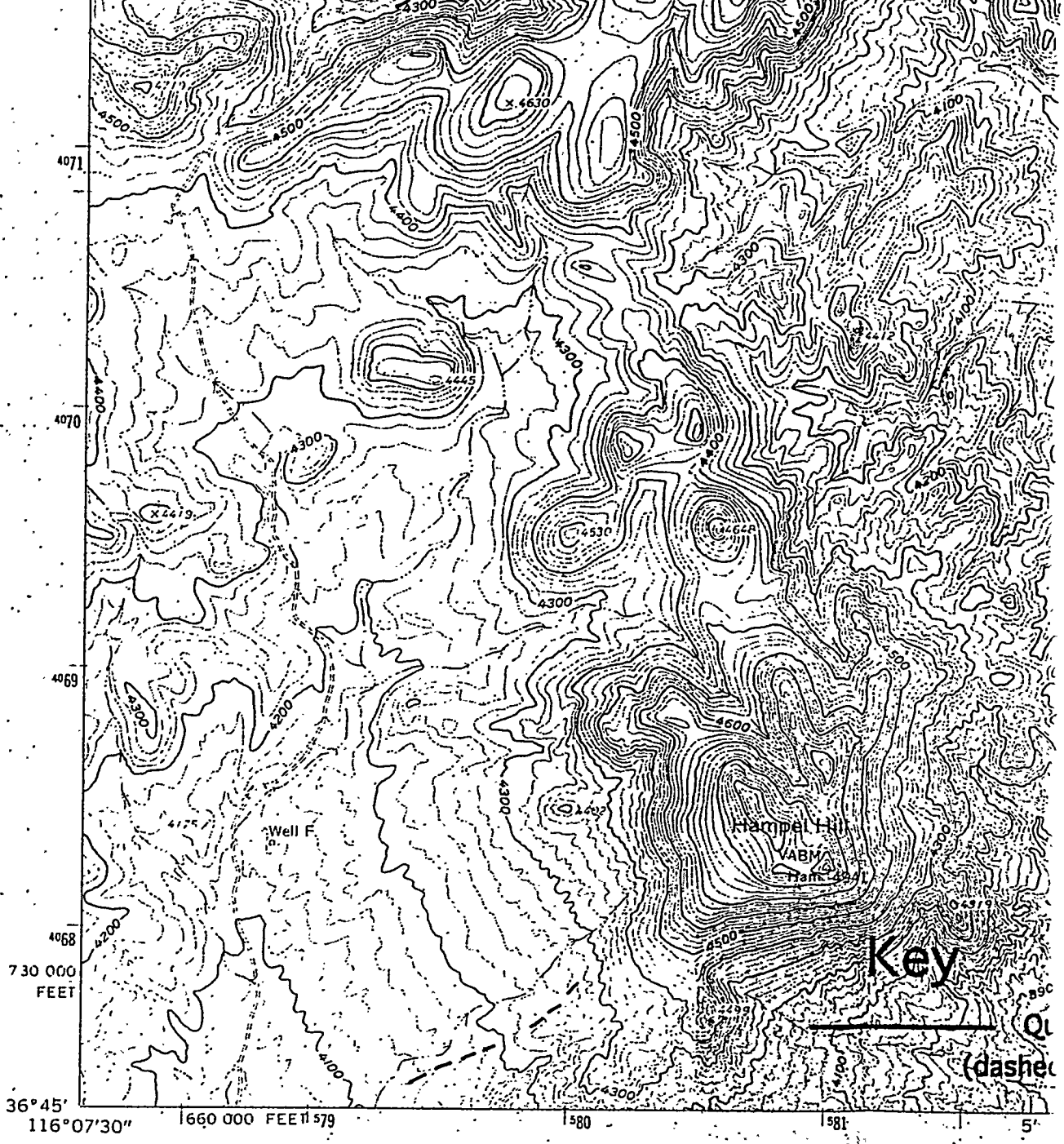

(SPECTER RANGE NW)
2757 II NW

Mapped, edited, and published by the Geological Survey
in cooperation with the Atomic Energy Commission

Control by USGS, USC&GS, USCE, and Atomic Energy Commission

Topography from aerial photographs by photogrammetric methods
Aerial photographs taken 1959. Field check 1961

Polyconic projection. 1927 North American datum
10,000-foot grid based on Nevada coordinate system, central zone
1000-metre Universal Transverse Mercator grid ticks, zone 11,
shown in blue

Fine dashed lines indicate selected fence lines

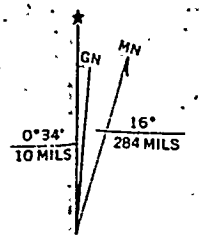

UTM GRID AND 1961 MAGNETIC NORTH
DECLINATION AT CENTER OF SHEET

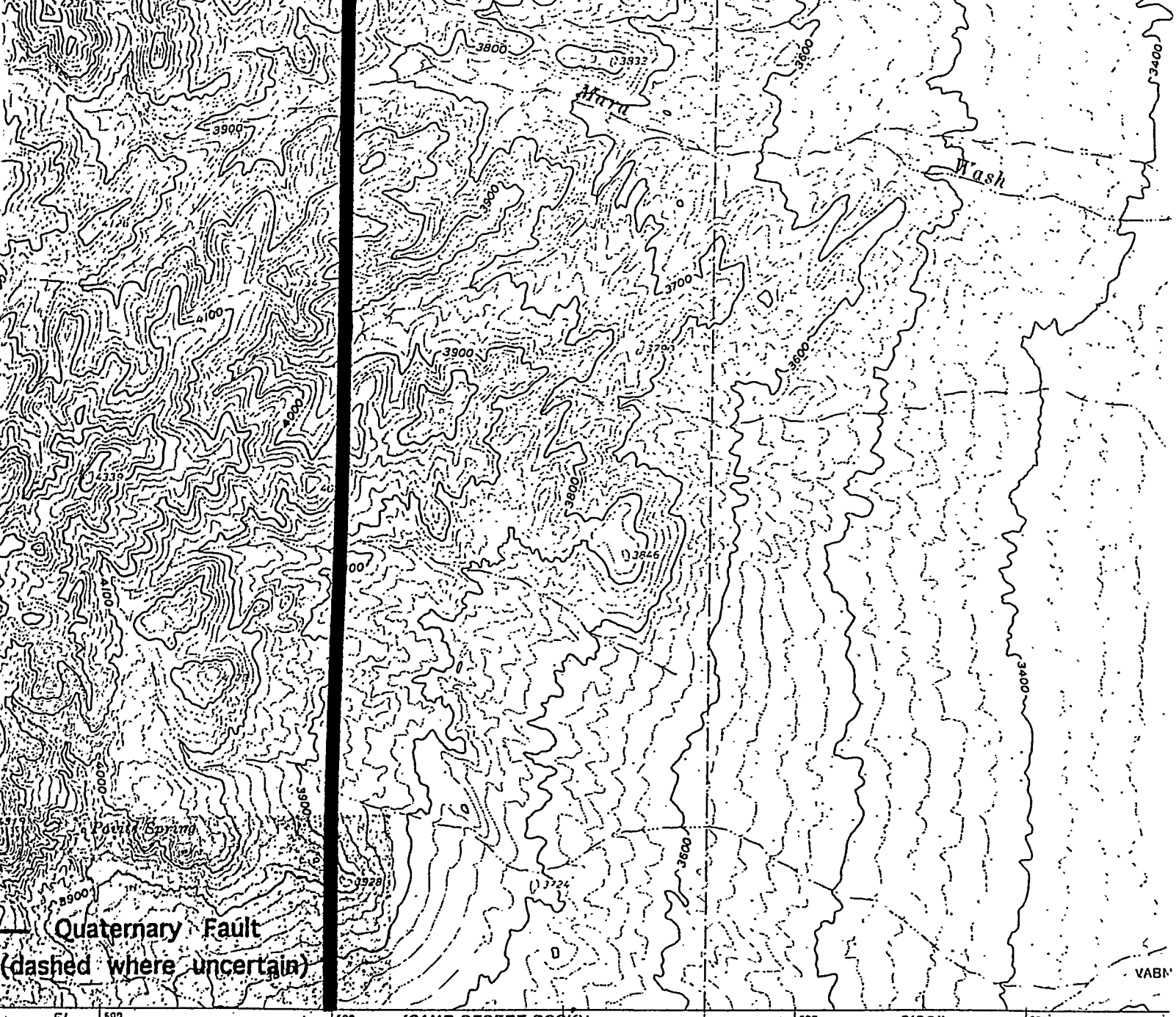
Wash
Quaternary Fault
(dashed where uncertain)
5'
582
583
(CAMP DESERT ROCK)
2757 II NE
585
2'30"
586
SCALE 1:24 000
1 0 1 MILE
1000 0 1000 2000 3000 4000 5000 6000 7000 FEET
1 5 0 1 KILOMETRE
CONTOUR INTERVAL 20 FEET
NATIONAL GEODETIC VERTICAL DATUM OF 1929
NEVADA
QUADRANGLE LOCATI

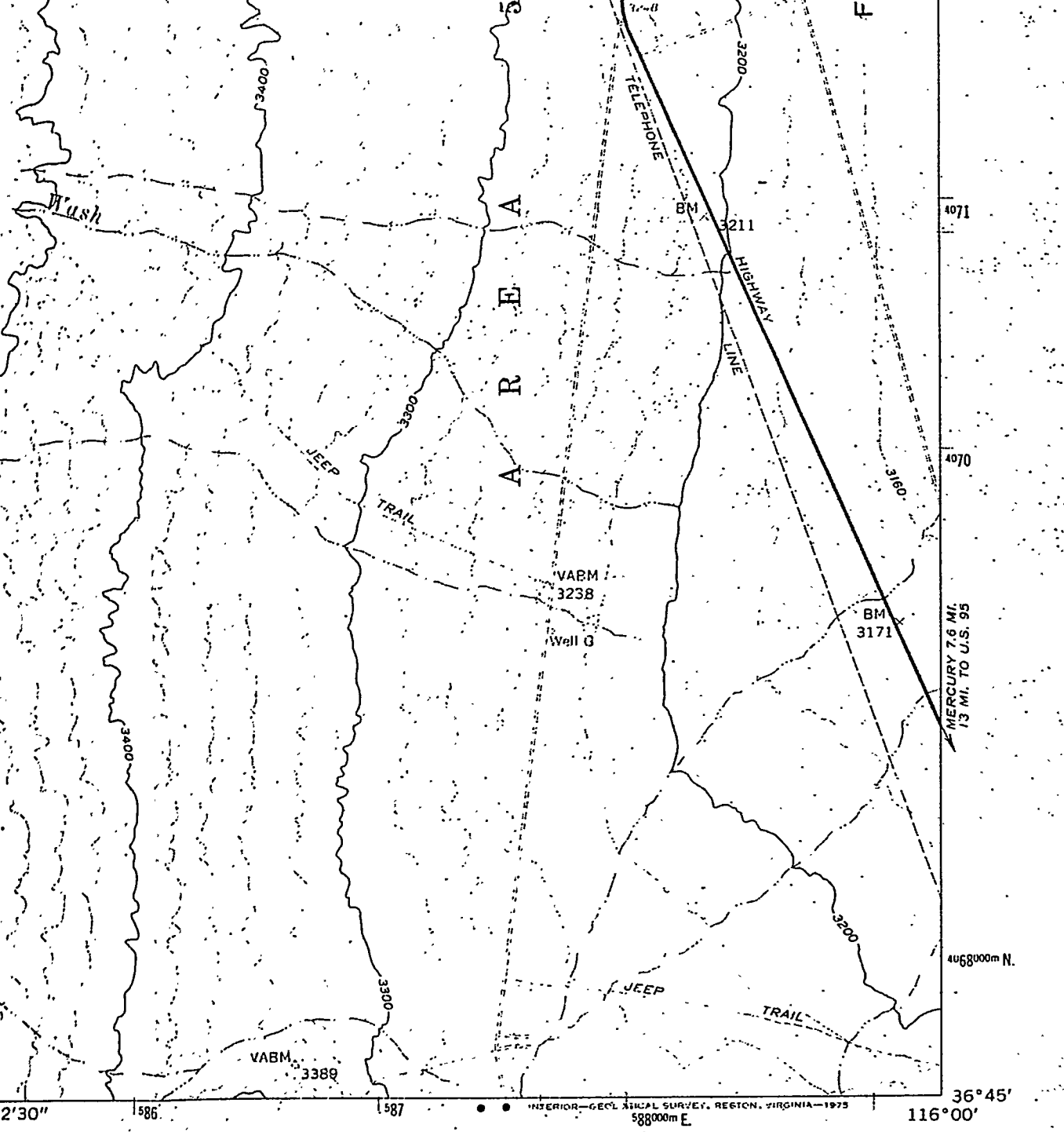

ROAD CLASSIFICATION

Heavy-duty ——— Light-duty ... .

Medium-duty — — Unimproved dirt - - - - -

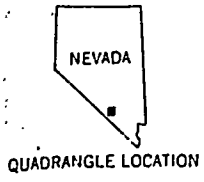

QUADRANGLE LOCATION

CANE SPRING, NEV.

SE/4 CANE SPRING 15' QUADRANGLE

N3645 – W11600/7.5

1961

AMS 2757 I SE—SERIES V896

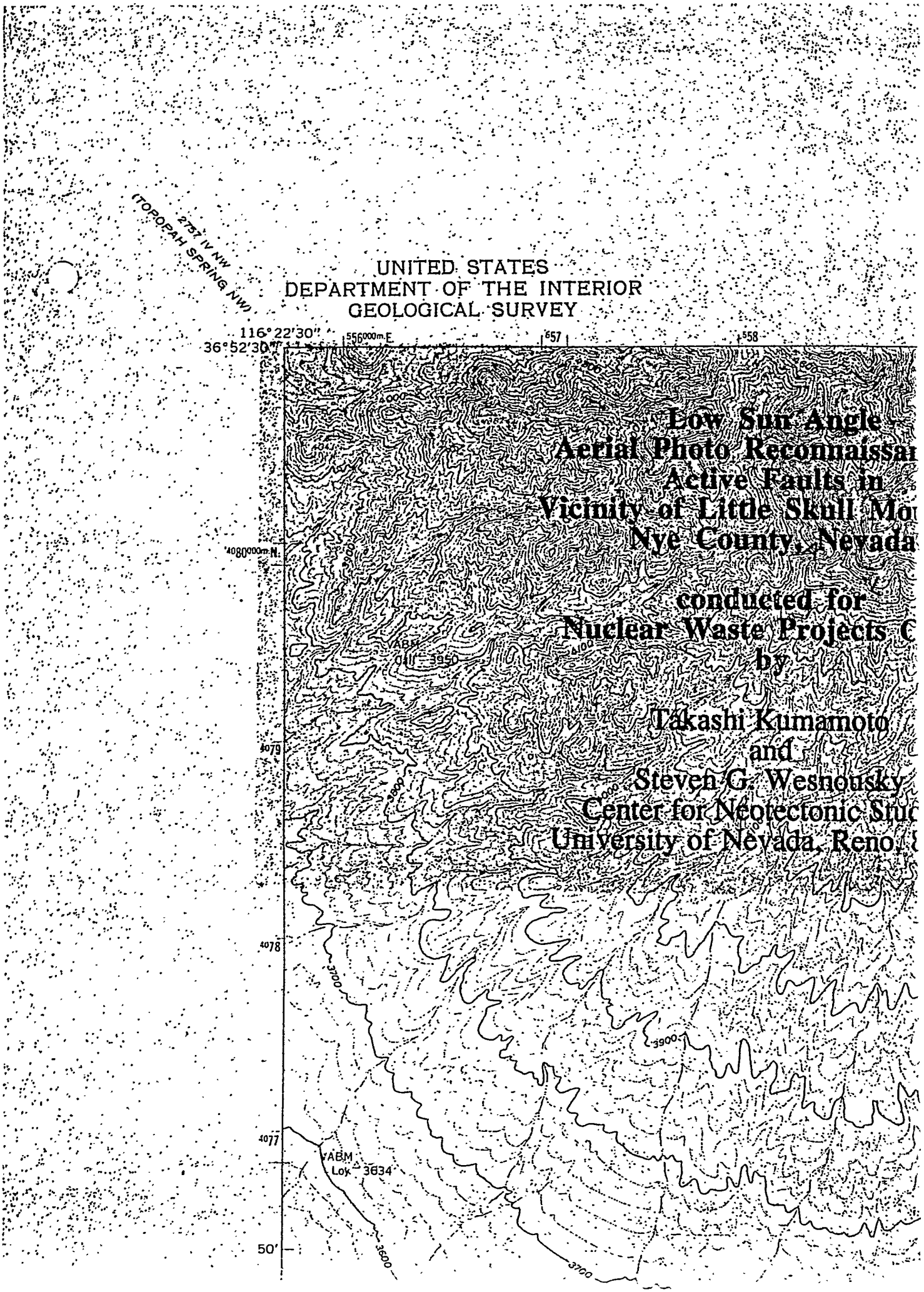
(TOPOPAH SPRING NW)
2757 IV NW
UNITED STATES
DEPARTMENT OF THE INTERIOR
GEOLOGICAL SURVEY
116°22'30"
36°52'30"
556000m.E
57
58
4080000m.N.
4079
4078
4077
50'
ABM
Lok 3950
ABM
Lok 3834
3600
3700
3800
3900
4000
4100
Low Sun Angle
Aerial Photo Reconnaissa
Active Faults in
Vicinity of Little Skull Mo
Nye County, Nevada
conducted for
Nuclear Waste Projects O
by
Takashi Kumamoto
and
Steven G. Wesnousky
Center for Neotectonic Stu
University of Nevada, Reno,

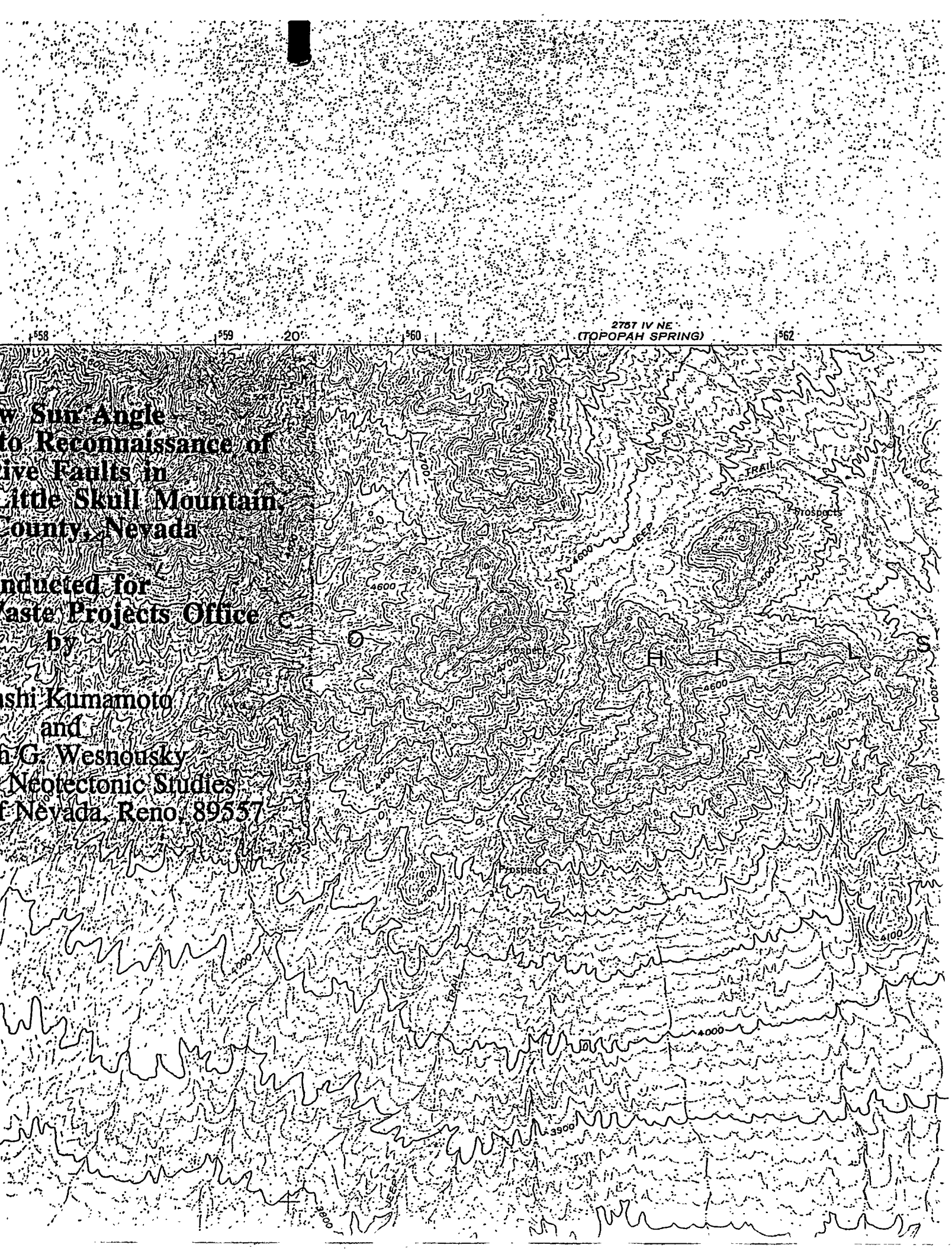

w Sun Angle
to Reconnaissance of
ive Faults in
ittle Skull Mountain,
ounty, Nevada

nducted for
Vaste Projects Office
by

shi Kumamoto
and
n G. Wesnousky
Neotectonic Studies
f Nevada, Reno, 89557

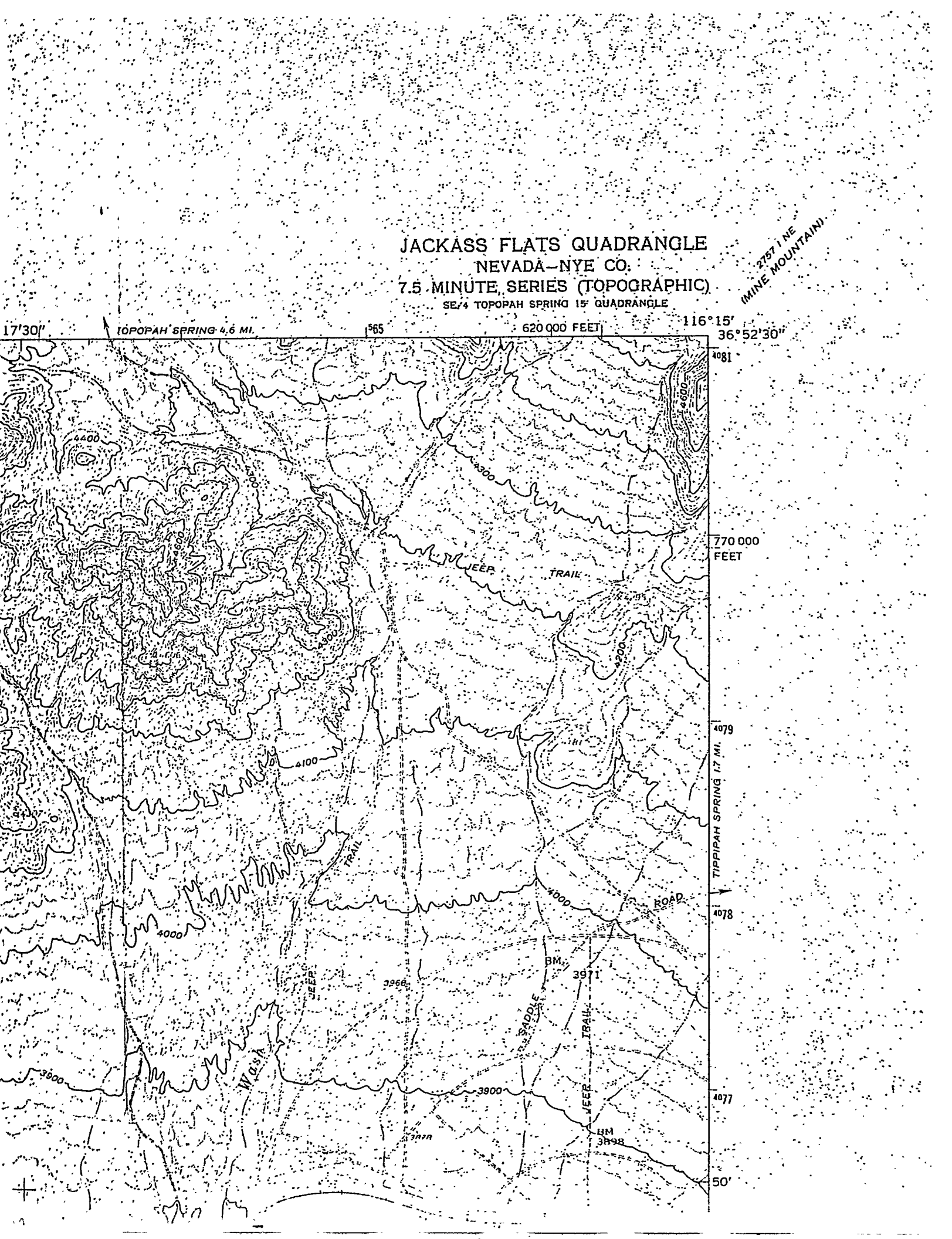
JACKASS FLATS QUADRANGLE
NEVADA—NYE CO.
7.5 MINUTE SERIES (TOPOGRAPHIC)
SE/4 TOPOPAH SPRING 15' QUADRANGLE
2757 I NE
(MINE MOUNTAIN)
17'30"
TOPOPAH SPRING 4.6 MI.
565
620 000 FEET
116°15'
36°52'30"
4081
4600
4400
4300
4200
4100
4000
3900
JEEP TRAIL
770 000 FEET
4079
TIPPIPAH SPRING 1.7 MI.
4078
ROAD
BM
3971
3966
SADDLE
JEEP TRAIL
Wash
4077
BM
3898
50'

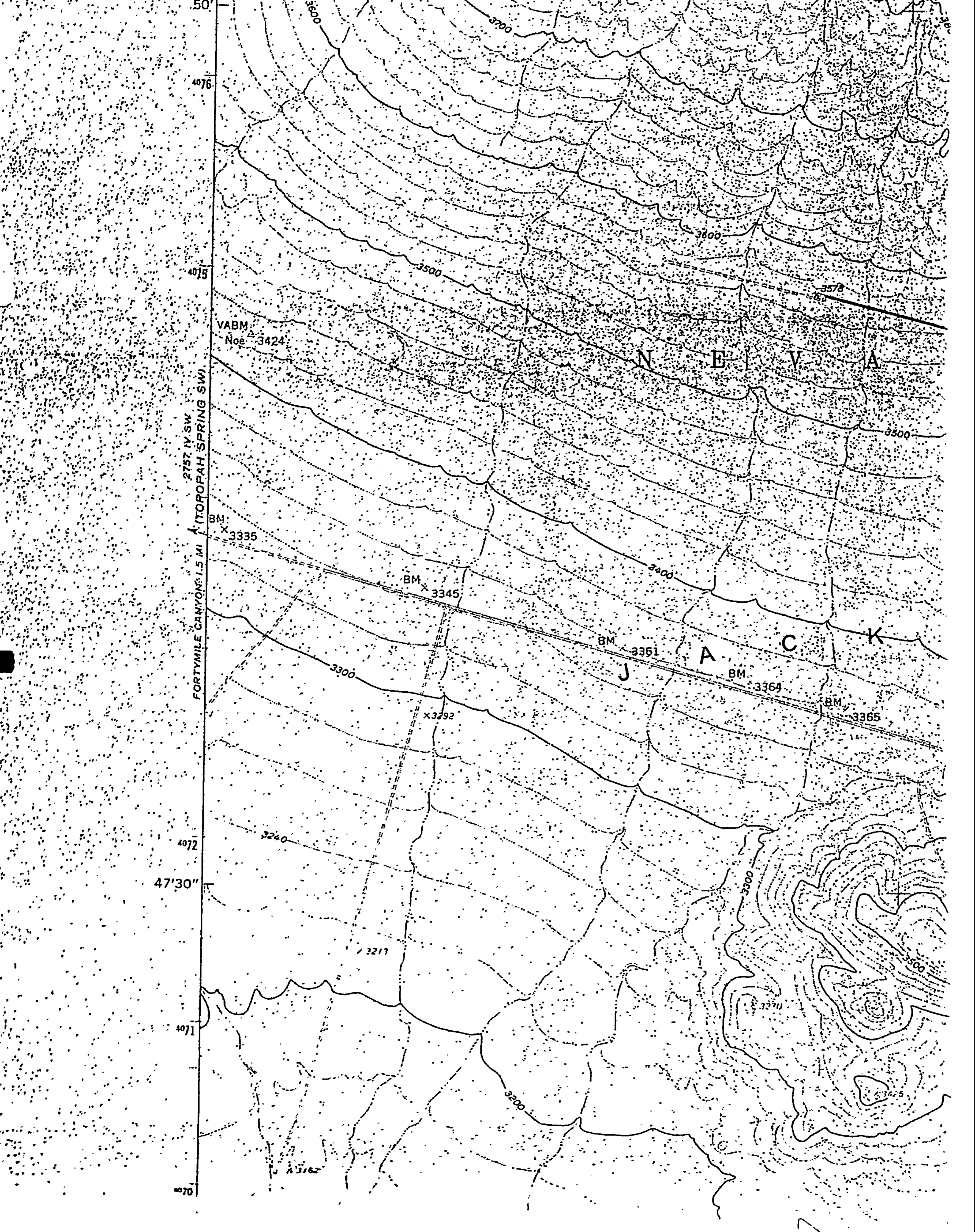

50'
3600
3700
4076
3600
3500
4075
3578
VABM
Noe 3424
N E V A
3500
2757 IV SW
FORTYMILE CANYON 1.5 MI (TOPOPAH SPRING SW)
BM
3335
3400
BM
3345
BM
3361
J A C K
BM
3364
BM
3365
3300
3292
3240
4072
47'30"
3300
3217
3500
4071
3200
4070

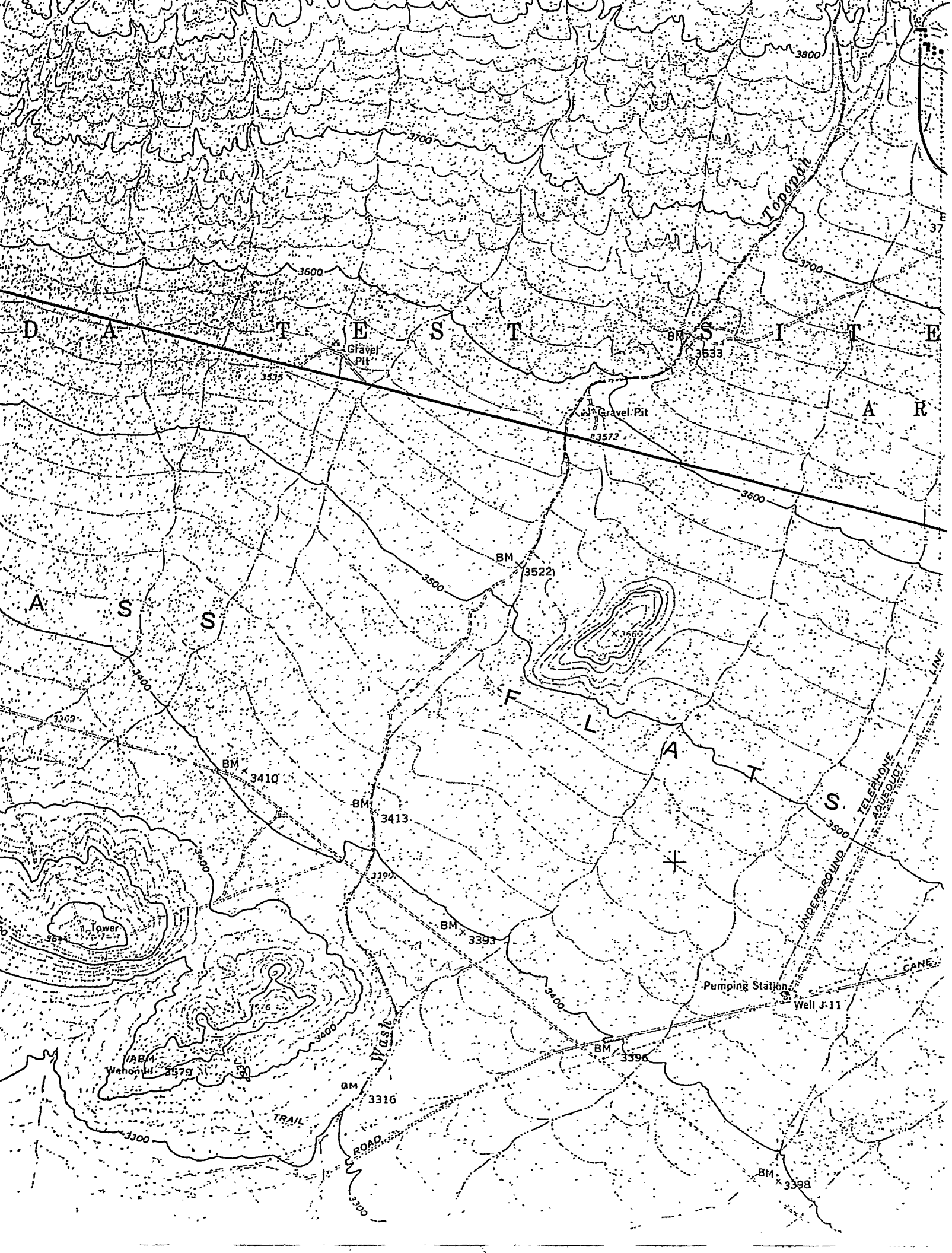
3800
3700
Topopah
3600
3700
D A T E S T
Gravel Pit
BM 3633
S I T E
3535
Gravel Pit
3572
A R
3600
BM 3522
3500
A S S
3660
F L A T S
3400
BM 3410
BM 3413
3400
3300
3500
TELEPHONE AQUEDUCT LINE
UNDERGROUND
Tower
3600
Pumping Station
Well J-11
CANE
3400
BM 3393
Wash
BM 3396
BM
Wahonu
3579
3600
BM 3316
TRAIL
3300
ROAD
3200
BM 3398

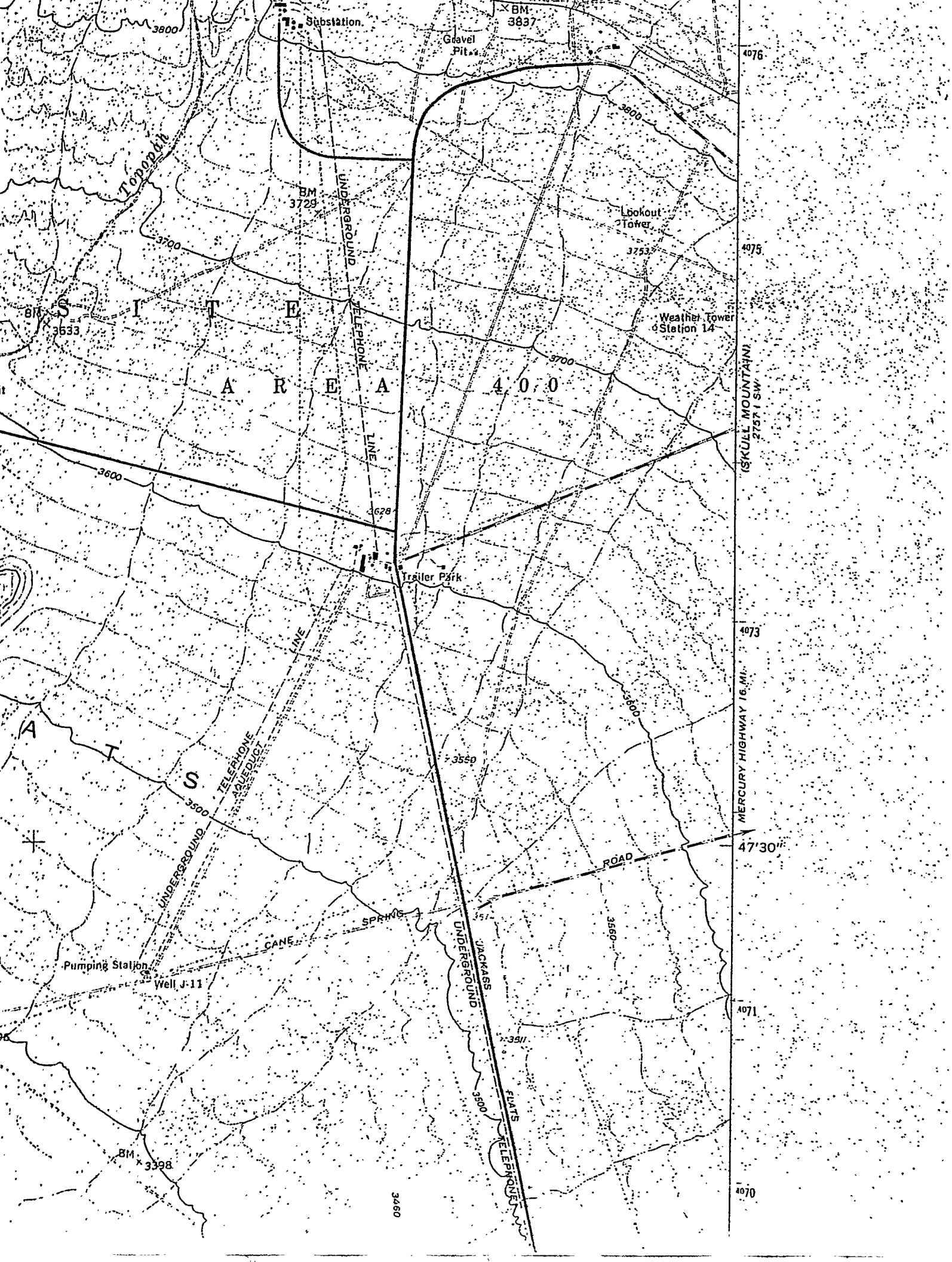
Substation
BM 3837
Gravel Pits
Lookout Tower
3753
Weather Tower Station 14
BM 3729
BM 3633
UNDERGROUND TELEPHONE LINE
TELEPHONE AQUEDUCT LINE
UNDERGROUND
Trailer Park
SITE AREA 400
SITES
MERCURY HIGHWAY 16 MI.
ROAD
47'30"
SPRING
CANE
JACKASS FLATS
UNDERGROUND TELEPHONE
Pumping Station
Well J-11
BM 3398
3628
3511
3460
(SKULL MOUNTAIN)
2757 I SW
4076
4075
4073
4071
4070
3800
3700
3600
3500
3660

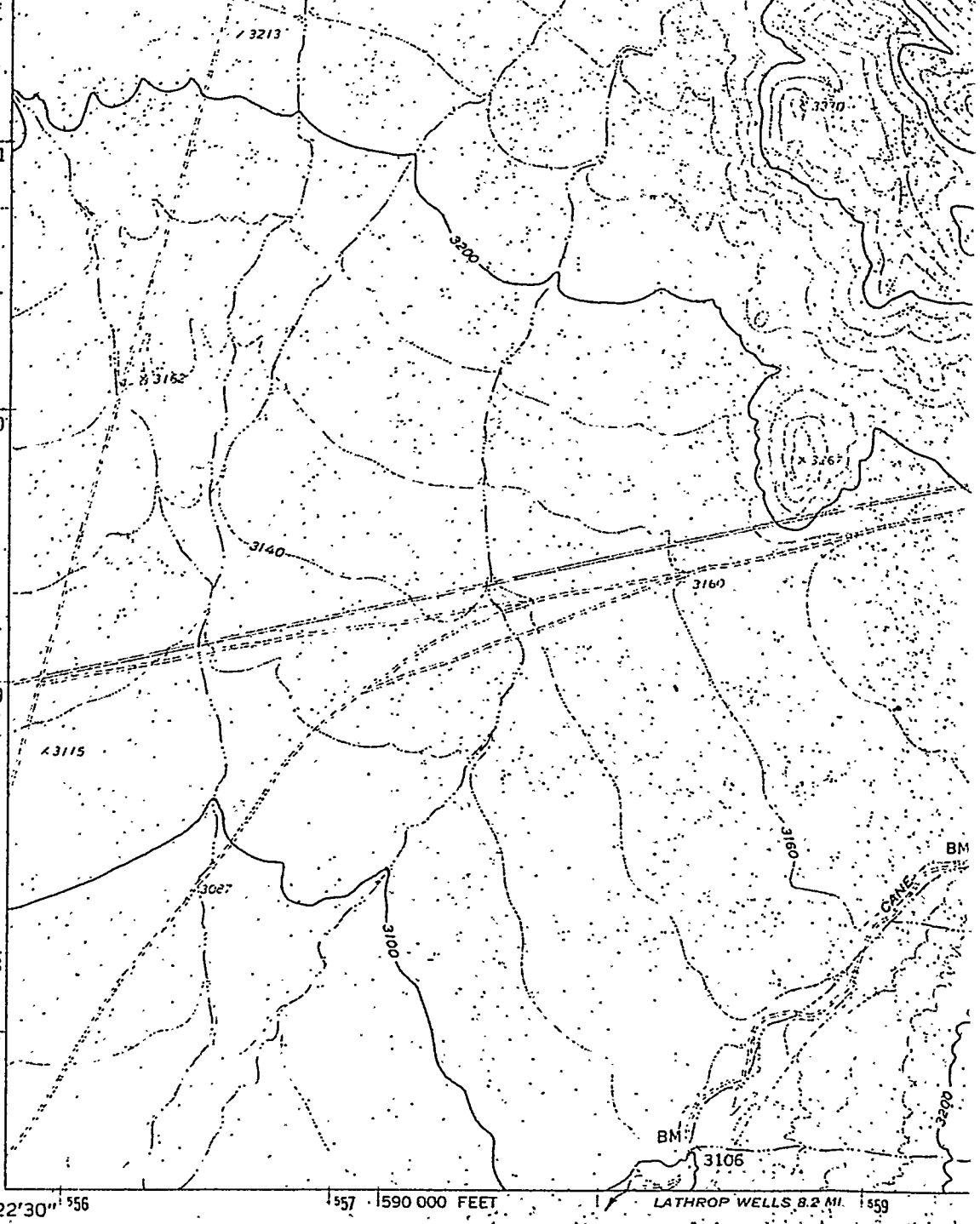

(LATHROP WELLS)
2757 III NW

Mapped, edited, and published by the Geological Survey
in cooperation with the Atomic Energy Commission

Control by USGS, USC&GS, and Atomic Energy Commission

Topography by photogrammetric methods from aerial photographs taken 1959. Field checked 1961

Polyconic projection. 1927 North American datum
10,000-foot grid based on Nevada coordinate system, central zone
1000-metre Universal Transverse Mercator grid ticks, zone 11, shown in blue

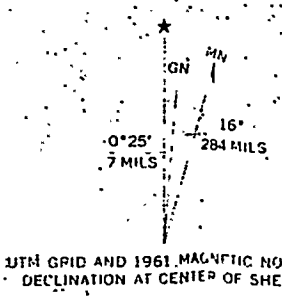

UTM GRID AND 1961 MAGNETIC NORTH
DECLINATION AT CENTER OF SHEET

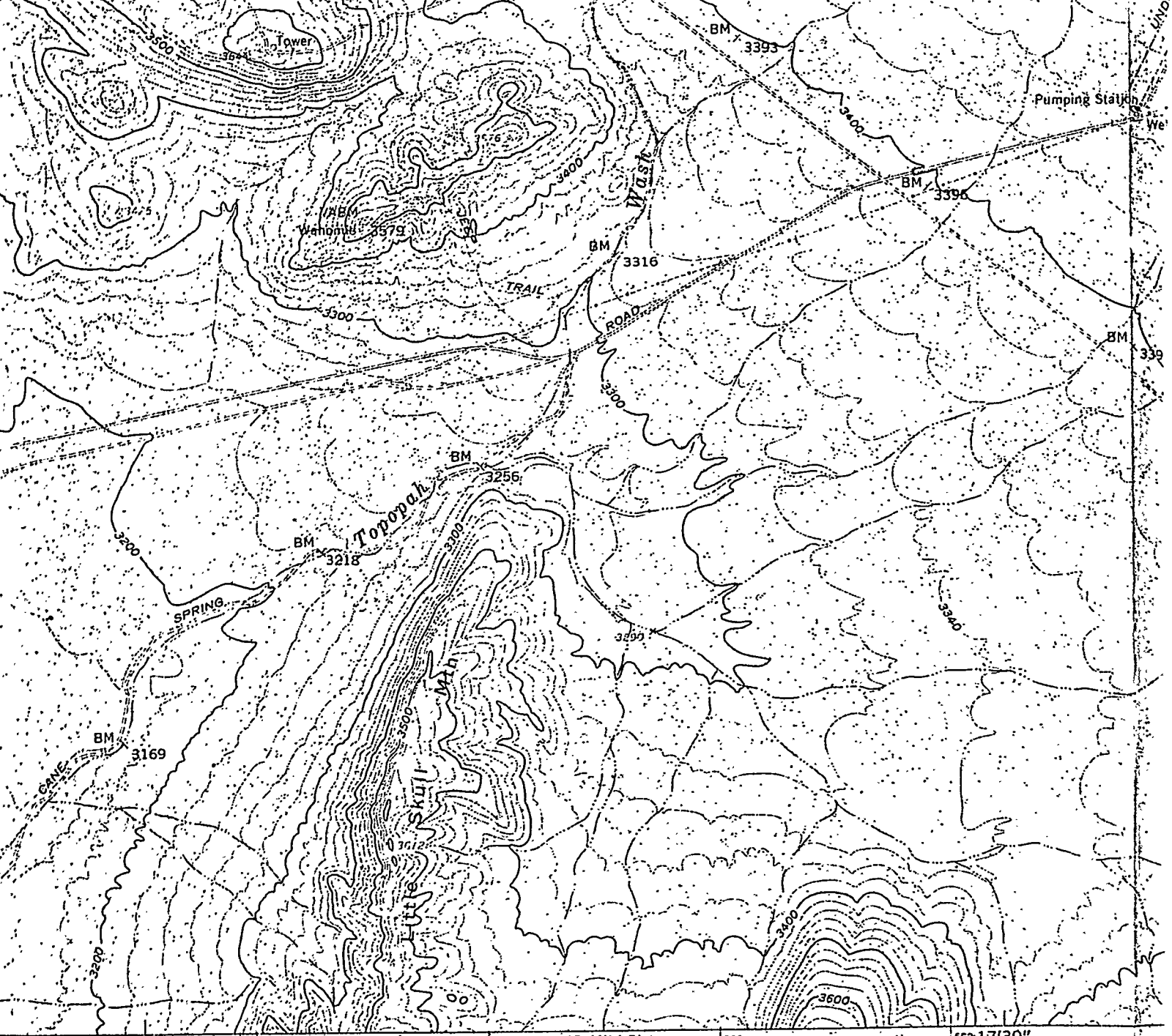
Tower
3644
3500
BM
3393
Pumping Station
3400
BM
3396
ABM
Wahonue
3579
3400
Wash
BM
3316
TRAIL
3300
ROAD
BM
339
3300
BM
3256
Topopah
3200
BM
3218
3300
SPRING
3340
3200
BM
3169
CANE
Skull Mtn
Little
3500
3400
3600
3200
559
20'
560
(STRIPED HILLS)
2757 III NE
562
563
17'30"
SCALE 1:24 000
0
1 MILE
1000 0 1000 2000 3000 4000 5000 6000 7000 FEET
.5 0
1 KILOMETRE
CONTOUR INTERVAL 20 FEET
NATIONAL GEODETIC VERTICAL DATUM OF 1929
16°
284 MILS
GNETIC NORTH
ER OF SHEET
QUADR

Progress Report

Task 1 Quaternary Tectonics

1 October 1993 to 30 September 1994

John W. Bell
Principal Investigator

Craig M. dePolo
Co-Investigator

SUMMARY OF ACTIVITIES CONDUCTED DURING THE CONTRACT PERIOD

During the contract period, the following activities were conducted by Task 1:

* C.M. dePolo completed and published the paper "The Maximum background Earthquake for the Basin and Range Province, Western North America" in the Seismological Society of America *Bulletin*, v. 84, p. 466-472.

* J.W. Bell completed and published with J.E. Faulds, D.L. Feuerbach, and A. Ramelli the map "Geologic Map of the Crater Flat Area, Nevada" as Nevada Bureau and Mines and Geology Map 101, scale 1:24,000.

* J.W. Bell completed the paper "Late Quaternary Geomorphology and Soils in Crater Flat, Yucca Mountain Area, Southern Nevada" which has been accepted for publication in the January 1995 issue of the Geological Society of America *Bulletin.*

* C.M. dePolo completed compilation of the maps showing ruptures associated with the 1932 Cedar Mountain earthquake. The maps will be initially open-filed at NBMG and the fully annotated version will be published as a NBMG map.

* C.M. dePolo completed the draft manuscript "Surface Faulting Associated with the 21 December 1932 Cedar Mountain Earthquake and Implications for Seismic Hazard Studies" which will be submitted to the Seismological Society of America *Bulletin.*

* C.M. dePolo presented the paper "Surface Faulting from the 1932 Cedar Mountain Earthquake" at the Annual Meeting of the Seismological Society of America.

* C.M. dePolo attended 2-day Nevada-sponsored field trip to Yucca Mountain to view trenches and the Sundance fault.

* C.M. dePolo attended the Technical Review Board meeting on probabilistic seismic hazard analyses.

* C.M. dePolo attended the American Geophysical Union and Geological Society of America, Cordilleran Section, annual meetings and observed presentations related to Yucca Mountain.

* C.M. dePolo participated in a field review of Quaternary surficial chronology organized by the U.S. Geological Survey at Yucca Mountain.

* C.M. dePolo attended the Nuclear Regulatory Commission review of exploratory trenches at Yucca Mountain in May 1994.

* C.M. dePolo participated in the 1994 U.S Geological Survey HARM campaign to establish high-precision GPS stations across Nevada.

* C.M. dePolo presented the papers "The 1932 Cedar Mountain Earthquake, Central Nevada, USA: a Major Basin and Range Province Earthquake that had a Widely Distributed Surface Rupturing Pattern" and "Estimating fault slip rates in the Great Basin, USA" at a paleoseismic conference sponsored by the American Geophysical Union.

* J.W. Bell conducted research on temporally clustered earthquake activity.

TECHNICAL REPORT

Technical studies conducted during the contract period consisted of several separate projects, some of which are still on-going. Below we summarize the results of the principal topics addressed during the period.

Preliminary Review of Bare Mountain Trench BMT-1

As part of the continuing field review of DOE exploratory trenching, the Bare Mountain trench BMT-1 excavated by the U.S. Bureau of Reclamation (USBR) was reviewed by Craig dePolo during the NRC field trip in May 1994. The principal conclusions drawn by USBR investigators were: 1) the rate of Quaternary faulting on the Bare Mountain fault is very low, and 2) the age of the most recent surface faulting event is significantly older than previously reported. The USBR reevaluated previous work (Reheis, 1988) which had concluded that there was evidence for Holocene activity on the Bare Mountain fault, and on the basis of trench exposures and fault scarp morphology they concluded that the most recent event was at least an order of magnitude older than previously believed-- on the order of 100 ka or older.

Based on the NRC field review and on a subsequent separate field review by John Bell, significant discrepancies have been found in the USBR conclusions regarding the age of the most recent surface faulting event. An analysis of low-sun angle aerial photography and examination of exposures in trench BMT-1 contradict USBR conclusions and strongly suggest that latest Pleistocene-Holocene activity has been high compared to the longer term late Quaternary rate. The following is a preliminary reinterpretation of structural-stratigraphic relations observed in the trench.

The trench exposes a major trace of the Bare Mountain fault which displaces deposits of several ages. The lowermost, and oldest, unit displaced by the fault is an alluvial-fan deposit containing a well-developed argillic Bt underlain by a strongly cemented petrocalcic horizon (Bqkm); this unit is equivalent to the Early Black Cone (Qfeb) unit of Peterson *et al.* (in press) and is on the order of 150-200 ka in age. This deposit is offset approximately 1-2 m by this fault trace.

Overlying the offset Qfeb unit is an alluvial deposit of mid- to late Holocene age that forms a broad terrace and fan apron across the piedmont surface radiating from the mouth of Tarantula

Canyon. This young alluvial unit is widely recognized on aerial photography and is exposed as a thin (< 1m) veneer in the other exploratory soil pits excavated by the USBR in the area. In the trench, this unit extends the length of the trench, thickening at the fault scarp. The USBR investigators attributed theses relations to eolian accumulations buttressed against the fault scarp. We believe, however, that these uppermost deposits are tectonically produced colluvial wedges.

The north wall of the trench exposes stratigraphy suggestive of 2, and possibly 3, colluvial deposits overlying the offset Qfeb soil. The uppermost grey silt is part of the most recent late Holocene sediment described above. It is horizontally laminated, and it is clearly uncut by the fault. The thickening of this silt at the fault contact, however, is suggestive of a colluvial wedge contact. Underlying this uppermost unit is 20 cm thick light grey silt that is similarly horizontally laminated. This unit, although partially recognized within the shear zone is apparently disrupted by shear fabric. Apparent displacement may be as much as 20 cm across the entire shear zone based on correlation of this unit through the zone. Underlying this silt is a brown-gray gravelly silt which lies directly on the displaced Early Black Cone argillic Bt. This silt is weakly laminated, with laminations dipping approximately 10° west toward the fault. This unit is in clear angular unconformity with the overlying silt unit.

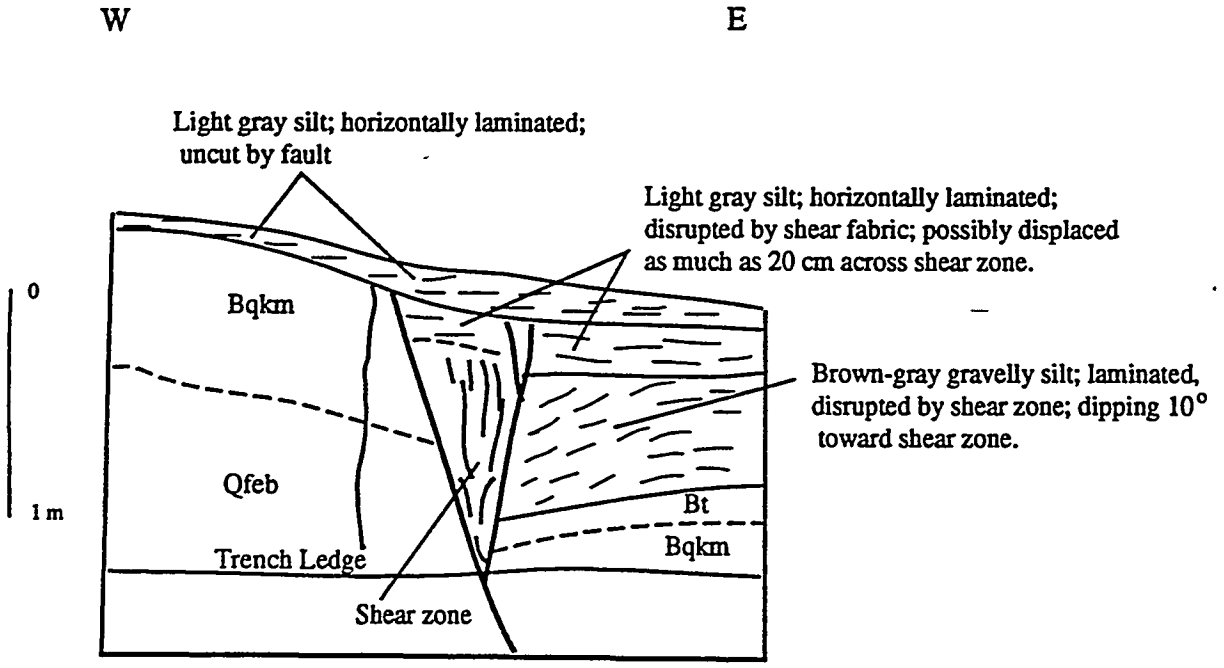

Sketch of deposits exposed in north wall of USBR trench BMT-1.

The two lower silt units exposed in the trench wall are tectonic colluvial deposits; they are thickest at the fault contact, and thin, or wedge out, downslope. Each wedge represents a single tectonic event. The lowermost gravelly silt is colluvium deposited after the Qfeb soil was displaced about 1 m. This gravelly silt was then offset and tilted by a later event which may have had a displacement of about 30-40 cm. The grey silt which overlies the tilted gravelly silt with angular unconformity is colluvium derived from this second event. This colluvium was then probably offset in the most recent event which had a displacement on the order of 20 cm. The uppermost unfaulted silt is likely the colluvium derived from this most recent faulting. A displacement on the scale of 20-30 cm is also suggested for the most recent event by the size of small scarps noted in numerous places along the Bare Mountain fault, including areas to the north of Tarantula where USBR investigations found no evidence of faulting.

The recognition of the three possible tectonic colluvial wedges overlying offset Qfeb soil strongly suggests that fault slip has been more freqent and more recent than concluded by USBR studies. The lack of any significant pedogenic development in the three silt deposits suggests that they are all of latest Pleistocene-Holocene age, and hence that the faulting events are likewise all of latest Quaternary age. The strong argillic soil developed on offset Qfeb deposits indicates that a long period of quiescence-- perhaps tens of thousands of years-- characterized the fault history up until the most recent activity. Such behavior is strongly suggestive of temporal clustering, a pattern of activity discussed later in this report.

Preliminary Detailed Lineament Map of the Southwestern Part of the Proposed Repository Block

It has long been known that Yucca Mountain has numerous internal faults of many different scales and sizes (Scott and Bonk, 1984; Barton and Larson, 1985), and recent studies have begun to delineate and characterize some of these faults. Mapping along the Ghost Dance fault led to the discovery of the northwest-trending Sundance fault and many other smaller faults (Spengler *et al.*, 1994).

For this contract period we have completed a preliminary detailed lineament map of the southwestern part of that block. The study area extended east from the crest of Yucca Mountain to the study area of Spengler *et al.* (1994) and north from Highway Ridge to Antler Ridge. A few lineaments had been previously mapped in this area by Wesling *et al.* (1992), but many more are apparent on existing large-scale photography. The photographs used for this preliminary map were USGS black and white photographs flown for the Yucca Mountain project in 1981 at a scale of 1:7,000 (DOE 24-05).

The preliminary lineament map consists mostly of tonal and vegetation lineaments, with a few bedrock scarps. Many are faint, and some may be lithologic, cooling, or otherwise non-tectonic in nature. However, field reconnassaince reveals that several of these lineaments correspond to fractures (zones), breccia zones, and possible small faults.

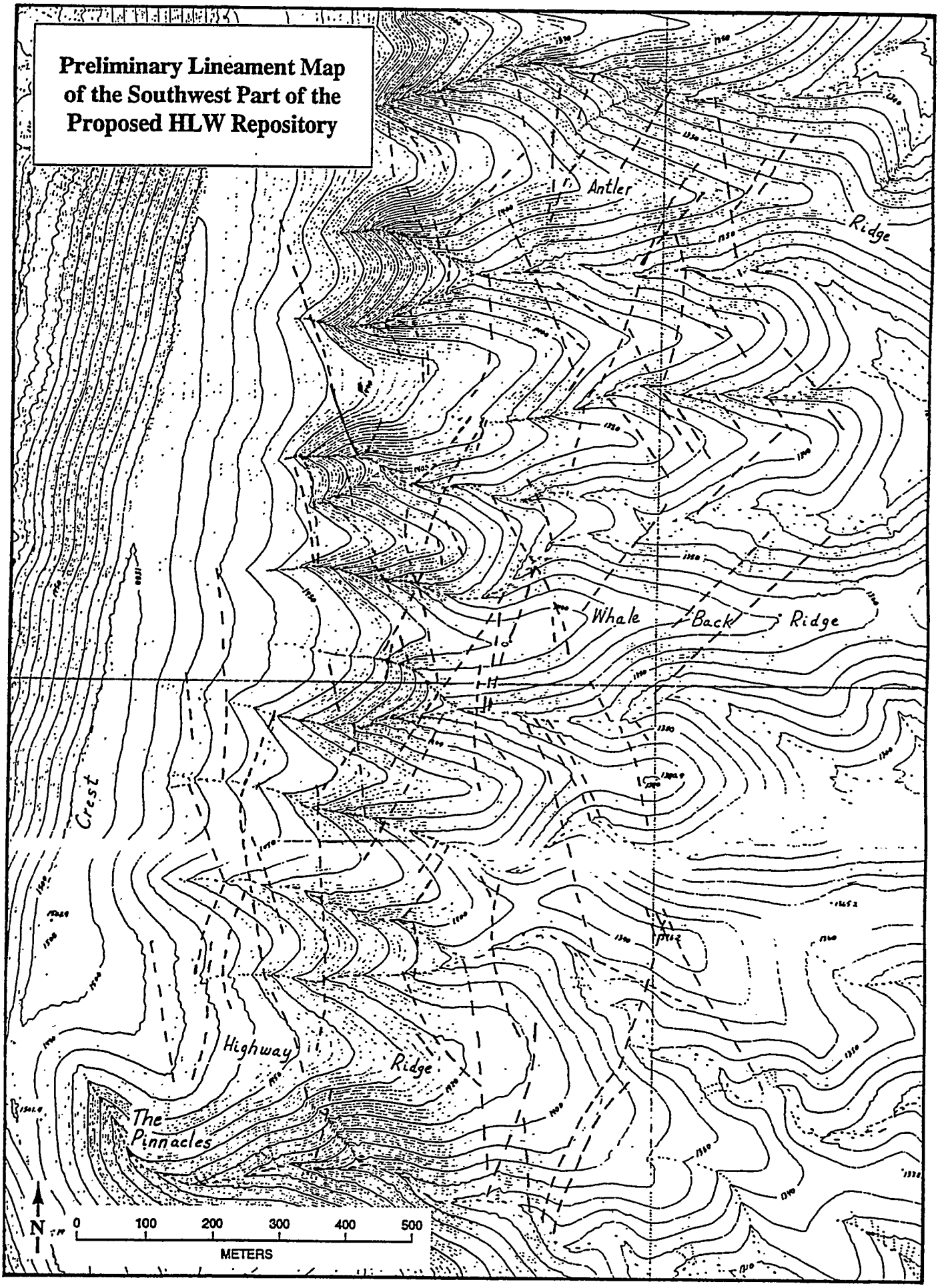
Preliminary Lineament Map of the Southwest Part of the Proposed HLW Repository
Antler
Ridge
Whale
Back
Ridge
Crest
Highway
Ridge
The Pinnacles
N
0
100
200
300
400
500
METERS

The mapped lineaments are short and discontinuous, although many are persistent and numerous throughout the study area. The orientations of these lineaments are trimodal, with northwest trends dominating and northeast-trending lineaments secondary. Northerly-trending lineaments are third most common, and become more prevalant in the southern part of the study area. These orientations mimic those found in the eastern Yucca Mountain region by Wesling *et al.* (1992).

The 1994 Double Spring Flat, Nevada earthquake (M6)

An earthquake of M_L=6.0, M_s=6.3 occurred on September 12, 1994 south of Minden, Nevada. Ground investigations were conducted by C.M. dePolo and J.W Bell, as well as by several other investigators (principal investigators, Alan Ramelli and Jim Yount). The epicentral area was examined and spot checks made along regional faults.

Local surface cracking was found distributed in a zone within 4 km of the epicenter, and two other areas of far-field sympathetic slip were found. This fracturing was probably secondary in nature, and it can be generally described as minor, ranging in opening from one to two millimeters, up to a centimeter wide. The longest zone of cracks was about 1 1/4 km long. Overall, cracks were found over a northwest-trending area 6 to 6 1/2 km in length and 2 km in width. Seven groups of cracks were found, all along faults with north or northwest trends. The far-field cracks are inferred to be sympathetic in nature, *i.e.*, dynamically triggered; both occur along faults with prior reports of fracturing. One area of sympathetic cracking is in Fish Spring Flat, east of Gardnerville, and it occurs along a fault having a history of aseismic creep. Other similar faults in the Fish Spring Flat area were surveyed and no additional evidence of cracking was found. The second area of sympathetic cracking occurred in northern Smith Valley, along a fault that is reported to have cracked previously during an earthquake around 1980.

Evidence for Temporal Clustering

The recently released DOE Topical Report "Methodology to Assess Fault Displacement and Vibratory Ground Motion Hazards At Yucca Mountain" highlights the importance of temporally-clustered earthquake behavior in estimating seismic hazard at the Yucca Mountain site. They note (p. A-13)

> "Temporal clustering may have a significant effect on the accuracy of recurrence rates that are based on fault slip rates."

This conclusion is based on the observation that faults which are presently in an actice cluster period will have higher recurrence intervals, and consequently higher hazards, than those either in a quiescent period or those characterized by the long-term average recurrence rate.

There is growing evidence form trench investigations at Yucca Mountain that some Yucca

Mountain faults exhibit clustered event behavior. Menges *et al.* (1994) found that trenches excavated across the Painbrush Canyon, Bow Ridge, and Stagecoach Road faults reveal evidence between 3 and 8 surface-rupturing events during the late Quaternary. A reinterpretation of the Midway Valley trench (MWV-T4) indicated that 4-5 events are recorded in offset colluvial wedge deposits, and that recurrence intervals may be less than 10^4 years based on the lack any significant soils within the colluvial wedge sequence. The Bare Mountain fault trench described above may also be an example of such activity.

These results together with similar results from several other trenches led Menges et al. (1994) to conclude that the presence or absence of temporal clustering in occurrence of earthquake ruptures at Yucca Mountain was a particularly important topic which needed to be addressed by future work. If temporal clustering is valid model for fault behavior at Yucca Mountain,, the seismic hazard estimated from this higher rate of activity could be as much as an order of magnitude greater than the hazard estimated from the presently used average values.

Due to the emerging importance of the temporal clustering model, we have investigated the evidence for the validity of this model on a global scale. While on sabbatical leave this past year, John Bell investigated the world-wide evidence for temporal clustering of paleoearthquakes in the paleoseismic record. This research was conducted while he was a visiting researcher at the Institut de Physique du Globe, Strasbourg, France. The preliminary report "Temporal Clustering of Paleoearthquakes" is included here.

References

Barton, C.C. and Larsen, E., 1985, Fractal geometry of two-dimensional fracture networks at Yucca Mountain, Southwestern Nevada: Proceedings of the International Symposium on Fundamentals of Rock Joints, Bjorkliden, Lapland, Sweden.

Menges, C.M., Swan, F.H., Oswald, J.A., Wesling, J.R., Coe, J.A., Whitney, J.W., and Thomas, A.P., Preliminary results of paleoseismic investigations of Quaternary faults on eastern Yucca Mountain, Nye County, Nevada: Proceedings of Fifth International Conference, High-level Radioactive Waste Management, 19 p.

Peterson, F.F., Bell, J.W., Dorn, R.I., Ramelli, A.R., and Ku, T.L., in press, Late Quaternary geomorphology and soils in Crater Flat, Yucca Mountain area, southern Nevada: Geological Society of America Bulletin.

Reheis, M.C., 1988, Preliminary study of Quaternary faulting on the east side of Bare Mountain, Nye County, Nevada, *in* Carr, M.D., and Carr, J.C., eds., Geologic and hydrlogic investigations of a potential nuclear waste disposal site at Yucca Mountain, southern Nevada: U.S. Geological Survey Bulletin 1790, p. 103-111.

Scott, R.B., and Bonk, J., 1984, Preliminary geologic map of Yucca Mountain with geologic sections, Nye County, Nevada: U.S. Geological Survey Open File Report 84-494, scale 1:12,000.

Spengler, R.W., Braun, C.A., Marin, L.G., and Weisenberg, C.W., 1994, The Sundance fault: a newly recognized shear zone at Yucca Mountain, Nevada: U.S. Geological Survey Open-File Report 94-49, 11 p.

NEVADA BUREAU OF MINES AND GEOLOGY

UNIVERSITY OF NEVADA RENO

Mail Stop 178
Reno, Nevada 89557-0088
Telephone: (702) 784-6691
FAX: (702) 784-1709

TEMPORAL CLUSTERING OF PALEOEARTHQUAKES

Preliminary Report to the Nevada Nuclear Waste Project Office

John W. Bell

TEMPORAL CLUSTERING OF PALEOEARTHQUAKES

John W. Bell

Introduction

The character of the earthquake cycle is important in understanding and modelling behavior of seismogenic sources. Of particular importance is the question of whether the cyclic tectonic loading and release process is periodic or aperiodic, because recurrence data are incorporated into most seismic hazard estimates (*cf.*, Scholz, 1990). Most probabilistic seismic hazard models utilize a periodic recurrence model (e.g., Bender and Perkins, 1987), in which it is assumed that the average long-term recurrence interval adequately represents real fault behavior. This is essentially the classical Reid concept where uniform stress accumulation is used to estimate the timing of regular, periodic earthquakes having uniform stress drops.

Within the last decade, however, a growing body of seismic data, largely derived from plate boundary faults, suggests that actual fault behavior is far more complex than that suggested by the original Reid concept, and that the seismic cycle is not so simple (cf., Wyss, 1990). For example, Shimazaki and Nakata (1980) proposed two additional earthquake recurrence models based on studies of less-regular Japanese earthquakes: the time-predictable and the slip-predictable models. Thatcher (1989, 1990) further illustrated that some major plate-boundary faults do not display periodic behavior as commonly assumed, and that such activity is actually the exception rather than the rule.

For intra-plate regions, such as the Basin and Range Province, seismic data are less able to define the nature of the earthquake cycle; seismicity is lower and more diffuse, distributed among hundreds of seismogenic faults. In addition, most faults have earthquake cycles that are one to three orders of magnitude longer than those on plate boundary faults. Within such regions, paleoseismic data are thus required to understand the earthquake cycle. Wallace (1987) first hypothesized that faults in the Basin and Range Province are characterized by irregular and varied patterns of activity (Fig. 1). In contrast to the conventional theory that regular, periodic earthquake cycles characterize fault behavior (Fig. 1B), Wallace (1987) proposed that the earthquake cycle in the Basin and Range is better represented by a grouping, or clustering, of events (Fig. 1A). Several earthquakes of similar size may cluster closely together in time with individual clusters separated by lengthy periods of fault quiescence, and although the bursts of clustered activity have short interseismic (recurrence) intervals, the long-term average recurrence interval remains the same as in the periodic recurrence model. Wallace (1987) referred to such behavior as temporal grouping, but it has more commonly been termed temporal clustering.

The occurrence and frequency of temporal clustering is a significant consideration in estimating earthquake hazard in the Basin and Range Province. At the proposed Yucca Mountain high-level nuclear waste repository, evidence for temporal clustering will be a major element in modelling

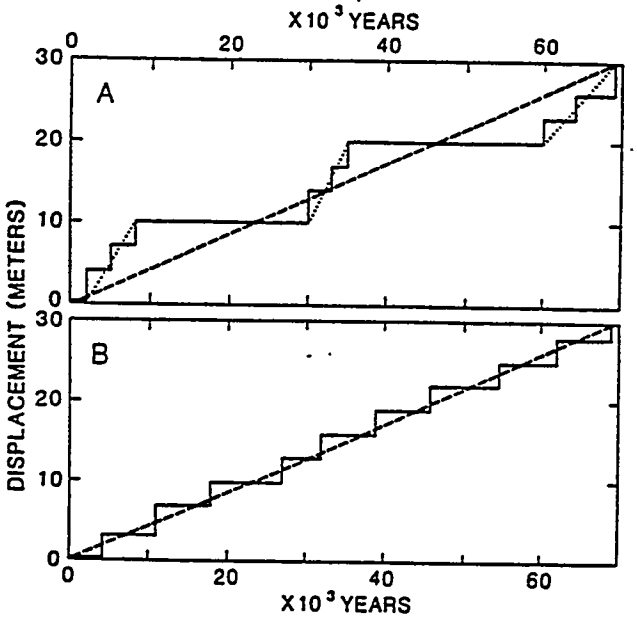

Figure 1. Diagrammatic graphs of two types of fault-displacement time histories. A) Temporal grouping of slip events separated by periods of quiescence. B) More regular recurrence of slip events. Dashed lines show average displacement rate which is the same in both examples (Wallace, 1987).

fault displacement within the repository (U.S. Department of Energy, 1994). Probabilistic logic tree analyses intended for use in characterizing seismic hazard at Yucca Mountain require that conditional probabilities be estimated for event clustering on repository faults (Electric Power Research Institute, 1993).

In this study, I have combined published world-wide data with independent field studies of selected faults to test the theory of temporal clustering. Preliminary results of this limited test indicate that although many faults exhibit periodic behavior, clustering appears to be a far more common behavior than generally believed. I present in this overview some of the best documented examples, and discuss the models that explain aperiodic fault behavior.

What is the Evidence for Earthquake Clustering?

Evidence from the Historical Seismicity Record

Examples of temporal clustering are frequently found in short- and long-term seismic records from both intra-plate and plate boundary settings. The long historical records of China and the

Mediterranean provide particularly useful insights into fault behavior (*cf.*, Allen, 1975), and suggest that clustered activity characterizes some major tectonic provinces. McGuire (1979) examined the Chinese seismic catalog which spans nearly 3000 years and found that earthquake activity was episodic. He concluded that earthquake activity cycles appear to occur on average every 300 years, separated by periods of quiescence. Ambraseys (1970) compiled data from more than 3000 earthquakes during the last 2000 years in Turkey, and found that alternating patterns of activity and quiescence could be identified on the Anatolian fault zone in Northern Turkey and on Red Sea-Dead Sea Border Zone of the eastern Mediterranean (Fig. 2).

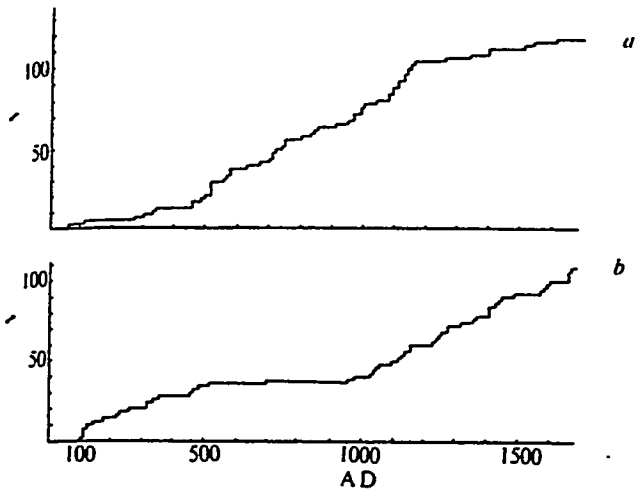

Figure 2. Time distribution of damaging earthquakes. a) Red Sea-Dead Sea Border fault zone. b) Anatolian fault zone. N, number of earthquakes (Ambraseys, 1971).

Some of the strongest evidence for clustering comes from plate boundary systems previously thought to exhibit periodic, characteristic earthquake behavior. A strong case for non-characteristic behavior of major plate boundary fault systems is made by several studies of historical seismic recurrence cycles. Thatcher (1989, 1990) examined seismic catalogues from 12 segments of circum-Pacific plate boundary faults, and found that while seismic strain release was relatively well ordered, the source dimensions, slip, and cumulative seismic moment varied considerably from cycle to cycle. Interevent times on individual boundary segments were found to be relatively uniform, but the seismic records were punctuated by temporal clusters of gap-filling events and cycle-to-cycle diversity among gap-filling events.

Kagan and Jackson (1991) examined several world-wide earthquake catalogues in order to compare relatively short-term and long-term records for evidence of clustering. They found that

the longer term record clearly displayed clustering, not periodicity, for all earthquakes regardless of focal depth. They concluded that circumstantial evidence strongly suggested that the long-term variation of seismicity is governed by a power-law temporal distribution which is scale-invariant.

As noted by Scholz (1990), who used the slip history of the San Andreas as an example, some earthquake behavior may be characterized as chaotic. Huang and Turcotte (1990) similarly described interactions between segments of major faults as chaotic in nature, and they compare simple slider-block laboratory simulations with patterns of seismicity on the San Andreas and Nankai trough of southeastern Japan. Hodder (1991) took the results of Huang and Turcotte (1990) and examined the behavior of the New Zealand plate boundary system. He found the New Zealand seismic record to be consistent with the chaotic model and concluded that there was evidence for clustered multi-events.

Nishenko and Buland (1987) compiled seismic recurrence data from California, Mexico, Japan, Chile, and Alaska to examine the relation between interevent and long-term recurrence intervals. They found that the ratio of the individual recurrence interval to the long-term average recurrence interval demonstrated non-periodic, non-linear, or chaotic fault interactions.

A Physical Model for Clustered Behavior

The concept of fractals appears to closely describe observed clustered behavior in the seismic record. As noted by Scholz (1990), the commonly used Gutenberg-Richter relation which describes earthquake frequency and moment is a power-law size distribution function which is typical of fractal sets. Such fractal characteristics are derived from the apparent self-similarity of earthquakes and the fracture process and suggest that earthquake clustering can be adequately modelled by fractal behavior.

Smalley *et al.* (1987) used fractal analysis to characterize the seismicity of the New Hebrides, and they found that the clustered seismic activity closely fit a fractal model. Relatively constant fractal dimensions suggested that there were significant deviations from the Poisonnian behavior normally attributed to earthquake recurrence. Kagan and Jackson (1991) also applied fractal theory and concluded that earthquake clustering on both short- and long-term scales was scale-invariant. They found that a fractal power-law distribution best described recurrence behavior, and that time-space clustering of earthquakes was apparently a universal phenomenon.

Fluctuating earthquake behavior has been modelled numerically by Rundle (1988) who concluded that earthquakes are perturbations or fluctuations on the long-term plate motion. He argued that interaction of neighboring fault segments is responsible for clustering of events. Similar arguments were made by Sykes and Jaumé (1990) based on seismic activity in the San Francisco Bay region.

Evidence From the Paleoseismic Record

Although temporal clustering of earthquakes appears to be frequently observed within the historical seismic record and can be adequately modelled using fractal concepts, well-documented examples in the paleoseismic record are comparatively few (Table 1). There are likely several reasons for this paucity of data. First, the concept of clustering only recently became a popular, widely discussed theory of paleoearthquake recurrence, thus many paleoseismic studies did not explicitly search for evidence of such behavior. In some cases, the evidence was not regarded as greatly significant and was only mentioned in passing (e.g., Zoback, 1979).

Second, not all faults exhibit evidence of clustered activity, and the periodic earthquake model still provides a credible explanation for some fault behavior. In a paleoseismic study of extensional faults in southern Tibet, Armijo *et al.* (1986) compared short- (Holocene) and long-term (60 ka) slip rates and found that although some faults had somewhat elevated Holocene rates, the short- and long-term rates were relatively comparable. Similar results were obtained by Peltzer *et al.* (1988) for the strike-slip Chang Ma fault in China. Based on offset terraces on the Wellington fault in New Zealand, Berryman (1990) concluded that the displacement rate of the terraces had been relatively constant over the last 150 ka. Pantosti *et al.* (1993) found that the Irpinia, Italy, fault exhibited characteristic earthquake behavior with 4 similar events preceding the 1980 rupture. Schwartz (1988) also found characteristic earthquake behavior in a paleoseismic study of the Cordillera Blanca fault in the Peruvian Andes.

Third, stratigraphic and age controls necessary for recognizing aperiodic fault slip are commonly not present or available in many paleoseismic studies. Although Wallace (1987) showed that temporal clustering and event migration were common characteristics of many Basin and Range faults, detailed data supporting this concept remain to be fully developed. For example, although Wallace (1987) effectively made the case for irregular earthquake occurrence in the Dixie Valley, Nevada areas on the basis surficial geologic evidence, detailed evidence of slip rate change was not available until detailed paleoseismic studies were conducted (Bell and Katzer, 1987, 1990).

Best World-wide Examples

The following four examples comprise some of the strongest cases for clustering of earthquake events in the paleoseismic record. These studies are all based on detailed determination and comparison of short- and long-term slip rates or recurrence intervals.

The Oued Fodda fault, Algeria

Paleoseismic studies of the Oued Fodda fault which ruptured in 1980 in association with a M7.3 earthquake were first conducted by Swan (1988). Exploratory trenching of the 1980 fault trace

Table 1. World-wide Examples of Temporal Clustering

Region	Fault and Type	Reference
Northern China	Several Unnamed; intraplate	Allen (1975)
Eastern China	Yishu; intraplate; strike-slip	Huang (1993)
Northern Turkey	Anatolian; intraplate; strike-slip	Ambraseys (1970; 1971)
Northern Algeria	Oued Fodda; intraplate; reverse	Swan (1988); Meghraoui *et al.* (1988)
South Island, New Zealand	Pisa-Grandview; intraplate; reverse	Beanland and Berryman (1989)
South Island, New Zealand	Alpine system; plate boundary; strike-slip	Knuepfer (1992)
North Island, New Zealand	Hikurangi system; plate boundary; reverse	Berryman *et al.* (1989)
U.S.		
Great Basin	Lost River, East Range, Dixie Valley; intraplate; normal	Wallace (1987)
Nevada	Dixie Valley; intrapate; normal	Bell and Katzer (1990)
Idaho	Lost River; intraplate; normal	Scott *et al.* (1985)
Utah	Wasatch; intraplate; normal	Machette *et al.* (1990)
California	San Andreas-Pallett Creek; plate boundary; strike-slip	Sieh *et al.* (1989)
California	San Andreas-Yucaipa; plate boundary; strike-slip	Harden and Matti (1989)
California	Sierra Nevada system; intraplate; normal	Bursik and Sieh (1989)
California	San Jacinto; plate boundary; strike-slip	Sharp (1981)
New Mexico	La Jencia; intraplate; normal	Machette (1986)
Oklahoma	Meers; intraplate; strike-slip	Crone and Luza (1990)
Tennessee	Reelfoot Lake; intraplate; strike-slip?	Zoback (1979)
Eastern U.S.	Charleston, New Madrid, Charlevoix, Meers; intraplate	Coppersmith (1988)

revealed evidence for three and possibly four previous events on the fault during the preceding 1.5 ka. Well-constrained dates on the previous events indicated that the average late Holocene recurrence interval on the fault was about 450 years and that the Holocene slip rate was on the order of 3 mm/yr. In contrast, Swan (1988) found that the longer term average late Quaternary recurrence interval determined by offset older alluvium was at least an order of magnitude longer and that the long-term slip rate was on the order of 0.3 mm/yr.

Meghraoui *et al.* (1988) also excavated exploratory trenches across the Oued Fodda and, although obtaining somewhat different slip rate and recurrence interval results than Swan (1988), they provided additional evidence for temporal clustering. They found evidence of six faulting events within the past 7,000 years and estimated the Holocene recurrence interval to be about 1061 years. Although Meghraoui *et al.* (1988) did not examine the longer late Quaternary record, they found that the dated paleoevents grouped together forming irregular patterns of activity (Fig. 3). Clusters of activity were observed at around 4000 years and within the last 1000 years.

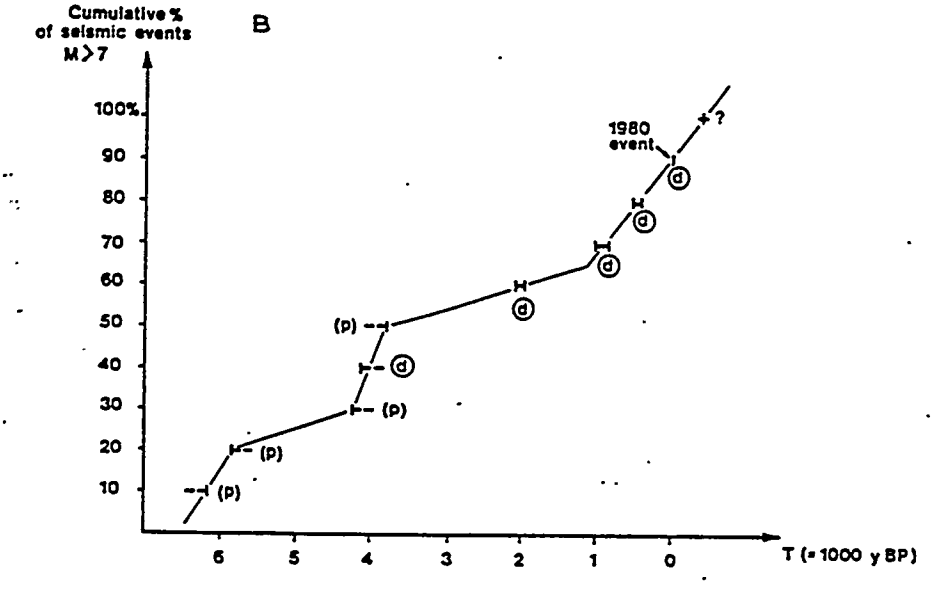

Figure 3. Distribution of events versus time that characterize the paleoseismic activity of the El Asnam fault. Horizontal lines are time boundaries for each event which is additionally characterized as definite (d) and possible (p). Seismic clusters around 4000 and 1000 years BP are alternating with periods of quiescence (Meghraoui *et al.*, 1988).

The Alpine Fault System, New Zealand

Based on estimates of late Quaternary slip in offset stream terraces and moraines crossing the Alpine fault system on the South Island of New Zealand, Knuepfer (1992) found that late Holocene slip rates differed significantly from longer term late Quaternary rates. Examination of the Wairau, Awatare, Clarence, Hope, Kekerengu, and Porters Pass faults showed all to have undergone substantial changes in slip rate during the last 3-5 kyr. On the Awatere fault, Knuepfer (1992) found that offset river terraces provided evidence that an early to mid-Holocene slip rate of 9.4 mm/yr had decreased to 3.8 mm/yr during the late Holocene (Fig. 4). Similarly, dated river terraces across the Hope exhibited evidence of a comparable reduction in the late Quaternary slip rate, declining from a very high rate of 60 mm/yr to about 4 mm/yr (Fig. 4).

Knuepfer (1992) also compared cumulative fault slip rates to the known plate boundary rate of 40 mm/yr and found that the sums of lateral motion during the 5-15 ka period exceeded the plate boundary rate, while the sum of activity for the late Holocene was less than half of the plate boundary rate. He concluded that the best explanation for these variations was that the slip across the plate boundary is episodic, varying over perhaps 5000 year intervals.

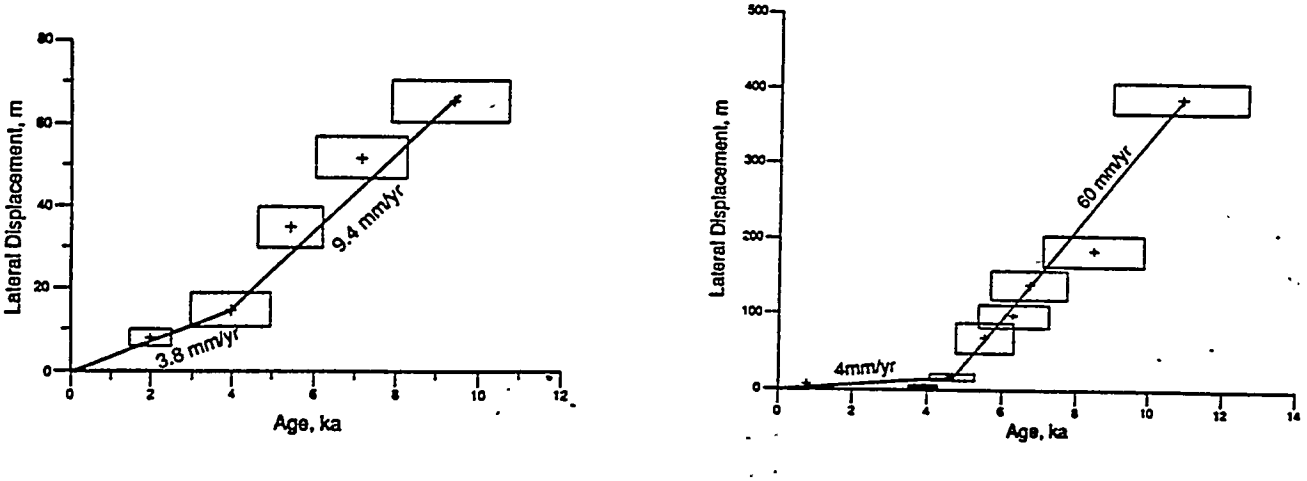

Figure 4. Left: Lateral offset of Saxton River terraces across the Awatere fault. Right: Lateral fault-slip data for the Charwell River terrace sequence, Hope fault. Crosses indicate position of most likely offset and age surface; boxes enclose uncertainties in both offset and age. (Knuepfer, 1992).

The San Andreas Fault

In the detailed paleoseismic study of the San Andreas fault at the Pallett Creek site, Sieh *et al.* (1989) document 10 episodes of faulting during the past 2000 years. Utilizing accelerator mass

spectrometry ages for 32 samples of peat collected from faulted deposits at Pallet Creek, Sieh *et al.* (1989) developed a detailed chronology for recurrent faulting along the San Andreas allowing the detection of clustered paleoseismic events. Although previous studies had revealed 12 events during the past 1800 years, the dates of individual events and the lengths of individual recurrence intervals were not well known, and the new refined dating allowed the discrimination of a more detailed slip history for the fault.

Sieh *et al.* (1989) found that the past 10 earthquakes occurred in four clusters, each consisting of two or three events (Fig. 5). They observed that earthquakes within the clusters were separated by several decades, but the clusters were separated by dormant periods of two to three centuries. Groupings of events occur around 1800 AD, 1400 AD, 1000-1100 AD, and 700-800

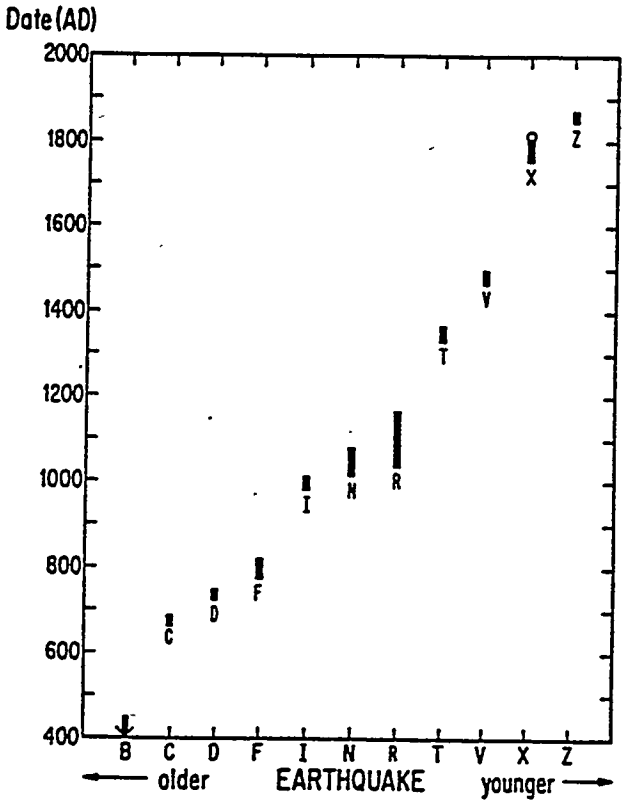

Figure 5. Estimates of the dates for earthquakes recorded in the sediments at Pallett Creek. Bars give 95% confidence intervals. Open circle on bar of event X indicates preferred date of AD 1812 (Sieh *et al.*, 1989).

AD. In comparison to the dated events at Wallace Creek (Sieh and Jahns, 1984), the Pallett Creek event clusters may correspond to large single events at that site.

(Note: Although Sieh *et al.* (1989) contend that the new radiocarbon dates from Pallet Creek are precise enough to allow the discrimination of clustered events-- a conclusion also supported by Jacoby *et al.* (1988), new statistical corrections of radiocarbon calibration ages by Biasi and Weldon (1994) suggest that the Pallett Creek ages may not be as clustered as indicated by Sieh *et al.* (1989)).

The Wasatch fault

Extensive exploratory trenching and related paleoseismic studies along the Wasatch fault system indicate that the system consists of 10 discrete fault segments which have been repeatedly active during the Holocene. Machette *et al.* (1990) summarized all recent studies and provided new interpretations of the faulting originally used by Schwartz and Coppersmith (1984) to define the concept of periodic, characteristic earthquakes. Although Machette *et al.* (1990) found that the long-term composite recurrence interval for the Wasatch is about the same as that estimated by Schwartz and Coppersmith (1984)-- about 400 years-- the frequency of large earthquakes during

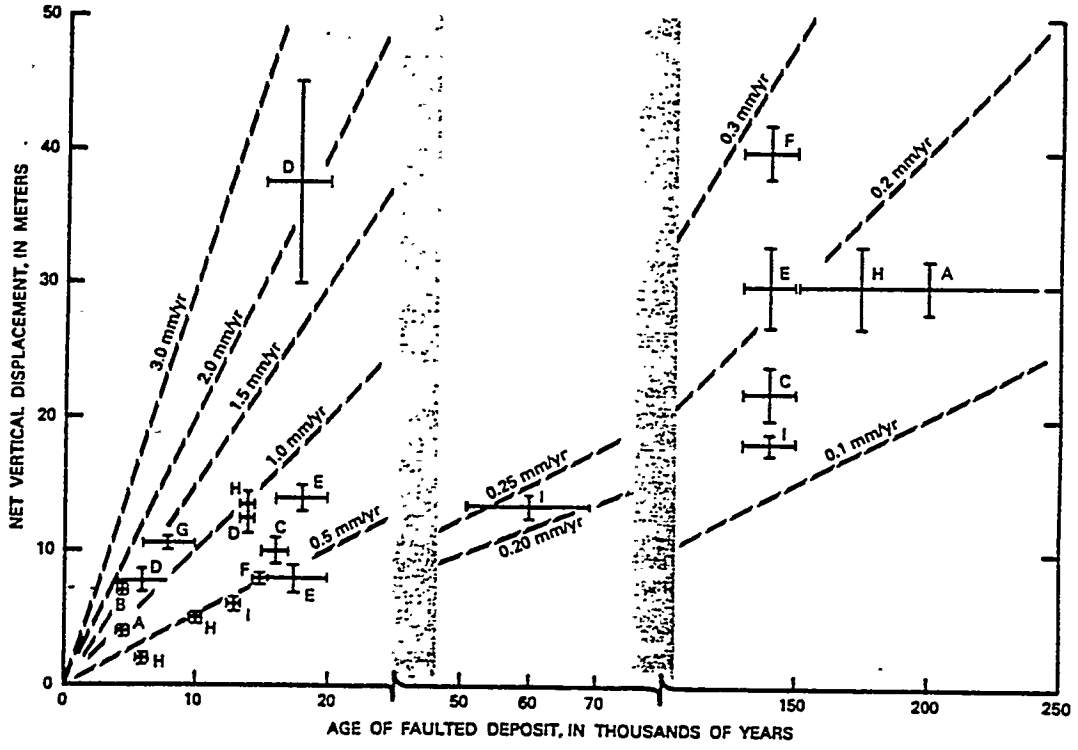

Figure 6. Slip rates on the Wasatch fault zone for different time intervals as determined from deposits of Holocene to middle Quaternary. Letters A through I indicate locations of slip-rate determinations. Vertical and horizontal bars indicate the range in probable amounts of displacement and ages of deposits. Dashed lines indicate different rates of slip (Machette *et al.*, 1990).

the late Holocene appears to be more frequent than suggested by the longer term rate. During the time period of 0.4-1.5 ka, at least six faulting events have occurred, yielding an average late Holocene recurrence interval of about 220 years. This recurrence is about half of the long-term rate. This observation together with the shortness of intervals between recent events and the long average recurrence intervals for individual fault segments (about 1900 years) led Machette *et al.* (1990) to conclude that major faulting events along the Wasatch fault system occurred in clusters interspersed with less-frequent random events between clusters.

Machette *et al.* (1990) also found that there were significant differences in slip rates for fault segments offsetting deposits which both pre-date and post-date the Lake Bonneville Lake cycles (Fig. 6). Comparing the net slip across faults for the last 200 ka, they found that several discrete rates could be discriminated. The slip rates during the past 15 ka were found to be distinctly higher by factors of 2 to 3 than the longer term average rates of 0.1-0.3 mm/yr determined from deposits older than the Lake Bonneville cycle.

New Field Data From the Nevada Basin and Range and Southeastern Spain

New data were collected from recent field studies in Nevada and southeastern Spain to further test the concept of temporal clustering. Previous data obtained from paleoseismic studies in the 1954 Dixie Valley, Nevada, earthquake (Bell and Katzer, 1987, 1990) were reevaluated for evidence of clustered behavior. Paleoseismic investigations recently completed on the Genoa fault (Ramelli *et al.*, 1994) provide new data on clustered activity of the Sierra Nevada fault system. A paleoseismic investigation of the Carboneras fault system in southeastern Spain provides new data for a tectonically active part of the western Mediterranean region where little paleoseismic data are available.

The 1954 Dixie Valley, Nevada, Earthquake Area

Exploratory trenching and drilling studies in the 1954 Dixie Valley earthquake (M6.9) showed that coseismic faulting occurred along two fault zones lying along the eastern flank of the Stillwater Range (Bell and Katzer, 1987). Cumulative displacements on these two zones were used to estimate both short- and long-term slip rates (Bell and Katzer, 1990). These cumulative displacements have been plotted here to examine the evidence for temporal clustering (Fig. 7).

Fault displacement associated with the 1954 earthquake was about 3 m, and a similar amount of displacement occurred during an event 1.5-6.8 ka ago. Beach gravels estimated to be 12 ka old exhibit the same offset as the younger alluvial fan deposits; intermediate-age alluvial fan deposits estimated to be of late Pleistocene (late Wisconsin) age are cumulatively offset about 8.5 m, and older alluvial fan deposits have more than 40 m of cumulative offset.

Figure 7 demonstrates that the most recent activity on the Stillwater fault zone has been clustered in comparison to the longer term level of activity. The 1954 earthquake and the event which

occurred between 1.5-6.8 ka ago together yield a relatively high recent slip rate (>1 mm/yr), in contrast to the cumulative offsets of both intermediate and older age alluvial deposits. Even by assuming conservatively young minimum ages for these alluvial-fan deposits (the maximum ages were preferred in previous studies), the late Holocene slip rate is significantly higher than the longer term rate, a strong indication that the most recent activity has been clustered.

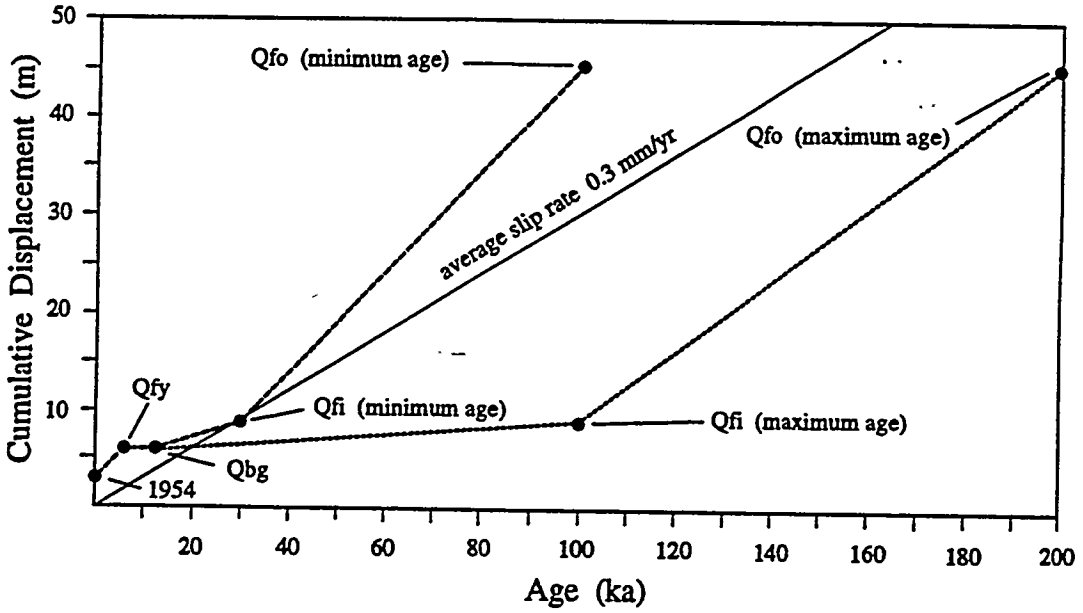

Figure 7. Plot of cumulative displacement on Dixie Valley faults and age of offset alluvial deposits. Dots represent approximate age and displacement: 1954, offset associated with the 1954 Dixie Valley earthquake; Qfy, young alluvial-fan deposits 1.5-6.8 ka in age; Qbg, 12-13 ka shoreline gravel deposits; Qfi, intermediate-age alluvial-fan deposits 30-100 ka in age; Qfo, older alluvial-fan deposits, 100-200 ka in age. Average slip rate of 0.3 mm/yr from Wallace and Whitney (1984).

The Genoa Fault

The Genoa fault is a principal trace of the Sierra Nevada fault segment extending from Markleeville, California, to Reno. Exploratory trenching across the Genoa fault at three locations revealed evidence for two large displacement (4-5 m each) events during the late Holocene (Ramelli *et al.*, 1994). Extensive radiocarbon dating of faulted deposits indicated that both events occurred within the last 3 ka, and the most recent event occurred about 500-600 years ago. At one trenching site (Walleys Hot Springs), Holocene stream terrace deposits which are offset about 9 m lie adjacent to older Quaternary alluvium cut by a large (18 m) scarp. Although the age of this older deposit is not precisely known, the presence of a thick (> 1m) argillic soil on the fan surface is indicative of at least an age of 100 ka. The Genoa fault can be traced discontinuously to Woodfords, California, where Tioga-age (12-35 ka) glacial stream deposits

are offset about 16 m.

Plotting cumulative slip along the Genoa fault based on trenching and exposures at the Woodfords site and Walleys Hot Springs site (Fig. 8), a higher rate of fault slip has occurred during the Holocene compared to the longer term rate represented by the older (> 100 ka) offset alluvial deposits at Walleys Hot Springs. If the two most recent events recorded on the Genoa fault were indeed indicative of the long-term event rate (> 1 mm/yr), the older scarp would exhibit a displacement on the order of 100 m, nearly an order of magnitude more than that observed.

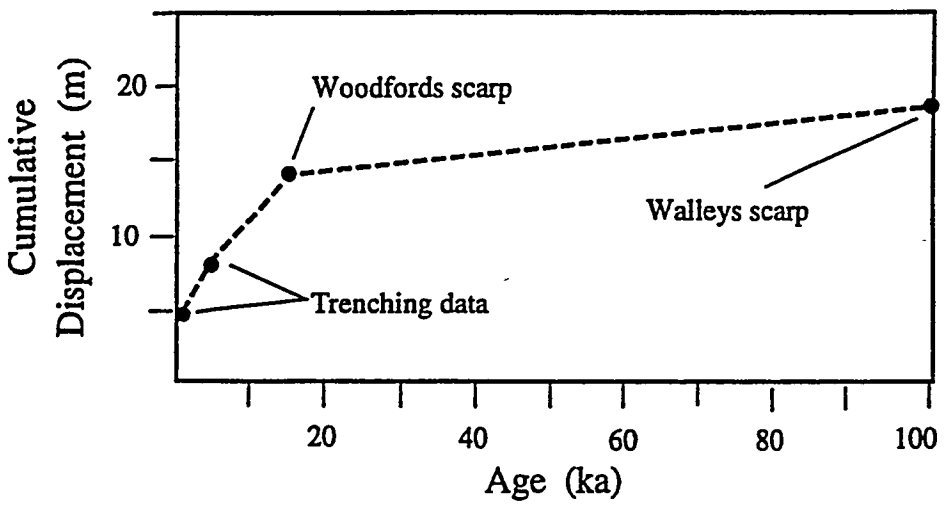

Figure 8. Plot of cumulative displacement across the Genoa fault and age of offset deposits. Dots represent approximate amount of displacement and age. Composite exploratory trenching data taken from three locations yielding radiocarbon ages; Woodfords and Walleys Hot Spring scarp data based on measured profiles and estimated ages based on glacial chronology and soil development (data from Ramelli *et al.*, 1994).

The Carboneras fault

The Carboneras fault is one of several large Quaternary strike-slip faults which comprise the Trans-Alboran fault system. This system trends across the western Mediterranean region coming on-shore in southeastern Spain and northern Africa, and it is part of the wide Europe-Africa plate boundary zone, a portion of which ruptured at the Oued Fodda site of the 1980 El Asnam, Algeria, earthquake described earlier. A paleoseismic investigation was conducted along the Carboneras fault in order to identify patterns and rates of late Quaternary faulting (Bell et al. 1994). Results indicated that a high rate of fault slip occurred during the mid-Quaternary, and

that this rate has substantially diminished during the late Quaternary.

This study found that 100-m left-lateral offsets of alluvial-fan streams occurred between 200-500 ka. The absence of offset late Quaternary alluvial-fan deposits indicates that little lateral displacement has occurred on the Carboneras fault during the past 35-100. Where the fault intersects the coastline, 100 ka marine shorelines are vertically displaced a maximum of 10 m, and there is circumstantial evidence of 1-3 m of vertical uplift along the fault at the coastline during the last few thousand years. These data suggest that the style of faulting has changed from strike slip to normal during the late Quaternary and that the rate of slip has declined substantially during the past 100-200 ka (Fig. 9). The 100-m stream offsets are confined to deposits older than 100-200 ka, and no discernible lateral displacements have occurred during the last 35 ka and probably during the last 100 ka. Marine terraces radiometrically dated at between about 85-125 ka exhibit no visible lateral offset component. At the same coastal locations, late Holocene (3 ka) stream channels flowing to the Mediterranean Sea are uplifted 1-3 m. These relations together strongly suggest that slip rates during the mid-Quaternary were comparatively high relative to those during latest Quaternary, and that the style of faulting has changed. A period of accelerated slip apparently characterized fault activity up until about 200 ka, after which time slip diminished by an at least an order of magnitude, suggesting that the fault is presently in a state of relative quiescence.

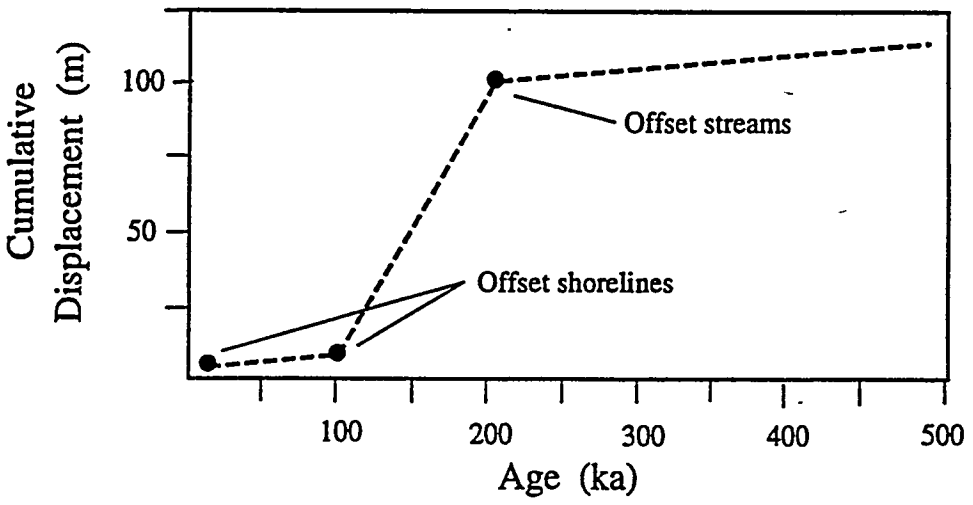

Figure 9. Plot of cumulative displacement and age of offset units along the Carboneras fault. Dots indicate approximate amount of displacement and age. Offset shorelines measured at locations where fault intersects marine terrace sequence; offset streams measured on alluvial fans crossing the fault.

Summary

The world-wide evidence for temporal clustering of earthquakes suggests that fault behavior in both plate boundary and intraplate settings is characterized commonly, but not universally, by periods of activity separated by periods of dormancy. The historical seismicity record provides substantial documentation of clustered activity, particularly in regions where the record dates back several millenia. Seismicity associated with principal plate boundary faults, such as those in the circum-Pacific region, has frequently been found to be punctuated by clusters of gap-filling events and cycle-to-cycle diversity. Comparisons of short- and long-term seismic records suggest that the long-term record is characterized by scale-invariant power-law temporal distributions, or clusters. The fractal concept has been found to closely describe this clustered behavior, and numerical laboratory models have been described which account for such aperiodic or irregular activity.

Although the historical seismic record has provided numerous examples of clustered activity, and the concept of fractals appears to adequately model such behavior, comparatively few examples of temporal clustering have been described in the paleoseismic literature. This is in part due to the fact that the periodic earthquake model still provides a credible explanation for some fault slip histories. But this is also due to the fact that paleoseismic investigations have only recently begun to collect and examine relevant data capable of discriminating clustering in the geologic record. In addition, detailed stratigraphic and age controls necessary for discriminating clustered events are not always present or available.

A list of about 20 examples from published literature provides the present basis for recognizing clustered activity in the paleoseismic record. The best examples from this list include the Oued Fodda fault in Algeria, the Alpine fault in New Zealand, the San Andreas fault, and the Wasatch fault. Of particular interest to characterizing fault behavior in the Basin and Range Province are the results of paleoseismic studies along the Wasatch fault. There, the extensive trenching and surficial geologic evidence appears to unequivocally point to clustered behavior during the Holocene.

In support of the concept of temporal clustering, new data are provided from investigations conducted during the last year. Previous slip data from the 1954 Dixie Valley, Nevada, earthquake area, Nevada, have been plotted to demonstrate the presence of clustered activity along the Stillwater fault during the Holocene. Similarly, recent trenching investigations along the Genoa fault in western Nevada indicate that this principal fault of the Sierra Nevada fault system exhibits strong evidence of clustered activity during the Holocene compared to the longer term Quaternary rate. Based on new paleoseismic studies along the strike-slip Carboneras fault of southeastern Spain, a tectonically active part of the western Mediterranean region, it is found that a high rate of fault slip occurred during the mid-Quaternary, but that this rate, and thus the frequency of events, has diminished substantially during the late Quaternary. This suggests that the fault is in a period of dormancy.

Selected Bibliography

Allen, C.R., 1975, Geological criteria for evaluating seismicity: Geological Society of America Bulletin, v. 86, p. 1041-1057.

Ambraseys, N.N., 1970, Some characteristic features of the Anatolian fault zone: Tectonophysics, v. 9, p. 143-165.

Ambraseys, N.N., 1971, Value of historical records of earthquakes: Nature, v. 232, p. 375-379.

Ambraseys, N.N., and Finkel, C.F., 1987, Seismicity of Turkey and neighbouring regions 1899-1915: Annales Geophys., v. 5B, p. 701-726.

Ambraseys, N.N., and Finkel, C.F., 1991, Long-term seismicity of Istanbul and the Marmara Sea region: Terra Nova, v. 3, p. 527-539.

Armijo, R., Tapponnier, P. Mercier, J.L., and Han, T.L., 1986, Quaternary extension in southern Tibet: field observations and tectonic implications: Journal of Geophysical Research, v. 91, p. 13,803-13,872.

Armijo, R., and Tapponnier, P., 1989, Late Cenozoic right-lateral strike-slip faulting in southern Tibet: Journal of Geophysical Research, v. 94, no. B3, p. 2787-2838.

Armijo, R., Lyon-Caen, H., and Papanastassiou, D., 1991, A possible normal-fault rupture for the 464 B.C. Sparta earthquake: Nature, v. 351, p. 137-139.

Armijo, R., Lyon-Caen, H., and Papanastassiou, D., 1992, East-west extension and Holocene normal-fault scarps in the Hellenic arc: Geology, v. 20, p. 491-494.

Beanland, S., and Berryman, K., 1989, Style and episodicity of late Quaternary activity on the Pisa-Grandview fault zone, central Toago, New Zealand: New Zealand Journal of Geology and Geophysics, v. 32, p. 451-461.

Bell, J.W. and Katzer, T., 1987, Surficial geology, hydrology, and late Quaternary tectonics of the IXL Canyon area, Nevada: Nevada Bureau of Mines and Geology Bulletin 102, 52 p.

Bell, J.W., and Katzer. T., 1990, Timing of late Quaternary faulting in the 1954 Dixie Valley earthquake area, central Nevada: Geology, v. 18, p. 622-625.

Bell, J.W., Amelung, F., and King, G.C.P., 1994, Results of preliminary paleoseismic studies in the Vera Basin region, southeastern Spain: Final Technical Report submitted to the European Community Desertification Project, 20 p.

Bellier, O., Dumont, J.F., Sébrier, M., and Mercier, J.L., 1991, Geological constraints on the kinematics and fault-plane solution of the Quiches fault zone reactivated during the 10 November 1946 Ancash earthquake, northern Peru: Seismological Society of America Bulletin, v. 81, no. 2, p. 468-490.

Bender, B., and Perkins, D.M., 1987, SEISRISK III: A computer program for seismic hazard estimation: U.S. Geological Survey Bulletin 1772.

Berryman, K.R., Ota, Y., and Hull, A.G., 1989, Holocene paleoseismicity in the fold and thrust belt of the Hikurangi subduction zone, eastern North Island, New Zealand: Tectonophysics, v. 163, p. 185-195.

Berryman, K., 1990, Late Quaternary movement on the Wellington fault in the Upper Hut area, New Zealand: New Zealand Journal of Geology and Geophysics, v. 33, p. 257-270.

Biasi, G.P., and Weldon, R., III, 1994, Quantitative refinement of calibrated ^{14}C distributions: Quaternary Research, v. 41, p. 1-18.

Bursik, M., and Sieh, K., 1989, Range front faulting and volcanism in the Mono Basin, eastern California: Journal of Geophysical Research, v. 94, no. B11, p. 15,587-15,609.

Cisternas, A., Dorel, J., and Gaulon, R., 1982, Models of the complex source of the Al Asnam earthquake: Seismological Society of America Bulletin, v. 72, p. 2245-2266.

Cluer, J.K., 1988, Quaternary geology of Willow Creek and some age constraints on prehistoric faulting, Lost River Range, east-central Idaho: Seismological Society of America Bulletin, v. 78, no. 2, p. 946-955.

Cowan, H.A., 1990, Late Quaternary displacements on the Hope fault at Glynn Wye, North Canterbury: New Zealand Journal of Geology and Geophysics, v. 33, p. 285-293.

Crone, A.J., and Luza, K.V., 1990, Style and timing of Holocene surface faulting on the Meers fault, southwestern Oklahoma: Geological Society of America Bulletin, v. 102, p. 1-17.

Crone, A.J., and Haller, K.M., 1991, Segmentation and the coseismic behaviour of Basin-and-Range normal faults: examples from east-central Idaho and southwestern Montana, U.S.A.: Journal of Structural Geology, v. 13, p. 151-164.

Dufaure, J.J., 1977, Néotectonique et morphogenèse dans une péninsule méditerranéenne: La Péloponnèse: Revue de Géographie Physique et de Géologie Dynamique, v. 19, p. 27-58.

Ebinger, C.J., 1989, Geometric and kinematic development of border faults and accommodation zones, Kivu-Rusizi rift, Africa: Tectonics, v. 8, p. 117-133.

Electric Power Research Institute, 1993, Earthquakes and tectonics expert judgment elicitation project: Electric Power Research Institute Report EPRI TR-102000.

Forman, S.L., Nelson, A.R., and McCalpin, 1991, Thermoluminescence dating of fault-scarp-derived colluvium: deciphering the timing of paleoearthquakes on the Weber segment of the Wasatch fault zone, north central Utah: Journal of Geophysical Research, v. 96, no. B1, p. 595-605.

Gardosh, M., Reches, Z., and Garfunkel, Z., 1990, Holocene tectonic deformation along the western margins of the Dead Sea: Tectonophysics, v. 180, p. 123-137.

Harden, J.W., and Matti, J.C., 1989, Holocene and late Pleistocene slip rates on the San Andreas fault in Yucaipa, California, using displaced alluvial-fan deposits and soil chronology: Geological Society of America Bulletin, v. 101, p. 1107-1117.

Hodder, A.P.W., 1991, Chaotic fault interactions: implications for seismic hazard in New Zealand: Terra Nova, v. 3, p. 628-630.

Huang, W., 1993, Morphologic patterns of stream channels on the active Yishi fault, southern Shandong Province, eastern China: implications for repeated great earthquakes in the Holocene: Tectonophysics, v. 219, p. 283-304.

Huang, J., and Turcotte, D.L., 1990, Evidence for chaotic fault interactions in the seismicity of the San Andreas fault and Nankai trough: Nature, v. 348, p. 234-236.

Jackson, J.A., King, G., and Vita-Finzi, C., 1982, The neotectonics of the Aegean: an alternative view: Earth and Planetary Science Letters, v. 61, p. 303-318.

Jackson, J.A., and McKenzie, D., 1983, The geometrical evolution of normal fault systems: Journal of Structural Geology, v. 5, p. 471-482.

Jackson, J.A., and White, N.J., 1989, Normal faulting in the upper continental crust: observations from regions of active extension: Journal of Structural Geology, v. 11, p. 15-36.

Jacoby, G.C., Jr., Sheppard, P.R., and Sieh, K.E., 1988, Irregular recurrence of large earthquakes along the San Andreas fault: evidence from trees: Science, v. 241, p. 196-199.

Kagan,Y.Y., and Jackson, D.D., 1991, Long-term earthquake clustering: Geophysical Journal International, v. 104, p. 117-133.

King, G.C.P., and Vita-Finzi, C., 1980, Active folding in the Algerian earthquake of 10 October 1980: Nature, v. 292, p. 22-26.

King, G.C.P., and Yielding, G., 1984, The evolution of a thrust fault system: processes of rupture initiation, propagation, and termination in the 1980 El Asnam (Algeria) earthquake: Geophysical Journal of the Royal Astronomical Society, v. 77, p. 915-933.

Kneupfer, P.L.K., 1987, Changes in Holocene slip rates in strike-slip environments: U.S. Geological Survey Open-file Report 87-673, p. 249-261.

Kneupfer, P.L.K., 1992, Temporal variations in latest Quaternary slip across the Australian-Pacific plate boundary, northeastern south Island, New Zealand: Tectonics, v. 11, no. 3, p. 449-464.

Lee, W., and Brillinger, D., 1979, On Chinese earthquake history-- an attempt to model an incomplete data set by point process analysis: Pure and Applied Geophysics, v. 117, p. 1229-1257.

Leeder, M.R., Seger, M.J., and Stark, C.P., 1991, Sedimentology and tectonic geomorphology adjacent to active and inactive normal faults in the Megara Basin and Alkyonides Gulf, Central Greece: Journal of the Geological Society of London, v. 148, p. 331-343.

Liew, P.M., Pirazzoli, P.A., Hsieh, M.L., Arnold, M., Barusseau, J.P., Fontugne, M., and Giresse, P., 1993, Holocene tectonic uplift deduced from elevated shorelines, eastern Coastal Range of Taiwan: Tectonophysics, v. 222, p. 55-68.

Lyon-Caen, H., and 11 others, 1988, The 1986 Kalamata (South Peloponnesus) earthquake: Detailed study of a normal fault, evidences for east-west extension in the Hellenic arc: Journal of Geophysical Research, v. 93, p. 14,967-15,000.

McCalpin, J., and Forman, S.L., 1991, Late Quaternary faulting and thermoluminescence dating of the east Cache fault zone, north-central Utah: Seismological Society of America Bulletin, v. 81, no. 1, p. 139-161.

McGuire, R.K., 1979, Adequacy of simple probability models for calculating felt-shaking hazard, using the Chinese earthquake catalog: Seismological Society of America Bulletin, v. 69, p. 877-892.

Machette, M.N., 1984, Preliminary investigations of the late Quaternary slip rates along the southern part of the Wasatch fault zone, central Utah, in Hays, W.W., and Gori, P.L., eds., Proceedings of Conference XXVI, A Workshop on "Evaluation of Regional and Urban Earthquake Hazards and Risks in Utah": U.S. Geological Survey Open-file Report 84-763, p. 391-406.

Machette, M.N., 1986, History of Quaternary offset and paleoseismicity along the La Jencia fault, central Rio Grande rift, New Mexico: Seismological Society of America Bulletin,

v. 76, no. 1, p. 259-272.

Machette, M.N., 1987, Changes in long-term versus short-term slip rates in an extensional environment, *in*, Crone, A.J., and Ohmdahl, E.M., eds., Proceedings of Conference 39--Directions in Paleoseismology: U.S. Geological Survey Open-file Report 87-673, p. 228-238.

Machette, M.N., Personius, S.F., and Nelson, A.R., 1990, Quaternary geology along the Wasatch fault zone-- segmentation, recent investigations, and preliminary conclusions: U.S. Geological Survey Professional Paper 1500.

Mariolakos, I., and Stiros, S.C., 1987, Quaternary deformation of the Isthmus of Corinthos (Greece): Geology, v. 15, p. 225-228.

Meghraoui, M. Cisternas, A., and Philip, H., 1986, Seismotectonics of the lower Cheliff basin: structural background of the El Asnam (Algeria) earthquake: Tectonics, v. 5, p. 809-836.

Meghraoui, M., Philip, H., Albarede, F., and Cisternas, A., 1988, Trench investigations through the trace of the 1980 El Asnam thrust fault: evidence for paleoseismicity: Seismological Society of America Bulletin, v. 78, p. 979-999.

Meghraoui, M., Jaegy, R., Lammali, K., and Albarede, F., 1988, Late Holocene earthquake sequences on the El Asnam (Algeria) fault: Earth and Planetary Science Letters, v. 90, p. 187-203.

Nishenko, S.P., and Buland, R., 1987, A generic recurrence interval distribution for earthquake forecasting: Bulletin of the Seismological Society of America, v. 77, p. 1382-1399.

Pantosti, D., Schwartz, D.P., and Valensise, G., 1993, Paleoseismicity along the 1980 surface rupture of the Irpinia fault: implications for earthquake recurrence in the southern Apennines, Italy: Journal of Geophysical Research, v. 98, no. B4, p. 6561-6577.

Papadopoulos, G., and Dedousis, V., 1992, Fractal approach of the temporal earthquake distribution in the Hellenic arc-trench system: PAGEOPH, V. 139, no. 2, p. 269-276.

Pearthree, P.A., and Calvo, S.S., 1987, The Santa Rite fault zone: evidence for large magnitude earthquakes with very long recurrence intervals, Basin and Range province of southeastern Arizona: Seismological Society of America Bulletin, v. 77, no.1, p. 97-116.

Peltzer, G., Tapponnier, P. Gaudemer, and Mayer, B., Shunmin, G., Kelun, Y., Zhitai, C., and Huagung, D., 1988, Offsets of late Quaternary morphology, rate of slip, and recurrence of large earthquakes on the Chang Ma fault (Gansu, China): Journal of Geophysical Research, v. 93, no. B3, p. 7793-7812.

Perkins, D.M., 1987, Contagious fault rupture, probabilistic hazard, and contagion observability, *in* Crone, A.J., and Omdahl, E.M., eds., Proceedings, of Conference XXXIX-- directions in paleoseismology: U.S. Geological Survey Open-file Report 887-673, p. 428-439.

Philip, H., Rogozhin, E., Cisternas, A., Bousquet, J.C., Borisov, B., and Karakhanian, A., 1992, The Armenian earthquake of 1988 December 7: faulting and folding, neotectonics and palaeoseismicity: Geophysical Journal International, v. 110, p. 141-158.

Ramelli, A.R., dePolo, C.M., and Bell, J.W., 1994, Synthesis of data and exploratory trenching along the Northern Sierra Nevada fault Zone: Final Technical Report submitted to the U.S. Geological Survey National Earthquake Hazard Reduction Program, 65 p.

Rice, J.R., 1993, Spatio-temporal complexity of slip on a fault: Journal of Geophysical Research, v. 98, no. B6, p. 9885-9907.

Roberts, S., and Jackson, J.A., 1991, Active normal faulting in central Greece: an overview, in, Roberts, A.M., Yielding, G., and Freeman, B., eds., The Geometry of Normal Faults: Geological Society Special Publication 56, p. 125-142.

Rundle, J., 1988, A physical model for earthquakes, 2, Application to southern California: Journal of Geophysical Research, v. 93, p.6255-6274.

Scholz, C.H., 1990, Earthquakes as chaos: Nature, v. 348, p. 197-198.

Scholz, C.H., 1990, The mechanics of earthquakes and faulting: Cambridge University Press, New York, 439 p.

Scott, W.E., Pierce, K.L., and Hait, M.H., 1985, Quaternary tectonic setting of the 1983 Borah Peak earthquake, central Idaho: Seismological Society of America Bulletin, v. 75, p. 1053-1066.

Sharp, R.V., 1981, Variable rates of late Quaternary strike slip on the San Jacinto fault zone, southern California: Journal of Geophysical Research, v. 86, no. B3, p. 1754-1762.

Sieh, K.E., 1981, A review of geological evidence for recurrence times of large earthquakes: American Geophysical Union Maurice Ewing Series, No. 4, p. 181-207.

Sieh, K.E., and Jahns, Holocene activity of the San Andreas fault at Wallace Creek, California: Geological Society of America Bulletin, v. 95, p. 883-896.

Sieh, K.E., Stuiver, M., and Brillinger, D., 1989, A more precise chronology of earthquakes produced by the San Andreas fault in southern California: Journal of Geophysical Research, v. 94, no. B1, p. 603-623.

Smalley, R.F., Jr., Chatelain, J-L., Turcotte, D.L., and Prévot, R., 1987, A fractal approach to the clustering of earthquakes: applications to the seismicity of the New Hebrides: Seismological Society of America Bulletin, v. 77, no. 4, p. 1368-1381.

Stein, R.S., Briole, P., Ruegg, J-C., and Tapponnier, P., 1991, Contemporary, Holocene, and Quaternary deformation of the Asal Rift, Djibouti: Implications for the mechanics of slow spreading ridges: Journal of Geophysical Research, v. 96, p. 21,789-21,806.

Stewart, I.S., and Hancock, P.L., 1991, Scales of structural heterogeneity within neotectonic normal fault zones in the Aegean region: Journal of Structural Geology, v. 13, p. 191-204.

Swan, F.H., 1988, Temporal clustering of paleoseismic events on the Oued Fodda fault, Algeria: Geology, v. 16, p. 1092-1095

Swan, F.H., 1989, Reply to Comment on "Temporal clustering of paleoseismic events on the Oued Fodda fault, Algeria": Geology, v. 17, p. 865-866.

Schwartz, D.P., 1988, Paleoseismicity and neotectonics of the Cordillera Blanca fault zone, northern Peruvian Andes: Journal of Geophysical Research, v. 93, no. B5, p. 4712-4730.

Thatcher, W., 1986, Cyclic deformation related to great earthquakes at plate boundaries: Bulletin Royal Society New Zealand, v. 24, p.245-272.

Thatcher, W., 1989, Earthquake recurrence and risk assessment in circum-Pacific seismic gaps: Nature, v. 341, p. 432-434.

Thatcher, W., 1990, Order and diversity in the modes of Circum-Pacific earthquake recurrence, Journal of Geophysical Research, v. 95B, p. 2609-2623.

Thommeret, Y., King, G.C.P., and Vita-Finzi, C., 1983, Chronology and development of the 1980 earthquake at El Asnam (Algeria): a postscript: Earth and Planetary Science Letters, v. 63, p. 137-138.

U.S. Department of Energy, 1994, Methodology to asses fault displacement and vibratory ground motion hazards at Yucca Mountain: U.S. Department of Energy, Office of Civilian Radioactive Waste Management Topical Report YMP/TR-002-NP, 20 p. with appendices.

Valensise, G., and Pantosti, D., 1992, A 125 Kyr-long geological record od seismic source repeatability: the Messina Straits (southern Italy) and the 1908 earthquake (Ms 7 1/2): Terra Nova, v. 4, p. 472-483.

Van Dissen, R., and Yeats, R.S., 1991, Hope fault, Jordan thrust, and uplift of the Seaward

Kaikoura Range, New Zealand: Geology, v. 19, p. 393-396.

Vita-Finzi, C., 1989, Comment on "Temporal clustering of paleoseismic events on the Oued Fodda fault, Algeria": Geology, v. 17, p. 865.

Vita-Finzi, C., 1992, Radiocarbon dating of late Quaternary fault segments and systems: Journal of the Geological Society, London: v. 149, p. 257-260.

Wallace, R.E., and Whitney, R.A., 1984, Late Quaternary history of the Stillwater seismic gap, Nevada: Seismological Society of America Bulletin, v. 74, p. 301-314.

Wallace, R.E., 1987, Grouping and migration of surface faulting and variations in slip rates on faults in the Great Basin: Seismological Society of America Bulletin, v. 77, p. 868-876.

Weldon, R.J., II, and Sieh, K.E., 1985, Holocene rate of slip and tentative recurrence interval for large earthquakes on the San Andreas fault, Cajon Pass, southern California: Geological Society of America Bulletin, v. 96, p. 793-812.

Wesnousky, S., 1988, Seismological and structural evolution of strike-slip faults: Nature, v. 335, p. 340-343.

Wesnousky, S., 1990, Seismicity as a function of geologic offset: some observations from southern California: Seismological Society of America Bulletin, v. 80, p. 1374-1381.

Winter, T., Avouac, J-P., and Lavenu, A., 1993, Late Quaternary kinematics of the Pallatanga strike-slip fault (central Ecuador) from topographic measurements of displaced morphological features: Geophysical Journal International, v. 115, p. 905-920.

Wyss, M., 1990, Seismic cycle not so simple: Nature, v. 345, p.290.

Yeats, R.S., and Berryman, K.R., 1987, South Island, New Zealand, and Transverse Ranges, California: a seismotectonic comparison: Tectonics, v. 6, p. 363-376.

Yielding, G., Jackson, J.A., King, G.C.P., Sinvhal, H., Vita-Finzi, C., and Wood, R.M., 1981, Relations between surface deformation, fault geometry, seismicity, and rupture characteristics during the El Asnam (Algeria) earthquake of 10 October 1980: Earth and Planetary Science Letters, v. 56, p. 287-304.

TASK 3: EVALUATION OF MINERAL RESOURCE POTENTIAL, CALDERA GEOLOGY, AND VOLCANO-TECTONIC FRAMEWORK AT AND NEAR YUCCA MOUNTAIN

REPORT FOR OCTOBER, 1993 - SEPTEMBER, 1994

Steven I. Weiss,[1] Donald C. Noble,[2] and Lawrence T. Larson[2]

Department of Geological Sciences, Mackay School of Mines, University of Nevada, Reno

[1] Research Associate
[2] Co-principal Investigators and Professors of Geology and Economic Geology

INTRODUCTION

This report summarizes the work of Task 3 that was initially discussed in our monthly reports for the period October 1, 1993 through September 30, 1994, and is contained in our various papers and abstracts, both published and in press or currently in review (see appendices). Our efforts during this period have involved the continuation of studies begun prior to October, 1993, focussed mainly on aspects of the caldera geology, magmatic activity, hydrothermal mineralization and extensional tectonics of the western and central parts of the southwestern Nevada volcanic field (SWNVF), studies of the subsurface rocks of Yucca Mountain utilizing drill-hole samples obtained in 1991 and 1992, and studies of veins and siliceous ledges cropping out in northwestern Yucca Mountain. These veins and ledges provide evidence for near-surface hydrothermal activity in northwestern Yucca Mountain during the Crater Flat Tuff period of volcanism.

During the period of this report we have concentrated our efforts on the production and publication of documents summarizing many of the data, interpretations and conclusions of Task 3 studies pertaining to hydrothermal activity and mineralization in the Yucca Mountain region and their relations to volcanism and tectonic activity. The resulting two manuscripts for journal publication and a compilation of radiometric age and trace-element geochemical data are appended to this report (see below).

The first manuscript, intended for publication in the journal *Economic Geology*, is entitled *Multiple episodes of hydrothermal activity and epithermal mineralization in the southwestern Nevada volcanic field and their relations to magmatic activity, volcanism and regional extension* and is included in this report as Appendix A (Weiss et al., 1995b). This lengthy paper provides both important general information, and a large amount of specific and detailed decriptive information, radiometric age data and our interpretations concerning the nature and timing of hydrothermal activity and associated mineralization in the Yucca Mountain region. Although an initial draft of this paper was completed in September, 1993, much time during the period of this report has been devoted to the construction of map figures and revisions of the text. In late March of 1994 the manuscript entered formal U.S. Geological Survey review. Such review is required prior to submission to a journal, due to the co-authorship on this paper of our colleague Edwin H. McKee of the Branch of Western Minerals Resources. Following constructive reviews by Brent Turrin and Roger Ashley of the U. S. Geological Survey, the manuscript was returned to us in September, 1994. The manuscript is more lengthy than is normally accepted by many journals, mainly as a result of our inclusion of data and discussion for all of the many known areas of hydrothermal activity and mineralization in the central, southern and western parts of the southwestern Nevada volcanic field. Presently we are attempting to shorten the manuscript.

STUDIES OF DRILL CORE AND CUTTINGS FROM THE SUBSURFACE OF YUCCA MOUNTAIN

Update on the Distribution, Origin and Significance of Pyrite in Tuffs of Yucca Mountain

An entirely new manuscript entitled *Pyritic ash-flow tuff, Yucca Mountain, Nevada--A discussion* has recently been prepared for submission to *Economic Geology* and is included in this report as Appendix B (Weiss et al., 1995a). The main objective of this paper is to dispute the interpretation of Castor et al. (1994) that pyrite in ash-flow tuff units in Yucca Mountain is mainly xenolithic material incorporated from previously altered wallrocks during the eruptions of the tuffs. Based on our studies of core and cuttings from the 12 drill holes that penetrate into and/or through the Crater Flat Tuff in Yucca Mountain, and detailed studies by personnel of the Los Alamos National Laboratory and the U. S. Geological Survey, we summarize our new information on the subsurface lateral and vertical distribution and textural characteristics of the pyrite, and consider phase stability relations and the conditions of major ash-flow eruptions that are inconsistent with the "lithic" origin of Castor et al. (1994). Our paper presents several lines of evidence that strongly support the *in-situ* formation of most, if not all, of the pyrite from hydrothermal fluids containing small, but geochemically significant, amounts of reduced sulfur. We explicitly point out that such fluids are clearly and unequivocally capable of transporting and depositing precious metals, that trace-elements associated with epithermal types of hydrothermal activity (e.g., As, Sb, Hg, Bi) are elevated with respect to fresh, unaltered rhyolitic ash-flow tuff at Yucca Mountain, and that the 12 existing deep drill holes are too widely spaced to rule out the presence of potentially attractive mineral resources beneath the proposed repository. Furthermore, as a progressively better understanding of the conditions of transport and deposition of gold, both in magmatic and hydrothermal systems (e.g., Connors et al., 1993) is obtained, it is clear that one critical factor in the formation of gold deposits is the existence of a gold-rich hydrothermal solution. An important corollary of this recognition is that the *absence* of gold in many areas of hydrothermal alteration does not demonstrate that a major deposit may not be present.

DATA COMPILATION

Appendix C consists of a data chart entitled *Compilation of radiometric age and trace-element geochemical data, Yucca Mountain and surrounding areas of southwestern Nevada* for use by the Nevada Nuclear Waste Project Office, their contractors and other interested groups. Part I of this document provides a compilation of presently available radiometric ages of pre-Quaternary volcanic rocks and hydrothermal activity in the southwestern Nevada volcanic field. Part II provides a compilation of trace-element analyses of surface and subsurface rocks in and near Yucca Mountain.

ROCK UNITS OF YUCCA MOUNTAIN AS HOSTS FOR PRECIOUS-METALS DEPOSITS

For some time it has been apparent to us that the same rock units that compose Yucca Mountain, such as the Lithic Ridge Tuff, and units of the Crater Flat, Paintbrush and Timber Mountain Tuffs, as well as underlying sedimentary rocks of pre-Cenozoic age, are the principal host rocks for economic and presently subeconomic precious-metal deposits in the surrounding Bare Mountain, Bullfrog, Wahmonie and Mine Mountain mining districts. This demonstrates that rock units composing Yucca Mountain are indeed suitable hosts for hydrothermal mineral resources. Direct radiometric dating of hydrothermal minerals and stratigraphic relations show that multiple, widespread pulses of Miocene hydrothermal activity and local precious-metal mineralization occurred in the Yucca Mountain region (Weiss et al., 1995b). At least one episode of hydrothermal activity took place in northwestern Yucca Mountain (and possibly in the repository area) between eruptions of the Tram Member and the 13.2 Ma Bullfrog Member of the Crater Flat Tuff (Weiss et al., 1993a), and at least one aerially extensive, laterally flowing hydrothermal system existed in the subsurface of Yucca Mountain coeval with widespread Timber Mountain magmatic activity (Aronson and Bish, 1987; Jackson et al., 1988; Bish and Aronson, 1993).

The fact that rocks of Yucca Mountain are suitable hosts for Au-Ag deposits and that multiple episodes of potentially mineralizing hydrothermal activity have occurred in or near Yucca Mountain (Weiss et al., 1995b) strengthen the possibility that mineral resources may have formed in the subsurface of Yucca Mountain and currently remain undiscovered. It is our opinion that estimates of the potential for undiscovered mineral resources and human interference at Yucca Mountain should explicitly recognize the demonstrated suitability of the rocks as hosts and that one, or more, possibly ore-forming episodes of hydrothermal activity have occurred. In an effort to draw attention to this, we prepared an abstract entitled *Potential for undiscovered mineral deposits at Yucca Mountain, NV: host rocks, timing and spatial distribution of nearby mineralization* (Weiss et al., 1994). This abstract has been accepted for presentation at the 1994 national meeting of the Geological Society of America (GSA) in Seattle, Washington. GSA has deemed our abstract to be of possible interest to the general public and has recently requested that we prepare a news release to provide additional information for the news media.

ADDITIONAL GEOCHEMICAL DATA FROM VEINS AND SILICEOUS DEPOSITS, NORTHWESTERN YUCCA MOUNTAIN

Additional trace-element data have been obtained from veins, altered rocks and siliceous ledges in northwestern Yucca Mountain and are reported in Table 1. Through a program of repeat and duplicate analyses, carried out blind to the analytical laboratory, the elevated concentrations of As, Bi, Hg, Sb and Tl reported last year (Weiss et al., 1993a) were corroborated and the effects of different sample pulverizing equipment were tested.

The data indicate that extremely hard, siliceous rocks gain as much as about 3.5 ppm Mo from pulverization in the shatterbox, relative to samples ground with steel plates in the rotary pulverizer at the Nevada Bureau of Mines and Geology (Table 1). Concentrations of the other elements analysed are not significantly affected by differences in the preparation equipment used. Analyses reported for surface and subsurface samples from Yucca Mountain by Weiss et al. (1990; 1991a; 1992) were from samples prepared in rotary pulverizers utilizing ceramic and steel plates and therefore do not reflect added Mo. Analyses reported last year (Weiss et al., 1993a) were, unfortunately, all on samples pulverized in the shatterbox, suggesting that Mo concentrations reported for the harder samples are from about 0.5 to 3.5 ppm too high. Nevertheless, "corrected" Mo concentrations of as much as about 4 ppm are present in veins of hydrothermal breccia and the siliceous ledges in northwestern Yucca Mountain (Table 1).

The elevated concentrations of As, Sb, Hg, Bi and Tl, ± Mo, (Weiss et al., 1993a; Table 1, this report) in veins, silicified siltstone and laminated silica (sinter) deposits are extremely difficult to ascribe to weathering or other surficial processes. We continue to view these data, as was stated last year (Weiss et al., 1993a), as evidence for the involvement of hydrothermal fluids in the formation of the veins and ledges. Similar concentrations of Hg and Sb, significantly elevated with respect to fresh tuff (Table 1), are locally present in argillically altered rocks of the Crater Flat Tuff and in thin veins of hydrothermal breccia in Windy Wash and in an altered area west of the siliceous ledges.

Analyses of rocks from altered and mineralized areas in Bare Mountain reported by Tingley (1984) were carried out by methods having poor sensitivity at low levels of concentration for Au, Ag, As, Sb, Bi, Mo and other trace elements. The analyses of Tingley (1984) also do not include data for elements such as Te and Tl, which are now recognized to be characteristic of certain classes of epithermal mineral deposits. We have obtained data on samples of the porphyry dikes, nearby wallrocks of Paleozoic sedimentary rocks, dikes of hydrothermal breccia and other rocks in Bare Mountain (Table 1) utilizing the much more highly sensitive methods of organic-extraction inductively-coupled plasma-emission spectrometry (ICP) that were unavailable to earlier studies such as Tingley (1984).

Our new data supplement the data of Tingley (1994) and are similar to the data of U.S. Precious Metals, Inc., from the Mother Lode mine as summarized by Weiss et al. (1993b). Altered rhyolitic porphyry dike rocks and, to a lesser degree, nearby Paleozoic carbonate wallrocks in the vicinity of Tarantula Canyon contain modest to low-level concentrations of added As, Hg, Sb, and Mo, ± Bi, ± Tl (Table 1). Silicified dikes of hydrothermal breccia from 0.3 to about 2 m in width that intrude Paleozoic rocks near the Telluride mine and in Joshua Hollow, and contain abundant volcanic rock fragments, have much greater concentrations of Ag and Au, and generally higher concentrations of As, Sb, Hg, Te, Mo and Tl than do the altered porphyry dikes. Breccia composed mainly of argillically altered carbonate rocks of the Nopah Formation that have been partly replaced by fluorite at the Goldspar/Diamond Queen mine contain 1.16 ppm Au, low Ag, and anomalous As, Bi, Hg, Sb, Te, Mo and Tl.

Differences in the style of mineralization and greater amounts of base metals, Ag and W in veins and altered rocks in western and southern Bare Mountain have led us to infer, following Tingley (1984) and Jackson (1988), that gold deposits in northern and eastern Bare Mountain reflect fundamentally different and likely younger hydrothermal events associated with the deeper parts of the large, genetically related porphyry magma system that we infer to underlie the porphyry dikes (Noble et al., 1989; 1991). We have proposed that the disseminated Au deposits of northern and eastern Bare Mountain formed from Carlin-type (or Carlin-like) hydrothermal activity genetically related to the porphyry-type magmatic activity (Weiss et al., 1993b; 1995). A sample containing macroscopic particles of gold along fractures in somewhat argillized dolomitic rock of the Wood Canyon Formation from the Gold Ace mine in western Bare Mountain was analyzed (Table 1). Other than the presence of visible gold, which is entirely absent in even the highest-grade ores of the Mother Lode and Sterling mines, and the relatively low contents of As and Sb, the Gold Ace sample differs little, geochemically, from ore-grade specimens of the disseminated Au deposits elsewhere in Bare Mountain.

UPDATE ON ANALOGUE STUDY OF THE BALD MOUNTAIN GOLD DEPOSITS

During the period of this report, additional age data were obtained on igneous rocks in the Bald Mountain district. The age dates show that igneous activity is clearly of Jurassic age. The age data and geologic information are presently being summarized in a new manuscript entitled *Geology and gold deposits of the Bald Mountain mining district, White Pine County, Nevada* (Hitchborn et al., in prep.). This paper will be submitted to the Geological Society of Nevada for publication in the symposium volume to be published for the 1995 Geological Society of Nevada Symposium entitled *Geology and Ore Deposits of the American Cordillera.*

PROGRESS IN RADIOMETRIC DATING STUDIES

Timing of Au-Ag mineralization at the Mother Lode mine, northern Bare Mountain

We have continued our efforts to better constrain the absolute age of gold mineralization in northern Bare Mountain and the timing of these gold deposits relative to porphyry magmatic activity. Our previous attempt, through K-Ar age determinations on illite-smectite at the Mother Lode mine, gave mixed results (Weiss et al., 1993a). Much of the ore at the Mother Lode mine is hosted by argillically altered silicic porphyry dikes. Similar dikes exposed nearby in Joshua Hollow, Tate's Wash and at a greater distance, in Tarantula Canyon, have given biotite K-Ar ages of 13.9 and 14.9 Ma (Marvin et al., 1989; Noble et al., 1991; Monsen et al., 1992). This spread in ages and the somewhat altered nature of the dated dikes has led us to question their reported ages and pursue additional dating of the age of dike emplacement using $^{40}Ar/^{39}Ar$ experiments.

Dike rocks exposed between the Telluride and Mother Lode mine are only weakly propylitically altered, containing phenocrysts of variably chloritized hornblende, clear sani-

dine, unaltered clinopyroxene and plagioclase partly replaced by turbid K-feldspar (adularia). Scanning electron microscope analyses of more strongly altered dike rocks from the Mother Lode mine show that the clear sanidine phenocrysts have compositions of about 27 to 34 mole % Na_2O, 0.25 to 0.5 mole % CaO and 1 to 2 mole % BaO, inconsistent with hydrothermal replacement by adularia. Using conventional magnetic, heavy liquid, hand-picking and acid treatment techniques, clear sanidine, turbid K-feldspar and unaltered hornblende grains were separated from the relatively weakly altered dike rock and sent to Dr. William McIntosh for $^{40}Ar/^{39}Ar$ dating in the laboratories of the New Mexico Bureau of Mines and Mineral Resources. Through a combination of step-heating and single-crystal laser fusion experiments we expect to better constrain the ages of dike emplacement and hydrothermal activity.

At this time the sanidine and turbid K-feldspar have not yet been analysed. Step heating of the hornblende gave an unusual, saddle-shaped Ar release spectra (Figure 1). The initial 10% and the last 16% of the Ar released gave apparent ages of between 35 and 53 Ma. Most of the Ar was released in the intermediate heating steps with an apparent age of about 19.2 Ma. The much older apparent ages of the initial heating steps suggest the presence of excess radiogenic Ar, perhaps trapped in fluid inclusions during growth of the hornblende, as has been documented for anomalously old hornblende crystallized from extremely volatile-rich mafic intrusions at the Porgera gold deposit in Papua, New Guinea (Richards and McDougall, 1990). Such excess radiogenic Ar suggests the 19.2 Ma age date is a *maximum* age for the dike. This raises the possibility that the biotite K-Ar ages may also in part reflect the presence of excess Ar. If this is the case, the 13.9 Ma ages should be considered *maximum* ages and the *ca.* 12.5 to 13 Ma hydrothermal activity suggested by adularia and alunite ages from nearby locations (Noble et al., 1991; McKee and Bergquist, 1993; Weiss et al., 1995b) may have occurred within, at most, about 1.5 Ma after magmatic activity. We hope that results from the clear sanidine and turbid K-feldspar grains will provide additional information bearing on this problem.

UPDATE ON MINING AND MINERAL EXPLORATION

Gold production continues from the main pit and the underground workings at the Lac Gold Bullfrog mine in the southern Bullfrog Hills. It is believed that only a few months of production of mill-grade ore from the main vein system remain accessible by open-pit mining methods. Stripping of overburden at the Montgomery-Shoshone mine is nearly complete and production from an open-pit resource is expected to begin in the next few weeks. In efforts to replace declining reserves, Lac Minerals Ltd., which is currently being acquired by American Barrick, has undertaken an aggressive program of detailed geologic mapping and continued exploratory drilling in the southern Bullfrog Hills, particularly in Bonanza Mountain west of the townsite of Rhyolite. Lac Minerals/American Barrick continues to hold extensive land positions in the northern Bullfrog Hills. Sunshine Mining and Pathfinder Exploration have dropped their leases on claims in the northern Bullfrog Hills held by D. Spicer and other individuals.

InterRock Exploration, a spin-off of Cordex Exploration Company, carried out two exploratory drilling programs in the upper reaches of Fluorspar Canyon and Tate's Wash in efforts to expand the presently subeconomic Secret Pass gold deposit. This currently subeconomic resource, hosted largely within the Crater Flat Tuff (Greybeck and Wallace, 1991), is located 19 km northwest of the proposed repository site.

HG Mining Inc. of Beatty, NV. continues production of cut stone products from ash-flow tuffs quarried within the geographic limits of the Timber Mountain caldera complex. Ash-flow units from which cut stone is currently produced include the glassy, partially welded caprock of the Rainier Mesa Member of the Timber Mountain Tuff in northern Crater Flat, the lower, lithic-rich, unwelded part of the Ammonia Tanks Member of the Timber Mountain Tuff in the Transvaal Hills, the tuff of Cut-off Road in the Transvaal Hills and the Pahute Mesa and Rocket Wash Members of the Thirsty Canyon Tuff in upper Oasis Valley.

REVIEWS, PUBLICATIONS AND PRESENTATIONS

Reviews

None

Publications

The following abstracts and articles resulting from Task 3 studies were produced and(or) published during the period covered by this report, and are contained in the appendices as follows:

Appendix A:

Weiss, S. I., Noble, D. C., Connors, K. A., Jackson, M. R., and McKee, E. H., Multiple episodes of hydrothermal activity and epithermal mineralization in the southwestern Nevada volcanic field and their relations to magmatic activity, volcanism and regional extension: (in revision following formal U.S. Geological Survey review, for submission to *Economic Geology*).

Appendix B:

Weiss, S. I., Larson, L. T., and Noble, D. C., Pyritic ash-flow tuff, Yucca Mountain, Nevada--A discussion: (for submission to *Economic Geology*).

Appendix C:

Weiss, S. I., Noble, D. C., and Larson, L. T., Compilation of radiometric age and trace-element geochemical data, Yucca Mountain and surrounding areas of southwestern Nevada: unpublished data compilation prepared for the Nevada Nuclear Waste Project Office by Task 3 of the Center for Neotectonic Studies, University of Nevada, Reno, 45 pp.

Appendix D:

Weiss, S. I., Noble, D. C., and Larson, L. T., 1994, Potential for undiscovered mineral deposits at Yucca Mountain, NV: host rocks, timing and spatial distribution of nearby mineralization [abst]: Geological Society of America Abstracts with Programs, v. 26, p. 311.

Presentations

D. C. Noble gave a presentation entitled *Mineral Resources and Potential and Related Human Interference at Yucca Mountain* to the meeting of the National Academy of Science Board on Radioactive Waste Management in Las Vegas, Nevada on November 9, 1993.

SUMMARY OF CONCLUSIONS AND RECOMMENDATIONS

New corroborating geochemical data confirms that elevated concentrations of As, Sb, Hg, Bi, Mo and Tl are present in veins and in altered rocks in northwestern Yucca Mountain, although measured Mo concentrations are as much as 0.5 to 3.5 ppm too high for some of the more siliceous samples. Elevated concentrations of this suite of elements are difficult to explain as the result of weathering or other surficial processes. The most reasonable explanation of the data is that hydrothermal fluids were involved in the formation of the veins, siliceous ledges and areas of alteration. As we stated last year, this hydrothermal activity must have occurred prior to deposition of the Bullfrog Member of the Crater Flat Tuff and therefore can not be detected by surface sampling in most of Yucca Mountain.

It is clear from stratigraphic relations and radiometric age data that multiple episodes of ore-forming and potentially ore-forming hydrothermal activity have occurred in large areas of the southwestern Nevada volcanic field, including the Yucca Mountain region (Weiss et al., 1995b). The pyritic rocks penetrated by the deep drill holes in Yucca Mountain provide important evidence, in addition to the large body of textural and mineralogical data on rock alteration reported in various papers by personnel of the Los Alamos National Laboratory and the U. S. Geological Survey, that one or more of these episodes has affected rocks deep within Yucca Mountain. More importantly, the presence of pyrite in these rocks indicates that the fluids contained small, but geochemically significant amounts of reduced sulfur and were therefore capable of transporting and depositing precious metals. The absence of elevated concentrations of precious-metals in drill hole samples analyzed to date does not mean that a major deposit may not be present, particularly when the wide

spacing of the existing deep drill holes is considered. We strongly disagree with the view of Castor et al. (1994) that pyrite in ash-flow units at Yucca Mountain is xenocrystic in origin.

We believe that the assessment of the potential for undiscovered mineral resources and possibly associated human interference at Yucca Mountain must include serious consideration of the fact that the same rock units that compose Yucca Mountain are the hosts for significant economic and potentially economic gold-silver deposits in neighboring mining districts, and that at least one episode of potentially mineralizing hydrothermal activity has occurred in Yucca Mountain. Our abstract entitled *Potential for undiscovered mineral deposits at Yucca Mountain, NV: host rocks, timing and spatial distribution of nearby mineralization*, to be presented to the annual meeting of the Geological Society of America in October, 1994, endeavors to draw attention to these observations.

As we have concentrated on the production and publication of papers based on results of our past work, we have postponed the start of new work on the hydrothermal dispersion of trace elements at volcanic-rock hosted precious metals deposits. During the coming year we hope to begin to investigate the trace-element contents of hydrothermally altered (but unmineralized) rocks from within and peripheral to several silicic volcanic-rock hosted epithermal mineral deposits. This would involve the same types of low-level, multi-element analyses reported in Table 1. We plan to obtain specimens and/or high-quality chemical data from rocks peripheral to a number of different types of deposits, including Round Mountain, Secret Pass, Rawhide, and Paradise Peak, Nevada, and perhaps Castle Mountain, California. The resulting data will provide important information for the evaluation of existing and future trace-element data from the subsurface of Yucca Mountain.

REFERENCES CITED AND OTHER PERTINENT LITERATURE

The following references were selected because of their direct bearing on the Cenozoic volcanic stratigraphy and caldera geology, hydrothermal activity, and mineral potential of Yucca Mountain and the surrounding region of the southwestern Nevada volcanic field. Additional pertinent references on mineral potential, and particularly unpublished data in files of the Nevada Bureau of Mines and Geology, are given by Bell and Larson (1982b). A compendium of information from the U.S. Geological Survey's Mineral Resource Data System is given by Bergquist and McKee (1991).

Ahern, R., and Corn, R.M., 1981, Mineralization related to the volcanic center at Beatty, Nevada: Arizona Geological Society Digest, v. XIV, p. 283-286.

Albers, J. P., and Stewart, J. H., 1972, Geology and mineral deposits of Esmeralda County, Nevada, Nevada Bur. Mines and Geol. Bull. 78, 80 p.

Ander, H.D., and Byers, F.M., 1984, Nevada Test Site field trip guidebook; Reno, Nevada, University of Nevada-Reno, Department of Geological Sciences, v. 2, 1984, 35 p.

Anderson, R.E., Ekren, E.B., and Healey, D.L., 1965, Possible buried mineralized areas in Nye and Esmeraldo Counties, Nevada: U.S. Geological Survey Professional Paper 525-D, p. D144-D150.

Anonymous, 1928, One strike of real importance made at Nevada's new camp: Engineering and Mining Journal, v. 125, no. 1, p. 457.

Aronson, J.L., and Bish, D.L., 1987, Distribution, K/Ar dates, and origin of illite/smectite in tuffs from cores USW G-1 and G-2, Yucca Mountain, Nevada, a potential high-level radioactive waste repository: Abstract of presentation at Clay Minerals Society Meeting, Socorro, NM, 1987.

Armstrong, R. L., Ekren, E. B., McKee, E. H., and Noble, D. C., 1969, Space-time relations of Cenozoic silicic volcanism in the Great Basin of the western United States: Am. Jour. Sci., v. 267, p. 478-490.

Bailey, E.H., and Phoenix, D.A., 1944, Quicksilver deposits in Nevada: Nevada Bureau of Mines and Geology Bulletin 41.

Barton, C.C., 1984, Tectonic significance of fractures in welded tuff, Yucca Mountain, Southwest Nevada: Geological Society of America, Abstracts with Programs, v. 16, p. 437.

Barton, P. B., and Skinner, B. J., 1979, Sulfide mineral stabilities: *in* Barnes, H. L., ed., Geochemistry of Hydrothermal Ore Deposits, Wiley and Sons, New York, 798 p.

Bath, G.D., and Jahren, C.E., 1984, Interpretations of magnetic anomalies at repository site proposed for Yucca Mountain area, Nevada Test Site: U.S. Geological Survey Open-File Report 84-120, 40 p.

Bath, G.D., and Jahren, C.E., 1985, Investigation of an aeromagnetic anomaly on west side of Yucca Mountain, Nye County, Nevada: U.S. Geological Survey Open-File Report 85-459, 24 p.

Beck, B. A., 1984, Geologic and gravity studies of the structures of the northern Bullfrog Hills, Nye County, Nevada: California State University at Long Beach, unpublished MSc Thesis, 86 p.

Bedinger, M.S., Sargent, K.A., and Langer, W.H., 1984, Studies of geology and hydrology in the Basin and Range Province, Southwestern United States, for isolation of high-level radioactive waste; characterization of the Death Valley region, Nevada and California: U.S. Geological Survey Open-File Report 84-743, 173 p.

Bedinger, M.S., Sargent, K.A., and Langer, W.H., 1984, Studies of geology and hydrology in the Basin and Range Province, Southwestern United States, for isolation of high- level radioactive waste; evaluation of the regions: U.S. Geological Survey Open-File Report 84-745, 195 p.

Bell, E.J., and Larson, L.T., 1982a, Overview of energy and mineral resources of the Nevada Nuclear Waste Storage Investigations, Nevada Test Site, Nye County, Nevada: U.S. Department of Energy Report NVO-250 (DE83001418), 64 p. plus maps.

Bell, E.J., and Larson, L.T., 1982b, Annotated bibliography, Overview of energy and mineral resources for the Nevada Nuclear Waste Storage Investigations, Nevada Test Site, Nye County, Nevada: U.S. Department of Energy Report NVO-251 (DE83001263), 30 p.

Benson, L.V. and McKinley, P.W., 1985, Chemical composition of the ground water in the Yucca Mountain area, Nevada: U.S. Geological Survey Open-File Report 85-484, 10 p.

Bentley, C.B., 1984, Geohydrologic data for test well USW G-4, Yucca Mountain area, Nye County, Nevada: U.S. Geological Survey Open-File Report 84-63, 67 p.

Bergquist, J. R., and McKee, E. H., 1991, Mines, prospects and mineral occurrences in Esmeralda and Nye Counties, Nevada, nera Yucca Mountain: U.S. Geological Survey Administrative Report to the Department of Energy, Yucca Mountain Project, 385 p.

Bish, D.L., 1987, Evaluation of past and future alteration in tuff at Yucca Mountain, Nevada based on clay mineralogy of drill cores USW G-1, G-2, and G-3: Los Alamos, New Mexico, Los Alamos National Laboratory Report LA-10667-MS, 42 p.

Bish, D. L., and Aronson, J. L., 1993, Paleogeothermal and paleohydrologic conditions in silicic tuff from Yucca Mountain, Nevada: Clays and Clay Minerals, v. 41, p. 148-161.

Bonham, H. F., Jr., and Garside, L. J., 1979, Geology of the Tonopah, Lone Mountain, Klondike and northern Mud Lake Quadrangles, Nevada: Nevada Bureau of Mines and Geology Bulletin 92, 142 p., 1:48,000.

Booth, M., 1988, Dallhold finalizes plans for huge Nevada mine: The Denver Business Journal, April 4, 1988, p. 10.

Boyle, R. W., 1979, The geochemistry of gold and its deposits: Geological Survey of Canada Bulletin 280, 584 p.

Boyle, R.W., and Jonasson, I.R., 1973, The geochemistry of arsenic and its use as an indicator element in geochemical prospecting: Journal of Geochemical Exploration, v. 2, p. 251-296.

Broxton, D. E., Vaniman, D., Caporuscio, F., Arney, B., and Heiken, G., 1982, Detailed petrographic descriptions and microprobe data fro drill holes USW-G2 and UE25b-1H, Yucca Mountain, Nevada: Los Alamos, New Mexico, Los Alamos National Laboratory Report LA-10802-MS, 168 p.

Broxton, D.E., Byers, F.M., Warren, R.G. and Scott, R.B., 1985, Trends in phenocryst chemistry in the Timber Mountain-Oasis Valley volcanic field, SW Nevada; evidence for isotopic injection of primitive magma into an evolving magma system: Geological Society of America, Abstracts with Programs, v. 17, p. 345.

Broxton, D. E., Warren, R. G., and Byers, F. M., Jr., 1989, Chemical and mineralogic trends within the Timber Mountain-Oasis Valley caldera complex, Nevada: Evidence for multiple cycles of chemical evolution in a long-lived silicic magma system: Journal of Geophysical Research, v. 94, p. 5961-5985.

Broxton, D.E., Warren, R.G., Byers, F.M., Jr., Scott, R.B., and Farner, G.L., 1986, Petrochemical trends in the Timber Mountain-Oasis Valley caldera complex, SW Nevada: EOS (American Geophysical Union Transactions), v. 67, p. 1260.

Broxton, D.E., Warren, R.G., Hagan, R.C. and Luedemann, G.,1986, Chemistry of diagenetically altered tuffs at a potential nuclear waste repository, Yucca Mountain, Nye County, Nevada: Los Alamos, New Mexico, Los Alamos National Laboratory Report LA-10802-MS, 160 p.

Byers, F. M., Jr., Carr, W. J., and Orkild, P. P., 1989, Volcanic centers of southwestern Nevada: evolution of understanding, 1960-1988: Journal of Geophysical Research, v.94, p. 5908-5924.

Byers, F.M., Jr., Carr, W.J., and Orkild, P.P., 1986, Calderas of southwestern Nevada-Evolution of understanding, 1960-1986: EOS (American Geophysical Union Transactions), v. 67, p. 1260.

Byers, F.M., Jr., Carr, W.J., Orkild, P.P., Quinlivan, W.D. and Sargent, K.A., 1976a, Volcanic Suites and related cauldrons of Timber Mountain-Oasis Valley caldera complex: U.S. Geological Survey Professional Paper 919, 70 p.

Byers, F.M., Jr., Carr, W.J., Christiansen, R.L., Lipman, P.W., Orkild, P.P., and Quinlivan, W.D., 1976b, Geologic map of the Timber Mountain Caldera area, Nye County, Nevada: U.S. Geological Survey Miscellaneous Investigations Series, I-891, sections, 1:48,000 scale.

Byers, F.M., Jr., Orkild, P.P, Carr, W. J., and Quinlivan, W.D., 1968, Timber Mountain Tuff, southern Nevada, and its relation to cauldron subsidence: Geological Society of America Memoir 110, p. 87-97.

Caporuscio, F., Vaniman, D.T., Bish, D.L., Broxton, D.E., Arney, D., Heiken, G., Byers, F.M., and Gooley, R., 1982, Petrologic studies of drill cores USW-G2 and UE25b-1H,Yucca Mountain, Nevada: Los Alamos, New Mexico, Los Alamos National Laboratory Report LA-9255-MS, 114 p.

Carr, M.D., and Monsen, S.E., 1988, A field trip guide to the geology of Bare Mountain: Geological Society of America Field Trip Guidebook, Cordilleran Section Meeting, Las Vegas, Nevada, p. 50-57.

Carr, M.D., Waddell, S.J., Vick, G.S., Stock, J.M., and Monsen, S.A., Harris, A.G., Cork, B.W., and Byers, F.M., Jr., 1986, Geology of drill hole UE25p-1: A test hole into pre-Tertiary rocks near Yucca Mountain, southern Nevada: U.S. Geological Survey Open File Report 86-175.

Carr, W.J., 1964, Structure of part of the Timber Mountain dome and caldera, Nye County, Nevada: U.S. Geological Survey Professional Paper 501-B, p. B16-B20.

Carr, W.J., 1974, Summary of tectonic and structural evidence for stress orientation at the NTS: U.S. Geological Survey Open-File Report 74-176, 53 p.

Carr, W.J., 1982, Volcano-tectonic history of Crater Flat, southwestern Nevada, as suggested by new evidence from drill hole USW-VH-1 and vicinity: U.S. Geological Survey Open-File Report 82-457, 23 p.

Carr, W.J., 1984a, Regional structural setting of Yucca Mountain, southwestern Nevada, and late Cenozoic rates of tectonic activity in part of the southwestern Great Basin, Nevada and California: U.S. Geological Survey Open-File Report 84-0854, 114 p.

Carr, W.J., 1984b, Timing and style of tectonism and localization of volcanism in the Walker Lane belt of southwestern Nevada: Geological Society of America, Abstracts with Programs, v. 16, p. 464.

Carr, W.J., 1988a, Styles of extension in the Nevada Test Site region, southern Walker Lane Belt: an integration of volcano-tectonic and detachment fault models: Geological Society of America, Abstracts with Programs, v. 20, p. 148.

Carr, W. J., 1988b, Volcano-tectonic setting of Yucca Mountain and Crater Flat, *in* Carr, M. D., and Yount, J. C., eds., Geologic and hydrologic investigations of a potential nuclear waste disposal site at Yucca Mountain, southern Nevada: U.S. Geol. Survey Bull. 1790, p. 35-49.

Carr, W.J., and Quinlivan, W.D., 1966, Geologic map of the Timber Mountain quadrangle, Nye County, Nevada: U.S. Geological Survey Geologic Quadrangle Map GQ-503, 1:24,000 scale, sections.

Carr, W.J., and Quinlivan, W.D., 1968, Structure of Timber Mountain resurgent dome, Nevada Test Site: Geological Society of America Memoir 110, p. 99-108.

Carr, W.J. and Parrish, L.D., 1985, Geology of drill hole USW VH-2, and structure of Crater Flat, southwestern Nevada: U.S. Geological Survey Open-File Report 85-475, 41 p.

Carr, W.J., Byers, F.M., and Orkild, P.P., 1984, Stratigraphic and volcano-tectonic relations of Crater Flat Tuff and some older volcanic units, Nye County, Nevada: U.S. Geological Survey Open-File Report 84-114, 97 p.

Carr, W.J., Byers, F.M., and Orkild, P.P., 1986, Stratigraphic and volcano-tectonic relations of Crater Flat Tuff and some older volcanic units, Nye County, Nevada: U.S. Geological Survey Professional Paper 1323, 28p.

Castor, S. B., and Weiss, S. I., 1992, Contrasting styles of epithermal precious-metal mineralization in the southwestern Nevada volcanic field, USA: Ore Geology Reviews, v. 7, p. 193-223.

Castor, Feldman and Tingley, 1990, Mineral evaluation of the Yucca Mountain Addition, Nye County, Nevada: Nevada Bureau of Mines and Geology, Open-file Report 90-4, 80 pp.

Castor, Feldman and Tingley, 1990, Mineral potential report for the U.S. Department of Energy, Serial No. N-50250: Nevada Bureau of Mines and Geology, University of Nevada, Reno, 24 pp.

Castor, S. B., Tingley, J. V., and Bonham, H. F., Jr., 1991, Yucca Mountain Addition subsurface mineral resource analysis: unpub. proposal to Science Applications International Corp., 10 p.

Castor, S. B., Tingley, J. V., and Bonham, H. F., Jr., 1992, Subsurface mineral resource analysis, Yucca Mountain, Nevada, Preliminary Report 1: Lithilogic logs: Nevada Bureau of Mines and Geology Open-file report 92-4, 11 p. plus appendices.

Castor, S. B., Tingley, J. V., and Bonham, H. F., Jr., (*in review*), Pyritic ash-flow tuff in Yucca Mountain: manuscript submitted in 1992 to Geology.

Castor, S. B., Tingley, J. V., and Bonham, H. F., Jr., (*in press*), Pyritic ash-flow tuff in Yucca Mountain: manuscript submitted in 1993 to Economic Geology.

Castor, S. B., Tingley, J. V., and Bonham, H. F., Jr., 1994, Pyritic ash-flow tuff, Yucca Mountain, Nevada: Economic Geology, v. 89, p. 401-407.

Christiansen, R.L., and Lipman, P.W., 1965, Geologic map of the Topopah Spring NW quadrangle, Nye County, Nevada: U.S. Geological Survey Geologic Quadrangle Map GQ-444, 1:24,000 scale, sections.

Christiansen, R.L., Lipman, P.W., Carr, W.J., Byers, F.M., Jr., Orkild, P.P., and Sargent, K.A., 1977: Timber Mountain-Oasis Valley caldera complex of southern Nevada: Geological Society of America Bulletin, v. 88, p. 943-959.

Christiansen, R.L., Lipman, P.W., Orkild, P.P., and Byers, F.M., Jr., 1965, Structure of the Timber Mountain caldera, southern Nevada, and its relation to basin-range structure: U.S. Geological Survey Professional Paper 525-B, p. B43-B48.

Connors, K. A., (*in preparation*), Studies in silicic volcanic geology: Part I: Compositional controls on the initial gold contents of silicic volcanic rocks; Part II: Geology of the western margin of the Timber Mountain caldera complex and post-Timber Mountain volcanism in the Bullfrog Hills: unpublished PhD dissertation, University of Nevada, Reno.

Connors, K.A., Weiss, S.I., Noble, D.C., and Bussey, S.D., 1990, Primary gold contents of some silicic and intermediate tuffs and lavas: evaluation of possible igneous sources of gold: Geological Society of America Abst. with Programs, v. 22, p. A135.

Connors, K.A., Noble, D.C., Weiss, S.I., and Bussey, S.D., 1991a, Compositional controls on the gold contents of silicic volcanic rocks: 15th International Geochemical Exploration Symposium Program with Abstracts, p. 43.

Connors, K. A., McKee, E. H., Noble, D. C., and Weiss, S. I., 1991, Ash-flow volcanism of Ammonia Tanks age in the Oasis Valley area, SW Nevada: Bearing on the evolution of the Timber Mountain calderas and the timing of formation of the Timber Mountain II resurgent dome: EOS, Trans. Am. Geophys. Union., v. 72, p. 570.

Connors, K., A., Noble, D. C., Bussey, S., D., and Weiss, S. I., 1993, Initial gold contents of silicic volcanic rocks: bearing on the behavior of gold in magmatic systems: Geology, v. 21, p. 937-940.

Cornwall, H.R., 1962, Calderas and associated volcanic rocks near Beatty, Nye County, Nevada: Geological Society of America, Petrologic Studies, A.F. Buddington Volume, p. 357-371.

Cornwall, H.R., 1972, Geology and mineral deposits of southern Nye County, Nevada: Nevada Bureau of Mines and Geology Bulletin 77, p. 49.

Cornwall, H.R., and Kleinhampl, F.J., 1961, Geology of the Bare Mountain quadrangle, Nevada: U.S. Geological Survey Geologic Quadrangle Map GQ-157, 1:62,500 scale.

Cornwall, H.R., and Kleinhampl, F.J., 1964, Geology of the Bullfrog quadrangle and ore deposits related to the Bullfrog Hills caldera, Nye County, Nevada, and Inyo County, California: U.S. Geological Survey Professional Paper 454-J, 25 p.

Cornwall, H.R., and Norberg, J.R., 1978, Mineral Resources of the Nellis Air Force Base and the Nellis Bombing and Gunnery Range, Clark, Lincoln, and Nye Counties, Nevada: U.S. Bureau of Mines Unpublished Administrative Report, 118 p.

Craig, R.W. and Robinson, J.H., 1984, Geohydrology of rocks penetrated by test well UE-25p#1, Yucca Mountain area, Nye County, Nevada, U.S. Geological Survey Water-Resources Investigations 84-4248, 57 p.

Craig, R.W., Reed, R.L., and Spengler, R.W., 1983, Geohydrologic data for test well USW H-6, Yucca Mountain area, Nye County, Nevada: U.S. Geological Survey Open-File Report 83-856, 52 p.

Crowe, B.M., 1980, Disruptive event analysis: Volcanism and igneous intrusion: Batelle Pacific Northwest Laboratory Report PNL-2822, 28 p.

Crowe, B.M., and Carr, W.J., 1980, Preliminary assessment of the risk of volcanism at a proposed nuclear waste repository in the southern Great Basin: U.S. Geological Survey Open-File Report 80-357, 15 p.

Crowe, B.M., Johnson, M.E., and Beckman, R.J., 1982, Calculation of probability of volcanic disruption of a high-level radioactive waste repository within southern Nevada, USA: Radioactive Waste Management and the Nuclear Fuel Cycle, v. 3, p. 167-190.

Crowe, B.M., Vaniman, D.J., and Carr, W.J., 1983b, status of volcanic hazard studies for the Nevada nuclear waste storage investigations: Los Alamos, New Mexico, Los Alamos National Laboratory Report LA-9325-MS.

Deino, A.L., Hausback, B.P., Turrin, B.T., and McKee, E.H., 1989, New $^{40}Ar/^{39}Ar$ ages for the Spearhead and Civet Cat Canyon Members of the of Stonewall Flat Tuff, Nye County, Nevada: EOS, Trans. American Geopphysical Union, v. 70, p. 1409.

Drexler, J. W., 1982, Mineralogy and geochemistry of Miocene volcanic rocks related to the Julcani Ag-Au-Cu-Bi deposit, Peru: Physiochemical conditions of a productive magma body: unpublished PhD dissertation, Houghton, Michigan Technical University, 250 p.

Eckel, E.B., ed., 1968, Nevada Test Site: Geological Society of America Memoir 110, 290 p.

Eichleberger, J. C., and Koch, F. G., 1979, Lithic fragments in the Bandelier Tuff, Jemez Mountains, New Mexico: Journal of Volcanology and Geothermal Research, v. 5, p. 115-134.

Ekren, E.B., and Sargent, K.A., 1965, Geologic map of Skull Mountain quadrangle at the Nevada Test Site, Nye County, Nevada: U.S. Geological Survey Geologic Quadrangle Map GQ-387.

Ekren, E.B., Anderson, R.E., Rodgers, C.L., and Noble, D.C., 1971, Geology of northern Nellis Air Force Base Bombing and Gunnery Range, Nye County, Nevada: U.S. Geological Survey Professional Paper 651, 91 p.

Feitler, S., 1940, Welded tuff resembling vitrophyre and pitchstone at Bare Mountain, Nevada: Geological Society of America Bulletin, v. 51, p. 1957.

Flood, T.P., and Schuraytz, B.C., 1986, Evolution of a magmatic system. Part II: Geochemistry and mineralogy of glassy pumices from the Pah Canyon, Yucca Mountain, and Tiva Canyon Members of the Paintbrush Tuff, southern Nevada: EOS Trans. American Geophysical Union, v. 67, p. 1261.

Foley, D., 1978, The geology of the Stonewall Mountain volcanic center, Nye County, Nevada: Ohio State University, Columbus Ohio, unpublished PhD Dissertation, 139 p.

Fouty, S.C., 1984, Index to published geologic maps in the region around the potential Yucca Mountain Nuclear Waste Repository site, southern Nye County, Nevada: U.S. Geological Survey Open-File Report 84-524, 31 p.

Fridrich, C. J., 1987, The Grizzly Peak cauldron, Colorado: structure and petrology of a deeply dissected resurgent ash-flow caldera: unpublished PhD dissertion, Stanford, Stanford University, 201 p.

Fridrich, C. J., Orkild, P. P., Murray, M., Price, J. R., Christiansen, R. L., Lipman, P. W., Carr, W. J., Quinlivan, W. D., and Scott, R. B., 1994, Geologic map of the East of Beatty Mountain Quadrangle, Nye County, Nevada: U.S. Geological Survey Open-file Report, 4 sheets, 1:12,000 (in review).

Frischknecht, F.C. and Raab, P.V., 1984, Time-domain electromagnetic soundings at the Nevada Test Site, Nevada, Geophysics, v. 49, p. 981-992.

Frizzell, Virgil, and Shulters, Jacqueline, 1986, Geologic map of the Nevada Test Site: EOS Trans. American Geophysical Union, v. 67, p. 1260.

Frizzell, Virgil, and Shulters, Jacqueline, 1990, Geologic map of the Nevada Test Site: U.S. Geological Survey Misc. Invest. Map I-2046, 1:100,000.

Gans, P. B., Mahood, G. A., and Schermer, E., 1989, Synextensional magmatism in the Basin and Range province; A case study from the eastern Great Basin: Geological Society of America Spec. Paper 233, 53 p.

Garside L.J. and Schilling, J.H., 1979, Thermal waters of Nevada: Nevada Bureau of Mines and Geology, Bulletin 91, 163 p.

Geehan, R.W., 1946, Exploration of the Crowell fluorspar mine, Nye County, Nevada: U.S. Bureau of Mines Report of Investigations 3954, 9 p.

Geldon, A. L., (in press) Preliminary hydrogeologic assessment of boreholes UE-25c #1, UE-25c #2 and UE-25c #3, Yucca Mountain, Nye County, Nevada: U.S. Geological Survey Water-Resources Investigations Report 91-XXX.

Greybeck, J. D., and Wallace, A. B., 1991, Gold mineralization at Fluorspar Canyon near Beatty, Nye County, Nevada: *in* Raines, G. L., Lisle,R. E., Shafer, R. W., and Wilkinson, W. W., eds., Geology and ore deposits of the Great Basin: Symposium Proceedings, Geol. Soc. of Nevada, sp. 935-946.

Hagstrum, J.T., Daniels, J.J., and Scott, J.H., 1980, Interpretation of geophysical well-log measurements in drill hole UE 25a-1, NTS, Radioactive Waste Program: U.S. Geological Survey Open-File Report 80-941, 32 p.

Hall, R.B., 1978, World nonbauxite aluminum resources--Alunite: U.S. Geological Survey Professional Paper 1076-A, 35 p.

Hamilton, W. B., 1988, Detachment faulting in the Death Valley region, California and Nevada, *in* Carr, M. D., and Yount, J. C., eds., Geologic and hydrologic investigations of a potential nuclear waste disposal site at Yucca Mountain, southern Nevada: U.S. Geol. Survey Bull. 1790, p. 51-86.

Hausback, B. P., and Frizzell, V. A. Jr., 1987, Late Miocene syntectonic volcanism of the Stonewall Flat Tuff, Nye County, Nevada [abs.]: Geological Society of America Abst. with Programs, v. 19, p. 696.

Hausback, B.P., Deino, A.L., Turrin, B.T., McKee, E.H., Frizzell, V.A., Noble, D.C., and Weiss, S.I., 1990, New $^{40}Ar/^{39}Ar$ ages for the Spearhead and Civet Cat Canyon Members of the Stonewall Flat Tuff, Nye County, Nevada: Evidence for systematic errors in standard K-Ar age determinations on sanidine: Isochron/West, No. 56, p. 3-7.

Harris, R.N., and Oliver, H.W., 1986, Structural implications of an isostatic residual gravity map of the Nevada Test Site, Nevada: EOS (American Geophysical Union Transactions), v. 67, p. 1262.

Heald, P., Foley, N.K., and Hayba, D.O., 1987, Comparative anatomy of volcanic-hosted epithermal deposits: acid-sulfate and adularia-sericite types: Economic Geology, v. 82, no. 1, p. 1-26.

Heikes, V.C., 1931, Gold, silver, copper, lead and zinc in Nevada--Mine report, in Mineral Resources of the U.S., 1928: U.S. Department of commerce, Bureau of Mines, pt. 1, p. 441-478.

Hildreth, E. W., 1977, The magma chamber of the Bishop Tuff: Gradients in temperature, pressure and composition: unpublished PhD dissertation, Univ. California-Berkely, 328 p.

Hill, J.M., 1912, The mining districts of the western U.S.: U.S. Geological Survey Bulletin 507, 309 p.

Hitchborn, A. D., Arbonies, D. G., Peters, S. G., McKee, E. H., Noble, D. C., Larson, L. T., and Beebe, J. S. (in preparation), Geology and gold deposits of the Bald Mountain mining district, White Pine County, Nevada: Geological Society of Nevada 1995 Symposium Volume, Geology and Ore Deposits of the American Cordillera.

Holmes, G.H., Jr., 1965, Mercury in Nevada, in Mercury potential of the United States: U.S. Bureau of Mines I.C., 8252, p. 215-300.

Hoover, D.L., Eckel, E.B., and Ohl, J.P., 1978, Potential sites for a spent unreprocessed fuel facility (SUREF), southwest part of the NTS: U.S. Geological Survey Open-File Report 78-269, 18 p.

Hoover, D. B., Chornack, M. P., Nervick, K. H., and Broker, M. M., 1982, Electrical studies at the proposed Wahmonie and Calico Hills Nuclear Waste Sites, Nye County, Nevada: U.S. Geol. Survey Open-File Rept. 82-466, 45 p.

Hudson, M. R., 1992, Paleomagnetic data bearing on the origin of arcuate structures in the Frenchman Peak - Massachusetts Mountain area of southern Nevada: Bull. Geol. Soc. Am., v. 104, p. 581-594.

Jackson, M. J., 1988, The Timber Mountain magmato-thermal event: an intense widespread culmination of magmatic and hydrothermal activity at the southwestern Nevada volcanic field: University of Nevada, Reno - Mackay School of Mines, Reno, Nevada, unpublished MSc Thesis.

Jackson, M.R., Noble, D.C., Weiss, S.I., Larson, L.T., and McKee, E.H., 1988, Timber Mountain magmato-thermal event: an intense widespread culmination of magmatic and hydrothermal activity at the SW Nevada volcanic field, Geol. Soc. Am. Abstr. Programs, v. 20, p. 171.

Jorgensen, D. K., Rankin, J. W., and Wilkins, J., Jr., 1989, The geology, alteration and mineralogy of the Bullfrog gold deposit, Nye County, Nevada: Soc. Mining Eng. Preprint 89-135, 13 p.

Kane, M.F., and Bracken, R.E., 1983, Aeromagnetic map of Yucca Mountain and surrounding regions, southwest Nevada: U.S. Geological Survey Open-File Report 83-616, 19 p.

Kane, M.F., Webring, M.W., and Bhattacharyya, B.K., 1981, A preliminary analysis of gravity and aeromagnetic surveys of the Timber Mountain areas, southern Nevada: U.S. Geological Survey Open-File Report 81-189, 40 p.

Keith, J. D., Dallmeyer, R. D., Kim, Choon-Sik, and Kowallis, B. J., 1991, The volcanic history and magmatic sulfide mineralogy of latites of the central East Tintic Mountains, Utah: *in* Raines, G. L., Lisle,R. E., Shafer, R. W., and Wilkinson, W. W., eds., Geology and ore deposits of the Great Basin: Symposium Proceedings, Geol. Soc. of Nevada, p. 461-483.

Kistler, R.W., 1968, Potassium-argon ages of volcanic rocks on Nye and Esmeralda Counties, Nevada: Geological Society of America Memoir 110, P. 251-263.

Knopf, A., 1915, Some cinnabar deposits in western Nevada: U.S. Geological Survey Bulletin 620-D, p. 59-68.

Kral, V.E., 1951, Mineral resources of Nye County, Nevada: University of Nevada Bulletin, v. 45, no. 3, Geological and Mining Series 50, 223 p..

Kullerude, G., and Yoder, H.S., 1959, Pyrite stability relations in the Fe-S sytem: Economic Geology, v. 54, p. 533-572.

Lahoud, R.G., Lobmeyer, D.H. and Whitfield, M.S., 1984, Geohydrology of volcanic tuff penetrated by test well UE-25b#1, Yucca Mountain, Nye County, Nevada: U.S. Geological Survey Water-Resources Investigations 84-4253, 49 p.

Larson, L. T., Noble, D. C., and Weiss, S. I., 1988, Task 3 report for January, 1987 - June, 1988: Volcanic geology and evaluation of potential mineral and hydrocarbon resources of the Yucca Mountain area: unpublished report to the Nevada Nuclear Waste Project Office, Carson City, Nevada.

Le Bas, M. J., Le Maitre, R. W., Streckheisen, A., and Zenettin, B., 1986, A chemical classification of volcanic rocks based on the total alkali-silica diagram: Journal of Petrology, v. 27, p. 745-750.

Lincoln, F.C., 1923, Mining districts and mineral resources of Nevada: Reno, Nevada, Nevada Newsletter Publishing Co., Reno, 295 p.

Lipman, P.W., Christiansen, R.L., and O'Connor, J.T., 1966, A compositionally zoned ash-flow sheet in southern Nevada: U.S. Geological Survey Professional Paper 524-F, p. F1-F47.

Lipman, P.W., and McKay, E.J., 1965, Geologic map of the Topopah Spring SW quadrangle, Nevada: U.S. Geological Survey Geologic Quadrangle Map GQ-439, 1:24,000 scale.

Lipman, P.W., Quinlivan, W.D., Carr, W.J., and Anderson, R.E., 1966, Geologic map of the Thirsty Canyon SE quadrangle, Nye County, Nevada: U.S. Geological Survey Geologic Quadrangle Map GQ-489, 1:24,000 scale.

Lobmeyer, D.H., Whitfield, M.S., Lahoud, R.G., and Bruckheimer, L., 1983, Geohydrologic data for test well UE-25bH, Nevada Test Site, Nye County, Nevada: U.S. Geological Survey Open-File Report 83-855, 54 p.

Luedke, R.G., and Smith, R.L., 1981, Map showing distribution, composition, and age of late Cenozoic volcanic centers in California and Nevada: U.S. Geological Survey Miscellaneous Investigation Series, I-1091-C, 2 sheets.

Maldonado, F., 1985, Late Tertiary detachment faults in the Bullfrog Hills, southwestern Nevada: Geol. Soc. Am. Abstr. Programs, 17, p. 651.

Maldonado, F., 1988, Geometry of normal faults in the upper plate of a detachment fault zone, Bullfrog Hills, southern Nevada: Geological Society of America, Abstracts with Programs, v. 20, P. 178.

Maldonado, F, 1990, Structural geology of the upper plate of the Bullfrog Hills detachment fault system, southern Nevada: Geological Society of America Bulletin, v. 102, p. 992-1006.

Maldonado, F, and Hausback, B.P., 1990, Geologic map of the northeastern quarter of the Bullfrog 15-minute quadrangle, Nye County, Nevada: U.S. Geological Survey Misc. Investigations Series Map I-2049, 1:24,000.

Maldonado, F, and Koether, S.L., 1983, Stratigraphy, structure, and some petrographic features of Tertiary volcanic rocks at the USW G-2 drill hole, Yucca Mountain, Nye County, Nevada: U.S. Geological Survey Open-File Report 83-732, 83 p.

Maldonado, F, Muller, D.C., and Morrison, J.N., 1979, Preliminary geologic and geophysical data of the UE25a-3 exploratory drill hole, Nevada Test Site, Nevada: U.S. Geological Survey Report, USGS-1543-6, 47 p.; available only from U.S. Department of Commerce, National Technical Information Service, Springfield, VA 22161.

Maldonado, Florian, Muller, D.C., and Morrison, J.N., 1979, Preliminary geologic and geophysical data of the UE25a-3 exploratory drill hole, Nevada Test Site, Nevada: U.S. Geological Survey Open-File Report 81-522.

Mapa, M.R., 1990 Geology and mineralization of the Mother Lode mine, Nye County, Nevada, *in* Hillmeyer, F., Wolverson, N., and Drobeck, P., 1990 spring fieldtrip guidebook, Volcanic-hosted gold deposits and structural setting of the Mohave region: Reno, Geol. Soc. Nevada, 4 p.

Marti, J., Diez-Gil, J. L., and Ortiz, R., 1991, Conduction model for the thermal influence of lithic clasts in mixtures of hot gases and ejecta: Journal of Geophysical Research, v. 96, p. 21,879-21,885.

Marvin, R.F., Byers, F.M., Mehnert, H.H., Orkild, P.P, and Stern, T.W., 1970, Radiometric ages and stratigraphic sequence of volcanic and plutonic rocks, southern Nye and western Lincoln Counties, Nevada: Geological Society of America Bulletin, v. 81, p. 2657-2676.

Marvin, R. F., and Cole, J. C., 1978, Radiometric ages: Compilation A, U.S. Geological Survey: Isochron/West, no. 22, p. 3-14.

Marvin, R. F., Mehnert, H. H., and Naeser, C. W., 1989, U.S. Geologic Survey radiometric ages - compilation "C", part 3: California and Nevada: Isochron/West, no. 52, p. 3-11.

McKague, H.L. and Orkild, P.P., 1984, Geologic Framework of the Nevada Test Site: Geological Society of America, Abstracts with Programs, v. 16, p. 589.

McKay, E.J., 1963, Hydrothermal alteration in the Calico Hills, Jackass Flats quadrangle, Nevada Test Site: U.S. Geological Survey Technical Letter NTS-43, 6 p.

McKay, E.J., and Sargent, K.A., 1970, Geologic map of the Lathrop Wells quadrangle, Nye County, Nevada: U.S. Geological Survey Geologic Quadrangle Map GQ-883, 1:24,000 scale.

McKay, E.J., and Williams, W.P., 1964, Geology of Jackass Flats quadrangle, Nevada Test Site, Nevada: U.S. Geological Survey Geologic Quadrangle Map GQ-368, 1:24,000 scale.

McKee, E.H., 1983, Reset K-Ar ages: evidence for three metamorphic core complexes, western Nevada: Isocron/West, no.38, p 17-20.

McKee, E. H., and Bergquist, J. M., 1993, New radiometric ages related to alteration and mineraliztion in the vicinity of Yucca Mountain, Nye County, Nevada: U. S. Geological Survey Open-file Report 93-538, 26 pp.

McKee, E. H., Noble, D. C., and Weiss, S. I., 1989, Very young silicic volcanism in the southwestern Great Basin: The late Pliocene Mount Jackson dome field, SE Esmeralda County, Nevada: EOS, Trans. Am. Geophys. Union., v. 70, p. 1420.

McKee, E. H., Noble, D. C., and Weiss, S. I., 1990, Late Neogene volcanism and tectonism in the Goldfield segment of the Walker Lane belt: Geological Society of America Abstracts with Programs, v. 22, p. 66.

Miller, D.C. and Kibler, J.E., 1984, Preliminary analysis of geological logs from drill hole UE-25p#1, Yucca Mountain, Nye County, Nevada: U.S. Geological Survey Open-File Report 84-649, 17 p.

Mills, J.G., Jr., and Rose, T.P., 1986, Geochemistry of glassy pumices from the Timber Mountain Tuff, southwestern Nevada: EOS (American Geophysical Union Transactions), v. 67, p. 1262.

Monsen, S.A., Carr, M.D., Reheis, M.C., and Orkild, P.P., 1990, Geologic map of Bare Mountain, Nye County Nevada: U.S. Geological Survey Open-file Report 90-25, 1:24,000.

Monsen, S.A., Carr, M.D., Reheis, M.C., and Orkild, P.P., 1992, Geologic map of Bare Mountain, Nye County Nevada: U.S. Geological Survey Miscellaneous Investigations Map I-2201, 1:24,000.

Morton, J. L., Silberman, M. L., Bonham, H. F., Garside, L. J., and Noble, D. C., 1977, K-Ar ages of volcanic rocks, plutonic rocks, and ore deposits in Nevada and eastern California - Determinations run under the USGS-NBMG cooperative program: Isochron/West, n. 20, p. 19-29.

Noble, D. C., and Christiansen, R. L., 1974, Black Mountain volcanic center, in Guidebook to the geology of four Tertiary volcanic centers in central Nevada: Nevada Bur. Mines Geol. Rept. 19, p. 22-26.

Noble, D. C., McKee, E. H., and Weiss, S. I., 1988, Nature and timing of pyroclastic and hydrothermal activity and mineralization at the Stonewall Mountain volcanic center, southwestern Nevada: Isochron/West, No. 51, p. 25-28.

Noble, D. C., Weiss, S. I., and Green, S. M., 1989, High-salinity fluid inclusions suggest that Miocene gold deposits of the Bare Mtn. district, NV, are related to a large buried rare-metal rich magmatic system: Geological Society of America Abs. with Programs, v. 21, p. 123.

Noble, D. C., Weiss, S. I., and McKee, E. H., 1990a, Style, timing, distribution, and direction of Neogene extension within and adjacent to the Goldfield section of the Walker Lane structural belt: EOS, Trans. American Geophysical Union, v. 71, p. 618-619.

Noble, D. C., Weiss, S. I., and McKee, E. H., 1990b, Magmatic and hydrothermal activity, caldera geology and regional extension in the western part of the southwestern Nevada volcanic field: Great Basin Symposium, Program with Abstracts, Geology and ore deposits of the Great Basin, Geol. Soc. of Nevada, Reno, p. 77.

Noble, D. C., Weiss, S. I., and McKee, E. H., 1991a, Magmatic and hydrothermal activity, caldera geology, and regional extension in the western part of the southwestern Nevada volcanic field: *in* Raines, G. L., Lisle,R. E., Shafer, R. W., and Wilkinson, W. W., eds., Geology and ore deposits of the Great Basin: Symposium Proceedings, Geol. Soc. of Nevada, p. 913-934.

Noble, D. C., Worthington, J. E., and McKee, E. H., 1991b, Geologic and tectonic setting and Miocene volcanic stratigraphy of the Gold Mountain-Slate Ridge area, southwestern Nevada: Geol. Soc. America Abstr. with Prog., v. 23, p. A247.

Noble, D. C., Sargent, K. A., Ekren, E. B., Mehnert, H. H., and Byers, F. M., Jr., 1968, Silent Canyon volcanic center, Nye County, Nevada: Geological Society of America Spec. Paper 101, p. 412-413.

Noble, D.C., Vogel, T. A., Weiss, S.I., Erwin, J.W., McKee, E.H., and Younker, L.W., 1984, Stratigraphic relations and source areas of ash-flow sheets of the Black Mountain and Stonewall Mountain volcanic centers, Nevada: Journal of Geophysical Research, v. 89, p. 8593-8602.

Norberg, J.R., 1977, Mineral Resources in the vicinity of the Nellis Air Force Base and the Nellis Bombing and Gunnery Range, Clark, Lincoln, and Nye Counties, Nevada: U.S. Bureau of Mines Unpublished Report, 112 p.

Orkild, P.P., 1968, Geologic map of the Mine Mountain quadrangle, Nye County, Nevada: U.S. Geological Survey Geologic Quadrangle Map GQ-746, 1:24,000 scale.

Orkild, P.P., and O'Connor, J.T., 1970, Geologic map of the Topopah Springs quadrangle, Nye County, Nevada: U.S. Geological Geologic Quadrangle Map GQ-849, 1:24,000 scale.

Odt, D. A., 1983, Geology and geochemistry of the Sterling gold deposit, Nye County, Nevada: Unpub. M.S. thesis, Univ. Nevada-Reno, 91 p.

Papike, J. J., Keith, T. E. C., Spilde, M. N., Galbreath, K. C., Shearer, C. K., and Laul, J. C., 1991, Geochemistry and mineralogy of fumarolic deposits, Valley of Ten Thousand Smokes, Alaska: bulk chemical and mineralogical evolution of dacite-rich protolith: American Mineralogist, v. 76, p. 1662-1673.

Papke, K.G., 1979, Fluorspar in Nevada: Nevada Bureau of Mines and Geology, Bulletin 93, 77 p.

Ponce, D.A., 1981, Preliminary gravity investigations of the Wahmonie site, Nevada Test Site, Nye County, Nevada: U.S. Geological Survey Open-File Report 81-522, 64 p.

Ponce, D.A., 1984, Gravity and magnetic evidence for a granitic intrusion near Wahmonie site, Nevada Test Site, Nevada, Journal of Geophysical Research, v. 89, p. 9401-9413.

Ponce, D.A., Wu, S.S. and Speilman, J.B., 1985, Comparison of survey and photogrammetry methods to positive gravity data, Yucca Mountain, Nevada: U.S. Geological Survey Open-File Report 85-36, 11 p.

Poole, F.G., 1965, Geologic map of the Frenchman Flat quadrangle, Nye, Lincoln, and Clark Counties, Nevada: U.S. Geological Survey Geological Quadrangle Map GQ-456, 1:24,000 scale.

Poole, F.G., Carr, W.J., and Elston, D.P., 1965, Salyer and Wahmonie Formations of southeastern Nye County, Nevada: U.S. Geological Survey Bulletin 1224-A, p. A44-A51.

Poole, F.G., Elston, D.P., and Carr, W.J., 1965, Geologic map of the Cane Spring quadrangle, Nye County, Nevada: U.S. Geological Survey Geological Quadrangle Map GQ-455, 1:24,000 scale.

Powers, P.S. and Healey, D.L., 1985, Free-air gradient observations in Yucca Flat, Nye County, Nevada: U.S. Geological Survey Open-File Report 85-530, 18 p.

Quade, J., and Tingley, J.V., 1983, A mineral inventory of the Nevada Test Site and portions of the Nellis Bombing and Gunnery Range, southern Nye County, Nevada: DOE/NV/10295-1, U.S. Department of Energy, Las Vegas.

Quade, J., and Tingley, J.V., 1984, A mineral inventory of the Nevada Test Site, and portions of Nellis Bombing and Gunnery Range southern Nye County, Nevada: Nevada Bureau of Mines and Geology Open File Report 82-2, 40 p. plus sample descriptions and chemical analyses.

Quade, J., and Tingley, J.V., 1986a, Mineral inventory and geochemical survey Groom Mountain Range Lincoln County, Nevada: Nevada Bureau of Mines and Geology Open File Report 86-9, 66 p. plus sample descriptions and chemical analyses.

Quade, J., and Tingley, J.V., 1986b, Mineral inventory and geochemical survey appendices F., G., & H Groom Mountain Range, Lincoln County, Nevada: Nevada Bureau of Mines and Geology Open File Report 86-10.

Quinlivan, W.D., and Byers, F.M., Jr., 1977, Chemical data and variation diagrams of igneous rock from the Timber Mountain-Oasis Valley caldera complex, southern Nevada: U.S. Geological Survey Open-File Report 77-724, 9 p.

Ramelli, A. R., Bell, J. W., and dePolo, C. M., Late Quaternary faulting at Crater Flat and Yucca Mountain, southern Nevada: Nevada Bureau of Mines and Geology (in review).

Raney, R. G., and Wetzel, N., Natural resource assessment methodologies for the proposed high-level nuclear waste repository at Yucca Mountain, Nye County, Nevada: U.S. Bureau of Mines report NRC FIN D1018, prepared for the Office of Nuclear Safety and Safeguards, U.S. Nuclear Regulatory Commission, 353 p.

Ransome, F.L., 1907, Preliminary account of Goldfield, Bullfrog, and other mining districts in southern Nevada: U.S. Geological Survey Bulletin 303, 98 p.

Ransome, F.L., Emmons, W.H., and Garrey, G.H., 1910, Geology and ore deposits of the Bullfrog district, Nevada: U.S. Geological Survey Bulletin 407, 130 p.

Reno Gazette-Journal, June 19, 1988, Gold report is favorable: Business page, Gold, J., Business editor.

Rhiele, J. R., 1973, Calculated compaction profiles of rhyolitic ash-flow tuffs: Geological Society of America Bulletin, v. 84, p. 2193-2216.

Richards, J. P., and McDougall, I., 1990, Geochronology of the Porgera gold deposit, Papua New Guinea: resolving the effects of excess argon on K-Ar and $^{40}Ar/^{39}Ar$ age estimates for magmatism and mineralization: Geochimica et Cosmochimica Acta, v. 54, p. 1397-1415.

Robinson, G.D., 1985, Structure of pre-Cenozoic rocks in the vicinity of Yucca Mountain, Nye County, Nevada; a potential nuclear-waste disposal site: U.S. Geological Survey Bulletin 1647, 22 p.

Rowe, J. J., and Simon, F. O., 1968, The determination of gold in geologic materials by neutron-activation analysis using fire assay for the radiochemical separations: U. S. Geological Survey Circular 559, 4 p.

Rush, F.E., Thordason, William, and Bruckheimer, Laura, 1983, Geohydrologic and drill-hole data for test well USW-H1, adjacent to Nevada Test Site, Nye County, Nevada: U.S. Geological Survey Open-File Report 83-141, 38 p.

Sander, M. V., 1988, Epithermal gold-silver mineralization, wall-rock alteration and geochemical evolution of hydrothermal fluids in the ash-flow tuff at Round Mountain, Nevada: Unpublished PhD. dissertation, Stanford University, Stanford, California, 283 p.

Sander, M. V., 1990, The Round Mountain gold-silver deposit, Nye County, Nevada: Geol. Soc. Nevada Symposium, Geology and Ore Deposits of the Great Basin, Field Trip Guidebook # 11, p. 108-121.

Sawyer, D. A., and Sargent, K. A., 1989, Petrologic evolution of divergent peralkaline magmas from the Silent Canyon caldera complex, southwestern Nevada volcanic field: Journal of Geophysical Research, v. 94, p. 6021-6040.

Sawyer, D. A., Fleck, R. J., Lanphere, M. A., Warren, R. G., and Broxton, D. E., 1990, Episodic volcanism in the southwest Nevada volcanic field: new $^{40}Ar/^{39}Ar$ geochronologic results: EOS, Transactions of the American Geophysical Union, v. 71, p. 1296.

Sawyer, D. A., Fleck, R. J., Lanphere, M. A., Warren, R. G., Broxton, D. E., and Hudson, M. R., 1994, Episodic caldera volcanism in the Miocene southwestern Nevada volcanic field: revised stratigraphic framework, $^{40}Ar/^{39}Ar$ geochronology, and implications for magmatism and extension: Geological Society of America Bulletin, *in press*.

Schoen, R., White, D.E., and Hemley, J.J., 1974, Argillization by decending acid at Steamboat Springs, Nevada: Clays and Clay Minerals, v. 22, p. 1-22.

Schneider, R. and Trask, N.J., 1984, U.S. Geological Survey research in radioactive waste disposal; fiscal year 1982: U.S. Geological Survey Water-Resource Investigation 84-4205, 116 p.

Schuraytz, B.C., Vogel, T.A., and Younker, L.W., 1986, Evolution of a magmatic system. Part I: Geochemistry and mineralogy of the Topopah Spring Member of the Paintbrush Tuff, southern Nevada: EOS, Transactions of the American Geophysical Union, v. 67, p. 1261.

Scott, R.B., 1984, Internal deformation of blocks bounded by basin-and-range-style faults: Geological Society of America, Abstracts with Programs, v. 16, p. 649.

Scott, R.B., 1986a, Rare-earth element evidence for changes in chemical evolution of silicic magmas, southwest Nevada: Transactions of the American Geophysical Union, v. 67, p. 1261.

Scott, R. B., 1986b, Extensional tectonics at Yucca Mountain, southern Nevada [abs.]: Geological Society of America Abs. with Programs, v. 18, p. 411.

Scott, R.B., 1988, Tectonic setting of Yucca Mountain, southwest Nevada: Geological Society of America, Abstracts with Programs, v. 20, p. 229.

Scott, R.B. and Bonk, J., 1984, Preliminary geologic map of Yucca Mountain, Nye County, Nevada, with geologic sections: U.S. Geological Survey Open-File Report 84-494, scale 1:12,000, plus 10 p.

Scott, R.B. and Castellanos, Mayra, 1984, Stratigraphic and structural relations of volcanic rocks in drill holes USW GU-3 and USW G3, Yucca Mountain, Nye County, Nevada: U.S. Geological Survey Open-File Report 84-491, 121 p.

Scott, R. B., and Whitney, J. W., 1987, The upper crustal detachment system at Yucca Mountain, SW Nevada [abs.]: Geological Society of America Abs. with Programs, v. 19, p. 332-333.

Scott, R.B., Byers, F.M. and Warren, R.G., 1984, Evolution of magma below clustered calderas, Southwest Nevada volcanic field [abstr.], EOS, Transactions of the American Geophysical Union, v.65, p. 1126-1127.

Scott, R.B., Spengler, R.W., Lappin, A.R., and Chornack, M.P., 1982, Structure and intracooling unit zonation in welded tuffs of the unsaturated zone, Yucca Mountain, Nevada, a potential nuclear waste repository: EOS, Transactions of the American Geophysical Union, v. 63, no. 18, p. 330.

Scott, R.B., Spengler, R.W., Diehl, S., Lappin, A.R., and Chornack, M.P., 1983, Geologic character of tuffs in the unsaturated zone at Yucca Mountain, southern Nevada: in Mercer, J.M., Rao, P.C. and Marine, W., eds., Role of the unsaturated zone in radioactive and hazardous waste disposal: Ann Arbor press, Ann Arbor, Michigan, p. 289-335.

Scott, R.B., Bath, G.D., Flanigan, V.J., Hoover, D.B., Rosenbaum, J.G., and Spengler, R.W., 1984, Geological and geophysical evidence of structures in northwest-trending washes, Yucca Mountain, southern Nevada, and their possible significance to a nuclear waste repository in the unsaturated zone: U.S. Geological Survey Open-File Report 84-567, 25 p.

Selner, G.I. and Taylor, R.B., 1988, GSDRAW and GSMAP version 5.0: prototype programs, level 5, for the IBM PC and compatible microcomputers, to assist compilation and publication of geologic maps and illustrations: U.S. Geological Survey Open File Report #88-295A (documentation), 130 p. and #88-295B (executable program disks).

Selner, G.I., Smith, C.L., and Taylor, R.B., 1988, GSDIG: a program to determine latitude/longitude locations using a microcomputer (IBM PC or compatible) and digitizer: U.S. Geological Survey Open File Report #88-014A (documentation) 16 p. and #88-014B (executable program disk).

Smith, C., Ross, H.P., and Edquist, R., 1981, Interpreted resistivity and IP section line W1 Wahmonie area, Nevada Test Site, Nevada: U.S. Geological Survey Open-File Report 81-1350, 14 p.

Smith, R.C., and Bailey, R.A., 1968, Resurgent Cauldrons: Geological Society of America Memoir 116, p. 613-662.

Smith, R.M., 1977, Map showing mineral exploration potential in the Death Valley quadrangle, California and Nevada: U.S. Geological Survey Miscellaneous Field Investigation Map MF-873, 1:250,000 scale.

Snyder, D.B., and Oliver, H.W., 1981, Preliminary results of gravity investigations of the Calico Hills, Nevada Test Site, Nye County, Nevada: U.S. Geological Survey Open-File Report 81-101, 42 p.

Snyder, D.B., and Carr, W.J., 1982, Preliminary results of gravity investigations at Yucca Mountain and vicinity, southern Nye County, Nevada: U.S. Geological Survey Open-File Report 82-701, 36 p.

Snyder, D.B. and Carr, W.J., 1984, Interpretation of gravity data in a complex volcano-tectonic setting, southwestern Nevada: Journal of Geophysical Research. B, v. 89, p. 10,193-10,206.

Spengler, R.W., Byers, F.M., Jr., and Warner, J.B., 1981, Stratigraphy and structure of volcanic rocks in drill hole USW-G1, Yucca Mountain, Nye County, Nevada: U.S. Geological Survey Open-File Report 82-1338, 264 p.

Spengler, R.W. and Chornack, M.P., 1984, Stratigraphic and structural characteristics of volcanic rocks in core hole USW G-4, Yucca Mountain, Nye County, Nevada: U.S. Geological Survey Open-File Report 84-789, 82 p.

Spengler, R.W., Muller, D.C., and Livermore, R.B., 1979, Preliminary report on the geology of drill hole UE25a-1, Yucca Mountain, Nevada Test Site: U.S. Geological Survey Open-File Report 79-1244, 43 p.

Spengler, R.W., and Rosenbaum, J.G., 1980, Preliminary interpretations of geologic results obtained from boreholes UE25a-4, -5, -6, and -7, Yucca Mountain, Nevada Test Site: U.S. Geological Survey Open-File Report 80-929, 35 p.

Spengler, R.W., and Rosenbaum, J.G., 1991, A low-angle breccia zone of hydrologic significance at Yucca Mountain, Nevada: Geological Society of America, Abstracts with Programs, v. 23, p. A119.

Stewart, J. H., 1988, Tectonics of the Walker Lane belt, western Great Basin-Mesozoic and Cenozoic deformation in a zone of shear, *in* Ernst, W. G., ed., Metamorphism and crustal evolution of the western United States, Rubey Vol. VII: Englewood Cliffs, New Jersey, Prentice Hall, p. 683-713.

Stuckless, J. S., Peterman, Z. E. and Muhs, D. R., 1991, U and Sr isotopes in groundwater and calcite, Yucca Mountain, Nevada: evidence against upwelling water: Science, v. 254, p. 551-554.

Sutton, V.D., 1984, Data report for the 1983 seismic-refraction experiment at Yucca Mountain, Beatty, and vicinity, southwestern Nevada: U.S. Geological Survey Open-File Report 84-661, 62 p.

Swadley, W.C., Hoover, D.L. and Rosholt, J.N., 1984, Preliminary report on late Cenozoic faulting and stratigraphy in the vicinity of Yucca Mountain, Nye County, Nevada: U.S. Geological Survey Open-File Report 84-788, 44 p.

Swolfs, H.S. and Savage, W.Z., 1985, Topography, stresses and stability at Yucca Mountain, Nevada, Proceedings - Symposium on Rock Mechanics: Research and engineering applications in rock masses, 26, p. 1121-1129.

Szabo, B.J. and Kyser, T.K., 1985, Uranium, thorium isotopic analyses and uranium-series ages of calcite and opal, and stable isotopic compositions of calcite from drill cores UE25a 1, USW G-2 and USW G-3/GU-3, Yucca Mountain, Nevada: U.S. Geological Survey Open-File 85-224, 30 p.

Szabo, B. J., and Kyser, T. K., 1990, Ages and stable-isotope compositions of secondary calcite and opal in drill cores from Tertiary volcanic rocks of the Yucca Mountain area, Nevada: Geological Society of America Bulletin, v. 102, p. 1714-1719.

Szabo, B.J. and O'Malley, P.A., 1985, Uranium-series dating of secondary carbonate and silica precipitates relating to fault movements in the Nevada Test Site region and of caliche and travertine samples from the Amargosa Desert: U.S. Geological Survey Open-File Report 85-0047, 17 p.

Taylor, E.M., and Huckins, H.E., 1986, Carbonate and opaline silica fault-filling in the Bow Ridge Fault, Yucca Mountain, Nevada -- deposition from pedogenic processes of upwelling ground water: Geological Society of America, Abstracts with Programs, v. 18, no. 5, p. 418.

Thordarson, William, Rush, F.E. , Spengler, R.W. and Waddell, S.J., 1984, Geohydrologic and drill-hole data for test well USW H-3, Yucca Mountain, Nye County, Nevada: U.S. Geological Survey Open-File Report 84-0149, 54 p.

Tingley, J.V., 1984, Trace element associations in mineral deposits, Bare Mountain (Fluorine) mining district, southern Nye County, Nevada: Nevada Bureau of Mines and Geology Report 39, 28 p.

Turrin, B. D., Champion, D., and Fleck, R. J., 1991, $^{40}Ar/^{39}Ar$ age of the Lathrop Wells volcanic center, Yucca Mountain Nevada: Science, v. 253, p. 654-657.

U.S. Department of Energy, 1986, Environmental Assessment Yucca Mountain Site, Nevada Research and Development Area, Nevada, v. 1: Washington, DC, Office of Civilian Radioactive Waste Management.

U.S. Department of Energy, 1988a, Consultation Draft Site Characterization Plan, Yucca Mountain Site, Nevada Research and Development Area, Nevada: Washington, DC,Office of Civilian Radioactive Waste Management, 347 p.

U.S. Department of Energy, 1988b, Site Characterization Plan, Yucca Mountain Site, Nevada Research and Development Area, Nevada: Washington, DC,Office of Civilian Radioactive Waste Management.

U.S. Geologic Survey, 1984, A summary of geologic studies through January 1, 1983 of a potential high-level radioactive waste repository site at Yucca Mountain, southern Nye County, Nevada: U.S. Geological Survey Open-File Report 84-792, 164 p.

Vaniman, D. T., 1991, Calcite, opal, sepiolite, ooids, pellets, and plant/fungal traces in laminar-fabric fault fillings at Yucca Mountain Nevada: Geological Society of America, Abstracts with Programs, v. 23, p. 117.

Vaniman, D.T., and Crowe, B.M., 1981, Geology and petrology of the basalts of Crater Flat: Applications to volcanic risk assessment for the Nevada nuclear waste storage investigations: Los Alamos, New Mexico, Los Alamos National Laboratory Report, LA-8845-MS, 67 p.

Vaniman, D.T., Crowe, B.M., and Gladney, E.S., 1982, Petrology and geochemistry of Hawaiite lavas from Crater Flat, Nevada: Contributions to Mineralogy and Petrology, v. 80, p. 341-357.

Vaniman, D.T., Bish, D.L., and Chipera, S., 1988, A preliminary comparison of mineral deposits in faults near Yucca Mountain, Nevada, with possible analogs: Los Alamos, New Mexico, Los Alamos National Laboratory Report LA-11298-MS, UC-70, 54 p.

Vaniman, D.T., Bish, D., Broxton, D., Byers, F., Heiken, G., Carlos, B., Semarge, E., Caporuscio, F., and Gooley, R., 1984, Variations in authigenic mineralogy and sorptive zeolite abundance at Yucca Mountain, Nevada, based on studies of drill cores USW GU-3 and G-3.

Vogel, T. A., Noble, D. C., and Younker, L. W., 1989, Evolution of a chemically zoned magma body: Black Mountain volcanic center, southwestern Nevada: Journal of Geophysical Research, v. 94, p. 6041-6058.

Vogel, T.A., Ryerson, R.A., Noble, D.C., and Younker, L.W., 1987, Constrains on magma mixing in a silicic magma body: disequilibrium phenocrysts in pumices from a chemically zoned ash-flow sheet: Journal of Geology, v. 95, in press.

Waddell, R.J., 1984, Geohydrologic and drill-hole data for test wells UE-29a#1 and UE-29a#2, Fortymile Canyon, Nevada Test Site: U.S. Geological Survey Open-File Report 84-0142, 25 p.

Wang, J.S.Y., and Narasimhan, T.N., 1985, Hydrologic mechanisms governing fluid flow in partially saturated, fractured, porous tuff at Yucca Mountain: University of California Lawrence Berkeley Laboratory Report SAND84-7202 (LBL-18473), 46 p.

Warren, R.G., and Broxton, D.E., 1986, Mixing of silcic and basaltic magmas in the Wahmonie Formation, southwestern Nevada volcanic field, Nevada: EOS (American Geophysical Union Transactions), v. 67, p. 1261.

Warren, R.G., Byers, F.M., and Caporuscio, F.A., 1984, Petrography and mineral chemistry of units of the Topopah Springs, Calico Hills and Crater Flat Tuffs, and some older volcanic units, with emphasis on samples from drill hole USW G-1, Yucca Mountain, Nevada Test site: Los Alamos, New Mexico, Los alamos National Laboratory Report LA-10003-MS.

Warren, R.G., Nealey, L.D., Byers, F.M., Jr., and Freeman, S.H., 1986, Magmatic components of the Rainier Mesa Member of the Timber Mountain Tuff, Timber Mountain-Oasis Valley Caldera Complex: EOS (American Geophysical Union Transactions), v. 67, p. 1260.

Warren, R. G., Byers, F. M., Jr., Broxton, D. E., Freeman, S. H., and Hagan, R. C., 1989, Phenocryst abundances and glass and phenocryst compositions as indicators of mag-

matic environments of large-volume ash flow sheets in southwestern Nevada: Journal of Geophysical Research, v. 94, p. 5987-6020.

Warren, R.G., McDowell, F.W., Byers, F.M., Broxton, D.E., Carr, W.J., and Orkild, P.P., 1988, Eposodic leaks from Timber Mountain caldera: new evidence from rhyolite lavas of Fortymile Canyon, southwestern Nevada Volcanic Field: Geological Society of America, Abstracts with Programs, v. 20, p. 241.

Weiss, S.I., 1987, Geologic and Paleomagnetic studies of the Stonewall and Black Mountain volcanic centers, southern Nevada: University of Nevada, Reno-Mackay School of Mines, Reno, Nevada, unpublished MSc Thesis, 67 p.

Weiss, S.I., and Noble, D.C., 1989, Stonewall Mountain volcanic center, southern Nevada: stratigraphic, structural and facies relations of outflow sheets, near-vent tuffs, and intracaldera units: Journal of Geophysical Research, v. 94, 6059-6074.

Weiss, S.I., Noble, D.C., and Mckee, E.H.,1984, Inclusions of basaltic magma in near-vent facies of the Stonewall Flat Tuff: product of explosive magma mixing: Geological Society of America, Abstracts with Programs, v. 16, p. 689.

Weiss, S. I., Noble, D. C., and McKee, E. H., 1988, Volcanic and tectonic significance of the presence of late Miocene Stonewall Flat Tuff in the vicinity of Beatty, Nevada: Geological Society of America Abs. with Programs, v. 20, p. A399.

Weiss, S. I., Noble, D. C., and McKee, E. H., 1989, Paleomagnetic and cooling constraints on the duration of the Pahute Mesa-Trail Ridge eruptive event and associated magmatic evolution, Black Mountain volcanic center, southwestern Nevada: Journal of Geophysical Research, v. 94, p. 6075-6084.

Weiss, S. I., Noble, D. C., and Larson, L. T., 1989, Task 3: Evaluation of mineral resource potential, caldera geology and volcano-tectonic framework at and near Yucca Mountain; report for July, 1988 - September, 1989: Center for Neotectonic Studies, University of Nevad-Reno, 38 p. plus appendices.

Weiss, S. I., Noble, D. C., and Larson, L. T., 1990, Task 3: Evaluation of mineral resource potential, caldera geology and volcano-tectonic framework at and near Yucca Mountain; report for October, 1989 - September, 1990: Center for Neotectonic Studies, University of Nevad-Reno, 29 p. plus appendices.

Weiss, S. I., Noble, D. C., and Larson, L. T., 1991a, Task 3: Evaluation of mineral resource potential, caldera geology and volcano-tectonic framework at and near Yucca Mountain; report for October, 1990 - September, 1991: Center for Neotectonic Studies, University of Nevad-Reno, 37 p. plus appendices.

Weiss, S. I., Noble, D. C., and Larson, L. T., 1992, Task 3: Evaluation of mineral resource potential, caldera geology and volcano-tectonic framework at and near Yucca Mountain; report for October, 1991 - September, 1992: Center for Neotectonic Studies, University of Nevad-Reno, 44 p. plus appendices.

Weiss, S. I., Noble, D. C., and Larson, L. T., 1993a, Task 3: Evaluation of mineral resource potential, caldera geology and volcano-tectonic framework at and near Yucca Mountain; report for October, 1992 - September, 1993: Center for Neotectonic Studies, University of Nevad-Reno, 41 p. plus appendices.

Weiss, S. I., Ristorcelli, S. J., and Noble, D. C., 1993b, Mother Lode gold deposit, southwestern Nevada: another example of Carlin-type mineralization associated with porphyry magmatism: Geological Society of America Abstracts with Programs, v. 25, p. 161.

Weiss, S. I., Noble, D. C., and Larson, L. T., 1994, Potential for undiscovered mineral deposits at Yucca Mountain, NV: host rocks, timing and spatial distribution of nearby mineralization [abst]: Geological Society of America Abstracts with Programs, v. 26, p. 311.

Weiss, S. I., Noble, D. C., and Larson, L. T., 1995a, Pyritic ash-flow tuff, Yucca Mountain, Nevada--A discussion: (for submission to Economic Geology).

Weiss, S. I., Connors. K. A., Noble, D. C., and McKee, E. H., 1990, Coeval crustal extension and magmatic activity in the Bullfrog Hills during the latter phases of Timber Mountain volcanism: Geological Society of America Abstracts with Programs, v. 22, p. 92-93.

Weiss, S. I., Noble, D. C., Worthington, J. E., IV., and McKee, E. H., 1993c, Neogene tectonism from the southwestern Nevada volcanic field to the White Mountains, California Part I. Miocene volcanic stratigraphy, paleotopography, extensional faulting and uplift between northern Death Valley and Pahute Mesa: *in* Lahren, M. M., Trexler, J. H., Jr., and Spinosa, C., eds., 1993, Crustal Evolution of the Great Basin and Sierra Nevada: Cordilleran/Rocky Mountain Section, Geological Society of America Guidebook, Department of Geological Sciences, University of Nevada, Reno, p. 353-369.

Weiss, S. I., McKee, E. H., Noble, D. C., Connors, K. A., and Jackson, M. R., 1991b, Multiple episodes of Au-Ag mineralization in the Bullfrog Hills, SW Nevada, and their relation to coeval extension and volcanism: Geological Society of America Abstracts with Programs, v. 23, p. A246.

Weiss, S. I., Noble, D. C., Connors, K. A., Jackson, M. R., and McKee, E. H., 1995b, Multiple episodes of hydrothermal activity and epithermal mineralization in the southwestern Nevada volcanic field and their relations to magmatic activity, volcanism and regional extension: (in revision following formal U.S. Geological Survey review; for submission to Economic Geology).

Wernicke, B. P., Christiansen, R. L., England, P. C., and Sonder, L. J., 1987, Tectonomagmatic evolution of Cenozoic extension of the North America Cordillera, *in* Coward, M. P., Dewey, J. F., and Hancock, P. L., eds., Continental extensional tectonics: Geol. Soc. London Spec. Pub. 28, p. 203-222.

White, A.F., 1979, Geochemistry of ground water associated with tuffaceous rocks, Oasis valley, Nevada: U.S. Geological Survey Professional Paper 712-E.

Whitney, J. A., and Stormer, J. C., Jr., 1983, Igneous sulfides in the Fish Canyon Tuff and the role of sulfur in calc-alkaline magmas: Geology, v. 11., p. 99-102.

Whitfield, M.S., Eshom, E.P., Thordarson, W., and Schaefer, D.H., 1985, Geohydrology of rocks penetrated in test well USW H-4, Yucca Mountain, Nye County, Nevada: U.S. Geological Survey Water-Resources Investigations Reports, 1985, 33 p.

Whitfield, M.S., Thordarson, W. and Eshom, E.P., 1984, Geohydrologic and drill-hole data for test well USW H-4, Yucca Mountain, Nye County, Nevada: U.S. Geological Survey

Worthington, J. E., IV., 1992, Neogene structural and volcanic geology of the Gold Mountain - Slate Ridge area, Esmeralda County, Nevada, unpublished MSc. thesis, Univ. Nevada, Reno, 76 p.

Worthington, J. E., IV., Noble, D. C., and Weiss, S. I., 1991, Structural geology and Neogene extensional tectonics of the Gold Mountain-Slate Ridge area, southwestern Nevada: Geol. Soc. America Abstr. with Prog., v. 23, p. A247.

Wu, S.S., 1985, Topographic Maps of Yucca Mountain area, Nye County, Nevada, 6 oversize sheets, scale 1:5,000: U.S. Geological Survey Open-File Report 85-0620.

Zartman, R. E., and Kwak, L. M., 1991, Lead isotopes in the carbonate-silica veins of Trench 14, Yucca Mountain, Nevada: Geological Society of America, Abstracts with Programs, v. 23, p. 117.

Table 1. Precious Metals and Indicator-Element Concentrations in Rocks from Northwestern Yucca Mountain and Bare Mountain, Nevada
(*Ag and Au values given in ppb, all others in ppm*)

Sample Id	comments	Ag	Au	As	Bi	Cd	Hg	Sb	Se	Te	Cu	Mo	Pb	Zn	Ga	Tl
	Northwestern Yucca Mtn.															
3SW-394A	brep675; opal-qtz vn w/Feox	13.7	0.459	12.7	0.154	0.183	0.677	2.72	-0.246	-0.049	5.58	3.4	8.74	10.6	0.849	1.03
3SW-394B	brep681B; Hbx vn of feox+silica	9.03	-0.198	139.0	0.293	0.562	0.18	8.9	-0.248	-0.05	9.05	1.8	44.8	29.6	2.69	-0.495
3SW-394C	brep681C; Hbx vn of feox+silica	8.22	-0.196	36.2	0.187	0.246	0.099	3.39	-0.245	-0.049	4.02	1.69	23.6	17.6	1.88	1.93
3SW-394D	brep685; silicif siltst, upper ledge	8.5	-0.2	6.59	0.070	0.625	0.233	1.27	-0.25	-0.05	5.16	3.33	4.54	14.3	0.343	4.95
3SW-394E	brep693; "sinter" lower ledge	12.8	-0.198	2.35	0.184	0.132	0.100	0.753	-0.248	-0.05	8.36	4.99	7.8	6.79	0.35	-0.495
3SW-394F	brep697; silicif siltst, upper ledge	7.04	-0.195	5.7	0.256	0.173	0.217	2.05	-0.244	0.057	6.36	8.11	51.9	104	0.329	0.637
X94A	bdup394F(697)	8.18	-0.199	5.5	0.261	0.172	0.229	1.89	-0.248	-0.05	6.09	7.92	50.7	102	0.104	0.667
NEEBM16	Tct w/qtz-opal vnlts	22.6	-0.196	40.0	0.096	0.135	0.041	3.89	-0.245	-0.049	14.0	2.27	16.1	35	1.63	0.829
3SW-717	Tct w/qtz-opal vnlts; bleached	18.5	-2.34	8.01	-0.049	0.063	-0.02	0.584	-0.247	-0.049	8.16	1.21	14	17.8	0.818	-0.494
3SW-719	Silica-Feox Hbx vns in Tct	19.7	-0.198	89.0	0.068	0.215	0.299	6.4	-0.247	-0.049	11.8	1.64	15	42	1.88	-0.495
3SW-721P	silicif silst +opal, upper ledge	8.06	-0.195	4.51	0.091	0.407	0.153	1.12	-0.243	-0.049	1.91	0.959	3.33	13.7	-0.097	1.67
X94C	bdup721S; silicif sltst, upper ledge	13.1	-0.199	5.64	0.130	0.428	0.150	1.32	-0.249	-0.05	12.5	4.45	4.36	22	0.353	1.83
3SW-723P	silicif silst +opal, upper ledge	10.2	0.291	7.63	0.144	0.192	0.091	0.4	-0.242	-0.048	1.73	0.614	22.5	88.5	0.196	1.05
X94D	bdup723S; silicif sltst, upper ledge	13.4	0.26	6.92	0.195	0.199	0.108	0.564	-0.244	-0.049	10.6	2.86	42.8	104	0.277	1.2
X94E	bdup723S; silicif sltst, upper ledge	14.1	0.23	6.79	0.200	0.192	0.107	0.586	-0.246	-0.049	10.5	2.78	41.5	105	0.289	1.18
3SW-725	alt. Tct	20.2	10.5	33.3	0.063	0.076	0.481	2.28	-0.25	-0.05	10.8	1.54	12	27.8	0.841	-0.5
3SW-121	Feox+silica hbx vns in Tc; Windy Wash	22.9	-0.2	5.53	0.088	0.075	0.065	2.14	-0.25	-0.05	8.61	1.25	9.11	22.9	0.793	-0.5
3MJ-184A	arg alt Tcp, head of Windy Wash	-2.93	-0.195	18.0	0.050	0.133	0.234	2.41	-0.244	-0.049	10.9	1.54	8.79	26	1.21	-0.488
3MJ-188	Feox-rich porous tuff	-2.91	-0.194	1.89	0.176	0.059	0.100	1.23	-0.243	-0.049	9.44	1.25	13.9	17.4	0.705	-0.485
	Bare Mountain															
3SW-633	arg alt Tip dike, Tungsten Canyon	11.1	1.06	2.34	-0.050	0.06	0.081	0.639	-0.248	-0.05	7.47	0.833	7.71	45.4	2.18	-0.495
3SW-641	alt Tip dike, Tarantula Canyon	11.8	0.265	2.41	-0.050	-0.02	0.037	0.08	-0.248	-0.05	8.54	1.09	3.48	11.1	0.531	-0.497
3SW-705	Dev ls wallrock <1 m from 641 dike	47.1	1.34	18.1	0.114	0.195	0.251	1.15	0.371	0.056	8.74	14.8	5.22	117	0.193	-0.49
3SW-645	alt Tip dike, Tarantula Canyon	41	-0.197	192.0	0.245	4.16	0.124	8.99	3.57	-0.049	15.2	14.8	14.6	84.6	1.17	-0.491
3SW-649	alt Tip dike N of Tarantula Canyon	11.1	0.398	55.3	0.074	-0.02	-0.020	0.17	-0.249	-0.05	8.04	2.15	4.18	7.55	0.941	-0.497

Table 1 continued

3SW-655A	hbx, margin of dike	24118	1603	163.0	0.153	0.044	5.22	22.4	-0.245	3.56	29.3	11.1	11.5	15.7	0.635	-0.49
3SW-655B	hbx, margin of dike	10488	1381	166.0	0.096	0.084	7.64	20.7	-0.247	2.09	29.1	9.62	16	34	0.241	0.537
872111	fluoritized brecciated Nopah, N pit	-2.96	1158	65.8	0.854	0.028	1.5	53.4	-0.247	0.097	4.76	118.0	5.65	16.6	3.12	1.55
SJH-2	Hbx dike, volc frags, in Pz carbs	164	1.87	4.59	0.134	0.193	0.322	2.76	-0.246	0.336	13.7	5.33	19.7	7.73	0.252	-0.491
SJH-3	Hbx dike, volc frags, in Pz carbs	49.3	0.96	1.24	-0.050	0.041	0.064	0.267	-0.248	-0.05	10.7	3.35	15.3	5.84	0.414	-0.497
TIPWW	alt Tjp, W wall ML pit, fresh bio	17.8	-0.199	4.02	-0.050	0.034	-0.02	-0.05	-0.249	-0.05	9.16	0.553	12.7	60.6	2.59	-0.497
3SW-659	alt Tjp, Joshua Hollow	21.9	-0.199	0.684	-0.050	0.068	-0.02	-0.05	-0.249	-0.05	5.96	0.843	12.6	52.8	4.29	-0.497
3SW-707	Sr ls wallrock <0.5 m W from dike	7.47	2.44	37.2	0.062	0.182	-0.02	1.13	-0.247	-0.049	9.87	1.30	4.53	24.7	0.1	0.543
3SW-709	Sr dolo ~350' W of 707	11.8	-0.197	17.4	-0.049	0.405	0.026	1.27	-0.246	-0.049	4.57	1.66	3.2	32.6	-0.098	-0.492
3SW-711A	brecc'd Sr dolo 0.5m W of dike	12.3	1.01	20.0	-0.049	0.359	-0.019	0.723	-0.244	-0.049	7.23	0.352	3.54	37.4	0.156	-0.487
3SW-711B	silicified Sr ~150' from 711A	36.4	0.365	25.0	0.073	0.073	0.037	1.38	-0.249	-0.05	10.3	2.45	2.96	22.4	-0.1	-0.498
3SW-713	cherty dolo w/fluor? near dike	246	0.627	84.0	0.208	1.400	0.569	11.3	2.56	0.081	40.9	23.8	4.84	117	0.276	-0.495
3MJ-160A	Gold Ace, Au-bearing Wood Canyon Fm	33010	110151	8.34	0.324	0.039	0.343	7.27	-0.249	0.069	14.5	9.75	12.3	25.8	-0.1	0.499
	"Blank" of fresh Tiva Canyon Mbr															
3SW-589p	new split prep'd in steel pulverizer	83.8	-0.194	1.99	-0.049	0.031	-0.019	-0.049	-0.243	-0.049	1.65	0.445	33.4	44.6	0.534	-0.485
X94B	new split prep'd in shatterbox	20.9	-0.195	1.93	-0.049	0.038	-0.02	-0.049	-0.244	-0.049	7.86	1.02	7.36	51.2	0.569	-0.488

brep= blind repeat analysis
bdup= blind duplicate analysis
hbx= hydrothermal breccia
vn= vein
Pz= Paleozoic
Sr= Roberts Mountain Formation
qtz= quartz
siltst= siltstone
vnlts= veinlets
alt= altered
ls= limestone
"p" following sample number denotes preparation in rotary pulverisor with steel plates; "s" denotes preparation in shatterbox with carbon-steel rings.
Tct= Tram Member of the Crater Flat Tuff
Tcp= Prow Pass Member of the Crater Flat Tuff
Tip and Tjp = porphyry dikes of Bare Mountain

Analyses by U. S. Mineral Laboratories, Inc., North Highlands, CA, using 15 gram digestions, organic liquid separation and inductively- coupled plasma-emission spectrography, except for Au which was determined by graphite-furnace atomic-absorption spectrometry. Values as reported by U. S. Mineral Laboratories. Number of significant figures does not indicate precision or accuracy of analyses.

"-" = less than.

Detection limits as quoted by U. S. Mineral Laboratories at 3 sigma confidence level:

Ag=	3 ppb	Bi=	0.050 ppm	Se=	0.25 ppm
Au=	0.2 ppb	Sb=	0.050 ppm	Zn=	0.25 ppm
Tl=	0.5 ppm	Te=	0.050 ppm	Cd=	0.020 ppm
As=	0.25 ppm	Pb=	0.050 ppm	Hg=	0.020 ppm
Cu=	0.010 ppm	Mo=	0.020 ppm		

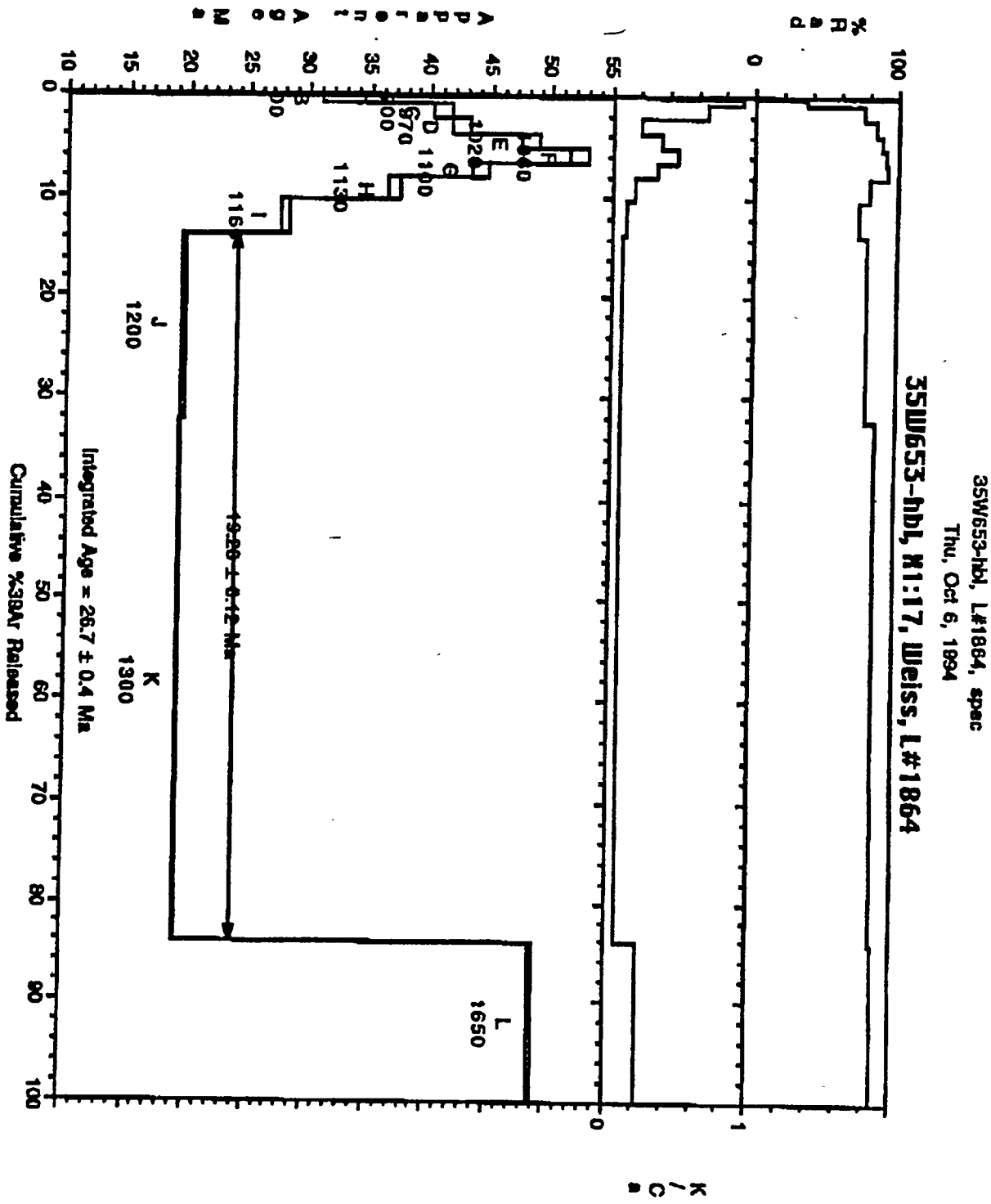

Figure 1. Argon release spectra for stepwise heating of hornblende separated from silicic porphyry dike in northern Bare Mountain; field sample number 3SW-653. Sample collected from dike outcrop about 1300 feet SSW from the open pit of the Mother Lode mine.

APPENDIX A

revised October 13, 1994 - SIW

Multiple Episodes of Hydrothermal Activity and Epithermal Mineralization in the Southwestern Nevada Volcanic Field and Their Relations to Magmatic Activity, Volcanism and Regional Extension

STEVEN I. WEISS, DONALD C. NOBLE, MAC ROY JACKSON[1] AND KATHERINE A. CONNORS
Mackay School of Mines, University of Nevada, Reno, Reno, Nevada, 89557
EDWIN H. MCKEE
U.S. Geological Survey, 345 Middlefield Road, Menlo Park, CA 94025

1 Present address: Newmont Exploration Ltd., P. O. Box 669, Carlin, NV, 89822-0669.

Abstract

Volcanic rocks of middle Miocene age and underlying pre-Mesozoic sedimentary rocks host widely distributed zones of hydrothermal alteration and epithermal precious metal, fluorite and mercury deposits within and peripheral to major volcanic and intrusive centers of the southwestern Nevada volcanic field (SWNVF) in southern Nevada, near the southwestern margin of the Great Basin of the western United States. Radiometric ages indicate that episodes of hydrothermal activity mainly coincided with and closely followed major magmatic pulses during the development of the field and together spanned more than 4.5 m.y. Rocks of the SWNVF consist largely of rhyolitic ash-flow sheets and intercalated silicic lava domes, flows and near-vent pyroclastic deposits erupted between 15.2 and 10 Ma from vent areas in the vicinity of the Timber Mountain calderas, and between about 9.4 and 7 Ma from the outlying Black Mountain and Stonewall Mountain centers. Three magmatic stages can be recogniz Three magmatic stages can be recognized: the main magm Mountain magmatic stage (11.7 to 10.0 Ma), and the late magmatic stage (9.4 to 7.5 Ma).

During the main magmatic stage most hydrothermal activity coincided with and closely followed eruption of the 12.8 to 12.7 Ma Paintbrush Tuff. Precious-metal vein deposits of adularia-sericite type formed in the Wahmonie-Salyer volcanic center at about 12.9 to 12.5 Ma, penecontemporaneous with, or at most a few tenths of a million years after, Wahmonie-Salyer volcanism. At about the same time, fluorite and disseminated gold deposits formed in northern and eastern Bare Mountain, about 1 to 2 Ma after the intrusion of a swarm of silicic porphyry dikes. This timing, together with high Mo, fluorine, Bi and Te, and the spatial association of much of the mineralization with the dikes, suggests a genetic relation to deeper porphyry-type magmatic activity. Alunite dated at about 12.9 Ma at the Thompson mine indicates that shallow, steam-heated acid-sulfate alteration and Hg mineralization took place peripheral to the margin of the Claim Canyon cauldron within at most a few tenths of a million years after eruption of the Paintbrush Tuff.

Hydrothermal activity was more widespread during the Timber Mountain stage, occurring within a few tenths of a million years after the climactic eruptions of the Timber Mountain Tuff and coeval with, to as much as 1 Ma after, the end of post-collapse volcanism of the Timber Mountain magma system. Steam-heated acid-sulfate alteration of units of the Timber Mountain Tuff and older

rocks at the Silicon mine and in the south flank of Mine Mountain took place at about 11.6 and 11.1 Ma, respectively. Identical, aerially extensive alteration in the Calico Hills, dated at about 10.3 Ma, closely preceded the eruptions of nearby and overlying rhyolite domes along the southeast margin of the Timber Mountain I caldera . Acid-sulfate alteration took place at Bailey's hot spring at about 10.2 Ma and in the Transvaal Hills at about 9.9 Ma. Quartz veins and adularia in Oasis Mountain formed under water-saturated conditions at about 10.6 Ma.

Two and possibly three periods of hydrothermal activity during the Timber Mountain stage are recognized in the Bullfrog Hills. Gold and silver-bearing, epithermal vein deposits of the low base-metal adularia-sericite type formed in faults cutting the Timber Mountain Tuff and older ash-flow sheets, and breccia deposits intercalated with the 10.5 to 10 Ma tuffs and lavas of the Bullfrog Hills (TLBH). Quartz-calcite veins at the Yellowjacket mine and north of the Pioneer mine formed within at most a few tenths of a million years after volcanism of the 11.45 Ma Ammonia Tanks Member of the Timber Mountain Tuff and the tuffs of Fleur de Lis Ranch. Younger and economically more important period(s) are represented by the Au-Ag bearing, multistage quartz-calcite fissure veins at the Original Bullfrog, Lac Gold Bullfrog, Montgomery-Shoshone, Gold Bar, Denver-Tramps and Mayflower mines. Adularia ages show that these deposits formed between about 10.0 to 9.5 Ma, and possibly as young as about 9.0 Ma, coeval with and as much as about 1 Ma after, volcanism of the TLBH.

Although hydrothermal activity took place within and adjacent to individual volcanic centers, deposits of economic significance were structurally controlled by normal faults related to regional extensional tectonism, rather than by volcano-tectonic structures such as caldera ring or radial faults, or faults formed by resurgent doming. In areas to the southeast, south and southwest of the central caldera complex two pulses of WNW-ESE directed extension are recognized and included the development of the Original Bullfrog-Fluorspar Canyon (OB-FC) fault system, a regional, presently low-angle system of normal faults separating highly faulted and tilted rocks of the SWNVF from pre-Cenozoic rocks. Fluorite and disseminated gold mineralization in Bare Mountain broadly coincided with the first pulse of faulting, bracketed between 12.8 and 11.7 Ma. Faults and fractures hosting the veins of the Wahmonie district may represent an early phase of this faulting. The later pulse

involved displacements along the Original Bullfrog segment of the OB-FC fault system and imbricate normal faulting and tilting of volcanic rocks to dips as steep as 90°, mainly to the southwest of the central caldera complex. The onset of this deformation took place after 11.45 Ma, but prior to the initial eruptions of the TLBH. Faulting and tilting in the Bullfrog Hills continued synchronously with, and after volcanism of the TLBH and some of the steeply dipping faults cut the low-angle OB-FC fault, indicating that brittle extension was not rooted in a shallow décollement, but also affected deeper levels of the crust. Faults formed during this pulse provided the sites of vein deposition in the Bullfrog Hills. Textural evidence shows that faulting took place during and after mineralization.

Spatial association and close temporal correspondence provide strong evidence for a genetic relation between magmatic and hydrothermal activity in the SWNVF. Faults related to regional extension were critical in localizing precious-metals deposits in the Bullfrog, Bare Mountain and probably the Wahmonie districts, as in other precious-metals districts of late Cenozoic age in the western Great Basin.

Introduction

Volcanic centers of the southwestern Nevada volcanic field (SWNVF) (Fig. 1) record 6 million years of intense Miocene igneous activity near the southwestern margin of the Great Basin in southern Nevada. Scattered epithermal precious-metal, fluorite and mercury deposits are present in widespread zones of hydrothermal alteration within rocks of the field and in underlying pre-Tertiary sedimentary and metasedimentary rocks contain (Fig. 2). These areas have attracted appreciable exploration and mining activity since the beginning of the 20th century, with total production plus reserves conservatively estimated at about 60 tons of gold and 150 tons of silver (Castor and Weiss, 1992). Although the volcanic stratigraphic framework, caldera geology and regional hydrology of the SWNVF and younger basaltic activity in the region have been intensively studied (e.g., Byers et al., 1989; Turrin et al., 1991), until recently little attention was directed toward understanding hydrothermal activity in the region either as a process associated with the development of individual volcanic centers or within the context of the development of the entire volcanic field. Initial studies of the timing and stratigraphic settings of hydrothermal alteration and mineralization (Jackson, 1988; Jackson et al., 1988) provided evidence for the broad correspondence of hydrothermal activity to

magmatic and volcanic events of the Timber Mountain caldera complex. Noble et al. (1991) proposed that hydrothermal activity and mineralization were associated with specific magmatic stages in the evolution of the field and Castor and Weiss (1992) emphasized the diverse nature and geologic settings of precious-metal deposits associated with the development of the SWNVF.

In this report we present and interpret geologic information and radiometric age data obtained on hydrothermal minerals from altered and mineralized areas of the SWNVF. This information demonstrates the long-lasting temporal and spatial association of hydrothermal activity and mineralization with magmatic and volcanic activity of the SWNVF, and their relations to pulses of extensional faulting in the region. We emphasize that multiple, widely distributed hydrothermal systems were broadly coeval with major culminations in magmatic activity of the field, unlike for example, parts of the San Juan volcanic field where hydrothermal mineralization followed caldera formation and major volcanism by 5 to 10 million years. Although hydrothermal activity took place within and adjacent to individual volcanic centers, structures related to regional extension were a more important element in the control of precious-metal deposits than were volcano-tectonic structures such as caldera ring-fracture systems.

Regional Setting and Volcanic-Stratigraphic Framework

The SWNVF forms part of a broad, discontinuous belt of volcanic rocks erupted around the periphery of the Great Basin during middle to late Miocene time. This belt is younger than, and in part overprints, southward migrating, ignimbrite-dominated Oligocene and Early Miocene volcanism. (Armstrong et al., 1969; Stewart and Carlson, 1976; Best et al., 1989). Situated near the southwestern margin of the Great Basin about 150 km NW of Las Vegas, Nevada (Fig. 1), the SWNVF consists largely of voluminous silicic ash-flow sheets and intercalated silicic lavas of middle to late Miocene age that were deposited on to late Miocene age that were deposited on sedimenta Miocene age and a complexly deformed and locally metamorphosed basement of Late Precambrian and Paleozoic sedimentary rocks (Ransome et al., 1910; Cornwall, 1972; Stewart, 1980; Carr, 1984a). The pre-Cenozoic rocks comprise a fairly complete sequence of Late Proterozoic through Mississippian clastic and carbonate continental shelf deposits (Monsen et al., 1990). Most of the volcanic

rocks were erupted between about 15.2 Ma and 10 Ma from vents within and peripheral to the central, long-lived complex of collapse-caldera volcanic centers in the Timber Mountain area, and between about 9 Ma and 7 Ma from the outlying Black Mountain and Stonewall Mountain centers (Fig. 1; Byers et al., 1989; Noble et al., 1991).

Major stratigraphic units and the volcanic development of the SWNVF are summarized in Table 1. Numerous radiometric ages constrain the timing of major volcanic events and individual eruptive centers within the field. All radiometric ages have been corrected, where necessary, using presently accepted abundance and decay constants (Steiger and Jager, 1977; Dalrymple, 1979).

Three distinct periods of magmatic activity may be recognized in the evolution of the SWNVF (Table 1) based on radiometric ages of rocks of the field, together with stratigraphic, petrologic and other geologic data (e.g., Byers et al., 1976a; Noble et al., 1984; Carr et al., 1986; Broxton et al., 1989). These periods have been termed by Noble et al. (1991) the *main magmatic stage*, extending from 15.2 Ma to about 12.7 Ma, the *Timber Mountain magmatic stage* from about 11.7 Ma to about 10 Ma and the *late magmatic stage* from about 9.4 Ma to 7.5 Ma. Within these time intervals, one or more successive ash-flow sheets and cogenetic lava units were erupted from petrologically related magma systems in short, episodic bursts that spanned only 0.1 to 0.4 million years (Sawyer et al., 1990; Noble et al., 1991). Small-volume basaltic cinder cones and lava flows of Pleistocene age in the region (e.g. Turrin et al., 1991) are unrelated to magmatic activity of the SWNVF.

At least nine major ash-flow sheets and many local ash-flow units of rhyolitic compositions were erupted during the main magmatic stage, with most of the volcanism occurring between about 14 and 12.7 Ma. Ash-flow units of this stage are commonly zoned from high-silica to low-silica rhyolite and range from calc-alkaline to peralkaline compositions. Magmatic activity culminated at about 12.8 to 12.7 Ma with the rapid eruption of the four ash-flow sheets of the Paintbrush Tuff, with a combined original minimum volume of more than 2000 km^3 (Scott et al., 1984).

Eruption of the Paintbrush Tuff was followed by a lull in volcanism of about 1 million years, during which only relatively small volumes of rhyolitic lava and associated pyroclastic deposits were erupted, mainly near the southern margin of the Claim Canyon cauldron. The Timber Mountain

stage began at about 11.7 to 11.6 Ma with the eruption of rhyolite domes and related pyroclastic aprons (Table 1), remnants of which are preserved within the Claim Canyon cauldron, in the lower part of Beatty Wash and northern Bare Mountain, and in the Bullfrog Hills. This activity was followed closely at 11.6 Ma by the eruption of the voluminous Rainier Mesa Member of the Timber Mountain Tuff and the formation of the Timber Mountain I caldera (Fig. 2) (Byers et al., 1976b; Noble et al., 1991). Eruption of the Ammonia Tanks Member of the Timber Mountain Tuff at 11.45 Ma was accompanied by the formation of the smaller, nested Timber Mountain II caldera. Uplift of intracaldera tuffs formed the prominent resurgent dome within, at most, 0.3 million years after eruption of the Ammonia Tanks Member (Connors et al., 1991). Magmatic activity then decreased, but continued for about 1 million years with the emplacement of moat-filling rhyolite tuffs and lavas in the southern part of the caldera (Byers et al., 1976a; 1976b), and the formation of extracaldera rhyolite domes such as those of Shoshone Mountain and in the Bullfrog Hills (Weiss et al., 1990b; Noble et al., 1991). By about 10.5 to 10 Ma, cooling and consolidation of the Timber Mountain magmatic system were sufficient to allow the ascent and eruption of the capping latitic to basaltic lavas in the Bullfrog Hills and the mafic lavas of Dome Mountain within the caldera moat.

Volcanism then shifted to areas northwest of the Timber Mountain caldera complex (Noble et al., 1991). From about 9.4 to about 7 Ma, major magmatic and volcanic activity were focussed in the outlying Black Mountain and Stonewall Mountain volcanic centers and in the vicinity of Obsidian Butte (Fig. 1). Three extensive and at least three more local units of ash-flow tuff of subalkaline to strongly peralkaline rhyolitic compositions were erupted during this *late magmatic stage*, as well as less voluminous units of silicic to mafic lava. Volcanic rocks of this stage partially filled the moats of the Timber Mountain I and II calderas and distal parts of the Stonewall Flat Tuff reached as far south as Beatty Wash and the southwestern Bullfrog Hills and as far west as the east side of northern Death Valley (Weiss et al., 1988; 1993c).

Relations to Walker Lane structures

The major volcanic centers of the SWNVF are situated near the eastern margins of the Goldfield and Mine Mountain - Spotted Range blocks of the Walker Lane belt (Stewart, 1988). Throughgoing NW-trending right-lateral strike-slip faults and shear zones of late Cenozoic age, which are characteristic of other parts of the Walker Lane belt, are poorly developed in the SWNVF and, where present, have experienced very little post-midddle Miocene offset. A major, northwest-trending, right-lateral strike slip fault of possible late Cenozoic age between Yucca Mountain and Bare Mountain has been inferred by Schweickert (1989) and northeast- and northwest-trending strike-slip faults have been recognized east of Timber Mountain in the Nevada Test Site (Carr, 1974; 1984a). Most of the movement on these structures appears to have taken place prior to the onset of volcanism of the SWNVF and only locally, as at Mine Mountain (Fig. 2), are rocks of the Timber Mountain Tuff offset (Orkild, 1968). In places, such as at the north end of Frenchmen Flat (Fig. 2), where faults cutting rocks as young as units of the Timber Mountain Tuff have been interpreted to define a northwest-trending zone of right-lateral flexural shear (Carr, 1984a), paleomagnetic data show little evidence of vertical-axis rotations and the fault pattern most likely defines an accommodation zone between oppositely tilted extensional domains (Hudson, 1992). Similarly, paleomagnetic data from volcanic strata in other parts of the SWNVF show no evidence for significant rotations about vertical axes that would be expected from major, right-lateral, Walker Lane tectonism during or after development of the SWNVF (Hudson et al., 1994).

It has been proposed that magmatic activity and the development of major volcanic centers of the SWNVF were focussed by deep seated pull-apart structures at right steps between northwest-trending, right-lateral shear zone segments along the eastern margin of the Walker Lane belt (Carr, 1974; 1984a; 1984b). There is little direct evidence to support this idea except, perhaps, for a north-trending gravity low inferred by Carr (1988; 1990) to mark a regional rift zone of middle Miocene age. Most structural features in the SWNVF can be attributed to volcano-tectonic processes, including magmatic tumescence, caldera collapse and resurgent doming (Christiansen et al., 1977), and to the effects of broadly coeval regional extensional tectonism.

Extensional faulting

Episodes of pre-Middle Miocene extension in southwestern Nevada are poorly known from fragmentary evidence (Ekren et al., 1968; Ekren et al., 1971; Schweikert and Caskey 1990; Noble et al., 1991). Basin-and-range style faulting along north-trending normal faults began in the northeastern part of the field between 17 Ma and 14 Ma (Ekren, 1968) and continued into Quaternary time (Ekren et al., 1971; Frizzell and Shulters, 1990). Basin-and-range fault displacements are small in much of the field and the large, distinct ranges and valleys of adjacent south-central Nevada pass southwards into the broad volcanic upland of Pahute Mesa. Much of the topography of the SWNVF reflects volcanic and pre-volcanic landforms buried to greater or lesser degrees by successive ash-flow sheets; the exceptionally well-preserved calderas and outflow sheets of the Black Mountain and Timber Mountain centers attest to relatively mild tectonism in the central and northern parts of the field since middle Miocene time.

South and west of the Timber Mountain caldera complex rocks of the SWNVF have been more steeply tilted than in areas to the east and north, locally to dips as steep as 90°, and normal faults are more numerous and more closely spaced (e.g., Carr, 1990). Much of this deformation is associated with the low-angle Original Bullfrog, Amargosa and Fluorspar Canyon normal faults (OB-FC, Fig. 2), which separate highly faulted and tilted rocks of the SWNVF from underlying pre-Cenozoic sedimentary and metamorphic rocks in the southern Bullfrog Hills and northern Bare Mountain (Ransome et al., 1910; Cornwall and Kleinhampl 1961; 1964; Maldonado, 1990a; 1990b; Maldonado and Hausback, 1990; Monsen et al., 1992). Recently some geologists have interpreted these faults as segments of a single, upper crustal, regional detachment fault that accommodated WNW-directed extension of upper-plate rocks, and propose that this fault probably cuts down-section to the southwest through pre-Cenozoic rocks in the Funeral Mountains (Fig. 2), where it is known as the Boundary Canyon fault (Maldonado, 1985; 1990a; 1990b; Carr and Monsen, 1988; Hamilton, 1988; Carr, 1990). Conformable relations between the units of the Timber Mountain Tuff and older, underlying ash-flow sheets in the southern Bullfrog Hills constrain the onset of major faulting and tilting along the Original Bullfrog and Amargosa segments of the OB-FC fault system to after 11.4 Ma (Carr, 1990; Maldonado, 1990a; 1990b; Maldonado and Hausback, 1990). Extensional faulting began ear-

lier above the Fluorspar Canyon segment of the OB-FC fault as shown by angular discordance of as much as 30° between the 12.7 Ma Tiva Canyon Member of the Paintbrush Tuff and the 11.6 Ma Rainier Mesa Member of the Timber Mountain Tuff (Carr and Monsen, 1988; Carr, 1990; Monsen et al., 1992). Extensional deformation between 12.7 Ma and 11.6 Ma also affected areas to the east, such as Yucca Mountain and the Calico Hills where units of the Paintbrush Tuff and older rocks were offset and tilted prior to deposition of the Rainier Mesa Member (McKay and Williams, 1964; Lipman and McKay, 1965; Orkild and O'Connor, 1970; Scott and Bonk, 1984; Carr, 1990).

In the Bullfrog Hills and near the north flank of Bare Mountain the Spearhead Member of the Stonewall Flat Tuff is interbedded with flat-lying conglomeratic deposits that overly and pinch out against the faulted and tilted middle Miocene rocks, indicating that major extension ceased in this area prior to 7.6 Ma (Weiss et al., 1988; 1990b). Most of the deformation associated with the OB-FC fault system and in areas to the east is therefore bracketed between 12.7 and 7.6 Ma. Structural relations in western Pahute Mesa show that extensional faulting in areas to the northwest of the Timber Mountain caldera complex began prior to 13.7 Ma (Minor et al., 1991). Post-7.5 Ma tectonic activity has involved mainly block uplift and faulting with little tilting in areas between northern Death Valley and Pahute Mesa (Noble et al., 1990; Weiss et al., 1993c).

The timing of major WNW-directed extension associated with the OB-FC fault system and in areas to the east corresponds closely to the timing of extension, tilting and basin development elsewhere in the southern Walker Lane belt. Large-magnitude extensional faulting and tilting took place in the Death Valley area between 14 Ma and 8.5 Ma (e.g., Cemen et al., 1985; Wright et al., 1991) and between about 12 and 9 Ma in the Lake Meade-Las Vegas Valley area to the south (Weber and Smith, 1987; Duebendorfer and Smith, 1991; Duebendorfer and Wallin, 1991). To the north in the Silver Peak-Weepah Hills region, detachment-style extension, core complex cooling and development of the Esmeralda basin took place between about 13 Ma and 6 Ma (McKee, 1983; Powers, 1983; Stewart and Diamond, 1990), coeval with much of the faulting and tilting in the Gold Mountain - Slate Ridge area of Esmeralda County (Worthington, 1992; Weiss et al, 1993c).

Timing and Nature of Hydrothermal Activity and Mineralization

Hydrothermal alteration and epithermal mineralization of Neogene age affected volcanic rocks of the SWNVF and underlying, basement rocks of pre-Mesozoic age (Fig. 2). Precious-metal and fluorite mines with significant present or past production include the Montgomery-Shoshone, Lac Gold Bullfrog, Sterling, Mother Lode, Gold Bar and Daisy mines (Fig. 2). The Wahmonie, Mine Mountain, northern Bullfrog Hills, Clarkdale and Tolicha districts have little recorded production, although rich ores are locally present. In addition, dozens of shallow prospect workings are scattered in areas of hydrothermal alteration near Sleeping Butte, Oasis Mountain, north of Bare Mountain and in the Transvaal Hills, the Calico Hills, and northwestern Yucca Mountain (Fig. 2). Various workers have reported on individual mines and prospects (e.g., Ransome et al., 1910; Cornwall and Kleinhampl, 1964; Odt, 1983; Tingley, 1984; Quade and Tingley, 1984; Jorgensen et al., 1989; Greybeck and Wallace, 1991). Castor and Weiss (1992) summarized the general styles of mineralization, alteration and ore mineral assemblages, geochemical characteristics and geologic settings of the Wahmonie, Mine Mountain, Bare Mountain, and Bullfrog districts (Fig. 2). Precious-metal mineralization in these four districts is of the low-sulfidation (adularia-sericite) class of epithermal deposits and includes disseminated deposits and vein systems generally of base metal-poor types. The deposits are hosted by felsic ash-flow tuff, lava, intercalated sedimentary rocks and intrusive rocks of the SWNVF, and by underlying sedimentary rocks of pre-Mesozoic age. In the case of Wahmonie and Bare Mountain, epithermal precious metal mineralization may be genetically related to deeper porphyry-type igneous activity (Noble et al., 1989; 1991; Castor and Weiss, 1992; Weiss et al, 1993b).

The timing of hydrothermal events is constrained by radiometrically dated rock units (Table 1) and by K-Ar and $^{40}Ar/^{39}Ar$ age determinations on adularia and alunite of hydrothermal origin obtained during this study (Table 2 and McKee and Bergquist, 1993). Alunite and adularia were concentrated using conventional magnetic and heavy liquid techniques. K-Ar and $^{40}Ar/^{39}Ar$ analyses were carried out in the Menlo Park, California, laboratories of the U.S. Geological Survey. The estimated analytical uncertainty at one standard deviation is based on experience with replicate analyses in the Menlo Park laboratories and reflects the uncertainty in the measurement of the argon isotopes, radiogenic ^{40}Ar, and K_2O, and for the $^{40}Ar/^{39}Ar$ analyses, an estimated J-value uncer-

tainty of ±0.5 percent. $^{40}Ar/^{39}Ar$ analyses of samples 10 and 11 were carried out on splits of the same concentrates used in the K-Ar analyses. Additional information concerning initial sample mineralogy and collection is given in Appendix 1 and in Mckee and Bergquist (1993).

Hydrothermal Activity Associated with the Main Magmatic Stage

Evidence for hydrothermal activity early in the development of the SWNVF is found in the vicinity of Sleeping Butte (Fig. 2), where tuffs of a thick, unnamed ash-flow unit that have undergone variable degrees of silicification and adularization are overlain by unaltered ash-flow tuff of the 13.7 Ma Grouse Canyon Member of the Belted Range Tuff (Noble et al., 1991). One or more early episodes of hydrothermal activity may have occurred south of the central caldera complex as well. Approximately 10 km northwest of drill hole USW G2, in the hills at the north end of Crater Flat (Fig. 2), numerous thin veins of hydrothermal breccia cemented by chalcedonic silica and iron oxides cut the Tram Member of the Crater Flat Tuff, but do not penetrate the overlying Bullfrog Member of the Crater Flat Tuff (Weiss et al., 1993a; Fridrich et al., 1994). In drill core from the subsurface of Yucca Mountain, portions of both the 14.0 Ma Lithic Ridge Tuff and a lithic-rich subunit of the Tram Member of the Crater Flat Tuff (age bracketed between 13.7 and 13.2 Ma) contain disseminated pyrite and veinlets of pyrite, locally with quartz, in lithic fragments that have been variably silicified, albitized and adularized (Weiss et al., 1990a; 1992; Castor et al., 1994). Veinlets in some of the altered fragments appear to be truncated by the edges of the fragments and may have formed prior to their incorporation in the pyroclastic units. Likely vent areas for these tuffs are located beneath northwestern Yucca Mountain and northern Crater Flat (Carr et al., 1986). Pyrite is also sparsely disseminated in the groundmass of these tuffs and in some cases can be found along edges of lithic fragments. This pyrite has the same fine-grained, anhedral to subhedral, commonly skeletal and pitted morphology as pyrite disseminated in propylitically altered silicic lavas beneath Yucca Mountain and probably reflects sulfidation by later hydrothermal solutions, most likely during the Timber Mountain stage (see below), more than 2 Ma after deposition of these ash-flow sheets (cf. Castor et al., 1994).

Wahmonie district: At the Wahmonie district in the southeastern part of the field (Fig. 2) Ag-Au ores at shallow depths were worked on a small scale intermittently prior to 1930 from a NE-trending swarm of quartz-calcite veins that locally contain small amounts of adularia. The veins are situated within a >30 km^2 area of propylitically and argillically altered andesitic to rhyodacitic lavas, tuffs and breccias of the Wahmonie and Salyer formations, and dikes and stocks of granodiorite porphyry, andesite and rhyolite (Ball, 1907; Ekren and Sargent, 1965; Castor and Weiss, 1992). These rocks comprise the Wahmonie-Salyer volcanic center (Poole et al., 1965), the eroded remnants of a composite central volcano or dome and flow field of mainly intermediate composition. Volcanism of this center, satellitic to the southeast margin of the Timber Mountain caldera complex, is bracketed between the Crater Flat Tuff and the rhyolite of Calico Hills (Broxton et al., 1989). K-Ar ages of about 13.2 Ma and 12.8 Ma have been obtained from rocks near the bottom and top, respectively, of the Wahmonie Formation (Kistler, 1968), consistent with stratigraphic constraints (Table 1). The dikes and stocks have volcanic and subvolcanic groundmass textures and, although not dated radiometrically, are reasonably interpreted as cogenetic with the surrounding extrusive rocks.

The veins at Wahmonie, as much as 1 to 2 m wide, and quartz-cemented breccia trend northeast and are exposed discontinuously for at least 1 km along strike. These veins contain electrum, hessite and other tellurium-bearing minerals, have bismuth contents as high as 211 ppm, moderately low base-metal contents and are characterized by gangue and selvages containing adularia and sericite (Quade and Tingley, 1984; Castor and Weiss, 1992). K-Ar ages of 12.9 ± 0.4 Ma and 12.6 ± 0.4 Ma (samples 1 and 2, Table 2) have been obtained from adularia separated from intensely adularized and silicified dacitic(?) wall rock with abundant, closely-spaced quartz ± adularia veinlets. These ages indicate that hydrothermal activity and mineralization took place in the Wahmonie-Salyer center coeval with, or very shortly after magmatic activity.

As pointed out by Noble et al. (1991) and Castor and Weiss (1992), several lines of evidence suggest the Ag-Au mineralization at Wahmonie may be related to an underlying porphyry system. An altered granodioritic porphyry stock with equigranular to granophyric groundmass texture is exposed <1 km north of the veins and locally contains abundant quartz veinlets carrying actinolite and pyrite, secondary hypersaline fluid inclusions in quartz phenocrysts and traces of secondary

biotite, consistent with the passage of highly saline hydrothermal fluids with a magmatic component. A large felsic pluton beneath and south of the stock is inferred from geophysical data to underly the district and induced polarization data suggest the presence of \2% sulfides below the water table at Wahmonie (Ponce, 1981; 1984; Hoover et al., 1982). In addition, a highly altered body of "intrusive breccia" (Ekren and Sargent, 1965) in the district and the presence of elevated concentrations of tellurium and bismuth in the veins (Castor and Weiss, 1992) are consistent with porphyry-related hydrothermal activity.

Mining activity in the Wahmonie district is believed to have taken place as early as 1853 (Quade eand Tingley, 1984), and three shafts to depths of as much as 150 m were sunk following high-grade discoveries in 1928. The stock market crash and ensuing depression in 1929 halted work and little ore was shipped (Cornwall, 1972). In 1940 the district was withdrawn from civilian access for inclusion in a part of the Tonopah Bombing and Gunnery Range that subsequently became part of the Nevada Test Site. The deepest shaft was used for the disposal of radioactive waste. Consequently, there has been no drilling or systematic geochemical sampling of the veins and workings in the district have been limited to shallow test pits and a few shallow shafts. Assays of reconnaissance samples from prospect dumps and vein outcroppings as high as 38.7 kg silver and 1.7 kg gold per ton (Quade and Tingley, 1984; Castor and Weiss, 1992), provide evidence for locally rich Ag-Au mineralization in the district. These data, together with the large lateral extent of the mostly unexplored veins and surrounding alteration zone, suggest a potential for economic Ag-Au mineralization despite the lack of appreciable past production.

Northern and eastern Bare Mountain: To the west, in the northern and eastern parts of Bare Mountain, epithermal fluorite and finely disseminated gold mineralization of approximately the same age as the Ag-Au veins in the Wahmonie district are hosted both by pre-Mesozoic clastic and carbonate rocks and by rocks of late Cenozoic age (Castor and Weiss, 1992) (Fig. 2). Small amounts of gold and mercury were produced intermittently from the Sterling gold mine and the Telluride gold-mercury camp between 1905 and the late 1970's. From 1980 through 1993 approximately 150,000 oz of gold were produced from disseminated deposits at the Sterling mine and the Mother Lode mine (Bonham and Hess, 1992; Randol, 1993). Currently subeconomic disseminated gold

deposits are present at the Goldspar mine, at and near the Mother Lode mine, the Secret Pass prospect and in the vicinity of the Daisy mine (Greybeck and Wallace, 1991; Castor and Weiss, 1992). Fluorite was produced from 1918 to 1989, mainly from the Daisy mine, with smaller production from the Goldspar and Mary mines (Papke, 1979; Castor and Weiss, 1992).

Most of Bare Mountain consists of complexly faulted sedimentary and low-grade metasedimentary rocks deposited on the North American continental shelf that underwent folding, metamorphism and thrust faulting during Mesozoic time and were exhumed by uplift associated with Cenozoic regional extension (Cornwall and Kleinhampl, 1961; Monsen, 1983; Hamilton, 1988; Monsen et al., 1992). In northern and eastern Bare Mountain the pre-Cenozoic rocks host a swarm of north-trending, steeply dipping, discontinuous, rhyolitic porphyry dikes that are exposed over a north-south distance of 13 km (Fig. 2). The dikes, generally less than 10 meters in thickness, are hydrothermally altered to greater or lesser degrees. Dikes between the Sterling mine and the Mary mine contain phenocrystic and primary groundmass feldspar that is partly to completely pseudomorphed by adularia; biotite exhibits little visible alteration. Strong biotite- and potassium feldspar-stable propylitic alteration affects the NNE-trending dike south of the Mother Lode mine. Seemingly unaltered biotite from several of the dikes has given K-Ar ages ranging from about 14.9 Ma to about 13.9 Ma (Marvin et al., 1989; Monsen et al., 1990; Noble et al., 1991), indicating emplacement during the main magmatic stage. Although the dikes are thin and contain varying amounts of quartz phenocrysts, they have coarsely granophyric groundmass textures and contain secondary, hypersaline fluid inclusions in quartz phenocrysts, consistent with the passage of a highly saline magmatic fluid phase after intrusion. These features, and the large lateral extent of the dikes, are not typical of other silicic dikes of the SWNVF, and strongly suggest that the dikes are unrelated to the magmatic system that produced the Crater Flat Tuff, as proposed by Carr et al. (1986). Instead, the silicic dikes probably represent the upper part of a large magmatic system (Noble et al., 1989; 1991), perhaps with petrochemical similarities to Late Cretaceous, lithophile-element rich stocks and plutons of the Great Basin (Barton and Trim, 1990).

Argillic alteration, bleaching and decarbonatization of the wallrocks accompany the dikes and also are present near the trace of the Fluorspar Canyon fault. Within these zones are areas of

fluorite and disseminated gold mineralization at the Sterling, Goldspar, Mary, Mother Lode, Telluride and Daisy mine areas (Fig. 2). A consistent trace element suite elevated in As, Hg, Sb, Ag, Mo, Tl, and with low concentrations of Cu, Pb, and Zn accompanies gold and fluorite (Odt, 1983; Tingley, 1984; Greybeck and Wallace, 1991; Castor and Weiss, 1992).

The fluorite deposits at the Goldspar, Mary and Daisy mines consist of banded fluorite veins and small replacement bodies, commonly with cinnabar, in early Paleozoic limestone and dolomite (Cornwall and Kleinhampl, 1964; Papke, 1979; Tingley, 1984). Finely disseminated gold is hosted by clastic and carbonate rocks of latest Precambrian and early Paleozoic age at the Sterling and Goldspar mines, and in the vicinity of the Daisy mine (Odt, 1983; Greybeck and Wallace, 1991). At the Mother Lode mine approximately 35,000 oz of Au were produced from the oxidized cap of a large, finely disseminated, sulfidic and refractory deposit hosted mostly by silicic porphyry dikes and adjacent tuffaceous sandstone, siltstone and interbedded carbonaceous marl and limestone of probable Early Miocene age (rocks of Joshua Hollow of Monsen et al., 1990) (Weiss et al., 1993b). Underlying Paleozoic sedimentary rocks are mineralized and a smaller, entirely separate deposit has been delineated nearby within quartzite and carbonate rocks probably of the Wood Canyon Formation and other early Paleozoic units (Ristorcelli and Ernst, 1991).

In all of these deposits alteration is dominantly argillic and quartz veins are not abundant. Silicification is typically absent or weak, although small jasperoid bodies are present near the Mother Lode mine. Base-metal concentrations are low (Cu+Pb+Zn generally < 150 ppm) and Ag is low, with Au:Ag ratios generally 1 to 10 for rocks containing 1 ppm or more Au (Odt, 1983; Geybeck and Wallace, 1991; Weiss et al., 1993b). Most sulfides at the Sterling mine are oxidized (Odt, 1983), but at the Mother Lode mine incompletely oxidized rocks contain veinlets and disseminated grains of pyrite, marcasite, arsenian pyrite, arsenopyrite and stibnite (S. I. Weiss and S. J. Ristorcelli, unpub. data, 1993). SEM studies and metallurgical tests on ores of the Mother Lode deposit show that gold is submicroscopic and resides within sulfide grains (Ristorcelli and Ernst, 1991; S.I. Weiss, unpub. data, 1993). Taken together, the overall style and mineralogy of Au mineralization and associated alteration, elevated As, Sb, Hg, and Tl, and low base-metals and Ag contents are typical of the broad class of epithermal, disseminated Au deposits often referred to as "Carlin-type" gold deposits else-

where in the Great Basin (e.g., Percival et al., 1988; Berger and Bagby, 1990). Unlike most sedimentary-rock hosted disseminated gold deposits, Bi and Te concentrations as high as 60 ppm and 5 ppm, respectively, have been found in rocks of the Mother Lode deposit (Weiss et al., 1993b).

Moderately to steeply dipping faults and fractures structurally below the Fluorspar Canyon fault system provided the principal structural controls and conduits for hydrothermal fluids at the Sterling mine and in the vicinity of the Daisy mine (Odt, 1983; Greybeck and Wallace, 1991). Although much of the Mother Lode deposit is situated adjacent to the northern part of the Fluorspar Canyon fault system, mainly in the hanging wall, exploration drilling has shown that the dikes provided the primary structural control, with relatively high grade ores (0.1 - 0.3 oz/ton Au) comprising a shell along and close to the top of the main dike (Weiss et al., 1993b).

Similar, but generally low grade, disseminated gold mineralization is hosted by the Bullfrog Member of the Crater Flat Tuff above the Fluorspar Canyon fault at the currently subeconomic Secret Pass deposit (Fig. 2). Silicification is generally weak and gold is associated with quartz, adularia, calcite, and pyrite (Greybeck and Wallace, 1991). Despite the difference in host-rock lithology, the trace-element assemblage of elevated As, Hg, Sb, Mo, Ag and Tl (Greybeck and Wallace, 1991) is the same as that of the Sterling, Mother Lode and Daisy mine gold deposits (Castor and Weiss, 1992).

Several lines of evidence indicate that hydrothermal activity and gold-fluorite-mercury mineralization in the northern and eastern parts of Bare Mountain took place during the main magmatic stage after emplacement of the porphyry dikes. Bleached rocks, argillic alteration and mineralization of the sedimentary rocks with high Mo, F, As, Sb, Hg, ± Tl, Au and Ag in eastern Bare Mountain are spatially closely associated with the dikes. The dikes are widely altered and contain sparse fluorite veins at the Goldspar and Mother Lode mines. Mineralized dike rock comprises a large proportion of the Mother Lode gold deposit and altered dikes near the Sterling mine locally contain strongly elevated Au, Ag, As, Sb, Mo and Hg concentrations. These relations indicate that much or all of the hydrothermal activity occurred after emplacement of the porphyry dikes. K-Ar and $^{40}Ar/^{39}Ar$ ages of about 12.9 Ma have been obtained from adularia that replaces igneous groundmass feldspar and phenocrysts in altered dike rock at the Goldspar mine (Noble et al., 1991),

suggesting that alteration and mineralization occurred near the end of the main magmatic stage, 1 to 2 million years after emplacement of the dikes. The similar style of fluorite and gold mineralization, alteration and trace-element signature in the vicinity of the Daisy mine lead us to infer, following Castor and Weiss (1992), a similar timing of hydrothermal acitivity at the Daisy mine area. This also is the case at Secret Pass, where Au-Ag mineralization must be no older than ca. 13.2 Ma, the age of the host rocks of the Bullfrog Member. Adularia- and illite-bearing alteration can be traced in outcrop into the lower part of the overlying, 12.8 Ma Topopah Spring Member of the Paintbrush Tuff, suggesting an even younger maximum age. A younger limit is provided by the timing of displacement along the Fluorspar Canyon fault which, according to Greybeck and Wallace (1991), truncated mineralization of the Secret Pass deposit and tilted the host rocks and overlying units of the Paintbrush Tuff as much as about 50° eastward prior to the deposition of onlapping, nearby flat-lying tuffs of the 11.6 Ma Rainier Mesa Member. The Secret Pass deposit therefore formed within a few hundred meters of the paleosurface, between 13.2 Ma and 11.6 Ma, and probably after 12.8 Ma.

The timing of Au-fluorite mineralization 1 to 2 million years after dike emplacement, together with the spatial association with the porphyry dike swarm in eastern Bare Mountain, the high Mo and F contents of altered rocks and the presence of significant Bi and Te at the Mother Lode deposit suggest that Carlin-type (or Carlin-like, cf. Seedorf, 1991) disseminated gold mineralization in Bare Mountain is related to the porphyry magmatic activity (Noble et al., 1989; 1991; Weiss et al., 1993b).

Interbedded ash-fall, surge and thin ash-flow tuffs associated with the pre-Rainier Mesa rhyolite domes are altered to alunite-, kaolinite-, and opal-bearing assemblages adjacent to the Mother Lode mine and similar acid-sulfate alteration is present southwest of the mine within older rocks along the Tates Wash segment of the Fluorspar Canyon fault. A K-Ar age of 12.2 ± 0.4 Ma has been obtained on fine-grained alunite separated from altered tuffaceous conglomerate of the rocks of Joshua Hollow beneath the pre-Rainier Mesa Member bedded tuffs along the Tates Wash fault (Table 2, sample 3). The alunitized conglomerate is part of a poorly exposed section of the sedimentary rocks of Joshua Hollow, which elsewhere underly units of the Crater Flat Tuff (Monsen et al., 1992) and the 12.2 Ma K-Ar age is therefore not unreasonable. Silurian dolomite along this portion of the fault is strongly silicified and subeconomic quantities of gold and mercury are report-

edly present along the fault at depth (D. Fanning, pers. commun., 1987). A short distance to the east, near the Telluride mine, a pipe-like body of hydrothermal breccia in silicified dolomite contains rounded, monomineralic clasts of fine-grained alunite. A K-Ar age of 11.2 ± 0.3 Ma has been obtained on this material (Table 2, sample 4). There is no evidence for the prior existence of significant amounts of sulfide minerals in topographically higher rocks nearby, or in rocks that would have overlain these localities, arguing against a supergene origin for this alunite. Moreover, the carbonate rocks would have buffered fluids associated with the weathering of sulfides. Our interpretation is that alunitic alteration along the Tates Wash segment and in the Telluride mine area reflects shallow hydrothermal activity producing weak gold-mercury mineralization at about 12-11 Ma. The high sulfate activity required for alunite formation perhaps was produced by acid condensates of H_2S-bearing steam. It is unclear to what extent this alteration reflects a continuation of the ca. 12.9 Ma activity, at shallow depths, or perhaps reflects a separate, later hydrothermal event. The shallow setting implied by this alteration is consistent with the shallow setting of the nearby Secret Pass deposit and requires that considerable uplift and erosion occurred between the time that the hypersaline fluid inclusions were trapped in the dikes, and about 12 to 11 Ma.

Base metals, in places accompanied by silver, are found in quartz veins in the western part of Bare Mountain (Cornwall, 1972, Tingley, 1984). These veins postdate cleavage and ductile and metamorphic fabrics of inferred Mesozoic age (Monsen, 1983; Monsen et al., 1990) within the upper Proterozoic Stirling Quartzite and the Wood Canyon Formation of lower Cambrian age. The quartz veins, in turn, are truncated by altered andesite dikes that have a minimum age of 26 Ma (Monsen et al., 1990), showing that base-metal mineralization in western Bare Mountain occurred more than 10 million years before, and is unrelated to, the emplacement of the silicic dikes and fluorite-Au-Hg mineralization elsewhere in Bare Mountain. At the Gold Ace mine (Fig. 2) coarse, macroscopically visible gold is present along bedding surfaces and compositional layering in marble of lower units of the Stirling Quartzite. Although the age of this deposit is not known, the difference in style of mineralization suggests it is unrelated to the fluorite, Hg and disseminated Au deposits described above.

Thompson mine: Small amounts of mercury were produced during the early 1900's from the Thompson mine, about 5.5 km north of Bare Mountain, near the northern end of Crater Flat (Fig. 2) (Cornwall, 1972; Tingley, 1984). The mine is situated within a large area of argillic and acid-sulfate altered rocks of the Crater Flat and Paintbrush Tuff. (U.S. Geological Survey, 1984; Jackson, 1988). Alteration is structurally controlled by post-Paintbrush, NE- and NNW-trending normal faults, is most intense at intersections between these two fault sets (Ristorcelli and Ernst, 1991), and near the Thompson mine affects rock units as young as the 12.7 Ma Tiva Canyon Member. Cinnabar is present as discontinuous stringers within veins composed of fine-grained alunite, halloysite and opaline silica, and as disseminated grains in ash-flow tuff replaced by porous, fine-grained intergrowths of alunite, opal-CT and kaolinite. We interpret the style and mineral assemblages of alteration and mercury mineralization in and surrounding the Thompson mine to reflect high-level acid alteration and mercury deposition in the vapor-dominated cap above a boiling hydrothermal system. A K-Ar age of 12.9 ± 0.5 Ma has been determined on fine-grained vein alunite probably of steam-heated origin (Rye, 1993) from the Thompson mine (Table 2, sample 5). This age is indistinguishable, within the limits of the analytical uncertainty, from the age of the host rocks and demonstrates that hydrothermal activity took place within, at most, a few tenths of a million years after deposition of the Tiva Canyon Member. In exposures of several square kilometers mainly to the northeast of the Thompson mine the alteration does not penetrate the uppermost 30 to 90 m of the Tiva Canyon Member, although the lower part of the ash-flow sheet is pervasively altered, showing that in some areas shallow, syn- to post-Paintbrush hydrothermal activity did not reach the paleosurface.

Hydrothermal activity associated with the Timber Mountain magmatic stage

Several areas of hydrothermal alteration and epithermal Au-Ag mineralization within and outside the margins of the Timber Mountain caldera complex provide a record of widespread, in part near-surface, hydrothermal activity penecontemporaneous with eruption of the 11.6 to 11.45 Ma Timber Mountain Tuff and genetically related local units of lava and tuff.

Silicon mine: Ceramic-grade silica was produced at the Silicon mine (Fig. 2) from steam-heated acid-sulfate altered rocks of the Rainier Mesa Member of the Timber Mountain Tuff (Fig. 3).

Alunite separated from alunite and opal-CT bearing tuff at the Silicon mine has given a K-Ar age of 11.6 ± 0.4 Ma (Table 2, sample 6), indicating that hydrothermal activity occurred near the margin of the Timber Mountain I caldera coeval with or, at most, a few tenths of a million years after eruption of the Timber Mountain Tuff. Near-surface activity occurred at about the same time 7 km to the south at the Telluride mine. Argillic alteration, opalization and pervasive reddish-orange colored iron-oxide staining surround the alunitic alteration of the Silicon mine and, except where hosted by the Rainier Mesa Member, are indistinguishable and have not been separated in Figure 2 from the older argillic and acid-sulfate alteration in the vicinity of the Thompson mine.

Calico Hills: Extensive areas of high-level argillic and advanced argillic alteration are exposed in the Calico Hills, largely within the eroded volcanic dome complex of lavas and near-vent tuffs of the rhyolite of Calico Hills, and overlying units of the Paintbrush Tuff (McKay, 1963; McKay and Williams, 1964; Jackson, 1988; Simonds, 1989). The volcanic rocks have been altered over wide areas to mixtures of alunite, kaolinite, quartz, opal-CT, and/or chalcedony, locally with sparse pyrite, and to porous acid-leached rock composed mainly of opaline silica. Tabular and irregular replacement bodies of chalcedony and opaline silica are present locally. This style of alteration is interpreted to result from high-level, acid-sulfate alteration in a steam-heated, largely vapor-dominated environment. Simonds and Scott (1990) reported the presence of adularia associated with silica and interpreted the alunitic alteration and opaline and chalcedonic silica replacement bodies to reflect areas of paleo hot spring activity. These silica bodies and the presence of adularia within an area of intense alunitic and argillic alteration likely reflect fluctuating water table levels during shallow hydrothermal activity. Argillic and alunitic alteration and silicification can be traced upwards into the Ammonia Tanks Member of the Timber Mountain Tuff in the eastern part of the Calico Hills, but in the central Calico Hills strongly altered rocks of the Paintbrush Tuff are directly overlain by unaltered flows of the rhyolite of Shoshone Mountain (Table 1). The rhyolite of Shoshone Mountain consists of rhyolite lava and tuff that represent a thick complex of overlapping and coalesced endogenous domes erupted along the margin of the Timber Mountain caldera complex at and perhaps slightly before 10.3 Ma, probably from the waning Timber Mountain magmatic system (Noble et al., 1991). These relations bracket hydrothermal activity in the Calico Hills between 11.4 Ma and

about 10.3 Ma. Identical K-Ar ages of 10.4 ± 0.3 Ma, have been determined on alunite from two widely separated localities (Table 2, samples 7 and 8) in the western and eastern parts of the Calico Hills, consistent with hydrothermal activity shortly before eruption of the rhyolite of Shoshone Mountain.

Beneath the altered volcanic rocks in the central part of the Calico Hills, units of Devonian carbonate rock lie in fault contact above shale and argillite of the Mississippian Eleana Formation (McKay and Williams, 1964; Orkild and O'Connor, 1970). Narrow rhyolitic dikes intrude the Eleana Formation and a large, shallow stock or pluton is inferred from geophysical data to underlie the area (Maldonado et al., 1979; Snyder and Oliver, 1981; Carr, 1984a). The Paleozoic rocks have locally undergone contact metamorphism, presumably associated with the inferred pluton (e.g., Carr, 1984a), and in places contain elevated concentrations of Au, Ag, Sb, As, Cu, Pb, and Zn, scattered base-metal bearing quartz veins, and replacement bodies and veins of brucite, magnesite, fluorite, barite and garnet (Quade and Tingley, 1984; Jackson, 1988; Simonds, 1989; Simonds and Scott, 1990). Although the pluton has been considered to be of late Mesozoic age (Carr, 1984a), a middle Miocene age was postulated by Simonds and Scott (1990) based on the fact that alteration and mineralization in both the pre-Cenozoic and Miocene rocks are roughly centered on the geophysically inferred location of the pluton. Further evidence is needed to resolve the relations, if any, between the acid alteration in the volcanic rocks, the contact metamorphism and hydrothermal activity in the underlying sedimentary rocks, and the inferred pluton.

Yucca Mountain: A number of deep drill holes have penetrated rocks of the Crater Flat Tuff, Lithic Ridge Tuff, older tuffs and intercalated flows of dacitic and rhyolitic lava that have been altered to zeolite- and illite/smectite-dominated assemblages over a lateral extent of at least 20 km^2 beneath Yucca Mountain (e.g. Spengler, 1981; Caporuscio et al., 1982; Maldonado and Koether, 1983; Bish 1987). Veins and irregular cavity fillings of fluorite, barite, quartz and calcite locally are present in these altered rocks and adularia and albite replace feldspar phenocrysts in some intervals (e.g. Warren et al., 1984). The silicic lavas in drill hole USW G2 are silicified, contain abundant veins of drusy quartz and locally calcite and fluorite, and have undergone pervasive quartz-albite-calcite, ±chlorite, ±pyrite (propylitic) alteration (Broxton et al., 1982; Caporuscio et al., 1982; Weiss et al.,

1992). Portions of the Tram and Bullfrog Members of the Crater Flat Tuff and the Lithic Ridge Tuff contain small amounts of finely disseminated pyrite in the groundmass, within argillicallly altered pumice fragments and partially replacing biotite (Weiss et al., 1992), as well as in lithic fragments. These relations provide strong evidence for sulfidation *after* deposition of the ash-flow units, in contrast to the interpretation of Castor et al. (1992; 1994). The degree of illite-smectite ordering and fluid inclusion homogenization data indicate that alteration temperatures of at least 275°C were reached in the deeper rocks penetrated in drill hole USW G2 and that maximum temperatures of 200°C and 100°C were reached in rocks of USW G1 and USW G3, respectively (Bish, 1987). K-Ar ages of 11 to 10 Ma have been obtained from illite (Aronson and Bish, 1987), consistent with alteration coeval with post-collapse volcanism and magmatic activity of the Timber Mountain II caldera to the north. These ages are 1.7 to 2.7 million years younger than the youngest altered unit and therefore can not reflect diagenetic or deuteric water-rock interaction during cooling of the host units as suggested by Castor et al. (1992). Taken together, the age data, mineralogy and textural features are best interpreted as the result of a large, south-flowing hydrothermal system driven by heat from magmatic activity in the nearby Timber Mountain caldera system.

Mine Mountain: Evidence for hydrothermal activity soon after eruption of the Timber Mountain Tuff is also preserved on the south flank of Mine Mountain, east of the Timber Mountain caldera complex (Figs. 2 and 4). Here argillic and alunitic alteration are present along a northwest-striking normal fault separating the Ammonia Tanks Member from pre-Paintbrush tuffs (Orkild, 1968). Alunite from this locality has given a K-Ar age of 11.1 ± 0.3 Ma (Table 2, sample 9), providing evidence for alteration within a few tenths of a million years of eruption of the Timber Mountain Tuff.

On the crest of Mine Mountain, about 1.5 km northeast of the area of alunitic alteration, zones of silicification, quartz and quartz-barite veins and hydrothermal breccia mainly within Devonian limestone and dolomite directly above the Mine Mountain thrust fault (Fig. 4) were prospected for silver and mercury during the 1920's (Orkild, 1968; Quade and Tingley, 1984; Castor and Weiss, 1992). This structure, originally considered part of a Mesozoic thrust fault system (Barnes and Poole, 1968), is now thought to have accomodated low-angle normal movement during Tertiary time

(Carr, 1984a; Caskey and Schweikert, 1992; Hudson and Cole, 1993). Geologic and geochemical data suggest similarities to the Candelaria, Nevada, silver district, or alternatively, overprinting of a Pb and Zn-rich base-metal system by later precious-metal and mercury mineralization (Castor and Weiss, 1992).

Structural relations suggest that some or all of this mineralization may be younger than the 11.4 Ma Ammonia Tanks Member of the Timber Mountain Tuff. The veins and hydrothermal breccia cut the Mine Mountain thrust fault, supporting a Tertiary age for hydrothermal activity. Quartz-barite veins both fill and are cut by moderately to steeply dipping minor faults and fractures that commonly have subhorizontal slickensides (S.I. Weiss and L.T. Larson, unpub. data, 1989). These relations most likely reflect strike-slip movements coeval with vein formation. On the south flank of Mine Mountain, units of the Timber Mountain Tuff and northwest-striking faults that cut them, are offset with apparent left-lateral displacement of about 1 km by closely spaced northeast-striking faults (Orkild, 1968) referred to by Carr (1984a) as the Mine Mountain fault (Fig. 4). The area of most numerous veins and intense silicification along the crest of Mine Mountain trends northeast, parallel to the Mine Mountain fault. Synmineralization strike-slip movements of faults and fractures in the zone of veins and silicification may have been kinematically related to the post-Ammonia Tanks displacement along the Mine Mountain fault. If this is the case, hydrothermal activity along the crest of Mine Mountain may be, at least in part, younger than 11.4 Ma, consistent with the 11.1 ± 0.3 Ma age obtained on the nearby alunite-bearing tuff.

Bullfrog Hills - Oasis Mountain area: Multiple episodes of Au-Ag mineralization during the Timber Mountain magmatic stage

The most important production in the SWNVF has been from gold and silver bearing vein deposits in the Bullfrog Hills, west of the Timber Mountain caldera complex, situated within large areas affected by post-Timber Mountain Tuff hydrothermal alteration (Fig. 2). Following the initial discovery of gold at the Original Bullfrog mine in 1904, gold and silver production from the Bullfrog district totalled at least $3 million by 1940 (Couch and Carpenter, 1943). Most production came from the Montgomery-Shoshone mine, with much smaller production from the Original Bullfrog and Gold Bar mines, several small mines near Rhyolite, and the Mayflower and Pioneer mines about 12

km to the north (Fig. 2). Exploration since the mid-1970's led to the delineation of bulk-mineable reserves at the Montgomery-Shoshone mine, open-pit production for three years at the Gold Bar mine, and the discovery and development of an entirely new deposit, now known as the Lac Gold Bullfrog mine, that is expected to produce at least 1.8 million ounces of gold (Jorgenson et al., 1989; Castor and Weiss, 1992).

The Bullfrog Hills largely consist of an upper structural plate of highly faulted and tilted Miocene volcanic and minor intercalated sedimentary rocks that are separated from underlying sedimentary and metamorphic rocks of Paleozoic and Proterozoic age by normal faults, including the low-angle Original Bullfrog segment of the OB-FC fault system (Ransome et al., 1910; Cornwall and Kleinhampl, 1964; Maldonado, 1985; 1990a). The volcanic units are mainly silicic ash-flow sheets erupted from volcanic centers of the SWNVF, including the Lithic Ridge Tuff, members of the Crater Flat, Paintbrush, and Timber Mountain Tuffs, and intercalated lavas of silicic to mafic composition. A local sequence of dominantly rhyolitic lava flows, domes and related near-vent pyroclastic deposits, in many places capped by flows of latitic to basaltic lava, overlies the Timber Mountain Tuff and older ash-flow sheets with apparent angular unconformity of as much as about 35° (Fig. 5) (cf. Maldonado, 1990a; Ahern and Corn, 1981; Weiss et al., 1990; S.I. Weiss and K.A. Connors, unpub. mapping 1989-1991). Radiometric ages show that this sequence, informally termed the tuffs and lavas of the Bullfrog Hills (TLBH) (Table 1), was erupted prior to about 10 Ma (Marvin et al., 1989; Noble et al., 1991).

Upper-plate rocks are cut and tilted, mainly to the east, as much as 90° by numerous north- to northeast-striking, generally west-dipping normal faults (Ransome et al., 1910; Cornwall and Kleinhampl, 1964; Maldonado, 1990b; Maldonado and Hausback, 1990; S.I. Weiss and K.A. Connors, unpub. mapping 1989-1991). Fault patterns and structural relations reflect numerous imbricated faults and suggest the presence of both planar-rotational and listric faults. This deformation has long been recognized as the result of strong WNW-ESE directed upper crustal extension estimated at about 25 percent (Ransome et al., 1910) to more than 100 percent (Maldonado, 1988; 1990a). Landslide and debris-flow deposits containing blocks of volcanic units and pre-Tertiary rocks as

much as 700 m in length interfinger with the TLBH and provide evidence for crustal instability and steep topography during this major pulse of extension (Weiss et al., 1990).

All of the Au-Ag production has come from quartz-calcite fissure veins hosted by the Original Bullfrog segment of the OB-FC fault and, more importantly, by moderately- to steeply-dipping normal faults within the upper plate (Fig. 5). The veins consist primarily of banded, crustiform and drusy quartz, bladed calcite, and quartz-calcite cemented breccia of vein fragments and highly altered wallrock fragments. Throughout the district the veins contain trace amounts of adularia, illite, pyrite (now largely oxidized), electrum and acanthite, and show textural evidence for multiple stages of fracturing, crustiform and banded vein filling, and brecciation (Ransome et al, 1910; Jorgenson et al., 1989; Castor and Weiss, 1992). Concentrations of Hg, As, Sb and base metals are generally low in the veins and altered wallrocks (Hg <0.25 ppm; As <50 ppm; Sb <4.0 ppm; Cu <50 ppm; Pb <25 ppm; Zn <50 ppm), although Cu concentrations as high as a few thousand ppm and Sb as high as a few hundred ppm have been reported for high-grade ores of the Original Bullfrog and Lac Gold Bullfrog mines (Castor and Weiss, 1992). Copper contents are generally greater than Pb or Zn (S. B. Castor and S. I. Weiss, unpub. data, 1990). Silver to gold ratios are low (8:1 at the Montgomery-Shoshone mine and 1:1 to 2:1 at the Lac Gold Bullfrog mine, Jorgenson et al., 1989). Wallrocks are mainly rhyolitic ash-flow units of the SWNVF and near-vein alteration is characterized by replacement of igneous alkali and plagioclase feldspar by adularia, silica flooding, and the presence of numerous quartz veinlets, disseminated pyrite and small amounts of illite. This alteration grades out initially into zones of adularia ±albite replacement of feldspar phenocrysts, thin discontinuous quartz veinlets and minor illite, and at greater distances into large areas of illitic alteration, where plagioclase phenocrysts and groundmass are partly to completely replaced by illite and calcite ±albite, ±adularia (Castor and Weiss, 1992). X-ray fluorescence analyses of a small number of samples from the Lac Gold Bullfrog and Montgomery-Shoshone mines show that potassium and rubidium concentrations are highly elevated with respect to unaltered host rocks and have a clear positive correlation, providing evidence for locally intense potassium and rubidium metasomatism within and near major veins (Fig. 6a). This metasomatism is particularly apparent considering that silicification has not reduced potassium contents through dilution (Fig. 6b). Metasomatized rocks are strongly

depleted in sodium (0.07 to 1.68 wt%) and calcium (0.02 to 0.89 wt%). Homogenization temperatures of about 200°C to 150°C and salinities of <1.5 wt% NaCl equivalent have been reported by Jorgenson et al. (1989) for fluid inclusions in samples from the Lac Gold Bullfrog and Montgomery-Shoshone mines. Together, the above characteristics indicate that mineralization in the Bullfrog district is of the low base metal type of the adularia-sericite (low-sulfidation) class of volcanic-hosted epithermal precious metal deposits, including Oatman, Arizona, Aurora, California, and Round Mountain, Sleeper and National, Nevada.

Southern Bullfrog Hills: The principal fissure vein at the Lac Gold Bullfrog mine (Fig. 2) follows a normal fault (Middle Plate fault of Jorgenson et al., 1989) dipping approximately 45° westward that brings an east-dipping hanging-wall section of Crater Flat Tuff, Paintbrush Tuff and Timber Mountain Tuff against rocks of the Crater Flat Tuff and an underlying unit of silicic lava that is widely exposed beneath the Crater Flat and Lithic Ridge Tuffs elsewhere in the Bullfrog Hills (cf. Maldonado and Hausback, 1990). The main vein (Fig. 7a) varies from about 10 to 60 m in width and consists of multiple generations of complexly cross-cutting and closely spaced veins and sheeted veins, and altered wallrock fragments and brecciated vein fragments surrounded by later stages of quartz and/or calcite. Some of the quartz is amethystine. These features provide strong evidence for multiple stages of vein deposition concurrent with repeated episodes of fracturing and brecciation and demonstrate fault movements during mineralization. Fragments of pre-Cenozoic sedimentary rock derived from below the deposit are locally not uncommon, requiring upward transport by hydrothermal fluids. Ore minerals include Ag-poor and Ag-rich electrum, acanthite and uytenbogaardtite (Ag_3AuS_2) in close paragenetic association, commonly accompanied by chrysocolla, suggesting final Au-Ag-S equilibration or reequilibration at temperatures near 113°C (Barton, 1980; Castor and Weiss, 1992; Castor and Sjoberg, 1993). Traces of tetrahedrite, chalcopyrite and galena have also been reported (Jorgenson et al., 1989). In higher levels of the mine well-developed subparallel fault surfaces form the upper and lower boundaries of the main vein, much of which is highly shattered (Fig. 7b); at deeper levels these fault surfaces become anastomosing and transect the main vein, indicating that movement of the host fault continued after the final stages of vein deposition (Weiss et al., 1991; Castor and Weiss, 1992). Adjacent hanging-wall rocks, largely of the Rainier

Mesa Member of the Timber Mountain Tuff, contain disseminated pyrite and abundant adularia as intergrowths with fine-grained, secondary quartz in the groundmass and abundant thin veins of quartz and calcite, locally with traces of adularia. Adularia, less commonly albite, and locally quartz replace the sanidine and plagioclase phenocrysts. Footwall lavas adjacent to the main vein are albitized, contain disseminated pyrite, and are cut by ore-grade stockwork zones of quartz-calcite-adularia veinlets and veins containing mixtures of hydrothermal breccia, solid black hydrocarbon, pyrite, quartz, chlorite and calcite (Fig. 7c).

Gold and silver were produced at the Montgomery-Shoshone mine 2 km to the north (Fig. 2) from quartz-calcite veins and vein-cemented fault breccia texturally, chemically and mineralogically similar to mineralization at the Lac Bullfrog deposit (Jorgenson, et al., 1989; Castor and Weiss, 1992). The veins at the Montgomery-Shoshone mine are hosted by steeply-dipping faults and fractures in the upper-plate, largely within the Ammonia Tanks Member of the Timber Mountain Tuff (Maldonado and Hausback, 1990). Alteration, including strong adularization and silica flooding within and adjacent to the veins, is identical to that observed at the Lac Gold Bullfrog mine and elsewhere in the southern Bullfrog Hills, such as at the Denver-Tramps and Gibraltar mines near Rhyolite (Fig. 2 and Fig. 5). At the Denver-Tramps and Gibraltar mines Au-Ag bearing quartz-calcite veins are also hosted by high-angle faults within units of the Paintbrush and Timber Mountain Tuffs, and are texturally, mineralogically and geochemically similar, if not identical, to those of the Montgomery-Shoshone and Lac Gold Bullfrog mines (Castor and Weiss, 1992).

At the Original Bullfrog mine in the western part of the district Au-Ag ore was mined along the shallowly north-dipping Original Bullfrog segment (Ransome et al., 1910) of the OB-FC fault within a shattered, tabular mass of complexly cross-cutting open-space quartz and calcite veins, brecciated veins and vein-encrusted and silicified wallrock fragments. Cross-cutting and textural relations reflect repeated episodes of fracturing, brecciation and open-space filling, consistent with fault movements during vein formation. Sheeted veins and quartz-calcite cemented breccia extend upward into adjacent adularized and silicified rocks of the moderately east dipping Lithic Ridge Tuff and underlying silicic lava, but the main body of vein material appears to be truncated against underlying, highly sheared Paleozoic clastic and carbonate rocks (Carr et al., 1986; Maldonado,

1990a). This truncation, along with the shattered nature of the vein, provides evidence for late movement of the Original Bullfrog fault after the final stages of vein deposition (Ransome et al., 1910). Ore and gangue mineralogy and textures, initially described by Ransome et al. (1910), and minor element signatures are remarkably similar to that of the Lac Gold Bullfrog mine, including the presence and close paragenetic association of uytenbogaardite replacing gold-poor electrum and intergrown with gold-rich electrum, acanthite and chrysocolla. (Castor and Weiss, 1992; Castor and Sjoberg, 1993).

Adularia separated from ore composed of a mixture of quartz-calcite veins and adularized wallrock fragments at the Lac Gold Bullfrog mine has given an $^{40}Ar/^{39}Ar$ age of 9.8 ± 0.3 Ma (Table 2, sample 16). This age is indistinguishable, within the limits of analytical uncertainty, from the K-Ar age of 9.5 ± 0.2 Ma reported by Morton et al. (1977) for adularia separated from vein and altered wallrock material at the Montgomery-Shoshone mine. The similarities in style of alteration and mineralization, structural and stratigraphic settings, and radiometric ages of adularia suggest mineralization at both mines was essentially contemporaneous and related to a single large hydrothermal system, rather than separate but similar systems. Veins and Au-Ag mineralization at the nearby Denver-Tramps and Gibraltar mines, 1.5 km west of the Lac Gold Bullfrog mine, also share the above similarities, consistent with deposition from the same hydrothermal system.

K-Ar and $^{40}Ar/^{39}Ar$ ages of 8.7 ± 0.3 Ma and 9.2 ± 0.3 Ma, respectively, have been obtained on two splits of adularia separated from a single specimen of thoroughly adularized and silicified Lithic Ridge Tuff at the Original Bullfrog mine (Table 2, sample 10). These ages are indistinguishable within the limits of the analytical uncertainty. Although $^{40}Ar/^{39}Ar$ age determinations of sanidine are in some cases considered to be more reliable than K-Ar ages (e.g. Hausback et al., 1990), on the basis of the analytical data alone it is difficult to assign greater weight to one determination over the other; a reasonable estimate of the age of hydrothermal activity and mineralization could be about 9 Ma. The $^{40}Ar/^{39}Ar$ age also overlaps the ages determined from adularia from the Lac Gold Bullfrog and Montgomery-Shoshone mines where mineralization is very similar in mineralogy, geochemistry and overall style. The presence of the rare mineral uytenbogaardtite in high-grade ores at both the Original Bullfrog and the Lac Gold Bullfrog mines provides additional evidence for a com-

mon origin for the veins. Following this line of reasoning, the older age of 9.2 ± 0.3 Ma would suggest a common age of mineralization of about 9.5 Ma for the Lac Gold Bullfrog, Montgomery-Shoshone, Original Bullfrog and rlated mines. Alternatively, the age data may reflect nearly identical hydrothermal activity and mineralization at the Original Bullfrog mine as much as a million years after that of the Lac Gold Bullfrog-Montgomery-Shoshone area.

Multi-stage quartz-calcite veins and vein-cemented breccia along normal faults in the upper plate were also mined for gold and silver at the Gold Bar mine, located about 4 km to the northwest of the Original Bullfrog mine (Fig. 2 and Fig. 5). Wallrocks include units of the Crater Flat Tuff and the Paintbrush Tuff, demonstrating that hydrothermal activity is younger than 12.8 to 12.7 Ma. The veins occupy faults that formed during the same pulse of extensional faulting, bracketed between 11.4 Ma and 7.6 Ma, and gangue mineralogy and textures, wallrock alteration style and assemblages and trace-element geochemistry are essentially identical to those at the Original Bullfrog, Lac Gold Bullfrog, and Montgomery-Shoshone mines. As pointed out by Ransome et al. (1910), slickensided fault surfaces and thin seams of gouge present within the veins and locally separating the veins from adjacent wallrocks indicate that faulting continued after deposition of the veins. Although not dated radiometrically, mineralization at the Gold Bar mine is inferred to have taken place at the same time as, and to be genetically related to, ore formation elsewhere in the southern part of the Bullfrog Hills.

Northern Bullfrog Hills and Oasis Mountain: The coarse landslide and debris-flow deposits that interfinger with the TLBH host gold and silver bearing quartz-calcite veins along fractures and normal faults at the Mayflower mine in the northern Bullfrog Hills (Fig. 2 and Fig. 5). These veins are texturally, mineralogically and geochemically similar to veins in the southern Bullfrog Hills (Castor and Weiss, 1992). North of the Mayflower mine, rocks of the Crater Flat and Paintbrush Tuffs are silicified and adularized in the vicinity of quartz, quartz-calcite and calcite veins hosted by normal faults and fractures. Silicified and adularia-bearing rocks are surrounded by areas in which sanidine has been preserved and plagioclase has been replaced by illite and/or kaolinite. Similar alteration is present at Oasis Mountain (Fig. 2) where quartz and quartz-calcite veins containing subeconomic concentrations of Au and Ag are present along a steeply dipping fault within a thick section of the

Ammonia Tanks Member of the Timber Mountain Tuff. Alteration to the south and southwest, between Oasis Mountain and Bailey's Hot Spring, is largely argillic, but includes areas of opal-alunite-kaolinite alteration, locally with pyrite, interpreted as the result of shallow, steam-heated acid-sulfate alteration above a fluctuating water table. This zone includes the area of intense alunitic alteration and silica leach-rock within the Ammonia Tanks Member of the Timber Mountain Tuff at Bailey's Hot Spring (Fig. 2).

Two splits of adularia from the same sample of adularized and silicified wallrock fragments incorporated in vein material from the Mayflower mine give K-Ar and $^{40}Ar/^{39}Ar$ ages of 10.0 ± 0.3 and 9.9 ± 0.3 Ma, respectively (Table 2, sample 11). These ages are identical to those of the Montgomery-Shoshone and Lac Gold Bullfrog mines, within the limits of the analytical uncertainty, and are about 0.7 Ma older than the $^{40}Ar/^{39}Ar$ age from the Original Bullfrog mine.

An earlier episode of hydrothermal activity is evident north of the Mayflower mine. At the Yellowjacket mine (Fig. 2) adularia separated from quartz-calcite-pyrite vein material containing fragments of adularized tuff has given an $^{40}Ar/^{39}Ar$ age of 11.3 ±0.3 Ma (Table 2, sample 17). A K-Ar age of 11.0 ±0.4 Ma has been obtained on adularia separated from metasomatized wallrock of Crater Flat Tuff along a quartz vein about 1.5 km south of the Yellowjacket mine (sample 12, Table 2). These ages reflect hydrothermal activity in the northern part of the Bullfrog Hills within at most a few tenths of a million years after deposition of the Ammonia Tanks Member and volcanism of the local tuffs of Fleur de Lis Ranch and tuff of Cut-off Road in the nearby, western part of the Timber Mountain I caldera.

A K-Ar age of 10.6 ±0.3 Ma determined on adularia separated from potassium and silica metasomatized tuff of the Ammonia Tanks Member adjacent to the veins in Oasis Mountain (sample 13, Table 2) falls between, and overlaps within the limits of the analytical uncertainty, both the K-Ar age from the Mayflower mine and the K-Ar age from the northern Bullfrog Hills. Alunite replacing phenocrysts and groundmass in the Ammonia Tanks Member at Bailey's Hot Spring has given a K-Ar age of 10.2 ±0.3 Ma (sample 14, Table 2). This age is identical, within the limits of the analytical uncertainty, to the age from Oasis Mountain and the ages from the Mayflower and Lac Gold Bullfrog mines. In contrast to the water-saturated conditions reflected by the veins and

adularia-stable alteration within the Ammonia Tanks Member at Oasis Mountain, vapor-dominated conditions south of Oasis Mountain between about 10 to 10.5 Ma are implied by the high-level acid-sulfate alteration within the same unit at Bailey's Hot Spring, and within overlying megabreccia deposits (presumeably deposited in topographically low areas) that are widely exposed west and northwest of Bailey's Hot Spring (Fig. 5). Stratigraphically equivalent megabreccia and conglomerate at the Mayflower mine apparently were below the water table at about 10 Ma.

Southeast of Oasis Mountain in the Transvaal Hills, argillic and alunitic alteration and silicification affect intracaldera units of the Timber Mountain Tuff and related, post-collapse lava and tuff within the Timber Mountain I and II calderas (Fig. 2). The altered rocks are locally overlain by unaltered basaltic lava and ash-flow sheets of the Thirsty Canyon Tuff (Byers et al., 1976b), demonstrating that hydrothermal activity ceased prior to about 9.4 Ma. Alunite lining fractures within acid-sulfate altered intracaldera-facies tuffs of the Rainier Mesa Member has given a K-Ar age of 9.9 ±0.4 Ma (sample 15, Table 2). This age is consistent with the ages of the host rocks and overlying units and is interpreted to reflect the timing of hydrothermal activity in the Transvaal Hills.

Hydrothermal activity poorly constrained in time

Areas of argillic alteration, quartz veins, opaline silicification, and/or locally abundant iron oxides after pyrite are present near the structural margin of the Claim Canyon cauldron in northern Yucca Mountain (Fig. 2). Units of the Crater Flat Tuff, Paintbrush Tuff and Paintbrush-related lava and caldera margin breccia (Byers et al., 1976b) are affected by this alteration. Accordingly, hydrothermal activity in these areas must at least in part be younger than 12.7 Ma, although earlier alteration of the Crater Flat Tuff can not be ruled out. These areas may represent stratigraphically and topographically higher parts of the large, *ca.* 11-10 Ma hydrothermal system in Yucca Mountain, where hydrothermal fluids perhaps ascended to higher stratigraphic and topographic levels along numerous faults and fractures near the structural margin of the Claim Canyon cauldron, and/or as a result of closer proximity to Timber Mountain magmatic activity.

Northwest of the Timber Mountain caldera complex, areas of hydrothermal alteration and precious-metal mineralization are present in Quartz Mountain and in the Clarkdale and Yellow

Gold mine areas (Cornwall, 1972; Quade and Tingley, 1984). Gold- and silver-bearing epithermal quartz veins are hosted by north- to northeast-trending faults and fractures (Quade and Tingley, 1984). Veins and silicification in the Quartz Mountain area are present in silicic lavas stratigraphically below the 13.7 Ma Grouse Canyon Member of the Belted Range Tuff (Noble and Christiansen, 1968) and possibly older than the 13.9 Ma tuff of Tolicha Peak (Minor et al., 1993). The Grouse Canyon Member is not present in the mineralized areas and it is not altered in exposures 1 to 2 km to the east; it is therefore impossible to place a lower limit on the age of mineraliztion. The stratigraphic position and timing of alteration and Au-Ag mineralization in the Clarksdale and Yellow Gold mine areas are less firmly constrained, but examination of aerial photographs and brief field reconnaissance of the southwestern edge of the altered area indicates that the alteration affects both the Rainier Mesa and Ammonia Tanks members of the Timber Mountain Tuff and may affect the rhyolite of Obsidian Butte (Minor et al., 1993).

Interrelations with Magmatic Activity, Volcanism and Extensional Faulting

Epithermal mineralization is found in areas of hydrothermal alteration within and marginal to volcanic and intrusive centers of the SWNVF (Fig. 2), as has been observed in other large intracontinental volcanic fields of late Cenozoic age, such as the Mogollon-Datil (Elston et al., 1973), San Juan (e.g., Lipman et al., 1976), Jemez (Gardiner et al., 1986; Woldegabriel and Goff, 1989) volcanic fields. This distribution around and within the Timber Mountain caldera complex, and initial K-Ar age determinations and stratigraphic information, led Jackson et al. (1988) and Jackson (1988) to propose that, with the exception of Wahmonie, the Thompson mine and possibly eastern Bare Mountain, most areas of hydrothermal activity and epithermal mineralization in the southern part of the field were related to the intense, widespread magmatic and volcanic activity of the Timber Mountain magmatic system. Further work led Noble et al. (1991) to emphasize the temporal and spatial association of hydrothermal activity and mineralization with magmatic events of *both* the main and Timber Mountain magmatic stages in the development of the SWNVF.

Radiometric ages of hydrothermal activity from the southern part of the field (Fig. 8) fall into two principal groups that overlap and closely follow the culminations of the main and Timber Moun-

tain magmatic stages at about 12.7 Ma and 11.45 Ma, respectively. During the main magmatic stage, silicic porphyry dikes in Bare Mountain and calc-alkaline, intermediate composition lavas, tuffs and intrusions at Wahmonie were derived from magma systems peripheral to the central caldera complex. Most fluorite and gold mineralization in the eastern part of Bare Mountain was associated with hydrothermal activity between about 13 Ma and 12.5 Ma that followed the emplacement of the silicic porphyry dikes by about 1 to 2 Ma. This time lag probably reflects continued and/or renewed magmatic activity of the deeper porphyry system. Shallow acid-sulfate alteration and epithermal mercury mineralization took place at the Thompson mine, near the southwestern margin of the Claim Canyon cauldron, within a few tenths of a million years after eruption of the Tiva Canyon Member of the Paintbrush Tuff, which marked the culmination of the main magmatic stage (Broxton et al., 1989; Noble et al., 1991). Epithermal Ag-Au vein deposits formed in the Wahmonie district at about the same time, coeval with the latter stages of, or shortly following, volcanism and igneous activity of the Wahmonie-Salyer volcanic center.

During the Timber Mountain magmatic stage, alunitic alteration formed at the Silicon mine, near the Telluride mine and at Mine Mountain, probably as the result of oxidation of H_2S and acid leaching in shallow, steam-heated portions of hydrothermal systems peripheral to the Timber Mountain caldera complex. The earliest episode of adularia-stable alteration and associated quartz-calcite vein formation in the northern Bullfrog Hills occurred at about 11.3 to 11 Ma, coeval with or at most a few tenths of a million years after eruption of the Ammonia Tanks Member, Tuffs of Fleur de Lis Ranch and the 11.4 Ma Tuff of Cut-off Road. South of the caldera complex, ages of from 11 to 10 Ma on illite from tuffs of pre-Paintbrush age in the subsurface of Yucca Mountain suggest that a hydrothermal system of large lateral extent was associated with the waning Timber Mountain magmatic system centered not far to the north. Alteration in northern and northwestern Yucca Mountain affected rocks as young the Paintbrush Tuff, and, although not radiometrically dated, may be of the same age. Hydrothermal fluids may have ascended to higher stratigraphic and topographic levels in northern Yucca Mountain along faults and fractures related to the Claim Canyon cauldron margin, and/or because of the close proximity to the Timber Mountain magma system.

Following collapse of the Timber Mountain II caldera and eruption of the Tuffs of Fleur de Lis Ranch and Tuff of Cut-off Road in the western part of the caldera complex, magmatic activity and volcanism continued until about 10 Ma with the eruption of mainly rhyolitic domes and related pyroclastic deposits, and smaller volumes of latitic and basaltic lavas in the Bullfrog Hills (see below) and within and adjacent to the southern margins of the complex. Shallow, steam-heated alunitic and argillic alteration in the Calico Hills, Transvaal Hills and at Bailey's Hot Spring, and adularization and quartz vein formation at Oasis Mountain were penecontemporaneous with this volcanism. In the southern Bullfrog Hills and at the Mayflower mine adularia ages of about 10 to 9 Ma indicate that alteration and epithermal Au-Ag mineralization were penecontemporaneous with, and continued for about 1 Ma after, the end of volcanism in the Bullfrog Hills.

Coeval extension, magmatic activity and volcanism, and precious-metal mineralization in the Bullfrog Hills-Oasis Mountain area

A simplified stratigraphic diagram showing major units, radiometric ages and structural relations of the TLBH to older and younger rocks in the Bullfrog Hills is given in Figure 9. Two principal units of interbedded ash-flow tuff and surge deposits, consisting of high-silica rhyolite, are each overlain and intruded by rhyolite plugs, domes and flows (Fig. 9). These two units of ash-flow tuff and surge deposits, and a number of the rhyolite plugs, domes and flows are petrographically and lithologically similar to tuffs of the Rainier Mesa Member of the Timber Mountain Tuff, containing abundant large phenocrysts of quartz and alkali feldspar, with lesser amounts of sodic plagioclase, accessory biotite and only traces of hornblende in some rocks. The pyroclastic rocks have abundant small- and large-scale cross bedding, scour-and-fill structures and discontinuous, extremely lithic-rich layers, and are best interpreted as near-vent, precursor pyroclastic deposits associated with the eruption of certain of the rhyolite domes and flows (Maldonado and Hausback, 1990; Weiss et al., 1990; Noble et al., 1991). Radiometric ages from rocks of the TLBH (Fig. 9), including thin flows of olivine basalt locally present at the base of the sequence, suggest that the entire sequence was erupted rapidly between about 10.5 to 10 Ma. The rhyolitic domes, flows and related tuffs of the TLBH are reasonably interpreted as products of the waning Timber Mountain magma system, based on their

ages, proximity to the western margin of the Timber Mountain caldera complex and similarities to the Rainier Mesa Member of the Timber Mountain Tuff (Noble et al., 1991).

Several lines of evidence indicate that extensional faulting and tilting in the Bullfrog Hills were coeval with the magmatic and volcanic activity of the TLBH, during the latter part of the Timber Mountain stage. No obvious angular discordance is present between the units of the Timber Mountain Tuff or underlying ash-flow sheets, constraining major faulting to be younger than 11.45 Ma. However, throughout the Bullfrog Hills the Ammonia Tanks Member and older units dip more steeply than do nearby younger rocks of the TLBH (Cornwall and Kleinhampl, 1964; Maldonado, 1990b; Maldonado and Hausback, 1990) and in widely separated locations, an angular discordance of as much as 35° is present between units of the TLBH and the underlying rocks (Fig. 5) (Ahern and Corn, 1981; Connors, Weiss and Noble, Plate 1 *in* Connors, 1994). This discordance most likely represents a district-wide angular unconformity (Fig. 9) and demonstrates that faulting and substantial tilting began prior to volcanism of the TLBH (cf. Maldonado, 1990a). Layers of coarse breccia that locally contain enormous blocks, including blocks of the Rainier Mesa and Ammonia Tanks Members of the Timber Mountain Tuff, tuffs of Fleur de Lis Ranch and the tuff of Cut-off Road, interfinger with units of the TLBH (Fig. 5 and Fig. 9). The unequivocal presence of blocks of the post-Ammonia Tanks units rules out an origin associated with collapse of the Timber Mountain I or II calderas. These breccia layers are interpreted as tectonic megabreccia, consisting of landslide and debris-flow deposits shed from steep topography, such as fault scarps, during deposition of the TLBH. A major scarp probably formed along the inferred fault or faults that have displaced the Ammonia Tanks Member of the Timber Mountain Tuff below the surface in Oasis Valley (Fig. 5), a throw of at least 2000 to 3000 feet. Further evidence for synvolcanic tectonism comes from the latitic lavas near the top of the TLBH (Fig. 9). Locally there is an upwards decrease in the dip of successive latite flows and in the northern Bullfrog Hills the latites drape fault scarps and irregular topography cut in underlying rhyolite flows and tuffs (Cornwall and Kleinhampl, 1964; Connors, Weiss and Noble, Plate 1 *in* Connors, 1994). Rhyolite plugs and dikes of the TLBH, which in some cases can be traced upwards into domes and flows, both intrude and are also cut by normal faults, providing evidence for the interaction of silicic magmas that fed eruptions of the TLBH with faults at

shallow levels in the upper plate. Basaltic dikes also intrude and are cut by faults in the upper plate in the southern Bullfrog Hills (Ransome et al., 1910) and at the 916 m level in the Lac Gold Bullfrog mine a thin, hydrothermally altered and brecciated basaltic dike can be seen to intrude and pinch out within the main fault and vein system.

Throughout the Bullfrog Hills numerous, generally west-dipping normal faults cut tilted sections of the TLBH, indicating that faulting and tilting continued or resumed after deposition of the sequence. Map patterns and exposed fault surfaces indicate that some of these faults are steeply dipping and in all probability cut the Original Bullfrog segment of the OB-FC fault system. Exploratory drilling in the southern Bullfrog Hills near Rhyolite and in the vicinity of the Lac Gold Bullfrog mine has demonstrated offsets of the OB-FC fault system of on the order of several hundreds of feet by faults such as the Lac Gold Bullfrog mine fault (middle plate fault of Jorgenson et al., 1989) and the Montgomery-Shoshone fault which have dips of 45 to 80°, respectively. (Jorgenson et al., 1989; J. Marr, pers. commun., 1990; T. Osmondson, pers. commun., 1992). A similar relationship is exposed 3 km east of the Mayflower mine (Figs. 5 and 10) where low-angle normal faults cut an east-facing, vertical to slightly overturned section of Lithic Ridge, Crater Flat and Paintbrush Tuffs and separate these units from underlying strata of Early Cambrian age. Although this situation is analogous to the truncation of the same sequence of east-dipping ash-flow units against pre-Cenozoic rocks near the Original Bullfrog mine by the gently north-dipping Original Bullfrog fault, east of the Mayflower mine the low-angle faults are offset as much as several hundred meters by younger, steeply-dipping faults (Fig. 10). The gently west-dipping to approximately 25° east dips of the low-angle faults in Figure 10 are inferred to result from the cumulative displacement of relatively late, down-to-the-west faults further to the east, perhaps following, or penecontemporanous with, isostatic rebound and flexure of the lower plate (e.g. Spencer, 1984; Buck, 1988). The offsets indicated by drilling in the southern Bullfrog Hills and the relations observed east of the Mayflower mine reflect extension at least in part accommodated by brittle structures that cut the OB-FC fault system. Such offsets and brittle deformation in the lower plate contradict the model of Maldonado (1990a, 1990b) and Maldonado and Hausback (1990), and argue for revisions to their cross-sections which show that all faults in the upper plate are inferred to merge with, and/or are truncated by, the Original Bullfrog

segment of the OB-FC fault system. The presence of dikes and plugs intruding some of these faults is consistent with a connection to deep structures, presumably also of extensional nature, that channeled magmas upward to, and/or above, the level of the OB-FC detachment fault system (Weiss et al., 1990).

The Au-Ag vein deposits in the Bullfrog Hills are hosted by shallowly to steeply-dipping faults and fractures that formed near the base of, and within, the upper plate during the pulse of post-Ammonia Tanks extensional faulting. The older ages of about 11.3 and 11.0 Ma for veins in the northern Bullfrog Hills are consistent with faulting and hydrothermal activity in the vicinity of the Yellow Jacket mine early during this interval of deformation. Vein textures at the Original Bullfrog, Lac Gold Bullfrog, Montgomery-Shoshone and Gold Bar mines reflect episodic brecciation and are best explained as a result of movements along the host faults during mineralization, although breccia of probable hydrothermal origin is present as well. The K-Ar and $^{40}Ar/^{39}Ar$ ages therefore provide evidence that the faults at the Lac Gold Bullfrog and Montgomery-Shoshone mines were active at about 9.8 (or possibly 9.5) Ma, and for faulting at the Original Bullfrog mine at about 9.0 Ma. The well-developed post-mineral fault surfaces and shattered nature of the vein at the Lac Gold Bullfrog mine indicate that fault movements in the upper plate continued after about 9.8 Ma. Veins at the Montgomery-Shoshone mine are both hosted within and truncated by the northeast-trending Montgomery-Shoshone fault that juxtaposes essentially unaltered units of the TLBH against altered and mineralized rocks of the Timber Mountain Tuff (Ransome et al., 1910; Maldonado and Hausback, 1990), indicating substantial fault displacement after about 9.5 (or possibly 9.8) Ma. Likewise, the shattered nature of the Original Bullfrog vein and its truncation against unmineralized rocks below the Original Bullfrog fault show that movement of the Original Bullfrog segment of the OB-FC fault system continued after about 9.0 Ma. These relations are consistent with the fact that entire sections of the *ca.* 10 to 10.5 Ma TLBH are commonly tilted as much as 35° and cut by numerous faults. Mineralization in the Bullfrog Hills was, therefore, penecontemporaneous with, as well as structurally controlled by, extensional faulting that continued after mineralization.

Discussion and Summary

Since the advent of radiometric dating numerous workers have demonstrated close space-time associations of hydrothermal activity and mineralization with volcanic and shallow igneous activity. In many cases, such as at Bodie, California, (Silberman et al., 1972), various deposits of the Maricunga belt, Chile (Sillitoe et al., 1991), Tavua caldera in Viti Levu, Fiji (Setterfield et al., 1992), Sleeper, Nevada (Conrad et al. 1993), Arcata, Peru (Candiotti de los Rios et al., 1990) and Orocopampa, Peru (McKee et al., 1994), it has been shown that hydrothermal activity took place toward the end of, or shortly after, volcanism and was presumably related to the emplacement and cooling of subjacent, late-stage magma bodies. Few studies of the duration of epithermal mineralization have been carried out using $^{40}Ar/^{39}Ar$ dating techniques and cross-cutting relations, but it has generally been accepted that individual hydrothermal systems responsible for volcanic-related epithermal precious-metal deposits have lifespans on the order of 0.5 Ma or less, to about 1.5 Ma (e.g., Silberman, et al., 1985). K-Ar and $^{40}Ar/^{39}Ar$ ages suggest that hydrothermal activity may have taken place over a period as long as 2 Ma at the volcanic dome-hosted Sleeper gold-silver deposit in northwestern Nevada (Conrad et al., 1993). Evidence for longer-lasting, episodic and/or more complex hydrothermal activity, in some cases involving multiple hydrothermal centers, comes from porphyry systems and large volcanic centers and intracontinental volcanic fields (e.g., Butte, Montana, Meyer et al., 1968; western San Juan caldera complex, Lipman et al., 1976; Julcani, Peru, Noble and Silberman, 1984; Jemez, New Mexico, Woldegabriel and Goff, 1989; Woldegabriel, 1990; Chila Cordillera, Peru, Swanson et al., 1993) where hydrothermal activity overlapped multiple periods of magmatic and volcanic activity.

In the SWNVF multiple hydrothermal systems were active over a period of at least 4.5 Ma, overlapping portions of the main and Timber Mountain magmatic stages. The earliest recognized hydrothermal activity occurred in the Sleeping Butte area early in the main magmatic stage, prior to the eruption of the 13.7 Ma Grouse Canyon Member, and possibly prior to 14.0 Ma in the vent area of the Lithic Ridge Tuff. Radiometric ages and stratigraphic relations indicate that presently known episodes of hydrothermal activity in large part were coeval with, and continued for 1 to 2 million years after, the climactic eruptions of the Paintbrush Tuff and Timber Mountain Tuff at about 12. 8

Ma and 11.5 Ma, respectively, and the main stage magmatic activity in Bare Mountain and the Wahmonie-Salyer center. In the southern Bullfrog Hills hydrothermal activity and mineralization may have taken place as late as about 9 Ma. No evidence has been recognized for hydrothermal activity 5 to 10 million years *after* the caldera cycles, as is the case, for example, with the Silverton and Summitville calderas of the San Juan volcanic field (Lipman et al., 1976; Bartos, 1993), and the Alunite Ridge-Deer Trail Mountain area of the Marysvale volcanic field (Cunningham et al., 1984; Beaty et al., 1986).

A broad spatial association between hydrothermal and magmatic activity in the SWNVF is shown by the distribution of alteration and mineralization within and peripheral to the southern and western margins of the Timber Mountain caldera complex and the older Claim Canyon cauldron, and in outlying centers of igneous and volcanic activity at Bare Mountain, and Wahmonie. Alteration is widespread in the Bullfrog Hills and the Calico Hills, in and adjacent to areas of extracaldera domes and flows erupted late in the Timber Mountain magmatic stage. The spatial association, in combination with the close temporal correspondence between magmatic-volcanic activity and hydrothermal activity, provides strong evidence in support of a genetic relation between pulses of magmatic activity and multiple episodes of hydrothermal alteration and mineralization.

Contrasting styles and types of epithermal precious-metal mineralization were produced during the main and Timber Mountain stages. Silver-rich precious metal-bearing quartz and quartz-calcite veins with abundant Te, and locally Bi, but modest base-metal contents, were deposited at the Wahmonie-Salyer center between about 13 to 12.5 Ma, possibly above a porphyry-type magmatic system near the end of, or shortly following, local volcanism. At about the same time, fluorite and disseminated Au mineralization formed in the northern and eastern parts of Bare Mountain in and near silicic porphyry dikes emplaced 1 to 2 m.y. earlier. The disseminated style of mineralization, abundant As, Sb, Hg, and Tl, low base metal concentrations and high Au:Ag ratios are features typical of sedimentary rock-hosted disseminated Au deposits commonly referred to as Carlin-type deposts elsewhere. At Bare Mountain the presence of hypersaline fluid inclusions in the altered dikes, abundant Mo, F and, locally, Bi and Te, and the timing of mineralization 1 to 2 Ma after dike emplacement, are consistent with a magmatic affinity, perhaps as distal products of deeper por-

phyry-type magmatic-hydrothermal activity (Noble et al., 1989; 1991; Weiss et al., 1993b). Structural relations suggest that silicification and deposition of quartz and quartz-barite veins containing high concentrations of base metals, Ag and Hg in Paleozoic rocks at Mine Mountain may have taken place at about 11.1 Ma. Excellent examples of adularia-sericite deposi place at about 11.1 Ma. Ex formed in the Bullfrog Hills during at least two periods of hydrothermal activity between 11.3 and about 9 Ma. A similar style of alteration and mineralization is inferred for the little-studied Au-Ag bearing veins in the Clarkdale and Tolicha-Quartz Mountain districts. Zones of alunitic and argillic alteration on the south flank of Mine Mountain, in the Calico Hills, Transvaal Hills, Silicon and Thompson mine area, near the Mother Lode and Telluride mines, and in areas of the Bullfrog Hills and Oasis Valley, including Bailey's Hot Spring, are interpreted as the result of steam-heated acid-sulfate processes near and/or above paleo-watertables, implying relatively shallow hydrothermal environments. In summary, altered and mineralized areas of the SWNVF are diverse in style, mineralogy, alteration and trace-element signatures, suggesting that in addition to differences in their geologic settings, the hydrothermal systems varied significantly in their composition and origin.

Two pulses of E-W to ESE-WNW regional extension of Miocene age are recognized in the southern and southwestern parts of the SWNVF. Based on the strikes of the silicic dikes in Bare Mountain, the least principal stress direction was oriented in a E-W to WNW-ESE direction at about 14 Ma. The first pulse coincided with the 1 Ma hiatus in volcanism between the main and Timber Mountain magmatic stages and involved tilting along N-S to NE-trending faults, mainly in areas south of the Timber Mountain caldera complex, including the area of Yucca Mountain and in the northern part of Bare Mountain. Extension was in part accommodated by the Fluorspar Canyon segment of the OB-FC fault system. The contrast between relatively shallow alunitic alteration and Hg mineralization in the Telluride - Mother Lode mine area and porphyry-type groundmass crystallization and hypersaline inclusions in the dikes suggests that considerable uplift, on the order of 1 to 2 km, took place in the northern part of Bare Mountain between 13.9 and 12.2 Ma. This uplift may have, in large part, resulted from tectonic denudation associated with the early pulse of extension and faulting along the Fluorspar Canyon segment, although some uplift prior to deposition of the 13.2 Ma Crater Flat Tuff is possible as well.

Major displacements along the Original Bullfrog segment of the OB-FC fault system, and the major tilting and imbricate normal faulting in the Bullfrog Hills took place during the younger pulse of extension between 11.4 Ma and 7.6 Ma. This younger deformation overlapped in time and space with magmatic activity and volcanism of the waning Timber Mountain system west of the Timber Mountain caldera complex. Precious-metal deposits at the Lac Gold Bullfrog, Montgomery-Shoshone, Rhyolite, Original Bullfrog, Gold Bar, Mayflower and Yellowjacket mines are structurally controlled by the Original Bullfrog fault and related, more steeply dipping faults in the upper plate that formed during the younger pulse of extension. Vein and breccia textures and structural relations show that mineralization took place concurrently with extensional faulting, and that faulting continued after mineralization. Radiometric ages indicate at least two periods of hydrothermal activity and vein deposition: one at about 11.3 to 11 Ma in the northern part of the Bullfrog Hills, and the second at about 10 to 9 Ma in the southern part of the Bullfrog Hills and at the Mayflower mine in the northern Bullfrog Hills. The older period closely followed eruption of the Ammonia Tanks Member and the tuffs of Fleur de Lis Ranch. The younger period, possibly consisting of two sub-episodes, began at about the end of volcanism of the TLBH and perhaps extended for about 1 Ma. The ages are consistent with mineralization at the Original Bullfrog mine at about 9 Ma, as much as 0.5 to 1 million years after formation of nearly identical deposits at the Lac Gold Bullfrog mine and elsewhere in the Bullfrog Hills. This suggests that mineralization in the southern Bullfrog Hills was episodic and may have been produced by similar, but separate, perhaps spatially overlapping hydrothermal systems. Nevertheless, the identical styles of alteration and mineralization, similar mineralogy and trace-element signatures, and the presence of uytenbogaardtite at both the Lac Gold Bullfrog and Original Bullfrog mines can be used to argue that widely separated, productive veins in the southern Bullfrog Hills were deposited in a single, aerially extensive hydrothermal system active between about 10 to 9.5 Ma. Such a large system may have developed in response to high heat flow over a wide area, resulting from the combination of extensional thinning of the crust, the rise of synextensional magmas that fed eruptions of the TLBH, and the high fracture permeability created by the numerous, closely spaced faults in the upper plate. High heat flow and high permeability could have persisted long after the end of local magmatic

activity as extensional faulting and tectonic denudation of the heated middle to upper crust continued, providing a potential mechanism for hydrothermal activity as late as about 9 Ma at the Original Bullfrog mine. The fact that productive veins are widely scattered in a large area of alteration suggests that gold and other metals may not have been evenly distributed through the hydrothermal fluids. For this reason, and considering the extremely low initial gold contents of the subalkaline rhyolitic rocks in the upper plate (~0.2 to 0.4 ppb Au, Connors et al., 1993), we speculate that ores in the district may reflect locallized inputs of gold to the hydrothermal system, possibly from magmatic fluids (e.g. Bartos, 1993).

The economically most important producers of precious metals in the SWNVF, the Bullfrog and Bare Mountain districts, are, along with the Wahmonie district, spatially and temporally associated with centers of igneous and volcanic activity. Nevertheless, in all three areas faults and fractures related to regional extension provided the most important structural controls for mineralization, rather than volcano-tectonic features such as ring fractures, caldera margin faults, or faults associated with resurgent doming. Veins in the Bullfrog Hills are hosted by, and were deposited during movements of, upper crustal extensional faults that were active during and after the waning stages of local magmatic and volcanic activity. At Wahmonie the veins formed within northeast trending high-angle faults and fractures associated with horst-and-graben structures (Ekren and Sargent, 1965) that developed shortly after volcanism of the Wahmonie-Salyer center. The gold and fluorite deposits of similar age in Bare Mountain were structurally controlled largely by north-south to northeast-southwest trending, moderately- to steeply-dipping faults and fractures mainly below the Fluorspar Canyon fault, as well as by the porphyry dikes, consistent with regional east-west to WNW-ESE extension. The importance of regional extension as a major factor in the genesis of precious metals deposits of early Miocene age in the southern Walker Lane belt, including Paradise Peak, Tonopah and Goldfield, Nevada, has recently been pointed out by John et al. (1989) and Seedorf (1991). We believe that this is also the case with the Bullfrog, Wahmonie and Bare Mountain districts in the SWNVF, where multiple episodes of magmatic activity, volcanism, extension and mineralization were closely interrelated during middle and late Miocene time.

Acknowledgments

This paper draws on studies carried out by K. A. Connors, M.R. Jackson, D.C. Noble, and S. I. Weiss under contracts from the Nevada Nuclear Waste Project Office (through the Center for Neotectonic Studies) and Cordex Exploration Company, (through the Department of Geological Science) at the Mackay School of Mines, University of Nevada, Reno. Additional support by a research grant to K. A. Connors from the Geological Society of America and a grant to S. I. Weiss from the Mackay Mineral Research Institute is gratefully acknowledged. The authors benefited from the insights of the many people who have contributed to understanding the volcano-tectonic framework of the SWNVF, and from lively discussions with M. D. Carr, W. J. Carr, S. B. Castor, B. Claybourne, D. Fanning, S. M. Green, J. D. Greybeck, L. T. Larson, T. Osmondson, J. M. Proffett, Jr., S. J. Ristorcelli, D. A. Sawyer and A. B. Wallace. We are particularly grateful for the interest and support provided by A.B. Wallace and thank Cordex Exploration Co., D and H Mining Inc., Gexa Gold Corp., Lac Minerals USA Inc., Saga Exploration Co., and US Precious Metals Inc., for access to their properties. Fieldwork in restricted areas of the Nevada Test Site was made possible by the cooperation of the staff at Operations Control and the Yucca Mountain Project Office at the Nevada Test Site. XXX and XXX provided useful and constructive reviews of the manuscript.

REFERENCES

Ahern, R., and Corn, R.M., 1981, Mineralization related to the volcanic center at Beatty, Nevada: Arizona Geological Society Digest, v. XIV, p. 283-286.

Armstrong, R.L., Ekren, E.B., McKee, E.H., and Noble, D.C., 1969, Space-time relations of Cenozoic silicic volcanism in the Great Basin of the western United States: Am. Jour. Science, v. 267, p. 478-490.

Aronson, J.L., and Bish, D.L., 1987, Distribution, K/Ar dates, and origin of illite/smectite in tuffs from cores USW G-1 and G-2, Yucca Mountain, Nevada, a potential high-level radioactive waste repository [abs.]: Program with Abstracts, 24th Annual Meeting, Clay Minerals Soc., Socorro, New Mexico, v. 25.

Ball, S.H., 1907, A geologic reconnaissance in southwestern Nevada and eastern California: U. S. Geol. Survey Bull. 308, 218 p.

Barnes, H., and Poole, F.G., 1968, Regional thrust-fault system in Nevada Test Site and vicinity, *in* Eckel, E.G., ed., Nevada Test Site: Geol. Soc. America Mem. 110, p. 233-238.

Barton, M.D., 1980, The Ag-Au-S system: Econ. Geol., v. 75, p. 306-316.

Barton, M.D., and Trim, H.E., 1990, Late Cretaceous two-mica granites and lithophile-element mineralization in the Great Basin [abs.]: Geology and Ore Deposits of the Great Basin, Reno/Sparks, Nevada, 1990, Program with Abstracts, p. 76.

Bartos, P.J., 1993, Comparison of gold-rich and gold-poor quartz-base metal veins, western San Juan Mountains, Colorado: the Mineral Point area as an example: Soc. Econ. Geol. Newsletter, no. 15.

Beaty, D.W., Cunningham, C.G., Rye, R.O., Steven, T.A., and Gonzalez-Urien, E., 1986, Geology and geochemistry of the Deer Trail Pb-Zn-Ag-Cu manto deposits, Marysvale district, west-central Utah: Econ. Geol., v. 81, p. 1932-1952.

Berger, B.R., and Bagby, W.C., 1990, The geology and origin of Carlin-type gold deposits: Jour. Geochem. Explor., v. 36, p. 210-248.

Best, M.G., Christiansen, E.H., Deino, A.L., Grommé, C.S., McKee, E.H., and Noble, D.C., 1989, Eocene through Miocene volcanism in the Great Basin of the western United States: New Mexico. Bur. Mines Mineral Res. Mem. 47, p. 91-133.

Bish, D.L., 1989, Evaluation of past and future alteration in tuff at Yucca Mountain, Nevada based on clay mineralogy of drill cores USW G-1, G-2, and G-3: Los Alamos Natl. Lab. Rept. LA-10667-MS, 41 p.

Bonham, H.F., Jr., and Hess, R.H., 1992, The Nevada mineral industry, 1992: Nevada Bur. Mines and Geol., Spec. Pub. MI-1992, 52 p.

Broxton, D.E., Vaniman, D., Caporuscio, F., Arney, B., and Heiken, G., 1982, Detailed petrographic descriptions and microprobe data fro drill holes USW-G2 and UE25b-1H, Yucca Mountain, Nevada: Los Alamos, New Mexico, Los Alamos Natl. Lab. Rept. LA-10802-MS, 168 p.

Broxton, D.E., Warren, R.G., and Byers, F.M., Jr., 1989, Chemical and mineralogic trends within the Timber Mountain-Oasis Valley caldera complex, Nevada: Evidence for multiple cycles of chemical evolution in a long-lived silicic magma system: Jour. Geophys. Res., v. 94, p. 5961-5985.

Buck, W.R., 1988, Flexural rotation of normal faults: Tectonics, v. 7, p. 959-973.

Byers, F.M., Jr., Carr, W.J., and Orkild, P.P., 1989, Volcanic centers of southwestern Nevada: evolution of understanding, 1960-1988: Jour. Geophys. Res., v. 94, p. 5908-5924.

Byers, F.M., Jr., Carr, W.J., Orkild, P.P., Quinlivan, W.D. and Sargent, K.A., 1976a, Volcanic Suites and related cauldrons of Timber Mountain-Oasis Valley caldera complex: U.S. Geol. Survey Prof. Paper 919, 70 p.

Byers, F.M., Jr., Carr, W.J., Christiansen, R.L., Lipman, P.W., Orkild, P.P., and Quinlivan, W.D., 1976b, Geologic map of the Timber Mountain Caldera area, Nye County, Nevada: U.S. Geol. Survey Misc. Invest. Map I-891, 1:48,000 scale.

Candiotti de los Rios, H., Noble, D.C., and McKee, E.H., 1990, Geologic setting and epithermal silver veins of the Arcata district, southern Peru: Econ. Geol., v. 85, p. 1473-1490.

Caporuscio, F., Vaniman, D.T., Bish, D.L., Broxton, D.E., Arney, D., Heiken, G., Byers, F.M., and Gooley, R., 1982, Petrologic studies of drill cores USW-G2 and UE25b-1H, Yucca Mountain, Nevada: Los Alamos Natl. Lab. Rept. LA-9255-MS, 114 p.

Carr, W.J., 1974, Summary of tectonic and structural evidence for stress orientation at the Nevada Test Site: U. S. Geol. Survey Open-file Rept. 74-176, 83 p.

Carr, W.J., 1984a, Regional structural setting of Yucca Mountain, southwestern Nevada, and late Cenozoic rates of tectonic activity in part of the southwestern Great Basin, Nevada and California: U.S. Geol. Survey Open-File Rept. 84-0854, 114 p.

Carr, W.J., 1984b, Timing and style of tectonism and localization of volcanism in the Walker Lane belt of southwestern Nevada [abs.]: Geol. Soc. America, Abstracts with Programs, v. 16, p. 464.

Carr, W.J., 1988, Volcano-tectonic setting of Yucca Mountain and Crater Flat, *in* Carr, M.D., and Yount, J.C., eds., Geologic and hydrologic investigations of a potential nuclear waste disposal site at Yucca Mountain, southern Nevada: U.S. Geol. Survey Bull. 1790, p. 35-49.

Carr, W.J., 1990, Style of extension in the Nevada Test Site region, southern Walker Lane belt; and integration of volcano-tectonic and detachment fault models, *in* Wernicke, B.P., ed., Basin and Range extensional tectonics near the latitude of Las Vegas, Nevada: Geol. Soc. America Mem. 176, Boulder, Colorado, p. 283-303.

Carr, W.J., Byers, F.M., and Orkild, P.P., 1986, Stratigraphic and volcano-tectonic relations of Crater Flat Tuff and some older volcanic units, Nye County, Nevada: U.S. Geol. Survey Prof. Paper 1323, 28 p.

Carr, M.D., and Monsen, S.E., 1988, A field trip guide to the geology of Bare Mountain, *in* Weide, D.L., and Faber, M.L., eds., This Extended Land: Geol. Soc. America Field Trip Guidebook, Cordilleran Section Meeting, Las Vegas, Nevada, p. 50-57.

Caskey, S.J., and Schweikert, R.A., 1992, Mesozoic deformation in the Nevada Test Site and vicinity: implications for the structural framework of the Cordilleran fold and thrust belt and Tertiary extension north of Las Vegas Valley: Tectonics, v. 11, p. 1314-1331.

Castor, S.B., and Weiss, S.I., 1992, Contrasting styles of epithermal precious-metal mineralization in the southwestern Nevada volcanic field, USA: Ore Geol. Rev., v. 7, p. 193-223.

Castor, S.B., and Sjoberg, J.J., 1993, Uytenbogaardtite, Ag_3AuS_2, in the Bullfrog mining district, Nevada: Canadian Mineralogist, v. 31, p. 89-98.

Castor, S.B., Tingley, J.V., and Bonham, H.F., Jr., 1992, Subsurface mineral resource analysis, Yucca Mountain, Nevada, Preliminary Report 1: Lithologic logs: Nevada Bur. Mines and Geol. Open-file Rept. 92-4, 11 p. plus appendices.

Castor, S.B., Tingley, J.V., and Bonham, H.F., Jr., 1994, Pyritic ash-flow tuff, Yucca Mountain, Nevada: Econ. Geol. (in press)

Cemen, I., Wright, L.A., Drake, R.E., and Johnson, F.C., 1985, Cenozoic sedimentation and sequence of deformational events at the southeastern end of the Furnace Creek strike-slip fault zone, Death Valley region, California, *in* Biddle, K.T., and Christie-Blick, N., eds., Strike-slip deformation, basin formation, and sedimentation: Society of Economic Paleontologists and Mineralogists Special Publication No. 37., p. 127-141.

Christiansen, R.L., Lipman, P.W., Carr, W.J., Byers, F.M., Jr., Orkild, P.P., and Sargent, K.A., 1977: Timber Mountain-Oasis Valley caldera complex of southern Nevada: Geol. Soc. America Bull., v. 88, p. 943-959.

Connors, K.A., 1994, Studies in silicic volcanic geology in the Great Basin of western North America: Unpub. Phd dissertation, Mackay School of Mines, University of Nevada, Reno, XX p. (in review)

Connors, K.A., McKee, E.H., Noble, D.C., and Weiss, S.I., 1991, Ash-flow volcanism of Ammonia Tanks age in the Oasis Valley area, SW Nevada: bearing on the evolution of the Timber Mountain calderas and the timing of formation of the Timber Mountain II resurgent dome [abs.]: EOS, Trans. Am. Geophys. Union., v. 72, p. 570.

Connors, K.A., Noble, D.C., Bussey, S.D., and Weiss, S.I., 1993, The initial gold contents of silicic volcanic rocks: bearing on the behavior of gold in magmatic systems, Geology, v. 21, p. 937-940.

Conrad, J.E., McKee, E.H., Rytuba, J.J., Nash, T.J., and Utterback, W.C., 1993, Geochronology of the Sleeper deposit, Humboldt County, Nevada: epithermal gold-silver mineralization following emplacement of a silicic flow-dome complex: Econ. Geol., v. 88, p. 317-327.

Cornwall, H.R., 1972, Geology and mineral deposits of southern Nye County, Nevada: Nevada Bur. Mines Geol. Bull. 77, p. 49.

Cornwall, H.R., and Kleinhampl, F.J., 1961, Geology of the Bare Mountain quadrangle, Nevada: U.S. Geol. Survey Map GQ-157, 1:62,500 scale.

Cornwall, H.R., and Kleinhampl, F.J., 1964, Geology of the Bullfrog quadrangle and ore deposits related to the Bullfrog Hills caldera, Nye County, Nevada, and Inyo County, California: U.S. Geol. Survey Prof. Paper 454-J, 25 p.

Couch, B.F., and Carpenter, J.A., 1943, Nevada's metal and mineral production: Nevada Bur. Mines Geol. Bull. 38, 159 p.

Dalrymple, G.B., 1979, Critical tables for conversion of K-Ar ages from old to new constants: Geology, v. 7., p. 558-560.

Duebendorfer, E.M., and Smith, E.I., 1991, Tertiary structure, magmatism, and sedimentation in the Lake Mead region, southern Nevada: *in* Seedorf, E., ed., 1991 Spring Field Trip Guide Book, Geol. Soc. Nevada Spec. Pub. 13, Reno, Nevada, p. 66-95.

Deubendorfer, E.M., and Wallin, E.T., 1991, Basin Development and syntectonic sedimentation associated with kinematically coupled strike-slip and detachment faulting, southern Nevada: Geology, v. 19, p. 87-90.

Ekren, E.B., Anderson, R.E., Rogers, C.L., and Noble, D.C., 1971, Geology of northern Nellis Air Force Base Bombing and Gunnery Range, Nye County, Nevada: U.S. Geol. Survey Prof. Paper 651, 91 p.

Ekren, E.B., Rodgers, C.L., Anderson, R.E., and Orkild, P.P., 1968, Age of Basin and Range faults in the Nevada Test Site and Nellis Air Force Range, *in* Eckel, E.B., ed., Nevada Test Site: Geol. Soc. America Mem. 110, Boulder, Colorado, p. 247-250.

Ekren, E.B., and Sargent, K.A., 1965, Geologic map of Skull Mountain quadrangle at the Nevada Test Site, Nye County, Nevada: U.S. Geol. Survey Geologic Quadrangle Map GQ-387, 1:24,000.

Elston, W.E., Damon, P.E., Coney, P.E., Rhodes, R.C., Smith, E.I., and Bikerman, M., 1973, Tertiary volcanic rock, Mogollon-Datil province, and surrounding region: K-Ar dates, patterns of eruption and periods of mineralization: Geol. Soc. America Bull., v. 84, p. 2259-2274.

Fleck, R. J., Lanphere, M. A., Turrin, B., and Sawyer, D. A., 1991, Chronology of late Miocene to Quaternary volcanism and tectonism in the southwest Nevada volcanic field [abs.]: Geol. Soc. America Abstracts with Programs, v. 23, p. 25.

Fridrich, C.A., Orkild, P.P., Murray, M., Price, J.R., Christiansen, R.L., Lipman, P.W., Carr, W.J., Quinlivin, W.D., and Scott, R.B., 1994, Geologic map of the East Of Beatty Mountain 7.5' Quadrangle, Nye County, Nevada: U. S. Geol. Survey Open-file Report, 1:12,000 scale, 4 sheets (in review).

Frizzell, V.A., Jr., and Shulters, J., 1990, Geologic map of the Nevada Test Site: U.S. Geol. Survey Misc. Invest. Map I-2046, 1:100,000.

Gardiner, J.N., Goff, F., Garcia, S., and Hagan, R.C., 1986, Stratigraphic relations and lithologic variations in the Jemez volcanic field, New Mexico: Jour. Geophys. Research, v. 91, p. 1763-1778.

Greybeck, J.D., and Wallace, A.B., 1991, Gold mineralization at Fluorspar Canyon near Beatty, Nye County, Nevada: *in* Raines, G.L., Lisle, R.E., Shafer, R.W., and Wilkinson, W.W., eds., Geology and ore deposits of the Great Basin: Symposium Proceedings, Geol. Soc. of Nevada, Reno, Nevada, p. 935-946.

Hamilton, W.B., 1988, Detachment faulting in the Death Valley region, California and Nevada, *in* Carr, M.D., and Yount, J.C., eds., Geologic and hydrologic investigations of a potential nuclear waste disposal site at Yucca Mountain, southern Nevada: U.S. Geol. Survey Bull. 1790, p. 51-86.

Hausback, B.P., Deino, A.L., Turrin, B.T., McKee, E.H., Frizzell, V.A., Noble, D.C., and Weiss, S.I., 1990, New $^{40}Ar/^{39}Ar$ ages for the Spearhead and Civet Cat Canyon Members of the Stonewall Flat Tuff, Nye County, Nevada: Evidence for systematic errors in standard K-Ar age determinations on sanidine: Isochron/West, No. 56, p. 3-7.

Hoover, D.B., Chornack, M.P., Nervick, K.H., and Broker, M.M., 1982, Electrical studies at the proposed Wahmonie and Calico Hills Nuclear Waste Sites, Nye County, Nevada: U.S. Geol. Survey Open-File Rept. 82-466, 45 p.

Hudson, M.R., 1992, Paleomagnetic data bearing on the origin of arcuate structures in the Frenchman Peak - Massachusetts Mountain area of southern Nevada: Geol. Soc. Am. Bull., v. 104, p. 581-594.

Hudson, M.R., and Cole, J.C., 1993, Kinematics of faulting in the Mine Mountain area of southern Nevada: evidence for pre-Middle Miocene extension [abs.]: Geol. Soc. America Abstracts with Programs, v. 25, p. 55.

Hudson, M.R., Sawyer, D.A., and Warren, R.G., 1994, Paleomagnetism and rotation constraints for the middle Miocene southwestern Nevada volcanic field: Tectonics, v. 13, no. 258-277.

Jackson, M.R., 1988, The Timber Mountain magmato-thermal event: an intense widespread culmination of magmatic and hydrothermal activity at the southwestern Nevada volcanic field: Unpub. M.S. thesis, Mackay School of Mines, Univ. Nevada, Reno, 46 p.

Jackson, M.R., Noble, D.C., Weiss, S.I., Larson, L.T., and McKee, E.H., 1988, Timber Mountain magmato-thermal event: an intense widespread culmination of magmatic and hydrothermal

activity at the SW Nevada volcanic field [abs.]: Geol. Soc. America Abstracts with Programs, v. 20, p. 171.

Jorgensen, D.K., Rankin, J.W., and Wilkins, J., Jr., 1989, The geology, alteration and mineralogy of the Bullfrog gold deposit, Nye County, Nevada: Soc. Mining Eng. Preprint 89-135, 13 p.

Kistler, R.W., 1968, Potassium-argon ages of volcanic rocks in Nye and Esmeralda Counties, Nevada: Geol. Soc. America Memoir 110, p. 251-263.

Lipman, P.W., and McKay, E.J., 1965, Geologic map of the Topopah Spring SW quadrangle, Nevada: U.S. Geological Survey Geologic Quadrangle Map GQ-439, 1:24,000 scale.

Lipman, P.W., Fisher, S.S., Mehnert, H.H., Naeser, C.W., Luedke, R.G., and Steven, T.A., 1976, Multiple ages of mid-Tertiary mineralization and alteration in the western San Juan Mountains, Colorado: Econ. Geol., v. 71, p. 571-588.

McKay, E.J., 1963, Hydrothermal alteration in the Calico Hills, Jackass Flats quadrangle, Nevada Test Site: U.S. Geological Survey Technical Letter NTS-43, 6 p.

McKay, E.J., and Williams, W.P., 1964, Geology of Jackass Flats quadrangle, Nevada Test Site, Nevada: U.S. Geological Survey Geologic Quadrangle Map GQ-368, 1:24,000 scale.

McKee, E.H., 1983, Reset K-Ar ages: evidence for three metamorphic core complexes, western Nevada: Isochron/West, no. 38, p 17-20.

McKee, E.H., and Bergquist, J.R., 1993, New radiometric ages related to alteration and mineralization in the vicinity of Yucca Mountain, Nye County, Nevada: U. S. Geol. Survey Open-File Rept. 93-538, 26 p.

McKee, E.H., Gibson, P.C., Noble, D.C., and Swanson, K.E., 1994, Timing of igneous activity, alteration and mineralization at the Orcopampa Ag-Au district, southern Peru [extended abs.]: U. S. Geol. Survey Circular 1103A, p. 65-66.

Maldonado, F., 1985, Late Tertiary detachment faults in the Bullfrog Hills, southwestern Nevada [abs.]: Geol. Soc. America Abstracts with Programs, v. 17, p. 651.

Maldonado, F., 1988, Geometry of normal faults in the upper plate of a detachment fault zone, Bullfrog Hills, southern Nevada [abs.]: Geol. Soc. America, Abstracts with Programs, v. 20, p. 178.

Maldonado, F., 1990a, Structural geology of the upper plate of the Bullfrog Hills detachment fault system, southern Nevada: Geological Society of America Bulletin, v. 102, p. 992-1006.

Maldonado, F., 1990b, Geologic map of the northwest quarter of the Bullfrog 15-minute quadrangle, Nye County, Nevada: U.S. Geol. Survey Misc. Invest. Map I-1985, 1:24,000.

Maldonado, F, and Hausback, B.P., 1990, Geologic map of the northeast quarter of the Bullfrog 15-minute quadrangle, Nye County, Nevada: U.S. Geol. Survey Misc. Invest. Map I-2049, 1:24,000.

Maldonado, F., and Koether, S.L., 1983, Stratigraphy, structure, and some petrographic features of Tertiary volcanic rocks at the USW G-2 drill hole, Yucca Mountain, Nye County, Nevada: U.S. Geological Survey Open-File Report 83-732, 83 p.

Maldonado, F., Muller, D.C., and Morrison, J.N., 1979, Preliminary geologic and geophysical data of the UE25a-3 exploratory drill hole, Nevada Test Site, Nevada: U.S. Geol. Survey Open-File Rept. 81-522.

Marvin, R. F., and Cole, J. C., 1978, Radiometric ages: compilation A, U. S. Geological Survey: Isochron/West, no. 22, p. 3-14.

Marvin, R.F., Mehnert, H.H., and Naeser, C.W., 1989, U.S. Geologic Survey radiometric ages - compilation "C", part 3: California and Nevada: Isochron/West, no. 52, p. 3-11.

Marvin, R.F., Byers, F.M., Mehnert, H.H., Orkild, P.P, and Stern, T.W., 1970, Radiometric ages and stratigraphic sequence of volcanic and plutonic rocks, southern Nye and western Lincoln Counties, Nevada: Geol. Soc. America, Bulletin, v. 81, p. 2657-2676.

Meyer, C., Shea, E.P., Goddard, C.C., Jr., and staff, 1968, Ore deposits at Butte, Montana: *in* Ridge, J.D., ed., Ore deposits of the United States, 1933-1967; Am. Inst. Mining, Met., and Pet. Eng., New York, v. 2, p. 1363-1416.

Minor, S.A., Sawyer, D.A., Orkild, P.P., Coe, J.A., Wahl, R.R., and Frizzell, V.A., Jr., 1991, Neogene migratory extensional deformation revealed on new map of the Pahute Mesa 1:100,000-scale quadrangle, southern Nevada [abs.]: EOS, Trans. Am. Geophys. Union, v. 72, p. 469.

Minor, S.A., Sawyer, D.A., Wahl, R.R., Frizzell, V.A., Jr., Schilling, S.P., Warren, R.G., Orkild, P.P., Coe, J.A., Hudson, M.R., Fleck, R.J., Lanphere, M.A., Swadley, W.C., and Cole, J.C., 1993, Preliminary geologic map of the Pahute Mesa 30' x 60' quadrangle, Nevada: U.S. Geol. Survey Open-file Rept. 93-299, 1:100,000.

Monsen, S.A., 1983, Structural evolution and metamorphic petrology of the Precambrian-Cambrian strata, northwestern Bare Mountain, Nevada: Unpub. M.S. thesis, Univ. California, Davis, 66 p.

Monsen, S.A., Carr, M.D., Reheis, M.C., and Orkild, P.P., 1990, Geologic map of Bare Mountain, Nye County Nevada: U.S. Geol. Survey Open-file Rept. 90-25, 1:24,000.

Monsen, S.A., Carr, M.D., Reheis, M.C., and Orkild, P.P., 1992, Geologic map of Bare Mountain, Nye County Nevada: U.S. Geol. Survey Misc. Invest. Map I-2201, 1:24,000.

Morton, J.L., Silberman, M.L., Bonham, H.F., Garside, L.J., and Noble, D.C., 1977, K-Ar ages of volcanic rocks, plutonic rocks, and ore deposits in Nevada and eastern California - Determinations run under the USGS-NBMG cooperative program: Isochron/West, n. 20, p. 19-29.

Noble, D.C., and Christiansen, R.L., 1968, Geologic map of the southwest quarter of the Black Mountain quadrangle, Nye County, Nevada: U.S. Geol. Survey Misc. Invest. Map I-562, 1:24,000.

Noble, D.C., Sargent, K.A., Ekren, E.B., Mehnert, H.H., and Byers, F.M., Jr., 1968, Silent Canyon volcanic center, Nye County, Nevada: Geol. Soc. America Special Paper 101, p. 412-413.

Noble, D.C., and Silberman, M.L., 1984, Evolucíon volcanica y hidrotermal y chronología de K/Ar del Distrito Minero del Julcani: Geol. Soc. Peru, Vol. Jubilar, 60 Aniv., Fasc. 5, 35 p.

Noble, D.C., Weiss, S.I., and Green, S.M., 1989, High-salinity fluid inclusions suggest that Miocene gold deposits of the Bare Mtn. district, NV, are related to a large buried rare-metal rich magmatic system [abs.]: Geol. Soc. America Abstracts with Programs, v. 21, p. 123.

Noble, D.C., Weiss, S.I., and McKee, E.H., 1990, Style, timing, distribution, and direction of Neogene extension within and adjacent to the Goldfield section of the Walker Lane structural belt: EOS, Trans. American Geophysical Union, v. 71, p. 618-619.

Noble, D.C., Weiss, S.I., and McKee, E.H., 1991, Magmatic and hydrothermal activity, caldera geology, and regional extension in the western part of the southwestern Nevada volcanic field, *in* Raines, G.L., Lisle, R.E., Shafer, R.W., and Wilkinson, W.W., eds., Geology and Ore Deposits of the Great Basin, Reno, Geol. Soc. of Nevada, p. 913-934.

Noble, D.C., Vogel, T.A., Weiss, S.I., Erwin, J.W., McKee, E.H., and Younker, L.W., 1984, Stratigraphic relations and source areas of ash-flow sheets of the Black Mountain and Stonewall Mountain volcanic centers, Nevada: Jour. Geophys. Res., v. 89, p. 8593-8602.

Odt, D.A., 1983, Geology and geochemistry of the Sterling gold deposit, Nye County, Nevada: Unpub. M.S. thesis, Univ. Nevada, Reno, 91 p.

Orkild, P.P., 1968, Geologic map of the Mine Mountain quadrangle, Nye County, Nevada: U.S. Geol. Survey Geologic Quadrangle Map GQ-746, 1:24,000 scale.

Orkild, P.P., and O'Connor, J.T., 1970, Geologic map of the Topopah Spring quadrangle, Nye County, Nevada: U.S. Geol. Survey Geologic Quadrangle Map GQ-849, 1:24,000 scale.

Papke, K.G., 1979, Fluorspar in Nevada: Nevada Bur. Mines Geol. Bull. 93, 77 p.

Percival, T.J., Bagby, W.C., and Radtke, A.S., 1988, Physical and chemical features of precious metal deposits hosted by sedimentary rocks in the western United States: *in* Schafer, R.W., Cooper, J.J., and Vikre, P.G., eds., Bulk Mineable Precious Metal Deposits of the Western United States, Geol. Soc. Nevada, Reno, p. 11-34.

Ponce, D.A., 1981, Preliminary gravity investigations of the Wahmonie site, Nevada Test Site, Nye County, Nevada: U.S. Geol. Survey Open-file Rept. 81-522, 64 p.

Ponce, D.A., 1984, Gravity and magnetic evidence for a granitic intrusion near Wahmonie, Nevada Test Site, Nevada: Jour. Geophys. Res., v. 89, p. 9401-9413.

Poole, F.G., Carr, W.J., and Elston, D.P., 1965, Salyer and Wahmonie Formations of southeastern Nye County, Nevada: U.S. Geol. Survey Bull. 1224-A, p. A44-A51.

Powers, S.L., 1988, Two lineation directions in the Mineral Ridge core complex, Esmeralda County, Nevada [abs.]: Geol. Soc. America Abstracts with Programs, v. 20, p. 222.

Quade, J., and Tingley, J.V., 1984, A mineral inventory of the Nevada Test Site, and portions of Nellis Bombing and Gunnery Range, southern Nye County, Nevada: Nevada Bur. Mines Geol. Open-file Rept. 82-2, 40 p. plus appendices.

RANDOL, 1993, Randol Mining Directory 1993/1994, U.S. mines and mining companies, Randol International, Ltd., Golden, Colorado, 734 p.

Ransome, F.L., 1907, Preliminary account of Goldfield, Bullfrog, and other mining districts in southern Nevada: U.S. Geol. Survey Bull. 303, 98 p.

Ransome, F.L., Emmons, W.H., and Garrey, G.H., 1910, Geology and ore deposits of the Bullfrog district, Nevada: U.S. Geol. Survey Bull. 407, 130 p.

Ristorcelli, S.J., and Ernst, D.R., 1991, Summary report: USNGS exploration 1990-1991, Nye County, Nevada, unpublished company report, U.S. Nevada Gold Search Joint Venture, Carson City, 104 p.

Rye, R.O., 1993, The evolution of magmatic fluids in the epithermal environment: the stable isotope perspective: Econ. Geol., v. 88, p. 733-753.

Sawyer, D.A., Fleck, R.J., Lanphere, M.A., Warren, R.G., and Broxton, D.E., 1990, Episodic volcanism in the southwest Nevada volcanic field: new $^{40}Ar/^{39}Ar$ geochronologic results [abs.]: EOS, Trans. Am. Geophys. Union, v. 71, p. 1296.

Sawyer, D.A., Fleck, R.J., Lanphere, M.A., Warren, R.G., Broxton, D.E., and Hudson, M.R., 1994, Episodic caldera volcanism in the southwestern Nevada volcanic field: revised stratigraphic framework, $^{40}Ar/^{39}Ar$ geochronology, and implications for magmatism and extension: Geol. Soc. America Bulletin (in review).

Sawyer, D.A., and Sargent, K.A., 1989, Petrologic evolution of divergent peralkaline magmas from the Silent Canyon caldera complex: Jour. Geophys. Res., v. 94, p. 6021-6040.

Schweikert, R.A., 1989, Evidence for a concealed dextral strike-slip fault beneath Crater Flat, Nevada [abs.]: Geol. Soc. America Abstracts with Programs, v. 21, p. A90.

Schweikert, R.A., and Caskey, S.J., 1990, Pre-Middle Miocene extensional history of the Nevada Test Site (NTS) region, southern Nevada [abs.]: Geol. Soc. America Abstracts with Programs, v. 22, p. 81.

Scott, R.B., 1988, Tectonic setting of Yucca Mountain, southwest Nevada [abs.]: Geol. Soc. America Abstracts with Programs, v. 20, p. 229.

Scott, R.B. and Bonk, J., 1984, Preliminary geologic map of Yucca Mountain, Nye County, Nevada, with geologic sections: U.S. Geol. Survey Open-file Rept. 84-494, scale 1:12,000, plus 10 p.

Scott, R.B., Byers, F.M. and Warren, R.G., 1984, Evolution of magma below clustered calderas, Southwest Nevada volcanic field [abs.], EOS, Trans. Am. Geophys. Union, v. 65, p. 1126-1127.

Seedorf, E.A., 1991, Magmatism, extension and ore deposits of Eocene to Holocene age in the Great Basin -mutual effects and preliminary proposed genetic relationships: *in* Raines, G.L., Lisle, R.E., Shafer, R.W., and Wilkinson, W.W., eds., Geology and Ore Deposits of the Great Basin, Reno, Geol. Soc. of Nevada, p. 133-178.

Setterfield, T.N., Mussett, A.E., and Oglethorpe, R.D.J., 1992, Magmatism and associated hydrothermal activity during the evolution of the Tavua caldera: ^{40}Ar- ^{39}Ar of the volcanic, intrusive, and hydrothermal events: Econ. Geol., v. 87, p. 1130-1140.

Silberman, M.L., Chesterman, C.W., Kleinhampl, F.J., and Gray, C.H., Jr., 1972, K-Ar ages of volcanic rocks and gold-bearing quartz-adularia veins in the Bodie mining district, Mono County, California: Econ. Geol., v. 67, p. 597-604.

Silberman, M.L., 1985, Geochronology of hydrothermal alteration and mineralization: Tertiary epithermal precious-metal deposits in the Great Basin: U. S. Geol. Survey Bull. 1646, p. 55-70.

Sillitoe, R.H., McKee, E.H., and Vila, T., 1991, Reconnaissance K-Ar geochronology of the Maricunga gold-silver belt, northern Chile: Econ. Geol., v. 86, p. 1261-1270.

Simonds, F.W., 1989, Geology and hydrothermal alteration in the Calico Hills, southern Nevada: Unpub. M.S. thesis, Univ. Colorado, Boulder, 136 p.

Simonds, F.W., and Scott, R.B., 1990, Hydrothermal alteration at the Calico Hills, Nye County, Nevada [abs.]: Geology and Ore Deposits of the Great Basin Program with Abstracts, Geol. Soc. Nevada, Reno, p. 126.

Smith, R.C., and Bailey, R.A., 1968, Resurgent Cauldrons: Geol. Soc. America Memoir 116, p. 613-662.

Snyder, D.B., and Oliver, H.W., 1981, Preliminary results of gravity investigations of the Calico Hills, Nevada Test Site, Nye County, Nevada: U.S. Geol. Survey Open-File Rept. 81-101, 42 p.

Spencer, J., 1984, Role of tectonic denudation in warping and uplift of low-angle normal faults: Geology, v. 12, p. 95-98.

Spengler, R.W., Byers, F.M., Jr., and Warner, J.B., 1981, Stratigraphy and structure of volcanic rocks in drill hole USW-G1, Yucca Mountain, Nye County, Nevada: U.S. Geol. Survey Open-File Rept. 82-1338, 264 p.

Steiger, R.H., and Jäger, 1977, Subcommission on geochronology- convention on the use of decay constants in geo- and cosmochronology: Earth and Planet. Sci. Letters, v. 36, p. 359-362.

Stewart, J.H., 1980, Geology of Nevada: Nevada Bur. Mines Geology Spec. Pub. 4, 136 p.

Stewart, J.H., 1988, Tectonics of the Walker Lane belt, western Great Basin-Mesozoic and Cenozoic deformation in a zone of shear, *in* Ernst, W.G., ed., Metamorphism and crustal evolution of the western United States, Rubey Vol. VII: Prentice Hall, Englewood Cliffs, p. 683-713.

Stewart, J.H., and Carlson, J.E., 1976, Cenozoic rocks of Nevada: Nevada Bur. Mines Geology Map 52, 1:1,000,000.

Stewart, J.H., and Diamond, D.S., 1990, Changing patterns of extensional tectonics; Overprinting of the basin of the middle and upper Miocene Esmeralda Formation in western Nevada by younger structural basins: Geol. Soc. America Memoir 176, p. 447-476.

Swanson, K.E., Noble, D.C., McKee, E.H., and Gibson, P.C., 1993, Collapse calderas and other Neogene volcanic and hydrothermal features of the Chila Cordillera and adjacent areas, southern Peru [abs.]: Geol. Soc. America Abstracts with Programs, v. 25, p. 153.

Tingley, J.V., 1984, Trace element associations in mineral deposits, Bare Mountain (Fluorine) mining district, southern Nye County, Nevada: Nevada Bur. Mines Geol. Rept. 39, 28 p.

Turrin, B.D., Champion, D.E., and Fleck, R.J., 1991, $^{40}Ar/^{39}Ar$ age of the Lathrop Wells volcanic center, Yucca Mountain, Nevada: Science, v. 253, p. 654-657.

Weber, M.E., and Smith, E.I., 1987 Structural and geochemical constraints on the reassembly of mid-Tertiary volcanoes in the Lake Mead area of southern Nevada: Geology, v. 15, p. 553-556.

Weiss, S.I., 1987, Geologic and paleomagnetic studies of the Stonewall and Black Mountain volcanic centers, southern Nevada: Unpub. M.S. thesis, Univ. Nevada, Reno, 67 p.

Weiss, S.I., Noble, D.C., and McKee, E.H., 1988, Volcanic and tectonic significance of the presence of late Miocene Stonewall Flat Tuff in the vicinity of Beatty, Nevada [abs.]: Geol. Soc. America Abstracts with Programs, v. 20, p. A399.

Weiss, S.I., Noble, D.C., and Larson, L.T., 1990a, Task 3: Evaluation of mineral resource potential, caldera geology and volcano-tectonic framework at and near Yucca Mountain; report for October, 1989 - September, 1990: Center for Neotectonic Studies, Univ. Nevada, Reno, 29 p. plus appendices.

Weiss, S.I., Noble, D.C., and Larson, L.T., 1992, Task 3: Evaluation of mineral resource potential, caldera geology and volcano-tectonic framework at and near Yucca Mountain; report for October, 1990 - September, 1991: Center for Neotectonic Studies, Univ. Nevada, Reno, 44 p. plus appendices.

Weiss, S.I., Noble, D.C., and Larson, L.T., 1993a, Task 3: Evaluation of mineral resource potential, caldera geology and volcano-tectonic framework at and near Yucca Mountain; report for October, 1991 - September, 1992: Center for Neotectonic Studies, Univ. Nevada, Reno, 41 p. plus appendices.

Weiss, S.I., Ristorcelli, S.J., and Noble, D.C., 1993b, Mother Lode gold deposit, southwestern Nevada: another example of Carlin-type mineralization associated with porphyry magmatism [abs.]: Geol. Soc. America Abstracts with Programs, v. 25, p. 161.

Weiss, S.I., Connors. K.A., Noble, D.C., and McKee, E.H., 1990b, Coeval crustal extension and magmatic activity in the Bullfrog Hills during the latter phases of Timber Mountain volcanism [abs.]: Geol. Soc. America Abstracts with Programs, v. 22, p. 92-93.

Weiss, S.I., McKee, E.H., Noble, D.C., Connors, K.A., and Jackson, M.R., 1991, Multiple episodes of Au-Ag mineralization in the Bullfrog Hills, SW Nevada, and their relation to coeval extension and volcanism [abs.]: Geol. Soc. America Abstracts with Programs, v. 23, p. A246.

Weiss, S.I., Noble, D.C., Worthington, J.E., IV, and McKee, E.H., 1993c, Neogene tectonism from the southern Nevada volcanic field to the White Mountains, California, Part I. Miocene volcanic stratigraphy, paleotopography, extensional faulting and uplift between northern Death Valley and Pahute Mesa: *in* Lahren, M.M., Trexler, J.H. Jr., and Spinosa, C., eds., Crustal Evolution of the Great Basin and Sierra Nevada: Cordilleran/Rocky Mountain Section, Geol. Soc. America Guidebook, Dept. Geol. Sci., Univ. Nevada, Reno, p. 353-382.

Woldegabriel, G., 1990, Hydrothermal alteration in the Valles caldera ring fracture zone and core hole VC-1: evidence for multiple hydrothermal systems: Jour. Volc. Geotherm. Res., v. 40, p. 105-122.

Woldegabriel, G., and Goff, F., 1989, Temporal relations of volcanism and hydrothermal systems in two areas of the Jemez volcanic field, New Mexico: Geology, v. 17, p. 986-989.

Wright, L.A., Thompson, R.A., Troxel, B.W., Pavlis, T.L., DeWitt, E.H., Otton, J.K., Ellis, M.A., Miller, M.G., and Serpa, L.F., 1991, Cenozoic magmatic and tectonic evolution of the east-central Death Valley region, California: *in* Walawender, M.J., and Hanan, B.B., eds., Geologic excursions in southern California and Mexico, Geol. Soc. America Field Trip Guidebook, San Diego, California, p. 93-127.

Worthington, J.E., IV, 1992, Neogene structural and volcanic geology of the Gold Mountain - Slate Ridge area, Esmeralda County, Nevada: Unpub. M.S. thesis, Univ. Nevada, Reno, 78 p.

Figure Captions:

Fig. 1 Map showing calderas and major volcanic centers of the southwestern Nevada volcanic field. Modified from Noble et al. (1991). SM = Stonewall Mountain; OB = Obsidian Butte; BM = Black Mountain; SC = Silent Canyon center; WS = Wahmonie-Salyer center; PP(?) = proposed Prospector Pass caldera of Carr et al. (1986). FLV-DV-FC FZ = Fish Lake Valley-Death Valley-Furnace Creek fault zone.

Fig. 2 Locations of mineral deposits, areas of hydrothermally altered rocks, caldera margins, and other structural and physiographic features of the southern part of the southwestern Nevada volcanic field. Porphyry dikes in Bare Mountain shown by dotted lines. OB-FC = the Original Bullfrog-Fluorspar Canyon fault system; BC = Boundary Canyon fault. B = Bailey's hot spring, BW = Beatty Wash, C = Clarkdale district, CH = Calico Hills, D = Daisy mine, G = Gold Bar mine, GA = Gold Ace mine, GD = Goldspar/Diamond Queen mine, LGB = Lac Gold Bullfrog mine, M = Mary mine, ML = Mother Lode mine, MM = Mine Mountain, MS = Montgomery-Shoshone mine, My = Mayflower mine, OB = Original Bullfrog mine, OM = Oasis Mountain, P = Pioneer mine, R = Denver-Tramps and Gibralter mines near Rhyolite, S = Sterling mine, Si = Silicon mine, SP = Secret Pass prospect, T = Telluride mine, Th = Thompson mine, TH = Transvaal Hills, TO = Tolicha-Quartz Mountain district, W = Wahmonie, YJ = Yellowjacket mine. O = Obsidian Butte, SB = Sleeping Butte. Small open dots labeled G1, G2 and G3 refer to deep drill holes USW-G1, USW-G2 and USW-G3. TM-I caldera associated with the eruption of the 11.6 Ma Rainier Mesa Member of the Timber Mountain Tuff; TM-II caldera associated with the eruption of the 11.45 Ma Ammonia Tanks Member of the Timber Mountain Tuff. Hammer and pick = active and recently producing mines, ë = historic mines, x = prospect.

Fig. 3 Residual silica and acid-leached rocks of the Rainier Mesa Member of the Timber Mountain Tuff near the Silicon mine, interpreted as the result of shallow, steam-heated acid-sulfate alteration.

Fig. 4 Geologic map of Mine Mountain showing structural features and the principal areas of alteration and mineralization. Modified from Orkild (1968) and Frizzell and Schulters (1990).

Fig. 5 Generalized geologic map of the Bullfrog Hills. Modified from Ransome et al. (1910), unpublished mapping of S. I. Weiss and K. A. Connors (1989-1991), Maldonado (1990b), Maldonado and Hausback (1990), and Monsen et al. (1992). Section A - A' shown in Figure 10. OBF = Original Bullfrog fault, AF = Amargosa fault, FC = Fluorspar Canyon fault and OVFZ = Oasis Valley fault zone. Mines and other features labeled as in Fig. 2. Zpu = Late Precambrian and Early Paleozoic sedimentary and metamorphic rocks, undivided; Tmo = Timber Mountain and older ash-flow sheets and units of lava and tuffaceous sedimentary rocks, Tpi = silicic, coarse-grained porphyritic dike of undetermined age; Tbh = tuffs and lavas of the Bullfrog Hills, m denotes landslide (megabreccia) deposits; Tri = rhyolitic plugs, dikes and domes of the tuffs and lavas of the Bullfrog Hill, includes post-Crater Flat Tuff phenocryst-poor rhyolitic plugs and dikes in the Pioneer - Yellowjacket area.

Fig. 6 Plot of A) K_2O vs. Rb and B) K_2O vs. SiO_2/Al_2O_3 for samples of altered wallrock at the Lac Gold Bullfrog and Montgomery-Shoshone mines. Dashed boxes show approximate range of values for unaltered high- and low-silica rhyolite of the Timber Mountain Tuff (Broxton et al., 1989). X's and +'s show rocks from the Montgomery-Shoshone and Lac Gold Bullfrog mines, respectively. Triangle shows banded quartz-calcite vein with about 25% wallrock fragments from the Polaris vein at the Montgomery-Shoshone mine. Analyses by X-ray fluorescence methods in the analytical laboratory of the Nevada Bureau of MInes and Geology under the supervision of P.J. Lechler.

Fig. 7 A) North wall of the open-pit, Phase I, at the Lac Gold Bullfrog mine showing the main vein (between arrows); view is to the northwest. B) West-dipping fault in northwest wall, Phase I, of open pit at the Lac Gold Bullfrog mine. Fault separates east-dipping, strongly silicified and potassium metasomatized ash-flow tuff of the Rainier Mesa Member of the

Timber Mountain Tuff, above, from underlying ore composed of brecciated quartz-calcite veins and altered wallrock fragments. C) Altered footwall lava cut by stockwork of dark colored veins and veinlets containing mixtures of quartz, black hydrocarbon, calcite, pyrite, chlorite and wallrock fragments. Carbonaceous veins are cut by light colored veins containing quartz, calcite, adularia and locally pyrite.

Fig. 8 Timing of hydrothermal activity in the southwestern Nevada volcanic field. Dots show radiometric age determinations, error bars at ±1 r. ** signifies $^{40}Ar/^{39}Ar$ ages. Open symbol shows timing constrained by stratigraphic relations. ö age recalculated from Morton et al. (1977); öö ages from Noble et al. (1991).

Fig. 9 Diagrammatic summary of volcanism, extensional faulting and hydrothermal activity of the Bullfrog Hills. Open diamonds show radiometric ages of volcanic rocks from Marvin and Cole (1978), Marvin et al. (1989), Hausback et al. (1990), Maldonado and Hausback, (1990), and Noble et al. (1991); solid diamonds show $^{40}Ar/^{39}Ar$ ages of adularia, x's show K-Ar ages of adularia; error bars at ±1 r. [1] = rhyolite of the Tracking Station (Marvin et al., 1989) and rhyolite of Sober Up Gulch (Maldonado and Hausback, 1990). [2] = latite of Donovan Mountain (Minor et al., 1993). [3] includes the rhyolite of Burton Mountain (Marvin and Cole,1978; Carr 1984a). AT = Ammonia Tanks Member of the Timber Mountain Tuff. NBH = northern Bullfrog Hills; SBH = southern Bullfrog Hills.

Fig. 10 Simplified cross section (A - A') in the northern Bullfrog Hills showing early, presently low-angle normal faults displaced and rotated by younger, higher-angle normal faults. Megabreccia deposits within the TLBH near the east end of A - A' dip approximately 18° to 20° to the east. cWu, cZ and cC refer, respectively, to the Early Cambrian upper Wood Canyon Formation, the Zabriskie Quartzite and the Carrera Formation, most recently described by Monsen et al. (1992) from more complete exposures at Bare Mountain. Tot = older tuffs; Tlr = Lithic Ridge Tuff; Tc = single cooling unit of the Crater Flat Tuff; Tpi = silicic porphyry intrusion containing sanidine phenocrysts as large as 1.5 cm in maximum

dimension. Tp = single cooling unit of the Paintbrush Tuff; m = coarse landslide (megabreccia) deposits within the TLBH; Tht_2 = unwelded, pumice-rich rhyolite ash-flow tuff and surge unit #2 of the TLBH (Fig. 9); Thri = rhyolite plug of the TLBH; Qac = Quaternary alluvium and colluvium.

APPENDIX

Descriptions of samples used in K-Ar and $^{40}Ar/^{39}Ar$ dating. Field numbers correspond to Table 2. Additional information concerning sample collection and sample localities is given by McKee and Bergquist (1993).

3MJ-224B: Mixture of quartz-adularia-calcite ± pyrite veins and altered wallrock fragments of aphyric andesite or dacite lava flow of the Wahmonie Formation, from outcrop about 800' NNW of the Hornsilver mine. Wallrock fragments are composed of fine-grained intergrowths of quartz, adularia and illite.

3SW-147: Altered porphyritic hornblende-biotite andesite or dacite lava flow of the Wahmonie Formation containing quartz ±adularia veinlets from outcrop about 650' NW of the Hornsilver mine. Biotite and hornblende phenocrysts are completely replaced by illite, plagioclase is pseudomorphed by adularia, and groundmass is composed of fine-grained intergrowths of quartz, illite and adularia.

3MJ-118: Alunitized, poorly sorted, matrix-supported tuffaceous conglomerate adjacent to the Tate's Wash segment of the Fluorspar Canyon fault, north flank of Bare Mountain. Volcanic clasts and matrix replaced by mixtures of fine-grained quartz, alunite and halloysite. Alunite comprises anhedral to blocky crystals of about 0.005 mm in maximum dimension. Conglomerate *underlies* pre-Rainier Mesa Member bedded ash-fall and ash-flow tuffs (cf. Jackson, 1988; Bergquist and McKee, 1993).

3MJ-130a: Angular to subrounded clasts composed of pure, very fine-grained alunite in matrix-supported breccia body cutting carbonate rocks of the Roberts Mountain Formation. Matrix consists of partially to completely alunitized porous tuff, including originally glassy pumice fragments. Alunite comprises anhedral to blocky crystals of about 0.010 mm in maximum dimension.

Thompson mine: Vein composed of 85% fine-grained alunite and 15% halloysite cutting altered rocks of the Paintbrush Tuff. Wallrocks altered to porous mixtures of opal-CT, kaolinite and alunite.

Silicon mine: Dense, alunitized and silicified rhyolitic ash-flow tuff containing small phenocrysts and phenocryst fragments of quartz and relict feldspar; sample is composed of about 35% alunite ($\leq$ 0.2 mm in maximum dimension) intergrown with about 65% fine-grained quartz and opal.

3MJ-216A: Vein containing about 95% fine-grained alunite and about 5% quartz within argillically altered ash-flow tuff of the Rainier Mesa Member of the Timber Mountain Tuff, eastern Calico Hills. Alunite comprises aggregates of anhedral to blocky crystals $\leq$ 0.010 mm in maximum dimension.

3SW-137A: Alunitized tuff of the rhyolite of Calico Hills; sample consists of a porous mixture of 50% fine-grained alunite, nearly 50% opal-CT, and traces of kaolinite. Alunite comprises anhedral to blocky crystals \ 0.010 mm in maximum dimension.

3SW-303: Alunitized, previously vitric, partially welded ash-flow tuff of the Ammonia Tanks Member of the Timber Mountain Tuff, south flank of Mine Mountain. Feldspar and mafic accessory phenocrysts and pumice fragments completely replaced by granular mosaics of blocky to bladed alunite (crystals \0.2 mm in maximum dimension), ± small amounts of kaolinite. Many large shards and pumice fragments replaced by finer-grained granular alunite; most of the groundmass glass is altered to kaolinite.

3MJ-176: Silicified lithic-rich ash-flow tuff of the Lithic Ridge Tuff adjacent to the main vein at the Original Bullfrog mine; contains numerous thin quartz and quartz-adularia veinlets. Groundmass replaced by fine-grained quartz, adularia and illite/smectite. Feldspar phenocrysts replaced by adularia, albite, illite and quartz.

Mayflower mine: Adularized nonwelded, crystal-rich, rhyolitic ash-flow tuff from dump at the Mayflower mine. Adularia crystals are present as coatings on fracture surfaces and feldspar phenocrysts are pseudomorphed by non-turbid adularia having mottled extinction; groundmass composed of fine-grained polygonal to granophyric intergrowths of quartz with anhedral to euhedral adularia.

Bullfrog Hills: Silicified and adularized rhyolitic ash-flow tuff of the Crater Flat Tuff adjacent to thin quartz vein along NE-striking fault between the Yellowjacket and Pioneer mines. Contains quartz veinlets and is composed of approximately 75% quartz, 20% adularia and 5% illite.

3MJ-74a: Silicified and adularized rhyolitic ash-flow tuff of the Ammonia Tanks Member of the Timber Mountain Tuff, adjacent to north-trending quartz vein in Oasis Mountain. Contains numerous veinlets of quartz. Feldspar phenocrysts pseudomorphed by adularia, albite and quartz, and mafic accessory phenocrysts replaced by illite. Groundmass consists of fine-grained intergrowths of quartz with sparse adularia and illite.

BAILEY'S: Alunitized Ammonia Tanks Member of the Timber Mountain Tuff near active, presently near-neutral hot spring. Feldspar and accessory phenocrysts replaced by granular mosaics of blocky to bladed alunite (\0.4 mm in maximum dimension). Groundmass altered to mixtures of fine-grained alunite, opal-CT, chalcedony, and kaolinite.

3MJ-6: Drusy veinlets of clear alunite crystals, as much as 0.5 mm in maximum dimension, along fractures in altered, originally glassy, densely welded, ash-flow tuff (vitrophyre) of the Rainier Mesa Member of the Timber Mountain Tuff, Transvaal Hills. Vitrophyre is altered to a fine-grained mixture of alunite, kaolinite and opal.

BBSF-2: Silicified and adularized wallrock fragment composed of ash-flow tuff cut by chalcedonic quartz veinlets, within vein ore of the upper silica-flooded zone, "middle-plate fault", west wall at 1018m level, Lac Gold Bullfrog mine. Feldspar phenocrysts pseudomorphed by adularia and quartz, and small amounts of illite and albite. Groundmass composed of granophyric intergrowths of secondary quartz with anhedral to euhedral, very fine-grained adularia and traces of illite.

3SW-357: Pyritic quartz vein containing silicified and adularized fragments of welded, rhyolitic ash-flow tuff of the Crater Flat Tuff, dump of the Yellowjacket mine. Feldspar phenocrysts pseudomorphed by adularia, quartz and illite; groundmass composed of quartz, anhedral adularia, illite/smectite and disseminated pyrite partly replaced by jarosite.

Table 1. Volcanic-Stratigraphic Framework and Geochronology of the Southwestern Nevada Volcanic Field

Major Ash-flow Units and Lavas		Radiometric	Volcanic Center/location
Formation	Member	Age (Ma)	
		Late Magmatic Stage	
Stonewall Flat Tuff	Civet Cat Canyon	7.5	Stonewall Mountain caldera complex
	Spearhead	7.6	
Rhyolite of Obsidian Butte		8.8	Obsidian Butte
Thirsty Canyon Tuff	Gold Flat	9.2	Black Mountain caldera complex
	Trail Ridge		
	Pahute Mesa		
	Rocket Wash	9.4	
		Timber Mountain Magmatic Stage	
mafic lavas			Timber Mountain caldera II; moat and periphery
Tuffs and Lavas of the Bullfrog Hills[1], Rhyolite of Shoshone Mountain		10.5-10.0	Periphery and west of Timber Mountain caldera II
Tuff of Cut-off Road, Rhyolite lavas of Beatty Wash, Tuffs of Fleur de Lis Ranch, Tuff of Buttonhook Wash		11.4	Western part of Timber Mountain caldera complex
Timber Mountain Tuff	Ammonia Tanks	11.45	Timber Mountain caldera II
	Rainier Mesa	11.6	Timber Mountain caldera I
pre-Rainier Mesa rhyolite lavas, domes		11.7-11.6	Periphery and west of Timber Mountain caldera I
		Main Magmatic Stage	
post-collapse rhyolite lavas, domes		12.7-12.5	South margin of Claim Canyon cauldron
Paintbrush Tuff	Tiva Canyon	12.7	Claim Canyon cauldron
	Yucca Mountain		All others from area of Timber
	Pah Canyon		Mountain caldera complex
	Topopah Spring	12.8	
Calico Hills Formation		12.9	Flow-dome complexes southeast of Claim Canyon cauldron and Area 20 caldera
Wahmonie and Salyer Formations		13.2-12.8	Wahmonie
Crater Flat Tuff	Prow Pass		Uncertain; likely sources include area of Timber Mountain, Silent Canyon-Area 20 caldera complex, NW Yucca Mountain, and/or proposed Prospector Pass caldera complex
	Bullfrog	13.2	
	Tram		
Belted Range Tuff	Grouse Canyon	13.7	Silent Canyon caldera complex
Tuff of Tolicha Peak		13.9	Uncertain; likely source area in the vicinity of Mount Helen
Dacitic lavas and breccias			Bullfrog Hills, periphery of Crater Flat
Lithic Ridge Tuff		14.0	Uncertain
Rhyolitic lavas and dikes; Silicic dikes of Bare Mountain		14 - 15?	Bullfrog Hills, periphery of Crater Flat, eastern Bare Mountain
Belted Range Tuff	Tub Spring	14.9	Silent Canyon caldera complex
"Older" tuffs			Unknown
Sanidine-rich tuff			Unknown
Tuff of Yucca Flat		15.1	Unknown
Red Rock Valley Tuff		15.2	Unknown

Table 1, continued.

Compiled from discussions given by Byers et al. (1976a, 1989), Christiansen et al. (1977), Noble et al. (1984, 1991), Carr et al. (1986), Sawyer and Sargent (1989), Weiss and Noble (1989) and radiometric age data of Kistler (1968), Noble et al. (1968), Marvin et al. (1970; 1989), Hausback et al. (1990), Fleck et al. (1991), Sawyer et al. (1990; 1994), Noble et al. (1991), Monsen et al. (1992) and Weiss et al. (1993c). Ages corrected for modern constants.

[1] Includes Rhyolite of Rainbow Mountain of Maldonado (1990) and Maldonado and Hausback (1990), as well as overlying latitic to basaltic lavas.

Table 2. Radiometric Age Data for Specimens from the Southern Portion of the Southwestern Nevada Volcanic Field

Conventional K-Ar Age Determinations

No.	Field number	Mineral dated	District/Area of Mineralization	Latitude N.	Longitude W.	K_2O wt.%	$^{40}Ar^*$ mole/g	$^{40}Ar^*/^{40}Ar$ (%)	Age $\pm 1\sigma$ (Ma)
1	3MJ-224B	Ad	Wahmonie	36°49.25'	116°10.03'	14.0	2.6018×10^{-10}	66.5	12.9 ± 0.4
2	3SW-147	Ad	Wahmonie	36°49.21'	116°10.07'	12.96	2.3657×10^{-10}	59.5	12.6 ± 0.4
3	3MJ-118	Al	Northern Bare Mountain	36°53.86'	116°39.5'	2.25	3.9508×10^{-11}	26.6	12.2 ± 0.4
4	3MJ-130a	Al	Northern Bare Mountain	36°53.66'	116°39.5'	10.65	1.7212×10^{-10}	71.3	11.2 ± 0.3
5	Thompson mine	Al	Northern Crater Flat	38°56.94'	116°38.0'	6.48	1.2085×10^{-10}	19.6	12.9 ± 0.5
6	Silicon mine	Al	Tram Ridge	36°57.51'	116°38.6'	6.89	1.1560×10^{-10}	52.3	11.6 ± 0.4
7	3MJ-216A	Al	Eastern Calico Hills	36°54.20'	116°14.28'	11.02	1.6491×10^{-10}	87.3	10.4 ± 0.3
8	3SW-137A	Al	Western Calico Hills	36°52.78'	116°21.47'	8.38	1.4028×10^{-10}	19.4	10.4 ± 0.3
9	3SW-303	Al	Mine Mountain	36°58.46'	116°9.83'	9.04	1.4483×10^{-10}	55.6	11.1 ± 0.3
10	3MJ-176	Ad	Original Bullfrog mine	36°54.06'	116°53.1'	12.4	1.5497×10^{-10}	49.5	8.7 ± 0.3
11	Mayflower	Ad	Northern Bullfrog Hills	36°59.73'	116°47.30'	13.71	1.9745×10^{-10}	78.7	10.0 ± 0.3
12	Bullfrog Hills	Ad	Northern Bullfrog Hills	37°0.80'	116°45.53'	11.19	1.7741×10^{-10}	65.7	11.0 ± 0.4
13	3MJ-74a	Ad	Oasis Mountain	37°2.6'	116°44.93'	5.32	8.1468×10^{-11}	43.4	10.6 ± 0.3
14	BAILEY'S	Al	Bailey's Hot Spring	36°58.58'	116°43.08'	7.89	1.1572×10^{-10}	60.2	10.2 ± 0.3
15	3MJ-6	Al	Transvaal Hills	37°1.07'	116°34.52'	9.05	1.2940×10^{-10}	37.0	9.9 ± 0.4

Table 2, continued.

$^{40}Ar/^{39}Ar$ Multigrain Resistance-furnace Fusion Determinations

No.	Field number	Mineral dated	District/Area of Mineralization	Latitude	Longitude	$^{40}Ar/^{39}Ar$	$^{36}Ar/^{39}Ar$	$^{37}Ar/^{39}Ar$	$^{40}Ar^{*}$ (%)	J	Age ±1σ (Ma)
16	BBSF-2*	Ad	Lac Gold Bullfrog mine	36°53.73'	116°48.84'	1.7893	2.6974×10^{-3}	3.3729×10^{-3}	51.8	0.00587	9.8± 0.3
10	3MJ-176**	Ad	Original Bullfrog mine	36°54.06'	116°53.1'	2.7466	5.0852×10^{-2}	1.4295×10^{-3}	45.3	0.00041	9.2± 0.3
11	Mayflower*	Ad	Mayflower mine	36°59.73'	116°47.30'	1.9522	3.0617×10^{-3}	1.9447×10^{-3}	50.3	0.00560	9.9± 0.3
17	3SW-357*	Ad	Yellowjacket mine	37°1.92'	116°47.64'	3.1573	6.7614×10^{-3}	2.3506×10^{-3}	34.7	0.00574	11.3± 0.3

Ad = adularia; Al = alunite

Constants: $^{40}K\lambda_{\epsilon} + {}^{40}K\lambda_{\epsilon'} = 0.581 \times 10^{-10}\ yr^{-1}$; $^{40}K_{\beta} = 4.962 \times 10^{-10}\ yr^{-1}$; atomic abundance $^{40}K/K_{total} = 1.167 \times 10^{-4}$ kmole/kmole.

* Reactor constants: $(^{36}Ar/^{37}Ar)_{Ca} = 0.000264$; $(^{39}Ar/^{37}Ar)_{Ca} = 0.000673$; $(^{40}Ar/^{39}Ar)_{K} = 0.065$.

** Reactor constants: $(^{36}Ar/^{37}Ar)_{Ca} = 0.000275$; $(^{39}Ar/^{37}Ar)_{Ca} = 0.000729$; $(^{40}Ar/^{39}Ar)_{K} = 0.002$.

**

Additional descriptive information on sample locations and sample mineralogy is given in the Appendix and in McKee and Bergquist (1993).

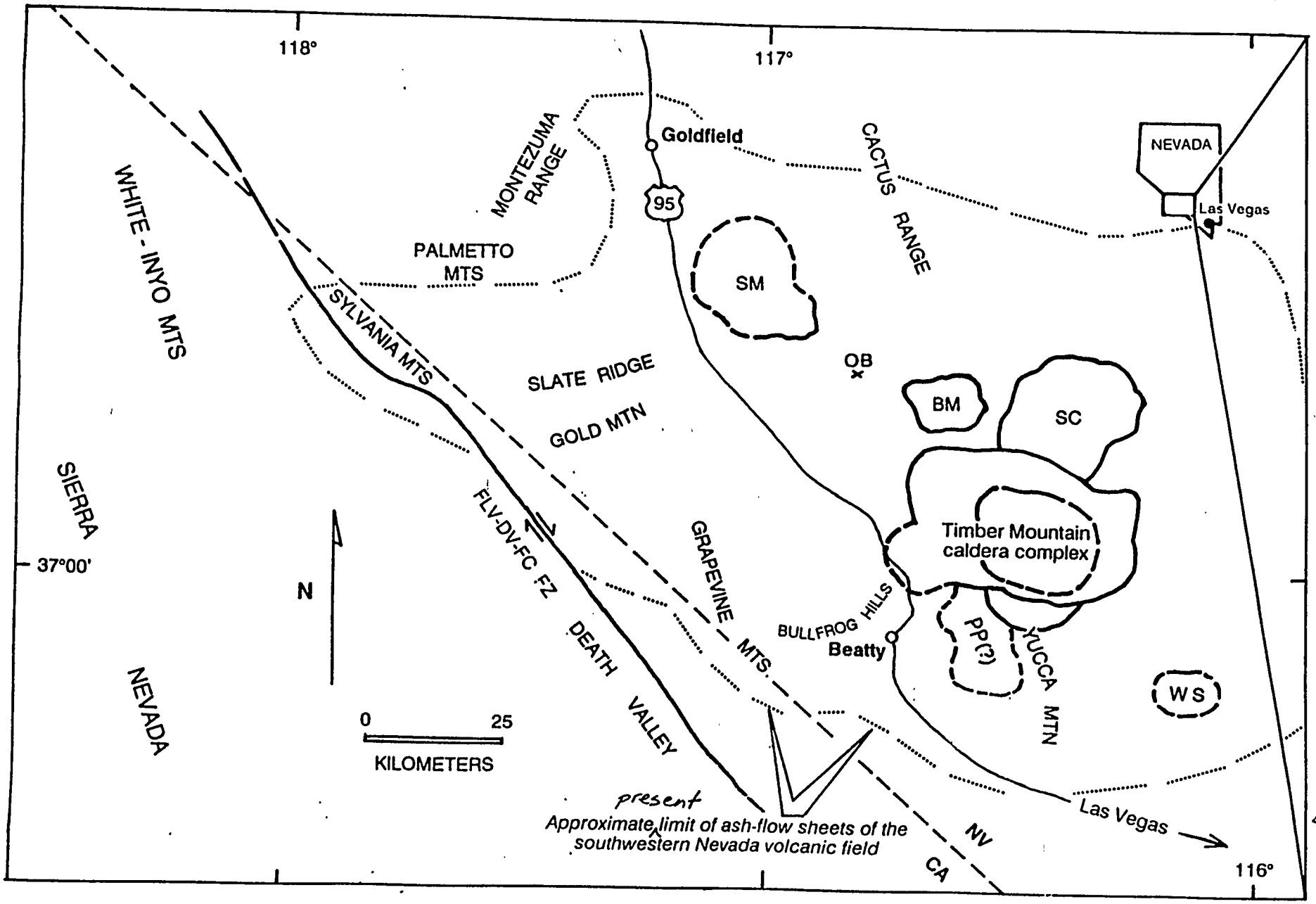
118°
117°
116°
37°00'
Goldfield
95
NEVADA
Las Vegas
MONTEZUMA RANGE
CACTUS RANGE
PALMETTO MTS
WHITE - INYO MTS
SYLVANIA MTS
SLATE RIDGE
GOLD MTN
SM
OB
BM
SC
Timber Mountain caldera complex
PP(?)
YUCCA MTN
WS
BULLFROG HILLS
Beatty
GRAPEVINE MTS
FLV-DV-FC FZ
DEATH VALLEY
SIERRA NEVADA
N
0
25
KILOMETERS
present
Approximate limit of ash-flow sheets of the southwestern Nevada volcanic field
NV
CA
Las Vegas

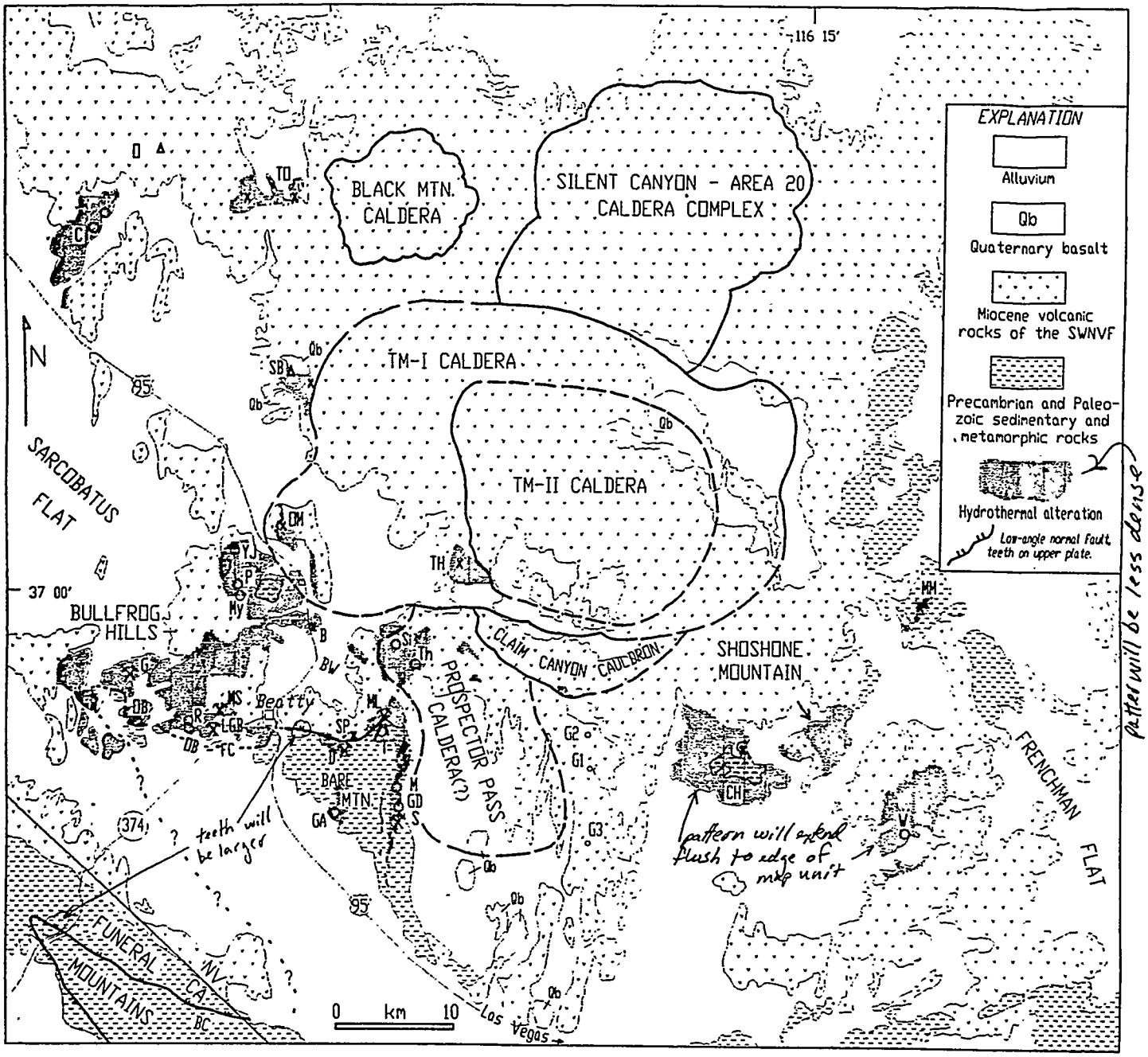
116 15'
BLACK MTN. CALDERA
SILENT CANYON - AREA 20 CALDERA COMPLEX
TM-I CALDERA
TM-II CALDERA
CLAIM CANYON CAULDRON
PROSPECTOR PASS CALDERA(?)
SARCOBATUS FLAT
BULLFROG HILLS
SHOSHONE MOUNTAIN
FRENCHMAN FLAT
FUNERAL MOUNTAINS
BARE MTN.
Beatty
Las Vegas
37 00'
N
0 km 10
EXPLANATION
Alluvium
Qb
Quaternary basalt
Miocene volcanic rocks of the SWNVF
Precambrian and Paleozoic sedimentary and metamorphic rocks
Hydrothermal alteration
Low-angle normal fault, teeth on upper plate.
teeth will be larger
pattern will extend flush to edge of mkp unit
pattern will be less dense

Fig. 3

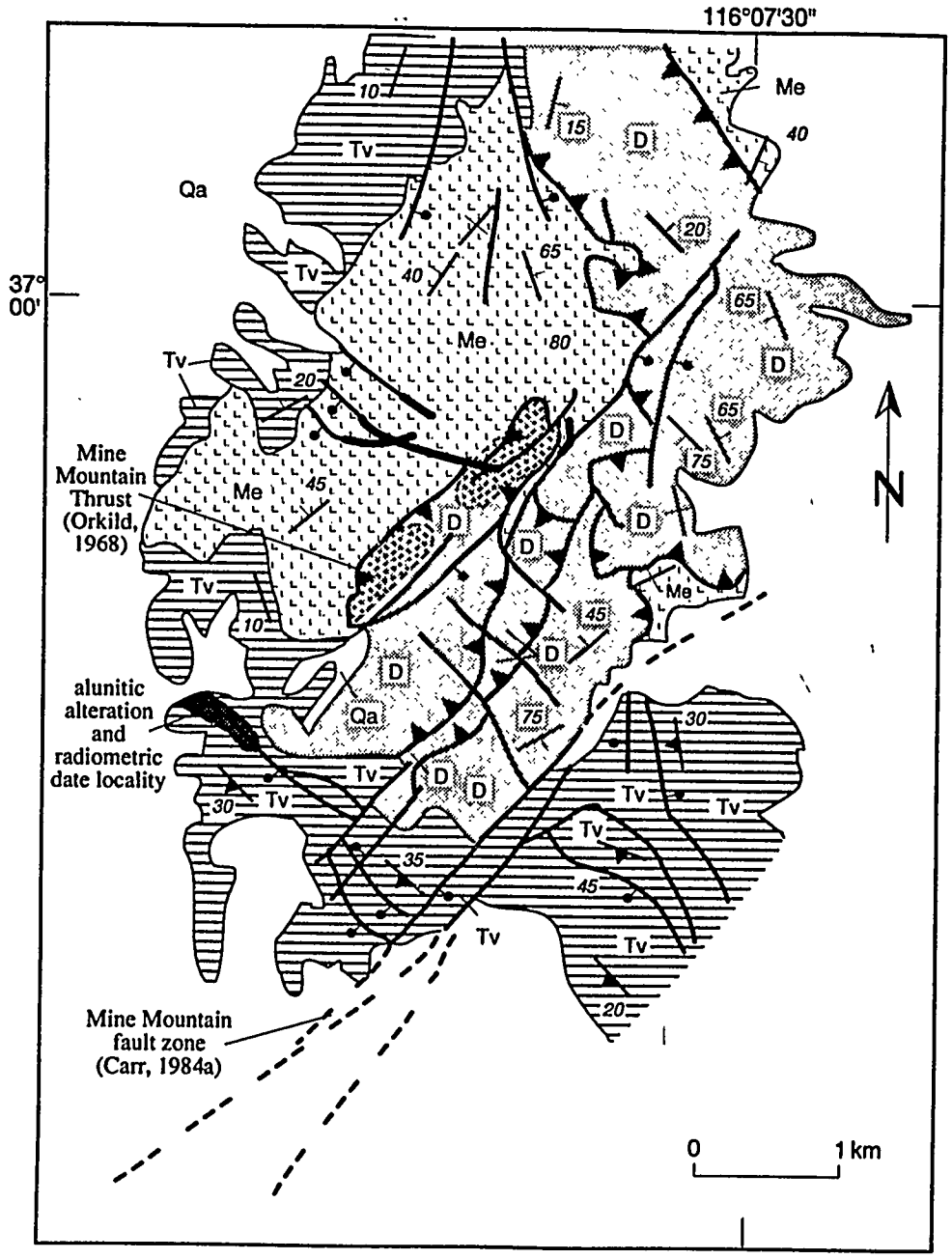

EXPLANATION

- Quaternary alluvium
- Miocene volcanic and sedimentary rocks
- Mississippian Eleana Formation
- Devonian limestone and dolostone
- Stipple shows principal areas of silicification, veins and hydrothermal and tectonic breccia along the crest of Mine Mountains
- Quartz and quartz-barite veins
- Strike and dip direction of beds
- 30 — Strike and dip direction of foliation in ash-flow tuff
- Mine Mountain "thrust." Teeth on upper plat

Patterns will be changed to: stipple for Tv
horizontal rule for Me
carbonate symbol for D

Fig. 4

Fig. 5

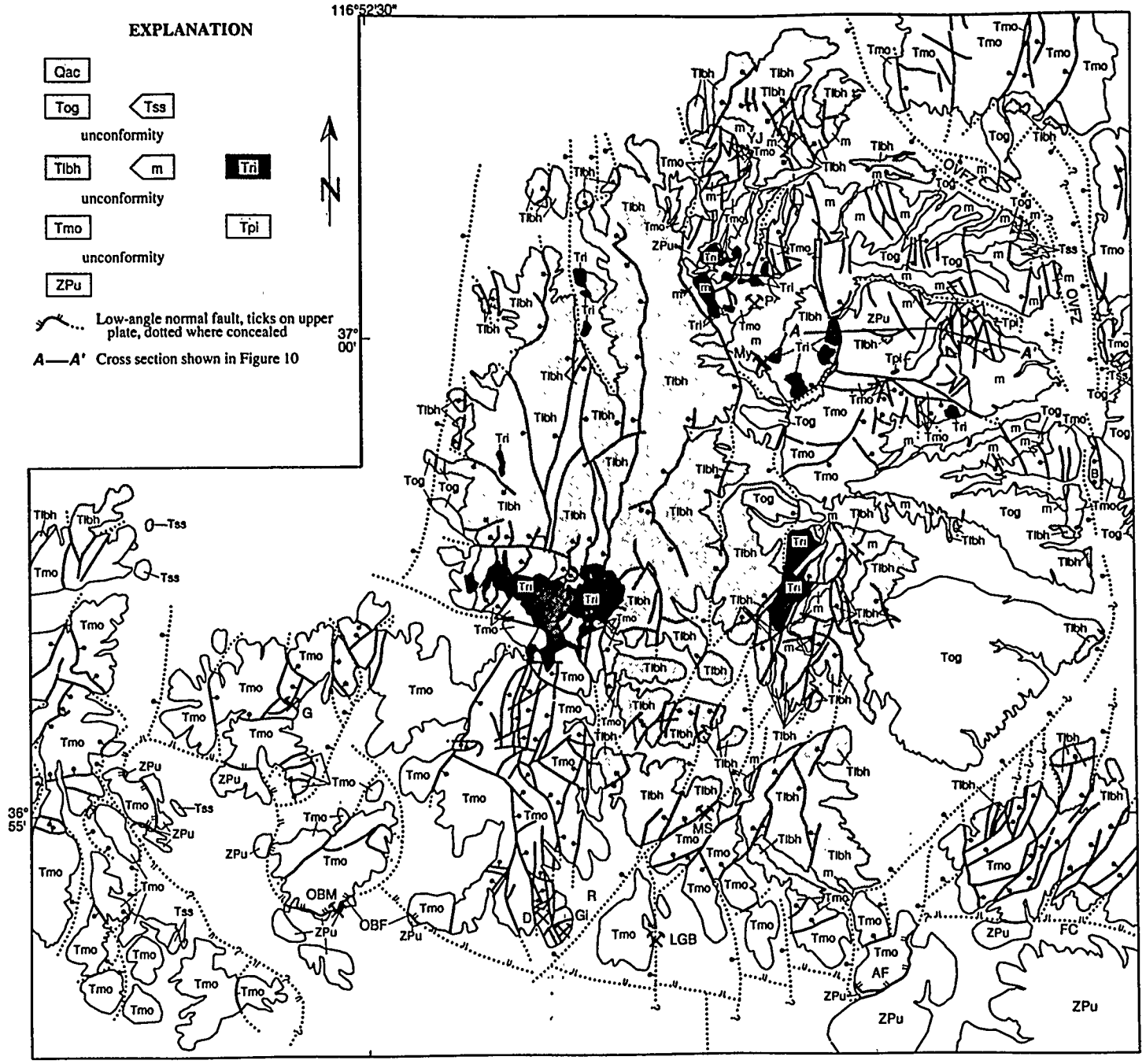
EXPLANATION
Qac
Tog
Tss
unconformity
Tlbh
m
Tri
unconformity
Tmo
Tpi
unconformity
ZPu
Low-angle normal fault, ticks on upper plate, dotted where concealed
A—A' Cross section shown in Figure 10
116°52'30"
37° 00'
36° 55'
N
Tlbh
Tmo
Tog
Tss
Tri
Tpi
ZPu
m
Q—Tss
G
OBM
OBF
D
Gl
R
LGB
MS
FC
AF
YJ
My
OVFZ
A
A'
B
B'

Fig. 5

fig. 6

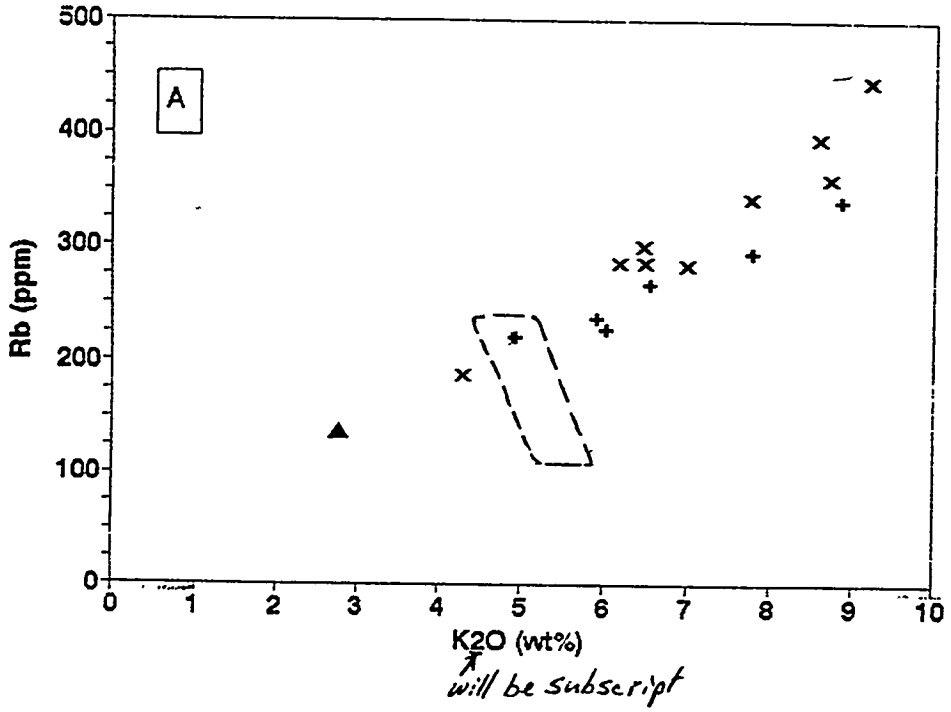
A
Rb (ppm)
500
400
300
200
100
0
0
1
2
3
4
5
6
7
8
9
10
K2O (wt%)
will be subscript

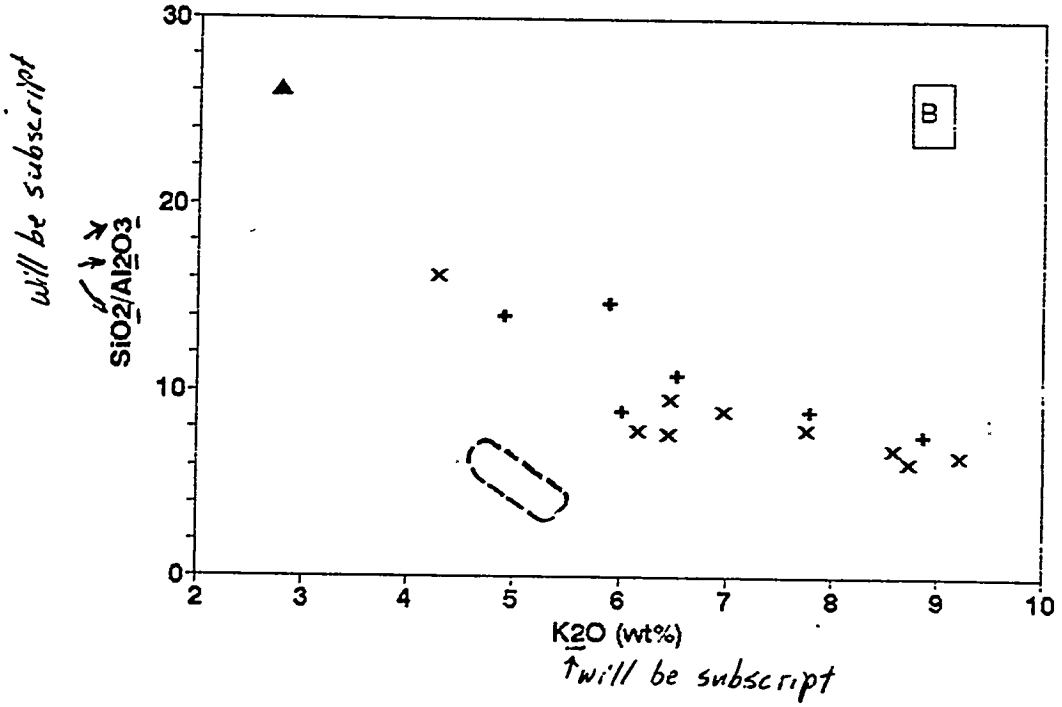
will be subscript
SiO2/Al2O3
B
30
20
10
0
2
3
4
5
6
7
8
9
10
K2O (wt%)
will be subscript

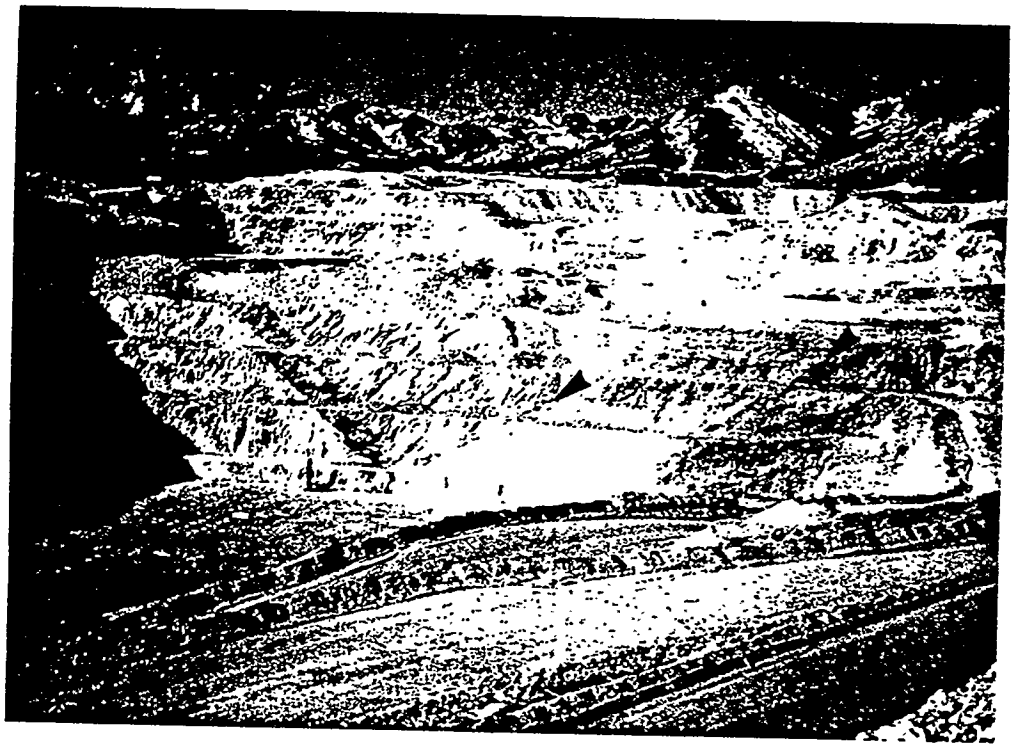

A

B

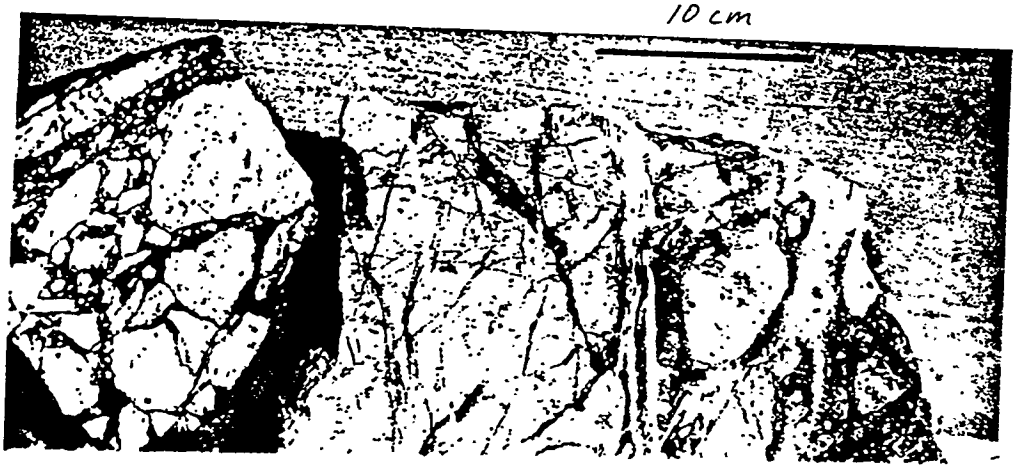

C

TIMING OF HYDROTHERMAL ACTIVITY AND MINERALIZATION, SOUTHERN PART OF THE SOUTHWESTERN NEVADA VOLCANIC FIELD

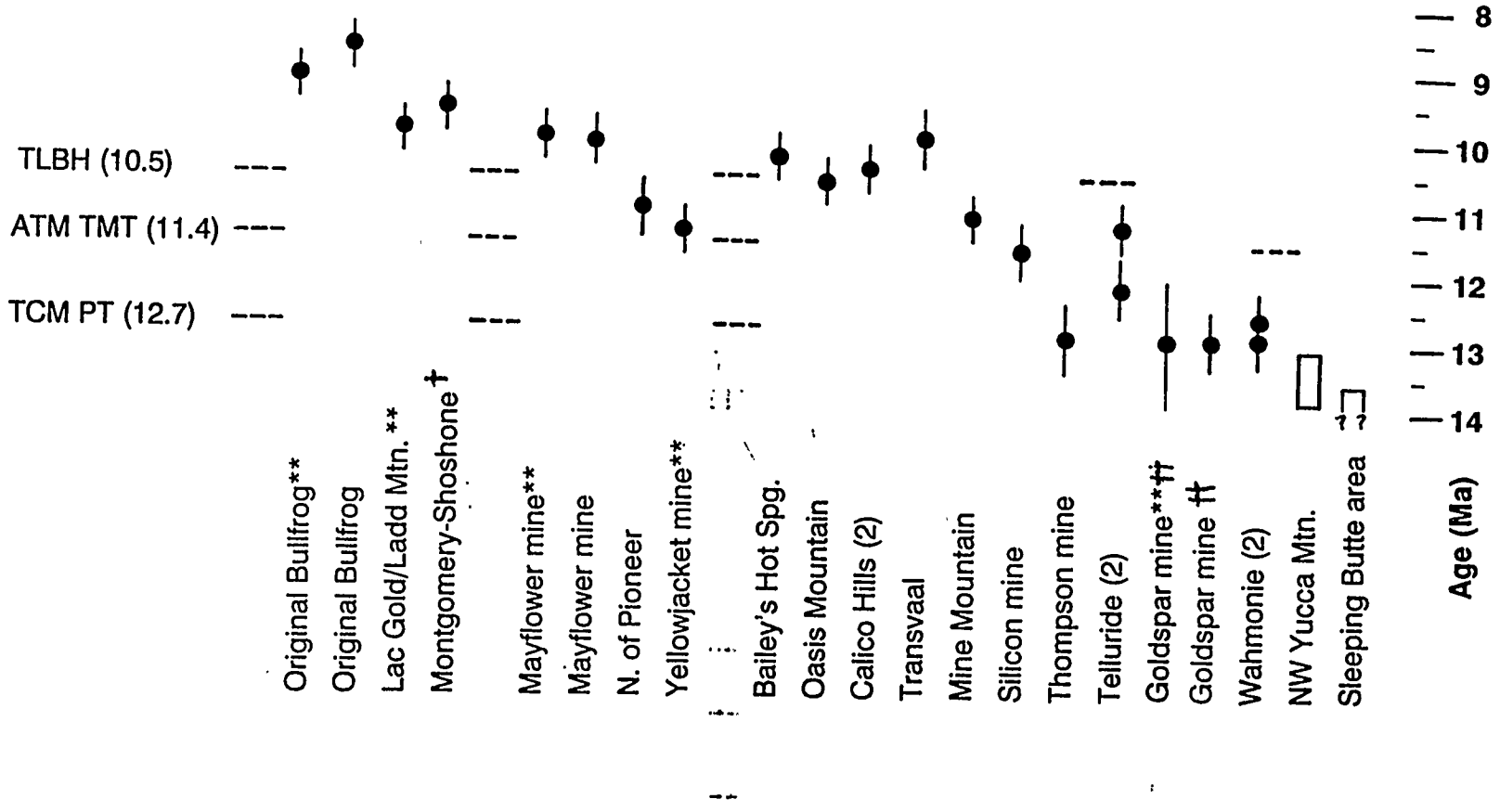

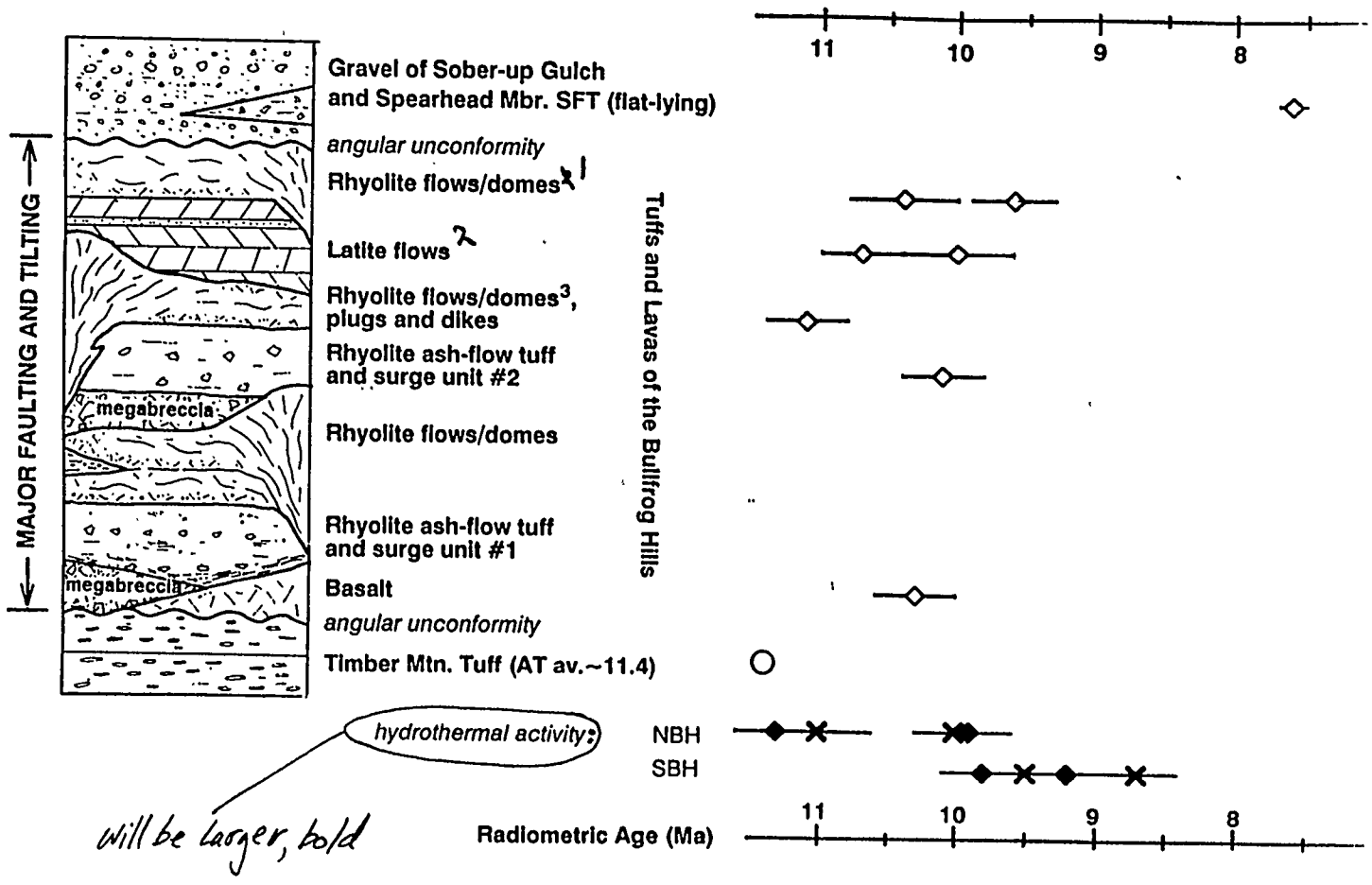
MAJOR FAULTING AND TILTING
megabreccia
megabreccia
Gravel of Sober-up Gulch
and Spearhead Mbr. SFT (flat-lying)
angular unconformity
Rhyolite flows/domes[1]
Latite flows[2]
Rhyolite flows/domes[3],
plugs and dikes
Rhyolite ash-flow tuff
and surge unit #2
Rhyolite flows/domes
Rhyolite ash-flow tuff
and surge unit #1
Basalt
angular unconformity
Timber Mtn. Tuff (AT av.~11.4)
Tuffs and Lavas of the Bullfrog Hills
11
10
9
8
hydrothermal activity:
NBH
SBH
will be larger, bold
Radiometric Age (Ma)
11
10
9
8

Fig. 9

Fig. 10

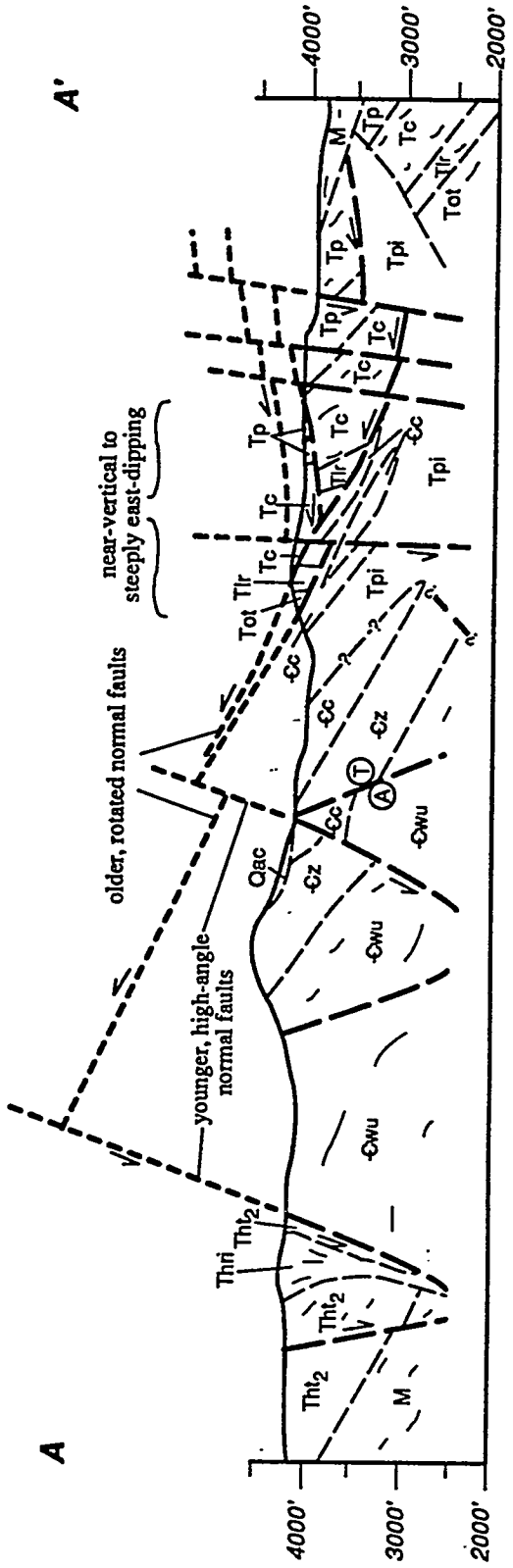
A
A'
4000'
3000'
2000'
near-vertical to steeply east-dipping
older, rotated normal faults
younger, high-angle normal faults
Tp
Tc
Tlr
Tot
Tpi
Qac
Qz
Qwu
Thr
Tht2
M

APPENDIX B

rev. October 13, 1994

PYRITIC ASH-FLOW TUFF, YUCCA MOUNTAIN, NEVADA--A DISCUSSION

Steven I. Weiss, Lawrence T. Larson, and Donald C. Noble

Department of Geological Science, Mackay School of Mines
University of Nevada, Reno, Reno, Nevada, 89557

Sir: Ample, well-documented textural and mineralogic evidence exists for at least one episode of widespread hydrothermal alteration of volcanic rocks deep in Yucca Mountain, Nevada (Broxton et al., 1982; Caporusio et al., 1982; Scott and Castellanos, 1984; Vaniman et al., 1984; Warren et al., 1984; Bish, 1987; Bish and Aronson, 1993). Despite this evidence, Castor et al. (1994) infer that most of the pyrite found in tuffs at Yucca Mountain was introduced as ejecta (lithic fragments) incorporated during the eruptions of the tuffs, rather than by *in-situ* hydrothermal activity. Their conclusions appear to be based on their observation that most of the pyrite resides in unaltered to variably altered and veined lithic fragments, whereas pyrite-bearing veins are absent in the tuff matrix, titanomagnetite and mafic phenocrysts in the matrix are generally not replaced by pyrite, and feldspar phenocrysts in the pyritic tuff matrix are generally unaltered. Castor et al. dismiss the much smaller quantities of pyrite disseminated in the tuff matrix, including relatively rare pyritized hornblende and biotite grains, as xenolithic as well.

The pyritic tuffs belong to large-volume, subalkaline rhyolite ash-flow units (ca. >150 to 250 km^3 each, Carr et al., 1986; Sawyer et al., 1994). The interpretation of Castor et al. (1994) has broad implications for the temperature, fO_2 and fS_2 of major ash flow eruptions. In addition, the origin of this pyrite also bears on the nature of past fluid flow and water-rock reactions at Yucca Mountain, which in turn are important factors in assessing the potential for currently undiscovered mineral resources in the area of the proposed nuclear waste repository. We have studied core and cuttings from the same drill holes studied by Castor et al., as well as other drill holes. It is our contention that the inconsistent lateral and stratigraphic distribution of the pyrite, textural features of the pyrite, and phase stability

considerations are incompatible with the "lithic" origin of Castor et al. (1994), and are more reasonably explained by *in-situ* formation from hydrothermal fluids containing low, but geochemically significant, concentrations of reduced sulfur.

Textural and stratigraphic evidence for in-situ origin of pyrite

Castor et al. (1994) state that pyrite in the tuff matrix is from "pulverized ejecta and is commonly in rounded grains (Fig 3.), probably due to abrasion during pyroclastic transport". We have not observed rounded pyrite grains. In fact, the pyrite (bright) grains shown in their Figure 3 and observed by us in our polished sections are not rounded, but are rather anhedral, have somewhat pitted to embayed margins, and have as many as two poorly developed crystal faces. The small, possibly subspherical voids surrounding two of these grains (dark in their Figure 3) are in the soft, clay-rich matrix and may be artifacts of grinding and polishing, particularly if the specimen was not impregnated with epoxy prior to grinding. Moreover, abrasion of the relatively hard pyrite grains is difficult to accept when, as shown in their Figure 3, the much more delicate points and cusps of the glass shards have not been destroyed. We note that phenocrysts in ash-flow tuffs are invariably angular and are commonly fractured, but are not rounded.

In lithic fragments and in the groundmass of the ash-flow units in Yucca Mountain the disseminated pyrite consists of anhedral to subhedral, generally pitted and wormy to seived, or skeletal(?), individual crystals and granular aggregates of from $<5\ \mu m$ to ~0.5 mm in maximum dimension (Fig. 1). In some grains pits and poikilitic texture appear to result from the presence of numerous inclusions of altered groundmass, whereas other grains, mainly those smaller than about $10\ \mu m$ in diameter, are not uncommonly subhedral in shape and free of pits. Propylitically altered silicic lava in drill hole USW G-2 contains disseminated pyrite grains having textures and morphology indistinguishable from those of the pyrite in the tuffs (Fig. 2). Fractures, not uncommon in granular pyrite in the tuffs, are present as well in pyrite grains in the altered lava. The pyrite in the lava is not lithic material,

demonstrating that fragmentation and degassing processes of ash-flow eruptions are not neccessarily responsible for the textures and morphology of the pyrite in the tuffs. Instead, as is clearly the case in the altered lavas, the observed textures of pyrite in the tuffs more likely result from *in-situ* precipitation and growth (± partial dissolution ?) from hydrothermal solutions.

Pyrite in tuffs at Yucca Mountain is identical within the range of textures and morphologies of pyrite formed during hydrothermal alteration of initially porous ash-flow tuff within and peripheral to precious-metal deposits such as Round Mountain, Divide and Lac Gold Bullfrog, Nevada (Fig. 3). In these and other districts (e.g. Tonopah, Bonham and Garside, 1979) intermediate to mafic volcanic fragments commonly have been preferentially pyritized, without pyrite rinds, and/or have greater pyrite contents relative to the surrounding groundmass of hydrothermally altered tuff (Fig. 3D). This is a common observation of geologists working in volcanic terranes and it is generally attributed to the greater abundance of iron in the fragments.

In Yucca Mountain drill hole USW G-2 (Fig. 4) small amounts of pyrite are disseminated in the altered dacitic lava and associated tuff that lies *between* the Lithic Ridge Tuff and the Tram Member at depths between 4072 to 4149 ft. Between 3457 and 3544 ft. partially to densely welded ash-flow tuff of the Bullfrog Member contains small amounts (< 1%) of pyrite disseminated in the groundmass, in altered pumice fragments (see below), in sparse lithic fragments and in and near thin quartz and quartz+calcite veinlets (Fig. 5). A steeply dipping, drusy quartz vein cutting the Bullfrog Member, although largely oxidized, contains traces of filmy pyrite on and intergrown with quartz (Fig. 6). This demonstrates that processes of in-situ formation of pyrite *have* occurred, at least locally, *after* the deposition of the ash-flow flow units in USW G-2, although the Lithic Ridge and Tram Member in this drill hole are largely barren of pyrite. Caporuscio et al. (1982) reported the presence of pyrite in bedded tuffs at the base of the Prow Pass and Tram Members, in the densely

welded, upper Lithic Ridge Tuff, and in the pre-Lithic Ridge rhyolitic lavas in USW G-2. We have examined these rocks and have not observed any pyrite.

Castor et al. (1994) imply that the pyritic tuffs are eruptive subunits, and apparently consider that the pyritic fragments and disseminated pyrite define distinctive lithic fragment assemblages that mark time-stratigraphic horizons. These proposed "subunits" must be discontinous on both regional and local scales, being restricted to certain areas of the Bullfrog Hills and certain drill holes in Yucca Mountain, (both are areas of recognized episodes of hydrothermal activity (e.g., Ransome et al., 1910; Carr et al., 1986; Bish, 1987; Bish and Aronson, 1993). Regionally, pyrite, lithic or otherwise, is not described by Carr et al. (1986) (or observed by our group) in the Lithic Ridge Tuff at the type locality 18 km northeast of Yucca Mountain or in exposures west of the Bullfrog Hills. We have not observed pyrite in the thick sections of the Tram Member exposed in northwestern Yucca Mountain (Fridrich et al., 1994).

At the local scale, in the subsurface of Yucca Mountain in drill hole USW G-1 (Fig. 4), pyrite is present in the lower part of the Tram Member, but is absent in the Lithic Ridge Tuff. Less than 0.5 km to the east in drill hole USW H-1 (Fig. 4) pyrite is present in the Lithic Ridge Tuff, but it is absent from the Tram Member. Pyrite is present in lower parts of the Bullfrog Member and in the *upper* part of the Tram Member at 3593 to 3595 ft. in USW G-2, approximately 2.5 km north of USW G-1 and H-1. In UE25B 1H, only 1.9 km southeast of USW H-1, pyrite appears again in the lower Tram Member, but is absent from the Lithic Ridge Tuff. Similarly, in USW G-3 (Fig. 4) pyrite is present in both the lower part of the Tram Member and the Lithic Ridge Tuff, but less than one kilometer to the north, only the lower Tram Member is pyritic in USW H-3. Less than 4 km east of USW H-3 pyrite is absent from both the Tram Member and the Lithic Ridge Tuff in UE25 P1, but is present in argillically altered tuffs below the Lithic Ridge Tuff. In USW H-4 we have observed pyrite

in welded and devitrified Crater Flat Tuff, probably within the Bullfrog Member, whereas in USW H-5 pyrite is absent.

The laterally discontinuous and stratigraphically inconsistent pyrite distribution, over distances of as little as 0.5 km, would require unrealistically abrupt and fortuitous differences in original deposition, or in subsequent preservation by variations in cooling, water-table elevations and/or weathering. We consider the pyrite distribution to have little, if any, relation to genetically meaningful stratigraphic units defined by primary depositional features (e.g., bedded tuff horizons, cooling and crystallization relations) and differences in phenocryst assemblages. Such irregular distribution is, however, reasonably attributable to the channeling of fluids having sufficient activity of reduced sulfur to precipitate pyrite, perhaps near faults, fractures and other zones of enhanced permeability.

Considerations of phase stability relations and conditions of ash-flow eruption and emplacement

Pyrite is not a stable phase in magmas of any composition; even the most sulfur-rich magmas do not contain pyrite. Blebs of pyrrhotite crystallized from magmatic sulfide solutions are present in trace amounts in many subalkaline silicic ash-flow tuffs and lavas (Hildreth, 1979; Whitney and Stormer, 1983), but survive eruption and cooling only when encapsulation in phenocryst phases and dense glass prevents breakdown by loss of S_2 gas (Keith et al., 1991). Therefore, pyrite disseminated in argillically-altered pumice fragments of the Bullfrog Member in USW G-2 and in the Tram Member in UE25 B1H (Figs. 5 and 7) must have formed *after* eruption and cooling from magmatic temperatures.

Pyrite exposed in vent walls is unlikely to survive the conditions of major ash flow eruptions. Subalkaline silicic magmas typically erupt at temperatures between about 720 and 900+°C. The principal units of the Paintbrush Tuff and the Timber Mountain Tuff have given Fe-Ti oxide equilibrium temperature estimates of between 700 and 900+°C (Warren et al., 1989). We see no reason for appreciably lower magma temperatures for the

earlier Crater Flat Tuff, Lithic Ridge Tuff and older tuffs units. *Within the vents* of major ash flow eruptions cooling is negligible from the incorporation of atmospheric gases and adiabatic expansion, owing to the overwhelming mass and energy flux of the magmatic volatiles and vesiculating magma fragments. The 742°C stability limit of pyrite mentioned by Castor et al. is the maximum temperature at which pyrite is stable in the Fe-S system, and requires the activity of $S^\circ = 1$ (ie. presence of S_{liq}), and the *absence* of O_2 (Kullerude and Yoder, 1959), conditions unlikely for most subalklaine rhyolite magmas and their exsolved gasses (Whitney, 1984). During initial degassing the dominant sulfur species is SO_2 (Whitney, 1984), but the gasses mainly comprise water vapor, CO_2, H_2, HCl, and HF, and would likely be corrosive to pyrite at temperatures well below 742°C.

Numerical models suggest that the incorporation of large volumes of lithic fragments in ash-flow tuffs will lower the bulk flow temperatures into the 500 to 650°C range over times on the order of minutes to months and may in some cases inhibit welding (Eichleberger and Koch, 1979; Marti et al., 1991), consistent with the common observation of envelopes of glassy tuff surrounding intracaldera slide blocks and wedges of megabreccia (e.g. Lipman, 1984, Fig. 10b; Fridrich, 1987). However, these models also indicate that lithic fragments less than a few millimeters in diameter are heated to the bulk flow temperature nearly instantaneously, with sub-millimeter fragments equilibrating in less than one second, *prior* to significant bulk cooling. The disseminated pyrite in the Yucca Mountain tuffs consists of grains less than 0.5 mm in diameter that would have been destroyed by heating to magmatic or near-magmatic temperatures in the presence of magmatic gasses during eruption and transport.

The lack of welding, low magnetic remanence and high magnetic susceptibility cited by Castor et al. (1994) as evidence for emplacement of the pyritic tuffs at temperatures below 550 to 580°C are, at best, weak arguments. Welding is a function of glass composition, water content and loading, as well as temperature and is thought to occur over minutes to years

(Rhiele, 1973; Eichleberger and Koch, 1979). According to Fisher and Schmincke (1984) temperatures of up to 645°C were measured in fumeroles in poorly welded ash-flow tuff in the Valley of Ten Thousand Smokes 7 years after deposition. Various pyroclastic deposits of the 1980 eruptions of Mount Saint Helens, all non-welded, glassy and 2 to 3 orders of magnitude smaller in volume than the pyritic units in Yucca Mountain, were emplaced at temperatures in the range of 750 to 850°C near the vent and between 300 to 730°C further away, with no significant decrease in temperatures along their flow paths (Banks and Hoblitt, 1981). Detailed rock magnetic and transmission electron microscope studies have shown that the bulk of the magnetic remanence and susceptibility characteristics in glassy ash-flow tuff, including that of the Paintbrush Tuff at Yucca Mountain, are carried by abundant Fe-Ti oxide microcrystals precipitated in the glass during cooling (Schlinger et al., 1988; 1991). In the pyritic units in Yucca Mountain the original quenched glass has largely been altered to clay, zeolites, silica and calcite (Bish, 1987; Broxton, et al., 1982; Caporuscio et al., 1982; Vaniman et al., 1984; Warren, et al., 1984). The low magnetic remanence and high magnetic susceptibility are equally consistent with, and more plausibly explained by, the destruction of the remanence carrying microcrystals during hydrothermal alteration of the glass, leaving only the large, high-susceptibility magnetite phenocrysts (± secondary(?) magnetite).

Trace-metal geochemistry

Concentrations of As, Bi, Hg, Mo, Sb, Te and Zn reported by Castor et al. (1994) for the Yucca Mountain drill core are as much as one to two orders of magnitude higher than the low levels found in surface samples of unaltered rhyolite ash-flow tuff in the Yucca Mountain area (Castor et al., 1990; Weiss et al., 1991; Castor and Weiss, 1992). Indeed, the elevated trace-metal concentrations in the drill hole samples are not unlike those reported by Castor and Weiss (1992) for altered volcanic rocks in the nearby Bullfrog, Bare Mountain and Wahmonie precious-metal districts when ore samples are excluded, and are comparable

to those of altered, but unmineralized rocks in other districts (e.g. Rawhide, (Black et al., 1991)). The 142 ppm As and 249 ppm Sb concentrations reported by Castor et al. in USW G-2 are from the weakly pyritic vein shown in our Figure 6. Castor et al. provide little explanation for the observed enrichments, which we believe are most simply explained by *in-situ* hydrothermal activity, rather than by derivation from altered lithic fragments.

Figure 5 of Castor et al. (1994) leads the reader to believe there is continuous assay data for the drill hole. This is not the case. Most samples, representing no more than a few tens of cm of core, are separated by distances of 10 to 70 m. Data points should have been shown as small dots or ticks to more accurately depict the sample spacing.

Although pyrite encapsulated *within* lithic rock fragments could perhaps retain sulfur and survive entrainment in major ash flow eruptions, in all probability unencapsulated grains of millimeter or smaller sizes would be destroyed by the near-instantaneous heating to magmatic and near-magmatic temperatures in magmatic gases, followed by cooling over minimum times of 10's of minutes to days or months. This probability, together with the textural similarities of the groundmass pyrite to that observed in altered lavas in USW G-2 and in altered porous tuffs in the Divide, Round Mountain and Bullfrog districts, the inconsistent lateral and stratigraphic distribution, the presence of pyrite locally in units overlying and underlying the Lithic Ridge and Tram Member, including propylitically altered silicic lava, the presence of pyrite in altered pumice fragments, and in and near silica veinlets in the Bullfrog Member in USW G-2, leads us to conclude that a much more simple and common process formed the pyrite in the groundmass of the tuffs: sulfidation of iron in the rocks from HS^- bearing hydrothermal fluids. Castor et al. considered this possibility an "untenable alternative" because of the generally unaltered feldspar phenocrysts, lack of pyritic veins and scarcity of pyritized titanomagnetite, hornblende and biotite phenocrysts in the tuffs. Within the tuff matrix, particularly under low permeability conditions within the clay-zeolite altered tuff matrix, fluids may have been buffered by the alteration of the rhyolitic glass to the

observed illite/smectite, silica, zeolite and carbonate minerals, allowing feldspar, biotite and hornblende phenocrysts to remain stable or metastable. Such stability would inhibit sulfidation and explain the scarcity of pyritized biotite and hornblende in the tuffs.

As pointed out by Castor et al. (1994), most of the pyritic lithic fragments consist of volcanic rocks of intermediate to mafic compositions. Fluids entering these fragments would encounter higher iron contents and would no longer be buffered by alteration of the tuff matrix, perhaps promoting preferential destabilization and sulfidation of the more abundant mafic silicate and Fe-Ti oxide phases. The uneven lateral and vertical distribution of pyrite can reasonably be attributed to the flow pathways of fluids that had activities of reduced sulfur species sufficient to sulfidize iron-rich phases in the rock mass. Pyrite in the lithic fragments is unlikely to have been dissolved in cool, dilute groundwater and re-precipitated in the tuff matrix.

Yucca Mountain is situated in a region containing presently and formerly producing precious-metal mines of middle and late Miocene age. Consequently, it is extremely important to assess the possibility of future human intrusion of the proposed high-level radioactive waste repository. A critical factor is the degree to which future generations perceive mineral potential beneath Yucca Mountain. It is therefore critical to determine the origin of the pyrite and the trace-metal enrichments. The textural, stratigraphic and phase stability relations discussed above are inconsistent with the interpretation of Castor et al. (1994) of a "lithic" origin related to major ash-flow eruptions. We believe that the evidence, including the trace-metal data, is internally consistent with, and strongly supports, in-situ formation from hydrothermal fluids containing reduced sulfur. Such bisulfide-bearing fluids may have been capable of carrying and depositing gold and silver. Although it is true that the pyritic rocks have been found only at depths of greater than 900 m, 11 of the 12 existing deep boreholes are situated from about 1.0 to more than 3.0 km apart (Fig. 4), a spacing far to great to rule out the potential presence of mineral deposits beneath the Paintbrush Tuff. Such

deposits, real or perceived, could well prove attractive to future explorationists. This is particularly true because the enormous amount of mined rock from excavation of the repository will indicate the existence of major underground workings, which could both suggest the possibility of previous mining and suggest relatively easy access to potential or perceived mineral deposits beneath Yucca Mountain.

October 13, 1994

REFERENCES

Banks, N. G., and Hoblitt, R., P., 1981, Summary of temperature studies of 1980 deposits: *in* Lipman, P. W., and Mullineaux, D. R., eds., The 1980 eruptions of Mount Saint Helens, Washington, U.S. Geological Survey Professional Paper 1250, p. 295-313.

Black, J. E., Mancuso, T. K., and Gant, J. L., 1991, Geology and mineralization at the Rawhide Au-Ag deposit, Mineral County, Nevada: *in* Raines, G.L., Lisle, R.E., Shafer, R.W., and Wilkinson, W.W., eds., Geology and Ore Deposits of the Great Basin, Reno, Geological Society of Nevada, p. 1123-1144.

Bish, D.L., 1987, Evaluation of past and future alteration in tuff at Yucca Mountain, Nevada based on clay mineralogy of drill cores USW G-1, G-2, and G-3: Los Alamos National Laboratory Report LA-10667-MS, 41 p.

Bish, D. L., and Aronson, J. L., 1993, Paleogeothermal and paleohydrologic conditions in silicic tuff from Yucca Mountain, Nevada: Clays and Clay Minerals, v. 41, p. 148-161.

Bonham, H. F., Jr., and Garside, L. J., 1979, Geology of the Tonopah, Lone Mountain, Klondike and northern Mud Lake Quadrangles, Nevada: Nevada Bureau of Mines and Geology Bulletin 92, 142 p., 1:48,000.

Broxton, D. E., Vaniman, D., Caporuscio, F., Arney, B., and Heiken, G., 1982, Detailed petrographic descriptions and microprobe data fro drill holes USW G2 and UE25b-1H, Yucca Mountain, Nevada: Los Alamos, New Mexico, Los Alamos National Laboratory Report LA-10802-MS, 168 p.

Caporuscio, F., Vaniman, D.T., Bish, D.L., Broxton, D.E., Arney, D., Heiken, G., Byers, F.M., and Gooley, R., 1982, Petrologic studies of drill cores USW G2 and UE25b-1H,Yucca Mountain, Nevada: Los Alamos, New Mexico, Los Alamos National Laboratory Report LA-9255-MS, 114 p.

Carr, W.J., Byers, F.M., and Orkild, P.P., 1986, Stratigraphic and volcano-tectonic relations of Crater Flat Tuff and some older volcanic units, Nye County, Nevada: U.S. Geological Survey Professional Paper 1323, 28p.

Castor, S. B., and Weiss, S. I., 1992, Contrasting styles of epithermal precious-metal mineralization in the southwestern Nevada volcanic field, USA: Ore Geology Reviews, v. 7, p. 193-223.

Castor, Feldman and Tingley, 1990, Mineral potential report for the U.S. Department of Energy, Serial No. N-50250: Nevada Bureau of Mines and Geology, University of Nevada, Reno, 24 pp.

Castor, S. B., Tingley, J. V., and Bonham, H. F., Jr., 1994, Pyritic ash-flow tuff, Yucca Mountain, Nevada: Economic Geology, v. 89, p. 401-407.

Eichleberger, J. C., and Koch, F. G., 1979, Lithic fragments in the Bandelier Tuff, Jemez Mountains, New Mexico: Journal of Volcanology and Geothermal Research, v. 5, p. 115-134.

Fridrich, C. J., 1987, The Grizzly Peak cauldron, Colorado: structure and petrology of a deeply dissected resurgent ash-flow caldera: unpublished PhD dissertion, Stanford, Stanford University, 201 p.

Fridrich, C. J., Orkild, P. P., Murray, M., Price, J. R., Christiansen, R. L., Lipman, P. W., Carr, W. J., Quinlivan, W. D., and Scott, R. B., 1994, Geologic map of the East of Beatty Mountain Quadrangle, Nye County, Nevada: U.S. Geological Survey Open-file Report, 4 sheets, 1:12,000 (in review).

Hildreth, W., 1979, The Bishop Tuff: Evidence for the origin of compositional zonation in silicic magma chambers: Geological Society of America Special Paper 180, p. 43-75.

Keith, J. D., Dallmeyer, R. D., Kim, C., and Kowallis, B. J., 1991, The volcanic history and magmatic sulfide mineralogy of latites of the central East Tintic Mountains, Utah: *in* Raines, G.L., Lisle, R.E., Shafer, R.W., and Wilkinson, W.W., eds., Geology and Ore Deposits of the Great Basin, Reno, Geological Society of Nevada, p. 461-483.

Kullerude, G., and Yoder, H. S., 1959, Pyrite stability relations in the Fe-S system: Economic Geology, v. 54, p. 533-572.

Lipman, P. W., 1984, The roots of ash flow calderas in western North America: windows into the tops of granitic batholiths: Journal of Geophysical Research, v. 89, p. 8801-8841.

Marti, J., Diez-Gil, J. L., and Ortiz, R., 1991, Conduction model for the thermal influence of lithic clasts in mixtures of hot gases and ejecta: Journal of Geophysical Research, v. 96, p. 21,879-21,885.

Ransome, F.L., Emmons, W.H., and Garrey, G.H., 1910, Geology and ore deposits of the Bullfrog district, Nevada: U.S. Geological Survey Bulletin 407, 130 p.

Rhiele, J. R., 1973, Calculated compaction profiles of rhyolitic ash-flow tuffs. Geological Society of America Bulletin, v. 84, p. 2193-2216.

Sawyer, D. A., Fleck, R. J., Lanphere, M. A., Warren, R. G., Broxton, D. E., and Hudson, M. R., 1994, Episodic caldera volcanism in the Miocene southwestern Nevada volcanic field: revised stratigraphic framework, $^{40}Ar/^{39}Ar$ geochronology, and implications for magmatism and extension: Geological Society of America Bulletin, *in press*.

Scott, R.B. and Castellanos, M., 1984, Stratigraphic and structural relations of volcanic rocks in drill holes USW GU-3 and USW G3, Yucca Mountain, Nye County, Nevada: U.S. Geological Survey Open-File Report 84-491, 121 p.

Schlinger, C. M., Rosenbaum, J. G., and Veblen, D. R., 1988, Fe-oxide microcrystals in welded tuff from southern Nevada: origin of remanence carriers by precipitation in volcanic glass: Geology, v. 16, p. 556-559.

Schlinger, C. M., Veblen, D. R., and Rosenbaum, J. G., 1991, Magnetism and magnetic mineralogy of ash flow tuffs from Yucca Mountain, Nevada: Journal of Geophysical Research, v. 96, p. 6035-6052.

Vaniman, D.T., Bish, D., Broxton, D., Byers, F., Heiken, G., Carlos, B., Semarge, E., Caporuscio, F., and Gooley, R., 1984, Variations in authigenic mineralogy and sorptive zeolite abundance at Yucca Mountain, Nevada, based on studies of drill cores USW GU-3 and G-3.

Warren, R.G., Byers, F.M., and Caporuscio, F.A., 1984, Petrography and mineral chemistry of units of the Topopah Springs, Calico Hills and Crater Flat Tuffs, and some older volcanic units, with emphasis on samples from drill hole USW G-1, Yucca Mountain, Nevada Test site: Los Alamos, New Mexico, Los alamos National Laboratory Report LA-10003-MS.

Warren et al., 1989 JGR

Weiss, S. I., Noble, D. C., and Larson, L. T., 1991, Task 3: Evaluation of mineral resource potential, caldera geology and volcano-tectonic framework at and near Yucca Mountain; report for October, 1990 - September, 1991: Center for Neotectonic Studies, University of Nevad-Reno, 37 p. plus appendices.

Whitney, J. A., 1984, Fugacities of sulfurous gases in pyrrhotite-bearing silicic magmas: American Mineralogist, v. 69, p. 69-78.

Whitney, J. A., and Stormer, J. C., Jr., 1983, Igneous sulfides in the Fish Canyon Tuff and the role of sulfur in calc-alkaline magmas: Geology, v. 11, p. 99-102.

Figure Captions

Figure 1 Pyrite in volcanic rocks of Yucca Mountain. A. XXX. B. XXX. C. XXX. D. XXXX. p = pyrite.

Figure 2 Disseminated pyrite in propylitically altered silicic lava from a depth of 5232.9 ft. in drill hole USW G-2. A. Large inclusion-bearing, pitted, subhedral pyrite grain. B. Small, subhedral pyrite grains and larger, embayed, anhedral grain. p = pyrite.

Figure 3 Disseminated pyrite in altered, porous ash-flow tuff near precious-metal deposits. Groundmass (A) and lithic fragment (B) of hydrothermally altered Tonopah Summit Member of the Fraction Tuff (Bonham and Garside, 1979) from dump of the Belcher-Divide mine, Divide mining district, Nevada. C. Altered porous Rainier Mesa Member of the Timber Mountain Tuff, within 30 m of ore, 916 bench, Phase IV, Lac Gold Bullfrog mine, Nevada. D. Porous type II ore, Round Mountain mine, Nevada. Note anhedral to subhedral, granular to embayed morphologies. p = pyrite.

Figure 4 Distribution of drill holes in Yucca Mountain showing spacing relative to the areal extent of selected volcanic-hosted Au-Ag deposits in Nevada. CFT = Crater Flat Tuff, PT = Paintbrush Tuff.

Figure 5 Pyrite in the Bullfrog Member of the Crater Flat Tuff in drill hole USW G-2. A. Pyrite disseminated in groundmass and in clay-altered pumice fragment at XXX ft. B. Pyrite along margin and within silica veinlet at 3459.4 ft. p = pyrite.

Figure 6 Filmy pyrite on quartz in drusy vein cutting the Bullfrog Member of the Crater Flat Tuff, drill hole USW G-2, 3260.8 ft.

Figure 7 Pyrite within clay ± zeolite altered pumice fragments. A. Tram Member of the Crater Flat Tuff, drill hole UE25 B1H, 3825.5 ft. B. Bullfrog Member of the Crater Flat Tuff, drill hole USW G-2, XXX ft. p = pyrite.

Fig. 4

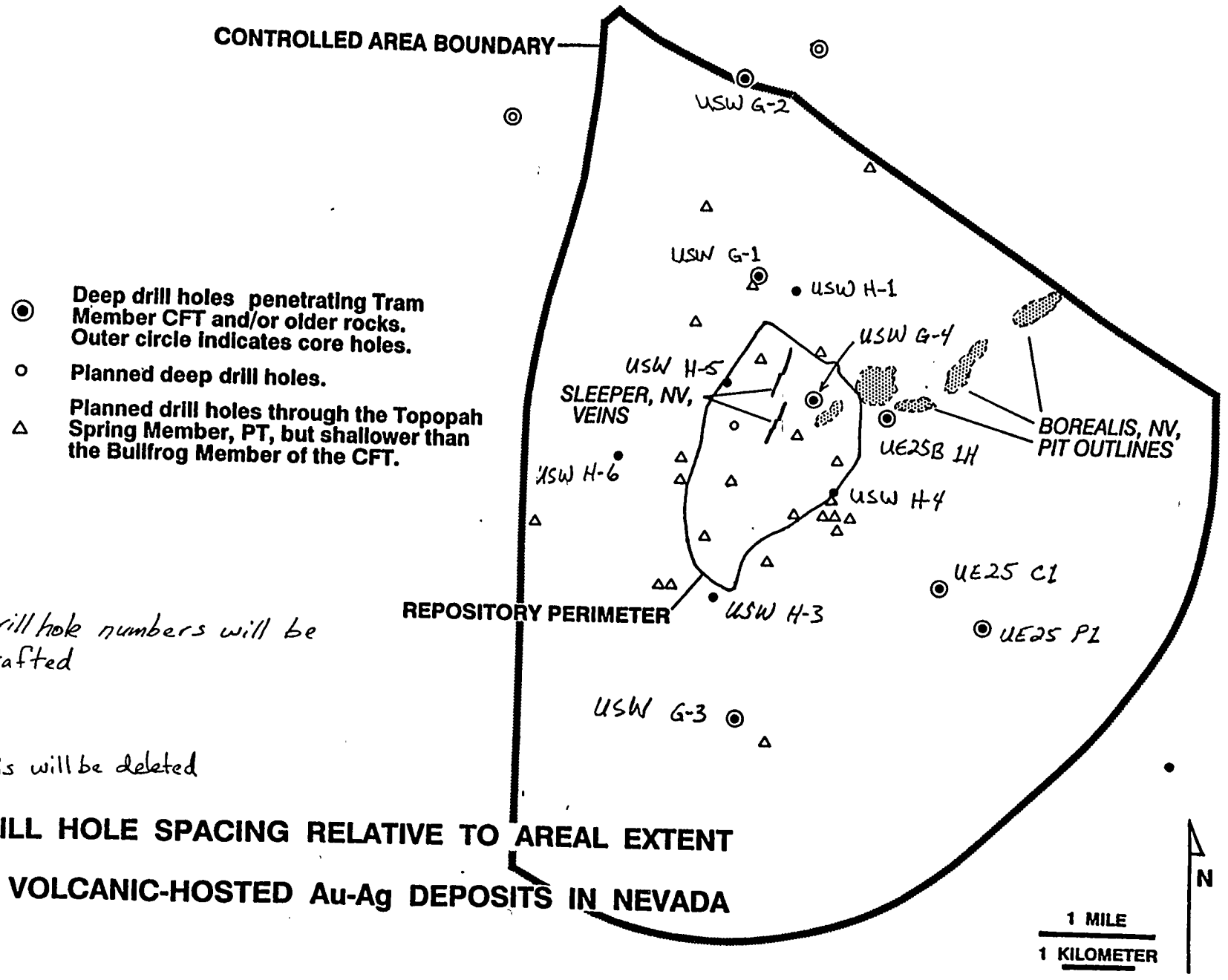

Drill hole numbers will be drafted

This will be deleted

↓

DRILL HOLE SPACING RELATIVE TO AREAL EXTENT OF VOLCANIC-HOSTED Au-Ag DEPOSITS IN NEVADA

APPENDIX C

Compilation of Radiometric Age and Trace-element Geochemical Data, Yucca Mountain and Surrounding Areas of Southwestern Nevada

Prepared by Task 3 of the Yucca Mountain Project,
Center for Neotectonic Studies, Mackay School of Mines,
University of Nevada, Reno

Steven I. Weiss - Research Associate
Donald C. Noble and Lawrence T. Larson
Co-Principal Investigators

September 31, 1994

Compilation of Radiometric Age and Trace-element Geochemical Data, Yucca Mountain and Surrounding Areas of Southwestern Nevada

This document is a compilation of available radiometric age and trace-element geochemical data for volcanic rocks and episodes of hydrothermal activity in Yucca Mountain and the surrounding region of southwestern Nevada. Only the age determinations considered to be geologically reasonable (consistent with stratigraphic relations) are listed below. A number of the potassium-argon (K-Ar) ages of volcanic rocks given by Kistler (1968), Marvin et al. (1970), Noble et al. (1984; 1988), Weiss et al. (1989a), and Noble et al. (1991) are not included as these ages have been shown to be incorrect or disturbed by hydrothermal alteration based on subsequent stratigraphic and/or petrographic data and the recognition of errors in K-Ar age determinations related to incomplete extraction of argon (e.g., Hausback et al., 1990). In cases where absolute ages are tightly constrained by high-precision $^{40}Ar/^{39}Ar$ ages and unequivocal stratigraphic relations (e.g. Hausback et al., 1990; Fleck et al., 1991; Sawyer et al., 1990; 1994), we have omitted the less precise K-Ar age data. Similarly, the more precise single-crystal laser-fusion $^{40}Ar/^{39}Ar$ age determinations of certain units are reported and less precise ages by multi-grain bulk-fusion $^{40}Ar/^{39}Ar$ methods are not included. This compilation does not include age data for basaltic rocks of Pliocene and Quaternary age in the Yucca Mountain region.

Part I

Radiometric Ages of Volcanic Rocks and Hydrothermal Minerals

Rock Unit	Age (Ma)	(± 1σ)	Type/mineral	Comments and References
Thirsty Canyon Tuff				
Gold Flat Member	9.15	0.03	Ar/Ar, sanidine	Fleck et al. (1991).
Rocket Wash Member	9.4	0.04	Ar/Ar, sanidine	Sawyer et al. (1990, 1994).
Rhyolite of Pillar Spring	8.9	0.3	K-Ar, whole-rock	Marvin et al. (1989).
	8.6	0.6	FT, zircon	Marvin et al. (1989).
Comendite of Ribbon Cliff	9.4	0.09	Ar/Ar, sanidine	Fleck et al. (1991).
Rhyolite dome, Grapevine Mts.	9.6	0.3	K-Ar, biotite	Weiss et al. (1990).
Microgranite dikes of Timber Mountain	9.9	0.8	K-Ar, alkali feldspar	Marvin and Dobson (1979).
Tracking Station rhyolite	10.4	0.4	K-Ar, biotite	Marvin et al. (1989).
	9.6	0.3	K-Ar, sanidine	Marvin et al. (1989).
Rhyolite of Shoshone Mtn.	10.3	0.4	K-Ar, obsidian	Near base of upper lava; Noble et al. (1991).
	9.3	0.3	K-Ar, nr	Base of lower lava; Marvin et al. (1989).
	8.8	nr	FT, zircon	Plug in Calico Hills; Simonds (1989).
Latite lava, Bullfrog Hills	10.0	0.4	K-Ar, biotite	East of Black Peak; Marvin et al. (1989).
	10.7	0.3	K-Ar, biotite	East of Black Peak; Morton et al. (1977).
Basalt, top of Kiwi Mesa	9.9	0.4	K-Ar, whole-rock	Marvin et al. (1989).
	10.0	0.4	K-Ar, whole-rock	Marvin et al. (1989).
Basaltic dike, Yucca Mtn.	10.0	0.4	K-Ar, whole-rock	Marvin et al. (1989).
Basalt, E of Beatty Mtn.	10.7	0.2	K-Ar, whole-rock	Monsen et al. (1992).
Basalt, Jackass Flats	11.1	0.5	K-Ar, whole-rock	Marvin et al. (1989).
	9.6	0.4	K-Ar, whole-rock	Marvin et al. (1989).

Ar/Ar = $^{40}Ar/^{39}Ar$ FT = fission track nr = not reported

Rock Unit	Age (Ma)	(± 1σ)	Type/mineral	Comments and References
Rhyolitic tuff, Burton Mtn.	10.1	0.3	K-Ar, biotite	Noble et al. (1991).
Rhyolite lava, Burton Mtn.	11.1	0.1	K-Ar, sanidine	Marvin and Cole (1978).
Rhyolite lavas in moat of the Timber Mtn. caldera	10.6	nr	nr	Warren et al. (1988).
	10.7	nr	nr	Warren et al. (1988).
Basalt, Little Skull Mtn.	11.2	0.5	K-Ar, whole-rock	Marvin et al. (1989).
	11.4	0.5	K-Ar, whole-rock	Marvin et al. (1989).
Tuff of Cutoff Road	11.4	0.10	Ar/Ar, sanidine	Noble et al. (1991).
Timber Mountain Tuff				
Ammonia Tanks Member	11.45	0.03	Ar/Ar, sanidine	Sawyer et al. (1994).
	11.44	0.03	Ar/Ar, sanidine	Fleck et al. (1991).
Rainier Mesa Member	11.6	0.03	Ar/Ar, sanidine	Sawyer et al. (1994).
Rhyolite of Pinnacles Ridge	11.5	nr	nr	Warren et al. (1988).
	11.7	0.03	Ar/Ar, sanidine	Fleck et al. (1991).
Rhyolite of Waterpipe Butte	12.5	0.01	Ar/Ar, sanidine	Fleck et al. (1991).
Rhyolite of the Loop	12.5	0.03	Ar/Ar, sanidine	Fleck et al. (1991), Sawyer et al. (1994).
Rhyolite of Delirium Canyon	12.6	nr	nr	Warren et al. (1988).
Rhyolite of Comb Peak	12.7	0.05	Ar/Ar, sanidine	Fleck et al. (1991).
Rhyolite of Vent Pass	12.7	0.02	Ar/Ar, sanidine	Fleck et al. (1991).
Paintbrush Tuff				
Tiva Canyon Member	12.7	0.03	Ar/Ar, sanidine	Sawyer et al. (1994).
Topopah Spring Member	12.8	0.03	Ar/Ar, sanidine	Sawyer et al. (1994).
Calico Hills Formation (rhyolite lava N of Timber Mtn.)	12.9	0.02	Ar/Ar, sanidine	Sawyer et al. (1994).

Ar/Ar = $^{40}Ar/^{39}Ar$ FT = fission track nr = not reported

Rock Unit	Age (Ma)	(± 1σ)	Type/mineral	Comments and References
Wahmonie Formation	13.0	0.1	Ar/Ar, biotite	Sawyer et al. (1994).
upper part??	12.8		K-Ar, biotite	Recalculated from Kistler (1968).
lower part??	13.2		K-Ar, biotite	Recalculated from Kistler (1968).
Crater Flat Tuff				
Bullfrog Member	13.25	0.04	Ar/Ar, sanidine	Sawyer et al. (1994).
Dead Horse Flat Formation	13.5	0.02	Ar/Ar, sanidine	Sawyer et al. (1994).
Belted Range Tuff				
Grouse Canyon Member	13.7	0.02	Ar/Ar, sanidine	Sawyer et al. (1994).
Comendite of Split Ridge	13.85	0.02	Ar/Ar, sanidine	Sawyer et al. (1994).
Tuff of Tolicha Peak	13.9	0.4	K-Ar, whole-rock	Weiss et al. (1991a, 1993b).
Lithic Ridge Tuff	13.85	nr	Ar/Ar, sanidine	Sawyer et al. (1990).
	14.0	0.07	Ar/Ar, sanidine	Sawyer et al. (1994).
Silicic porphyry dikes of				
Bare Mountain	13.9	0.5	K-Ar, biotite	Tarantula Canyon; Marvin et al. (1989).
	13.9	0.1	K-Ar, biotite	Joshua Hollow; Monsen et al. (1992).
	13.8	0.2	K-Ar, biotite	Tarantula Canyon; Monsen et al. (1992).
	14.9	0.5	K-Ar, biotite	Tate's Wash exposure; Noble et al. (1991).
Belted Range Tuff				
Tub Spring Member	14.9	0.04	Ar/Ar, sanidine	Sawyer et al. (1990, 1994).
Tuff of Yucca Flat	15.1	0.06	Ar/Ar, sanidine	Sawyer et al. (1990, 1994).
Red Rock Valley Tuff	15.2	0.06	Ar/Ar, sanidine	Sawyer et al. (1990, 1994).

Ar/Ar = $^{40}Ar/^{39}Ar$ FT = fission track nr = not reported

Rock Unit	Age (Ma)	(± 1σ)	Type/mineral	Comments and References
Tuff of Oriental Wash	14.2	0.6	K-Ar, hornblende	Weiss et al. (1991a).
Tuff of Gold Coin mine	15.3	0.5	K-Ar, biotite	Worthington (1992).
Tuff of Mount Dunfee	16.7	0.4	K-Ar, biotite	Worthington (1992), Weiss et al. (1993b).
	16.8	0.5	K-Ar, biotite	Worthington (1992), Weiss et al. (1993b).
Metadiorite, Bullfrog Hills	14.6	0.9	K-Ar, hornblende	Marvin et al. (1989), Monsen et al. (1992).
Gneiss, Bullfrog Hills	16.3	0.4	K-Ar, muscovite	Marvin et al. (1989), Monsen et al. (1992).
Diorite dike, Bare Mtn.	26.1	1.7	K-Ar, hornblende	Monsen et al. (1992).
	16.6	1.2	K-Ar, biotite	Monsen et al. (1992).

Ar/Ar = $^{40}Ar/^{39}Ar$ FT = fission track nr = not reported

Radiometric Ages of Hydrothermal Activity, Southwestern Nevada

Rock Unit	Age (Ma)	(± 1σ)	Type/mineral	Comments and References
Bullfrog Hills - Oasis Valley area				
Original Bullfrog mine	8.7	0.3	K-Ar, adularia	Jackson (1988), McKee and Bergquist (1993), Weiss et al. (1995).
Original Bullfrog mine	9.2	0.3	Ar/Ar, adularia	Weiss et al. (1991b, 1995), McKee and Bergquist (1993).
Montgomery-Shoshone mine	9.5	0.2	K-Ar, adularia	Morton et al. (1977).
Lac Gold Bullfrog mine	9.8	0.3	Ar/Ar, adularia	Weiss et al. (1991b, 1995), McKee and Bergquist (1993).
Mayflower mine	9.9	0.3	Ar/Ar, adularia	Weiss et al. (1991b, 1995), McKee and Bergquist (1993).
Mayflower mine	10.0	0.3	K-Ar, adularia	Jackson (1988), McKee and Bergquist (1993), Weiss et al. (1995).
Bailey's (Hicks) Hot Spring	10.2	0.3	K-Ar, alunite	McKee and Bergquist (1993), Weiss et al. (1995).
Oasis Mountain	10.6	0.3	K-Ar, adularia	Jackson (1988), McKee and Bergquist (1993), Weiss et al. (1995).
North of Pioneer mine	11.0	0.4	K-Ar, adularia	Jackson (1988), McKee and Bergquist (1993), Weiss et al. (1991b, 1995).
Yellowjacket mine	11.3	0.3	Ar/Ar, adularia	Weiss et al. (1991b, 1995), McKee and Bergquist (1993).
Transvaal Hills - Tram Ridge - northern Crater Flat				
Transvaal Hills	9.9	0.4	K-Ar, alunite	Jackson (1988), McKee and Bergquist (1993), Weiss et al. (1995).
Silicon mine, Tram Ridge	11.6	0.4	K-Ar, alunite	Jackson (1988), McKee and Bergquist (1993), Weiss et al. (1995).
Thompson mine, N Crater Flat	12.9	0.5	K-Ar, alunite	Jackson (1988), McKee and Bergquist (1993), Weiss et al. (1995).

Ar/Ar = $^{40}Ar/^{39}Ar$ I/S = illite/smectite nr = not reported

Rock Unit	Age (Ma)	(± 1σ)	Type/mineral	Comments and References
Bare Mountain District				
Telluride mine area	11.2	0.3	K-Ar, alunite	Jackson (1988), McKee and Bergquist (1993), Weiss et al. (1995).
Telluride mine area	12.2	0.4	K-Ar, alunite	Jackson (1988), McKee and Bergquist (1993), Weiss et al. (1995).
Mother Lode mine	12.2	0.4	K-Ar, I/S	G. Woldegabriel and S.I. Weiss, unpub. data, 1993; Weiss et al. (1993a).
Mother Lode mine	13.1	0.3	K-Ar, I/S	G. Woldegabriel and S.I. Weiss, unpub. data, 1993; Weiss et al. (1993a).
Mother Lode mine	26.9	0.6	K-Ar, I/S	G. Woldegabriel and S.I. Weiss, unpub. data, 1993; Weiss et al. (1993a).
Goldspar/Diamond Queen mine	12.9	0.4	K-Ar, adularia	Noble et al. (1989, 1991).
Goldspar/Diamond Queen mine	12.9	0.8	K-Ar, adularia	Noble et al. (1989, 1991).
Other Areas				
Northern Stonewall Mountain	6.7	0.2	K-Ar, adularia	North face of Stonewall Mtn.; Weiss et al. (1989b).
Calico Hills, west	10.4	0.3	K-Ar, alunite	Jackson (1988), McKee and Bergquist (1993), Weiss et al. (1995).
Calico Hills, east	10.4	0.3	K-Ar, alunite	Jackson (1988), McKee and Bergquist (1993), Weiss et al. (1995).
Mine Mountain, south flank	11.1	0.3	K-Ar, alunite	McKee and Bergquist (1993), Weiss et al. (1995).
Wahmonie	12.6	0.4	K-Ar, adularia	Jackson (1988), McKee and Bergquist (1993), Weiss et al. (1995).
Wahmonie	12.9	0.4	K-Ar, adularia	

Ar/Ar = $^{40}Ar/^{39}Ar$ I/S = illite/smectite nr = not reported

Subsurface of Yucca Mountain

Drill Hole #, Unit	Depth (m)	Age(Ma)(± 1σ)		Type/mineral	Comments and References
USW G1, Older Tuffs	1511.2	9.9	0.5	K-Ar, I/S	I/S: R = 1; Bish and Aronson (1993).
USW G1, Older Tuffs	1511.2	10.1	0.5	K-Ar, I/S	duplicate of above; Bish and Aronson (1993).
USW G1, Older Tuffs	1718.2	10.9	0.6	K-Ar, I/S	I/S: R ≥ 3; Bish and Aronson (1993).
USW G2, Tram Member	1133.9	8.7	0.4	K-Ar, I/S	I/S: R = 1; Bish and Aronson (1993).
USW G2, Tram Member	1133.9	9.7	0.6	K-Ar, I/S	duplicate of above; Bish and Aronson (1993).
USW G2, Tram Member	1133.9	9.9	0.6	K-Ar, I/S	duplicate of above; Bish and Aronson (1993).
USW G2, Tram Member	1181.1	11.0	0.6	K-Ar, I/S	I/S: R ≥ 3; Bish and Aronson (1993).
USW G2, Tram Member	1198.8	11.7	0.7	K-Ar, I/S	I/S: R ≥ 3; Bish and Aronson (1993).
USW G2, Tram Member	1198.8	11.3	0.5	K-Ar, I/S	duplicate of above; Bish and Aronson (1993).
USW G2, pre-Tram Member lava	1246.6	10.9	0.5	K-Ar, I/S	I/S: R = 0; Bish and Aronson (1993).
USW G2, pre-Lithic Ridge lava	1508.5	10.0	0.5	K-Ar, I/S	I/S: R = 0; Bish and Aronson (1993).
USW G2, pre-Lithic Ridge lava	1576.1	11.0	0.6	K-Ar, illite	Bish and Aronson (1993).

Ar/Ar = $^{40}Ar/^{39}Ar$ I/S = I/S nr = not reported

References Cited in Part I

Bish, D. L., and Aronson, J. L., 1993, Paleogeothermal and paleohydrologic conditions in silicic tuff from Yucca Mountain, Nevada: Clays and Clay Minerals, v. 41, p. 148-161.

Fleck, R. J., Lanphere, M. A., Turrin, B., and Sawyer, D. A., 1991, Chronology of late Miocene to Quaternary volcanism and tectonism in the southwest Nevada volcanic field [abs.]: Geol. Soc. America Abstracts with Programs, v. 23, p. 25.

Hausback, B.P., Deino, A.L., Turrin, B.T., McKee, E.H., Frizzell, V.A., Noble, D.C., and Weiss, S.I., 1990, New $^{40}Ar/^{39}Ar$ ages for the Spearhead and Civet Cat Canyon Members of the Stonewall Flat Tuff, Nye County, Nevada: Evidence for systematic errors in standard K-Ar age determinations on sanidine: Isochron/West, No. 56, p. 3-7.

Jackson, M. J., 1988, The Timber Mountain magmato-thermal event: an intense widespread culmination of magmatic and hydrothermal activity at the southwestern Nevada volcanic field: University of Nevada, Reno - Mackay School of Mines, Reno, Nevada, unpublished MSc Thesis.

Kistler, R.W., 1968, Potassium-argon ages of volcanic rocks on Nye and Esmeralda Counties, Nevada: Geological Society of America Memoir 110, P. 251-263.

Marvin, R. F., and Cole, J. C., 1978, Radiometric ages: Compilation A, U.S. Geological Survey: Isochron/West, no. 22, p. 3-14.

Marvin, R. F., and Dobson, S. W., 1979, Radiometric ages: Compilation B, U. S. Geological Survey: Isochron/West, no. 26, p. 3-32.

Marvin, R. F., Mehnert, H. H., and Naeser, C. W., 1989, U.S. Geologic Survey radiometric ages - compilation "C", part 3: California and Nevada: Isochron/West, no. 52, p. 3-11.

Marvin, R.F., Byers, F.M., Mehnert, H.H., Orkild, P.P, and Stern, T.W., 1970, Radiometric ages and stratigraphic sequence of volcanic and plutonic rocks, southern Nye and western Lincoln Counties, Nevada: Geological Society of America Bulletin, v. 81, p. 2657-2676.

McKee, E. H., and Bergquist, J. M., 1993, New radiometric ages related to alteration and mineraliztion in the vicinity of Yucca Mountain, Nye County, Nevada: U. S. Geological Survey Open-file Report 93-538, 26 pp.

McKee, E. H., Noble, D. C., and Weiss, S. I., 1989, Very young silicic volcanism in the southwestern Great Basin: The late Pliocene Mount Jackson dome field, SE Esmeralda County, Nevada: EOS, Trans. Am. Geophys. Union., v. 70, p. 1420.

Minor, S.A., Sawyer, D.A., Wahl, R.R., Frizzell, V.A., Jr., Schilling, S.P., Warren, R.G., Orkild, P.P., Coe, J.A., Hudson, M.R., Fleck, R.J., Lanphere, M.A., Swadley, W.C., and Cole, J.C., 1993, Preliminary geologic map of the Pahute Mesa 30' x 60' quadrangle, Nevada: U.S. Geol. Survey Open-file Rept. 93-299, 1:100,000.

Monsen, S.A., Carr, M.D., Reheis, M.C., and Orkild, P.P., 1992, Geologic map of Bare Mountain, Nye County Nevada: U.S. Geological Survey Miscellaneous Investigations Map I-2201, 1:24,000.

Morton, J. L., Silberman, M. L., Bonham, H. F., Garside, L. J., and Noble, D. C., 1977, K-Ar ages of volcanic rocks, plutonic rocks, and ore deposits in Nevada and eastern California - Determinations run under the USGS-NBMG cooperative program: Isochron/West, n. 20, p. 19-29.

Noble, D. C., McKee, E. H., and Weiss, S. I., 1988, Nature and timing of pyroclastic and hydrothermal activity and mineralization at the Stonewall Mountain volcanic center, southwestern Nevada: Isochron/West, No. 51, p. 25-28.

Noble, D. C., Weiss, S. I., and Green, S. M., 1989, High-salinity fluid inclusions suggest that Miocene gold deposits of the Bare Mtn. district, NV, are related to a large buried rare-metal rich magmatic system: Geological Society of America Abs. with Programs, v. 21, p. 123.

Noble, D. C., Weiss, S. I., and McKee, E. H., 1991, Magmatic and hydrothermal activity, caldera geology, and regional extension in the western part of the southwestern Nevada volcanic field: *in* Raines, G. L., Lisle,R. E., Shafer, R. W., and Wilkinson, W. W., eds., Geology and ore deposits of the Great Basin: Symposium Proceedings, Geol. Soc. of Nevada, p. 913-934.

Noble, D.C., Vogel, T. A., Weiss, S.I., Erwin, J.W., McKee, E.H., and Younker, L.W., 1984, Stratigraphic relations and source areas of ash-flow sheets of the Black Mountain and Stonewall Mountain volcanic centers, Nevada: Journal of Geophysical Research, v. 89, p. 8593-8602.

Sawyer, D. A., Fleck, R. J., Lanphere, M. A., Warren, R. G., and Broxton, D. E., 1990, Episodic volcanism in the southwest Nevada volcanic field: new $^{40}Ar/^{39}Ar$ geochronologic results: EOS, Transactions of the American Geophysical Union, v. 71, p. 1296.

Sawyer, D. A., Fleck, R. J., Lanphere, M. A., Warren, R. G., Broxton, D. E., and Hudson, M. R., 1994, Episodic caldera volcanism in the Miocene southwestern Nevada volcanic field: revised stratigraphic framework, $^{40}Ar/^{39}Ar$ geochronology, and implications for magmatism and extension: Geological Society of America Bulletin, *in press*.

Simonds, F.W., 1989, Geology and hydrothermal alteration in the Calico Hills, southern Nevada: Unpub. M.S. thesis, Univ. Colorado, Boulder, 136 p.

Warren, R.G., McDowell, F.W., Byers, F.M., Broxton, D.E., Carr, W.J., and Orkild, P.P., 1988, Eposodic leaks from Timber Mountain caldera: new evidence from rhyolite lavas of Fortymile Canyon, southwestern Nevada Volcanic Field: Geological Society of America, Abstracts with Programs, v. 20, p. 241.

Weiss, S. I., Noble, D. C., and McKee, E. H., 1989a, Paleomagnetic and cooling constraints on the duration of the Pahute Mesa-Trail Ridge eruptive event and associated magmatic evolution, Black Mountain volcanic center, southwestern Nevada: Journal of Geophysical Research, v. 94, p. 6075-6084.

Weiss, S. I., Noble, D. C., and Larson, L. T., 1989b, Task 3: Evaluation of mineral resource potential, caldera geology and volcano-tectonic framework at and near Yucca Mountain; report for July, 1988 - September, 1989: Center for Neotectonic Studies, University of Nevad-Reno, 38 p. plus appendices.

Weiss, S. I., Noble, D. C., and Larson, L. T., 1990, Task 3: Evaluation of mineral resource potential, caldera geology cano-tectonic framework at and near Yucca Mountain; report for October, 1989 - September, 1990: Center for Neotectonic Studies, University of Nevad-Reno, 33 p. plus appendices.

Weiss, S

Weiss, S. I., Noble, D. C., and Larson, L. T., 1991a, Task 3: Evaluation of mineral resource potential, caldera geology and volcano-tectonic framework at and near Yucca Mountain; report for October, 1990 - September, 1991: Center for Neotectonic Studies, University of Nevad-Reno, 37 p. plus appendices.

Weiss, S. I., McKee, E. H., Noble, D. C., Connors, K. A., and Jackson, M. R., 1991b, Multiple episodes of Au-Ag mineralization in the Bullfrog Hills, SW Nevada, and their relation to coeval extension and volcanism: Geological Society of America Abstracts with Programs, v. 23, p. A246.

Weiss, S. I., Noble, D. C., and Larson, L. T., 1993a, Task 3: Evaluation of mineral resource potential, caldera geology and volcano-tectonic framework at and near Yucca Mountain; report for October, 1992 - September, 1993: Center for Neotectonic Studies, University of Nevad-Reno, 41 p. plus appendices.

Weiss, S. I., Noble, D. C., Worthington, J. E., IV., and McKee, E. H., 1993b, Neogene tectonism from the southwestern Nevada volcanic field to the White Mountains, California Part I. Miocene volcanic stratigraphy, paleotopography, extensional faulting and uplift between northern Death Valley and Pahute Mesa: *in* Lahren, M. M., Trexler, J. H., Jr., and Spinosa, C., eds., 1993, Crustal Evolution of the Great Basin and Sierra Nevada: Cordilleran/Rocky Mountain Section, Geological Society of America Guidebook, Department of Geological Sciences, University of Nevada, Reno, p. 353-369.

Weiss, S. I., Noble, D. C., Connors, K. A., Jackson, M. R., and McKee, E. H., (1995), Multiple episodes of hydrothermal activity and precious-metal mineralization in the southwestern Nevada volcanic field and their relations to magmatic activity, volcanism and regional extension: *in U.S.G.S. review for submission to Economic Geology.*

Worthington, J. E., IV., 1992, Neogene structural and volcanic geology of the Gold Mountain - Slate Ridge area, Esmeralda County, Nevada, unpublished MS thesis, Univ. Nevada, Reno, 76 p.

Part II

Major and Trace-element Geochemical Data

Precious Metals and Indicator-Element Concentrations in Rocks from Northwestern Yucca Mountain and Bare Mountain, Nevada
(Ag and Au values given in ppb, all others in ppm)

Sample Id	comments	Ag	Au	As	Bi	Cd	Hg	Sb	Se	Te	Cu	Mo	Pb	Zn	Ga	Tl
	Northwestern Yucca Mtn.															
3SW-394A	brep675; opal-qtz vn w/Feox	13.7	0.459	12.7	0.154	0.183	0.677	2.72	-0.246	-0.049	5.58	3.4	8.74	10.6	0.849	1.03
3SW-394B	brep681B; Hbx vn of feox+silica	9.03	-0.198	139	0.293	0.562	0.18	8.9	-0.248	-0.05	9.05	1.8	44.8	29.6	2.69	-0.495
3SW-394C	brep681C; Hbx vn of feox+silica	8.22	-0.196	36.2	0.187	0.246	0.099	3.39	-0.245	-0.049	4.02	1.69	23.6	17.6	1.88	1.93
3SW-394D	brep685; silicif siltst, upper ledge	8.5	-0.2	6.59	0.07	0.625	0.233	1.27	-0.25	-0.05	5.16	3.33	4.54	14.3	0.343	4.95
3SW-394E	brep693; "sinter" lower ledge	12.8	-0.198	2.35	0.184	0.132	0.1	0.753	-0.248	-0.05	8.36	4.99	7.8	6.79	0.35	-0.495
3SW-394F	brep697; silicif siltst, upper ledge	7.04	-0.195	5.7	0.256	0.173	0.217	2.05	-0.244	0.057	6.36	8.11	51.9	104	0.329	0.637
X94A	bdup394F(697)	8.18	-0.199	5.5	0.261	0.172	0.229	1.89	-0.248	-0.05	6.09	7.92	50.7	102	0.104	0.667
NEEBM16	Tct w/qtz-opal vnlts	22.6	-0.196	40	0.096	0.135	0.041	3.89	-0.245	-0.049	14	2.27	16.1	35	1.63	0.829
3SW-717	Tct w/qtz-opal vnlts; bleached	18.5	-2.34	8.01	-0.049	0.063	-0.02	0.584	-0.247	-0.049	8.16	1.21	14	17.8	0.818	-0.494
3SW-719	Silica-Feox Hbx vns in Tct	19.7	-0.198	89	0.068	0.215	0.299	6.4	-0.247	-0.049	11.8	1.64	15	42	1.88	-0.495
3SW-721P	silicif silst +opal, upper ledge	8.06	-0.195	4.51	0.091	0.407	0.153	1.12	-0.243	-0.049	1.91	0.959	3.33	13.7	-0.097	1.67
X94C	bdup721S; silicif sltst, upper ledge	13.1	-0.199	5.64	0.13	0.428	0.15	1.32	-0.249	-0.05	12.5	4.45	4.36	22	0.353	1.83
3SW-723P	silicif silst +opal, upper ledge	10.2	0.291	7.63	0.144	0.192	0.091	0.4	-0.242	-0.048	1.73	0.614	22.5	88.5	0.196	1.05
X94D	bdup723S; silicif sltst, upper ledge	13.4	0.26	6.92	0.195	0.199	0.108	0.564	-0.244	-0.049	10.6	2.86	42.8	104	0.277	1.2
X94E	bdup723S; silicif sltst, upper ledge	14.1	0.23	6.79	0.2	0.192	0.107	0.586	-0.246	-0.049	10.5	2.78	41.5	105	0.289	1.18
3SW-725	alt. Tct	20.2	10.5	33.3	0.063	0.076	0.481	2.28	-0.25	-0.05	10.8	1.54	12	27.8	0.841	-0.5
3SW-121	Feox+silica hbx vns in Tc; Windy Wash	22.9	-0.2	5.53	0.088	0.075	0.065	2.14	-0.25	-0.05	8.61	1.25	9.11	22.9	0.793	-0.5
3MJ-184A	arg alt Tcp, head of Windy Wash	-2.93	-0.195	18	0.05	0.133	0.234	2.41	-0.244	-0.049	10.9	1.54	8.79	26	1.21	-0.488
3MJ-188	Feox-rich porous tuff	-2.91	-0.194	1.89	0.176	0.059	0.1	1.23	-0.243	-0.049	9.44	1.25	13.9	17.4	0.705	-0.485
	Bare Mountain															
3SW-633	arg alt Tip dike, Tungsten Canyon	11.1	1.06	2.34	-0.05	0.06	0.081	0.639	-0.248	-0.05	7.47	0.833	7.71	45.4	2.18	-0.495
3SW-641	alt Tip dike, Tarantula Canyon	11.8	0.265	2.41	-0.05	-0.02	0.037	0.08	-0.248	-0.05	8.54	1.09	3.48	11.1	0.531	-0.497
3SW-705	Dev ls wallrock <1 m from 641 dike	47.1	1.34	18.1	0.114	0.195	0.251	1.15	0.371	0.056	8.74	14.8	5.22	117	0.193	-0.49
3SW-645	alt Tip dike, Tarantula Canyon	41	-0.197	192	0.245	4.16	0.124	8.99	3.57	-0.049	15.2	14.8	14.6	84.6	1.17	-0.491
3SW-649	alt Tip dike N of Tarantula Canyon	11.1	0.398	55.3	0.074	-0.02	-0.02	0.17	-0.249	-0.05	8.04	2.15	4.18	7.55	0.941	-0.497
3SW-655A	hbx, margin of dike	24118	1603	163	0.153	0.044	5.22	22.4	-0.245	3.56	29.3	11.1	11.5	15.7	0.635	-0.49

3SW-655b	hbx, margin of dike	10488	1381	166	0.096	0.084	[illegible]4	20.7	-0.247	2.09	29.1	9.62	16	34	0.241	0.537
872111	fluoritized brecciated Nopah, N pit	-2.96	1158	65.8	0.854	0.028	1.5	53.4	-0.247	0.097	4.76	118	5.65	16.6	3.12	1.55
SJH-2	Hbx dike, volc frags, in Pz carbs	164	1.87	4.59	0.134	0.193	0.322	2.76	-0.246	0.336	13.7	5.33	19.7	7.73	0.252	-0.491
SJH-3	Hbx dike, volc frags, in Pz carbs	49.3	0.96	1.24	-0.05	0.041	0.064	0.267	-0.248	-0.05	10.7	3.35	15.3	5.84	0.414	-0.497
TIPWW	alt Tjp, W wall ML pit, fresh bio	17.8	-0.199	4.02	-0.05	0.034	-0.02	-0.05	-0.249	-0.05	9.16	0.553	12.7	60.6	2.59	-0.497
3SW-659	alt Tjp, Joshua Hollow	21.9	-0.199	0.684	-0.05	0.068	-0.02	-0.05	-0.249	-0.05	5.96	0.843	12.6	52.8	4.29	-0.497
3SW-707	Sr ls wallrock <0.5 m W from dike	7.47	2.44	37.2	0.062	0.182	-0.02	1.13	-0.247	-0.049	9.87	1.3	4.53	24.7	0.1	0.543
3SW-709	Sr dolo ~350' W of 707	11.8	-0.197	17.4	-0.049	0.405	0.026	1.27	-0.246	-0.049	4.57	1.66	3.2	32.6	-0.098	-0.492
3SW-711A	brecc'd Sr dolo 0.5m W of dike	12.3	1.01	20	-0.049	0.359	-0.019	0.723	-0.244	-0.049	7.23	0.352	3.54	37.4	0.156	-0.487
3SW-711B	silicified Sr ~150' from 711A	36.4	0.365	25	0.073	0.073	0.037	1.38	-0.249	-0.05	10.3	2.45	2.96	22.4	-0.1	-0.498
3SW-713	cherty dolo w/fluor? near dike	246	0.627	84	0.208	1.4	0.569	11.3	2.56	0.081	40.9	23.8	4.84	117	0.276	-0.495
3MJ-160A	Gold Ace, Au-bearing Wood Canyon Fm	33010	110151	8.34	0.324	0.039	0.343	7.27	-0.249	0.069	14.5	9.75	12.3	25.8	-0.1	0.499
	"Blank" of fresh Tiva Canyon Mbr															
3SW-589p	new split prep'd in steel pulverizer	83.8	-0.194	1.99	-0.049	0.031	-0.019	-0.049	-0.243	-0.049	1.65	0.445	33.4	44.6	0.534	-0.485
X94B	new split prep'd in shatterbox	20.9	-0.195	1.93	-0.049	0.038	-0.02	-0.049	-0.244	-0.049	7.86	1.02	7.36	51.2	0.569	-0.488

brep= blind repeat analysis
bdup= blind duplicate analysis
hbx= hydrothermal breccia
vn= vein
Pz= Paleozoic
Sr= Roberts Mountain Formation
"p" following sample number denotes preparation in rotary pulverisor with steel plates; "s" denotes preparation in shatterbox with carbon-steel rings.
Tct= Tram Member of the Crater Flat Tuff
Tcp= Prow Pass Member of the Crater Flat Tuff
Tip and Tjp = porphyry dikes of Bare Mountain

qtz= quartz
siltst= siltstone
vnlts= veinlets
alt= altered
ls= limestone

Analyses by U. S. Mineral Laboratories, Inc., North Highlands, CA, using 15 gram digestions, organic liquid separation and inductively- coupled plasma-emission spectrography, except for Au which was determined by graphite-furnace atomic-absorption spectrometry. Values as reported by
U. S. Mineral Laboratories. Number of significant figures does not indicate precision or accuracy of analyses.
"-" = less than.
Detection limits as quoted by U. S. Mineral Laboratories at 3 sigma confidence level:

Ag=	3 ppb	Bi=	0.050 ppm
Au=	0.2 ppb	Sb=	0.050 ppm
Tl=	0.5 ppm	Te=	0.050 ppm
As=	0.25 ppm	Pb=	0.050 ppm
Se=	0.25 ppm	Cd=	0.020 ppm
Zn=	0.25 ppm	Hg=	0.020 ppm
Cu=	0.010 ppm	Mo=	0.020 ppm

Weiss et al. (1993)

Precious Metals and Indicator-Element Concentrations in Rocks from Northwestern Yucca Mountain and the Lac Gold Bullfrog mine

(Ag and Au values given in ppb, all others in ppm)

	Field #	Ag	Au	As	Bi	Cd	Hg	HgAA	Sb	Se	Te	Cu	Mo	Pb	Zn	Tl
1	3SW675	11	0.43	11.2	0.173	0.19	0.712	0.824	2.77	<0.25	0.06	5.9	3.32	9.1	11.0	1.000
2	3SW677	9	<0.20	15.3	0.067	0.04	<0.020	0.023	0.63	<0.25	<0.05	3.4	1.15	10.1	39.0	<0.498
3	3SW679A	63	<0.20	21.0	0.095	0.18	0.026	0.045	3.77	<0.25	<0.05	10.4	3.19	13.9	39.9	<0.496
4	3SW679B	23	0.56	11.7	0.105	0.14	0.039	0.056	1.17	<0.25	<0.05	9.6	3.71	12.5	25.5	0.546
5	3SW681A	5	<0.20	46.1	0.149	0.28	0.070	0.106	2.83	<0.25	<0.05	3.8	1.14	20.9	36.1	<0.487
6	3SW681B	<3	0.36	109.0	0.337	0.59	0.189	0.259	9.44	<0.25	<0.05	9.5	1.86	47.0	31.6	<0.493
7	3SW681C	5	<0.20	31.4	0.230	0.26	0.114	0.151	3.63	<0.25	0.05	4.2	1.73	25.2	18.0	2.040
8	3SW683	8	0.56	34.0	0.056	0.05	<0.020	0.038	2.83	<0.25	<0.05	3.1	1.42	16.1	17.8	<0.492
9	3SW685	4	<0.20	6.0	0.075	0.70	0.246	0.304	1.40	<0.25	0.05	5.5	3.41	5.1	16.1	5.460
10	3SW687	4	<0.20	2.4	0.092	0.07	0.034	0.038	3.07	<0.25	0.05	4.5	9.47	1.3	2.3	<0.497
11	3SW689	7	<0.20	3.6	0.099	0.10	0.040	0.045	0.14	<0.25	<0.05	5.9	2.97	11.8	15.7	<0.495
12	3SW691	4	<0.20	11.9	0.178	0.26	0.063	0.069	0.31	<0.25	<0.05	4.4	2.47	16.1	10.9	<0.486
13	3SW693	11	<0.20	2.3	0.208	0.15	0.124	0.139	0.83	<0.25	<0.05	9.9	5.55	9.2	7.9	<0.491
14	3SW695	10	<0.20	5.4	0.078	0.05	0.035	0.043	0.48	<0.25	0.05	6.6	2.80	4.7	12.7	<0.489
15	3SW697	<3	<0.20	4.9	0.256	0.17	0.227	0.274	1.96	<0.25	0.06	6.3	7.56	53.6	107.0	0.626
	Unaltered devitrified Tiva Canyon Member of the Paintbrush Tuff															
16	3SW589	25	0.59	1.6	<0.049	0.04	<0.02	0.017	<0.05	<0.25	<0.05	5.0	1.33	7.3	53.4	<0.495
	Hydrothermally altered Rainier Mesa Member, Timber Mountain Tuff at the Lac Gold Bullfrog mine															
17	3SW699	282	156.00	2.5	0.275	0.211	<0.019	0.010	0.90	<0.243	<0.05	6.8	0.60	32.1	35.0	<0.486
18	893X	232	71.30	2.5	0.282	0.212	<0.020	nd	0.88	<0.249	<0.05	6.7	0.59	32.0	35.2	<0.497

nd = not determined.

HgAA = Hg analyses carried out by the Nevada Mining Analytical Laboratory using hydride-generator atomic absorption methods with 10 gram digestions, M. O. Desilets, analyst. All other values from analyses by U. S. Mineral Laboratories, Inc., (formerly MB Associates) North Highlands, CA, using 15 gram digestions, organic liquid separation and inductively-coupled plasma emission spectrography, except for Au which was determined by graphite furnace - atomic absorption spectrometry. Values as reported by U.S. Mineral Laboratories except Ag rounded to nearest 1 ppb, Au rounded to nearest 0.01 ppb, As, Cu Pb and Zn rounded to nearest 0.1 ppm, and Cd, Sb, Se, Te and Mo rounded to nearest 0.01 ppm. Number of significant figures does not indicate precision or accuracy of analyses.

Detection limits as quoted by U.S. Mineral Laboratories at 3 sigma confidence level:

Ag = 3 ppb; Au = 0.2 ppb; Tl = 0.5 ppm; As, Se and Zn = 0.25 ppm; Bi, Sb, Te and Pb = 0.050 ppm; Cd, Hg and Mo = 0.020 ppm; Cu = 0.010 ppm.

1 Northeast-trending, banded, 1 - 5 cm wide light grey opal-quartz vein with center filled by a mixture of very fine grained reddish iron-oxide and silica.

2 Densely welded, devitrified ash-flow tuff of the Tram Member of the Crater Flat Tuff; contains no veins.

3 Northeast-trending, clear to white, banded opal and fine grained quartz vein largely <3 cm wide; specimen includes about 50 volume % wallrock tuff.

4 Northeast-trending, 3 cm wide dark grey to white banded opal vein; specimen includes about 50 volume % wallrock tuff.

5 Welded and devitrified ash-flow tuff of the Tram Member with fracture coatings of limonite and soft, tabular barite(?) crystals; specimen includes about 25 volume % thin veins composed of iron oxide and silica cemented wallrock tuff fragments.

6 Northwest-trending 2 cm wide vein filled with reddish brown mixture of iron oxide silica and wallrock tuff fragments.

7 East-west to northwest-trending vein as much as 3 cm wide composed of reddish brown mixture of iron oxide silica and wallrock tuff fragments.

8 Bleached, light grey welded and devitrified ash-flow tuff of the Tram Member with thin veins (<3 cm wide) of opal and granular quartz. Partial to complete adularization of feldspar phenocrysts. Float from vein zone about 250' to the north.

9 Dark brownish grey, silicified thin-bedded siltstone with interbeds and veinlets of white opaline silica; upper ledge.

10 Brecciated, coarsely layered reddish brown, clear and white opal containing fine-grained drusy quartz; upper ledge.

11 Silicified unwelded, previously glassy tuff adjacent to WNW-striking, steeply dipping opal and chalcedony vein about 5 cm wide; lower ledge, stratigraphically above silica sinter or sinter-like strata of specimen 13. Partial adularization of feldspar phenocrysts and pervasive replacement of glass shards and pumice by very fine grained mixture of chalcedony, quartz and adularia.

12 WNW-striking, steeply south-dipping vein about 5 cm wide consisting, from the wallrock inward, of banded opal surrounding a core of silica-cemented breccia of opal vein fragments and silicified wallrock fragments; lower ledge, stratigraphically above silica sinter or sinter-like strata of specimen 13.

13 Finely to coarsely layered reddish brown, clear, white and grey opaline silica; silica sinter or sinter-like strata at old prospect; lower ledge.

14 Silicified, unwelded, previously glassy ash-flow tuff with clear to white chalcedony and fine grained granular quartz veins and veinlets to about 1 cm wide; tuff overlies silica sinter or sinter-like strata, lower ledge.

15 Dark greyish brown to black, fine grained, silicified siltstone with irregular pods and boudin-shaped opal bodies; upper ledge.

16 Unaltered, devitrified rhyolite ash-flow tuff of the Tiva Canyon Member of the Paintbrush Tuff prepared and analysed with the other specimens to monitor analytical precision at low concentrations and to confirm the effectiveness of clean preparation procedures. Previous analyses of other splits from same 10 kg specimen given by Weiss et al. (1992).

17 Hydrothermally altered porous ash-flow tuff, lower part of the Rainier Mesa Member of the Timber Mountain Tuff, from unmineralized horse within fault-bounded vein system exposed in the 916 bench, Phase IV, Lac Gold Bullfrog mine, Rhyolite, NV. Sample location is within 30 m of Au-Ag orebody.

18 893X = blind duplicate analysis of split of specimen 17 (3SW699).

Major and Trace-element Analyses of Siliceous Strata, Northwestern Yucca Mountain

	Major Elements in Weight %										
Field #	SiO2	TiO2	Al2O3	Fe2O3	MnO2	MgO	CaO	Na2O	K2O	P2O5	Total
3SW685	92.0	0.04	5.16	1.05	0.53	0.14	0.57	0.10	0.31	0.1	100.30
3SW687	96.1	0.03	2.08	1.60	0.04	0.12	0.05	bd	0.03	bd	100.04
3SW693	96.6	0.04	1.93	0.98	0.11	0.12	0.08	0.09	0.17	bd	100.12

	Trace Elements in ppm								
	Zr	Y	Sr	Rb	Th	Ba	Cu	Pb	Zn
3SW685	20	5	49	10	8	458	21	13	23
3SW687	7	1	9	bd	2	45	14	9	bd
3SW693	21	4	11	8	5	17	18	3	5

Analyses carried out in the Nevada Mining Analytical Laboratory by X-ray fluorescence methods on pressed-powder pellets; M. O. Desilets and P. J. Lechler analysts. bd = below detection.

3SW685 Dark brownish grey, silicified thin-bedded siltstone with interbeds and veinlets of white opaline silica; upper ledge.

3SW687 Brecciated, coarsely layered reddish brown, clear and white opal containing fine-grained drusy quartz; upper ledge.

3SW693 Finely to coarsely layered reddish brown, clear, white and grey opaline silica; lower ledge sinter or sinter-like strata at old prospect.

Weiss et al. (1992)

Precious Metals and Indicator-Element Abundances in Core and Rotary Cuttings Samples from the Subsurface of Yucca Mountain

Ag and Au values given in ppb, all others given in ppm

Hole #	SMF ID#	Ag	Au	As	Bi	Cd	Hg	HgAA	Sb	Se	Te	Cu	Mo	Pb	Zn	Tl
UE25B-1H	16854	38.0	0.492	4.2	0.451	0.202	0.066	0.023	<0.05	0.355	0.208	2.8	0.38	13.5	37.4	<0.492
UE25B-1H	16855	34.5	0.233	4.8	0.554	0.132	0.063	0.022	0.22	0.456	0.413	3.3	0.47	17.0	37.0	<0.500
UE25B-1H	16856	37.9	<0.200	7.8	0.442	0.118	0.068	0.037	0.23	0.416	0.428	3.5	0.33	15.8	38.4	<0.500
UE25B-1H	16857	33.7	0.230	5.2	0.450	0.196	0.078	0.021	<0.05	0.556	0.268	3.2	0.69	14.1	38.2	<0.493
UE25B-1H	16859	34.1	0.596	7.9	0.445	0.118	0.080	0.024	<0.05	0.464	0.202	3.1	0.27	16.5	39.7	<0.496
	16860	33.3	0.324	0.7	0.182	0.324	0.153	0.106	<0.05	<0.243	<0.049	5.8	0.23	7.7	54.1	<0.486
	YMX-2	40.1	1.10	<0.75	0.167	0.355	0.142	nd	<0.15	<0.753	<0.151	6.5	0.41	7.9	53.2	<1.51
UE25B-1H	16861	28.6	<0.200	0.5	0.183	0.082	0.060	0.040	0.14	<0.250	0.112	2.4	0.23	8.7	41.4	<0.500
UE25B-1H	16862	33.6	0.230	0.3	0.057	0.037	<0.020	<0.010	<0.05	<0.246	<0.049	0.9	<0.02	8.0	36.4	<0.493
UE25 P1	16954	41.1	0.360	5.2	0.156	0.320	0.140	0.120	<0.07	<0.338	<0.068	1.7	1.18	14.9	30.8	<0.675
UE25 P1	16955	27.1	<0.198	2.7	0.154	0.089	0.053	0.038	0.42	<0.248	0.085	2.6	0.79	22.6	125	<0.495
UE25 P1	16956	29.6	<0.197	3.4	0.105	0.082	0.039	0.022	0.52	<0.247	0.062	1.7	0.62	14.1	21	<0.493
UE25 P1	16958	54.0	0.519	47.8	0.123	0.127	0.092	0.061	1.84	<0.243	0.055	1.6	2.86	11.7	29.4	<0.487
UE25 P1	16959	93.0	2.13	63.2	0.051	0.253	0.129	0.136	0.39	<0.242	<0.048	1.4	1.32	5.6	42.5	<0.484
UE25 P1	16960	29.8	<0.198	14.3	0.164	0.107	0.060	0.027	1.14	<0.247	0.157	1.4	0.82	13.0	21.5	<0.494
UE25 P1	16961	91.3	0.794	9.7	<0.050	0.035	0.056	0.046	1.35	0.268	<0.050	1.1	2.19	1.9	12.8	<0.496
	16962	51.3	<0.196	3.7	<0.049	0.030	0.025	0.031	0.77	0.363	<0.049	0.8	1.92	2.3	11.7	<0.489
	YMH-X5	54.7	<0.199	3.9	<0.050	0.031	0.031	nd	0.86	0.318	0.065	0.9	1.78	2.3	11.8	<0.498
UE25 P1	16963	139.0	4.83	25.9	1.92	0.469	0.585	nd	12.7	0.687	0.091	38.6	208	900	227	2.44
	16963B*	173.0	7	38.2	1.65	0.208	0.815	0.714	20.1	1.38	<0.526	64.9	286	1358	304	3.05
UE25 P1	16964	49.2	0.328	4.5	0.053	0.037	0.051	0.051	1.23	<0.246	<0.049	1.6	16.2	9.7	15	<0.492
USW G1	16904	41.8	<0.196	8.0	0.340	0.079	0.073	0.023	0.15	0.404	0.439	4.3	0.37	16.1	21.2	<0.491
USW G1	16905	39.1	2.72	6.8	0.427	0.173	0.070	0.023	<0.05	0.526	0.206	3.9	0.64	18.3	37.9	<0.486
USW G1	16907	36.7	0.396	8.4	0.381	0.224	0.069	0.016	<0.05	0.687	0.325	4.7	0.68	15.0	37.4	<0.495
USW G1	16914	33.3	0.327	2.6	0.070	0.045	0.054	<0.010	<0.05	<0.245	<0.049	2.0	<0.02	10.1	57.3	<0.490
USW G2	16871	14.8	1.47	18	<0.049	0.416	0.649	0.786	5.31	<0.246	<0.049	1.7	0.46	9.5	36.8	<0.491
	16871							0.681								
USW G2	16887	28.4	0.332	68.8	<0.050	0.100	0.192	0.118	<0.05	<0.249	<0.050	3.9	0.59	12.1	50.1	<0.498
USW G2	16888	26.2	<0.197	85.2	0.064	0.119	0.220	0.152	0.40	<0.247	0.073	3.5	1.16	17.2	81.9	<0.493
USW G2	16889	28.7	0.232	47.1	0.081	0.126	0.220	0.123	<0.05	<0.248	<0.050	3.1	2.05	16.9	52	<0.497
	YMX-1	34.9	1.14	50	<0.132	0.132	0.188	nd	<0.132	<0.66	<0.132	3.5	2.2	16.5	51.8	<1.32
USW G2	16890	27.9	<0.198	38.6	<0.050	0.163	0.081	0.037	0.34	<0.248	0.067	3.7	0.18	22.3	86.8	<0.496
USW G2	16895	43.0	0.360	1.6	<0.049	0.092	0.061	0.016	0.17	<0.246	0.067	12.6	0.18	9.3	76.8	<0.491
USW G2	16896	38.6	<0.197	0.5	<0.049	0.100	0.178	0.021	<0.25	<0.246	<0.049	11.2	<0.02	7.2	78.8	<0.492
USW G3	16932	36.7	<0.198	1.5	0.196	0.153	0.078	0.046	<0.05	<0.248	<0.050	1.8	0.13	9.3	12.7	<0.496
	X-1							0.050								
USW G3	16933	36.7	<0.194	1.3	0.152	0.071	0.091	0.063	0.11	<0.243	0.130	1.0	0.30	10.5	32.8	<0.486
USW G3	16934	40.2	0.328	1.2	0.268	0.215	0.110	0.079	<0.05	<0.246	<0.049	1.7	0.15	10.6	31.7	<0.492
USW G3	16935	41.3	0.329	1.1	0.177	0.144	0.111	0.066	<0.05	<0.247	<0.049	1.6	0.12	10.8	29.8	<0.493
USW G3	16936	34.4	<0.199	1.1	0.179	0.077	0.053	0.046	0.24	<0.249	0.115	1.7	0.29	14.8	27.7	<0.498
UE25 C1	20064	8.5	<0.198	18.1	0.106	0.119	0.042	0.033	15.1	<0.247	<0.049	0.8	1.25	9.9	40.6	<0.494
UE25 C2	20065	6.5	0.295	5.5	1.110	0.050	<0.020	0.017	<0.05	<0.246	0.083	0.5	<0.02	13.9	17.0	<0.491
UE25 C2	20066	12.4	<0.225	22.4	0.122	0.057	0.026	0.018	3.72	<0.282	<0.056	0.6	8.83	6.2	9.3	<0.563

UE25 C2	20067	10.1	0.276	20.4	0.277	0.120	0.050	0.021	0.47	<0.345	<0.069	0.8	12.5	6.5	27.3	<0.689
UE25 C3	20068	12.5	0.328	77.4	0.163	0.292	0.075	0.062	1.49	<0.246	<0.049	0.6	0.98	10.9	39.1	<0.491
UE25 C3	20069	21.1	0.395	34.3	1.970	0.083	0.153	0.045	3.37	<0.247	0.134	0.5	193	11.1	20.8	<0.494
	20069R	10.0	<0.199	37.7	1.240	0.092	0.113	0.045	3.67	<0.249	0.188	0.7	207	11.3	23.6	<0.499
	X-2							0.050								
	20069B	9.9	<0.199	23	0.674	0.067	0.065	0.030	2.35	<0.248	0.090	0.4	110	9.2	19.3	<0.497
	YMH-X4	10.4	<0.198	22.7	0.744	0.066	0.064	0.045	2.3	<0.248	0.107	0.6	109	9.0	19.1	<0.496
UE25 C3	20070	4.5	0.261	35.3	<0.049	0.063	0.041	0.058	4.67	<0.244	<0.049	0.7	0.29	2.8	12.8	<0.489
	Fresh tuff reference samples															
BMCF-D		10.1	<0.199	5.3	<0.050	0.062	0.024	0.013	0.26	<0.249	0.055	1.0	1.36	2.0	47.9	<0.497
3SW-589		9.7	0.265	2.7	<0.050	0.037	<0.020	0.015	<0.05	<0.249	<0.050	1.4	0.89	4.9	49.0	<0.497
YMH-X3		13.1	<0.198	2.6	<0.049	0.044	0.023	0.014	0.12	<0.247	0.053	1.2	0.64	4.5	50.5	<0.495
X-3								0.012								

SMF ID # denotes sample identification assigned to each interval by staff of Sample Management Facility, Area 25, Nevada Test Site; ID numbers beginning with YM and X were assigned by Task 3 to denote blind duplicates. nd = not determined.

py = pyrite, fluor = fluorite; cal = calcite; qtz = quartz; vns = veins, alt = altered, mod = moderately, dissem = disseminated.

Srm = Roberts Mountain Formation, Slm = Lone Mountain Dolomite; Tot = pre-Lithic Ridge sequence of ash-flow and bedded tuffs, Trl = pre-Lithic Ridge silicic lavas, Tlr = Lithic Ridge Tuff; Tct, Tcb and Tcp = Tram, Bullfrog, and Prow Pass members of the Crater Flat Tuff, respectively; Tc = Crater Flat Tuff undivided; Tpc = Tiva Canyon Member of the Paintbrush Tuff.

Hole #	SMF ID#	Unit	Py?	Vns?	Comments
UE25B-1H	16854	Tct	Y	N	lithology similar to Round Mountain type II ore
UE25B-1H	16855	Tct	Y	N	
UE25B-1H	16856	Tct	Y	Y	cal vns
UE25B-1H	16857	Tct	Y	Y	cal vns; dissem py in groundmass and in lithics; minor py in cal vn.
UE25B-1H	16859	Tct	Y	Y	cal + green to clr fluor?? vein, possible fluid inclusions.
UE25B-1H	16860	Tct?	N	Y	cal + green phase in vn; no py seen
	YMX-2				(blind duplicate 16860)
UE25B-1H	16861	Tlr	?	N	
UE25B-1H	16862	Tlr	N	Y	cal vn
UE25 P1	16954	Tot	N	?	
UE25 P1	16955	Tot	Y	?	alt volc frags, some w/py
UE25 P1	16956	Tot	N	?	alt Tot, no py seen, contains drill tool fragments
UE25 P1	16958	Tot	Y	?	mixed Tot/Slm
UE25 P1	16959	fault?	?	?	
UE25 P1	16960	Tot/Slm	Y	?	mixed Tot/Slm, 90% Tot fragments contain sparse py
UE25 P1	16961	Slm	N	Y	cal + fluor? vns
UE25 P1	16962	Srm	N	Y	cal+fluor?+qtz? vn frags
	YMH-X5				(blind dup. 16962)
UE25 P1	16963	Srm	Y	Y	contains drill tool fragments; py and fluor vn or vug fragments
	16963B*				(powder from 2nd split of chips; 5 gram GXPL)
UE25 P1	16964	Srm	Y	Y	qtz, py, fluor? vns + dissem py in some fr, contains drill tool fragments;
USW G1	16904	Tct	Y	N	
USW G1	16905	Tct	Y	Y	clear qtz vn; pyritic lithics and groundmass.
USW G1	16907	Tct	Y	N	pyritic lithics and groundmass.
USW G1	16914	Tot	N	N	xtal-rich, milky fldsp phenocrysts

USW G2	16871	Tcb	N	Y	Mn-ox filled fracture.
	16871				(second split of original powder)
USW G2	16887	Trl	Y	Y	propylitic alt, cal-chlor-silica vns., albitized feldspar phenos
USW G2	16888	Trl	N	Y	as above
USW G2	16889	Trl	Y	Y	propylitic alt, cal-chlor-silica vns., albitized feldspar phenos
	YMX-1				(blind dup. 16889)
USW G2	16890	Trl	N	Y	fault surfaces, sheared cal+green clay? vn
USW G2	16895	Trl	N	Y	cal vns
USW G2	16896	Trl	N	Y	cal vns
USW G3	16932	Tlr	Y	N	py in lithics and groundmass
	X-1				X-1 (blind dup. 16932 for Hg by AA)
USW G3	16933	Tlr	Y	N	very sparse py in few lithics; lithology similar to Round Mtn type II
USW G3	16934	Tlr	Y	N	v. sparse py in few lithics; good match for RM typeII ore
USW G3	16935	Tlr	Y	N	v. sparse py in few lithics; good match for RM typeII ore
USW G3	16936	Tlr	?	N	
UE25 C1	20064	Tc	N	Y	rubble zone frags w/breccia veins
UE25 C2	20065	Tc	N	N	strong reddish Feox stain
UE25 C2	20066	Tc	N	Y	bleached, Feox breccia vns
UE25 C2	20067	Tc	N	Y	breccia veins as in 20064; bleached, biotite fresh
UE25 C3	20068	Tc	N	Y	breccia veins, clear calcite+dark grey calcite veins
UE25 C3	20069	Tc	N	Y	breccia vns; fluor+
					montmorill. in cavities; vfg qtz+fluor? vns, no ca
	20069R				(2nd analysis of powder from original split of 20069)
	X-2				(blind dup. 20069 for Hg by AA)
	20069B				(powder from second split of 20069 excluding cut surfaces)
	YMH-X4				(blind dup. 20069B)
UE25 C3	20070	Tc	N	N	bleached to mustard color
BMCF-D		Tcb			mod. welded, devit; S end Yucca Mtn NW of Lathrop Wells cinder cone
3SW-589		Tpc			fresh, dense, devit, minor caliche in lithophys.; Exile Hill
YMH-X3					(blind dup. 3SW-589)
X-3					(blind duplicate 3SW-589 for Hg by AA)

Analyses by MB Associates, North Highland, CA, using inductively-coupled plasma emission spectrography for all elements except Au which was carried out by graphite furnace - atomic absorption spectrometry; * = 5 gram digestion, all other analyses used 15 gram digestion. Values as reported by MB Associates except Ag rounded to nearest ppb, As, Sb and Cu rounded to nearest 0.1 ppm, and Mo to nearest 0.01 ppm. Number of significant figure does not indicate precision or accuracy of analyses.

HgAA = analyses carried out by the Nevada Mining Analytical Laboratory using hydride-generator type atomic absorption methods, M. O. Desilets, analyst.

nd = not determined.

Weiss (1992)

X-Ray Fluorescence Analyses of Rocks of the Mount Jackson Dome Field
major elements given in weight percent, minor elements in ppm

Sample #	383A	383A*	383B	385	387	387*	MJ-SE	MJ-W	DWLJ-1
SiO2	75.6	72.9	74.4	74.5	72.6	72.8	67.0	65.6	74.6
Al2O3	12.6	12.2	12.4	12.1	12.7	12.7	14.4	15.2	12.8
MgO	0.20	0.24	0.23	0.18	0.19	0.18	0.72	0.87	0.11
CaO	0.66	1.52	0.79	0.82	0.76	0.85	2.49	2.92	0.70
Na2O	4.26	4.03	4.08	4.06	4.05	4.06	3.70	4.14	3.74
K2O	4.48	4.53	4.56	4.25	4.85	4.83	4.16	3.77	4.55
P2O5	0.02	0.04	0.03	0.03	0.02	0.02	0.11	0.12	0.02
TiO2	0.161	0.141	0.145	0.131	0.135	0.127	0.380	0.367	0.118
MnO	0.08	0.08	0.08	0.08	0.08	0.08	0.06	0.06	0.07
Fe2O3	0.97	0.83	0.87	0.84	0.92	0.87	2.13	2.30	0.58
Cr	-10	13	-10	-10	-10	-10	-10	-10	-10
Rb	172	189	187	316	157	159	138	95	237
Sr	-10	-10	-10	19	13	21	715	977	-10
Y	27	34	28	42	-10	16	14	-10	14
Zr	119	112	114	100	129	102	162	130	93
Nb	35	50	47	73	32	53	39	30	40
Ba	31	57	63	91	77	72	1230	1650	41
LOI(%)	0.85	2.65	2.10	2.80	2.95	3.00	2.90	2.95	2.20
SUM(%)	99.9	99.2	99.7	99.9	99.3	99.6	98.3	98.6	99.5

Analyses Recalculated "Anhydrous"

Sample #	383A	383A*	383B	385	387	387*	MJ-SE	MJ-W	DWLJ-1
SiO2	76.2	74.9	76.0	76.6	74.8	75.1	69.0	67.6	76.3
Al2O3	12.7	12.5	12.7	12.4	13.1	13.1	14.8	15.7	13.1
MgO	0.20	0.25	0.23	0.19	0.20	0.19	0.74	0.90	0.11
CaO	0.67	1.56	0.81	0.84	0.78	0.88	2.57	3.01	0.72
Na2O	4.30	4.14	4.17	4.18	4.17	4.19	3.81	4.27	3.82
K2O	4.52	4.65	4.66	4.37	5.00	4.98	4.29	3.89	4.65
P2O5	0.02	0.04	0.03	0.03	0.02	0.02	0.11	0.12	0.02
TiO2	0.162	0.145	0.148	0.135	0.139	0.131	0.392	0.378	0.121
MnO	0.08	0.08	0.08	0.08	0.08	0.08	0.06	0.06	0.07
Fe2O3	0.98	0.85	0.89	0.86	0.95	0.90	2.19	2.37	0.59
Cr	-10	13	-10	-10	-10	-10	-10	-10	-10
Rb	173	194	191	325	162	164	142	98	242
Sr	-10	-10	-10	20	13	22	737	1007	-10
Y	27	35	29	43	-10	16	14	0	14
Zr	120	115	116	103	133	105	167	134	95
Nb	35	51	48	75	33	55	40	31	41
Ba	31	59	64	94	79	74	1267	1701	42

All samples contained small amounts of secondary carbonate minerals (caliche). To minimize the CaO contributed by caliche most samples were crushed to -20 mesh and leached for 10 minutes with 5% acetic acid in a sonic cleaner. * indicates samples not leached in 5% acetic acid. Total iron as Fe2O3.

Analyses carried out by XRAL Ltd., using fused disk (lithium metaborate flux) X-ray fluorescence methods.

Weiss et al. (1991)

GOLD CONTENTS OF SUBALKALINE RHYOLITIC ROCKS OF THE SOUTHWESTERN NEVADA VOLCANIC FIELD
(values given in parts per billion)

Sample #	Au	Sample type	Unit and location
3SW-171A	0.2	vitrophere	Red Rock Valley Tuff; east side of Eleana Range
K-190	0.5	vitrophere	Bullfrog Member, Crater Flat Tuff; south end of Yucca Mountain
K-192	0.7	devitrified	Bullfrog Member, Crater Flat Tuff; south end of Yucca Mountain
CP4-2OB	0.4	vitrophere	Topopah Spring Member, Paintbrush Tuff; Yucca Mountain
BB9-15	0.8	vitrophere	Topopah Spring Member, Paintbrush Tuff; Yucca Mountain
BB8-45	0.4	vitrophere	Topopah Spring Member, Paintbrush Tuff; Yucca Mountain
3SW-519G	0.1	vitrophere	Tiva Canyon Member, Paintbrush Tuff; Yucca Mountain
3SW-519GU	0.2	vitrophere	Tiva Canyon Member, Paintbrush Tuff; Yucca Mountain
3SW-521	0.1	devitrified	Tiva Canyon Member, Paintbrush Tuff; Yucca Mountain
3SW-433NA	0.5	devitrified	Tiva Canyon Member, Paintbrush Tuff; Yucca Mountain (Exile Hill)
3SW-435NA	0.6	devitrified	Tiva Canyon Member, Paintbrush Tuff; Yucca Mountain (Exile Hill)
3SW-437NA	0.6	devitrified	Tiva Canyon Member, Paintbrush Tuff; Yucca Mountain (Exile Hill)
3DCN8-82	0.2	vitrophere	Rainier Mesa Member, Timber Mountain Tuff; SE of Sleeping Butte
3SW-523GL	0.1	vitrophere	Rainier Mesa Member, Timber Mountain Tuff; NW of Scotty's Junction
3SW-525	0.1	devitrified	Rainier Mesa Member, Timber Mountain Tuff; NW of Scotty's Junction
SJW-81-ATV	0.3	vitrophere	Ammonia Tanks Member, Timber Mountain Tuff; NW of Scotty's Junction
3DN8-21	0.2	vitrophere	Ammonia Tanks Member, Timber Mountain Tuff; SE of Sleeping Butte
THR-1	0.3	vitrophere	post-Ammonia Tanks rhyolite lava #1, Bullfrog Hills
THR-2	<0.1	vitrophere	post-Ammonia Tanks rhyolite lava #2, Bullfrog Hills
3DN9-24	0.1	vitrophere	post-Ammonia Tanks rhyolite lava #1, Bullfrog Hills
3DN8-20	0.2	vitrophere	"tracking station" rhyolite, northern Bullfrog Hills
FCT-1	0.1	vitrophere	post-Ammonia Tanks tuff; between Fluorspar Canyon and Beatty Wash
OBS-B	0.2	obsidian	Rhyolite lavas of Obsidian Butte
3SW-173TR	0.4	obsidian	Rhyolite lavas of Shoshone Mountain

Analyses by XRAL Activation Services Inc., using instrumental neutron activation prior to fire assay concentration and radiochemical analyses (Rowe and Simon, 1968; Connors et al., 1990; 1991).

Weiss et al. (1991)

MERCURY CONTENTS OF ROCK-CHIP SAMPLES FROM YUCCA MOUNTAIN
M(*values given in parts per billion as the means of replicate analyses*)

Sample#	Hg	2 sigma	n	Description/location
Bow Ridge fault at Trench 14				
3SW-569	22.0	0.0	2	Rainier Mesa Member, N wall; caliche impregnated, weak argillic alteration, adjacent to main carbonate-silica vein.
3SW-571	40.5	3.0	2	brecciated Tiva Canyon Member, N wall, ~30" E of main vein; drusy quartz, silica ±caliche veins xcut drusy quartz.
3SW-573	40.5	3.0	2	brecciated Tiva Canyon Member, N wall, E of 3SW-571; w/ drusy quartz.
3SW-575	26.5	1.0	2	brecciated Tiva Canyon Member, N wall, E of 3SW-573; w/ fng drusy quartz ±caliche in lithophysae.
3SW-577	22.0	4.0	2	brecciated Tiva Canyon Member, S wall, ~18"E of main vein; w/ drusy quartz + caliche.
3SW-579	45.5	3.0	2	breccia of Tiva Canyon Member fragments in carbonate-silica matrix, S wall, adjacent to E edge of main vein.
3SW-581	<10		4	partially opalized Tiva Canyon Member , S wall, between splays of main vein.
Solitario Canyon fault				
3SW-599A	63.0	10.5	4	reddish, FeOx-rich opalized? bedded tuff w/caliche coating, ~100' W of Solitario Canyon fault splay*a*.
3SW-599B	67.7	7.5	3	dark rusty brown, porous bedded tuff ~12'WNW from 3SW-599A.
3SW-603	35.5	3.0	2	caliche vein, N wall of Trench 8, Solitario Canyon fault splay.
3SW-605	58.0	6.0	2	fault breccia of dark purplish brown fragments of Topopah Spring Member, minor opal in fractures; E end Trench 8.
3SW-607	33.3	10.3	4	siliceous, strain-hardened? fault breccia of Topopah Spring Member adjacent to caliche vein at E end Trench 8
Bow Ridge fault near Bow Ridge				
3SW-593A	19.5	5.0	2	opal? cemented fault breccia of dense Tiva Canyon Member, Bow Ridge below saddle W of Bow Ridge
3SW-593B	13.0	0.0	2	opal-veined fault breccia/gouge,~2' E of 3SW-593A; fragments of dark Topopah Spring Member? in siliceous matrix.
Fault system NW of Busted Butte				
3SW-595A	11.0	0.0	2	siliceous fault gouge or vein?, fault in saddle S of Dune Wash, ~2050' SW of hill 3834.
3SW-595B	10.0	2.0	2	FeOx-rich Topopah Spring Member? in footwall of fault in saddle S of Dune Wash, adjacent to 3SW-595A.
"Fresh" Tiva Canyon Member				
3SW-583	31.2	14.0	6	Tiva Canyon Member, densely welded, devitrified, caliche in lithophysal cavities; E side Exile Hill.
3SW-585	<10		2	Tiva Canyon Member, densely welded, devitrified, caliche in lithophysal cavities; E side Yucca Mtn., NW of Exile Hill.
3SW-589	12.0	2.0	2	Tiva Canyon Member, densely welded, devitrified, w/caliche in lithophysal cavities; ridge E of Bow Ridge.
3SW-591	16.5	2.0	2	Tiva Canyon Member, densely welded, devitrified, w/caliche in lithophysal cavities; just W of Bow Ridge.
3SW-597	35.5	9.6	4	Tiva Canyon Member, densely welded, devitrified, w/caliche in lithophysal cavities; ~2000' SE of 3SW-595A/595B.
Hydrothermally altered rock in Claim Canyon				
3SW-587A	827.5	65.4	4	silicified and partially adularized rhyolite lava between units of the Paintbrush Tuff; ~3600' N35°E from Prow Pass.

Analyses carried out by M. Desilets, analyst, Nevada Bureau of Mines Analytical Laboratory on 10 gram digestions using atomic absorption spectrometry with hydride generation methods.

Uncertainty expressed in parts per billion Hg at 2 Sigma level; n = number of replicate analyses.

Detection limit is estimated to be 10 parts per billion based on the results of standard addition analysis and intrarun comparison to synthetic control samples.

a = sample is from same outcrop as SC-52 of Castor et al. (1989).

Weiss et al. (1991)

PRECIOUS METALS AND INDICATOR-ELEMENT ABUNDANCES IN ROCK-CHIP SAMPLES FROM YUCCA MOUNTAIN
(Ag and Au expressed in parts per billion, all other elements given in parts per million)

Sample #	Ag	Au	As	Bi	Cd	Hg	Sb	Se	Cu	Mo	Pb	Zn	Ga
Bow Ridge fault at Trench 14													
3SW-569	12	7.3	4.22	0.132	0.030	0.026	0.227	<0.244	0.977	0.280	4.15	11.3	1.29
3SW-571	11	0.5	9.88	0.086	0.031	0.050	0.317	<0.249	0.799	0.555	8.41	32.0	0.595
3SW-573	14	1.2	11.8	0.093	0.032	0.038	0.267	<0.246	0.931	0.604	9.20	32.5	0.431
3SW-579	6	1.1	6.65	<0.050	0.036	0.048	0.169	0.412	1.64	0.232	4.10	17.8	0.282
3SW-581	4	0.9	3.83	0.057	0.020	0.025	0.139	0.323	0.673	0.483	0.790	41.2	0.540
Solitario Canyon fault													
3SW 599A*	<9	1.1	1.68	3.99	0.077	<0.058	0.300	<0.723	1.72	1.86	70.5	43.0	1.69
3SW-599B*	<9	<0.6	<0.750	1.35	0.065	<0.060	0.160	<0.750	1.15	0.570	3.32	12.7	0.989
3SW-605	4	0.4	1.67	0.335	0.034	0.024	0.089	<0.247	0.263	0.389	1.59	27.4	0.812
X-15[t]	5	<0.2	2.26	0.334	0.037	0.022	0.132	<0.247	0.255	0.383	1.49	26.2	0.760
Fault system NW of Busted Butte													
3SW-595B	5	0.5	1.87	1.77	0.047	0.038	0.388	0.377	0.268	2.27	17.3	8.11	2.10
X-16[u]	6	0.5	2.32	1.81	0.045	0.024	0.410	<0.246	0.313	2.34	18.0	9.48	2.27
Densely welded lithophysal "fresh" tuff													
3SW-585	25	<0.2	6.00	0.094	0.073	<0.019	0.183	<0.242	0.597	1.2	9.98	52.9	0.608
58991[#]	14	0.3	2.41	0.066	0.040	0.030	0.126	0.326	0.832	0.591	3.58	47.4	0.543
3SW-433NA[v]		0.5											
3SW-435NA[v]		0.6											
3SW-437NA[v]		0.6											
Fault system west side of Boomerang Point													
3SW-519G[x]	0.1												
3SW-519GU[y]	0.2												
3SW-521[z]	0.1												
Claim Canyon													
3SW-587A	13	0.5	7.78	0.073	0.047	0.515	0.849	<0.246	0.580	0.308	3.80	26.3	0.618

Analyses by Geochemical Services Inc. using inductively-coupled plasma emission spectrography for all elements except Au which was carried out by graphite furnace - atomic absorption spectrometry; * = 5 gram digestion, all other analyses used 15 gram digestion. Values as reported by G.S.I. except Ag rounded to nearest ppb and Au rounded to nearest 0.1 ppb; number of significant figures does not indicate precision or accuracy of analyses.

Measured tellurium contents were <0.25 ppm in all samples. Measured thallium contents were <0.50 ppm in all samples except 3SW-599A and 3SW-599B which were <1.50 ppm.

[t] denotes blind duplicate sample of 3SW-605.

[u] denotes blind duplicate sample of 3SW-595B.

[v] analyses by XRAL Activation Services, Inc. using instrumental neutron activation (INAA) methods.

[x] middle part of vitrophere of Tiva Canyon Member; INAA analysis by XRAL Activation Services, Inc.

[y] upper part of vitrophere of Tiva Canyon Member; INAA analysis by XRAL Activation Services, Inc.

[z] devitrified Tiva Canyon Member just above vitrophere; INAA analysis by XRAL Activation Services, Inc.

58991 is composite sample of equal parts 3SW-589 and 3SW-591.

Detection limits quoted by G.S.I. based on intrarun standards and blanks as follows:

Ag	3.00 ppb	Hg	0.020 ppm	Mo	0.020 ppm
Au	0.20 ppb	Sb	0.050 ppm	Pb	0.050 ppm
As	0.250 ppm	Se	0.250 ppm	Zn	0.250 ppm
Bi	0.050 ppm	Te	0.050 ppm	Ga	0.100 ppm
Cd	0.020 ppm	Cu	0.010 ppm	Tl	0.500 ppm

Weiss ... (1990)

PRECIOUS METALS AND INDICATOR-ELEMENT ABUNDANCES IN ROCK-CHIP SAMPLES FROM TRENCH 14 AND VICINITY
(expressed in parts per million)

	Ag	As	Au	Cu	Hg	Mo	Pb	Sb	Tl	Zn	Bi	Ga	Se	Te
1)	0.423	110	0.005	27.9	0.799	65.3	154	24.6	<0.49	33.2	<0.249	1.90	<0.995	<0.497
1a)	0.129	10.0	0.002	6.49	0.202	1.11	15.0	0.763	<0.487	44.6	<0.243	1.15	<0.973	<0.487
1b)	-	-	-	-	0.036	-	-	-	-	-	-	-	-	-
2)	0.048	15.6	0.004	11.1	0.373	1.23	16.4	10.1	<0.488	90.8	<0.244	<0.488	<0.977	<0.488
2a)	-	-	-	-	0.085	-	-	-	-	-	-	-	-	-
3)	<0.015	5.89	0.001	2.71	0.349	1.80	10.7	2.90	<0.498	147	<0.249	<0.498	<0.996	<0.498
3a)	-	-	-	-	0.012	-	-	-	-	-	-	-	-	-
4)	0.048	11.2	0.001	4.11	0.553	2.29	14.8	6.36	<0.492	75.5	<0.246	<0.492	<0.984	<0.492
4a)	-	-	-	-	0.048	-	-	-	-	-	-	-	-	-
5)	0.049	11.2	0.002	2.95	2.02	1.58	46.6	2.89	<0.492	892	<0.246	<0.492	<0.983	<0.492
5a)	-	-	-	-	0.012	-	-	-	-	-	-	-	-	-
6)	0.141	14.1	0.001	14.4	3.08	2.54	78.6	8.69	<0.487	344	<0.244	<0.487	<0.975	<0.487
6a)	-	-	-	-	0.024	-	-	-	-	-	-	-	-	-
7)	0.054	1.77	0.001	2.35	0.160	0.759	3.27	<0.247	<0.494	50.0	<0.247	0.845	<0.987	<0.494
7a)	0.054	1.83	<0.0005	3.11	0.185	0.686	3.49	<0.245	<0.49	46.3	<0.245	0.799	<0.979	<0.49
7b)	0.049	1.57	0.001	1.68	0.170	0.637	2.93	<0.25	<0.5	49.4	<0.25	0.576	<0.999	<0.5
7c)	-	-	-	-	<0.050	-	-	-	-	-	-	-	-	-
8)	0.04	3.09	<0.0005	1.28	0.214	0.688	4.02	<0.245	<0.49	41.1	<0.245	0.606	<0.979	<0.49
8a)	0.055	3.05	<0.0005	1.31	0.184	0.712	4.02	<0.248	0.523	44.0	<0.248	0.684	<0.992	<0.496
8b)	0.053	3.51	0.001	1.57	0.177	0.883	4.31	<0.245	<0.491	44.7	<0.245	0.650	<0.982	<0.491
8c)	-	-	-	-	<0.050	-	-	-	-	-	-	-	-	-
9)	0.048	4.34	<0.0005	1.23	0.154	0.703	3.68	<0.247	<0.494	43.1	<0.247	0.535	<0.989	<0.494
9a)	0.051	3.84	<0.0005	1.17	0.178	0.698	3.60	<0.244	<0.488	38.8	<0.244	0.524	<0.976	<0.488
9b)	0.047	4.09	<0.0005	1.16	0.171	0.680	3.49	<0.246	<0.491	41.1	<0.246	0.559	<0.982	<0.491
9c)	-	-	-	-	<0.050	-	-	-	-	-	-	-	-	-

1) x3SW195B: north wall, fractured Tiva Canyon Member with weak silicification, ± drusy quartz in lithophysae, analysis from Weiss et al. (1989) **
1a) Split of hand-sample remaining from 3SW-195B. **
1b) z Later split of hand-sample remaining from 3SW-195B.
2) x3SW329: south wall, siliceous buff to white carbonate vein filling. *
2a) zSplit of hand-sample remaining from 3SW329.
3) x3SW331: south wall, dark purplish, silicified breccia of Tiva Canyon Member between calcareous veins. *
3a) zSplit of hand-sample remaining from 3SW331.
4) x3SW333: south wall, siliceous margin of 1-2 cm thick white calcareous vein. Margin is composed of buff to light brown silica vein material containing small, dark colored, silica-replaced fragments of Tiva Canyon Member. *
4a) zSplit of hand-sample remaining from 3SW333.
5) x3SW335: north wall, silicified breccia of Tiva Canyon Member with bleached groundmass surrounding drusy quartz-lined lithophysal cavities, ~ 2 meters east of thick, white, calcareous vein. *
5a) zSplit of hand-sample remaining from 3SW335.
6) x3LT029: south wall, silicified breccia of Tiva Canyon Member, purplish rock fragments in buff siliceous matrix. *
6a) zSplit of hand-sample remaining from 3LT029.
7) 3SW433; dense, lithophysal Tiva Canyon Member, east side of Exile Hill. **
7a) Duplicate split of 3SW433. **
7b) Triplicate split of 3SW433. **
7c) zSplit of hand-sample remaining from 3SW433.
8) 3SW435; dense, lithophysal Tiva Canyon Member, east side of Exile Hill. **
8a) Duplicate split of 3SW435. **
8b) Triplicate splite of 3SW435. **

8c) [z]Split of hand-sample remaining from 3SW435.
9) 3SW437; dense, lithophysal Tiva Canyon Member, east side of Exile Hill. **
9a) Duplicate split of 3SW437. **
9b) Triplicate splite of 3SW437. **
9c) [z]Split of hand-sample remaining from 3SW437.

Except as noted, analyses by Geochemical Services Inc., using inductively-coupled plasma emission spectrography; * = 10 gram digestion; ** = 15 gram digestion; k = x103. Values as reported by G.S.I.; number of significant figures does not indicate precision or accuracy of analyses.

[x] denotes analyses from Weiss et al. (1989b).

[z] denotes mercury analyses by the Nevada Mining and Analytical Laboratory, Nevada Bureau of Mines and Geology, using atomic absorption methods.

Castor et al. (1990)

Chemical Analyses, in ppm, of Samples From the Yucca Mountain Addition and Surrounding Mining Districts

Sample No.	Ag	As	Au	Cu	Hg	Mo	Pb	Sb	Tl	Zn	Bi	Cd	Ga	Pd	Se	Te
	Yucca Mountain															
YMSC 1	0.020	3.79	0.001	10.20	<0.099	2.380	3.740	<0.249	<0.497	22.20	<0.249	0.413	0.900	<0.497	<0.994	<0.497
YMSC 2	<0.015	<1.00	<0.0005	14.50	0.228	1.600	2.820	0.297	<0.500	21.00	<0.250	<0.100	0.616	<0.500	<0.999	<0.500
YMSC 2A†	0.036	<0.99	<0.0005	1.44	<0.099	0.472	1.890	<0.247	<0.494	26.40	<0.247	0.115	<0.494	<0.494	<0.987	<0.494
YMSC 3	0.025	<1.00	<0.0005	13.90	0.112	1.400	1.670	<0.251	<0.501	20.60	<0.251	<0.100	<0.501	<0.501	<1.000	<0.501
YMSC 4	0.028	5.52	0.002	10.90	<0.100	0.982	1.400	<0.251	<0.502	9.93	<0.251	0.202	<0.502	<0.502	<1.000	<0.502
YMSC 5A†	0.039	6.63	<0.0005	4.04	<0.098	0.487	1.090	<0.246	<0.491	4.66	<0.246	<0.098	<0.491	<0.491	<0.982	<0.491
YMSC 5B†	0.037	5.56	<0.0005	4.17	<0.098	0.316	1.200	0.259	<0.488	4.35	<0.244	<0.098	<0.488	<0.488	<0.976	<0.488
YMSC 5C	0.028	6.13	0.004	6.86	<0.105	0.213	1.900	<0.263	<0.526	5.31	<0.263	0.118	0.612	<0.526	<1.050	<0.526
YMSC 5H	0.022	3.97	0.002	7.98	<0.112	0.211	0.834	0.301	<0.561	2.78	<0.281	0.140	<0.561	<0.561	<1.120	<0.561
YMSC 6	0.023	<1.00	<0.0005	15.80	<0.100	1.650	2.420	0.294	<0.502	22.50	<0.251	<0.100	0.636	<0.502	<1.000	<0.502
YMSC 7	0.036	8.29	0.001	10.60	<0.101	1.070	7.650	<0.252	<0.505	22.40	<0.252	0.136	<0.505	<0.505	<1.000	<0.505
YMSC 7A†	0.040	9.00	0.001	3.71	<0.098	0.316	3.760	0.369	<0.492	10.20	<0.246	0.120	<0.492	<0.492	<0.984	<0.492
YMSC 8	0.031	7.70	0.001	9.28	<0.101	1.100	6.180	<0.252	<0.503	33.10	<0.252	<0.101	<0.503	<0.503	<1.000	<0.503
YMSC 9	0.034	3.14	0.001	12.60	<0.100	1.370	8.120	0.397	<0.501	33.70	<0.251	0.102	0.642	<0.501	<1.000	<0.501
YMSC 10	0.026	1.62	<0.0005	11.70	0.131	1.220	5.010	<0.250	<0.501	29.70	<0.250	0.108	0.633	<0.501	<1.000	<0.501
YMSC 11	0.021	1.08	<0.0005	14.30	<0.100	1.680	5.060	<0.251	<0.502	29.90	<0.251	<0.100	<0.502	<0.502	<1.000	<0.502
YMSC 12	0.023	<1.00	0.001	5.27	<0.100	0.551	4.890	<0.251	<0.501	24.90	<0.251	0.260	<0.501	<0.501	<1.000	<0.501
YMSC 12X	0.019	1.66	0.001	5.34	<0.100	0.789	10.100	<0.250	<0.500	34.30	<0.250	0.166	1.130	<0.500	<0.999	<0.500
YMSC 13	0.026	1.44	0.002	12.90	<0.100	1.670	7.270	<0.251	<0.501	32.40	<0.251	<0.100	<0.501	<0.501	<1.000	<0.501
YMSC 14	0.032	12.90	0.006	5.08	<0.109	0.286	1.260	<0.273	<0.546	18.00	<0.273	0.215	<0.546	<0.546	<1.090	<0.546
YMSC 14A†	0.042	11.10	0.003	3.56	<0.098	0.288	1.460	0.269	<0.492	20.10	<0.246	0.221	<0.492	<0.492	<0.984	<0.492
YMSC14B	0.042	10.80	0.006	4.94	<0.096	0.734	1.890	0.328	<0.481	8.26	<0.240	0.241	<0.481	<0.481	<0.962	<0.481
YMSC 14C	0.367	1.36	<0.0005	2.59	<0.099	0.468	2.290	<0.246	<0.493	27.70	<0.246	0.134	0.515	<0.493	<0.985	<0.493
YMSC 14C*	0.520	1.53	0.003	3.77	<0.099	0.505	2.630	0.273	<0.496	35.60	<0.248	0.172	1.330	<0.489	<0.978	<0.496
YMSC 15	0.028	2.58	0.001	10.10	<0.100	1.420	9.070	<0.250	<0.500	35.20	<0.250	<0.100	<0.500	<0.500	<0.999	<0.500
YMSC 16	0.021	<1.00	<0.0005	5.64	<0.100	0.663	2.760	<0.250	<0.500	20.00	<0.250	0.101	0.517	<0.500	<0.999	<0.500
YMSC 17	0.052	4.73	<0.0005	15.00	<0.101	1.600	8.430	<0.251	<0.503	31.30	<0.251	<0.101	0.665	<0.503	<1.000	<0.503
YMSC 18	0.022	<1.00	<0.0005	12.00	<0.101	1.250	1.640	<0.251	<0.503	15.60	<0.251	0.109	0.620	<0.503	<1.000	<0.503
YMSC 19	0.025	<1.00	<0.0005	13.80	<0.101	1.410	2.630	<0.251	<0.503	19.00	<0.251	0.107	<0.503	<0.503	<1.000	<0.503
YMSC 20	0.027	3.94	0.001	5.13	<0.099	0.462	3.330	<0.248	<0.496	23.30	<0.248	0.115	0.592	<0.496	<0.992	<0.496
YMSC 21	0.021	<1.00	0.001	14.70	<0.100	1.430	3.280	0.257	<0.499	24.00	<0.250	<0.100	0.702	<0.499	<0.998	<0.499
YMSC 22	0.019	2.59	0.001	9.13	<0.100	1.120	20.300	0.323	1.840	63.60	3.190	0.263	1.400	<0.499	<0.998	<0.499
YMSC 22A†	0.032	2.88	0.008	2.57	<0.098	0.523	22.500	0.309	1.990	96.70	3.620	0.273	1.870	<0.488	<0.976	<0.488
YMSC 22S	0.019	3.01	<0.0005	8.79	<0.101	0.799	8.360	<0.252	<0.503	38.40	0.894	0.110	0.560	<0.503	<1.000	<0.503
YMSC 22SA†	0.022	3.43	0.001	0.89	<0.100	0.234	23.700	<0.249	<0.498	56.10	1.840	0.156	<0.498	<0.498	<0.996	<0.498
YMSC 23	0.034	1.40	0.002	15.50	<0.101	1.830	5.060	0.294	<0.503	27.80	<0.252	<0.101	<0.503	<0.503	<1.000	<0.503
YMSC 24	0.033	5.12	0.002	7.56	<0.101	0.495	0.859	<0.252	<0.504	13.90	<0.252	0.102	<0.504	<0.504	<1.000	<0.504
YMSC 24A†	0.029	6.45	<0.0005	2.74	<0.098	0.275	2.330	<0.245	<0.489	13.50	<0.245	0.101	<0.489	<0.489	<0.978	<0.489
YMSC 25	0.021	9.14	0.002	8.79	<0.103	0.650	2.370	<0.256	<0.513	13.20	<0.256	<0.103	<0.513	<0.513	<1.020	<0.513
YMSC 25A†	0.030	10.30	0.003	3.53	<0.098	0.411	3.480	0.269	<0.488	20.60	<0.244	0.105	<0.488	<0.488	<0.977	<0.488
YMSC 26	0.017	<1.00	<0.0005	15.20	<0.100	1.500	6.010	<0.250	<0.501	17.60	<0.250	<0.100	0.978	<0.501	<1.000	<0.501

Sample No.	Ag	As	Au	Cu	Hg	Mo	Pb	Sb	Tl	Zn	Bi	Cd	Ga	Pd	Se	Te
YMSC 27	0.020	<1.00	<0.0005	13.20	<0.100	1.250	2.260	<0.250	<0.501	13.80	<0.250	<0.100	0.924	<0.501	<1.000	<0.501
YMSC 28	0.051	16.20	0.003	1.95	<0.101	0.138	2.380	<0.252	<0.504	4.09	<0.252	0.343	<0.504	<0.504	<1.000	<0.504
YMSC 28A†	0.052	6.58	0.002	2.00	<0.097	0.364	3.800	<0.243	<0.486	17.70	<0.243	0.159	<0.486	<0.486	<0.972	<0.486
YMSC 29	0.027	2.11	<0.0005	12.20	<0.100	1.080	2.210	<0.250	<0.501	26.90	<0.250	<0.100	0.837	<0.501	<1.000	<0.501
YMSC 30	0.028	5.16	0.003	8.48	<0.100	0.284	0.479	<0.250	<0.501	2.18	<0.250	<0.100	<0.501	<0.501	<1.000	<0.501
YMSC 31	0.020	10.40	0.001	9.6	<0.100	1.460	21.800	<0.251	0.580	59.60	0.614	0.133	1.770	<0.502	<1.000	<0.502
YMSC 31A†	0.027	1.77	0.002	1.92	<0.098	1.020	29.100	<0.246	<0.491	67.90	0.916	0.099	0.981	<0.491	<0.982	<0.491
YMSC 31B	0.041	26.70	<0.0005	1.44	<0.099	0.296	5.230	0.271	<0.497	4.71	0.334	0.105	1.320	<0.497	<0.993	<0.497
YMSC 32	0.020	<1.00	<0.0005	13.90	<0.100	1.480	2.130	<0.251	<0.501	31.80	<0.251	<0.100	0.719	<0.501	<1.000	<0.501
YMSC 33	<0.015	2.41	<0.0005	11.60	<0.100	1.080	1.210	<0.251	<0.502	31.80	<0.251	<0.100	0.743	<0.502	<1.000	<0.502
YMSC 34	0.037	16.00	0.001	8.85	<0.111	0.256	6.000	<0.278	<0.556	10.50	<0.278	0.120	0.783	<0.556	<1.110	<0.556
YMSC 34A†	0.039	17.90	0.002	7.32	<0.099	0.252	5.830	<0.247	<0.493	8.03	<0.247	0.105	<0.493	<0.493	<0.986	<0.493
YMSC 35	0.023	3.91	<0.0005	9.86	<0.101	0.906	2.610	<0.252	<0.503	22.80	<0.252	<0.101	1.110	<0.503	<1.000	<0.503
YMSC 36	0.042	11.90	<0.0005	6.15	<0.100	0.318	1.670	<0.251	<0.501	5.46	<0.251	0.102	0.632	<0.501	<1.000	<0.501
YMSC 36A†	0.029	16.10	0.001	5.28	<0.100	0.233	1.450	<0.249	<0.498	4.06	<0.249	<0.100	<0.498	<0.498	<0.995	<0.498
YMSC 37	0.029	3.64	<0.0005	10.80	<0.100	1.040	4.770	<0.250	<0.501	27.30	<0.250	0.146	0.730	<0.501	<1.000	<0.501
YMSC 38	0.049	4.45	0.001	9.73	<0.100	0.750	3.950	<0.251	<0.501	26.20	<0.251	0.147	0.652	<0.501	<1.000	<0.501
YMSC 39	0.031	3.03	<0.0005	9.88	<0.100	1.300	8.440	<0.250	<0.500	39.50	<0.250	<0.100	0.721	<0.500	<0.999	<0.500
YMSC 40	0.022	4.14	0.001	7.53	<0.101	0.929	6.300	<0.251	<0.503	36.00	<0.251	0.111	0.874	<0.503	<1.000	<0.503
YMSC 41	0.029	3.51	<0.0005	14.50	<0.100	1.410	6.610	<0.250	<0.500	27.40	<0.250	<0.100	0.943	<0.500	<1.000	<0.500
YMSC 42	0.026	7.79	0.003	6.03	<0.101	0.254	0.674	<0.251	<0.503	7.36	<0.251	<0.101	<0.503	<0.503	<1.000	<0.503
YMSC 42A†	0.050	12.30	0.001	7.82	<0.100	0.326	2.000	0.294	<0.499	11.90	<0.249	0.122	<0.499	<0.499	<0.997	<0.499
YMSC 43	0.026	1.97	<0.0005	13.50	<0.100	1.470	2.720	<0.250	<0.500	32.30	<0.250	0.146	0.839	<0.500	<1.000	<0.500
YMSC 44	0.032	4.12	0.001	6.41	<0.100	0.258	0.567	<0.251	<0.501	6.67	<0.251	<0.100	<0.501	<0.501	<1.000	<0.501
YMSC 45	0.114	7.40	0.001	6.90	<0.101	0.223	1.560	0.304	<0.505	8.47	<0.252	0.143	0.875	<0.505	<1.000	<0.505
YMSC 45A†	0.092	7.28	<0.0005	3.19	0.141	0.268	1.050	0.332	<0.499	11.20	<0.249	<0.100	<0.499	<0.499	<0.997	<0.499
YMSC 46A	0.017	<1.00	0.001	4.47	<0.100	0.407	4.920	<0.250	<0.500	12.00	<0.250	0.155	<0.500	<0.500	<1.000	<0.500
YMSC 47	<0.015	<1.00	<0.0005	10.90	<0.100	1.140	1.430	<0.250	<0.501	19.50	<0.250	<0.100	0.958	<0.501	<1.000	<0.501
YMSC 48	0.019	<1.00	<0.0005	13.00	<0.100	1.530	1.250	<0.251	<0.501	25.80	<0.251	<0.100	0.862	<0.501	<1.000	<0.501
YMSC 48C	0.027	1.33	0.001	10.20	<0.100	1.180	1.180	<0.250	<0.501	30.70	<0.250	<0.100	1.000	<0.501	<1.000	<0.501
YMSC 49	0.028	4.41	<0.0005	10.50	<0.100	1.110	7.020	<0.251	<0.502	17.30	<0.251	<0.100	0.737	<0.502	<1.000	<0.502
YMSC 49C	0.022	2.47	<0.0005	11.20	<0.100	2.710	3.690	<0.250	<0.500	21.00	<0.250	<0.100	1.450	<0.500	<0.999	<0.500
YMSC 50S	0.029	2.12	<0.0005	17.40	<0.101	2.390	4.190	0.275	<0.505	18.60	<0.252	<0.101	1.220	<0.505	<1.000	<0.505
YMSC 50SA†	0.049	1.80	<0.0005	3.28	<0.100	1.160	5.310	0.340	<0.499	21.90	<0.249	<0.100	0.819	<0.499	<0.997	<0.499
YMSC 50CS	0.021	5.52	<0.0005	7.88	<0.101	0.234	0.743	<0.252	<0.504	5.18	<0.252	<0.101	0.561	<0.504	<1.000	<0.504
YMSC 50CSA†	0.032	6.33	<0.0005	6.52	<0.100	0.474	2.130	<0.250	<0.499	13.90	<0.250	0.102	0.756	<0.499	<0.998	<0.499
YMSC 50CS2	0.024	1.81	<0.0005	11.60	<0.100	1.040	1.240	<0.251	<0.501	20.00	<0.251	<0.100	1.010	<0.501	<1.000	<0.501
YMSC 50CS2A†	0.042	2.71	0.001	3.56	<0.099	0.365	2.280	0.251	<0.497	20.90	<0.248	<0.099	<0.497	<0.497	<0.993	<0.497
YMSC 51	0.035	1.65	0.001	12.20	<0.100	1.210	1.550	0.321	<0.502	19.30	<0.251	<0.100	0.717	<0.502	<1.000	<0.502
YMSC 52	<0.015	1.71	<0.0005	10.50	<0.100	2.870	109.000	0.274	<0.501	39.20	4.320	<0.100	1.280	<0.501	<1.000	<0.501

Sample No.	Ag	As	Au	Cu	Hg	Mo	Pb	Sb	Tl	Zn	Bi	Cd	Ga	Pd	Se	Te
YMSC 52A†	0.028	1.92	<0.0005	2.41	<0.099	4.030	145.000	0.300	<0.497	59.30	6.100	<0.099	1.930	<0.497	<0.993	<0.497
YMSC 53	0.017	1.47	<0.0005	9.73	<0.100	1.050	2.890	<0.250	<0.500	27.80	<0.250	<0.100	0.668	<0.500	<0.999	<0.500
YMSC 54	<0.015	1.38	<0.0005	9.24	<0.100	0.977	0.774	<0.250	<0.501	23.10	<0.250	<0.100	0.661	<0.501	<1.000	<0.501
YMSC 55	0.022	2.02	<0.0005	3.52	<0.100	0.266	1.460	<0.250	<0.501	14.20	<0.250	0.109	<0.501	<0.501	<1.000	<0.501
YMSC 56	0.025	3.11	<0.0005	7.55	<0.100	1.030	15.300	<0.251	<0.502	29.20	<0.251	0.108	1.620	<0.502	<1.000	<0.502
YMSC 57	0.023	1.34	<0.0005	7.16	<0.100	4.490	10.200	<0.251	<0.502	35.50	<0.251	<0.100	2.650	<0.502	<1.000	<0.502
YMSC 58	0.029	2.80	<0.0005	11.80	<0.100	1.390	2.870	<0.251	<0.502	20.50	<0.251	<0.100	0.799	<0.502	<1.000	<0.502
YMSC 59	0.023	1.82	<0.0005	13.80	<0.100	1.900	2.240	<0.251	<0.502	13.00	<0.251	0.122	0.790	<0.502	<1.000	<0.502
YMSC 60	0.042	5.78	<0.0005	18.20	<0.100	1.840	5.520	0.255	<0.501	23.00	<0.250	<0.100	0.653	<0.501	<1.000	<0.501
YMSC 61	0.020	3.41	<0.0005	10.30	<0.100	1.100	1.640	<0.251	<0.501	8.20	<0.251	<0.100	<0.501	<0.501	<1.000	<0.501
YMSC 62	0.025	2.15	0.001	12.10	<0.100	1.330	1.760	<0.251	<0.501	15.60	<0.251	<0.100	0.557	<0.501	<1.000	<0.501
YMSC 63	0.029	1.27	<0.0005	16.30	<0.100	1.660	1.160	0.287	<0.501	14.60	<0.250	<0.100	0.503	<0.501	<1.000	<0.501
YMSC 64	0.021	2.15	<0.0005	12.30	<0.100	1.250	9.190	<0.250	<0.500	19.10	<0.250	<0.100	0.801	<0.500	<1.000	<0.500
YMSC 65	<0.015	3.37	<0.0005	2.46	<0.097	1.550	7.950	<0.244	<0.487	30.40	<0.244	<0.097	<0.487	<0.487	<0.975	<0.487
YMSC 66	0.026	2.56	0.026	2.07	<0.097	1.980	6.260	<0.242	<0.483	24.80	<0.242	<0.097	<0.483	<0.483	<0.966	<0.483
YMSC 66*	0.025	1.57	0.003	2.35	<0.096	0.619	6.210	<0.241	<0.481	28.60	<0.241	<0.096	0.702	<0.481	<0.962	<0.481
YMSC 66A†	0.018	1.60	<0.0005	1.71	<0.100	0.776	6.350	0.305	<0.500	26.50	<0.250	<0.100	<0.500	<0.500	<0.999	<0.500
YMSC 66A*	0.020	1.17	0.002	1.43	<0.099	0.644	5.440	<0.247	<0.494	22.50	<0.247	<0.099	<0.494	<0.494	<0.988	<0.494
YMSC 67	0.026	6.87	0.001	1.88	<0.099	0.639	3.330	<0.248	<0.496	10.90	<0.248	0.126	0.651	<0.496	<0.992	<0.496
YMSC 68	<0.015	4.95	0.001	1.48	<0.097	0.670	4.480	0.514	<0.487	7.58	<0.243	0.642	<0.487	<0.487	<0.974	<0.487
YMSC 69	0.028	12.00	0.001	2.47	<0.100	0.909	6.080	<0.249	<0.498	18.90	<0.249	0.115	0.626	<0.498	<0.996	<0.498
YMSC 69*	0.021	3.42	0.002	2.30	0.110	0.575	7.120	0.348	<0.492	25.70	<0.246	<0.098	0.972	<0.492	<0.984	<0.492
YMSC 69A†	0.033	5.18	<0.0005	2.15	<0.100	0.672	6.810	<0.250	<0.500	22.50	<0.250	<0.100	<0.500	<0.500	<0.999	<0.500
YMSC 70	0.033	3.41	0.002	2.38	<0.096	2.020	6.070	<0.239	<0.479	24.70	<0.239	<0.096	0.587	<0.479	<0.958	<0.479
YMSC 71	0.030	3.11	0.002	2.94	<0.096	0.724	5.260	<0.240	<0.481	29.90	<0.240	0.135	0.528	<0.481	<0.962	<0.481
YMSC 72	0.079	1.27	0.001	2.18	<0.099	2.940	5.370	<0.248	<0.497	31.40	<0.248	<0.099	0.497	<0.497	<0.993	<0.497
YMSC 73	0.030	4.70	0.002	4.19	<0.097	1.090	5.450	<0.243	<0.485	27.30	<0.243	<0.097	<0.485	<0.485	<0.971	<0.485
YMSC 74	0.024	3.08	0.001	2.26	<0.096	2.970	6.970	0.794	<0.479	28.80	<0.239	<0.096	3.320	<0.479	<0.958	<0.479
YMSC 75	0.025	4.10	0.001	3.12	<0.096	1.780	7.240	0.239	<0.478	28.20	<0.239	0.126	0.627	<0.478	<0.955	<0.478
YMSC 76	0.030	3.38	0.002	4.53	<0.098	2.280	8.440	0.547	0.583	34.30	<0.245	<0.098	0.860	<0.489	<0.978	<0.489
YMSC 77	0.035	2.04	0.001	2.73	<0.096	1.230	1.370	<0.239	<0.479	27.70	<0.239	0.114	0.806	<0.479	<0.958	<0.479
YMSC 78	0.043	3.27	0.001	2.73	<0.100	2.130	1.980	0.351	<0.498	44.30	<0.249	0.156	0.970	<0.498	<0.996	<0.498
YMSC 79	0.020	<0.99	0.001	1.30	<0.099	2.100	2.040	0.278	<0.496	17.30	<0.248	0.126	0.882	<0.496	<0.992	<0.496
YMSC 80	0.028	2.18	<0.0005	2.51	<0.099	1.650	2.030	1.510	<0.496	31.90	<0.248	0.141	0.832	<0.496	<0.991	<0.496
YMSC 81	0.025	1.33	0.001	1.29	<0.099	1.590	1.530	<0.247	<0.494	19.20	<0.247	<0.099	0.677	<0.494	<0.987	<0.494
YMSC 81*	<0.015	<0.99	<0.0005	0.87	<0.099	0.351	1.650	<0.247	<0.493	17.30	<0.247	<0.099	0.553	<0.493	<0.986	<0.493
YMSC 82	0.024	2.18	0.001	1.47	<0.097	1.560	1.410	<0.242	<0.483	25.90	<0.242	<0.097	0.821	<0.483	<0.966	<0.483
YMSC 83	0.022	<0.98	0.001	1.21	<0.097	1.800	1.610	<0.244	<0.487	13.30	<0.244	<0.097	0.649	<0.487	<0.975	<0.487
YMSC 84	0.039	5.21	0.001	2.93	<0.096	1.300	6.670	<0.241	0.696	27.50	<0.241	<0.096	<0.482	<0.482	<0.963	<0.482
YMSC 85	0.034	6.35	0.005	2.82	0.360	<0.099	2.840	<0.247	0.969	7.52	0.289	0.433	0.728	<0.494	<0.988	<0.494

Sample No.	Ag	As	Au	Cu	Hg	Mo	Pb	Sb	Tl	Zn	Bi	Cd	Ga	Pd	Se	Te
YMSC 85*	0.051	7.12	0.005	3.58	<0.099	0.165	3.100	<0.248	0.683	7.86	<0.248	0.475	0.858	<0.495	<0.990	<0.495
YMSC 85*	0.092	7.74	0.005	3.91	<0.098	0.191	3.030	0.370	0.713	7.55	<0.245	0.487	1.180	<0.489	<0.978	<0.489
YMSC 86	<0.015	1.98	0.002	1.86	<0.100	0.284	5.400	<0.249	<0.498	28.90	<0.249	<0.100	0.715	<0.498	<0.995	<0.498
YMSC 87	<0.015	3.06	<0.0005	0.59	0.186	0.144	2.330	<0.245	<0.490	15.00	0.353	<0.098	0.735	<0.490	<0.098	<0.490
YMSC 88	0.017	3.94	<0.0005	2.83	0.105	0.324	1.670	0.256	<0.499	15.00	0.993	0.145	1.750	<0.499	<0.998	<0.499
YMSC 89	0.021	1.71	<0.0005	2.03	<0.096	0.820	4.460	<0.241	<0.482	12.70	<0.241	<0.096	1.010	<0.482	<0.963	<0.482
YMSC 90	<0.015	1.16	<0.0005	1.33	0.126	0.899	2.660	<0.246	<0.492	10.90	<0.246	<0.098	0.761	<0.492	<0.984	<0.492
YMSC 91	<0.015	<0.99	0.001	1.06	<0.100	0.414	1.070	<0.247	<0.493	27.80	<0.247	0.270	0.559	<0.493	<0.986	<0.493
YMSC 92	<0.015	<0.98	0.001	0.97	<0.097	0.614	3.320	<0.244	0.908	12.60	0.948	<0.097	0.847	<0.487	<0.975	<0.487
YMSC 93	<0.014	<0.97	0.001	0.97	<0.097	0.156	2.350	<0.241	<0.483	17.60	<0.241	<0.097	0.947	<0.483	<0.965	<0.483
YMSC 94	<0.015	1.16	0.001	1.86	<0.098	0.473	6.340	<0.244	<0.489	38.20	<0.244	0.170	0.672	<0.489	<0.978	<0.489
YMSC 95	<0.015	1.55	<0.0005	1.25	<0.100	0.252	1.670	<0.250	<0.500	19.90	<0.250	<0.100	1.000	<0.500	<0.999	<0.500
YMSC 96	0.029	5.82	0.005	4.80	<0.100	0.163	1.590	0.440	<0.499	9.22	<0.250	<0.100	0.723	<0.499	<0.998	<0.499
YMSC 96*	0.035	5.07	0.003	4.03	<0.099	0.182	1.490	<0.247	<0.494	6.34	<0.247	<0.099	0.650	<0.494	<0.987	<0.494
YMSC 97	0.040	6.33	0.003	3.22	<0.970	0.109	1.130	0.348	<0.485	6.62	<0.242	<0.097	0.759	<0.485	<0.970	<0.485
YMPG 1	0.033	1.46	0.001	19.10	<0.101	2.230	7.140	<0.251	<0.503	27.60	<0.251	<0.101	<0.503	<0.503	<1.000	<0.503
YMPG 2	0.029	1.29	<0.0005	14.50	<0.100	1.520	7.430	<0.251	<0.502	24.20	<0.251	<0.100	0.570	<0.502	<1.000	<0.502
YMPG 3	0.028	<1.01	<0.0005	7.00	<0.101	0.878	5.150	<0.253	<0.506	26.70	<0.253	0.112	0.557	<0.506	<1.010	<0.506
YMPG 3A	0.031	1.30	<0.0005	7.14	<0.100	0.820	4.880	<0.250	<0.501	27.20	<0.250	0.127	0.642	<0.501	<1.000	<0.501
YMPG 4	0.028	1.37	<0.0005	6.71	<0.100	0.761	7.300	<0.250	<0.500	28.00	<0.250	0.115	0.744	<0.500	<1.000	<0.500
YMPG 5	0.027	3.64	<0.0005	10.40	<0.100	0.997	8.680	<0.250	<0.500	38.00	<0.250	0.105	0.881	<0.500	<1.000	<0.500
YMPG 6	0.026	3.54	<0.0005	14.20	<0.100	1.630	8.890	0.295	<0.501	32.00	<0.251	0.115	<0.501	<0.501	<1.000	<0.501
YMPG 7	0.023	1.88	<0.0005	14.90	<0.100	1.750	7.180	0.258	<0.500	25.10	<0.250	<0.100	<0.500	<0.500	<1.000	<0.500
YMPG 7*	0.027	2.08	<0.0005	15.30	<0.100	1.830	7.340	<0.250	<0.501	26.30	<0.250	<0.100	<0.501	<0.501	<1.000	<0.501
YMPG 8	0.020	2.09	<0.0005	11.70	<0.100	1.480	5.900	0.272	<0.501	23.60	<0.250	0.105	<0.501	<0.501	<1.000	<0.501
YMPG 9	0.036	1.65	<0.0005	21.10	<0.100	2.150	6.160	0.407	<0.501	27.30	<0.251	<0.100	0.556	<0.501	<1.000	<0.501
YMPG 10	0.026	3.06	<0.0005	10.70	<0.100	1.040	5.170	<0.251	<0.501	23.70	<0.251	<0.100	0.631	<0.501	<1.000	<0.501
YMPG 11	0.028	1.37	<0.0005	13.20	<0.100	1.470	6.570	<0.251	<0.501	22.40	<0.251	<0.100	<0.501	<0.501	<1.000	<0.501
YMPG 12	0.027	1.32	<0.0005	15.00	0.102	1.660	6.950	<0.251	<0.502	23.30	<0.251	<0.100	0.786	<0.502	<1.000	<0.502
YMPG 13	0.019	1.19	<0.0005	14.10	<0.100	1.390	5.270	<0.250	<0.501	24.90	<0.250	<0.100	<0.501	<0.501	<1.000	<0.501
YMPG 14	0.022	3.86	0.002	10.20	<0.101	0.949	12.300	<0.252	<0.504	31.90	<0.252	0.119	1.320	<0.504	<1.000	<0.504
YMPG 15	0.024	1.60	<0.0005	9.58	<0.100	0.996	8.030	<0.250	<0.500	23.30	<0.250	<0.100	1.040	<0.500	<1.000	<0.500
YMPG 16	0.021	2.22	0.002	6.78	<0.100	0.809	5.330	<0.251	<0.502	23.80	<0.251	0.121	0.719	<0.502	<1.000	<0.502
YMPG 17	0.035	6.23	0.002	9.97	0.106	0.578	2.310	<0.252	<0.504	14.70	<0.252	0.120	0.807	<0.504	<1.000	<0.504
YMPG 18	0.022	1.98	0.006	9.84	<0.100	1.160	8.820	<0.250	<0.501	29.30	<0.250	<0.100	0.878	<0.501	<1.000	<0.501
YMPG 18A†	<0.015	1.72	0.004	1.27	<0.097	0.417	7.480	<0.243	<0.486	29.70	<0.243	<0.097	0.675	<0.486	<0.973	<0.486
YMPG 19	0.017	2.40	0.003	4.15	<0.100	0.220	2.540	<0.250	<0.500	14.30	<0.250	0.130	0.545	<0.500	<1.000	<0.500
YMPG 19A†	0.018	3.25	0.001	2.14	<0.096	0.318	3.390	<0.240	<0.481	22.10	<0.240	<0.096	<0.481	<0.481	<0.962	<0.481
YMPG 20	0.038	2.01	0.001	8.20	<0.100	0.933	5.470	<0.251	0.659	30.50	<0.251	0.114	0.891	<0.501	<1.000	<0.501
YMPG 21	0.030	3.61	<0.0005	6.08	<0.101	0.670	3.950	<0.251	0.565	25.40	<0.251	0.127	0.719	<0.503	<1.000	<0.503
YMPG 22	0.037	4.99	<0.0005	15.70	<0.100	1.780	6.370	0.477	<0.501	29.10	<0.250	<0.100	0.779	<0.501	<1.000	<0.501

Sample No.	Ag	As	Au	Cu	Hg	Mo	Pb	Sb	Tl	Zn	Bi	Cd	Ga	Pd	Se	Te
YMSC 85*	0.051	7.12	0.005	3.58	<0.099	0.165	3.100	<0.248	0.683	7.86	<0.248	0.475	0.858	<0.495	<0.990	<0.495
YMSC 85*	0.092	7.74	0.005	3.91	<0.098	0.191	3.030	0.370	0.713	7.55	<0.245	0.487	1.180	<0.489	<0.978	<0.489
YMSC 86	<0.015	1.98	0.002	1.86	<0.100	0.284	5.400	<0.249	<0.498	28.90	<0.249	<0.100	0.715	<0.498	<0.995	<0.498
YMSC 87	<0.015	3.06	<0.0005	0.59	0.186	0.144	2.330	<0.245	<0.490	15.00	0.353	<0.098	0.735	<0.490	<0.098	<0.490
YMSC 88	0.017	3.94	<0.0005	2.83	0.105	0.324	1.670	0.256	<0.499	15.00	0.993	0.145	1.750	<0.499	<0.998	<0.499
YMSC 89	0.021	1.71	<0.0005	2.03	<0.096	0.820	4.460	<0.241	<0.482	12.70	<0.241	<0.096	1.010	<0.482	<0.963	<0.482
YMSC 90	<0.015	1.16	<0.0005	1.33	0.126	0.899	2.660	<0.246	<0.492	10.90	<0.246	<0.098	0.761	<0.492	<0.984	<0.492
YMSC 91	<0.015	<0.99	0.001	1.06	<0.100	0.414	1.070	<0.247	<0.493	27.80	<0.247	0.270	0.559	<0.493	<0.986	<0.493
YMSC 92	<0.015	<0.98	0.001	0.97	<0.097	0.614	3.320	<0.244	0.908	12.60	0.948	<0.097	0.847	<0.487	<0.975	<0.487
YMSC 93	<0.014	<0.97	0.001	0.97	<0.097	0.156	2.350	<0.241	<0.483	17.60	<0.241	<0.097	0.947	<0.483	<0.965	<0.483
YMSC 94	<0.015	1.16	0.001	1.86	<0.098	0.473	6.340	<0.244	<0.489	38.20	<0.244	0.170	0.672	<0.489	<0.978	<0.489
YMSC 95	<0.015	1.55	<0.0005	1.25	<0.100	0.252	1.670	<0.250	<0.500	19.90	<0.250	<0.100	1.000	<0.500	<0.999	<0.500
YMSC 96	0.029	5.82	0.005	4.80	<0.100	0.163	1.590	0.440	<0.499	9.22	<0.250	<0.100	0.723	<0.499	<0.998	<0.499
YMSC 96*	0.035	5.07	0.003	4.03	<0.099	0.182	1.490	<0.247	<0.494	6.34	<0.247	<0.099	0.650	<0.494	<0.987	<0.494
YMSC 97	0.040	6.33	0.003	3.22	<0.970	0.109	1.130	0.348	<0.485	6.62	<0.242	<0.097	0.759	<0.485	<0.970	<0.485
YMPG 1	0.033	1.46	0.001	19.10	<0.101	2.230	7.140	<0.251	<0.503	27.60	<0.251	<0.101	<0.503	<0.503	<1.000	<0.503
YMPG 2	0.029	1.29	<0.0005	14.50	<0.100	1.520	7.430	<0.251	<0.502	24.20	<0.251	<0.100	0.570	<0.502	<1.000	<0.502
YMPG 3	0.028	<1.01	<0.0005	7.00	<0.101	0.878	5.150	<0.253	<0.506	26.70	<0.253	0.112	0.557	<0.506	<1.010	<0.506
YMPG 3A	0.031	1.30	<0.0005	7.14	<0.100	0.820	4.880	<0.250	<0.501	27.20	<0.250	0.127	0.642	<0.501	<1.000	<0.501
YMPG 4	0.028	1.37	<0.0005	6.71	<0.100	0.761	7.300	<0.250	<0.500	28.00	<0.250	0.115	0.744	<0.500	<1.000	<0.500
YMPG 5	0.027	3.64	<0.0005	10.40	<0.100	0.997	8.680	<0.250	<0.500	38.00	<0.250	0.105	0.881	<0.500	<1.000	<0.500
YMPG 6	0.026	3.54	<0.0005	14.20	<0.100	1.630	8.890	0.295	<0.501	32.00	<0.251	0.115	<0.501	<0.501	<1.000	<0.501
YMPG 7	0.023	1.88	<0.0005	14.90	<0.100	1.750	7.180	0.258	<0.500	25.10	<0.250	<0.100	<0.500	<0.500	<1.000	<0.500
YMPG 7*	0.027	2.08	<0.0005	15.30	<0.100	1.830	7.340	<0.250	<0.501	26.30	<0.250	<0.100	<0.501	<0.501	<1.000	<0.501
YMPG 8	0.020	2.09	<0.0005	11.70	<0.100	1.480	5.900	0.272	<0.501	23.60	<0.250	0.105	<0.501	<0.501	<1.000	<0.501
YMPG 9	0.036	1.65	<0.0005	21.10	<0.100	2.150	6.160	0.407	<0.501	27.30	<0.251	<0.100	0.556	<0.501	<1.000	<0.501
YMPG 10	0.026	3.06	<0.0005	10.70	<0.100	1.040	5.170	<0.251	<0.501	23.70	<0.251	<0.100	0.631	<0.501	<1.000	<0.501
YMPG 11	0.028	1.37	<0.0005	13.20	<0.100	1.470	6.570	<0.251	<0.501	22.40	<0.251	<0.100	<0.501	<0.501	<1.000	<0.501
YMPG 12	0.027	1.32	<0.0005	15.00	0.102	1.660	6.950	<0.251	<0.502	23.30	<0.251	<0.100	0.786	<0.502	<1.000	<0.502
YMPG 13	0.019	1.19	<0.0005	14.10	<0.100	1.390	5.270	<0.250	<0.501	24.90	<0.250	<0.100	<0.501	<0.501	<1.000	<0.501
YMPG 14	0.022	3.86	0.002	10.20	<0.101	0.949	12.300	<0.252	<0.504	31.90	<0.252	0.119	1.320	<0.504	<1.000	<0.504
YMPG 15	0.024	1.60	<0.0005	9.58	<0.100	0.996	8.030	<0.250	<0.500	23.30	<0.250	<0.100	1.040	<0.500	<1.000	<0.500
YMPG 16	0.021	2.22	0.002	6.78	<0.100	0.809	5.330	<0.251	<0.502	23.80	<0.251	0.121	0.719	<0.502	<1.000	<0.502
YMPG 17	0.035	6.23	0.002	9.97	0.106	0.578	2.310	<0.252	<0.504	14.70	<0.252	0.120	0.807	<0.504	<1.000	<0.504
YMPG 18	0.022	1.98	0.006	9.84	<0.100	1.160	8.820	<0.250	<0.501	29.30	<0.250	<0.100	0.878	<0.501	<1.000	<0.501
YMPG 18A†	<0.015	1.72	0.004	1.27	<0.097	0.417	7.480	<0.243	<0.486	29.70	<0.243	<0.097	0.675	<0.486	<0.973	<0.486
YMPG 19	0.017	2.40	0.003	4.15	<0.100	0.220	2.540	<0.250	<0.500	14.30	<0.250	0.130	0.545	<0.500	<1.000	<0.500
YMPG 19A†	0.018	3.25	0.001	2.14	<0.096	0.318	3.390	<0.240	<0.481	22.10	<0.240	<0.096	<0.481	<0.481	<0.962	<0.481
YMPG 20	0.038	2.01	0.001	8.20	<0.100	0.933	5.470	<0.251	0.659	30.50	<0.251	0.114	0.891	<0.501	<1.000	<0.501
YMPG 21	0.030	3.61	<0.0005	6.08	<0.101	0.670	3.950	<0.251	0.565	25.40	<0.251	0.127	0.719	<0.503	<1.000	<0.503
YMPG 22	0.037	4.99	<0.0005	15.70	<0.100	1.780	6.370	0.477	<0.501	29.10	<0.250	<0.100	0.779	<0.501	<1.000	<0.501

Sample No.	Ag	As	Au	Cu	Hg	Mo	Pb	Sb	Tl	Zn	Bi	Cd	Ga	Pd	Se	Te
YMDD 31	0.026	5.61	0.001	8.64	<0.100	0.715	1.340	0.517	<0.502	8.32	<0.251	0.113	0.928	<0.502	<1.000	<0.502
YMDD 32	0.022	7.81	0.002	6.10	<0.100	0.405	1.400	0.305	<0.502	4.22	<0.251	<0.100	0.911	<0.502	<1.000	<0.502
YMDD 34	0.019	3.14	0.002	9.33	<0.100	1.820	2.540	0.352	<0.500	17.30	<0.250	<0.100	1.150	<0.500	<1.000	<0.500
YMDD 35	0.029	1.32	0.001	14.60	<0.100	1.740	2.760	0.556	<0.500	17.30	<0.250	<0.100	1.090	<0.500	<1.000	<0.500
YMDD 36	0.024	4.63	0.003	8.85	<0.100	0.728	3.860	0.459	<0.501	13.60	<0.251	<0.100	1.150	<0.501	<1.000	<0.501
YMDD 36A	0.018	32.30	<0.0005	2.11	0.158	0.413	123.000	<0.245	<0.491	41.10	1.050	0.130	0.809	<0.491	<0.981	<0.491
YMDD 37	0.035	4.55	0.003	3.81	<0.099	1.740	6.820	<0.249	<0.497	26.00	<0.249	<0.099	<0.497	<0.497	<0.994	<0.497
YMDD 38	0.072	6.70	0.003	4.40	<0.097	0.744	4.570	0.251	<0.484	9.63	<0.242	<0.097	0.766	<0.484	<0.967	<0.484
YMDD 38*	<0.015	2.56	0.002	1.44	<0.097	0.835	6.930	<0.243	<0.487	33.80	<0.243	<0.097	<0.487	<0.487	<0.974	<0.487
YMDD 38A	0.016	<0.99	0.001	2.41	<0.099	0.835	8.230	<0.247	<0.493	32.80	<0.247	<0.099	0.629	<0.493	<0.986	<0.493
YMDD 39	0.084	3.22	<0.0005	6.56	<0.096	1.550	8.350	<0.239	<0.478	35.40	<0.239	<0.096	0.485	<0.478	<0.957	<0.482
YMDD 40	0.017	3.62	<0.0005	5.35	<0.096	1.470	7.370	<0.241	<0.482	30.20	<0.241	0.110	<0.482	<0.482	<0.964	<0.482
YMDD 41	0.024	3.08	0.001	5.07	<0.100	1.050	6.460	<0.249	<0.498	43.10	<0.249	0.128	0.504	<0.498	<0.995	<0.498
YMDD 42	0.020	2.19	<0.0005	1.56	<0.096	1.190	1.700	<0.240	<0.481	30.20	<0.240	<0.096	<0.481	<0.481	<0.962	<0.481
YMDD 43	<0.015	7.16	0.001	5.55	<0.100	0.221	0.912	<0.249	<0.498	13.10	<0.249	<0.100	<0.498	<0.498	<0.995	<0.498
YMDD 43*	0.021	8.77	<0.0005	5.92	0.099	0.142	0.971	<0.245	<0.489	9.25	<0.245	<0.098	<0.489	<0.489	<0.978	<0.489
YMDD 44	<0.015	1.72	<0.0005	1.45	<0.098	1.310	1.870	<0.245	<0.490	33.40	<0.245	<0.098	<0.490	<0.490	<0.980	<0.490
YMDD 45	0.022	8.84	0.004	7.08	<0.099	0.322	3.540	<0.247	<0.495	7.82	<0.247	0.158	<0.495	<0.495	<0.989	<0.495
YMDD 45A†	<0.015	6.68	0.001	4.05	<0.098	0.516	4.070	<0.246	<0.492	18.20	<0.246	<0.098	<0.492	<0.492	<0.983	<0.492
YMDD 46	0.020	4.37	0.001	2.42	<0.097	1.880	3.690	<0.242	<0.484	28.70	<0.242	<0.097	<0.484	<0.484	<0.968	<0.484
YMDD 47	<0.015	4.09	<0.0005	2.65	<0.097	1.390	8.720	<0.242	<0.484	40.90	<0.242	<0.097	<0.484	<0.484	<0.969	<0.484
YMDD 48	<0.014	5.23	0.001	2.81	<0.097	1.390	5.630	<0.242	<0.483	36.50	<0.242	<0.097	<0.483	<0.483	<0.966	<0.483
YMDD 49	0.017	2.87	<0.0005	4.81	<0.097	1.030	7.510	<0.243	<0.485	31.70	<0.243	<0.097	0.512	<0.485	<0.971	<0.485
YMDD 50	<0.015	1.92	<0.0005	2.40	<0.099	2.550	4.000	<0.247	<0.495	63.80	<0.247	<0.099	<0.495	<0.495	<0.989	<0.495
YMDD 51A	<0.015	1.82	0.001	5.08	<0.099	0.995	3.030	<0.247	<0.494	15.50	<0.247	<0.099	0.764	<0.494	<0.988	<0.494
YMDD 51B	<0.015	2.74	0.001	2.72	<0.098	2.020	1.980	<0.244	<0.489	14.90	<0.244	<0.098	0.868	<0.489	<0.978	<0.489
YMDD 52	0.019	3.71	0.001	4.26	<0.097	1.050	1.830	<0.242	<0.483	13.00	<0.242	0.097	0.783	<0.483	<0.966	<0.483
YMDD 53	0.015	9.41	0.003	17.90	0.116	0.499	1.060	<0.242	<0.483	12.00	<0.242	0.124	<0.483	<0.483	<0.966	<0.483
YMDD 54	0.027	1.57	0.001	3.94	<0.096	1.570	4.400	<0.239	<0.478	12.20	<0.239	<0.096	0.968	<0.478	<0.956	<0.478
YMDD 55A	0.018	6.18	<0.0005	3.52	<0.096	1.040	1.970	<0.240	<0.480	28.50	<0.240	0.134	0.640	<0.480	<0.961	<0.480
YMDD 55B	<0.014	1.28	0.001	3.89	<0.096	1.130	1.770	<0.240	<0.481	7.36	<0.240	<0.096	0.633	<0.481	<0.962	<0.481
YMDD 55C	<0.015	7.75	0.001	3.25	<0.099	0.826	1.060	<0.247	<0.495	21.00	<0.247	<0.099	<0.495	<0.495	<0.989	<0.495
YMDD 56	0.015	9.26	<0.0005	3.14	<0.099	0.396	1.310	<0.249	<0.497	12.50	<0.249	<0.099	<0.497	<0.497	<0.994	<0.497
YMDD 56*	0.044	5.29	0.002	5.93	0.099	0.241	1.270	<0.239	<0.479	22.80	<0.239	<0.096	0.619	<0.479	<0.958	<0.479
YMDD 57	0.030	6.98	0.003	13.90	<0.097	0.762	1.800	<0.241	<0.483	16.40	<0.241	0.172	0.749	<0.483	<0.965	<0.483
YMDD 58	0.019	4.35	0.001	2.72	<0.095	0.860	0.856	<0.238	<0.477	6.27	<0.238	<0.095	<0.477	<0.477	<0.953	<0.477
YMDD 59	0.033	5.48	0.001	2.40	<0.097	0.397	3.380	<0.242	<0.484	22.50	<0.242	0.148	<0.484	<0.484	<0.967	<0.484
YMDD 60	0.022	1.81	0.001	3.20	<0.098	1.200	2.570	<0.245	<0.490	9.81	<0.245	0.107	0.656	<0.490	<0.979	<0.490
YMJT 1	<0.015	3.60	0.001	1.74	<0.100	0.170	28.700	<0.250	<0.500	22.00	<0.250	<0.100	0.519	<0.500	<0.999	<0.500
YMJT 2	0.016	2.01	0.001	1.55	<0.097	0.529	7.210	<0.241	<0.483	26.10	<0.241	0.136	0.622	<0.483	<0.965	<0.483

Sample No.	Ag	As	Au	Cu	Hg	Mo	Pb	Sb	Tl	Zn	Bi	Cd	Ga	Pd	Se	Te
YMJT 3	0.021	5.59	0.001	6.36	<0.099	0.158	2.080	<0.246	<0.493	9.76	<0.246	0.137	0.501	<0.493	<0.985	<0.493
YMJT 4	<0.015	7.43	0.001	4.57	<0.099	0.141	0.824	<0.247	<0.493	4.40	<0.247	0.130	<0.493	<0.493	<0.986	<0.493
YMJT 5	<0.015	1.64	<0.0005	2.06	0.101	0.475	6.240	<0.242	<0.484	21.20	<0.242	<0.097	<0.484	<0.484	<0.969	<0.484
YMSF 6	0.015	2.29	<0.0005	1.48	<0.097	0.638		<0.243	<0.486	27.50	<0.243	<0.097	0.576	<0.486	<0.972	<0.486
	Bullfrog District															
BH 1	<0.015	4.97	0.001	1.34	<0.097	5.180	10.700	<0.243	<0.487	16.90	<0.243	<0.097	1.310	<0.487	<0.974	<0.487
BH 2	0.821	1.63	0.030	15.00	<0.096	6.120	5.220	<0.241	0.730	33.20	<0.241	0.172	<0.482	<0.482	<0.964	<0.482
BH 3	0.032	<0.96	0.017	0.92	<0.096	2.190	10.800	<0.239	<0.478	6.80	<0.239	<0.096	<0.478	<0.478	<0.956	<0.478
BH 4	5.610	<0.96	4.990	3.07	0.171	4.430	24.700	<0.240	<0.480	6.70	0.335	<0.096	<0.480	<0.480	<0.961	10.900
BH 5	0.171	7.32	0.098	1.84	<0.098	10.100	5.650	0.324	<0.489	10.40	<0.245	<0.098	<0.489	<0.489	<0.978	<0.489
BH 5**	0.179	84.50	0.113	3.11	0.114	5.130	6.560	2.920	<0.485	12.80	<0.242	<0.097	1.070	<0.485	<0.970	<0.485
BH 6	0.163	<0.99	0.189	1.95	<0.099	3.170	6.800	<0.248	<0.495	7.00	<0.248	<0.099	<0.495	<0.495	<0.990	<0.495
BH 7	0.356	2.47	0.110	2.52	<0.099	9.240	5.190	<0.248	<0.496	13.30	<0.248	<0.099	<0.496	<0.496	<0.991	<0.496
BH 8	0.268	3.15	0.144	1.53	1.430	8.960	10.200	<0.244	<0.488	20.40	<0.244	<0.098	0.759	<0.488	<0.977	<0.488
BH 8**	0.292	6.84	0.139	2.38	<0.099	4.440	14.900	0.562	<0.494	21.30	<0.247	<0.099	1.360	<0.494	<0.987	<0.494
BH 9	0.305	<0.96	0.150	2.14	0.186	12.600	0.620	<0.240	<0.480	4.30	<0.240	<0.096	<0.480	<0.480	<0.961	<0.480
BH 10	0.484	18.10	1.310	1.54	0.133	3.780	8.560	0.367	<0.488	75.70	<0.244	<0.098	0.542	<0.488	<0.976	<0.488
BH 11	0.046	5.88	0.023	1.76	<0.097	8.990	10.400	<0.241	<0.483	28.00	<0.241	<0.097	1.630	<0.483	<0.965	<0.483
BH 12	0.075	<0.96	0.047	1.63	<0.096	5.070	2.330	<0.241	<0.482	49.90	<0.241	<0.096	<0.482	<0.482	<0.963	<0.482
BH 13	0.032	6.30	0.005	1.83	<0.096	8.350	12.100	<0.240	<0.480	5.00	<0.240	<0.096	0.506	<0.480	<0.961	<0.480
BH 13A	0.223	24.30	0.014	3.33	0.107	2.350	21.800	1.370	<0.482	22.00	<0.241	<0.096	1.680	<0.482	<0.963	<0.482
BH 14	0.034	8.13	0.002	2.02	<0.099	2.480	9.370	0.314	<0.493	12.00	<0.247	<0.099	0.862	<0.493	<0.986	<0.493
BH 14**	0.069	19.00	0.004	3.28	<0.100	1.350	16.900	0.944	<0.499	13.00	<0.250	<0.100	1.570	<0.499	<0.998	<0.499
BH 15	0.464	2.16	0.020	27.90	<0.099	5.590	8.690	1.050	0.890	18.70	0.929	<0.099	<0.493	<0.493	<0.985	<0.493
BH 16	1.790	7.71	0.079	121.00	<0.099	4.480	8.120	1.970	0.766	16.90	1.290	<0.099	<0.494	<0.494	<0.988	<0.494
BH 18	3.860	11.70	0.023	63.30	<0.098	8.520	6.210	1.730	1.250	18.90	0.801	0.118	<0.490	<0.490	<0.980	5.020
BH 19	1.630	15.30	0.106	87.20	<0.098	3.180	3.350	3.360	0.530	28.90	<0.244	0.260	<0.488	<0.488	<0.976	<0.488
BH 20	1100.000	355.00	117.000	5160.00	<0.100	8.100	91.300	494.000	<0.500	26.60	19.100	1.420	<0.500	<0.500	<1.000	<0.500
BH 21	5.230	30.30	1.350	26.70	<0.098	5.490	9.340	4.890	<0.488	10.50	<0.244	<0.098	<0.488	<0.488	<0.977	<0.488
BH 21B	5.700	<0.98	0.171	34.20	<0.098	7.750	5.140	6.280	0.556	2.70	0.516	<0.098	<0.489	<0.489	<0.978	<0.489
BH 22	2.530	3.36	0.463	4.57	0.268	3.990	9.850	0.717	0.551	10.80	<0.244	<0.097	<0.487	<0.487	<0.975	<0.487
BH 23	1.090	5.73	0.060	7.28	<0.096	9.260	15.500	1.350	1.330	58.60	<0.241	0.213	<0.482	<0.482	<0.964	<0.482
BH 24	0.669	17.50	0.466	2.97	<0.097	6.260	7.310	3.190	0.556	15.80	0.298	<0.097	<0.486	<0.486	<0.973	<0.486
BH 25	0.417	<0.96	0.025	3.16	<0.096	4.810	6.670	0.628	0.509	4.40	<0.239	<0.096	<0.478	<0.478	<0.956	<0.478
BH 25**	0.090	4.30	0.012	2.55	<0.097	1.040	4.830	0.549	<0.484	5.90	<0.242	<0.097	1.080	<0.484	<0.969	<0.484
BH 26	0.678	<0.98	1.220	1.82	<0.098	3.960	1.680	<0.244	0.657	3.40	<0.244	<0.098	<0.488	<0.488	<0.976	<0.488
BH 27	0.258	4.46	0.003	2.67	<0.099	2.650	5.400	0.561	<0.493	6.00	<0.247	<0.099	1.000	<0.493	<0.986	<0.493
BH 28	1.290	26.00	0.300	4.14	<0.100	3.660	12.500	0.995	<0.498	19.80	<0.249	<0.100	0.648	<0.498	<0.996	<0.498
BH 29	0.170	44.00	0.087	3.35	1.080	2.450	10.000	1.190	<0.481	33.40	<0.241	<0.096	1.410	<0.481	<0.962	<0.481
BH 29B	0.370	32.50	0.466	3.27	1.220	2.980	6.810	1.190	<0.494	28.30	<0.247	0.100	1.160	<0.494	<0.987	<0.494

Sample No.	Ag	As	Au	Cu	Hg	Mo	Pb	Sb	Tl	Zn	Bi	Cd	Ga	Pd	Se	Te
BH 29V	0.412	5.74	0.421	2.70	<0.097	3.140	1.740	0.849	<0.487	11.90	<0.243	<0.097	1.010	<0.487	<0.974	<0.487
BH 29V**	0.949	2.43	1.520	2.68	<0.098	2.210	1.290	0.527	<0.489	7.50	<0.245	<0.098	0.530	<0.489	<0.978	<0.489
BH 30	0.089	9.01	0.012	4.22	<0.096	1.570	13.600	0.851	0.520	52.30	<0.241	0.109	5.370	<0.482	0.966	<0.482
BH 31	0.207	25.40	<0.0005	11.30	<0.099	3.670	12.100	2.100	<0.494	39.80	0.429	<0.099	1.830	<0.494	<0.988	0.587
BH 32	0.031	2.70	0.001	2.19	<0.099	0.670	8.040	0.783	<0.494	26.70	<0.247	0.147	2.510	<0.494	1.060	<0.494
BH 33	0.037	2.89	0.001	2.21	<0.097	1.190	12.000	0.844	<0.487	9.50	<0.244	<0.097	1.490	<0.487	<0.975	<0.487
BH 34	0.035	3.87	<0.0005	1.47	<0.097	0.990	9.900	0.451	<0.486	33.70	<0.243	<0.097	1.510	<0.486	<0.972	<0.486
BH 34G	0.044	1.87	<0.0005	2.22	<0.098	1.160	5.060	0.389	<0.490	11.40	<0.245	<0.098	1.540	<0.490	<0.979	<0.490
BH 35	0.053	9.16	<0.0005	1.82	<0.100	1.100	8.370	0.676	<0.500	19.60	<0.250	<0.100	2.000	<0.500	<1.000	<0.500
BH 37	0.059	15.80	<0.0005	2.43	<0.098	1.240	16.700	1.640	<0.492	64.00	<0.246	<0.098	3.170	<0.492	<0.983	<0.492
BH 36	<0.015	<0.97	0.001	3.59	0.106	8.780	53.000	<0.242	<0.485	48.90	<0.242	2.030	1.160	<0.485	<0.970	<0.485
BH 38	0.051	5.42	<0.0005	13.70	0.216	0.580	4.690	0.560	<0.483	39.90	<0.241	<0.097	1.920	<0.483	<0.965	<0.483
BH 39	0.852	4.23	1.050	2.74	<0.096	0.810	24.600	0.609	<0.482	7.40	<0.241	<0.096	1.930	<0.482	<0.964	<0.482
BH 39**	0.026	7.90	0.012	2.20	<0.097	1.900	15.300	0.519	<0.487	8.20	<0.243	<0.097	1.660	<0.487	<0.974	<0.487
BH 40	0.037	1.50	<0.0005	0.98	<0.097	0.760	5.690	0.290	<0.485	6.60	<0.242	<0.097	1.190	<0.485	<0.970	<0.485
BH 41	0.052	3.85	<0.0005	1.79	<0.098	1.860	6.620	0.737	<0.491	10.80	<0.246	<0.098	1.350	<0.491	<0.982	<0.491
BH 42	0.042	5.73	<0.0005	2.39	<0.098	1.070	15.600	0.594	<0.491	13.60	<0.245	<0.098	1.490	<0.491	1.030	<0.491
BH 43	0.034	2.41	<0.0005	0.86	<0.098	1.130	6.740	0.405	<0.488	8.20	<0.244	<0.098	1.550	<0.488	<0.977	<0.488
	Mother Lode Mine, surface samples															
GEXA 1	0.190	121.00	0.031	4.10	<0.100	4.840	4.110	6.930	<0.500	33.80	<0.250	0.124	0.819	<0.500	1.010	<0.500
GEXA 2	0.165	122.00	0.029	4.25	<0.098	3.820	4.090	8.220	<0.491	33.50	<0.246	0.129	0.753	<0.491	<0.982	<0.491
GEXA 3	1.990	713.00	3.510	4.75	0.246	0.950	8.360	23.400	0.999	2.60	<0.243	<0.097	2.060	<0.485	<0.971	1.810
GEXA 4	0.081	521.00	0.048	7.37	0.405	2.390	7.110	19.700	<0.488	31.20	<0.244	<0.098	1.680	<0.488	1.660	<0.488
GEXA 5	3.870	3874.00	7.470	33.10	4.020	13.500	21.900	64.500	5.150	171.00	<0.243	0.378	0.993	<0.486	2.030	5.220
GEXA 6	0.305	550.00	0.783	10.00	0.188	2.190	17.900	23.300	1.270	87.50	<0.248	0.137	1.290	<0.496	1.160	0.585
GEXA 7	0.283	117.00	0.462	2.25	0.103	0.820	9.570	16.200	<0.500	4.50	<0.250	<0.100	1.280	<0.500	<1.000	0.701
GEXA 8	1.380	696.00	0.276	3.99	0.712	1.570	7.990	21.300	0.997	247.00	<0.242	0.109	1.310	<0.484	<0.986	0.564
GEXA 9	2.260	328.00	1.070	17.60	0.890	5.150	93.700	2077.00	3.570	91.20	<0.244	0.440	<0.487	<0.487	<0.975	2.700
GEXA 10	2.400	289.00	1.590	16.30	1.890	3.460	32.400	673.000	0.780	45.60	<0.246	0.123	<0.491	<0.491	<0.982	1.320
GEXA 11	0.029	7.53	0.010	1.27	<0.099	0.450	4.120	14.300	<0.497	3.60	<0.249	<0.099	1.710	<0.497	<0.994	<0.497
GEXA 11A	0.047	12.70	0.013	1.04	<0.096	0.830	9.150	6.250	<0.482	3.80	<0.241	<0.096	20.000	<0.482	<0.964	<0.482
GEXA 11A**	<0.015	8.42	0.016	1.21	<0.099	1.260	6.290	<0.248	<0.497	1.90	<0.248	<0.099	11.900	<0.497	<0.993	<0.497
GEXA 12	0.162	339.00	0.003	7.19	5.250	2.010	10.200	7.630	<0.499	33.10	<0.249	<0.100	<0.499	<0.499	<0.997	<0.499
GEXA 12A	0.544	1581.00	0.110	6.70	4.780	3.310	15.100	21.400	<0.497	95.40	<0.249	0.149	<0.497	<0.497	8.320	<0.497
GEXA 13	0.038	156.00	0.026	4.60	4.030	6.110	2.130	9.170	<0.479	261.00	<0.239	0.651	<0.479	<0.479	<0.958	<0.479
GEXA 14	0.071	68.20	0.237	6.09	0.110	0.910	2.800	3.340	<0.488	6.70	<0.244	<0.098	<0.488	<0.488	<0.977	<0.488
GEXA 15	0.241	89.30	0.175	6.02	<0.100	0.360	3.060	2.470	<0.500	4.90	<0.250	0.102	<0.500	<0.500	<1.000	<0.500
GEXA 16	0.769	38.70	0.172	2.58	0.361	0.430	5.240	3.050	<0.494	11.60	<0.247	0.639	<0.494	<0.494	<0.988	<0.494
GEXA 17	0.033	5.77	0.006	1.26	<0.099	1.380	3.860	0.515	<0.494	3.20	<0.247	<0.099	<0.494	<0.494	<0.988	<0.494
GEXA 18	0.045	17.00	0.005	1.32	<0.098	4.110	2.910	1.750	<0.490	3.00	<0.245	<0.098	4.530	<0.490	<0.980	<0.490
GEXA 19	0.121	44.30	0.001	2.85	0.368	8.610	4.490	1.730	<0.496	51.10	<0.248	1.030	3.290	<0.496	5.080	0.553
GEXA 20	0.025	14.00	0.002	5.35	<0.097	1.200	17.700	0.867	<0.487	32.20	<0.243	<0.097	<0.487	<0.487	<0.974	<0.487

Sample No.	Ag	As	Au	Cu	Hg	Mo	Pb	Sb	Tl	Zn	Bi	Cd	Ga	Pd	Se	Te
GEXA 21	0.065	2.49	0.004	5.22	<0.100	8.510	3.470	1.440	<0.498	6.00	<0.249	<0.100	<0.498	<0.498	<0.996	<0.498
GEXA 22	0.220	1.63	0.001	2.72	<0.099	5.100	9.240	0.492	<0.493	3.10	<0.247	<0.099	<0.493	<0.493	<0.986	<0.493
GEXA 23	0.038	12.50	0.001	2.30	<0.099	5.930	6.820	0.733	<0.494	4.80	<0.247	<0.099	5.180	<0.494	<0.988	<0.494
GEXA 24	0.297	27.30	0.869	1.62	<0.098	0.520	6.850	1.230	<0.490	<1.00	<0.245	<0.098	<0.490	<0.490	<0.979	<0.490
GEXA 25	0.134	8.49	0.003	2.97	<0.098	4.630	0.580	<0.246	<0.492	1.20	<0.246	<0.098	0.838	<0.492	<0.983	<0.492
GEXA 26	<0.014	17.40	0.006	1.84	<0.096	2.160	4.120	0.284	<0.482	2.40	<0.241	<0.096	2.070	<0.482	<0.964	<0.482
GEXA 27	0.046	5.08	0.035	4.04	<0.098	1.030	2.360	<0.245	<0.491	7.30	<0.245	<0.098	0.886	<0.491	<0.981	<0.491
GEXA 28	0.060	4.42	0.018	1.35	0.483	16.300	1.520	1.340	<0.500	4.10	<0.250	<0.100	<0.500	<0.500	<1.000	<0.500
GEXA 29	0.170	10.00	0.152	2.56	1.050	32.900	2.810	2.690	<0.491	13.70	<0.246	0.127	<0.491	<0.491	<0.982	<0.491
GEXA 30	0.167	44.40	0.091	5.69	0.317	45.200	4.420	2.970	<0.495	10.60	<0.247	<0.099	<0.495	<0.495	<0.989	<0.495
GEXA 31	0.096	5.00	0.271	7.35	5.870	1.950	1.690	1.110	<0.492	5.50	<0.246	<0.098	0.706	<0.492	<0.983	<0.492
GEXA 33	<0.015	53.70	0.054	2.71	1.090	7.510	14.400	6.270	<0.487	<1.00	1.680	<0.097	1.290	<0.487	1.470	<0.487
GEXA 34	0.312	2225.00	3.070	41.50	1.640	34.400	10.400	41.000	<0.480	18.90	<0.240	0.282	<0.480	<0.480	5.510	1.620
FC 1	<0.015	35.10	0.223	2.10	0.449	2.070	9.350	3.250	<0.486	40.70	<0.243	<0.097	0.616	<0.486	<0.973	<0.486
Montgomery-Shoshone Mine																
MS 1	95.500	31.30	13.900	4.70	0.133	8.910	4.440	0.709	<0.489	13.90	<0.244	<0.098	0.806	<0.489	1.910	<0.489
MS 2	4.280	45.40	0.908	3.30	<0.099	4.520	14.600	1.180	<0.496	30.20	<0.248	<0.099	2.200	<0.496	<0.992	<0.496
MS 3	12.700	13.70	3.140	3.31	<0.098	5.670	2.330	0.960	<0.491	17.80	<0.245	<0.098	0.673	<0.491	<0.981	<0.491
MS 3**	6.640	24.00	0.730	2.99	0.145	2.650	6.390	0.450	<0.497	24.60	<0.249	<0.099	2.380	<0.497	<0.994	<0.497
MS 4	4.880	12.40	0.239	3.46	0.344	8.300	5.950	0.621	<0.488	49.50	<0.244	<0.098	0.752	<0.488	<0.976	<0.488
MS 5	3.720	5.09	0.067	2.01	0.199	4.810	2.280	0.852	<0.500	10.80	<0.250	<0.100	<0.500	<0.500	<0.999	<0.500
MS 5VN	1.120	71.70	0.115	4.52	<0.098	429.000	37.600	3.120	<0.492	34.60	<0.246	0.157	<0.492	<0.492	<0.984	<0.492
MS 6	0.095	18.40	0.011	25.80	<0.098	4.500	5.790	0.477	<0.492	64.00	<0.246	0.133	9.550	<0.492	<0.984	<0.492
Gold Bar Mine																
GB 1	0.053	5.39	0.006	2.48	<0.098	0.530	7.480	<0.245	<0.490	24.00	<0.245	<0.098	<0.490	<0.490	<0.980	<0.490
GB 2	0.331	1.82	0.016	4.38	<0.097	3.650	11.100	0.488	<0.484	12.00	<0.242	<0.097	<0.484	<0.484	<0.968	<0.484
GB 3	0.266	3.02	0.019	3.49	<0.100	2.810	12.200	0.418	<0.499	14.40	<0.250	<0.100	<0.499	<0.499	<0.998	<0.499
GB 4	0.244	5.08	0.080	14.40	<0.098	0.750	2.550	1.000	<0.488	34.40	<0.244	<0.098	5.110	<0.488	<0.976	<0.488
GB 5	0.144	1.65	0.018	13.10	<0.100	0.700	2.570	0.810	<0.500	34.40	<0.250	0.127	4.060	<0.500	<1.000	<0.500
Wahmonie District																
W 1	0.148	1.13	0.004	2.80	<0.097	2.980	1.820	0.495	<0.487	1.10	<0.243	<0.097	<0.487	<0.487	<0.974	<0.487
W 2	0.048	48.70	0.010	5.93	<0.097	6.760	17.800	2.140	<0.487	14.90	0.703	<0.097	0.575	<0.487	<0.974	1.070
W 3	0.142	36.10	0.002	45.00	0.193	4.640	22.500	3.720	<0.489	19.50	1.140	<0.098	0.529	<0.489	1.390	1.920
W 4	0.106	42.70	0.006	29.00	0.160	3.470	4.860	9.870	<0.490	19.50	0.610	<0.098	0.527	<0.490	<0.979	0.790
W 5	3.470	8.44	0.445	5.20	0.293	3.870	2.150	1.570	<0.495	3.50	1.600	<0.099	<0.495	<0.495	<0.990	6.240
W 6	0.080	23.20	0.004	3.14	<0.097	3.180	6.500	1.640	<0.484	4.30	<0.242	<0.097	0.675	<0.484	<0.969	0.546
W 7	1.340	360.00	0.080	10.40	0.180	2.940	9.170	1.030	<0.491	5.60	1.290	0.268	0.514	<0.491	2.000	2.600
W 8	0.076	106.00	0.002	13.00	<0.098	8.340	9.960	3.010	<0.492	10.10	<0.246	<0.098	1.050	<0.492	1.720	1.480
W 9	0.174	11.20	0.001	4.49	<0.098	4.060	30.500	0.246	<0.489	<1.00	1.450	<0.098	<0.489	<0.489	1.100	0.806
W 10	0.404	117.00	0.013	12.20	<0.099	1.680	5.480	3.110	<0.495	3.80	0.502	<0.099	0.782	<0.495	1.120	1.340
W 11	2.210	49.30	0.012	24.30	<0.100	2.610	6.850	1.910	<0.500	1.40	6.470	<0.100	<0.500	<0.500	1.070	4.450
W 12	45.900	7.38	0.202	2.24	1.820	4.690	1.450	0.742	<0.497	20.20	<0.248	<0.099	<0.497	<0.497	<0.993	10.300

† analysis of resampled material
* reanalysis of original sample
** reanalysis of hand sample
See Castor et al. (1990) for sample descriptions and analytical methods.

Weiss et al. (1989)

PRECIOUS METALS AND INDICATOR-ELEMENT ABUNDANCES IN ROCK-CHIPSAMPLES FROM TRENCH 14
(expressed in parts per million)

	Ag	As	Au	Cu	Hg	Mo	Pb	Sb	Tl	Zn	Bi	Ga	Se	Te
1)	0.034	7.93	0.004	7.16	0.122	0.587	7.75	<0.247	<0.494	23.8	0.504	<0.494	<0.988	<0.494
2)	0.423	110	0.005	27.9	0.799	65.3	154	24.6	<0.49	33.2	<0.249	1.90	<0.995	<0.497
3)	0.031	7.31	0.002	4.52	0.147	0.422	5.31	<0.245	<0.497	19.0	<0.245	<0.49	<0.979	<0.49
4)	0.048	15.6	0.004	11.1	0.373	1.23	16.4	10.1	<0.488	90.8	<0.244	<0.488	<0.977	<0.488
5)	<0.015	5.89	0.001	2.71	0.349	1.80	10.7	2.90	<0.498	147	<0.249	<0.498	<0.996	<0.498
6)	0.048	11.2	0.001	4.11	0.553	2.29	14.8	6.36	<0.492	75.5	<0.246	<0.492	<0.984	<0.492
7)	0.049	11.2	0.002	2.95	2.02	1.58	46.6	2.89	<0.492	892	<0.246	<0.492	<0.983	<0.492
8)	0.141	14.1	0.001	14.4	3.08	2.54	78.6	8.69	<0.487	344	<0.244	<0.487	<0.975	<0.487

1) 3SW195A: north wall, silicified breccia of Tiva Canyon Member with light brown silica veins. **

2) 3SW195B: north wall, fractured Tiva Canyon Member with weak silicification, ± drusy quartz in lithophysae. **

3) 3SW197: south wall, silicified breccia of Tiva Canyon Member with light brown silica veinlets and later(?) buff-colored silica-carbonate fillings. **

4) 3SW329: south wall, siliceous buff to white carbonate vein filling. *

5) 3SW331: south wall, dark purplishsilicified breccia of Tiva Canyon Member between calcareous veins. *

6) 3SW333: south wall, siliceous margin of 1-2 cm thick white calcareous vein. Margin is composed of buff to light brown silica vein material containing small, dark colored, silica-replaced fragments of Tiva Canyon Member. *

7) 3SW335: north wall, silicified breccia of Tiva Canyon Member with bleached groundmass surrounding drusy quartz-lined lithophysal cavities, ~ 2 meters east of thick, white, calcareous vein. *

8) 3LT029: south wall, silicified breccia of Tiva Canyon Member, purplish rock fragments in buff siliceous matrix. *

Analyses by Geochemical Services Inc., using inductively-coupled plasma emission spectrography; * = 10 gram digestion; ** = 15 gram digestion; k = x103. Values as reported by G.S.I.; number of significant figures does not indicate precision or accuracy of analyses.

Weiss . (1989)

PRECIOUS METALS AND INDICATOR-ELEMENT ABUNDANCES IN ROCK-CHIP AND SOIL SAMPLES FROM MINE MOUNTAIN
(expressed in parts per million)

	Ag	As	Au	Cu	Hg	Mo	Pb	Sb	Tl	Zn	Bi	Cd	Ga	Se	Te
1)	0.038	<0.97	0.004	18.8	0.389	0.767	1.85	<0.243	<0.485	1.51	1.22	<0.097	<0.485	<0.97	<0.485
2)	0.033	6.94	0.002	3.18	0.44	0.884	7.95	1.16	<0.495	2.32	<0.247	0.138	0.878	<0.989	<0.495
3)	1.41	782	0.203	92.7	38.4	0.647	180	51.4	<0.484	259	<0.242	6.34	6.55	1.64	<0.484
4)	7.56	11.2k	0.578	464	201	1.54	14.8k	459	<5	3019	<2.5	211	<5	17.9	<5
5)	2.18	8998	0.301	267	18.2	<1	17.6k	2722	<5	1771	<2.5	48.7	<5	12.9	<5
6)	0.028	27.9	0.011	76	0.206	2.06	14.2	1.84	<0.496	145	<0.248	0.14	2.19	<0.991	<0.496
7)	3.62	374	0.132	35.6	11.2	4.62	2812	448	<0.484	1541	<0.242	25.6	2.32	1.92	0.679
8)	1.14	163	0.054	7.04	4.29	17.7	689	181	0.871	42.4	<0.25	0.764	1.23	<0.999	<0.5
9)	18.8	320	0.063	531	624	21.8	7340	301	<4.58	100k	<2.29	864	<4.58	<9.17	<4.58
10)	1.97	1508	0.113	41.8	16.8	4.34	4108	754	<0.49	705	0.410	17.5	2.22	5.48	<0.49
11)	0.245	85.4	0.06	45.9	8.09	3.08	130	12.1	<0.491	1385	<0.245	10.5	0.982	1.50	<0.491
12)	0.694	7357	0.183	33.7	3.50	5.95	186	22.3	1.07	1529	<0.241	12.2	0.866	3.53	<0.483
13)	0.04	14.8	<0.0005	2.31	0.815	0.319	28.3	2.33	<0.49	186	<0.245	1.12	<0.49	<0.98	<0.49
14)	0.147	30.4	0.014	64.0	0.561	6.18	17.2	2.45	<0.491	156	<0.246	0.395	0.879	2.50	<0.491
15)	0.124	59.4	0.004	2.51	2.23	15.7	47.4	185	<0.484	223	<0.242	2.14	4.04	<0.967	<0.484
16)	0.242	408	0.014	12.7	16.5	23.2	213	301	<0.488	573	<0.244	1.97	<0.488	<0.977	<0.488
17)	7.58	110	<0.005	55.5	272	<0.926	4630	195	<4.63	146k	<2.31	269	<4.63	<9.25	<4.63
18)	7.64	315	0.022	15.5	22.7	10.8	5100	572	<0.5	1106	<0.25	18.0	0.621	<0.999	<0.5
19)	0.406	82	0.023	6.90	16.7	14.1	268	131	0.483	399	<0.238	1.64	2.17	<0.952	<0.476
20)	77.9	389	0.073	40.6	428	324	23.2k	2920	<0.5	6805	<2.5	74.6	<5	34.7	<5
21)	0.873	688	0.004	11.0	22.9	22.9	410	130	1.54	7358	<0.249	10.2	9.23	3.27	0.753

1) 3SW191: silicified, partly acid-leached Ammonia Tanks Mmbr.(?), S flank of Mine Mtn.**

2) 3SW201: argillic altered Topopah Springs Mmbr.(?), S flank of Mine Mtn.**

3) 3SW207: quartz-calcite cemented hydrothermal breccia cutting shaly Eleana Fm.**

4) 3SW209: same structure as 3SW207.**

5) 3SW211: quartz-calcite stockwork along same high-angle structure as host to 3SW207.**

6) 3SW215: "soil" of altered shaly Eleana Fm.**

7) 3SW279: barite-quartz vein near retort by Mine Mtn. road.**

8) 3SW281: hydrothermal breccia within silicified Ddn.**

9) 3SW305: leached and silicified porous Ddn, visible cinnabar.*

10) 3SW307: Quartz vein along high-angle structure in shaly Eleana visible cinnabar.*

11) 3SW311: altered Eleana Fm., NW of hilltop 5443, NW flank of Mine Mtn.*

12) 3SW313: silicified breccia in Eleana Fm., NW flank of Mine Mtn.*

13) 3SW319B: calcite veined massive Ddn.*

14) 3SW323A: "soil" of Eleana Fm.*

15) 3SW327A: dark, siliceous hydrothermal breccia with fragments of barite, "blow-out" in Ddn at SW-most shaft on Mine Mtn.*

16) 3LT005: silicified Ddn in adit on crest of Mine Mtn.*

17) 3LT017: silicified, Feox-rich Ddn, crest of Mine Mtn.*

18) 3LT019: barite- and quartz-veined silicified Ddn, crest of Mine Mtn.*

19) 3LT023: Feox-rich hydrothermal breccia in altered Ddn, crest of Mine Mtn.*

20) 3LT025: dump sample, portal of adit near crest of Mine Mtn., cinnabar yellow specks and grey sulphide(?).*

21) 3LT027: vuggy gossan associated with hydrothermal breccia at southwesternmost shaft, "blow-out" in Ddn.*

Analyses by Geochemical Services Inc., using inductively-coupled plasma emission spectrography * = 10 gram digestion; ** =15 gram digestion; k = x103. Values as reported by G.S.I.; number of significant figures does not indicate precision or accuracy of analyses.

References Cited in Part II

Castor, S. B., Feldman, S., and Tingley, J. V., 1990, Mineral evaluation of the Yucca Mountain Addition, Nye County, Nevada: Nevada Bureau of Mines and Geology, Open-file Report 90-4, 80 pp.

Weiss, S. I., Noble, D. C., and Larson, L. T., 1989, Task 3: Evaluation of mineral resource potential, caldera geology and volcano-tectonic framework at and near Yucca Mountain; report for July, 1988 - September, 1989: Center for Neotectonic Studies, University of Nevad-Reno, 38 p. plus appendices.

Weiss, S. I., Noble, D. C., and Larson, L. T., 1990, Task 3: Evaluation of mineral resource potential, caldera geology and volcano-tectonic framework at and near Yucca Mountain; report for October, 1989 - September, 1990: Center for Neotectonic Studies, University of Nevad-Reno, 33 p. plus appendices.

Weiss, S. I., Noble, D. C., and Larson, L. T., 1991, Task 3: Evaluation of mineral resource potential, caldera geology and volcano-tectonic framework at and near Yucca Mountain; report for October, 1990 - September, 1991: Center for Neotectonic Studies, University of Nevad-Reno, 37 p. plus appendices.

Weiss, S. I., Noble, D. C., and Larson, L. T., 1992 Task 3: Evaluation of mineral resource potential, caldera geology and volcano-tectonic framework at and near Yucca Mountain; report for October, 1991 - September, 1992: Center for Neotectonic Studies, University of Nevad-Reno, 44 p. plus appendices.

Weiss, S. I., Noble, D. C., and Larson, L. T., 1993, Task 3: Evaluation of mineral resource potential, caldera geology and volcano-tectonic framework at and near Yucca Mountain; report for October, 1992 - September, 1993: Center for Neotectonic Studies, University of Nevad-Reno, 41 p. plus appendices.

Weiss, S. I., Noble, D. C., and Larson, L. T., 1994, Task 3: Evaluation of mineral resource potential, caldera geology and volcano-tectonic framework at and near Yucca Mountain; report for October, 1993 - September, 1994: Center for Neotectonic Studies, University of Nevad-Reno, XXX p. plus appendices.

TASK 4 ANNUAL REPORT
October 1993 - September 1994
James N. Brune and Rasool Anooshehpoor

OBJECTIVES

1. YUCCA MOUNTAIN MICROEARTHQUAKE NETWORK OPERATION AND DATA ANALYSIS

2. THREE-STATION BROADBAND REGIONAL NETWORK OPERATION AND DATA ANALYSIS

Objective 1: Yucca Mountain Microearthquake Network (YMMN) Operation and Data Analysis

Instrumentation

Most previous microearthquake studies have been carried out with temporary portable seismographs. However, because of the importance of the site, we felt microearthquakes should be monitored as close to continuously as possible. Therefore we decided to transmit data continuously back to the Seismological Laboratory at the University of Nevada, Reno. This was accomplished via radio links to a nearby microwave relay station (see Fig. 1). Four sites were selected, two on Yucca Mountain near the Solitario Canyon fault (YNB and YYM), one about 5 km to the west in Crater Flat (YCF), and one still further west on Black Cone (YBC) near the center of Crater Flat. The instrumentation and telemetry setup are discussed in Brune et al. (1992). The actual useful sensitivity of the system depends on the background seismic noise level. During windy periods we often reduced the sensitivity. Several stations of a permanent recording network (Southern Great Basin Seismic Network, or SGBSN) are also located in this same area. Data from this network is also telemetered to Reno, and it is prcoessed through a realtime detection system called CUSP. Sensors of this network do not pass as high frequencies as those of the four microearthquake stations.

Seismograms

Typical records are shown in Figures 2a and 2b. Figure 2a shows an event arriving from the west (first at YBC) with an S-P time of about 2 sec at YBC. This event did not trigger the CUSP system. Figure 2b shows a more distant event (about 15-sec S-P time) along with an explosion sonic that could have been confused with an earthquake if four recording stations had not been available. The use of four stations is critical for identifying small events when the noise level is relatively high. Sonic events show a slow moveout (slow sonic velocity), whereas

earthquakes arrive nearly simultaneously at the stations, and a seismic observer quickly learns to distinguish earthquakes from sonic bursts and other noise.

Figure 3 shows typical events with short S-P times on the Yucca Mountain microearthquake array (YMNN). None of these events triggered the automated CUSP system.. These events are relatively rare. The magnitudes are estimated to be about 0 to -1. Qualitative observation confirms a very low rate of microearthquake activity at Yucca mountain, consistent with the low seismicity observed by Rogers et al. (1987), Gomberg (1991) and Von Seggern and Brune (1994). Of particular note is the lack of events with short S-P times (less than 3 sec.) Oliver et al. (1966) found that, in seismically active areas in Nevada, most events had S-P times of less than 3 sec, as might be expected because of the rapid attenuation of 30-Hz energy with distance. This qualitative observation with short S-P times further emphasizes the relatively low microearthquake activity in the immediate vicinity of the microearthquake stations at Yucca Mountain.

Because we wished to validate the operation of our systems, and the qualitative arguments given above, we temporarily transferred the recording of continuous data to four stations in the Mammoth Lakes region (Red Slate Mountain, Casa Diablo Hot Springs, Deadman Pass, and Montgomery Pass), with filters applied to give approximately the same response shape as the Yucca Mountain stations. As expected from this highly active area, the great majority of events has S-P times of less than 3 sec, and microearthquake rates were orders of magnitude higher than at Yucca Mountain (over 100 events per day, Brune et al. 1992). A very similar result was obtained in the aftershock zone of the Little Skull Mountain earthquake.

Microearthquake Magnitude Detection Threshold

Brune et al. (1992) derived a magnitude definition curve based on observed trace amplitudes of the microearthquake network and magnitudes given by the USGS-operated Southern Great Basin Seismic Network (SGBSN) data reports. There was very little data for events in the immediate neighborhood of Yucca Mountain, and thus the curve was uncertain at close distances. Assuming R^{-1} for geometrical spreading and a Q at 20 Hz of 400, they estimated the magnitude detection threshold as M approximately -1.5 at distances of 10 km (for the quietest noise level periods). They concluded that, if many events with magnitudes greater than -1 were occurring at Yucca Mountain, they would have been observed. The fact that only one microearthquake was observed with an S-P time less than 2 sec in 600 hours of low noise recording indicated a very low rate of microearthquake activity.

Two occurrences since the Brune et al. (1992) paper was published allow further checks on the microearthquake detection threshold: the occurrence of the Little Skull Mountain earthquake with its aftershock sequence, and the occurrence of a $M_D = 2.1$ earthquake in the northeast Crater Flat region (M_D = duration magnitude).

The Little Skull Mountain earthquake of June 29, 1992, (M = 5.6) produced an aftershock

sequence of microearthquakes which still continues. Since the surface geology at Little Skull Mountain is similar to that at Yucca Mountain, (layered tuffs over paleozoic basement), the attenuation and site effects properties are probably quite similar; and thus we can estimate the detection threshold at Yucca Mountain by establishing it at Little Skull Mountain. After the earthquake, UNRSL installed 7 local telemetered stations around Little Skull Mountain, in addition to the Little Skull Mountain (LSM) station installed years earlier by the USGS. These stations have continued to operate to the present. In order to use these stations to estimate microearthquake rates and threshold magnitudes, we band-pass filtered the transmitted signals from 4 stations (LSM, LMT, KRV and LTS) and recorded the signals on strip chart recorders similar to those recording the YMMN. The microearthquake rates were very high, up to over 100 events per day. In order to calibrate the stations, we operated them at 20 times lower gain for several weeks in January 1994 to obtain on-scale recordings of events with magnitudes high enough to be reported by the regular network (coda magnitude, M_D). The formula used by UNRSL is somewhat different than that used previously by the USGS. Comparison of magnitudes during the overlap period of September 1992 indicated a small systematic difference, ~ 0.25 units (VonSeggern, 1993). The coda magnitude is set up to be similar to the Richter magnitude M_L for magnitudes near 4, but may differ significantly for lower magnitudes; we discuss this further below.

In order to establish the magnitude threshold for each station we computed mean values using:

$$\text{Log}_{10} A - M_D = \text{Log}_{10} A_o \qquad (1)$$

for three filtered stations: LMT, LSM and KRV. A suite of 11 earthquakes, located in the center of the aftershock region, was used. M_D magnitudes were provided by the SGBSN. A_o is the estimated trace amplitude for a magnitude zero event. M_D is the coda duration magnitude and A is the peak amplitude recorded on the strip chart recorder when it is set at 1 volt full scale (full scale = 112.5 mm). We also include an estimate of Log_{10} A for these same events at the Yucca Mountain station YNB. For this station many of the events were clipped, but we could estimate the peak amplitude from the coda amplitude and the average coda shape for smaller events.

Average values of $\text{Log}_{10} A_0$ for the suite of events was about 0.8 mm at LMT and KRV, about 1.2 mm at LSM (all three at epicentral distances less than 10km) and about 0.4 mm at YNB (epicentral distance about 22 km). Based on these values, an event with amplitude 1 mm (the lowest amplitude readable with essentially no noise present) has a magnitude of about -0.8 at LMT and KRV and about -1.2 at LSM. For the station YNB at a distance of about 22 km the corresponding 1 mm magnitude is about -.4, but if we make an approximate distance correction (based on the curve in Brune et al., 1992) of about 0.5 magnitude units, we obtain a 1 mm trace amplitude magnitude of about -0.9. For the Brune et al. (1992) study, the estimated 1 mm magnitude at distances of about 10 km was about -1.5, but was quite uncertain because of the large extrapolations involved. Differences could be caused by differences in instrument gain, site effects, as well as differences in magnitude definition (Brune et al., 1992, used the USGS SGBSN

definition, and here we use the UNRSL SGBSN coda magnitude definition).

Calibration with M_D = 2.1 Northeast Crater Flat Event

The M_D = 2.1 northeast Crater Flat event occurred only a few km from the YMMN (Fig. 4). The seismogram was recorded on the new digital recording system, as well as on the strip charts used from August 1990 until September 1994, and thus allows a calibration of the network sensitivity relative to this event. The strip chart recordings for this event were clipped but the digital recordings were on scale (Fig. 5). By matching the coda amplitudes for the strip chart recording and the digital recording, we determined the true peak amplitudes that would have been recorded on the strip chart recordings if they had had a higher dynamic range. For the YMMN station YCF this was about 924 mm. Thus $Log_{10} A_0 = Log_{10} A - M_D$ was about 1.0, and the estimated magnitude for a 1 mm amplitude event would be about -1.

For the station YNB the sensitivity has been increased since the Brune et al. (1992) study by placing an L4 seismometer 75' down a drill hole very near the previous site (~100'), and increasing the gain by about a factor of 2 to take advantage of the decreased noise level. For this event $Log_{10} A_0$ was about 1.3 and the corresponding 1 mm amplitude event was about -1.3. Thus for events with the same geometry as the M_D = 2.1 northeast Crater Flat event, the YMMN should be able to detect events at distances of about 10 km with magnitudes M_D about -1 (during periods of low background noise level). This result is consistent with the results for the Little Skull Mountain test described above.

Adjustment of USGS SGBSN and UNRSL SGBSN Magnitudes

As mentioned above, the USGS SGBSN M_D magnitudes were calculated with a different formula than the UNRSL SGBSN magnitudes. Von Seggern (1993) made a comparison of these magnitudes for the one month overlap test period of September 1992. The UNRSL M_D magnitudes were about 0.2 - 0.3 units higher than the USGS average magnitudes. Since Brune et al. (1992) used USGS magnitudes, whereas the above comparisons use UNRSL magnitudes, for strict comparisons we should decrease the above magnitudes by about 0.25 units. This makes the comparison of threshold 1 mm magnitudes between the two studies better (-1.5 for Brune et al. 1992 study and -1.3 for the adjusted UNRSL M_D magnitude).

Comparison with M_L Magnitudes

The original Richter M_L magnitude definition was based on peak amplitudes as a function of distance, whereas M_D magnitudes are based on coda amplitude durations above a certain defined amplitude, to first order independent of distance (because the distance travelled by the scattered energy at times long after the S wave arrival time is to first order independent of distance between epicenter and recording station, but rather dependent on the travel path of the scattered energy, which is to first order proportional to the time after the origin time).

However, for small magnitude events the coda lengths are too short to be independent of distance and thus coda length magnitude definitions are cast in doubt (For the M_D = 2.1 northeast Crater Flat event the coda durations were only about 20 seconds). Furthermore, the USGS and UNRSL coda magnitude definitions were both adjusted to agree approximately with M_L at magnitudes above 3.5 and thus may not agree with M_L at lower magnitudes. These potential differences may become important at small magnitudes when attempting to estimate quantitative source parameters, such as seismic moment, source size and stress drop.

Savage and Anderson (1994) determined M_L attenuation curves for $M_L > 3.5$ for the Great Basin, including the Southern Great Basin, and found nearly perfect agreement with the standard Richter M_L attenuation curves, thus giving confidence in the use of M_L to estimate seismic moment, M_0, based on results from California. However, they noted an apparent discrepancy in plots of M_D vs M_L for the SGBSN, with M_L values apparently averaging about 0.4 magnitude units less than M_D values at M_D about 3.5, and scattering about 1 unit. However they cautioned that this could have been due to a bias problem because no events with M_D less than 3.5 were used in the regression.

Von Seggern and dePolo (1994) made a similar comparison for M_D events down to M_D about 3.0, and found a similar result, with average M_L values being about 0.6 magnitude units less than M_D values at $M_D \sim 3$. This seems to confirm that the discrepancy of values at small magnitudes is real. Since the M_L magnitudes determined at close distances and small magnitudes are nearly directly proportional to $Log_{10} M_0$, where M_0 is seismic moment, it will be important to obtain a direct estimate of seismic moment, M_0, relative to M_L and M_D. We plan to do this in the coming year. For the present we will make a preliminary estimate of M_0 based on the current data.

If we project the results of Von Seggern (1993) to $M_D \sim 2.1$, the M_D magnitude of the northeast Crater Flat event, we conclude that M_L is approximately one unit less than M_D, or about 1. Direct determination of M_L at five close stations gives $M_L \sim 0.3$ (within the range of scatter of M_L vs M_D points indicated in the Von Seggern, 1993, plots).

If we take -1 as a preliminary estimate of the correction to go from M_D to M_L at these small magnitudes, we obtain, using the threshold estimates above, corresponding M_L thresholds of about $M_L \sim -2.0$. Recent regressions of M_D vs M_L (Bakun, 1989, Vidal and Mungia, 1991), and the data of Woods et al. (1993) give the moment for $M_L = 2$ as about 3×10^{19} dyne-cm. For a detection threshold event of $M_L \sim -2$, M_0 would be about 3×10^{15} dyne -cm. Using the standard formulas $\sigma = (7/16) M_0/r^3$, where σ is the stress drop and r is the source radius, gives, for σ = 100 bars, a source radius of about 2 meters. We conclude that the YMMN current detection threshold corresponds to ruptures of a few meters in dimension. Since the surface rocks at Yucca Mountain appear to have fractures on this scale, there is no known reason why events of this size could not occur if the stresses were high enough.

Microearthquakes and b-values near Yucca Mountain

The empirical relationship between earthquake magnitude and frequency of occurrence proposed by Gutenberg and Richter [1944] is well known:

$$\text{Log}(N) = a - bM \qquad (2)$$

where N is the number of earthquakes which occur in a given area and time period, larger than magnitude M. The constant *a* is a measure of the level of seismicity and the constant *b* is typically close to 1. This relationship has been found to hold globally from about magnitude 3 to 6.5, and is consistent with a self similarity of earthquake sources in this size range. Magnitude-frequency statistics from earthquake catalogues, however, typically depart from the constant *b*-value at low magnitudes. This departure has traditionally been attributed to the detection threshold of the recording network, under the assumption that many small earthquakes occur undetected. Some recent studies, however, have proposed that this decrease in number of small earthquakes, compared to that expected from a constant *b*-value, is not just an artifact of the recording system but is due to the fact that there really are fewer small earthquakes than self similarity predicts. Abercrombie and Brune (1994) presented evidence that in California (including Baja California and the Mammoth Lakes region) the *b* value (from equation 2) was essentially constant down to magnitudes of about zero. We have verified that this is also true for aftershocks of the Little Skull Mountain earthquake. We filtered the traces for the station LMT near Yucca Mountain and recorded it on a strip chart recorder like that used for the Yucca Mountain Microearthquake Network (described above). We then counted all microearthquakes with trace amplitudes above 5 mm for the period 15 Dec 1993 to 5 Jan 1994 and determined a microearthquake rate for this magnitude (M_D about 0.3). This value is plotted as the large open circle with error bars in Figure 6 (the error bars are rough estimates of the errors in determining magnitude and in estimating earthquake rates). For comparison we plotted cumulative numbers of Little Skull Mountain aftershocks as a function of magnitude for various time periods (taken from the Southern Great Basin Seismic Network catalog). Microearthquake activity has been progressively decreasing since the earthquake, as indicated by the curves, but there are local fluctuations in activity over shorter periods of time, including bursts of increased activity lasting a few days. From Figure 6 we can see that the counted microearthquake rate is roughly consistent with extrapolations of the seismicity rates from the catalog, with no indication of a negative deviation from the curve at low magnitudes (We also made a rough count of events with trace amplitude above 1 mm on the station LSM which had a somewhat higher magnification and verified that the curve continues to smaller magnitudes with more or less the same slope). Based on this result, and similar results from Abercrombie and Brune (1994), we expect formula (2) to extend to lower magnitudes; and thus the numbers of events will continue to increase with a *b*-value of about 1 if we increase the sensitivity of the system. Equation (2) may not be applicable to predicting the frequency of larger earthquakes, although it has often been used to do this.

The seismicity rate near Yucca Mountain (distances less than 15 km) is very low (Rogers et al., 1987; Gomberg, 1991; Von Seggern and Brune, 1994). At the microearthquake level, Brune et al. (1992) recorded only one microearthquake with magnitude greater than zero at Yucca Mountain

during a period of 25 days quiet recording time. This one event is not sufficient to establish a microearthquake rate, however it is roughly consistent with the catalog rates of seismicity extrapolated to the microearthquake level. Fig. 7 (from Von Seggern and Brune, 1994) compares the catalog b-value curve for events within 10 km of the Exploratory Studies Facility at Yucca Mountain with the general *b*-value curve for the whole SGBSN. As can be seen from this figure, the seismicity rate in the immediate vicinity of Yucca Mountain is more than an order of magnitude lower than that for the entire southern great basin region (the downward pointing arrows indicate that some of the smallest events in the catalog have been found to be noise bursts rather than true earthquakes). Also, the one microearthquake reported by Brune et al. (1992) is roughly consistent with the extrapolation of the curve (open circle above M = -1).

Microearthquakes and Stress Level

When rocks are stressed to near the failure point they almost always begin to undergo small scale fracturing prior to the main failure. In the laboratory the small events are called acoustic emissions. In mining operations they are called rockbursts. It is uncertain how to extrapolate these results to the scale of earthquakes, even microearthquakes. Many large earthquakes are preceded by foreshocks, which may represent the same phenomenon; but for many large earthquakes there is apparently no foreshock sequence, although this often could be a consequence of lack of sensitive recording equipment in the hypocentral region prior to the earthquake. The concept of foreshock, or foreshock sequence, is not well defined. In particular there is no generally accepted interval time preceding an earthquake during which events are labelled foreshocks. Also, it is well known that there is often a seismic quiescence prior to a large earthquake, evidently due to "locking up" of the tectonic system. The time scale of periods of quiescence or increased activity vary greatly; and, in areas like the Basin and Range where the repeat times of major earthquakes may be thousands of years, the whole historical record might be included in one of these periods. Nevertheless, there is a general tendency for earthquakes to nucleate in regions that have had relatively high recent activity, even though the majority of the rupture may then propagate into regions which have had little prior seismic activity. The Little Skull Mountain earthquake of June 29, 1992, occurred in or near an area of relatively high small-magnitude activity and also had a clear foreshock sequence. We may assume that areas of currently high small-magnitude earthquake activity are likely sites for future earthquakes.

Hydrofracture experiments at Yucca Mountain have been interpreted to indicate possible incipent normal faulting at shallow depths by Stock et al. (1985). If the rocks are indeed stressed to near failure, one would expect microearthquakes at some magnitude level. Watters et al. (1990) found that, near the failure point, Yucca Mountain tuffs began to yield acoustic emissions typical of most rocks, with the character of the acoustic emissions depending on the porosity and other properties of the rock. On the other hand Brune et al. (1992) found no evidence of microearthquake activity above the magnitude zero level. This would suggest that the rocks at Yucca Mountain are not near the failure point. Possible explanations of these contradictory indications include: (1) the hydrofracture interpretation may be incorrect, (2) microearthquakes may be occurring at a magnitude level too low to be detected with current equipment, and (3) there may be special circumstances

which make it inappropriate to extrapolate laboratory results to actual field conditions. We feel that it is important to reduce the microearthquake detection threshold to magnitudes as small as possible in order to provide further understanding of the state of stress in the Yucca Mountain area, as well as to establish a background base-level of microearthquake activity for comparison with possible future increases in microearthquake activity caused by tunneling activities or possible future heating by storage of radioactive materials.

Lack of microearthquake activity in a local area such as Yucca Mountain, which is in the otherwise tectonically active region of southern Nevada, might be a result of several conditions: (1) the local stress level may be permanently low due to more or less permanent complex variations in rock elastic properties or fault geometry, (2) magmatic activity may be absorbing the elastic strain (Parsons and Thompson, 1991), or (3) the stress level may be temporarily low due to complex changes in the stress field due to ongoing tectonic processes (e.g., reduction in stress by prior earthquakes or fault creep). These considerations lead to four possible hypotheses concerning microearthquake and earthquake activity at Yucca Mountain:

1. There will never (at least for > 10,000 years) be any significant seismic energy release at the site.

2. Microearthquake activity will increase prior to the next major earthquake in the area.

3. Microearthquake activity will increase prior to any rupture which might "nucleate" in the area, but may not increase prior to all earthquakes rupturing the area because the nucleation point of ruptures may be outside the area, or a rupture may be triggered by other ruptures outside the immediate area.

4. Microearthquake activity will not increase even if there is nucleation of a large earthquake in the immediate vicinity of Yucca Mountain.

At the present time we cannot definitely prove or disprove any of these hypotheses. However either (3) or (1) seems the most likely. Further study may improve our understanding of the situation. Irregardless, microearthquakes will continue to be one of several possible indicators of major changes in stress level at the site, caused either by tectonic changes or changes induced by human activities such as tunneling and radioactive storage.

Description of the New Digital Recording System

Since July 1994 a new digital recording system has replaced the strip chart recorder. The data acquisition system consists of a 486 PC equipped with a state-of-the-art 330 kHZ analog-to-digital board (DAP 1200e/6 manufactured by Microstar Laboratories). The DAP 1200e/6 has an on-board processor and 1 Mb of memory for real-time data processing.

The analog data from YMMN transmitted to the Seismological Laboratory at UNR, along with a time channel (IRIG-E), is continuously digitized and transferred to a SUN workstation every 5 minutes (the digital data consists of 12-bit, 200 sample-per-second data). The data is then

demultiplexed (separating data for each station) and written in SAC format into separate files identified by the time at the beginning of the 5-minute files and the channel numbers corresponding to each station (e.g. JJJ.HH.MM.SS.CH). The digitized time channel is saved as well. A PASSCAL Quick Look (PQL) program is used to look at each Julian day's data in order to monitor the microseismic activities in the Yucca Mountain region. Finally, two copies of the compressed data of each Julian day are saved on digital cassette tapes and stored in a safe place. See Figure 5 for an example of the recorded data.

Objective 2: 3 Station Broadband Digital Network

Three broadband digital stations near Troy Canyon, NV, Nelson, NV, and Deep Springs, CA, (Fig. 8) were originally installed by UNRSL and the Institute of Geophysics and Planetary Physics (IGPP), University of California, San Diego, in 1986, with funding from the Natural Resources Defense Council. In 1988 operation of these stations was taken over by UNRSL under funding from the Nevada Nuclear Waste Projects Office (NWPO) and operated as part of Task 4 of the UNR Neotectonics Project of NWPO. The stations have broadband sensors located in 30 m boreholes, and the data is transmitted by radio and microwave to UNRSL. The stations have operated more or less continuously since 1988 (except for down time due to floods, vandalism, etc.), and have collected a large amount of data useful for crustal structure studies, as well as for earthquake source mechanism studies. The data has only begun to be utilized. The data will provide an important compliment to the data from DOE Broadband Digital Upgrade Network, scheduled to be operational in 1995 or 1996.

As a preliminary test of the usefulness of the data, we have examined a number of $M_D > 3$ Little Skull Mountain and Rock Valley aftershocks recorded on the broadband network. We have made rough measurement of signal/noise ratios, peak broadband amplitude, and peak amplitude through a 0.2 - 0.5 Hz bandpass filter.

Figure 9 shows approximate signal/noise ratios plotted as a function of M_D. The larger events have high signal/noise ratios (> 3), but for smaller events the ratio approaches 1., as the signals become no larger than the noise. It is well known that signal/noise can often be improved by narrowband filtering. To check this, we have narrowband filtered the records with a two-pole Butterworth band-pass filter, with corners at 0.2 and 0.5 Hz. Signal/noise ratios for magnitudes near 3.0 were significantly improved in some cases. Of course signal/noise ratios depend not only on earthquake size but also on ambient noise conditions (storms, wind).

One of the uses of the broadband data is to determine linearity of scaling relationships, e.g., between magnitude, M_L or M_D, and moment, M_0. As a preliminary test of this, we have plotted peak broadband amplitude and peak filtered amplitude as a function of magnitude M_D (Fig. 10, Little Skull Mountain events, and Fig. 11, Rock Valley events). These relationships should be linear to first order, with the bandpass filtered data more linear. As can be seen, the plots indicate approximate linearity down to $M \sim 3.5$. However, at small magnitudes there is a serious deviation, with observed peak amplitudes falling significantly below a line projected with slope 1. Since peak amplitude should

scale approximately linearly with M_L, these results again indicate that M_D values are high relative to M_L at magnitudes below $M_D = 3.5$. This is consistent with the M_L vs M_D data discussed above.

References

Abercrombie, R.E. and J.N. Brune, 1994. Evidence for a constant *b*-value above magnitude 0 in the southern San Andreas, San Jacinto and San Miguel fault zones, and at the Long Valley caldera, California, Geophys. Res. Letts., vol. 21, no. 15, pp 1647-1650.

Bakun, W.H., 1984. Seismic moments, local magnitudes, and coda-duration magnitudes for earthquakes in Center California, Bull. Seismol. Soc Am. vol. 74, no. 2 pp 439-458.

Brune, J.N., W. Nicks, A. Aburto, 1992. Microearthquakes at Yucca Mountain, Nevada, Bull. Seismol. Soc. of Amer. vol. 82 no. 1 pp 164-174.

Gomberg, J., 1991. Seismicity and detection/location threshold in the southern Great Basin Seismic Network, J. Geophys. Res., vol. 95, no. 16, pp 4-46, 414.

Oliver, J., A. Ryall, J.N. Brune and D.B. Slemmons, 1966. Microearthquake activity recorded by portable seismographs of high sensitivity, Bull. Seismol. Soc. Am., vol. 56 pp 899-924.

Parsons, T. and G.A. Thompson, 1991. The role of magma overpressure in suppressing earthquakes and topography: worldwide examples, Science vol. 253, pp. 1399-1402.

Rogers, A.M., S.C. Harmsen, M.E. Meremonte, 1987. Evaluation of the seismicity of the southern Great Basin and its relationship to the tectonic framework of the region, U.S. Geol. Surv. Open-File Rept. pp. 87-408.

Savage, M.K. and J.G. Anderson, 1994. A local magnitude scale for the Western Great Basin-Eastern Sierra Nevada from synthetic Wood-Anderson seismograms, Bull. Seismol. Soc. Am., in press.

Stock, J.M., J.H. Healy, S.H. Hickman and M.D. Zoback, 1985. Hydraulic fracturing stress measurement at Yucca Mountain,, Nevada, and relationship to the regional stress field, J. Geophys. Res., vol. 90, pp 8691-8706.

Vidal, A. and L. Munguia, 1991. Local magnitude and source parameters for earthquakes in the peninsular ranges of Baja California, Mexico, Bull. Seismol. Soc. Am. vol. 81, no. 6, pp 2254-2267.

von Seggern, D. H. 1993. Seismicity for the southern Great Basin of Nevada and California in 1992, Appendix B: Comparison of USGS and UNR seismic bulletins for the month of September 1992.

von Seggern, D. and J.N. Brune, 1994. Seismicity in the Southern Great Basin, 1868-1992, USGS Circular on the Yucca Mountain Tectonics Workshop, Jan. 24-26, 1994, in press.

von Seggern, D.H., and D. dePolo, 1994. Seismicity for the southern Great Basin of Nevada and California in 1993, U. Nevada, Reno, Seismological Laboratory report to the U.S. Geological Survey, Yucca Mountain Project Branch, Denver, CO.

Watters, R.J., J.R. Carr and D.M. Chuck, 1990. New techniques in rock mass classification: application to welded tuffs at the Nevada Yucca Mountain, Int'l J. Min. and Geol. Engr., vol. 8, pp 241-260.

Woods, B.B., S. Kedar and D.V. Helmberger, 1993. M_L:M_0 as a regional seismic discriminant, Bull. Seismol. Soc. Am., vol. 83, no. 4 pp 1167-1183.

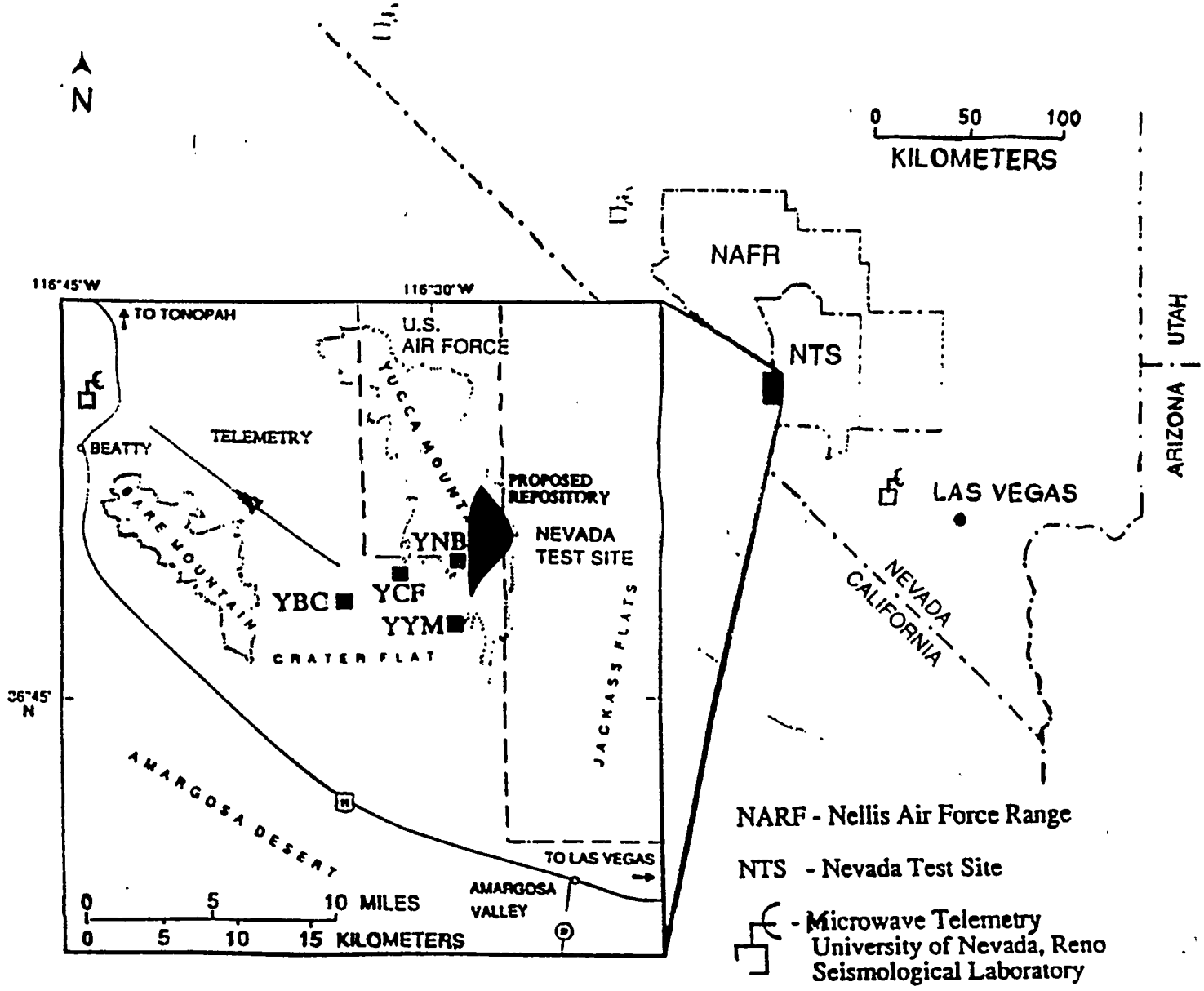

Figure 1. Location Map for Yucca Mountain Microearthquake Net (YMMN)

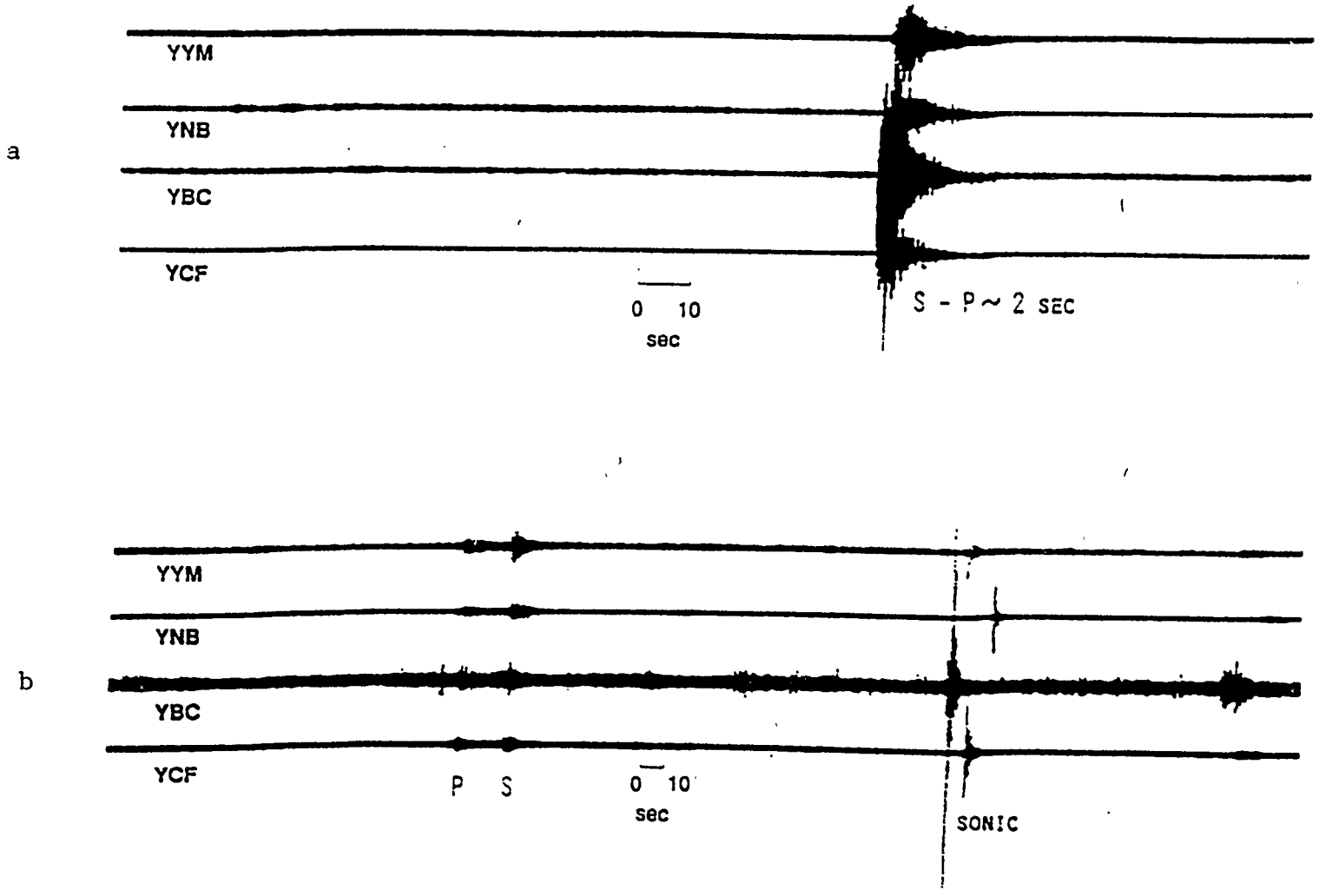

FIG. 2 Examples of microearthquake recordings and noise, including a sonic, at two different chart speeds.

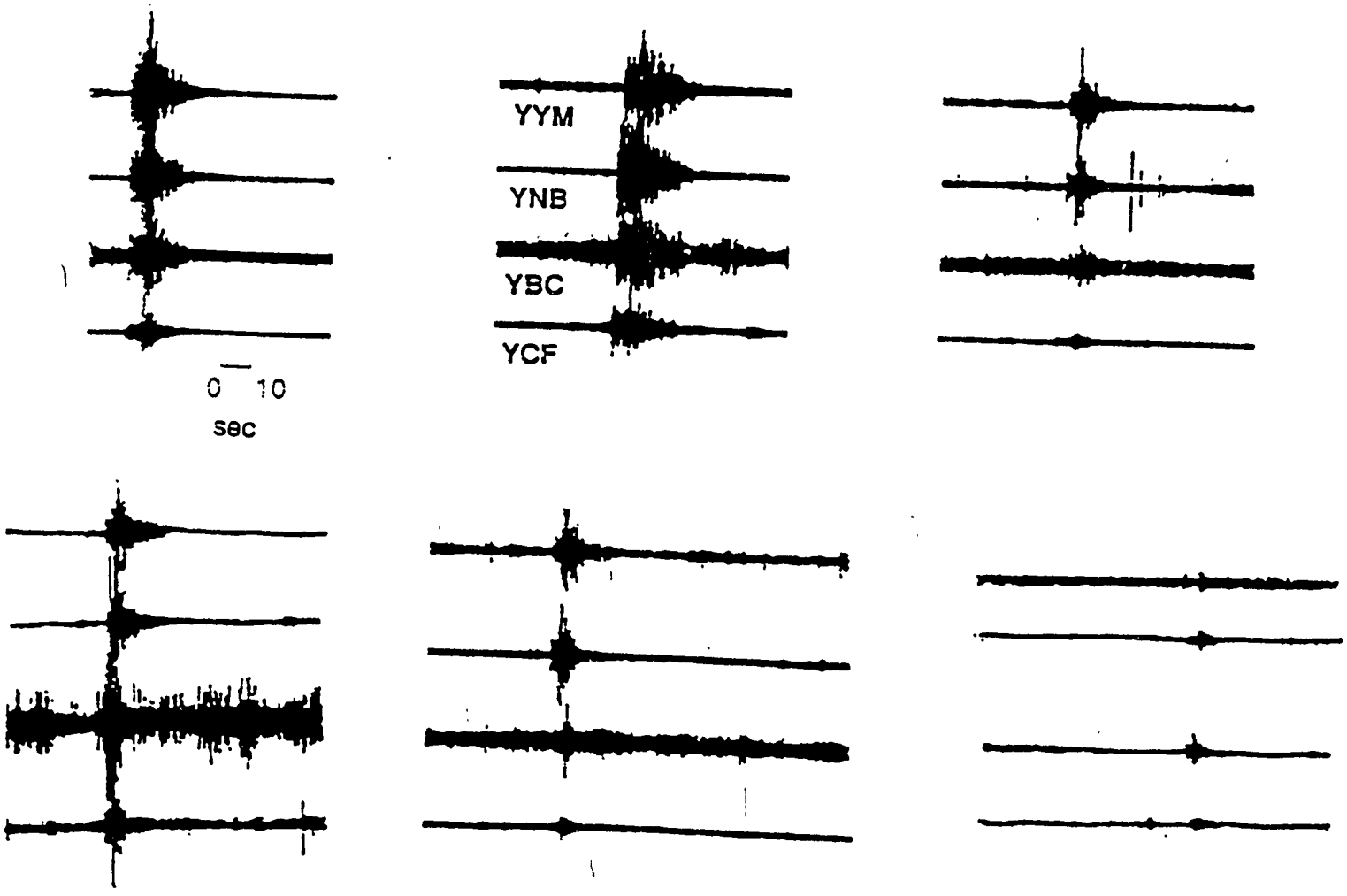

FIG. 3 Examples of recordings of the relatively rare events in the neighborhood of Yucca Mountain (*S-P* times of less than about 5 sec).

Date: 14 July 1994
Time: 23:28:76.91 GMT
Epicenter: 36N53.68 116W33.06 (P-wave), 36N53.58 116W33.18 (S-wave)
Depth: 4.92 km (P-wave), 5.80 km (S-wave)
M = 2.11

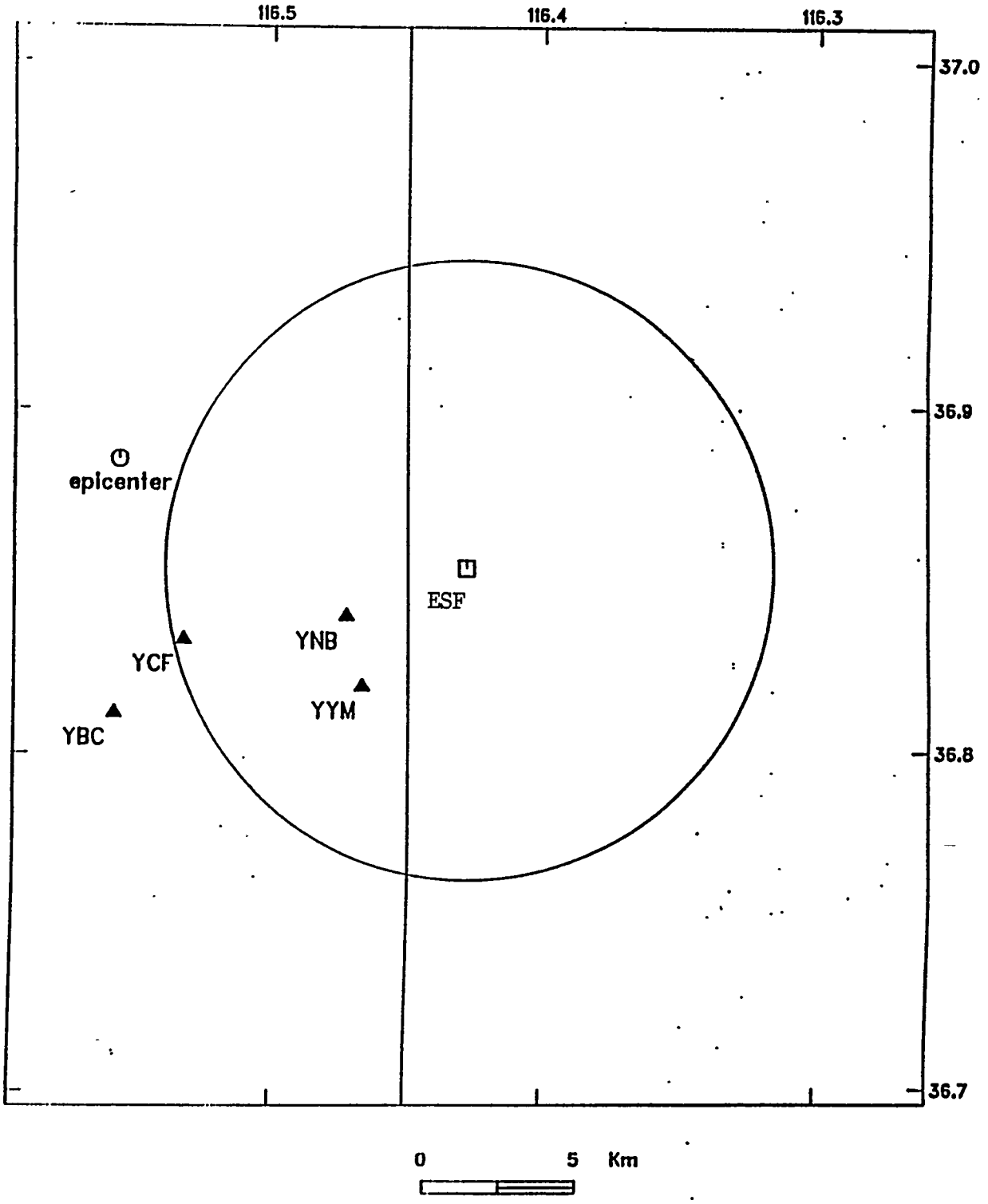

Figure 4 Location of 14 July 1994 Northeast Crater Flat event relative to microearthquake stations and proposed Exploratory Studies Facility

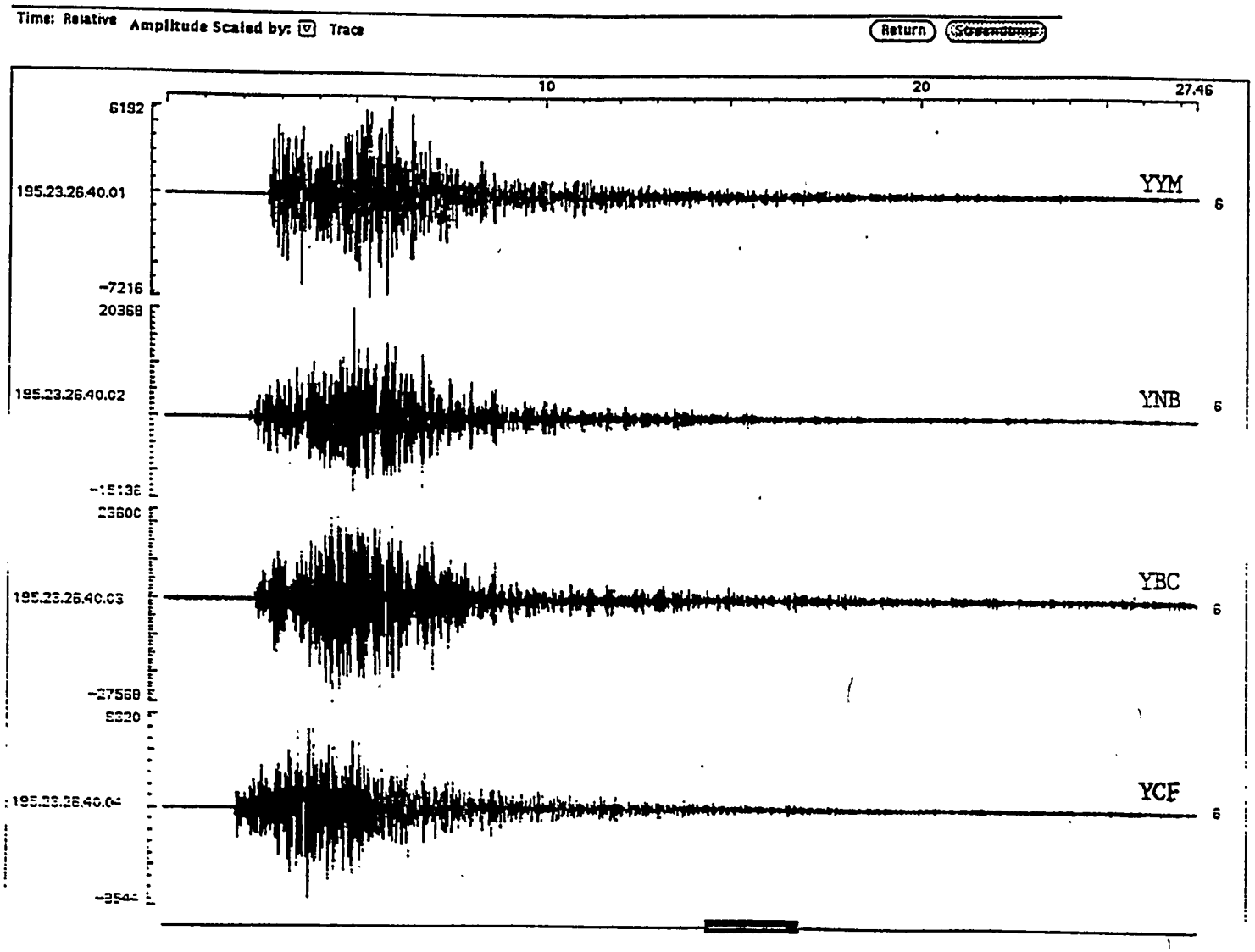

Figure 5 Digital recordings of 14 July 1994 Northeast Crater Flat earthquake

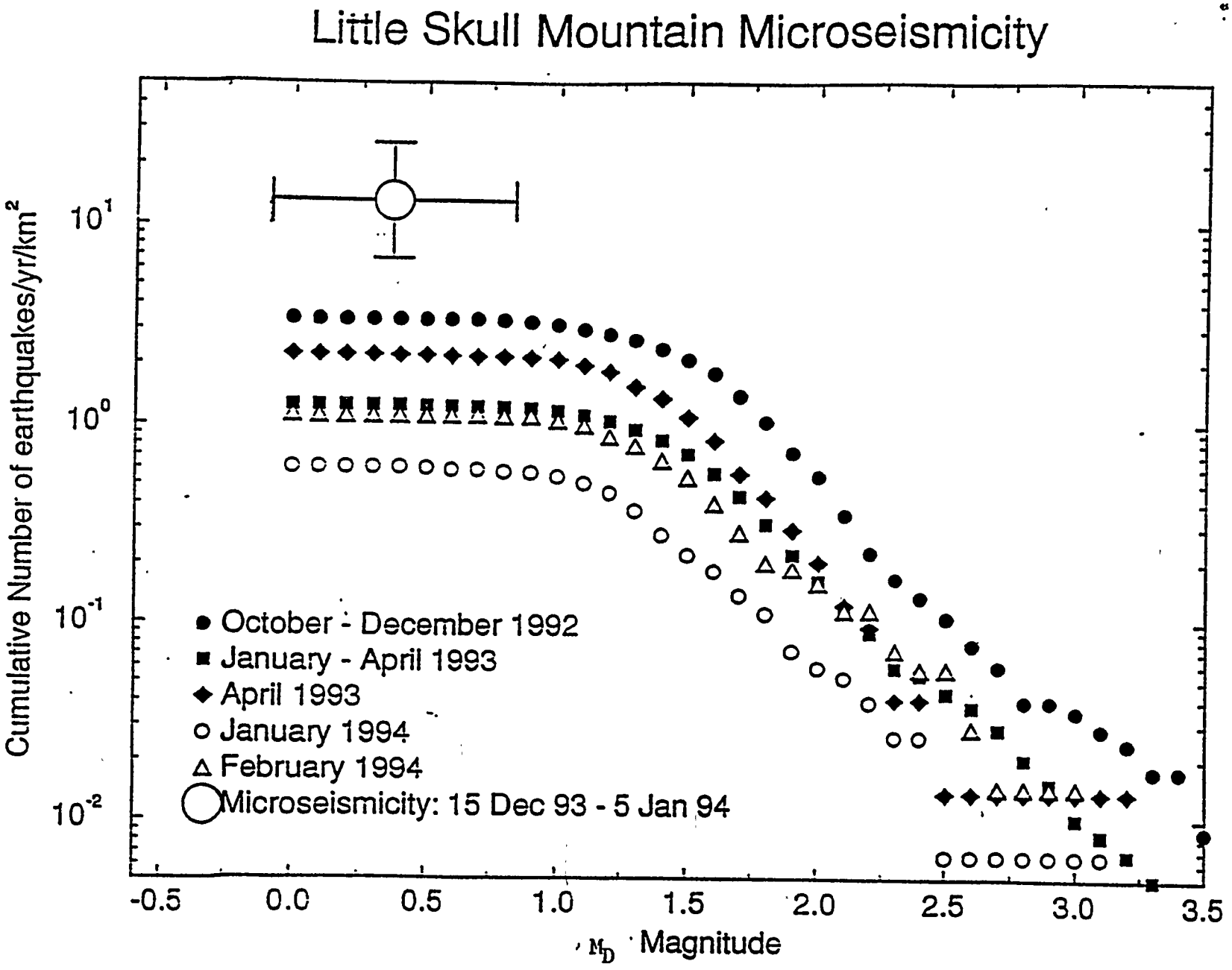

Figure 6 Cumulative number vs M_D plot for Little Skull Mountain aftershocks, compared with microearthquake rate

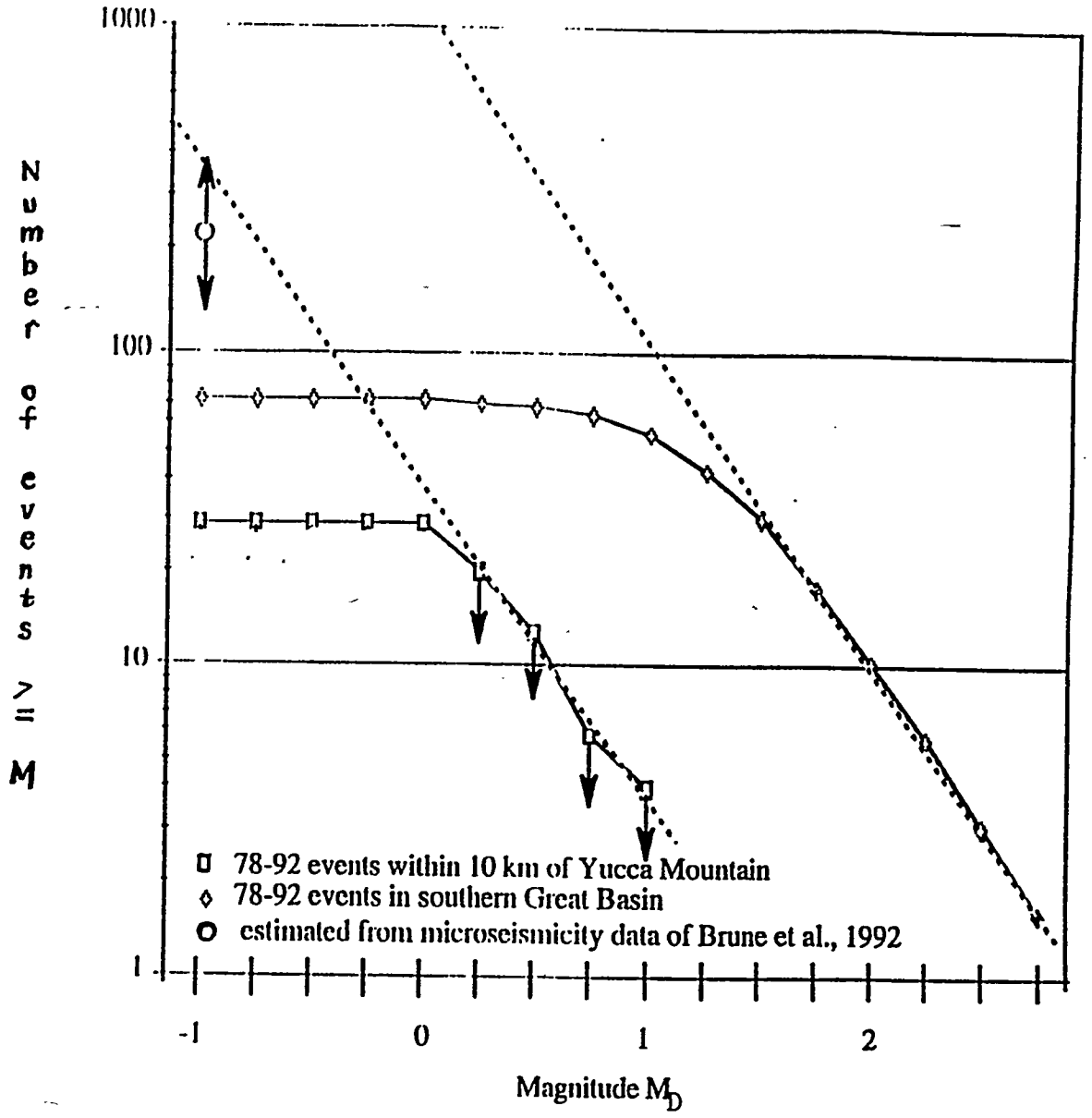

Figure 7 Cumulative number of events vs M_D for Southern Great Basin, and for area within 10 km of Yucca Mountain, normalized for area.

UNIVERSITY OF NEVADA, RENO
DIGITAL SEISMIC NETWORK

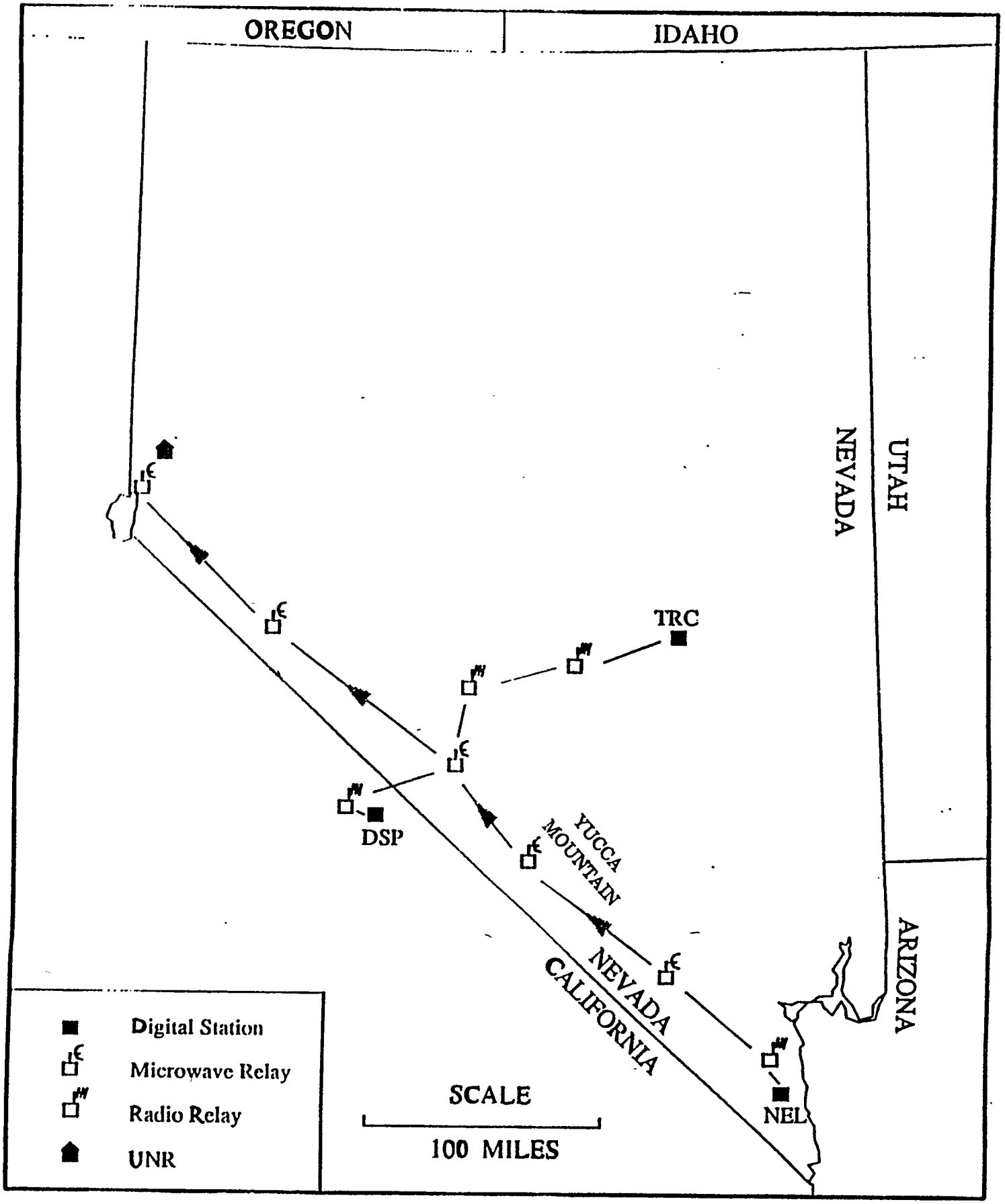

Figure 8 Location map for three broadband stations TRC, NEL, and DSO

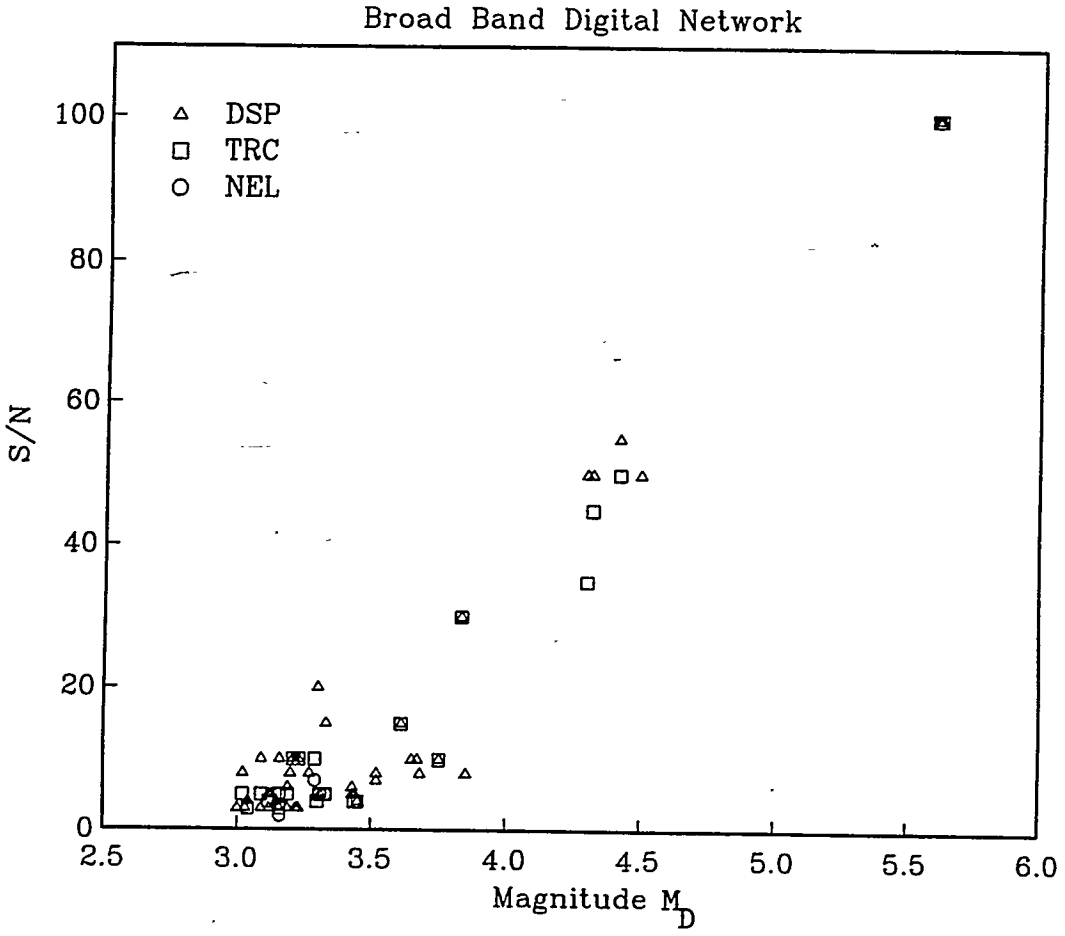

Figure 9a Signal/noise ratios plotted vs M_D for Little Skull Mountain aftershocks

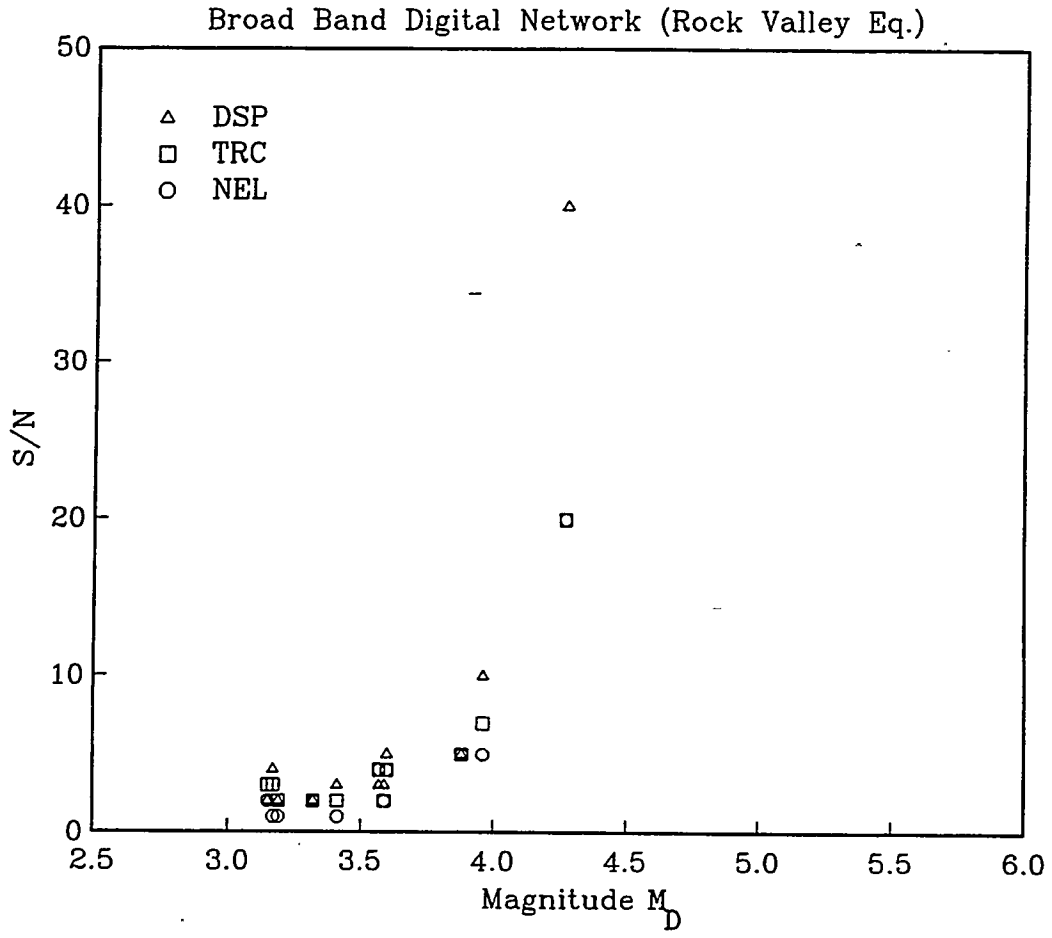

Figure 9b Signal/noise ratios vs M_D for Rock Valley events

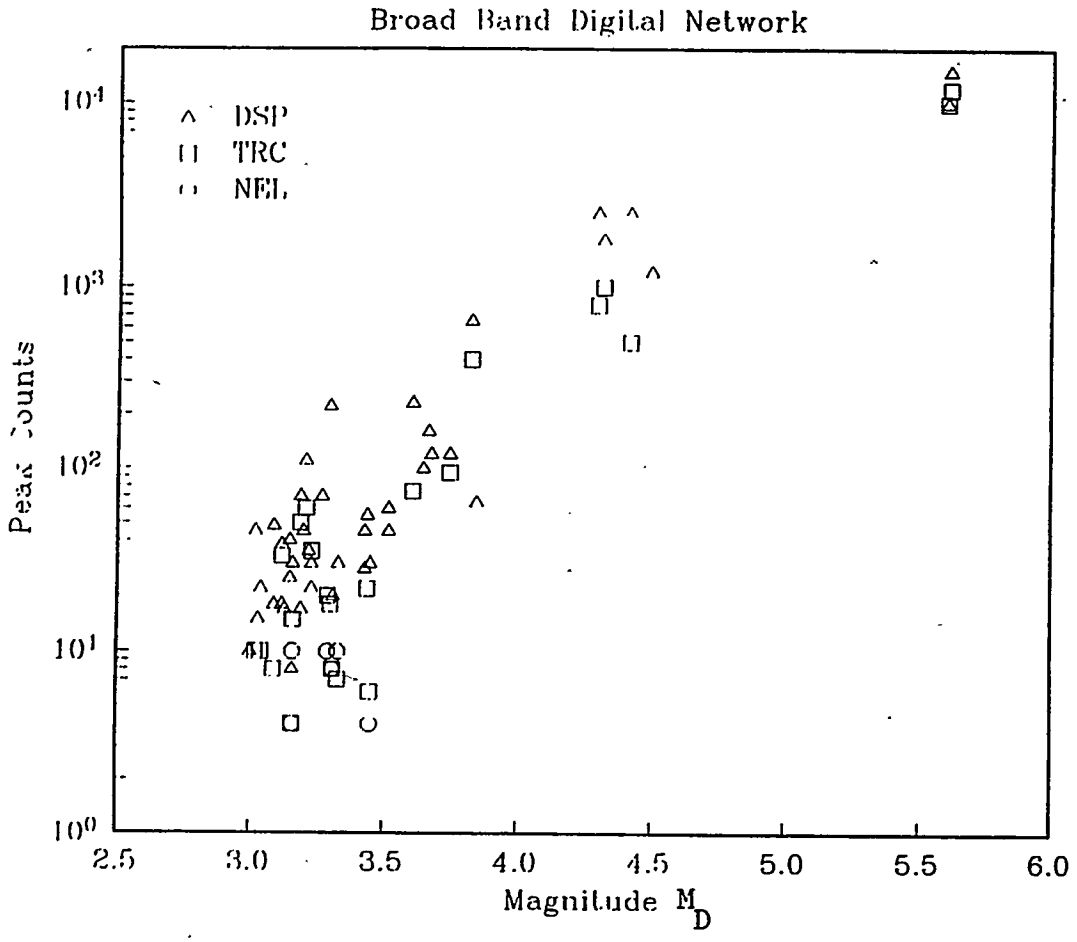

Figure 10a Peak counts vs M_D for Little Skull Mountain aftershocks

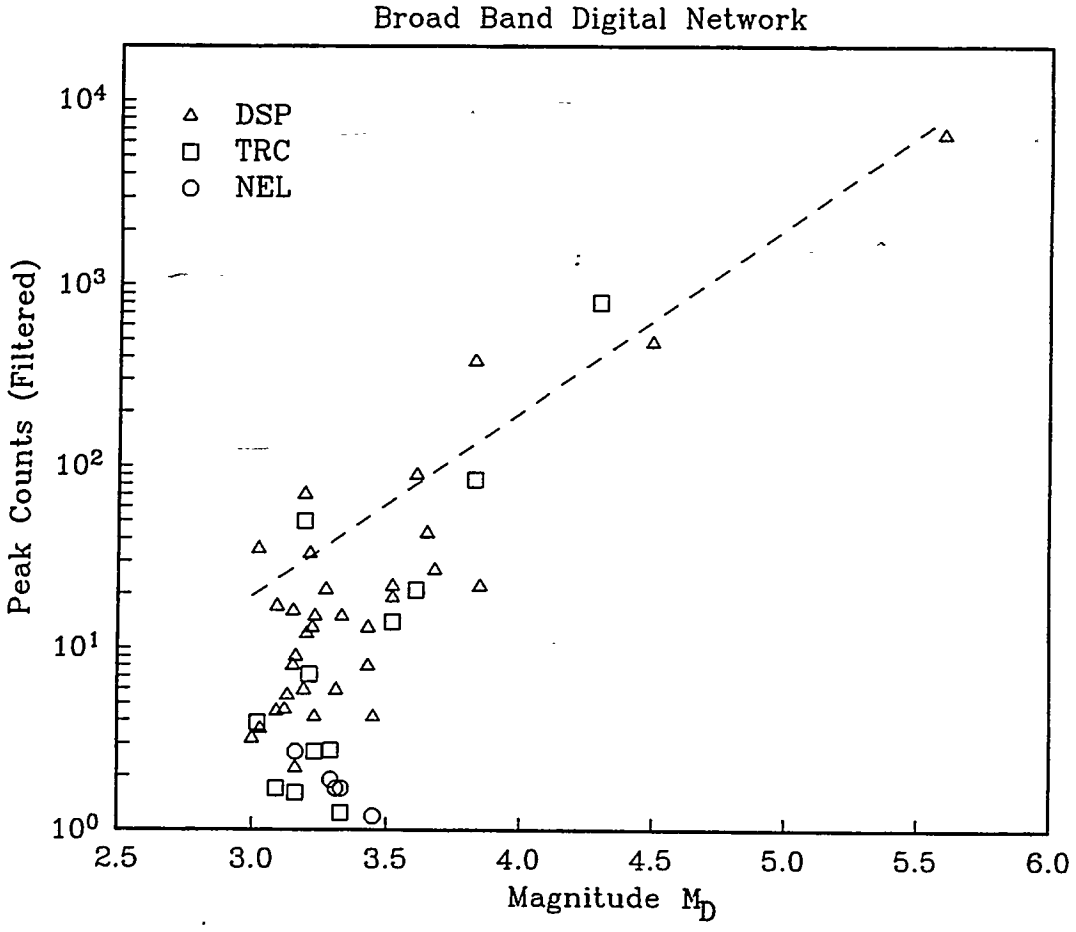

Figure 10b Peak counts through filter, vs M_D, for Little Skull Mountain aftershocks

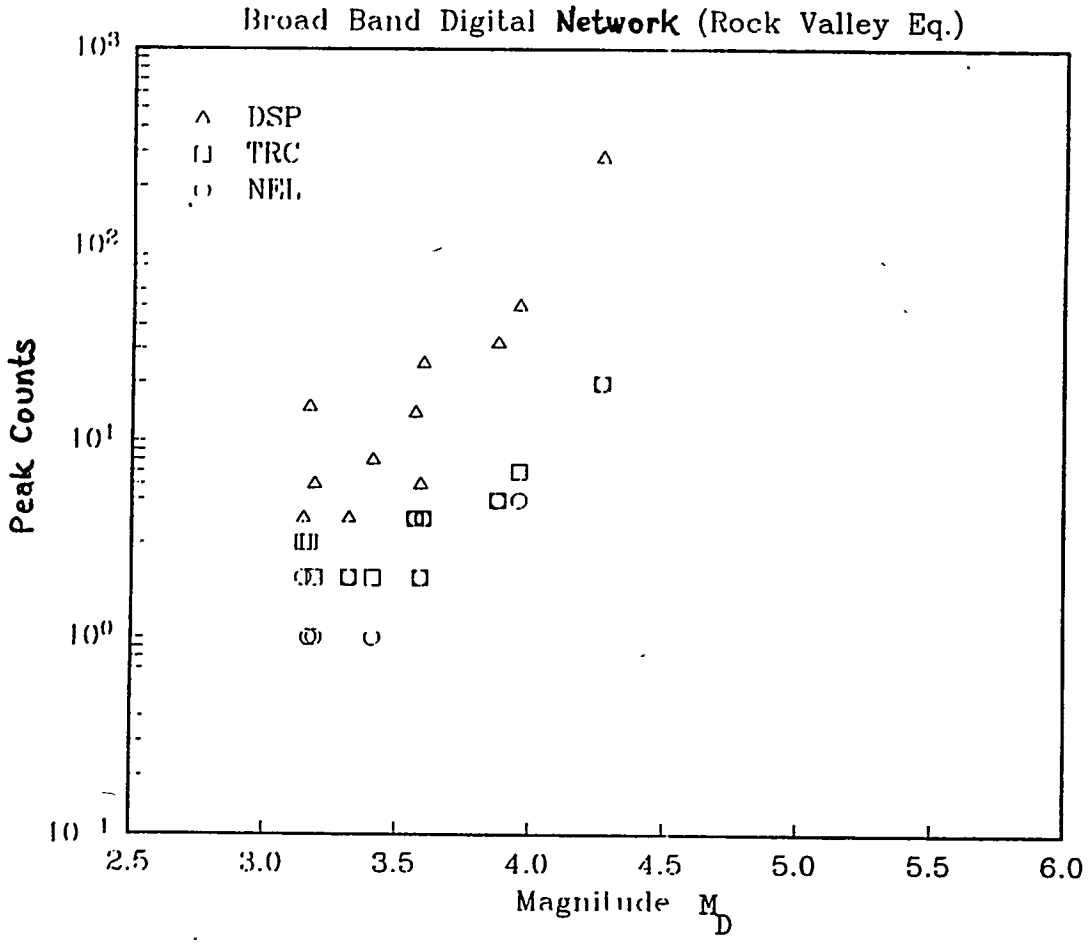

Figure 11a Peak counts vs M_D for Rock Valley events

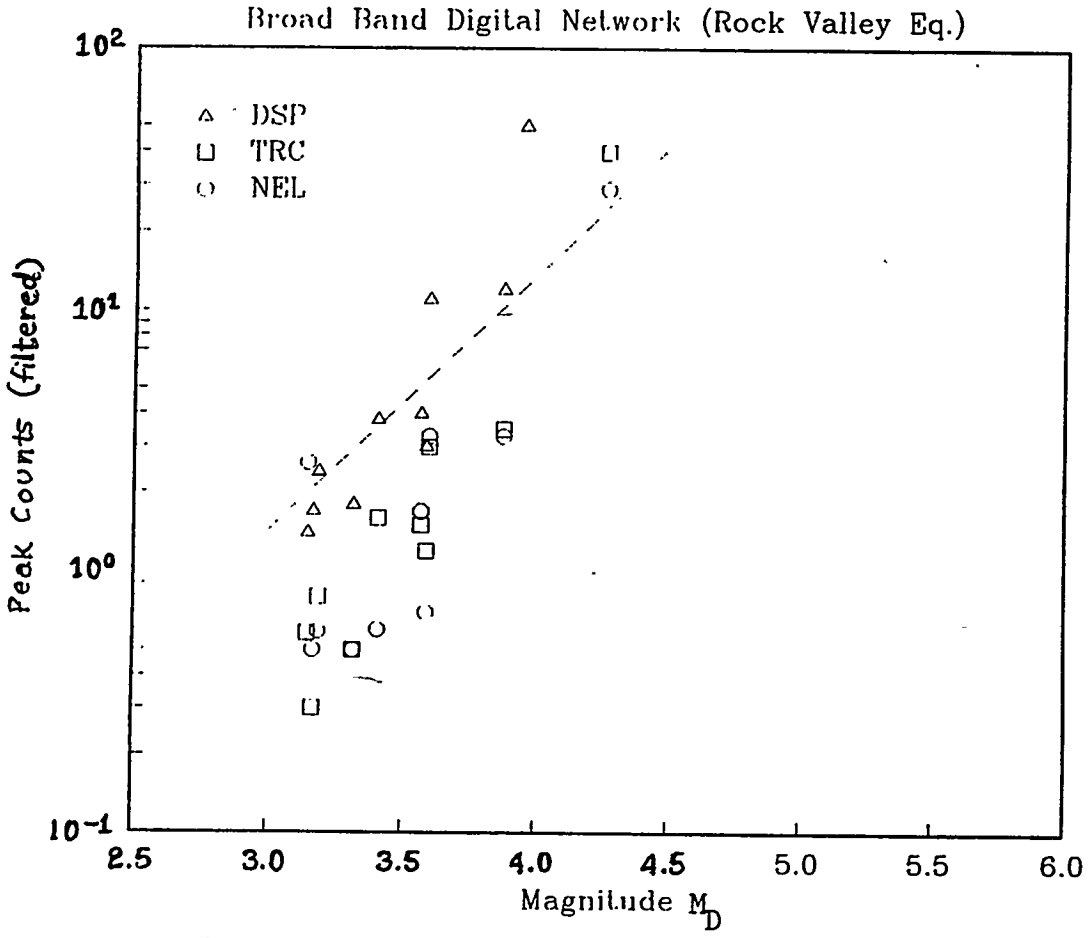

Figure 11b Peak counts through filter, vs M_D, for Rock Valley events

PROGRESS REPORT--OCTOBER 1, 1993 TO SEPTEMBER 30, 1994

TASK 5--Tectonic and Neotectonic framework of the Yucca Mountain Region

Personnel

Principal Investigator: Richard A. Schweickert

Research Assistant Professor: Mary M. Lahren, July, 1994 to September, 1994

Graduate Research Assistants:

a. **Zhang, Y.--October, 1993-September, 1994**
b. **Wellman, E.--August-September, 1994**
c. **Plank, G.--August-September, 1994**

Part I. *Highlights of research accomplishments*

a. Completion of new manuscript on the Amargosa fault system
b. Structural studies in Grapevine Mountains, Bullfrog Hills, and Bare Mountain
c. Publication of abstract based upon research funded under Task 5: Schweickert and Lahren (1994 GSA National Meeting, Seattle).
d. Preliminary results of U-Pb isotopic analysis of pegmatites and orthogneisses in Bullfrog Hills and Funeral Mountains

Part II. *Research projects*

This section highlights the research projects conducted by Task 5 personnel.

1. *Regional overview of structure and geometry of Mesozoic thrust faults and folds in the area around Yucca Mountain*; R. A. Schweickert and M. M. Lahren.

The purpose of this study is to provide information about the deep structural geometry of Paleozoic units and their bounding faults, which is

necessary both for understanding of Tertiary faults and for the correct formulation of regional hydrologic models. This study has also provided critical new evidence for a previously unknown strike-slip fault beneath Crater Flat, and for the existence of major pre-Middle Miocene extension in the NTS region. The study involves new field work in selected areas and a synthesis of structural relations in areas both east and west of Yucca Mountain, including the CP Hills-Mine Mountain area to the east, and Bare Mountain-Bullfrog Hills-Grapevine Mountains to the west.

2. *Kinematic analysis of low and high angle normal faults and strike-slip faults in the Bare Mountain area, study of metamorphic rocks, and comparison of structures with the Grapevine Mountains* Y. Zhang and R. Schweickert

Bare Mountain is a direct analog of the deep structure beneath Cenozoic ash flow tuffs at Yucca Mountain. The purpose of this study is to determine the structural evolution of Bare Mountain by field analysis of the timing and slip directions of high and low-angle normal faults exposed there, and by integrating field data into structural cross-sections. This work has provided better constraints on the displacement histories of the faults. A number of deep cross-sections have been constructed through Bare Mountain to build up a model of the structural evolution of the area. In addition, metamorphic fabrics are being studied in metamorphic rocks in the northern parts of the mountain and traced to lower grade rocks in the southern part of the mountain. Finally, the development of these structures will be compared with possible analogs in the Grapevine Mountains and the CP Hills to develop firm constraints on the deep structure beneath the Yucca Mountain area.

3. *Evaluation of pre-Middle Miocene structure of Grapevine Mountains and its relation to Bare Mountain.* R. Schweickert and M.M. Lahren

The goal of this study is to establish the Mesozoic and Cenozoic structural geometry and timing of deformation in the Grapevine Mountains, which developed in close proximity to the Bullfrog Hills and Bare Mountain areas, prior to post-10 Ma displacement on the Bullfrog Hills-Boundary Canyon detachment fault. This study is clarifying the significance of pre-

Middle Miocene and possibly pre-Tertiary extension and detachment faulting on crustal structure in the area between the NTS and Death Valley, and beneath Yucca Mountain.

4. *Evaluation of paleomagnetic character of Tertiary and pre-Tertiary units in the Yucca Mountain region, as tests of the Crater Flat shear zone hypothesis and the concept of oroclinal bending.* S. Gillett, R. Karlin, Y. Zhang, and R. A. Schweickert.

Paleomagnetic data from various volcanic units at Yucca Mountain show that up to 30° of progressive north-to-south clockwise rotation has occurred since mid-Miocene. These studies are geographically relatively limited; one of the goals of this study is to expand the data base to various Paleozoic and Mesozoic units to understand the regional variations of magnitude and timing of rotations.

5. *Late Quaternary fault patterns in southern Amargosa Valley, Stewart Valley, and Pahrump Valley.* M.M. Lahren and R.S. Schweickert.

This project involves the compilation of all available data on the distribution and style of late Quaternary faults in the region, primarily from mapping by Donovan and Hoffard (M.S. Theses completed under Task 5) and USGS mapping. This compilation will reveal the nature of the late Quaternary structural setting of Yucca Mountain. Field checking of certain key areas is not complete.

6. *Tectonics and Neotectonics of the Pahranagat shear zone, Lincoln County, Nevada;* (R. Elwood and T. Reynolds, formerly supported here, have both left UNR; R. Elwood plans to complete her studies by December 0f 1994).

The rationale for this study has been that the Pahranagat shear zone lies on trend with the Spotted Range - Mine Mountain structural zone, which is composed of seismically active, ENE-striking, sinistral faults, and which lies immediately south of Yucca Mountain. Studies of the Pahranagat shear zone have been undertaken to evaluate whether the two zones are parts of a related zone of crustal weakness that may be active.

In addition, the Pahranagat shear zone shows clear evidence that

shortening occurs within the Basin and Range province. Such shortening may be manifest as thrust earthquakes and (or) as shortening through aseismic folding. Elwood's part of this project was completed in 1991, and her thesis report is in progress.

Part III.

Brief summaries of research results during FY 1994

This section presents a summary of progress to date. Because these projects are long-term and field-intensive, the results are still preliminary, and should not be quoted without permission. Many of our interpretations are speculative.

1. Regional overview of structure and geometry of Mesozoic thrust faults and folds in the area around Yucca Mountain. and ***Quaternary fault patterns and basin history of Pahrump and Stewart Valleys, Nevada and California.*** (Also see 1993 progress report)

R. A. Schweickert and M. M. Lahren.

(See preprint and abstract by Schweickert and Lahren; Appendix 1).

We summarize evidence based upon gravity, seismic, paleomagnetic, structural, stratigraphic, volcanic, spring, and stratigraphic data that a major N24W-trending dextral strike-slip system passes beneath Crater Flat and Yucca Mountain. This is one of several active systems in the southern part of the Walker Lane belt, based upon evidence of Quaternary faults in southern Amargosa Valley that provide a connection from the Pahrump-Stateline fault zones to Crater Flat. It represents the principal zone of late Quaternary fault movements in the area east of Death Valley. Both normal faults and late Cenozoic volcanic cones in Crater Flat appear to be manifestations of this strike-slip fault system.

3. Evaluation of pre-Middle Miocene structure of Grapevine Mountains and its relation to Bare Mountain. **R. Schweickert and M.M. Lahren. (see 1993 progress report).**

New field work was done in March on a 3-day trip to Death Valley, Panamint Valley, and Amargosa Valley, March 18-20, 1994, with R.A. Schweickert and M.M. Lahren. Contacts between the Oligocene Titus Canyon Formation and underlying Cambrian rocks were examined in upper Titanothere Canyon and determined to be depositional, confirming

observations of FY 1993. Clast compositions of the Titus Canyon Formation were also studied.

Prelimary results of U-Pb isotopic dating indicate that deformed and undeformed granitoids in the Bullfrog Hills are associated with metamorphic rocks in the footwall of the Bullfrog Hills detachment fault are of Late Cretaceous age (J. D. Walker, oral commun., 1994), suggesting the metamorphic rocks there may be analogous to those in the Funeral Mountains.

4. Kinematic analysis of low and high angle normal faults in the Bare Mountain area, and comparison of structures with the Grapevine Mountains Y. Zhang has continued to work on a new structural model for Bare Mountain (Fig. 1).

Bare Mountain provides evidence that the deep structures of Paleozoic rocks that lie beneath Yucca Mountain include major top to the southeast low angle normal faults and pre-14 Ma N-S striking dextral strike-slip faults.

Geologic map compilations and cross-section constructions on the basis of field data and air-photo information are approximately 3/4 complete. These maps and sections will show the structural patterns and Mesozoic and Cenozoic geologic history of Bare Mountain.

A model of structural evolution of Bare Mountain has been developed by analysis of kinematic data, truncation relationships and styles of various structures, especially faults, at Bare Mountain. A number of cross-sections and geological maps, constructed by integrating field data, provide new insights into the structural evolution at Bare Mountain. Highlights of the geological chronology are listed below.

1)Panama thrust

This is the oldest fault at Bare Mountain and is of Mesozoic age. The north-vergent thrust emplaced Proterozoic and Cambrian rocks over Paleozoic rocks. A couple of klippen of upper plate rocks rest upon Paleozoic rocks as young as Mississippian age. The klippe resting on Mississippian rocks near the north end of Bare Mountain was probably dismembered from the Panama thrust root zone by east-dipping oblique-slip normal faults during the Tertiary.

2)Meiklejohn Peak thrust

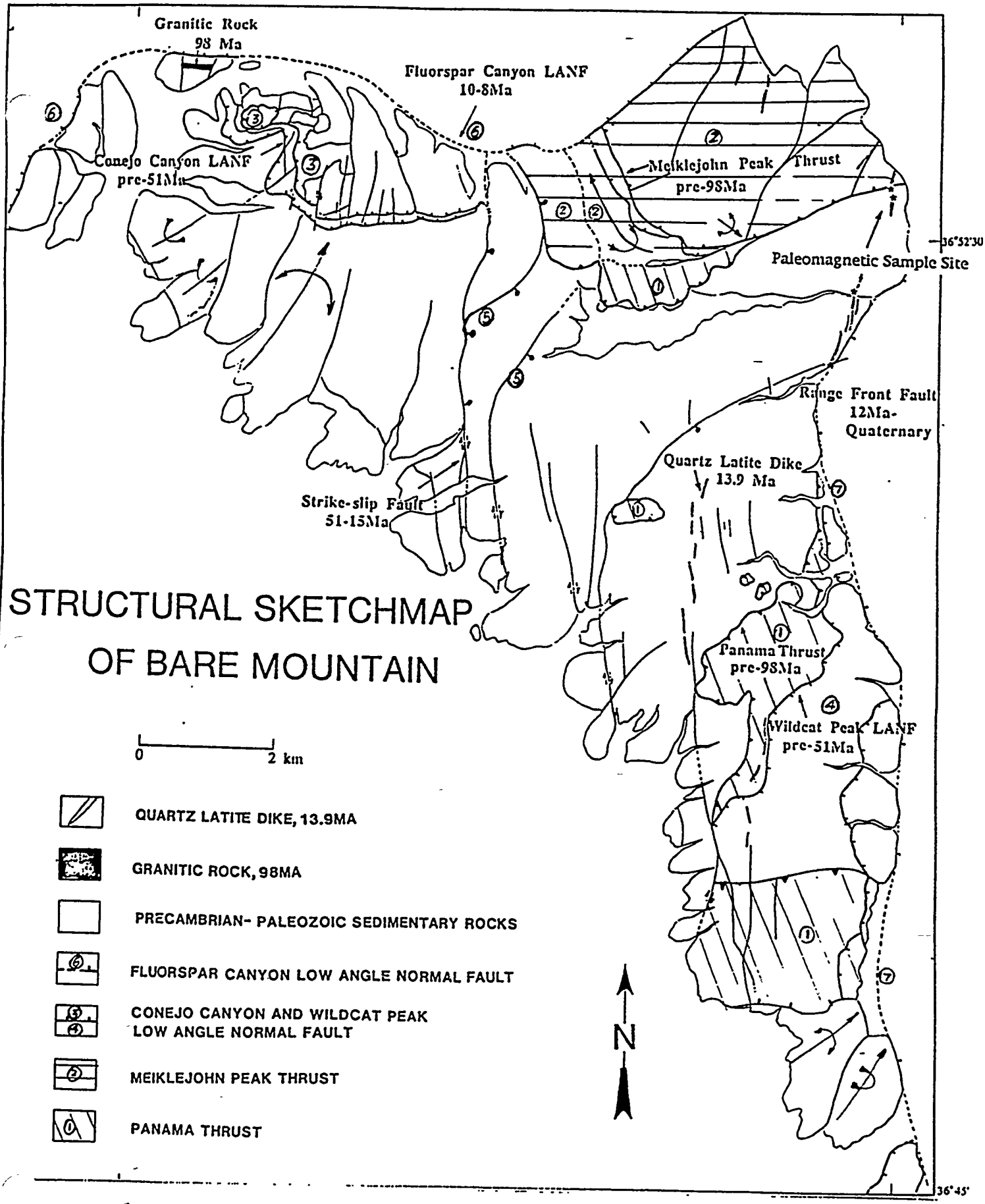

Figure 1. Structural sketchmap of Bare Mountain showing fault types, timing of faults and relations of various structures recognized at Bare Mountain.

This south-vergent thrust formed northeast of Bare Mountain and emplaced Ordovician-Silurian rocks upon a south-facing footwall syncline of Devonian-Mississippian rocks. Drag folds in the upper plate indicate southward movement of the upper plate. The rocks and structures of both upper plate and lower plate of the thrust are distinctly different from the rest of Bare Mountain. This implies that the entire Meiklejohn Peak thrust sheet and part of its footwall may have been transported from an area north of Bare Mountain during Mesozoic or early Cenozoic deformation.

3)Conejo Canyon detachment fault

The oldest detachment fault at Bare Mountain is exposed in the footwall of the Fluorspar Canyon detachment fault in the northwest part of Bare Mountain. Kinematic and structural data indicate that the Conejo Canyon detachment fault roots to the south. The Conejo Canyon fault was responsible for much of the denudation of amphibolite-facies rocks in the area, although Monsen (1982) reported that metamorphic minerals also occur in the upper plate of the detachment. The unroofing and detachment faulting could range back to the late Mesozoic based upon analogies with the Funeral and Grapevine Mountains.

4)Wildcat Peak detachment fault

Overturned Upper Cambrian rocks rest upon Precambrian rocks at the south end of Bare Mountain along the Wildcat Peak detachment fault. The detachment fault truncated the Panama thrust and emplaced both upper and lower plates of the Panama thrust to the south. Black Marble Butte at the south end of Bare Mountain may be part of the upper plate of the detachment fault. The consistent orientation of 13.9 Ma dikes in the eastern parts of Bare Mountain indicates that Wildcat Peak detachment fault may be pre-13.9 Ma. Structural relations indicate that this fault formed at a much higher structural level than the Conejo Canyon fault.

5)North-south striking, oblique-slip faults

The north-south striking faults at Bare Mountain have a unique style: they are steeply east-dipping, right lateral oblique-slip faults with downthrown blocks to the southeast. Some may have several km of dextral displacement. These faults displaced unmetamorphosed, high level rocks from the western parts of Bare Mountain to the southeast. These faults truncate both Mesozoic thrusts and older detachment faults like the

Conejo Canyon and Wildcat Peak faults. They may be responsible for both uplift of the northwest parts of Bare Mountain and for regional extension in the Miocene. Most displacement on these faults appears to predate 13.9 Ma dikes.

5. Evaluation of paleomagnetic character of Tertiary and pre-Tertiary units in the Yucca Mountain region, as tests of the Crater Flat shear zone hypothesis and the concept of oroclinal bending. S. Gillett, R. Karlin, Y. Zhang, and R. A. Schweickert.

(See 1993 progress report; no new work on this phase of the study was done in 1994)

Part IV. *Other activities of Task 5 personnel*

1. Technical review of reports for the Center

None formally assigned; reviewed new publications by Brocher and others, 1993, Faulds and others, 1994, Hudson and others, 1994, Snow and Prave, 1994, Coplen and others, 1994; Savage and others, 1994, and Sawyer and others, 1994:

Brocher, T. M., Carr, M. D., Fox, K. F., and Hart, P. E., 1993, Seismic reflection profiling across Tertiary extensional structures in the eastern Amargosa Desert, southern Nevada, Basin and Range rovince: Geol Soc. America Bull., v. 105, p. 30-46.

Hudson, M. R., Sawyer, D. A., and Warren, R. G., 1993, Paleomagnetism and rotation constraints for the middle Miocene southwestern Nevada volcanic field: Tectonics, v. 13, p. 258-277.

Faulds, J. E., Bell, J. W., Feuerbach, D. L., and Ramelli, A., 1994, Nevada Bureau of Mines and Geology, Map 101.

Snow, J. K., and Prave, A. R., 1994, Covariance of structural and stratigraphic trends: Evidence fof anticlockwise rotation within the Walker Lane belt Death Valley region, California and Nevada: Tectonics, v. 13, p. 712-724.

Coplen, T. B., Winograd, I. J., Landwehr, J. M., and Riggs, A. C., 1994, 500,000-year stable carbon isotopic record from Devils Hole, Nevada: Science, v. 263, p. 361-365.

Savage, J. C., Lisowski, M., Gross, W. K., King, N. E., and Svarc, J. L., 1994,

Strain accumulation near Yucca Mountain, Nevada: Jour. Geophys. Res., v. 99, p. 18103-18107.

Sawyer, D. A., Fleck, R. J., Lanphere, M. A., Warren, R. G., Broxton, D. E., and Hudson, M. R., 1994, Episodic caldera volcanism in the Miocene southwestern Nevada volcanic field: Revised stratigraphic framework, 40Ar-39Ar geochronology, and implications for magmatism and extension: Geol. Soc. America Bull., v. 106, p. 1304-1318.

2. *Meetings attended in relation to the Yucca Mountain Project and the Center for Neotectonic Studies*

a. Advisory Committee on Nuclear Waste, Bethesda, Maryland, June 28-30, 1994; Schweickert presented a paper on Tectonics Research on Yucca Mountain Project for State of Nevada, emphasizing alternative structural models.

b. Geological Society of America, National Meeting, Seattle, Washington, October, 23-27, 1994 (attended by Schweickert and Wellman; see abstract of paper presented by Schweickert and Lahren)

4. *Professional reports provided to NWPO*

a. None

5. *Abstracts published*

a. Schweickert, R.A., and Lahren, M. M., 1994, Amargosa fault system near Yucca Mountain, Nevada (abs.): Geol. Soc. America Abs. with Programs, v. 26, p. A250.

6. *Papers accepted for publication in peer-reviewed literature*

a. None

7. *Graduate theses supported by NWPO*

a. Zhang, Y., in progress, Structural and kinematic analysis of Mesozoic and Cenozoic structures at Bare Mountain, Nye County, Nevada

Appendix I.

University of Nevada, Reno
Center for Neotectonic Studies

Task 8: Evaluation of Hydrocarbon Potential

Report of Investigations
October, 1993 through September, 1994

Principal Investigators:
Patricia H. Cashman
James H. Trexler, Jr.

EXECUTIVE SUMMARY

The goal of research performed by Task 8 is to evaluate the potential for hydrocarbon (oil or gas) reserves in the rocks in the vicinity of Yucca Mountain. We have pursued this goal in several ways:

- Evaluate the bedrock stratigraphy of the region in terms of source rock and reservoir rock potential.
- Refine the Paleozoic stratigraphic data base in the Yucca Mountain region in order to better understand the distribution of strata with hydrocarbon potential.
- Reconstruct the structural history by mapping visible structures and identifying cryptic ones through stratigraphic control.

Our results to date can be summarized as follows:

1. The only stratigraphic unit in the area that has potential as a hydrocarbon source is the Mississippian Chainman Shale. This unit is a hydrocarbon source elsewhere in the state, but had not previously been recognized near Yucca Mountain. It crops out in a belt from the Calico Hills northeast toward Groom Lake, and has significant hydrocarbon content in strata that are in the oil and gas "maturity window".

2. The Mississippian Eleana Formation represents the siliciclastic Antler foreland basin in southern Nevada. It comprises a thick section of conglomerate and sand that is mid- to late Mississippian in age. It has been telescoped eastward along internal thrust faults that also juxtapose it against the coeval Chainman Shale. The Eleana Formation has no source rock potential, but could be a reservoir rock under the right conditions.

3. Important, high-angle faults trending mainly north-south place different Paleozoic units together that were originally widely separated. These faults cut the low-angle thrusts, and are in turn cut by Tertiary low-angle extensional faults. Paleogeographic reconstruction of controls on the distribution of the Chainman Shale will rely on understanding of these faults.

4. Prior to our work, upper Paleozoic stratigraphy in the NTS area was poorly constrained, and based mainly on reconnaisance-level lithostratigraphy. We have systematically improved our understanding of these strata by careful depositional facies mapping and biostratigraphy. Our age control on these units continues to improve, with the addition of 'in-house' experts Mira Kurka (conodonts) at UNR and Betty Skipp (endothyrids and calcareous algae) who works with colleague Jim Cole at the USGS in Denver.

Our ultimate goal is to project Paleozoic strata and structure southwestward under Yucca Mountain. In order to do this, we will have to gain substantially better understanding of the faults that both juxtapose and dismember the strata. In the coming year we will pursue this understanding through more and better stratigraphic control, and geophysical data analysis where possible.

INTRODUCTION

Our studies focus on the stratigraphy of Late Devonian to early Pennsylvanian rocks at the NTS, because these are the best potential hydrocarbon source rocks in the vicinity of Yucca Mountain. In the last year, our stratigraphic studies have broadened to include the regional context for both the Chainman and the Eleana formations. New age data based on biostratigraphy constrain the age ranges of both Chainman and Eleana; accurate and reliable ages are essential for regional correlation and for regional paleogeographic reconstructions. Source rock analyses throughout the Chainman establish whether these rocks contained adequate organic material to generate hydrocarbons. Maturation analyses of samples from the Chainman determine whether the temperature history has been suitable for the generation of liquid hydrocarbons. Structural studies are aimed at defining the deformation histories and present position of the different packages of Devonian - Pennsylvanian rocks.

This report summarizes new results of our structural, stratigraphic and hydrocarbon source rock potential studies at the Nevada Test Site and vicinity. Stratigraphy is considered first, with the Chainman Shale and Eleana Formation discussed separately. New biostratigraphic results are included in this section. New results from our structural studies are summarized next, followed by source rock and maturation analyses of the Chainman Shale. Directions for future work are included where appropriate.

STRATIGRAPHY

Chainman Shale

The primary focus of Task 8's stratigraphic work this year was the internal stratigraphy and regional extent of the Mississippian Chainman Shale in southern Nevada. Our previous understanding of the Chainman (see Task 8 progress report 9/93) was based on relatively poor surface exposures in the vicinity of the Eleana Range, and on the UE17e core from the northern end of Syncline Ridge (Fig. 1). New information for this report comes from surface exposures at Shoshone Mountain, the Calico Hills, and the Spotted Range, and from drillholes at the Calico Hills, the Syncline Ridge vicinity, and the western part of Yucca Flat. More work remains to be done with the available drillhole data.

There were several breakthroughs this year in Task 8's work on the Chainman Shale on the NTS. The depositional base (previously unknown in the area) has been observed in a core and probably also in outcrop. The underlying carbonate has been sampled for conodonts, and has provisionally been dated. The Late Devonian - Early Mississippian depositional history recorded by the rocks between the Devonian carbonate and the typical Chainman mudstone is consistent with the lower Mississipian regional record. At the east edge of the NTS, the Chainman Shale is

exposed in the Spotted Range. Here, the Chainman section comprises calcareous siltstones and mudstones in a thin interval truncated at the top by a regional thrust fault. There is no evidence of carbonaceous shales (potential source rocks) in the Spotted Range, suggesting that they are confined to a present geographic area between Mercury Ridge and the Eleana Range.

The Chainman Shale was deposited on Devonian (?) laminated carbonates. The depositional base can be observed in the core from drillhole UE25a-3 in the Calico Hills; these carbonates have been sampled for dating. This core was logged for Task 8 by consulting petroleum geologist Donna Herring; her lithologic log is shown in Fig. 2. The lower part of the section contains graded sandstone. This was not found in the UE17e core (Fig. 3), and presumably represents a part of the section that was not reached in UE17e. The Chainman mudstone that makes up the bulk of the core resembles the extensive lower mudstone section in the UE17e core at Syncline Ridge (see Task 8 progress report 9/93). The relatively thin section of siltstone, fossiliferous limestone and interbedded mudstone that characterizes the top of the UE17e core does not occur in UE25a-3, but does crop out at the surface in the vicinity of the UE25a-3 drill pad, supporting a correlation between the rocks in these two cores.

The Late Devonian - Early Mississippian section at Shoshone Mountain (Fig. 4) is probably a surface exposure of the lower part of the Chainman Shale. If so, it is the only surface exposure we have found. Karst is developed at the top of the Devonian Guilmette Formation at Shoshone Mountain. This is overlain by shallow marine or fluvial sands with wood debris, and then by argillite and mudstone. Two limestone horizons occur in the mudstone, a lower grainstone interbedded with chert, and an upper laminated micrite. Conodonts from the upper limestone are late Kinderhookian (with reworked Famennian forms), based on identifications by Mira Kurka. Forams in the upper limestone are probably middle Mississippian (Osage-Meramec), based on preliminary identifications by Betty Skipp.

The Shoshone Mountain measured section and new dates document the Late Devonian and Early Mississippian depositional history there: Sea-level lowstand in late Devonian time resulted in erosion and karsting of the Devonian carbonate surface, and deposition of quartz sand in a subareal environment. The surface was drowned in the early Mississippian, and fine-grained siliceous mud was deposited. In Kinderhookian time, carbonate debris was transported in as turbidite beds. These in turn were buried by an unknown thickness of siliceous shale.

Work is in progress to test the correlation of the Shoshone Mountain section with the base of the Chainman, by comparing the ages of the carbonates: The carbonate at the bottom of the UE25a-3 core has been sampled for conodont dating. A small amount of carbonate is also present at the bottom of the UE1l drillhole, from the east side of Syncline Ridge; this may be datable based on forams. Both UE25a-3 and UE1l contain thick sections of Chainman Shale, so an age from either one would date the base of the Chainman.

Eleana Formation

The Eleana Formation does not have hydrocarbon source rock potential, so our objectives in further studying it are to: (1) determine the internal stratigraphy of the several structural slices and (2) interpret the depositional history, in order to (3) describe the regional paleogeography, incoporating the records in both the Chainman and the Eleana. These stratigraphic data will enable us to unravel the complex structure of the area. We have summarized our work to date in a paper on the stratigraphy, depositional environment, and basin history of the Eleana Formation; this paper has been submitted to the AAPG Bulletin.

New information this year on the Eleana Formation includes: (1) the history of the base of the Eleana section, and (2) the recognition of an Eleana section at Mine Mountain that appears to be transitional between the Eleana and the Chainman. The history of the base of the section is based on exposures at Bare Mountain and on samples and descriptions (J.C. Cole, pers. commun., 1994) of the type section at Carbonate Wash. The history of the base of the section is also recorded in the transitional section at Mine Mountain. We have new dates for samples from the Mine Mountain section, based on Mira Kurka's conodont identifications Anita Harris's conodont identifications, and Betty Skipp's foram identifications.

The biggest breakthrough in Task 8's study of the Eleana Formation is the recognition of a transitional Eleana section at Mine Mountain (Figs. 5, 6). This section is generally finer grained than other Eleana sections, and it contains some compositional characteristics of the Chainman, particularly near the top of the section. It appears to have been deposited geographically between the typical Eleana, as seen in the Eleana Range, and the typical Chainman, as seen in core UE17e near Syncline Ridge. A complete section is preserved relatively intact, from the depositional base on Late Devonian carbonates through the bioclastic debris turbidites that were deposited in Late Mississippian (Chesterian) time. Limestones interbedded with fine-grained clastic rocks at the base of the Mine Mountain section are Kinderhookian (with reworked Famennian forms), based on conodonts identified by both Harris and Kurka. In the same horizon, abundance of radiosphaerids, as identiified by Skipp, suggests a late Devonian through Kinderhook-Osage age. Endothyrids from sandy packstones in the upper part of the Mine Mountain section are upper Mississippian in age (Skipp, pers. comm., 1994). A distinctive pebbly mudstone occurs near the top of the section; it appears in the core from the UE1m drillhole (Fig. 6), and is exposed on the surface at the northeastern end of the range. More work is needed to determine the source and depositional environment of this unit.

A new interpretation, based on these data and on regional sequence stratigraphy, is that the coarse clastic part of the Eleana Formation was probably deposited in middle Misisippian time, rather than ranging in age from latest Devonian to latest Mississippian.

Also new this year is a good description of the base of the Eleana section. The type section of the lowest part of the Eleana is at Carbonate Wash, on the Nellis Air

Force Range, and has therefore been inaccessible to us. In the last year, however, it has been described, photographed and sampled for us by our colleague Jim Cole (USGS). The lowest part of the Eleana crops out again at Bare Mountain, west of the NTS. At both places, the Eleana Formation overlies Devonian carbonates. The base of the Eleana Formation (as originally described at both localities) is marked by a sedimentary breccia, followed by quartz sand interbedded with carbonates. After a hiatus, there is an influx of chert lithic sand and conglomerate. These chert lithic sediments seem to have been derived from the northeast, and to be equivalent to the bulk of the Eleana section in the Eleana Range. At Bare Mountain to the southwest the section is thinner and finer grained, and thus is interpreted to be a much more distal version of the section at Carbonate Wash.

Based on the Bare Mountain and Carbonate Wash sections, we can interpret the Late Devonian - Early Mississippian history of the Eleana Formation: The breccia and quartz sand at the bottom of the section seem to reflect the earliest tectonic uplift due to the Antler orogeny (possibly time equivalent to the karsting event recorded in the Shoshone Mountain and Mine Mountain sections farther east). A hiatus in middle Mississippian was followed by down-axis filling of a northeast-trending trough. Objectives for future work on the tectonic history recorded by the Eleana include a measured section and conodont samples from Bare Mountain, and, if possible, samples and paleocurrents from the Carbonate Wash type section.

It is now clear that the "Eleana Formation" as originally defined includes several upper Devonian and lower Mississippian units that have separate histories. These units were juxtaposed by east-west shortening, and by additional faulting which is not yet completely understood. However, in addition to the structural complications, it is clear that there were dramatic east-to-west facies changes in this syntectonic basin stratigraphy. The paleogeography was the primary control on the distribution of the more easterly, organic-rich, Chainman Shale.

STRUCTURAL GEOLOGY

Structural studies for Task 8 focus on the deformational histories of the different Late Devonian - Early Pennsylvanian sections, and particularly on the fault relationships between them. New work summarized in this report includes (1) structure of the transitional Eleana section at Mine Mountain (worked out with Jim Cole of the USGS), (2) fault relationships between the Eleana and the Chainman in the Calico Hills, (3) thrusting between the Eleana and the Chainman Shale, and within the Eleana Formation, in the Eleana Range, (4) extensional faulting in the Eleana Range, and (5) distribution of the Chainman and Eleana formations under Yucca Flat, based on drillhole information. In addition, our new stratigraphic interpretation (specifically, the presence of a transitional Eleana section at Mine Mountain) requires a significant unrecognized fault between Mine Mountain and Syncline Ridge; future work is planned to identify this structure.

The biggest structural breakthrough this year is the recognition that there is no Mine Mountain thrust (Cole and others, 1994). Northwest-dipping beds, which comprise the western limb of a broad anticline, contain an essentially intact lower Devonian to upper Mississippian section, although the Devonain-Mississippian contact was originally mapped as the "Mine Mountain thrust". At its type location, this "thrust" is a low-angle normal fault complex that transports dismembered slabs of the middle Paleozoic carbonate section southwestward over the Mississippian siliciclastic section (Hudson and Cole, 1993). Throw on this fault complex is regionally insignificant.

At the Calico Hills, a thin, fault-bounded slice of the Eleana Formation overlies a deformed but intact section of Chainman Shale. The Eleana rocks are from the upper part of the Eleana section, and include bioclastic limestones which are Chesterian in age (Mamet, personal communication, 1993). Although there is no unequivocal evidence for the nature of the fault contact, it apears to be an extensional fault. The presence of Devonian carbonates in low-angle extensional fault contact over the Chainman here (and, locally, over the Eleana as well) support this interpretation.

New mapping in the southern Eleana Range documents several styles of structures that have accommodated east-vergent thrusting. Locally, near the Eleana-Chainman contact, slices of Eleana and Chainman are imbricated along sub-horizontal surfaces. However, most exposures of this contact show a steeply west-dipping fault with local overturning in hanging wall and/or footwall. Elsewhere, east-vergent folding is associated with a moderately to steeply west-dipping thrust within the Eleana. This thrust occurs in the core of a macroscopic hanging-wall anticline Throughout, cleavage (where developed) dips steeply west, and fold axes plunge gently south-southwest (Fig. 7).

Extensional faulting truncates the Paleozoic section along the west side of the southern Eleana Range, just below the Tertiary volcanic cover (Fig. 7). Numerous kinematic indicators document top-to-the-west motion. This deformation may be fairly local, and may be related to the presence of several large Tertiary calderas immediately to the west of the Eleana Range.

Drillhole information along the west side of Yucca Flat shows that the Chainman Shale extends northward well beyond where it can be mapped from surface exposures. Numerous shallow drillholes (designed to stop after drilling into bedrock) penetrated a few tens to hundreds of feet of black or brown shale interpreted to be Eleana unit j ... which we would now call Chainman. In addition, there are several deeper (1500' -6000') drillholes in the vicinity of Syncline Ridge which we have not yet examined in detail. We plan to examine the cuttings from these holes, to confirm the unit identification. Rock distributions under the basin fill of Yucca Flat may constrain the position and orientation of the both Eleana/Chainman contact, and also the previously unrecognized fault that we have hypothesized between Syncline Ridge and Mine Mountain.

SOURCE ROCK AND MATURATION ANALYSES OF THE CHAINMAN SHALE

Samples from the two most complete cores of Chainman Shale were analysed for source rock potential and maturation history. Unweathered core samples are preferable to surface samples for this purpose. Total organic carbon (TOC) content is measured; TOC > 0.5% is generally considered to be of interest in oil industry exploration. Maturation history can be evaluated from Tmax, a measurement of the temperature at which hydrocarbons are driven off from the sample. Tmax values for immature, overmature and "oil window" rocks are shown in Fig. 8. A regional heating event -- e.g. stratigraphic or structural burial -- results in heating throughout the section, with highest temperatures reached in the deepest part of the section. Local heating -- e.g., due to hydrothermal fluids moving through fractures -- results in heating histories that are much less systematic.

Analysis of 27 Chainman Shale samples from the UE17e drillhole (see Fig. 1 for location) documents that TOC content is within the range for hydrocarbon source rocks throughout the length of the core. TOC is greater than 0.5% for virtually all of the samples, and is substantially higher than that for some of them (Fig. 9). Although most of the samples were selected because of their black color -- usually an indicator of high organic content -- the other samples had TOC values within the same range as the black ones. This suggests that source rock potential is good throughout the section at UE17e.

Maturation studies on the same samples show that although many have been heated past the best temperatures for oil production, there are scattered immature results, including some from near the bottom of the core (Fig. 9). This shows that the heating recorded by the other samples is a local, not a regional, event.

TOC contents of twelve Chainman Shale samples from the Calico Hills (UE25a-3 core) are within the some range as those from the UE17e core (Fig. 10). This suggests that the Chainman contains good source rocks throughout a large areal and vertical extent. Maturation results from these samples cannot be used: S2 values are low enough that Tmax estimates are not reliable. S2 values are generally an order of magnitude lower than those in the UE17e core; with S2 values this low, Tmax results are also low, possibly by as much as 200°.

FIGURE CAPTIONS

Figure 1: Location map showing drillholes and geographic localities mentioned in the text.

Figure 2: Consultant D.M Herring's lithologic log of drillhole UE25a-3, Calico Hills (Chainman Shale).

Figure 3: Consultant D.M Herring's lithologic log of drillhole UE17e, north Syncline Ridge (Chainman Shale).

Figure 4: J.H. Trexler's measured section at Shoshone Mountain (base of the Chainman Shale (?)).

Figure 5: J.H. Trexler's measured section at Mine Mountain (transitional Eleana Formation).

Figure 6: Consultant D.M Herring's lithologic log of drillhole UE1m, northeast Mine Mountain (upper part of the transitional Eleana Formation).

Figure 7: Geologic map of east-verging folding and thrusting in the Eleana Formation in the southern Eleana Range. Stereograms show poles to bedding, poles to cleavage (where present), and computed fold axes for: (a) the macroscopic hanging-wall anticline; n = 18; (b) mesoscopic folds at the base of the hanging-wall anticline, adjacent to the thrust; n = 13; (c) mesoscopic folds associated with imbricate faulting in the core of the hanging-wall anticline; n = 13; and (d) poles to bedding at the south end of the hanging-wall anticline; n = 27.

Figure 8: Correlation of maturation indices, showing Tmax values for hydrocarbon generation.

Figure 9: TOC (total organic carbon) and maturation results for samples from drillhole UE17e; analyses performed at the USGS lab of Charlie Barker.

Figure 10: TOC (total organic carbon) and maturation results for samples from drillhole UE25a-3; analyses performed by MicroStrat, Inc.

Figure 1

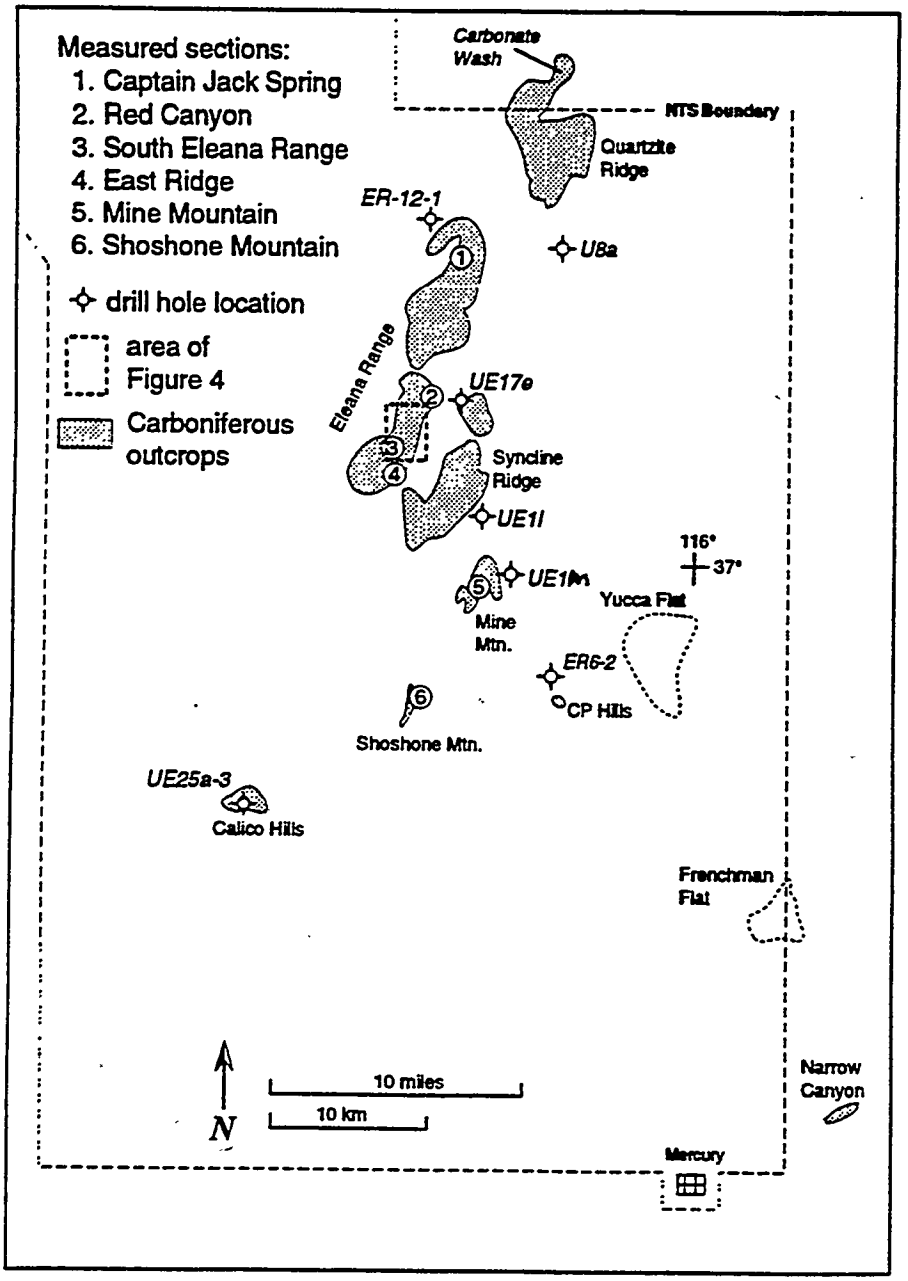
Measured sections:
1. Captain Jack Spring
2. Red Canyon
3. South Eleana Range
4. East Ridge
5. Mine Mountain
6. Shoshone Mountain
drill hole location
area of Figure 4
Carboniferous outcrops
Carbonate Wash
NTS Boundary
Quartzite Ridge
ER-12-1
U8a
Eleana Range
UE17e
Syncline Ridge
UE1l
116°
37°
UE1m
Yucca Flat
Mine Mtn.
ER6-2
CP Hills
Shoshone Mtn.
UE25a-3
Calico Hills
Frenchman Flat
Narrow Canyon
Mercury
N
10 miles
10 km

Figure 2

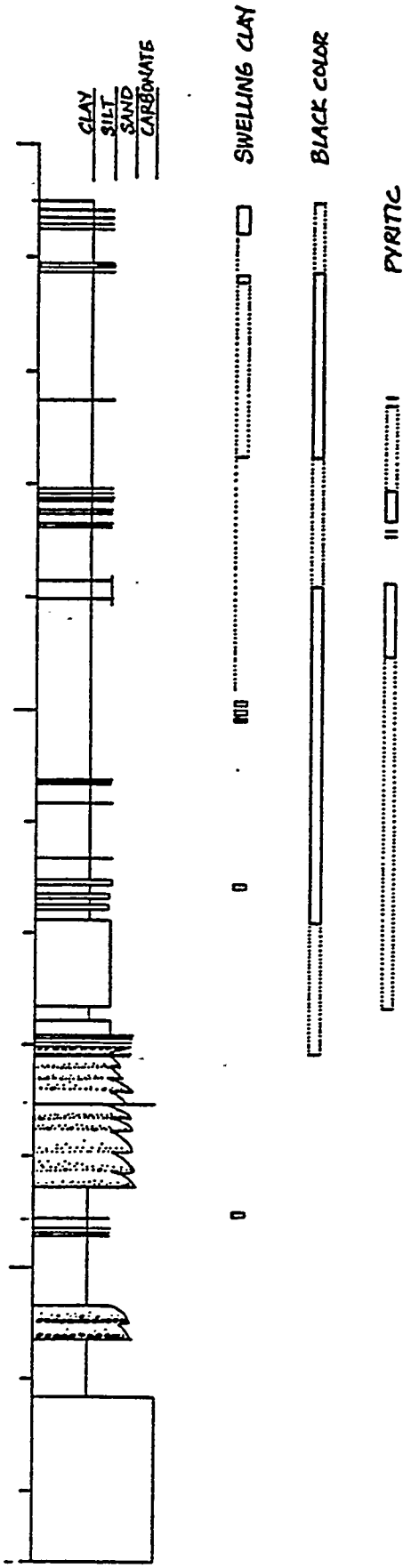

DRILLHOLE UE25a-3

Donna M. Herring
REECO NV
March 1994

Figure 3

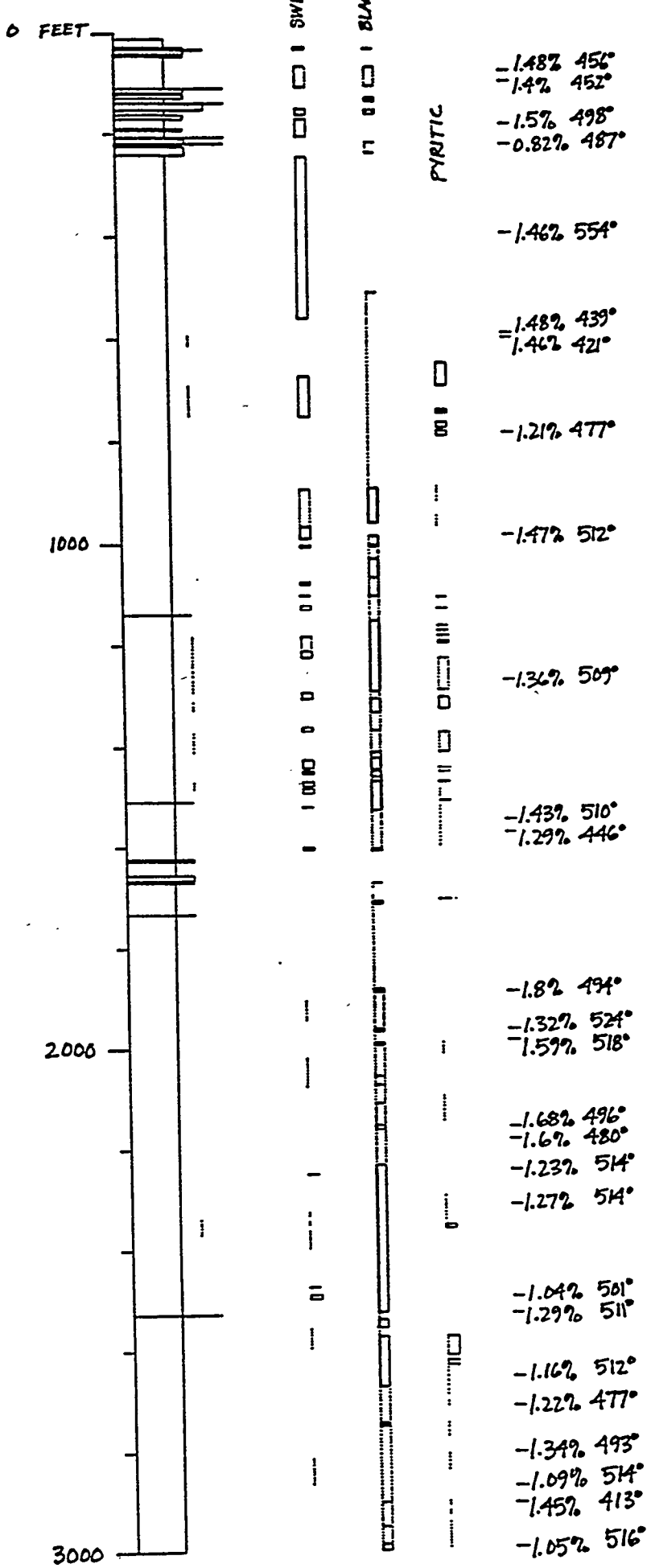

DRILLHOLE UE17e

Donna H. Herr
Reno NV
March 1994

Location Shoshone Mtn., east flank

Name Shoshone Mtn Section

Date 5/9/94 Initials JT

Figure 4

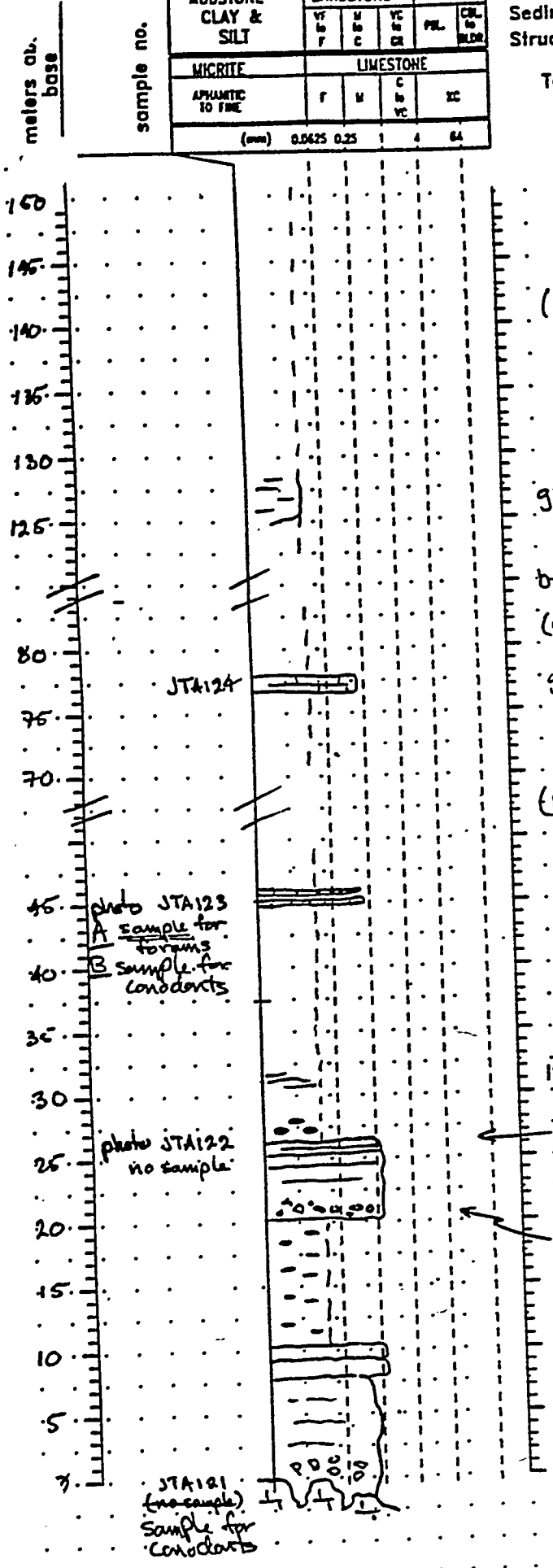

(cover)

gray-green chippy shale

break & offset - continuous section not certain

(cover)

gray laminated limestone - fine micrite

(break)

(gray shale in chippy rubble)

cover

interbedded grainstone & chert

cover

lite-gray chippy shale } float
black chert

rusty indurated top is slightly irregular, very sharp (flooding surface?) with rip-up clasts & wood debris (photo)

breccia disappears upward, is strata bound here

angular, poorly sorted breccia, not sedimentary?

cover - float is thin-bedded black argillite/chert

qtzite w/ coherent beds, no fabric, poss hard-ground tops (dark & indurated)

brecciated qtzite; some faint lamination

carbonate - karsted unconformity, brecciated

Location Shoshone Mtn east flank

Name Shoshone Mtn section

Date 5/9/94 Initials JT

Figure 4

meters above base	sample no.	CLAY & SILT	VF to F	M to C	VC to GR	PEB.	COBBLE to BLDR	Sedimentary Structures/ Taxa
		MICRITE	LIMESTONE					
		APHANITIC TO FINE	F	M	C to VC	XC		
		(mm)	0.0625	0.25	1	4	64	

230

JTA 127

Tert. volcanic cover

poorly exposed, blocky to chippy wx, green on fresh & wx surfaces, stained to brown where indurated, "broken china" sound when walked on.

210

no vertical variation seen

200

195

distinctive green shale

190

break - cover

160

JTA126

A foram sample

gtz grains in laminated beds v.w.sel & clean, wx carbonates in grains

nodular chert

B con. sample

155

black micrite wx lite gray, laminated on wx surface

JTA125

cover

Figure 5

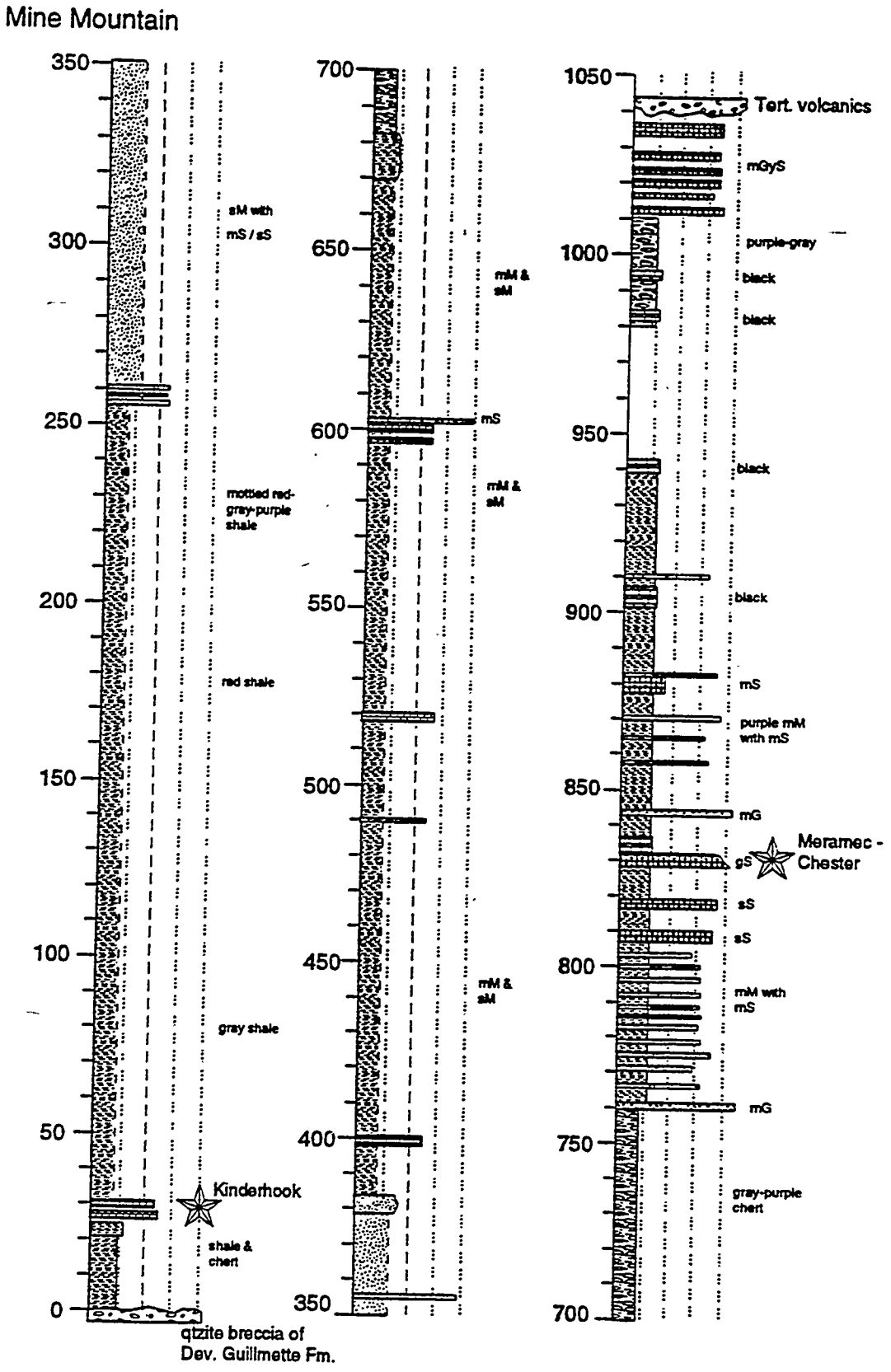
Mine Mountain
350
300
250
200
150
100
50
0
sM with mS / sS
mottled red-gray-purple shale
red shale
gray shale
Kinderhook
shale & chert
qtzite breccia of Dev. Guilmette Fm.
700
650
600
550
500
450
400
350
mM & sM
mS
mM & sM
mM & sM
1050
1000
950
900
850
800
750
700
Tert. volcanics
mGyS
purple-gray
black
black
black
black
mS
purple mM with mS
mG
gS
Meramec - Chester
sS
sS
mM with mS
mG
gray-purple chert

1"=200'

feet

meters

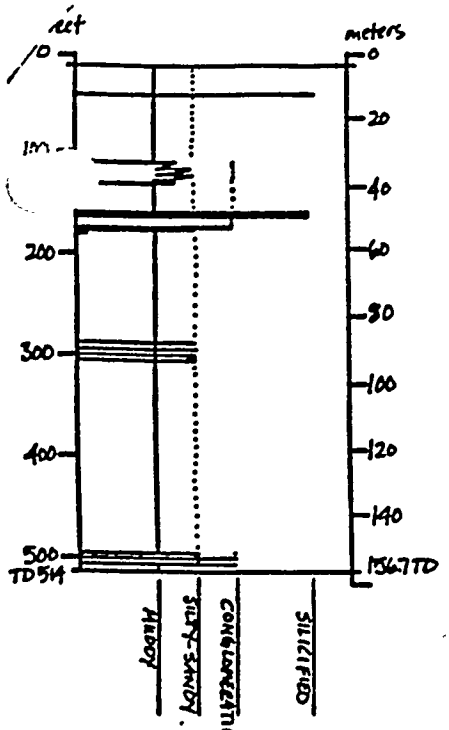

1"=100'

Figure 6

meters

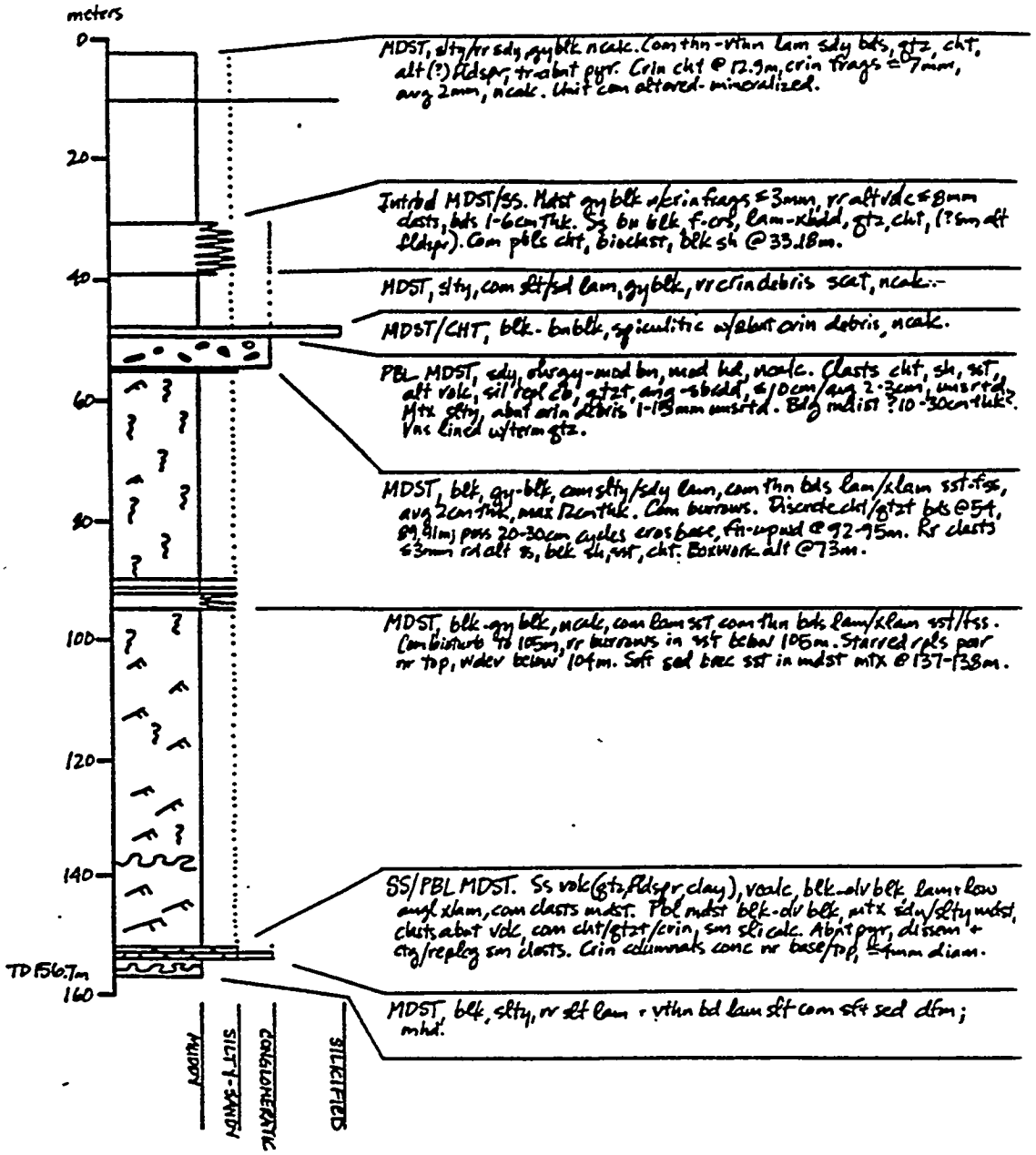

starved ripples

calcareous

soft-sediment deformation

bioturbation

NTS DRILLHOLE UE1m

Donna M. Herring
June 1994

Figure 7

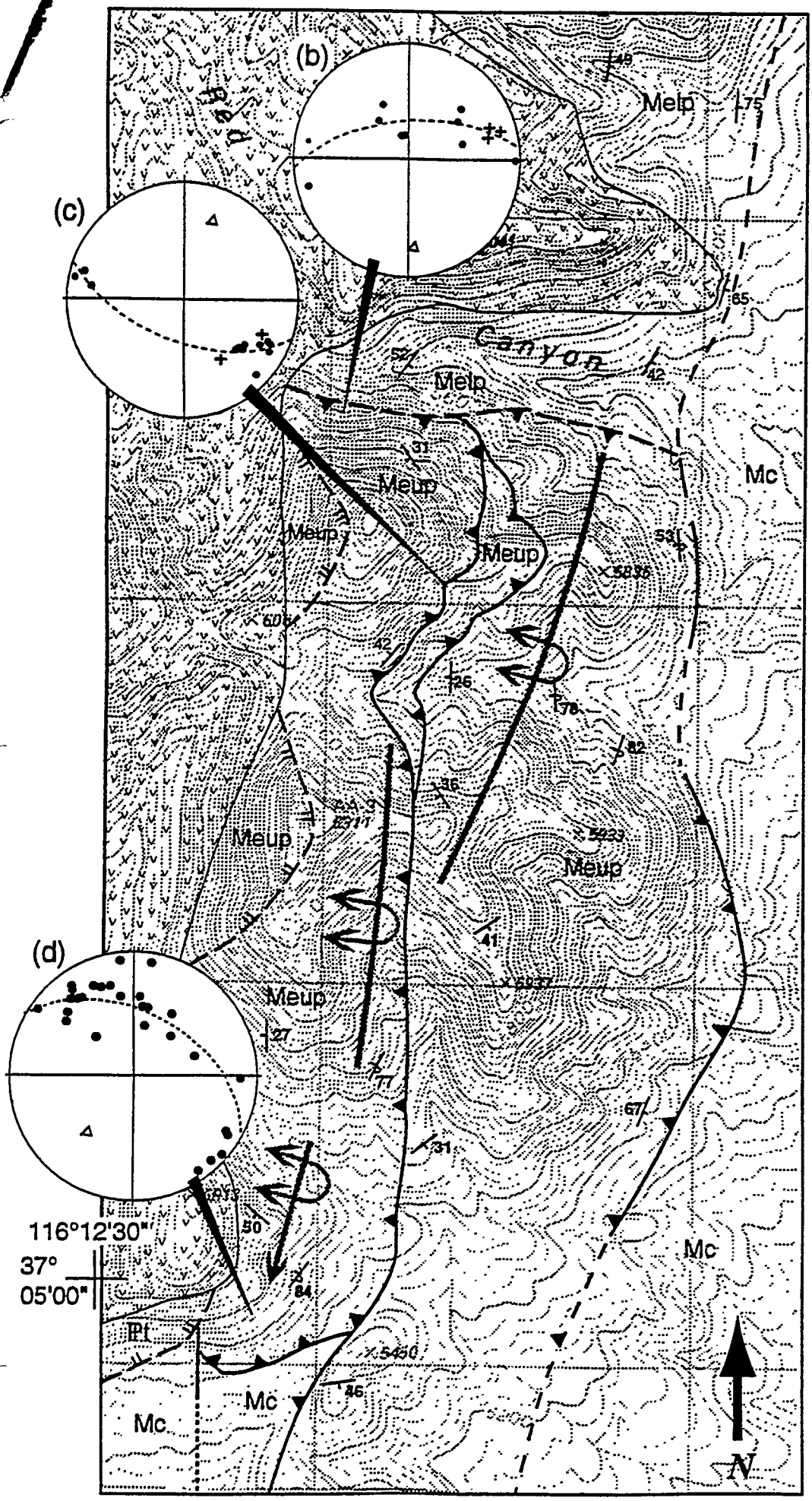

Tertiary volcanic cover

Pt – Penn. Tippipah Ls.

Meup -- Miss. Eleana Fm. upper structural plate

Melp -- Miss. Eleana Fm. lower structural plate

Mc -- Miss. Chainman Fm.

stratigraphic contact

fault (dashed where inferred)

thrust fault

low-angle extensional fault

plunge

overturned anticline

contour interval 20 feet

0.5 km

symbols on stereonets:

- • poles to bedding
- o poles to bedding (overturned)
- △ fold axes
- \+ poles to cleavage

Figure 8.

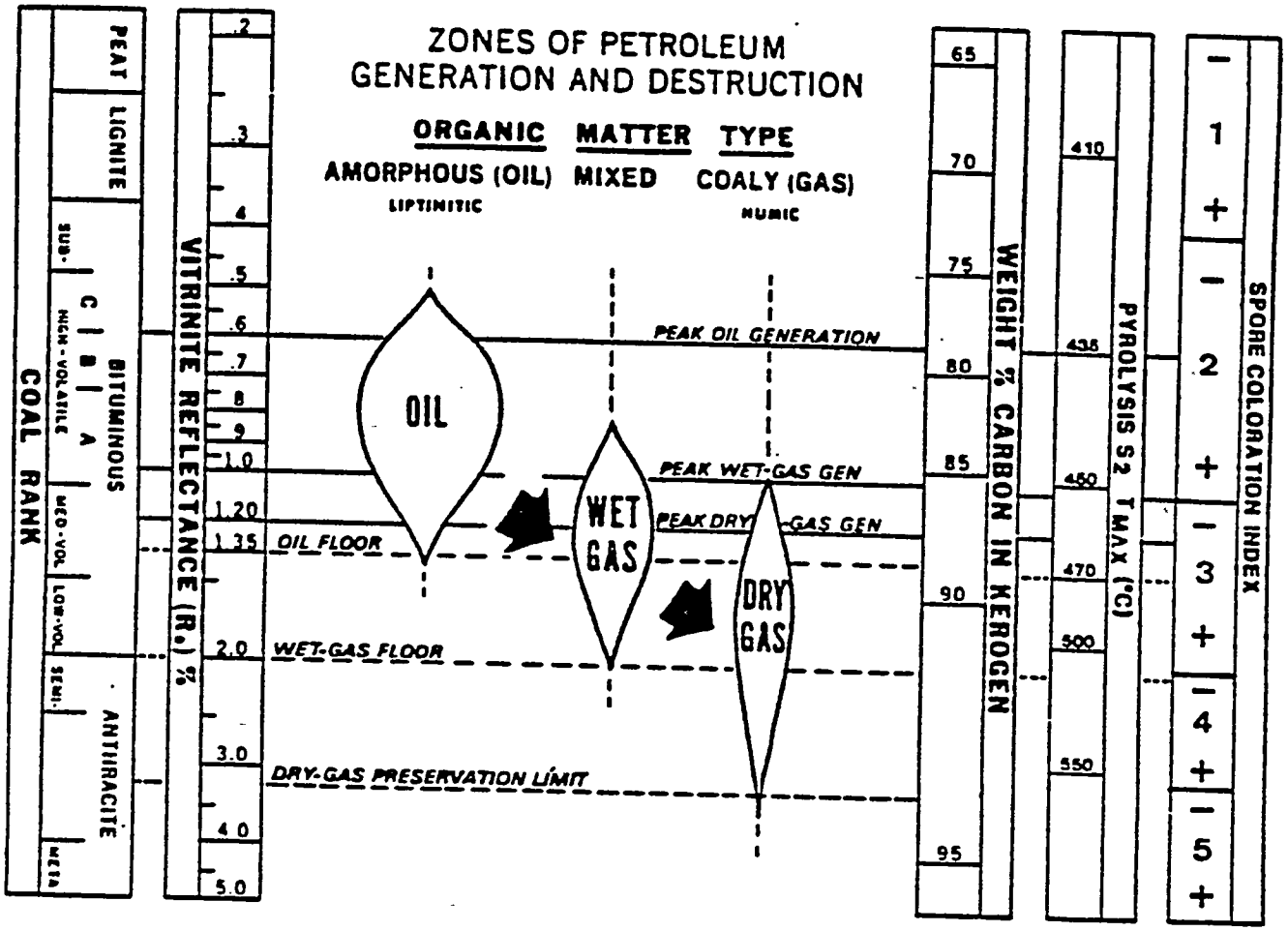

CORRELATION OF VARIOUS MATURATION INDICES AND ZONES OF PETROLEUM GENERATION AND DESTRUCTION.

Figure 9.

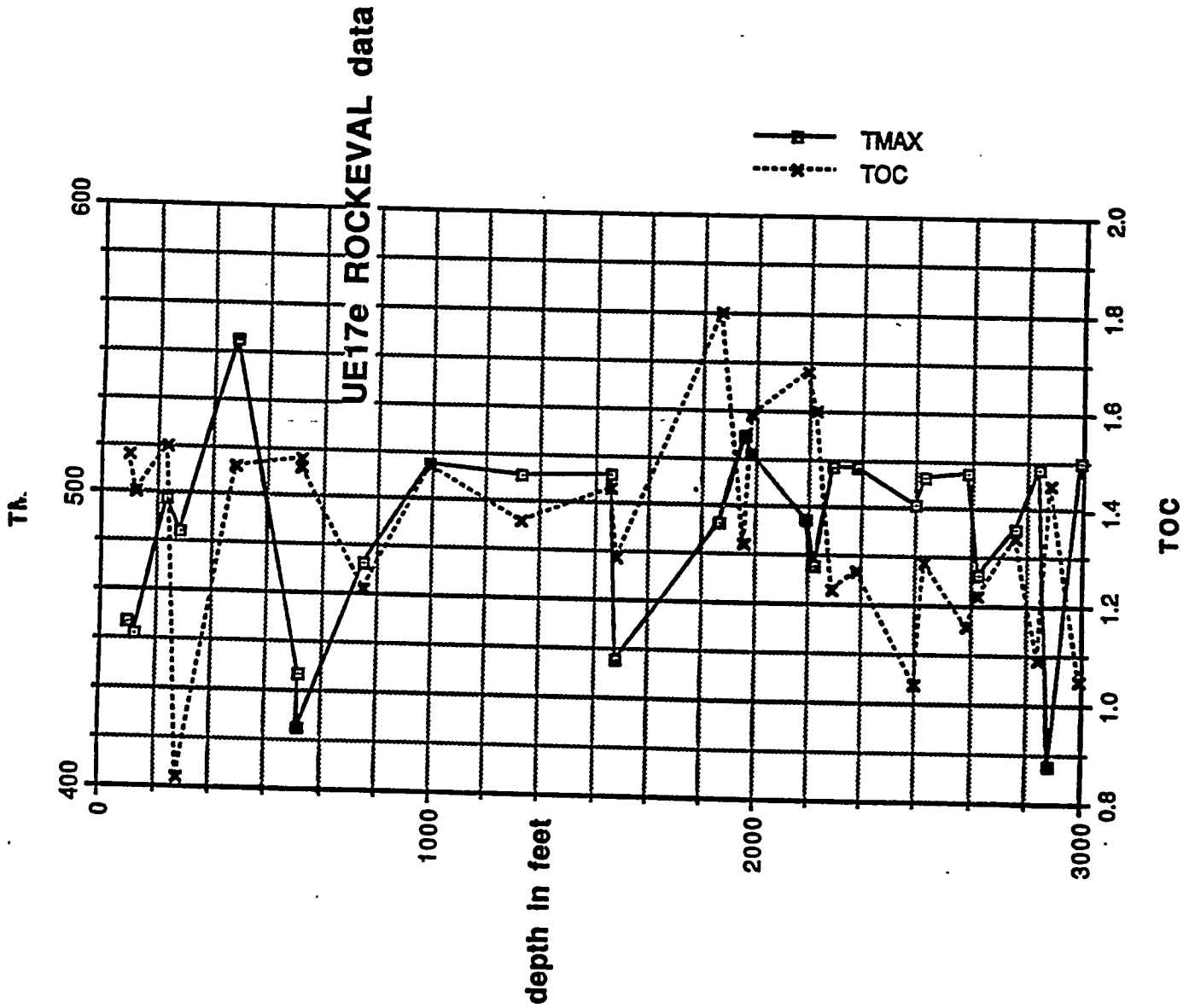
UE17e ROCKEVAL data
TMAX
TOC
Th.
TOC
depth in feet
400
500
600
0
1000
2000
3000
0.8
1.0
1.2
1.4
1.6
1.8
2.0

MICRO-STRAT INC.

PROJECT NUMBER: MSI-94-28

SAMPLE NO.	SAMPLE DESCRIPTION	DEPTH 1 (m)	DEPTH 2 (m)	TOC AND ROCK-EVAL DATA					INTERPRETIVE RATIOS					NOTES	
				TOC	S1	S2	S3	TMAX	HI	OI	S2/S3	PI	S1/TOC	Check	Pyrogram
1	VE25A-3	129.0	129.2	1.17	0.03	0.06	0.15	472 *	5	13	0.40	0.33	3		n
2	VE25A-3	237.3	237.7	1.48	0.03	0.05	0.08	535 *	3	5	0.63	0.38	2		n
3	VE25A-3	339.4	339.6	1.48	0.03	0.08	0.09	480 *	5	6	0.89	0.27	2	c	n
4	VE25A-3	376.1	376.3	1.86	0.06	0.04	0.09	472 *	2	5	0.44	0.60	3		n
5	VE25A-3	410.1	410.3	1.41	0.02	0.01	0.08	347 *	1	6	0.13	0.67	1		n
6	VE25A-3	484.3	484.4	1.75	0.06	0.09	0.13	431 *	5	7	0.69	0.40	3	c	n
7	VE25A-3	551.5	551.7	1.51	0.04	0.03	0.10	307 *	2	7	0.30	0.57	3		n
8	VE25A-3	809.4	809.6	1.52	0.01	0.02	0.08	349 *	1	5	0.25	0.33	1		n
9	VE25A-3	993.1	993.3	1.02	0.05	0.07	0.09	382 *	7	9	0.78	0.42	5		n
10	VE25A-3	1091.0	1091.2	1.23	0.03	0.04	0.12	361 *	3	10	0.33	0.43	2		n
11	VE25A-3	1237.4	1237.6	0.63	0.06	0.09	0.10	334 *	14	16	0.90	0.40	10		n
12	VE25A-3	1544.0	1544.1	1.36	0.06	0.06	0.11	335 *	4	8	0.55	0.50	4	c	n

* Tmax data not reliable due to low S2 values

TOC = weight percent organic carbon
S1,S3 = mg hydrocarbons/g rock
S3 = mg carbon dioxide/g rock
Tmax = Degree C

HI = S2*100/TOC
OI = S3*100/TOC
PI = S1/(S1+S2)
S1/TOC = S1*100/TOC

NOTES:
Check
c = sample analysis confirmed
Pyrogram
n = normal

Figure 10

REFERENCES CITED

Cashman, P.H. and Trexler, J.H., Jr., 1994, The case for two, coeval, Mississippian sections at the Nevada Test Site: p. 76 - 81, *in* McGill, S.F. and Ross, T.M. (eds.), Geological Investigations of an Active Margin, GSA Cordilleran Section Guidebook, San Bernardino, CA, March 21-23, 1994.

Cole, J.C., Trexler, J.H., Jr., Cashman, P.H., and Hudson, M.R., 1994, Structural and stratigraphic relations of Mississippian rocks at the Nevada Test Site: p. 66 - 75, *in* McGill, S.F. and Ross, T.M. (eds.), Geological Investigations of an Active Margin, GSA Cordilleran Section Guidebook, San Bernardino, CA, March 21-23, 1994.

Cole, J.C., Trexler, J.H., Jr., and Cashman, P.H., 1994, Reinterpretation of Mesozoic contractile structures in southern NyeCounty, NV (abs) *submitted to fall AGU meeting*

Hudson, M.R. and Cole, J.C., 1993, Kinematics of faulting in the Mine Mountain area of southern Nevada: evidence for pre-middle Miocene extension: Geol. Soc. America Abs. with Programs, v. 25, no. 5, p. 55.

Trexler, J.H., Jr., and Cashman, P.H., (in review), The southern Antler Foreland Basin: the Mississippiam Eleana Formation, Nevada Test Site: submitted to AAPG Bulletin

preprints, preprint and abstracts removed. ds